Structural and chemical controls on melting in high grade metapelites, SW Finland

Amanda Voase

Thesis submitted for the degree of Doctor of Philosophy

University of Edinburgh

2000

Abstract

The Turku granulite terrain of southern Finland is located within the south-west corner of the Svecofennian Schist Belt, part of the Scandinavian Svecofennian Orogenic Belt. The field area is a representative slice of an island arc system which collided against the northern Baltic Shield at 1890 Ma. This resulted in amphibolite-granulite facies metamorphism in the time interval 1890-1870 Ma when two phases of compression (D1 and D2) deformed the Turku rocks into recumbent isoclinal folds, with axial traces striking NW-SE.

A second thermal pulse within the Turku terrain was accompanied by a gentler period of compression (D3) and rotation that produced folds with axial traces orientated NE-SW. Maximum pressure and temperature estimates (from three garnet/cordierite barometers, five Fe-Mg exchange thermometers and an internally consistent thermodynamic dataset) are 750°C and 5-5.5 kbar.

Under these P-T conditions the pelitic supracrustals partially melted, producing felsic segregations and a restite rich in garnet, cordierite and biotite. Two different generations of garnet and cordierite are linked to D2 and D3. The melting started during late D2 and was continuous right through D3, during which time most of the melting occurred. The leucosomes that were produced throughout this period ranged from syenogranites to granodiorites, based on their normative quartz and feldspar components. They all have A/CNK values of >1.10 and thus are peraluminous in composition, in accordance with melts produced experimentally within pelitic systems. FeO + MgO contents of leucosomes range from 0.31 to 12 wt%; above 3 wt% the leucosomes are also enriched in Zr and Th. This suggests that either entrainment of restitic material occurred during inefficient melt segregation, or that the leucosomes are themselves restitic after further melt migration, i.e. they are enriched in 'cumulate' phases.

The composition of the leucosomes and the presence of garnet and cordierite poikiloblasts suggests that melting proceeded via incongruent melting reactions involving the breakdown of biotite and sillimanite to produce garnet, cordierite, K-feldspar and melt. Volatiles, liberated through the breakdown of biotite, will partition directly into melt and cordierite: the total volatile contents and the X_{CO2} (CO_2/CO_2+H_2O) of cordierite were analysed to distinguish between fluid-present and fluid-absent conditions, and to allow calculation of fluid species activities. Total measured H_2O contents of cordierite (0.2-0.6 moles per formula unit) are lower than experimentally calibrated saturation values at the relevant PT conditions. This suggests that the melts in equilibrium with the cordierite were water-undersaturated. The melts would have contained around 3-3.5 wt% water, using D*w* (H_2O melt/H_2O cordierite) values of 3. These values are much lower than those for water-saturated felsic melts that would have had water contents of 11 wt% at 5.5 kbar and 750°C. This is borne out by low calculated water activities of 0.15-0.5. These values are heterogeneous on a sample scale but are fairly homogeneous across the terrain.

$\delta^{13}C$ values from cordierite CO_2 (-7 to -25‰) indicate mixing of original sedimentary carbon with an external fluid source, and in some cases the total CO_2 m.p.f.u of cordierite are close to experimentally-calibrated saturation curves. It appears that melt production in the Turku terrain has occurred by two processes. Some leucosomes are representative of locally controlled dehydration melting that produced volatile undersaturated melts. Cordierites that are close to saturation and that have heavy $\delta^{13}C$ values are evidence for the presence, at some localities, of a CO_2-rich fluid introduced by melts in an open system.

Acknowledgements.

Primary thanks must go to my supervisors, Professor Simon Harley and Professor Ben Harte. Cheers to Shimon for sharing the delights of shell shuits, Shean and Shpinel. Thanks to Ben for being my ceilidh partner, introducing me to cigars and for being a 'smashing' supervisor. Oh and thanks to them both for the moped experience!

Thanks for helpful advice in all things academic must go to, in no particular order, Professor Ian Parsons, Professor Godfrey Fitton, Professor Colin Graham, Dr John Craven, Dr Peter Hill, Dr Paula McDade, Dr Dodie James, Dr Pentti Höltta, Dr Markku Väisänen, Steph Lewis, Clare Bond and John Dale. For helping me to untangle the joy that is THERMOCALC I have to thank Dr Tim Holland and Dr Roger Powell. Thanks must also go to Roger for introducing me to the fine wines that British Airways have to offer. Analytically speaking, I must praise the help of those that let me loose on their beautiful shiny instruments and gave me tea and plain chocolate hobnobs. Cheers, John, Pete, Simon and Paula.

Thanks to Bob, Ted, Pat, Terry, Brian, Jim, Gary, Keith and Dave for always being there and making life more fun.

I must of course thank all those who have been true friends for my adulthood! Thanks to Cleggy for always being on the end of the phone, for sharing her cheesy chips and for introducing me to the delights of the heaving metropolis that is Leyland. Big thanks to Clair and Carolyn, for sitting next to me that fateful day, for sharing many alcohol fuelled evenings and for agreeing to share George with me. I look forward to the desert island!. Cheers Marky, for being a great pal for the last seven years, you always know how to cheer me up! Thanks to Alistair, for gainfully taking over Wednesday nights, being my beach buddy and for the proposal!

Thanks to all those people that have shared office space with me. The lads, Mark, Tim, Al, Sandy and Jase, thanks for bike maintenance afternoons, penguin kidnapping and your manly advice. Equally I thank Lisa, Lesley and Nicky for bringing girlieness to the office and for sharing their chocolate ice cream!

All those people that have made Edinburgh such fun over the last four years I thank you, Paula 'Clydebank' McDade, Clare 'nice packaging' Bond, Steph 'secret smile' Lewis, and Ned 'vegetable' Pegler! Cheers for red wine fuelled evenings, for fun weekends amongst the hills and for all your help and support. I couldn't have managed it without you all. Oh, and Paula, sorry about the prune donut and diet coke! Cheers also to Lisa, Nicky, Lesley, Zoe, Kathryn and Sue for all their friendships. Special thanks to Mark 'levels of squidginess' Hutchison for being my first friend in Edinburgh, for assisting in Finland and for improving my Ceilidh dancing!

Special thanks have to go to Jonny, thanks for your advice, help and encouragement. You gave me confidence in my abilities and introduced me to aspects of myself I didn't know I had. Thank you.

Finally my biggest thanks have to go to my family. To Grandad and Nanny for always supporting everything I've done (and to Grandma and Grandpa for helping me through my formative years, I'm sure you've both been watching over me!). Cheers to Rob for his brotherly advice, his Playstation lessons and for allowing me to 'put away'! Thanks for absolutely everything must go to Mum and Dad. They've been my biggest supporters, financial backers and friends! Thanks for being everybody's Aunty Linda and Uncle Peter. I am indebted to you both.

List of symbols and abbreviations

Minerals

Amph	Amphibolite	Kfs	K-feldspar
And	Andalusite	Qtz	Quartz
Bt	Biotite	Saph	Sapphirine
Chl	Chlorite	Sil	Sillimanite
Crd	Cordierite	Spl	Spinel
Grt	Garnet		
Gr	Graphite		

Additional phases

L	Silicate melt	V	Volatile fluid

Mineral components

Ab	Albite	Hc	Hercynite
Alm	Almandine	Mag	Magnetite
Ann	Annite	Or	Orthoclase
An	Anorthite	Plag	Plagioclase
Chr	Chromite	Prp	Pyrope
East	Eastonite	Spl	Spinel
Gah	Gahnite	Spss	Spessartine
Gal	Galaxite	Usp	Ulvöspinel
Grs	Grossular	Uvr	Uvarovite

Chemical elements

Standard symbols are used for chemical elements and compounds (e.g. Fe, CO_2 etc.).

Chemical systems

KMASH	K_2O- MgO-Al_2O_3-SiO_2-H_2O
KFASH	K_2O-FeO- Al_2O_3-SiO_2-H_2O
KFMASH	K_2O-FeO-MgO-Al_2O_3-SiO_2-H_2O

Thermodynamic symbols

R	universal gas constant (equal to $8.314 JK^{-1}$
P	Pressure

T	Temperature
n_i	number of moles of component i
a_i	activity of a component
f_i	fugacity of a component
K	equilibrium constant for a reaction
K_D	distribution coefficient of two cations between two phases

Miscellaneous

D_i	refers to a deformational event
S_i	refers to a planar fabric
F_i	folds associated with D1
AFM	projection onto Al_2O_3-FeO-MgO plane from quartz, K-feldspar and H_2O
$\delta^{13}C$	$10^3 [(^{13}C/^{12}C)_x-(^{13}C/^{12}C)_{std}]/(^{13}C/^{12}C)_{std}$ where *x* is the unknown specimen and *std* is the standard material (PDB for carbon)

"Finland, Finland, Finland,

The country where I want to be....."

"your treetops so lofty, your mountains so tall"

'Monty Python Sings' (1989)

Contents

Chapter 1

Introduction and geological background

Chapter 1 - Introduction and geological background

1.1 - A brief introduction to granulites and their study

The study of granulite facies rocks provides an insight into the conditions of their formation and the processes operating in the lower crust, such as PT conditions, fluid regimes, melting processes, deformation at high temperatures and P-T-t evolution. Granulites may span a range of rock compositions from basaltic to pelitic and granitic, and a range of recorded pressures and temperatures from 700-1100° and 5-11 kbar (Harley, 1989, 1992, 1998). The study of granulites currently falls into four main areas of research. These are discussed in further detail later on in this chapter.

1. Modelling of the tectonic and thermal processes required to produce the range of pressures and temperatures recorded from granulites (Loosveld and Etheridge, 1990; Sandiford and Powell, 1991), and the P-T-t evolution paths as models for granulite formation (Bohlen, 1987; 1991; Harley 1989; 1991; 1992; Warren and Ellis 1996), such as ITD (isothermal decompression) and IBC (isobaric cooling) paths.
2. Understanding and interpreting the low water activities and abundance of CO_2-rich fluid inclusions which are characteristic of granulites, and which contrast with fluid inclusions and activities in most other metamorphic facies. CO_2 fluxing has been proposed as a mechanism of desiccating the lower crust (Newton et al, 1980; Shreurs, 1985; Frost and Frost, 1987). However recent workers have argued against CO_2 flushing as a standard method of stabilising granulites based upon several lines of evidence, i.e. misidentification of peak inclusions, variable inclusion barometry results and heterogeneous isotope compositions within terrains (Lamb et al, 1987; Lamb, 1990; Valley et al, 1990; Bhowmik et al, 1995).

   H_2O-NaCl brines have been proposed as an alternative to CO_2 rich fluids to explain the low water activities of most granulites, supported by recent experimental results (Aranovich and Newton, 1996; Shmulovich and Graham, 1996; Aranovich and Newton, 1997; Aranovich and Newton, 1999; Shmulovich and Graham, 1999). In the H_2O-CO_2-NaCl system, water activity is greatly

reduced and CO_2 activity relatively increased. The presence of crustal brines could therefore be responsible for the low a_{H2O} values and high a_{CO2} values of granulite terrains.

The third alternative discussed in this thesis is the lowering of a_{H2O} by partial melting. Melting following the breakdown of hydrous phases will liberate water which may be selectively removed by a melt (Powell, 1982; Waters and Whales, 1984; Waters; 1988; Harley, 1989, 1992; Harley and Hensen, 1990), thus lowering a_{H2O}. Evidence for melting is found within many granulite terrains and so this is currently the most widely cited method for lowering a_{H2O}.

3. In order to constrain the position of key melting reactions in P-T-X space, theoretical and experimentally constrained petrogenetic grids have been derived for certain chemical systems, e.g. KFMASH (Thompson, 1982, 1996; Henson and Harley; 1990; Powell and Downs, 1990, Carrington and Harley, 1995; Holland et al., 1996). The construction of these grids and their related pseudosections furthers the understanding of lower crustal processes, particularly melting and dehydration of the crust
4. Migmatite terrains may be the source area for S-type granites (Sawyer, 1996) and so methods for segregating and extracting melt from granulite terrains need to be understood. Controls on melt extraction can be chemical e.g. H_2O contents (Brown et al., 1995; Clemens and Droop, 1998) or physical, i.e. deformation and stress (Collins and Sawyer, 1996). Shear zones are often thought to be paths for melt movement (Collins and Sawyer, 1996).

This project studies the low pressure granulite terrain of Turku, SW Finland and aims to model melting within pelitic compositions and constrain the fluid regime at the time of melting.

1.2 - Aims of this study

Previous work on the Turku granulite terrain has established a well-constrained metamorphic history and structural framework (Hietanen, 1947; Höltta, 1986; Van Duin and Nieman, 1993; Väisänen et al. 1994; Väisänen and Höltta, in press). The

terrain represents a slice of an island arc system that collided with the Baltic shield >1890 Ma. During collision the resulting compression and deformation of the terrain led to amphibolite to granulite facies metamorphism (Van Duin and Nieman, 1993; Väisänen et al. 1994; Väisänen and Höltta, in press). This metamorphic event is associated with large volumes of granitic material (leucosomes) now found at many Turku localities. Whilst previous work on the terrain has suggested that the leucosomes represent melts formed through dehydration melting of the local pelites, there has been no previous attempt to classify the range of leucosome types, or to define quantitatively the conditions under which melting and melt segregation took place. This study aimed to constrain these features and derive a model for melting within the Turku terrain. It attempted to confirm the PT estimates from previous work on the area and whether the reported PT gradient (700°C/4-5kbar – 800°/6kbar) exists (Van Duin and Nieman, 1993; Väisänen et al, 1994). The final aim was to ascertain the presence, composition and nature of any peak metamorphic fluid.

There were three main research approaches were adopted within the project in order to derive a single model for melting within the Turku terrain:

a) Classification of the temporal relationships of leucosomes within the structural framework defined by Väisänen et al. (1994).
b) Petrological studies of metamorphic assemblages and mineral textures as evidence for partial melting, combined with a compositional classification of leucosome types based upon mineral assemblages, bulk compositional data and trace element geochemistry.
c) A definition of the external factors that control melting such as P, T, a_{H2O} and a_{CO2}.

1.2.1 – a) Fieldwork approaches

In the field a basic framework for the model had to be derived. Fieldwork concentrated on outcrops (road cuttings or flat glaciated hummocks) from three main zones in the north, middle and south of the terrain in order to investigate the reported PT gradients of Höltta (1986), Van Duin and Nieman (1993), and Väisänen et al.

(1994). Detailed field techniques will be presented in chapter 2. A preliminary field season of three weeks was undertaken in September of 1995 and a further 6 weeks in the summer of 1996. During the two field seasons care was taken to:

1) Document leucosome characteristics, size, mineralogy, grain size and relation to the deformation fabric.
2) Document the amount of leucosome material present at any one outcrop.
3) Decipher relationships of different leucosomes and determine crosscutting relationships.
4) Observe and interpret the mesosome assemblages and textures.
5) Check structural observations against previous studies.

1.2.2 – b) Petrological studies

Following the examination of numerous outcrops, eleven were selected as priority localities for detailed work on the basis of the features observed. Approximately 200 samples were collected from across the terrain (Appendix 3.1). Thin sections were made from all leucosome and mesosome samples and those from the identified key localities were studied petrographically. A Cameca CAMEBAX microprobe at Edinburgh University was used to determine major element mineral compositions. XRF analysis identified the major and trace element contents of the different leucosome generations distinguished from the fieldwork.

1.2.3 – c) Geothermobarometric and fluid studies

Compositional data were combined with knowledge of equilibrium assemblages from petrological studies in order to constrain pressure and temperature. Various Fe-Mg exchange thermometers and barometers combined with the internally consistent dataset of Powell and Holland (1988) were utilised. In order to gain an understanding of the fluid conditions under which melting took place, the channel volatiles of cordierite have been analysed using SIMS (secondary ion mass spectrometry) at Edinburgh University. Cordierite is a good fluid monitor as it can contain volatile fluid species within the large channels in its structure. With PT information from this study and earlier studies, the ratio and amount of CO_2 and H_2O

can be used to calculate a_{H2O} and a_{CO2} in the terrain during melting, based on approaches developed by Harley (1994); Carrington and Harley (1996); Harley and Carrington (in press) and Harley et al. (unpubl. data). The possible sources of CO_2 have been examined using $\delta^{13}C$ of cordierite channel volatiles as measured using stepped heating mass spectrometry at Royal Holloway, University of London.

1.3 - Structure of the thesis

The rest of this chapter consists of two main sections (Figure 1.1):

1) Introduction to granulites and the problems associated with their research

2) The tectonic history of the Finnish Svecofennian, and in particular the position that the Turku terrain has in tectonic models.

Following this chapter introducing the Svecofennian of Finland, the Turku terrain and this thesis, Chapter 2 presents the fieldwork data (including detailed maps and traces of the outcrops), whilst Chapter 3 considers the mineral assemblage evolution and textural relations as deduced from petrographic observations.

Chapter 4 presents mineral chemistry based on electron probe data whereas the bulk-rock geochemistry results are presented in Chapter 5. The mineral chemistry data is used in chapter 6 to determine equilibration pressures and temperatures using a range of geothermobarometric equilibria. In Chapters 7 and 8 data on volatile contents and isotopic compositions in cordierite is presented with SIMS (Chapter 7) and stepped heating methods (Chapter 8). Chapter 9 concludes the thesis and suggests a model for melt processes in the Turku granulite terrain.

1.4 – Section 1 - Granulite formation, previous work

Granulites are also found to have a range of compositions from mafic and felsic orthogneisses to pelitic, calcareous and psammitic paragneisses (Fitzsimons, 1991). Figure 1.2 illustrates the P-T range over which granulite phase assemblages are stable. The granulite field is bound by eclogite facies at higher pressures and amphibolite

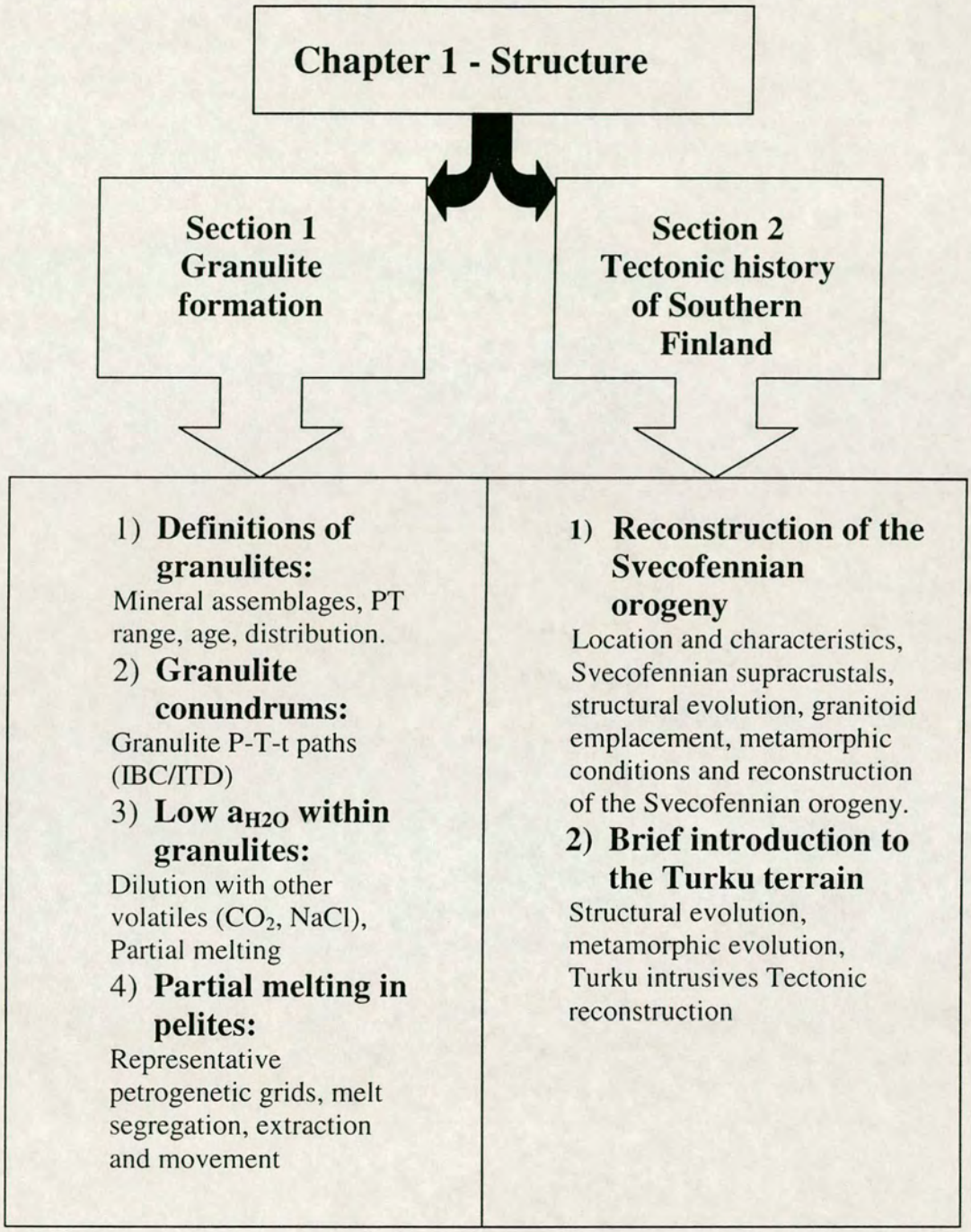

Figure 1.1 – Structure of Chapter 1.

facies at lower temperatures, and some granulite terrains may show a facies transition across these borders.

The transition from amphibolite to granulite facies metamorphism is seen in several metamorphic terrains e.g. South Greenland, the Svecofennian of Finland, Broken Hill Australia and central Canada, (Philips, 1980; Harley, 1989; Fitzsimons, 1991; Spear 1994). The transition is generally marked by an increase in temperature and by a decrease in a_{H2O}. In different lithologies this transition is marked by the incoming of certain mineral assemblages, or key indicator minerals.

Mafic: Amphibole → Orthopyroxene

Felsic: Biotite + amphibole → Orthopyroxene

Pelitic: Biotite + sillimanite + K-feldspar → Garnet + cordierite

Although some workers on granulites identified a narrow range of peak granulite facies temperatures and pressures for most terrains of 750±50°C and 7.5 ± 1 kbar (Bohlen, 1987; Bohlen, 1991), a wider study of recent literature indicates that approximately 50% of granulite terrains fall outside of this narrow P-T box (Harley, 1989). Some granulites record ultra-high temperature metamorphism, others very high P, and yet others high T/low P conditions. Figure 1.3 incorporates data taken from Harley (1989, 1992) and more recent data that are presented in Table 1.1. Some of the key mineral assemblages used to distinguish the ultra-high temperature subfacies of granulite metamorphism, at both higher (opx + sil ± qtz) and lower pressures (spr + qtz, spl + qtz) are illustrated in the petrogenetic grids of Figure 1.4.

1.4.1 - Age of granulite terrains

Although it was once thought that granulites were constrained to Precambrian terrains it is now known that granulites are found within tectonic belts from the Archaean to the Phanerozoic (Harley, 1989; 1992). There is a potential bias to the preservation of Proterozoic belts as Archaean belts have often been reworked. Phanerozoic belts are also more rare due to the difficulties involved in granulite exhumation over shorter timescales (Fitzsimons, 1991), but important granulites of Variscan, Hercynian and Alpine ages are exposed in Europe

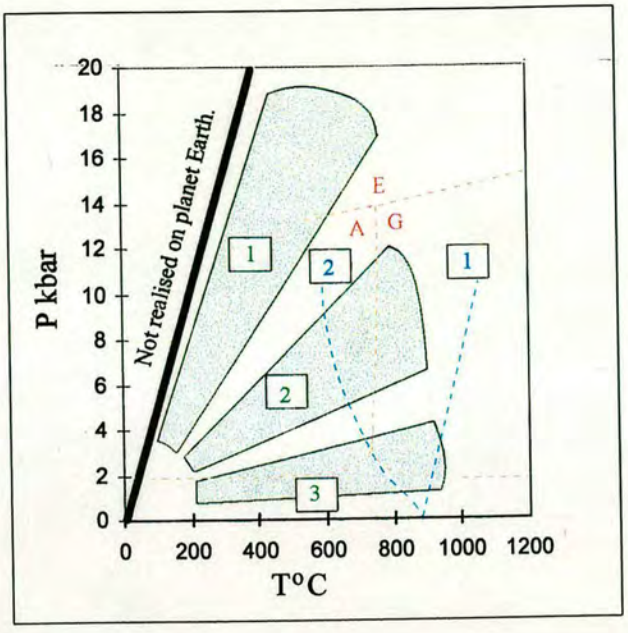

Figure 1.2 - P-T boundaries of granulite facies (G) against neighbouring amphibolite (A) and eclogite (E) facies (After Yardley, 1989). Tectonic settings are superimposed onto the graph: 1 - subduction zones, 2 - continental orogenic belts, 3 - island arcs, ocean ridges, contact aureoles Dry (1) and wet (2) granite melting curves are also included. After Spear, 1993).

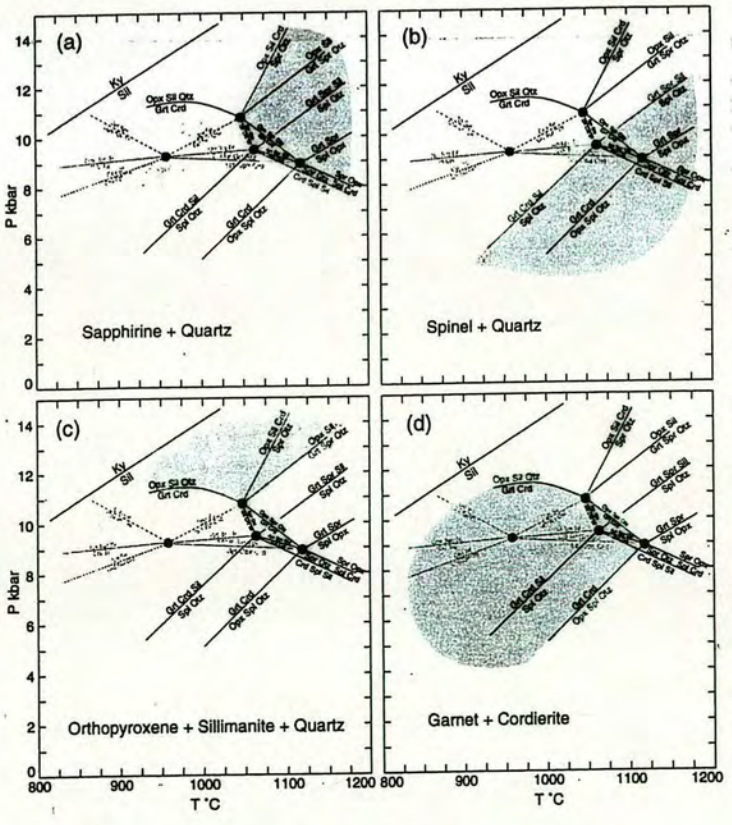

Figure 1.4- Petrogenetic grids for the FMAS system illustrating the P-T stability fields of : A - saph + qtz (high P/high T), B - spl + qtz (high T/low P), C - opx + sill ± qtz (high P/low T), 4 - grt + crd (lower P+T). After Hensen and Green (1973).

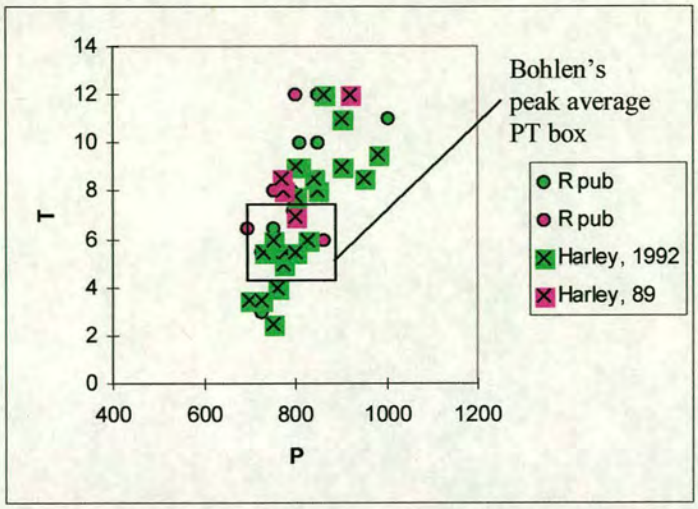

Figure 1.3 - Average peak pressures (kbar) and temperatures (°C) of granulites. Green symbols represent Proterozoic terrains and pinks symbols represent Archaean terrains.

.

Author	Temperature (°C)	Pressure (kbar)
Archaean and Proterozoic		
Raith et al., 1997	850	12
Buick et al., 1998	775	5.2
Stuwe and Powell, 1989	750	6.5
Baba, 1998	850	10
Appel et al., 1998	810	10
Kraus and Menard, 1997	750	5.5
Hand, 1992	725	5.5
Dempster et al., 1991	725	3
Harley and Fitzsimons, 1991	1000	11
Ring et al., 1997	800	5.5
Raith and Harley, 1998	785	5.5
Hand et al., 1994	800	7.5
Phanerozoic		
Sawyer et al., 1998	800	12
Osanai et al., 1998	795	7.2
Gibson and Ireland, 1995	790	8
Ibarguchi and Martinez, 1982	695	6.5
Fitzsimons, 1996	860	6
Carson et al., 1997	800	7
Barth and May, 1992	750	8
Bucher-Nurminen and Ohta, 1993	750	8

Table 1.1 - Recent pressure/temperature estimates from granulite terrains

Granulites are mainly found within three different tectonic settings (Bohlen, 1987; 1991; Ellis, 1987; Harley, 1989; 1992; Fitzsimons, 1991):-

1) Precambrian basement in continental shields represent the largest expanses of granulite facies rocks, examples being the East-Antarctic Shield, Greenland and southern India. Within this type are two subsets:-

a) Massive terrains that were equilibrated entirely within the granulite facies.

b) Transitional terrains where rocks record a metamorphic gradient from amphibolite to granulite facies, e.g. Svecofennian of southern Finland, Van Duin and Nieman (1993); Väisänen and Höltta (in press). Broken Hill in Australia and southern India (Philips, 1980).

2) Within Phanerozoic mountain belts granulites are found as tectonically emplaced blocks, e.g. within the Hercynian Belt (Harley, 1989). These are emplaced in two ways:

a) Granulites that were metamorphosed in an earlier event are thrust upwards during a later deformation event e.g. Cucamonga, southern California (Barth and May, 1992)

b) Other granulites are formed and tectonically uplifted within the same orogenic event, Manicouagan Imbricate Zone (Indares, 1997).

3) Finally, granulites are found as xenoliths within basaltic and kimberlitic magmas Dawson et al. (1997),

1.4.2 - Granulite conundrums

Over the last twenty years advances in the development of thermobarometers and the construction of petrogenetic grids have allowed for tighter constraints on the pressures and temperatures of granulite metamorphism. From this, and correct identification of mineral inclusions and reaction textures, P-T-t paths can be extrapolated. From the calculated paths the likely tectonic settings of granulite formation can be inferred. The detailed interpretation of P-T-t paths is a major problem that is still faced by those who study granulites.

Granulites preserve temperatures that cannot be simply explained by a normal regional metamorphic thermal gradient, (Bohlen, 1987, 1991; Harley, 1989, 1992; Fitzsimons 1991) and so a variety of environments have been suggested for granulite formation, e.g. crustal thickening, continental collision, magmatic accretion and crustal extension. (Bohlen, 1987, 1991; Harley, 1989, 1992; Windley, 1991). However because of the range of P-T-t paths reported in the literature, it is clear that there is no one model that can account for granulite formation, and that granulites may form in a variety of settings and through a combination of processes. Notwithstanding this, researchers have identified some end member granulite P-T-t paths (Ellis, 1987; Bohlen, 1987; Harley, 1989, 1991; Harley and Hensen 1990).

The two main P-T-t paths involve either post-peak near isothermal decompression (ITD), or post-peak near isobaric cooling (IBC), (Harley, 1989; 1992). The nature of these P-T-t paths is based upon retrograde textures that indicate either a decrease in pressure or temperature from peak conditions. In order to better infer a tectonic setting for the terrain, some knowledge is needed about the prograde path but evidence for this can be notoriously difficult to find (Harley, 1989). However studies on transitional terrains and inclusion assemblages can provide clues on the metamorphic evolution of the terrain before the peak of metamorphism. This has lead to a further subdivision of granulite paths, anti-clockwise (ACW) and clockwise (CW) (Bohlen, 1987; 1991; Harley 1989; 1991; 1992; Warren and Ellis 1996). Figure 1.5 illustrates the range of end member P-T-t paths. In a clockwise path the terrain attains peak pressure before its thermal maximum whereas the reverse is true for anti-clockwise paths.

As the granulite terrain of Turku, which forms the basis of this study, is representative of a low-pressure granulite terrain (5-6 kbar, Höltta, 1986; Van Duin and Nieman, 1993; Väisänen et al., 1994), the next section aims to explore the problem of defining the crustal conditions needed to attain such high temperatures (750-800°C) at low pressures. There are a number of low-pressure granulite terrains on different continents including: Bunger Hills, East Antarctica (Stüwe and Powell,

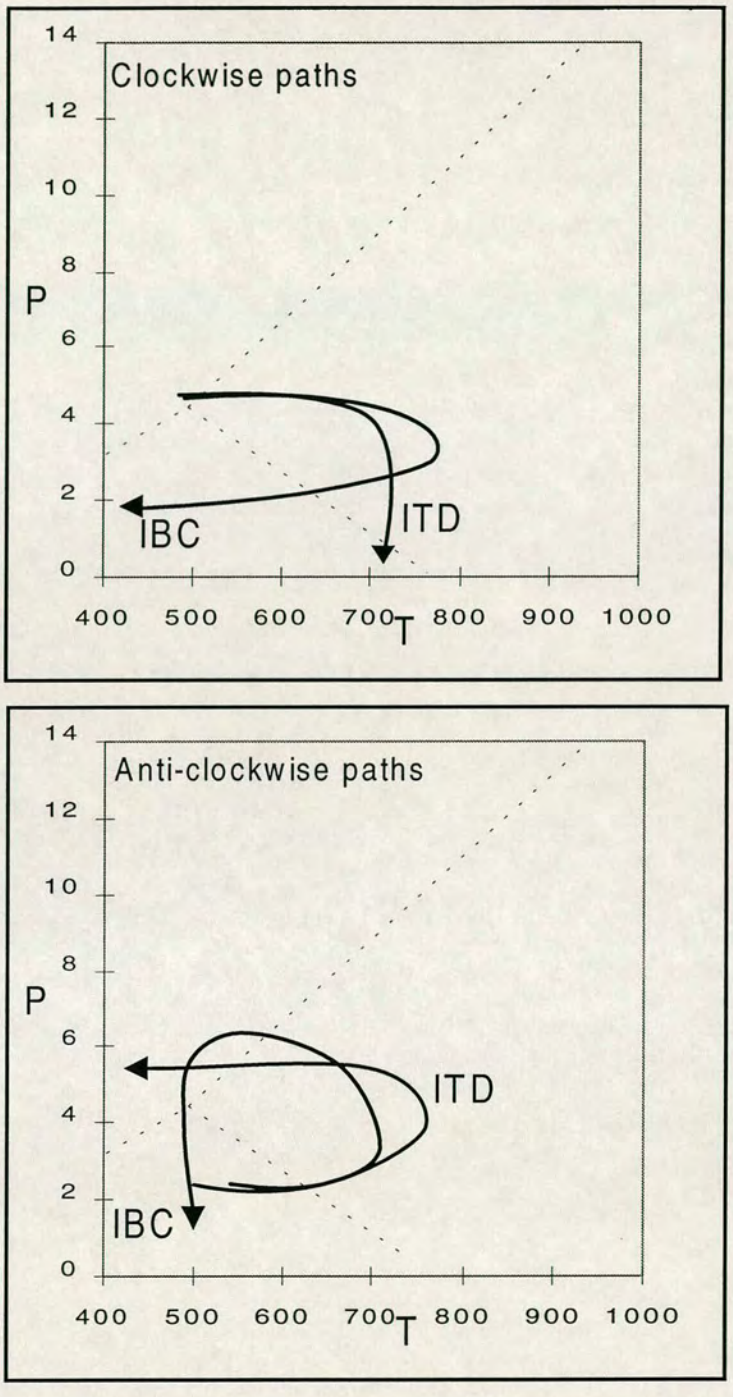

Figure 1.5- End member P-T paths based on work by Bohlen (1987, 1991);Ellis (1987); Harley (1989). P-T paths can either be clockwise or anti-clockwise depending upon whether a terrain reached it's thermal maximum before or after peak pressure. The retrogressive path can follow either isobaric cooling or isothermal decompression (Harley, 1989).

1989); Dronning Maud Land, Antarctica (Bucher-Nurminen and Ohta, 1993); Reynolds Range, Australia (Buick et al., 1998); Malawi, Africa (Ring et al., 1997).

There are two main tectonic processes that have been proposed to explain granulite formation: continental collision (crustal thickening) or continental extension (crustal thinning) both processes may also include the added effects of magmatic accretion.

ITD paths

ITD paths are thought to result in granulites formed in dominantly collisional events (Harley, 1989). It has been recognised however that thickening alone is not enough to produce granulite facies conditions, and that high temperatures would only be obtained somewhat after deformation. This is a feature that is inconsistent with structural data from many granulite terrains in which compressional deformation and higher temperature metamorphism are coeval (Loosveld and Etheridge, 1990; Sandiford and Powell, 1991). The high heat flow needed may be aided by the thickening of already 'hot' crust, i.e. already thinned, underplated crust, or by the addition of hot mantle-derived magmas which would help to advect heat into the lower crust (Bohlen, 1987; 1991; Harley, 1989). However magmatic accretion is generally short lived or less efficient if substantial volumes of old crust are present, and so for certain terrains other processes need to be explored (Harley, 1989; Sandiford and Powell, 1991).

Houseman and McKenzie (1981) suggested that under tectonic shortening the mantle lithosphere would shorten also, forcing colder lithosphere into the warmer asthenosphere. This may lead to instability and collapse (convective removal of the thermal boundary layer), allowing upwelling of warmer asthenosphere material closer to the base of the remaining crust and mantle (Figure 1.6). This would in turn instigate crustal melting, which would help to transfer heat upwards. Looseveld and Etheridge (1990) and Sandiford and Powell (1991) both propose that in order to produce granulite facies metamorphism coeval with deformation the whole mantle part of the lithosphere would need to be convectively removed. Simultaneous

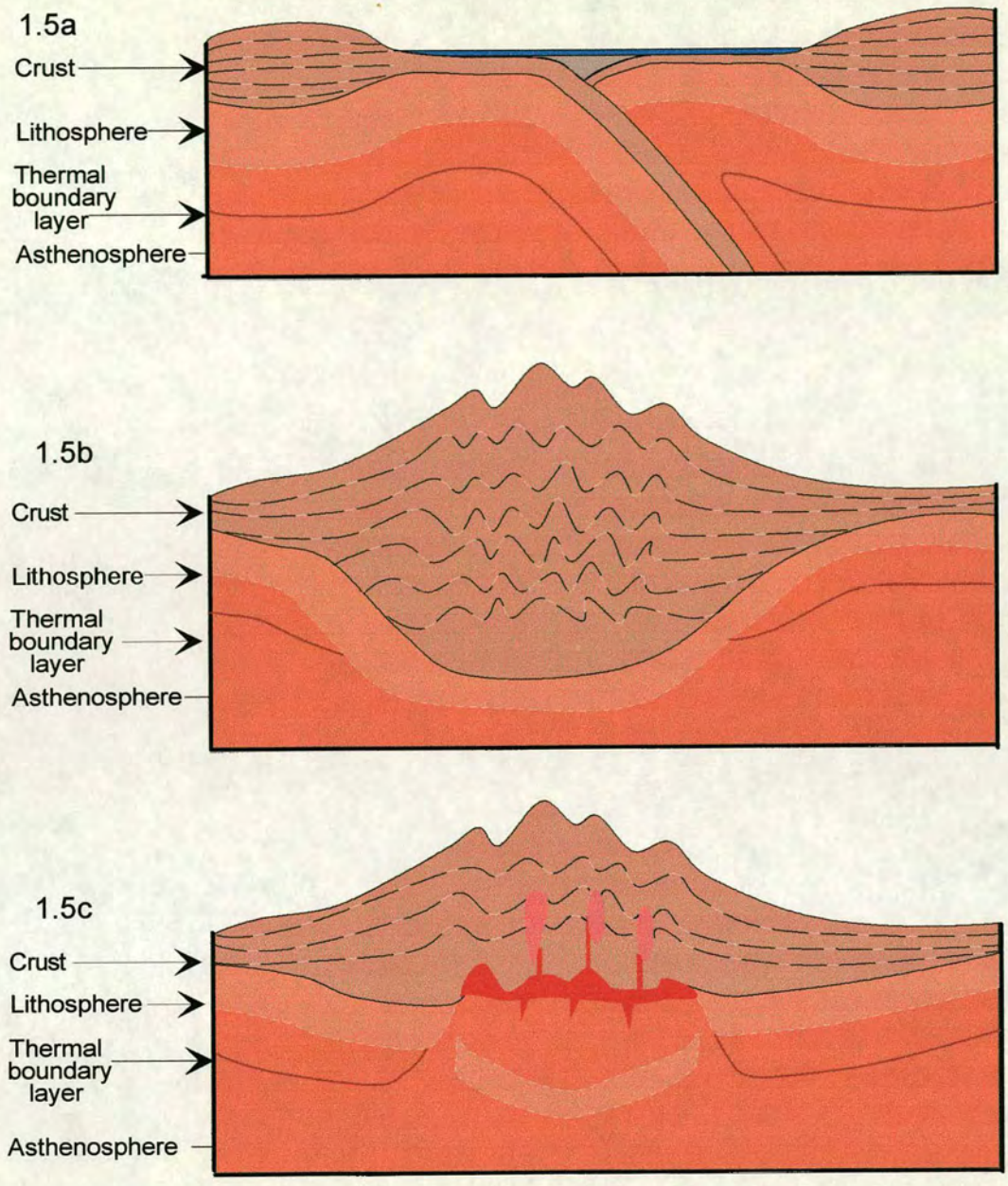

Figure 1.6 - Crustal thickening and resulting lithospheric delamination after the models of Houseman and McKenzie (1981), Looseveld and Etheridge (1990), and Sandiford and Powell (1991)(a) Pre-collision phase, the thermal boundary layer beneath the continents is undisturbed. (b) Due to tectonic shortening the comparatively cool lithosphere is shortened and pushed into the warmer asthenosphere. (c) Due to instability and collapse the thermal boundary layer is removed and the lithosphere is delaminated. Upwelling of asthenosphere and mantle melts heat the base of the crust causing crustal melting.

thickening of the crust with thinning of the lithosphere would provide a significant heat source to the lower crust. This model also helps to explain the conundrum of structural evidence pointing to collisional tectonics coeval with low-pressure granulite metamorphism. Recent work by Sandiford and Hand (1998) has suggested that burial of rocks rich in heat producing elements like Th and U may account for high temperatures over long time spans under a collisional regime.

IBC paths

In order to obtain high temperature (e.g. >700°C) isothermal decompression, a terrain needs to be exhumed swiftly, and probably quicker than by simple erosion. Thus tectonic thinning due to extensional collapse of the orogen has been suggested (Harley, 1989). Further extension of a terrain may be aided by the production of anatectic melts which act as lubricants along shear zones, in some cases allowing the movement of large blocks in tectonic surges (Hollister and Crawford, 1986).

IBC paths are also associated with low- and medium-pressure granulites and are recorded from a number of terrains: e.g. Fiordland, New Zealand (Gibson and Ireland, 1995); Sri Lanka (Schumacher et al., 1990); Vestfold Hills and Napier Complex, Antarctica (Harley and Hensen, 1990); Basin and Range (Sandiford and Powell, 1986). These terrains may reflect a number of tectonic settings (Harley 1989) and their interpretation is still controversial. In order to obtain an IBC path an elevated geothermal gradient is required that has had the chance to evolve towards a steady state without a change in depth (Spear, 1993) and so the following settings are proposed (Harley, 1989).

1. Magmatic accretion and intrusion at the base of and into continental crust, (Ellis, 1987; Bohlen, 1987; 1991). This can often form the ACW paths of Bohlen (1987; 1991) and is attributed to episodes of crustal growth, (e.g. via arc accretion).
2. Extension of the continental crust accompanied by magmatic underplating. This effectively thickens the crust and could take place within back-arc or continental arc settings. Stüwe and Powell (1989) use this model to explain the IBC path of the Bunger Hills, Antarctica. This area shows some compression in the cooling

path, linked by Stüwe and Powell (1989) to gravitational backflow within the hot, weak, extended crust.

3. Extension of normal thickness crust without additional magmatic input, (Sandiford and Powell, 1986).
4. Tectonic thickening of extended crust back to normal thickness.
5. Extension of previously thickened crust.
6. Thermal relaxation of the lower crust in a collisionally thickened crustal section due to erosion.

Therefore to establish the tectonic setting that produced any given terrain, an understanding is needed of the mineral assemblages and textures, the timescale of the event and the structural regime (Selverstone and Chamberlain, 1990).

In some terrains the P-T-t path contains elements of both IBC and ITD trends, usually with ITD preceding the IBC phase. In these instances the proposed model is one of tectonic thinning or extension of the crust after crustal collision (Harley, 1989). If extension is fast enough then isothermal decompression will occur, initially leading to a crust of near normal thickness that would later equilibrate under isobaric conditions, an example of this being the Basin and Range (Sandiford and Powell, 1986). Some paths are shown to loop in a clockwise direction (South Harris, Baba, 1998) and others anticlockwise (SW U.S.A, Williams and Karlstrom, 1996). These are both attributed to crustal collisional tectonics with the size of the loop governed by the interplay between crustal thickening and magmatic heating.

Erroneous P-T-t paths can be very misleading and care has to be taken where a terrain has undergone polymetamorphism: e.g. British Columbia and New Hampshire, U.S.A (Selverstone and Chamberlain, 1990); Rauer Group, Antarctica (Harley and Fitzsimons, 1991); Jetty Peninsula, Antarctica (Hand et al., 1992). Erroneous P-T-t paths could be determined by linking unrelated events e.g. the Arunta inlier, Australia (Hand et al., 1992). In contrast, at Jetty Peninsula one continuous decompression path with fluctuating temperatures initially gave the impression of two separate metamorphic events with one overprinting the other

suggesting an isobarically cooled terrain. It is therefore vital to integrate all pieces of petrological (geothermobarometry, mineral reaction textures and zoning, petrogenetic grids, isotope and volatile analysis, geochronology) and field evidence (structural data) in order to correctly derive the P-T-t path that the terrain truly followed (Hensen and Zhou, 1995)

1.5 - Section 1 - Fluids and their influence on crustal melting

The other area of granulite research that has been open to misinterpretation is the a_{H2O} of granulites (Harley, 1989, 1992). Granulites for the most part preserve anhydrous assemblages and low water activities (Powell, 1982; Waters and Whales, 1984; Waters; 1988; Harley, 1989, 1992; Harley and Hensen, 1990) compared to lower grade rocks, even within the same terrains. The lowering of a_{H2O} within a transitional terrain defines the boundary between granulite and amphibolite facies (along with aforementioned assemblage transitions). Most lithologies in contact with a free, water-rich fluid would melt under the extreme metamorphic conditions of granulite facies. As a consequence, three main methods have been proposed for the lowering of a_{H2O}.

1. Dilution by a pervasive, mantle derived carbonic fluid or by crustal brines
2. Partitioning of fluid into a melt (which is not saturated with H_2O).
3. Early, pre-granulite metamorphism and desiccation of the terrain (not discussed in this chapter.

The role of fluids in granulite formation and their influence on lower crustal melting are considered here.

CO_2 flushing

The main evidence for carbonic metamorphism (Newton et al, 1980) is the presence of high-density CO_2 rich fluid inclusions within peak assemblages. In many transitional amphibolite/granulite terrains early fluid inclusions in the granulites are characteristically carbonic (CO_2) in contrast to H_2O rich inclusions found within amphibolites. This is seen in the Adirondack Mountains, USA (Valley et al, 1987;

Lamb, 1990; Valley et al, 1991) and the West Uusimaa complex, SW Finland (Shreurs, 1985).

Using the density of fluid inclusions, pressures and temperatures can be extrapolated (Touret, 1985; Shreurs, 1985), as high-density inclusions plot on isochors that pass through the PT conditions of inclusion formation. These isochors often record apparent 'peak' granulite pressures and temperatures which has lead workers to propose 'flushing' of CO_2 fluids through the lower crust as a method for stabilising the low a_{H2O} conditions of granulites. The source for these CO_2 rich fluids is often thought to be the emplacement of mafic magmas within or at the base of the crust (Frost and Frost, 1987).

However recent literature (Lamb et al, 1987; Lamb, 1990; Valley et al, 1990; Bhowmik et al, 1995) has shown that there are several lines of evidence against CO_2 infiltration as a general method for stabilising granulite faces conditions.

1) Some inclusions that have been deemed primary are often found not to have formed at the peak of metamorphism. Lamb (1990) investigated a suite of fluid inclusions from the Adirondack Mountains (USA) and found that many inclusions were present as trails that crossed a multitude of grains within a peak assemblage. Although the density of these inclusions provide peak pressures and temperatures the above texture suggested that they represented later fluids that penetrated the rocks after the peak of metamorphism.
2) Using CO_2 densities to extract pressures and temperatures can often give a scattered set of results. As Lamb (1987) and others argue, fluid inclusion barometry has often been misleading because of mis-identification of 'peak' fluid inclusions. Another problem is that the densities of CO_2 inclusions can vary across a terrain, which leads to a wide range of apparent pressures calculated from fluid density isochors. When compared to mineral assemblage barometers this range is not seen (Lamb, 1990). As mentioned

previously many of the inclusions are probably secondary or post-peak inclusions based upon textural evidence.

3) Another line of evidence that suggests that fluid inclusions were not coeval with granulite facies metamorphism are low values of f_{O2}. CO_2 is only stable at high f_{O2} (Valley et al, 1990), illustrated in Figure 1.7. In the Adirondacks the peak mineral assemblage of graphite + tremolite + calcite + quartz yield low f_{O2} values (Valley et al, 1990). Low values of f_{O2} and f_{H2O} or f_{CO2} and f_{H2O} indicate fluid absent conditions, ruling out the presence of a pervasive CO_2 rich fluid. A study of CO_2 and H_2O producing reactions suggest variable X_{CO2} and f_{CO2} on a regional scale.

4) Carbon and oxygen isotopes also provide evidence against pervasive CO_2 fluids as a method for stabilising granulite facies (Vry et al; 1988; Valley et al, 1990; Bhowmik et al, 1995). The CO_2 in a mantle fluid has a $\delta^{13}C$ value around -7‰ (Vry et al; 1988) and only a small amount of CO_2 is required to reset sedimentary carbon values of –25-30‰. For CO_2 infiltration to be effective in dehydrating the crust it must be pervasive along all grain boundaries and be 10-25% of the mass of the affected crust in order to homogenise isotope signatures across a terrain. However many terrains i.e. Adirondacks (USA), Eastern Ghats (India) preserve their pre-metamorphic $\delta^{13}C$ values (Lamb et al., 1987; Lamb, 1990; Valley et al., 1990; Bhowmik et al., 1995). The isotopes are heterogeneous across lithological boundaries, which argues against blanket infiltration of a CO_2 rich fluid. Detailed isotopic work from the granulites of the Eastern Ghats has shown that different calc-silicate bands preserve original, pre-metamorphic isotopic gradients, indicating local fluid buffering (Bhowmik et al., 1995). Later shear zones show evidence of a post-peak fluid influx that moved through the shear zones (Bhowmik et al., 1995). The high dihedral angles of granulites create difficulties for fluid flow through the lower crust but high strain within shear zones allows for movement of a CO_2 bearing fluid phase due to dynamic recrystallisation (Stevens and Clemens, 1993).

5) The mineral cordierite can trap volatiles within its crystal structure and the composition of these volatiles have been used as evidence for CO_2 infiltration as a method of stabilising granulite facies conditions. Some cordierites i.e. those from the Lapland Granulites, contain high CO_2 values (2-3 wt %) and heavy $\delta^{13}C$ values (-7‰), (Armbruster et al, 1982) and this has been used as an argument for CO_2 flushing. However other cordierites preserve low total volatiles, low X_{CO2} and have light $\delta^{13}C$ (Vry et al, 1988, 1990). Also it is possible that these values may have been reset by later fluid influx.
6) There may also be errors in the measurements of the ratios of volatile species within fluid inclusions. H_2O is often concentrated in the tips of irregular shaped inclusions and thus may be missed during analysis. This can lead to a lower measured H_2O/CO_2 ratio than is actually present in the inclusions (Hollister, 1988).

Thus whilst there is evidence for CO_2 flushing at some localities, it cannot be accepted as a uniform method for stabilising granulite conditions. However CO_2 is not the only recorded volatile species other than water in granulite and lower crustal fluid inclusions.

Crustal brines

Touret (1985) first recorded primary crystalline salt inclusions from the Bambok Region, south Norway. Crustal fluids have since been found to have variable, but often large, concentrations of dissolved salts such as NaCl, KCl etc (Shmulovich and Graham, 1990, Aranovich and Newton, 1997). The salinity of some fluid inclusions can range up to 65 wt% and it is thought that their source may be evaporites contained within subducted continental margin sequences

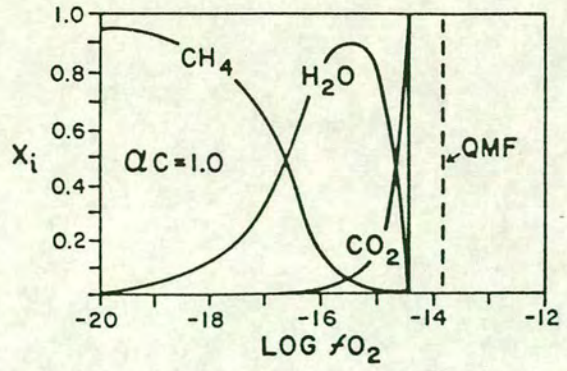

Figure 1.7 – Mole fractions of CO_2, H_2O and CH_4 vs log f_{O2} at 800°C and 8 kbar. The vertical line is the reaction $C + O_2 = CO_2$ with graphite stable to the left. The QMF buffer is dashed. (Valley et al, 1990)

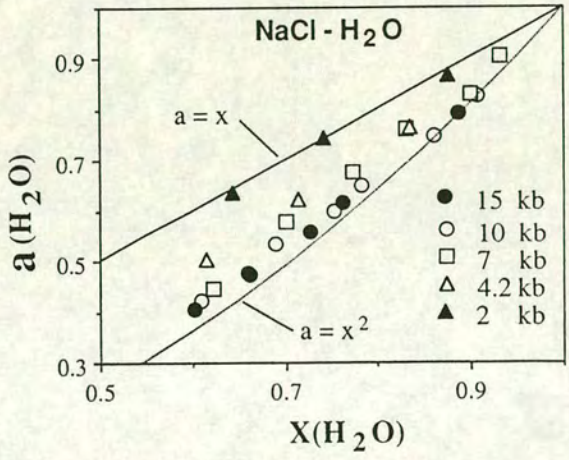

Figure 1.8 – Activity of H_2O (a_{H2O}) as a function of H_2O mole fraction (X_{H2O}) calculated from the brucite-periclase data of Aranovich and Newton (1996). The diagram shows the affect of increasing pressure within the H_2O-NaCl system.

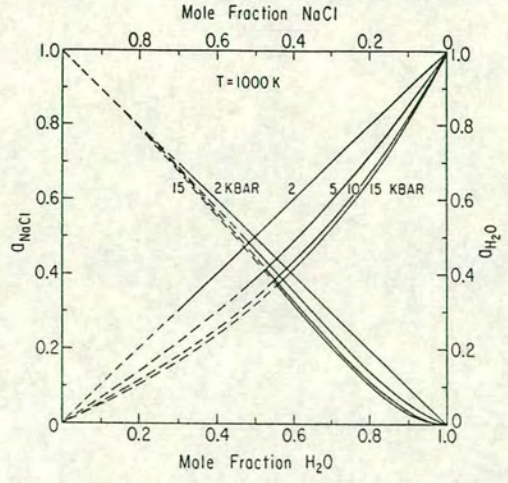

Figure 1.9 – Activity-composition relations of H_2O and NaCl in the binary join (Aranovich and Newton, 1996). The curves are dashed in their metastable portions.

Many workers agree that concentrated salt in crustal fluids can play an important role in many petrogenetic processes in the deep crust e.g. PT location of mineral-fluid-melt equilibrium (Jacobs and Kerrick, 1981; Aranovich and Newton, 1996; Shmulovich and Graham, 1996; Aranovich and Newton, 1997; Aranovich and Newton, 1999; Shmulovich and Graham, 1999). Aranovich and Newton (1996) investigated the effect of NaCl on a_{H2O}. H_2O activities in concentrated NaCl solutions were measured within PT conditions of 600-900°C and 2-12 kbar and in relation to the depression of brucite-periclase dehydration equilibrium. The experiments showed that at low pressures NaCl has no effect on a_{H2O} (Figure 1.8), and that $a_{H2O} = X_{H2O}$ which would suggest ideal mixing in both systems. As pressure increases this relationship changes, so that at 15 kbar (Figure 1.8) $a_{H2O} = X_{H2O}^2$. Thus an increase in NaCl and small decrease of X_{H2O} will lead to a direct decrease in water activity.

The work of Shmulovich and Graham (1996) on the H_2O - NaCl system has shown that at low pressures salts exist as neutral molecular species. When pressure is increased aqueous electrolytes become strongly dissociated into simple ionic speciations and are then solvated by water molecules. This leads to a decrease in a_{H2O} and therefore increasing non-ideality between the two species. This pressure effect can be seen in Figure 1.9.

Melting under granulite facies pressures and temperatures is a common phenomena (Powell, 1982; Le Breton and Thompson, 1988; Waters, 1988, 1994; Carrington and Harley, 1995) and as mentioned previously the presence of crustal brines could affect melting equilibria. Shmulovich and Graham (1996) carried out a range of experiments designed to study the melting of albite in the presence of H_2O-NaCl fluids. The experiments were carried out between 700-900°C and at 5 and 9.2 kbar. The effect of NaCl-H_2O dissociation and the consequent lowering of water activity can be clearly seen in Figures 10a and b. During melting the NaCl will partition into the fluid rather than into the melt. The associated dissolution of water into the melt

phase means that the NaCl content of the fluid increases. At high pressures this will have the effect of buffering the melting process and thus limiting the amount of melting.

Another consequence of the presence of crustal brines is to enhance a_{CO2} within granulites. Jacobs and Kerrick (1981) studied H_2O-CO_2-NaCl mixtures at 6 kbar and found that in comparison to H_2O-CO_2 fluids, the presence of small amounts of NaCl (5-10 wt%) significantly increase a_{CO2} for H_2O rich compositions. This effect was also seen in the experiments of Aranovich and Newton (1999) where the increase of a_{CO2} and decrease of a_{H2O} led to miscibility of the two volatiles and an enhancement of the salinity of the brine. Shmulovich and Graham (1999) experimentally explored the same ternary system, binary joins and miscibility gap. They found that there is a large stability field of CO_2 rich fluid with halite (Figure 1.11). Thus CO_2 rich fluid inclusions do not necessarily require a CO_2 rich fluid and CO_2 may be in equilibrium with an H_2O-NaCl brine and halite. Recent work by Markl and Bucher (1999) has shown granulites from the Lofoten Islands, Norway to contain halite and sylvite within fluid inclusions. Further work on granulite fluid inclusions will provide information on the frequency with which these salts are found.

However the current popular method for lowering water activities within granulites is through partial melting. This method will be discussed in the next section.

Partial melting

During partial melting any fluid phase present would partition dominantly into the melt, and the removal of this melt and subsequent recrystallisation of the residual assemblage would then effectively lower the a_{H2O} in the system (Powell, 1983). Thus a_{H2O} could be locally controlled by the extent of the melting process and melt extraction (Powell, 1982, Waters and Whales, 1984, Waters, 1988, Harley 1989).

Melting therefore provides internal lithological control of volatile activities without the need for any external fluid buffer (Stevens and Clemens, 1993). H_2O is much

more soluble in a silicate melt than CO_2 (Johannes and Holtz, 1996) and this differential solubility would progressively enrich any coexisting fluid phase in CO_2 (Waters and Whales, 1984).

The amount of melt produced in any system is a function of pressure, temperature, bulk composition and a_{H2O} as can be seen from experiments within the haplogranitic system, (Waters and Whales, 1984; Clemens and Vielzeuf, 1987; Le Breton and Thompson, 1988; Johannes and Holtz, 1996). Experimental work has shown that the solidii of pelitic and quartzo-feldspathic rocks are close to that of the haplogranite system (Clemens and Vielzeuf, 1987). The following section will therefore be based on the experimental work of Johannes and Holtz (1996). Where a_{H2O} is equal to one, the temperature of the solidus decreases as pressure increases at low pressures; thus the slope of the melting curve is strongly negative, (Figure 1.12a). H_2O saturated melts could form in the mid to lower crust at temperatures as low as 630°C, but would crystallise as they ascend because they would very quickly intersect their solidus.

There is a large temperature difference between the dry melting curve and the wet melting curve within the same system, and the dry curve has a positive *dP/dT* slope, (Figure 1.12b). At temperatures between the wet and dry solidii, a protolith could produce a melt that has an H_2O content determined by the a_{H2O} of the system, which is in turn determined dominantly by the temperature of the system.

The maximum water solubility in granitic melts increases with increasing pressure whereas temperature has little effect on maximum water solubility. For a given H_2O availability the effect of this increased water solubility is to decrease the amount of H_2O-saturated melt that could be produced from a protolith at given a_{H2O}. However at lower a_{H2O} it is still possible to undergo extensive melting. Conversely, a decrease in pressure can lead to an increase in the amount of melt produced, a phenomenon often termed decompression melting (Fitzsimons, 1996; Carson et al., 1997).

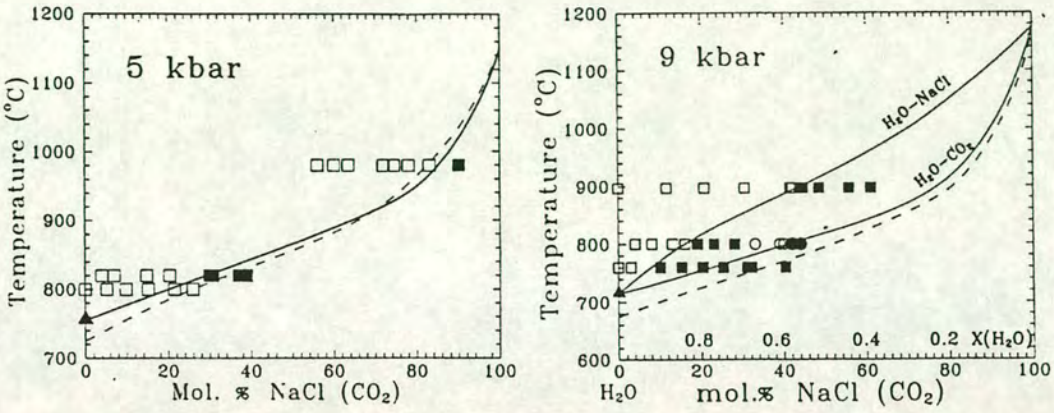

Figure 1.10 – a) Melting curves in the systems H_2O-CO_2 and H_2O-NaCl at 5 kbar, based on the experiments of Schmulovich and Graham (1996). Open squares are melt ± albite, and closed symbols are albite only. b) The same system at 9 kbar illustrating the effect of pressure increase on the two curves, moving the H_2O-NaCl curve to higher temperatures.

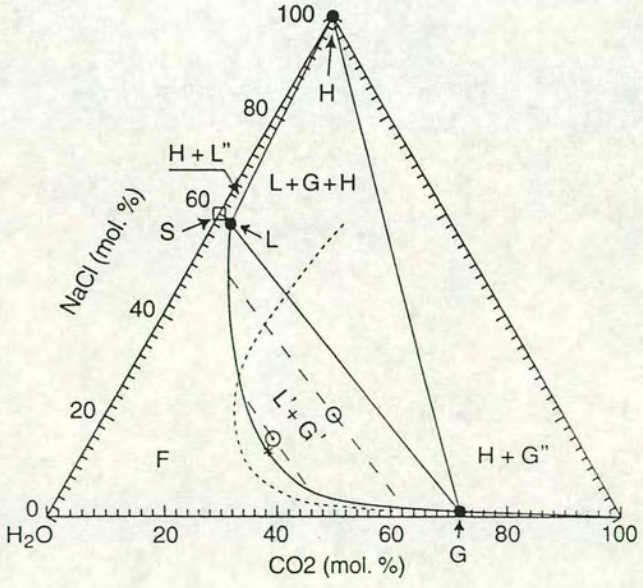

*Figure 1.11 – A phase diagram for the H_2O-CO_2-NaCl system calculated from the experiments of Schmulovich and Graham (1999) at 9 kbar and 800°C, in mol%. **S**-saturation point in binary system H_2O-NaCl, **L**- halite saturation point for ternary systems, **G** – maximum CO_2 concentration in phase **G'**, which can coexist with phase L (more CO_2-rich compositions, phase **G''** and with halite, **H**, solid).*

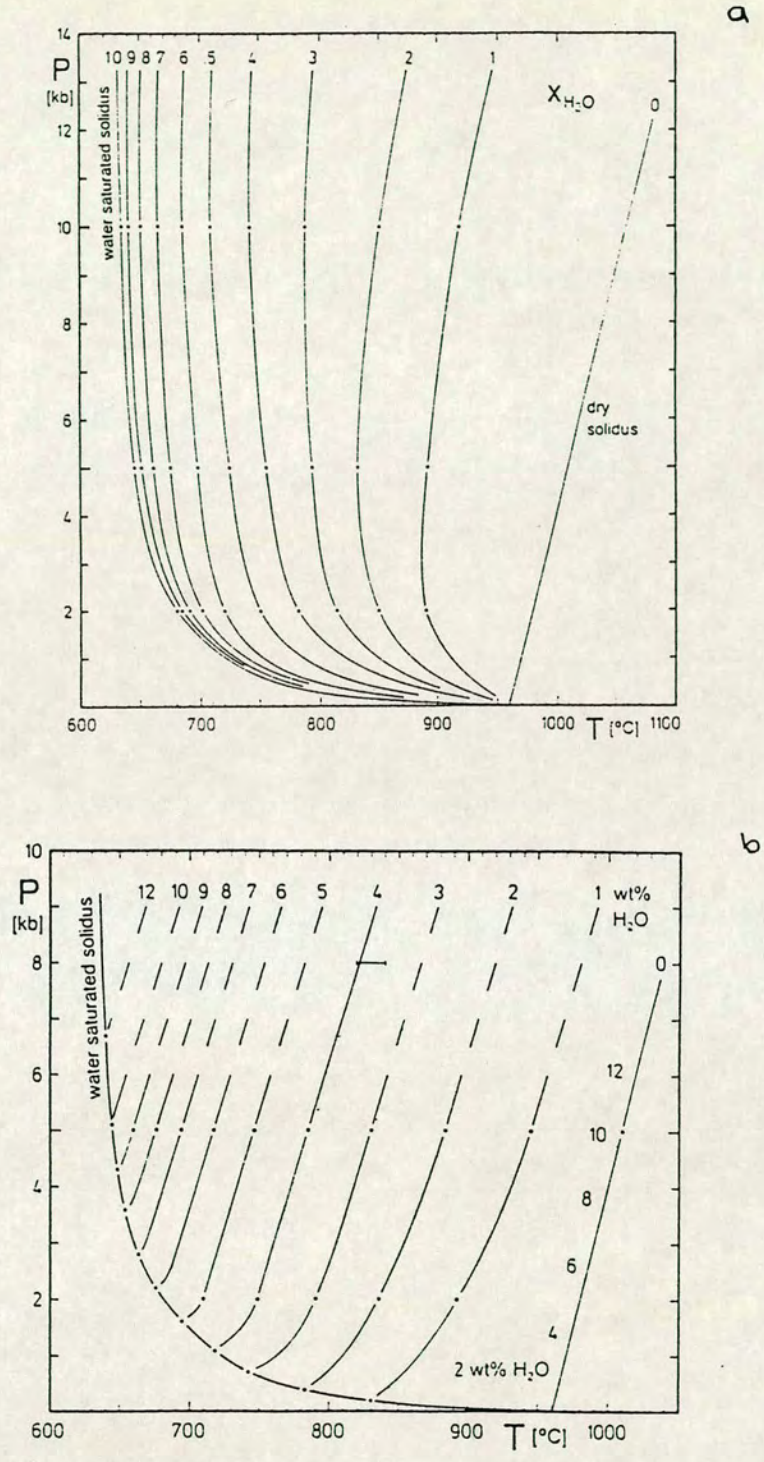

Figure 1.12 - Solidus and melting curves for the haplogranitic system, After Johannes and Holtz, (1996). (a) Solidus curves for the Qz-Ab-Or-H2O-CO2 system for a range of XH2O. (b) Liquidus curves of the system Qz-Ab-Or for minimum melts at a range of specified water contents

Hence the pressure, temperature and a_{H2O} content all affect the degree of melting and the water content of the melt. Rocks in the lower crust have low porosity, probably 0.1 vol% or less (Etheridge et al, 1984). If such a porosity were to represent voids filled with pure water it would amount to a maximum of 0.03 wt% water (Clemens and Vielzeuf, 1987). Therefore early fluid-present melting would produce a small melt percentage, and extraction of such a melt would quickly lead to reduced a_{H2O} in the residual assemblage as it evolves to higher temperatures.

Under low a_{H2O} conditions hydrous minerals such as micas and amphiboles break down and react with non-hydrous phases to produce H_2O-undersaturated melts and potentially a restite. The breakdown of hydrous phases leads to water being liberated directly into the melt, (Thompson, 1982; Stevens and Clemens, 1993). As this project concentrates on melting within pelites the compositions explored next are within the pelitic system. The melting of pelitic rocks is considered to contribute to the formation of peraluminous S-type granites, leaving behind a residuum rich in Al-, Fe- and Mg-bearing minerals (e.g. biotite, cordierite, garnet).

When Al is introduced to the haplogranitic system it lowers the temperature of eutectic melting and also increases the normative quartz content of the melt.
Aluminous melts can also have more H_2O dissolved in them at higher pressures than pure haplogranitic melts (Clemens and Vielzeuf, 1987). When Fe and Mg are involved, the MgO content of the melt increases with temperature.

Melting in granulite facies pelitic systems generally follows the reaction :-

Biotite + sillimanite + quartz + plagioclase = garnet ± cordierite + K-feldspar + melt

(Waters and Whales, 1984; Le Breton and Thompson, 1988; Waters, 1988; Thompson, 1989, 1996). The amount of melt produced in these situations is linked to the proportion of biotite in the protolith (Clemens and Vielzeuf, 1987; Le Breton and Thompson, 1988) in addition to pressure, temperature and a_{H2O} as noted above.

Melting of pelites though biotite dehydration-melting reactions occurs from 750°C (Clemens and Vielzeuf, 1987) upwards, with major amounts of melt (> 20%) produced above 850°C (Thompson, 1982). Other temperature estimates of peak melt productivity include those of Vielzeuf and Holloway (1988) -850-875°C; Patino Douce and Johnson (1991) -850-900°C; and Stevens and Clemens (1993) -700-900°C. A great deal of experimental work and modelling has been undertaken to try to quantify the amount of melt that can be produced from a given protolith composition under varying PT conditions (Thompson, 1982; Clemens and Vielzeuf, 1987; Le Breton and Thompson, 1988; and Waters and Whales, 1984).

Clemens and Vielzeuf (1987) modelled melt production from a range of rock compositions as a function of their modal proportions of hydrous phases. They calculated the H_2O available if the hydrous phases were to liberate all of their water, and then modelled the subsequent wt% melt produced at both 5 and 10 kbar. Le Breton and Thompson (1988) carried out similar experiments on pelitic bulk compositions with varying wt% biotite. Unlike Clemens and Vielzeuf (1987) they kept the pressure of their experiments constant at 10 kbar but varied temperature from 780-860°C. The result of both experimental studies are summarised in Table 1.2.

Those assemblages with the high percentage of hydrous phases are able to contribute a higher amount of water to the melting reaction. This leads to an increase in the amount of melt produced, as the wt% H_2O in the melt is governed by the a_{H2O} imposed by the melting reaction at the specified P and T (Johannes and Holtz, 1996). An increase in pressure for all of the points calculated by Clemens and Vielzeuf leads to lower melt percentages. At a constant pressure (10 kbar) a temperature increase leads to an increase in the melt production and the % of H_2O in the equilibrium melt decreases.

Clemens and Vielzeuf (1987)				
Sample	**Wt% hydrous phase**	**Wt% H_2O**	**Wt% melt**	**Wt% melt**
		(From hydrous phases)	**5 kbar/900°C**	**10 kbar/920°C**
PEL A	Ms 10 Bt 20	1.23	50	30
PEL B	Bt 27	1.05	43	26
Le Breton and Thompson (1988)				
Sample	**Wt% hydrous phase**	**Wt% H_2O**	**Wt% melt**	**Wt% melt**
		(From hydrous phases)	**10 kbar/860°C**	**10 kbar/780°C**
MIX 1	Bt 31	1.24	24.3	15.9
MIX 2	Bt 55.3	2.21	43.3	28.3
MIX 3	Bt 28.03	1.12	21.9	14.35

Table 1. 2 - Results of the melting experiments of Clemens and Vielzeuf (1987) on the two pelitic bulk compositions they studied (PEL A and PEL B) and the three pelites of Le Breton and Thompson (1988).

Melts produced through the dehydration melting of pelites are typically peraluminous granites with a small excess of FeO and MgO (Fitzsimons 1996). Generally the melt composition has an X_{Mg} intermediate between the garnet and biotite of the reaction (Le Breton and Thompson, 1988

1.6 - Section 1 - Migmatite formation

Many granulite terrains show some degree of partial melting in the form of migmatised areas, within which leucosomes representing melt are seen in conjunction with mesosomes and/or restites (residues of melting). Modelling of melting within pelites usually occurs within the KFMASH system (K_2O-FeO-MgO-Al_2O_3-SiO_2-H_2O). Melting reactions are most commonly represented by petrogenetic grids and associated pseudosections. Petrogenetic grids are powerful tools for understanding metamorphic terrains and many theoretical grids have been constructed for melting within pelites (Thompson, 1982, 1996; Henson and Harley; 1990; Powell and Downs, 1990). There have also been more recent attempts to experimentally constrain these grids (Carrington and Harley, 1995; Holland et al, 1996). The experimental grid of Carrington and Harley (1995) looked at high PT reactions in pelites from 840-1000° and 5-12.5 kbar. These high temperature

reactions are not seen in the Turku Granulite Terrain as the maximum temperatures and pressures recorded are 800°C and 6 kbar (Väisänen et al, 1994).

As mentioned earlier the melting reaction at the PT conditions of the Turku terrain is bt + sil+ qtz = melt + kfs + grt + crd. The theoretical grid of Henson and Harley (1990) illustrates the above reaction emanating to lower pressures from the (Spr, Spl) absent point in the KFMASH system (+ K-feldspar + melt, X_{Mg} melt>X_{Mg} grt). The right hand side of the reaction is the higher temperature side (Figure 1.13). Powell and Downes (1990) constructed theoretical grids for melting within Broken Hill, Australia. The effect of bulk composition on the position of melt reactions can be seen by superimposing KMASH and KFASH grids over a KFMASH grid (Figure 1.14). This clearly illustrates the effect the bulk composition will have on the products of the melting reaction, cordierite is favoured by Mg rich bulk compositions whereas garnet is the product of melting reactions within KFASH. Melting in intermediate compositions, seen in the KFMASH system, will produce both garnet and cordierite.

A pseudosection from Holland et al (1996) who modelled melting within the KFMASH system, shows that PT conditions also affect the products of the melting reactions assuming a set bulk composition (Figure 1.15). Garnet is favoured by higher pressures and temperatures than cordierite + garnet which in turn form at

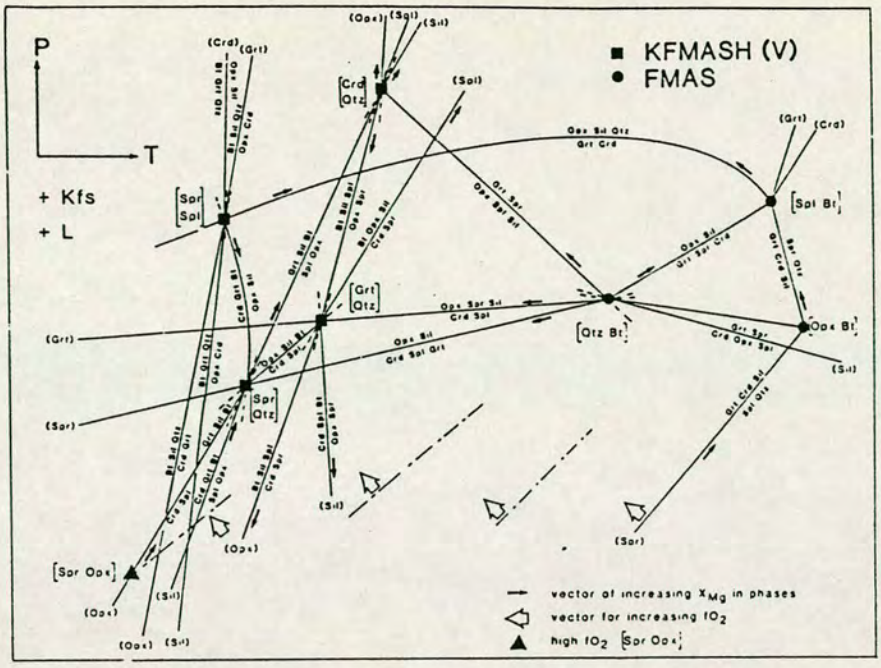

Figure 1.13 – Theoretical PT grid for vapour absent-dehydration melting reactions in the system KFMASH(O). The phase relations are projected from K-feldspar and liquid (L). The left hand side of the grid is stable at highoxygen fugacity whilst the right hand side is seen at lowoxygen fugacities (Hensen and Harley, 1990).

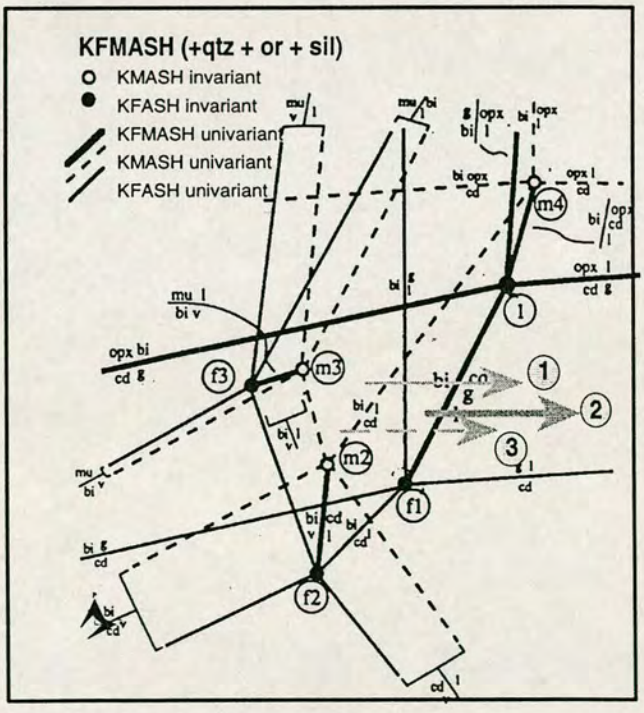

Figure 1.14 - Dehydration melting reactions within the KFMASH system.
1 = KFMASH melting reaction in intermediate compositions to produce crd+grt+melt.
2 = KFASH melting reaction in Fe-rich compositions to produce grt+melt.
3 = KMASH melting reaction in Mg-rich compositions to produce crd+melt.
(After Powell and Downes, 1991).

higher PT conditions than just cordierite. Thus the X_{Mg} of the bulk composition will control the amount of melt produced for a given rise in temperature (Carrington and Harley, 1995).

Most leucosomes within high grade pelites contain high temperature mafic porphyroblasts such as garnet, cordierite or orthopyroxene. These represent the aforementioned solid products of incongruent melt-forming reactions (Powell and Downes, 1990). Large garnets that are often poikiloblastic in texture are observed within leucosomes in a number of granulite terrains: e.g. Namaqualand, S Africa (Waters and Whales, 1984; Waters, 1988), Broken Hill, Australia (Powell and Downes, 1991). Inclusions of sillimanite and biotite in garnets occurring in leucosomes in the Reynolds Range, Australia, are consistent with the origin of the garnets as products of a dehydration melting reaction (Buick et al., 1998).

Powell and Downes (1990) suggest that melt that was produced through the same dehydration melting reaction would grow around a garnet poikiloblast as a diffusion

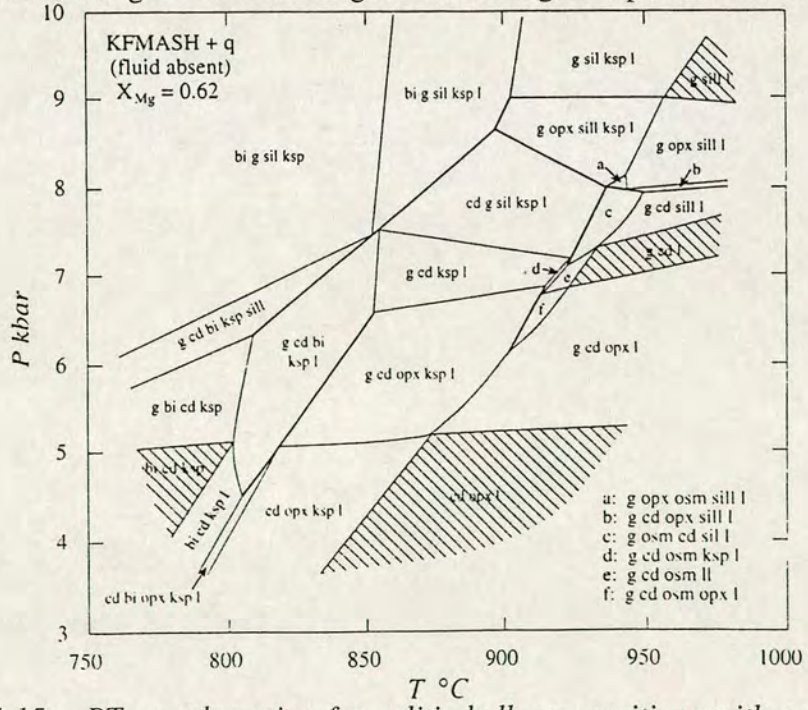

Figure 1.15 – PT pseudosection for pelitic bulk compositions with an X_{Mg} of 0.62. This was extrapolated by Holland et al (1996) using the experimental data of Carrington and Harley (1995).

-controlled texture. If the melt remained in-situ a back reaction would be expected upon crystallisation of the melt. As any retrogressive features are minimal in most cases it seems likely that melt extraction on some scale is common in most granulite terrains (Harley, 1989, Powell and Downes, 1991). The high amount of ferromagnesian phases in the LG2 leucosomes mentioned previously may represent material left behind after extraction of such melt (Fitzsimons, 1996).

Thus melting under low a_{H2O} conditions is a common phenomenon in granulite terrains, but whether melts will move up through the crust is dependent on the temperature and water content of the melt, which is in turn governed by the conditions of its source. This is summarised in Figure 1.16 with the data of Stevens and Clemens (1993). However there are also physical mechanisms that dictate the nature and scales of melt extraction and segregation as well as the potential melt transport processes. In some terrains such physical conditions may be appropriate for the generation of S-type peraluminous granites (Sawyer, 1996).

Initial small-scale melt segregation is governed by convection of the melt and solid components of the system according to Brown et al. (1995). The model consists of convection within a two-phase viscous flow model defined by melt and solid. At larger melt volumes Brown et al. (1995) suggest that melt is segregated by filter pressing of the two phases. The melt moves by porous flow as a consequence of the differential stresses that the two phases undergo. Melt in migmatite terrains can be concentrated in folds, boudins, parallel to layering and in fracture arrays. As Figure 1.17 shows, high strain areas favour stromatic leucosomes and low strain areas patchy leucosomes (Collins and Sawyer, 1996).

Whether a melt stays in-situ or whether there is melt movement, is dependent upon its volume change or the ΔV of the melting reaction (Clemens and Droop, 1998; Brown et al., 1995). Fluid present reactions generally have negative *dP/dT* slopes (over the range 0.1-1.0 GPa) and are accompanied by bulk volume reductions (negative $\Delta V_{melting}$), taking account of total volume of solids, melt and pore-filling

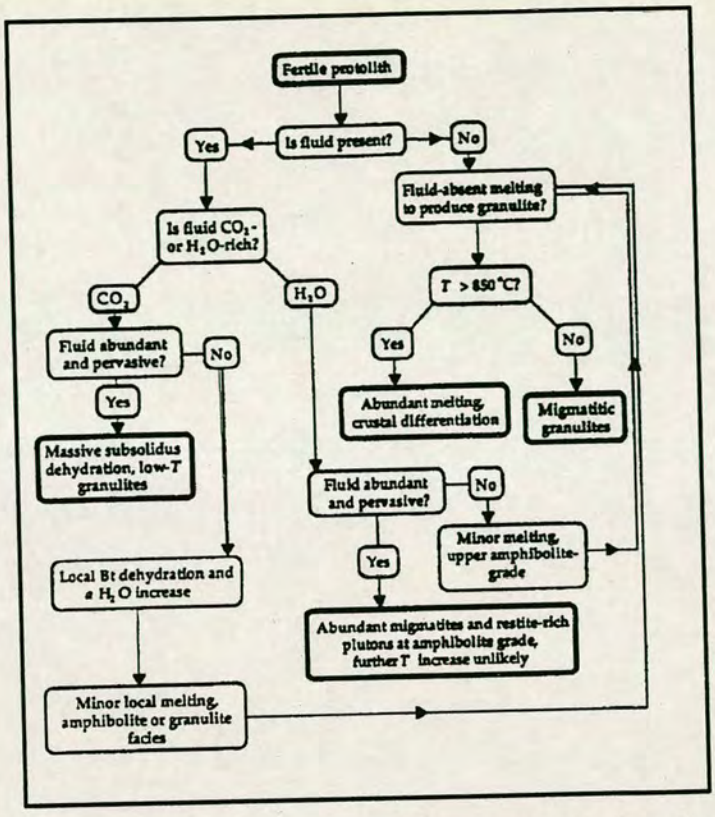

Figure 1.16- Flow diagram demonstrating the different paths taken by melts in the lower crust governed by the availability of H_2O. (After Stevens and Clemens, 1993).

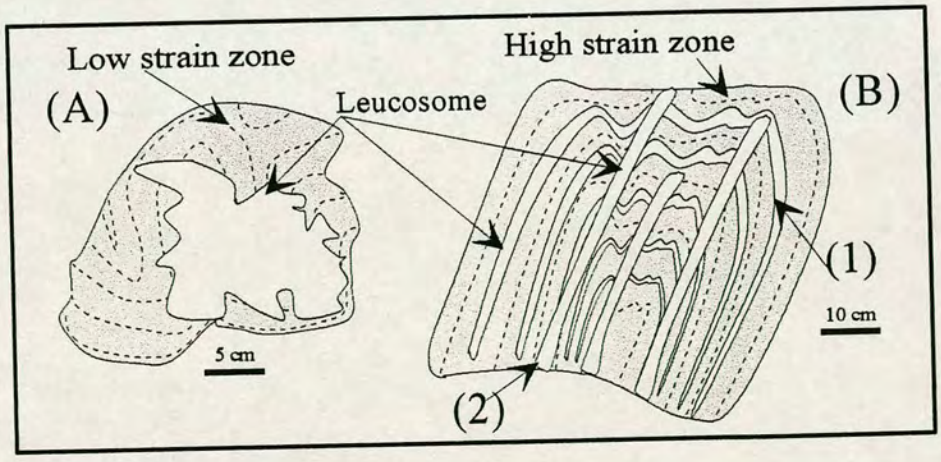

Figure 1.17 - The effect of deformation on leucosome style. In low strain zones (A) melt can pond and will form patchy leucosomes. Where strain is high (B) the melt segregates out into elongate leucosome that form at 90° to the principal stress field. In this case an early leucosome set has formed parallel to the first foliation (1). This has since been folded and a new set of leucosomes (2) have segregated parallel to the axial trace of the later fold. This diagram is representative of leucosome styles observed by Carson et al. (1997) at Larsemann Hills, East Antarctica.

a.

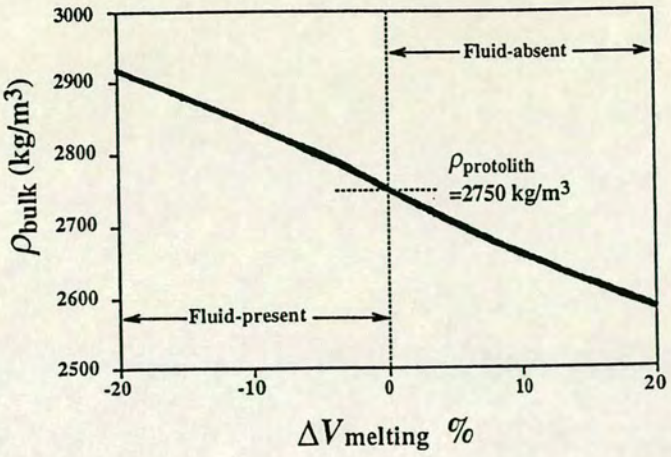

b. Fluid-present melting

$\Delta V_{melting}$ -ve

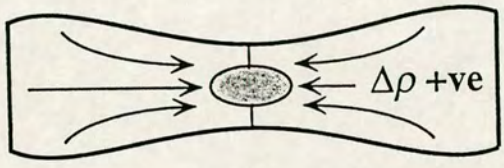

c. Fluid-absent melting

$\Delta V_{melting}$ +ve

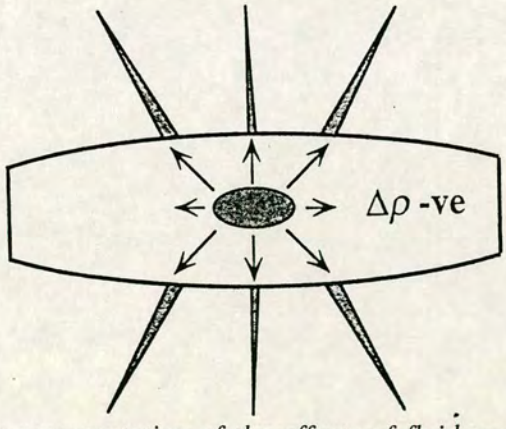

Figure 1.18 – A diagrammatic representation of the effects of fluid presence or absence during partial fusion on the physical behaviour of a partially molten rock mass (Clemens and Droop, 1998).

a. *A graph to represent how the density (ρ) of a rock mass changes on partial malting. Positive and negative changes are shown in %.*

b. *The deformed rectangle is the rock mass and the shaded area is the location of most intense melting. Fluid present melting indicates a negative volume change, an increase in density and melt flow focussed into the rock mass.*

c. *The deformed rectangle is the rock mass and the shaded area is the location of most intense melting. There is a positive change for fluid absent melting accompanied by expansion of the protolith, failure of the envelope and expulsion of melt into the fractures.*

fluid present. In contrast, fluid-absent reactions have positive *dP/dT* slopes and are accompanied by bulk volume increases (positive $\Delta V_{melting}$). In fluid present conditions the melt is somewhat denser than the surrounding rock and will pool inwards. The positive volume change in fluid absent melting is representative of a decrease in density and thus expansion of the protolith, brittle failure of the envelope and melt expulsion into external fractures (Figure 1.18).

Other methods for melt escape include pre-existing or synchronous shear zones and diapiric magma migration. Once melt has escaped, how it will travel is largely governed by temperature and H_2O content, with hot, dry magmas being less viscous and so able to move more readily (Clemens and Vielzeuf, 1987).

The RCMP (rheologically critical melt percentage) is often used to distinguish between terrains that contain local migmatites, and those that produce magma bodies, with 30-40% volume melt being the accepted RCMP value (Vielzeuf and Clemens, 1987). A link between migmatite and granitoid intrusions is present within the Mt. Hay region of central Australia. There is an evident link between the small scale leucosomes that represent local melts and the metres wide charnockite intrusions that are located within thrust structures, fold necks and fractures (Collins and Sawyer, 1996). This is taken as evidence that melt can migrate through non-coaxial compressional deformation of the crust to feed the granitoid intrusions of structurally higher regions.

1.7 - Section 2 - The Svecofennian orogeny of Southern Finland

1.7.1 - Location and characteristics

The Turku granulite terrain of this study is one of three granulite terrains (Figure 1.19) within the Svecofennian schist belt (SSB) of southern Finland (Van Duin and Nieman, 1993). The SSB is an east-west trending schist belt within the Svecofennian Domain (SD, Korja, 1995) in the south of the Fennoscandian shield (Figure 1.19). The Svecofennian Domain is bordered by the Caledonides in the north and by Phanerozoic sediments in the south (Korja et al., 1993) and stretches across Finland

and Sweden. To the north the Archaean Fennoscandian in Finland consists of three main greenstone belts (Front and Nurmi, 1987), the Kola, Belmorian and Karelian domains (Nironen, 1997). The Karelian Domain occurs to the NE of the Svecofennian Domain and consists of small linear greenstone and schist belts that are separated from each other by migmatite-granitoid areas (Korja, 1995), and associated tonalites that have been dated to 2.8±0.18 Ga. The Svecofennian Domain is separated from the Karelian block in the east by the Ladoga-Bothnian Bay Zone (Figure 1.19), which represents the palaeosuture between the Archaean and Proterozoic cratons (Nironen, 1997).

The Svecofennian Domain is dominated in the north by the Central Finland Granitoid Complex (CFGC), which occupies an area of more than 35,000 km^2 (Front and Nurmi, 1987). The CFGC is composed of a large number of plutons that vary in size and in composition from gabbroic to granitic. The CFGC is bounded by the Bothnia Belt to the west and the Savo Belt to the east, whilst to the south it is bound by the Tampere Schist Belt (TSB, Lahtinen and Huhma, 1997). The TSB is composed of various metasediments and metavolcanics cut by dominantly granitoid intrusions (Pajunen, 1994).

Between the SSB in the south and the TSB further north is the Tonalite Migmatite Zone, (TMZ, Lahtinen and Huhma, 1997). In the TMZ the mesosome is usually psammitic in composition with an assemblage of plagioclase, biotite and quartz. These psammites have produced a leucosome suite with trondjhemitic, granodioritic and tonalitic compositions. The semi-pelite is quite homogeneous and volcanogenic rocks seen in other schist belts are rare (Koistinen et al., 1996).

South of the TMZ, within the SSB (Figure 1.19), is the Potassium Granite Migmatite Zone, (PGMZ, Koistinen et al., 1996; Lahtinen and Huhma, 1997) or the Late Granite Migmatite Zone (LGMZ) of Ehlers et al. (1993). Generally this southern zone is characterised by a supra-crustal sequence of pelitic gneisses interlayered with metavolcanic rocks (Van Duin and Nieman, 1993). The supracrustals produced

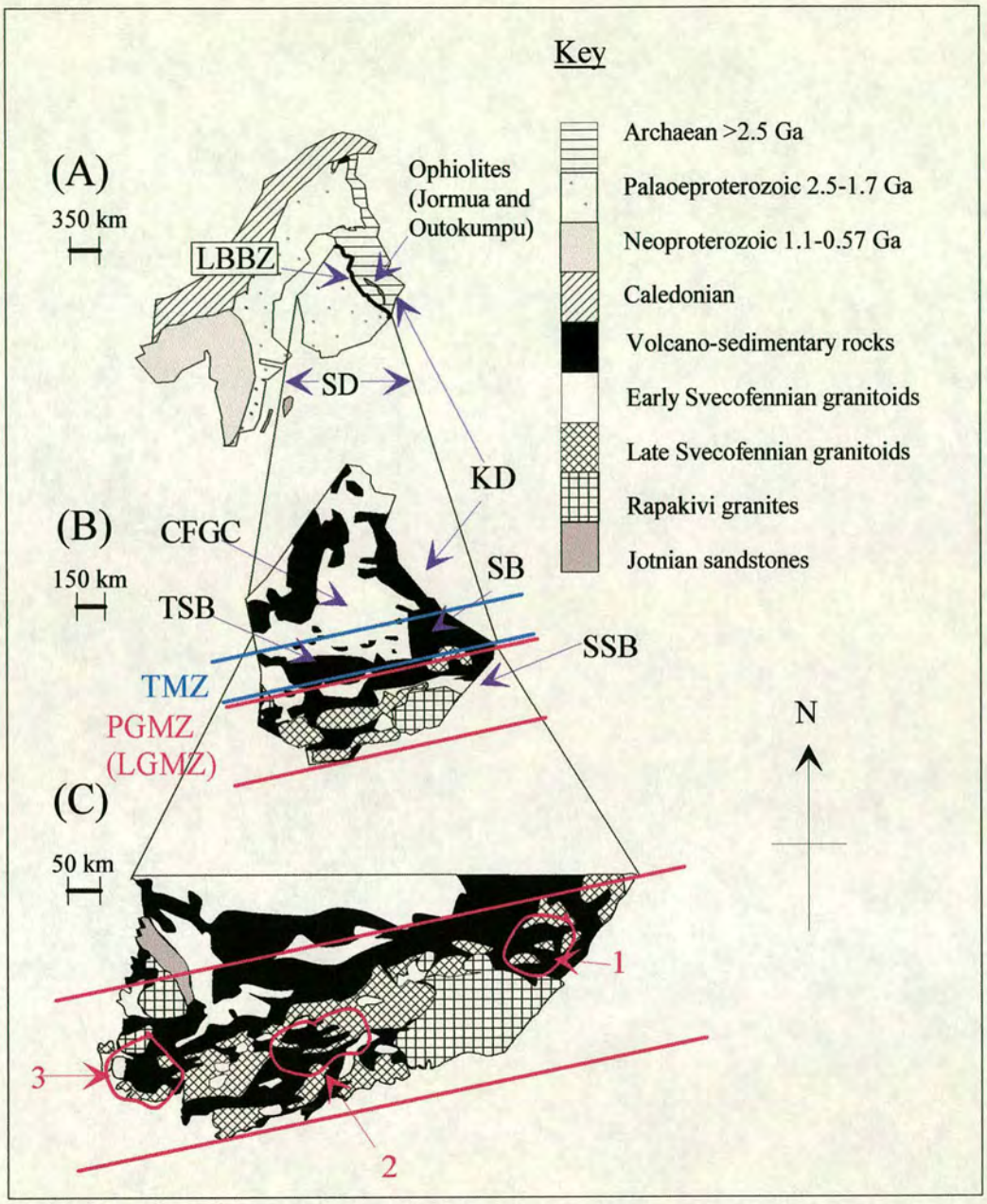

LBBZ = Ladoga Bothnian Bay Zone
KD = Karelian Domain
TSB = Tampere Schist Belt
SD = Svecofennian Domain
SB = Savo Belt
CFGC = Central Finland Granitoid Complex
TMZ = Tonalite Migmatite zone

SSB = Svecofennian Schist Belt (Van Duin and Nieman, 1993)
PGMZ = Potassium Granite Migmatite zone (Koistinen et al., 1996)
LGMZ = Late Granite Migmatite Zone (Ehlers et al., 1993)

Figure 1.19 - Position of Svecofennian tectonic, igneous and metamorphic terrains. (A) After Patchet and Kuovo, (B) after Lahtinen and Huhma, 1997, (C) after Van Duin and Nieman, 1993. The Svecofennian Schist Belt contains three granulite terrains; (1) Sulkava area (2) West Uusimaa Complex (3) Turku area.

migmatites of a granitic composition that contain aluminous phases such as garnet and cordierite (Koistinen et al., 1996). Previous studies of such rocks have shown that the Svecofennian metamorphism occurred at low pressure and high temperature, 760-750°C and 4-5 kbar (Höllta, 1986; Väisänen et al., 1994; Koistinen et al., 1996). The Turku Granulite terrain is found in the SW of this southern belt of rocks.

Two main deformation phases can be seen within the SSB (Van Duin and Nieman, 1993; Ehlers et al., 1993). D1 is present as recumbent isoclinal folds with axial traces orientated NW/SE. These folds can be up to several kilometres in amplitude. The earliest episodes of high-grade metamorphism are synchronous with this phase of deformation (Ehlers et al., 1993; Van Duin and Nieman, 1993). D1 has subsequently been refolded by gentler E-W trending open folds, F2. Open F2 folding is responsible for the overall E-W trend of the SSB (Ehlers et al., 1993). Peak metamorphism linked to the production of potassic migmatites is associated with this phase of deformation.

The SSB is also typified by two main generations of granitoid intrusions (Ehlers et al., 1993; Van Duin and Nieman, 1993; Koistinen et al., 1996). The early granitoids are dated at 1.89-1.88 Ga (Ehlers et al., 1993) and comprise I-type rocks ranging from diorites through to red microcline granites. Some of the intrusives of this suite were affected by D1. A later suite of S-type granites dated at 1.84-1.83 Ga (Ehlers et al., 1993) is deformed by D2. Much later granitoids in the area include the Rapakivi intrusive suite dated to 1.6±0.1 Ga (Laitakari et al., 1996).

The first attempts to devise a tectonic model for the Svecofennides originates with Hietanen (1975), who proposed that a simple arc system was thrust against the Archaean, Karelian continent in the early Proterozoic. The model has since increased in complexity. In order to explain the tectonic history of the Svecofennian it is imperative to start with the origin of the Svecofennian supracrustal suite.

1.7.2 - Svecofennian supracrustals

Detailed stratigraphy is difficult in this belt of rocks due to the intense deformation and related migmatisation (Laajoki, 1986). However, in broad terms the Svecofennide supracrustals are characterised by a metagreywacke-metabasalt association with minor but distinctive calc-alkalic volcanics and very minor quartzites. Laajoki (1986) has postulated that the calc-alkaline affinity of the volcanics and the immaturity of the sediments is linked to their formation in an island arc environment that formed offshore of an Archaean continent. The SSB is split into two main belts, the Häme Belt and the Uusimaa Belt (Nironen, 1997), illustrated in Figure 1.20. The chemistry of the volcanics within the SSB and TSB are characteristic of varied tectonic settings i.e. rift, arc, back-arc and continental-arc affiliations. Hietanen (1947) describes successions of rocks with volcanic origins, with some of the mafic layers containing deformed amygdales, suggesting an origin as relic lava flows.

Thus the earliest rocks within the Svecofennian domain are indicative of a number of potential island arc systems typified by eruptions of lava. Periods of volcanism were separated by deposition of sandstones, shales and occasional limestones. Väisänen et al. (1994) interpret the sedimentary rocks as turbidite sequences deposited on an unstable shelf.

1.7.3 - Structural evolution

Following the growth of the island arc systems referred to above, the arcs slowly moved towards the Karelian basement to the NE. The deformation within the Svecofennian is attributed to the collision of the island arcs against the Archaean craton (Korja et al., 1993, Nironen, 1996). The 'suture' is considered to correspond with the Ladoga-Bothnian Bay Zone, which cuts NW-SE across middle to southern Finland (Koistinen et al., 1996). The suture zone is not a single structure but a complex tectonic junction believed to provide evidence for convergent plate tectonic movement (Koistinen et al., 1996).

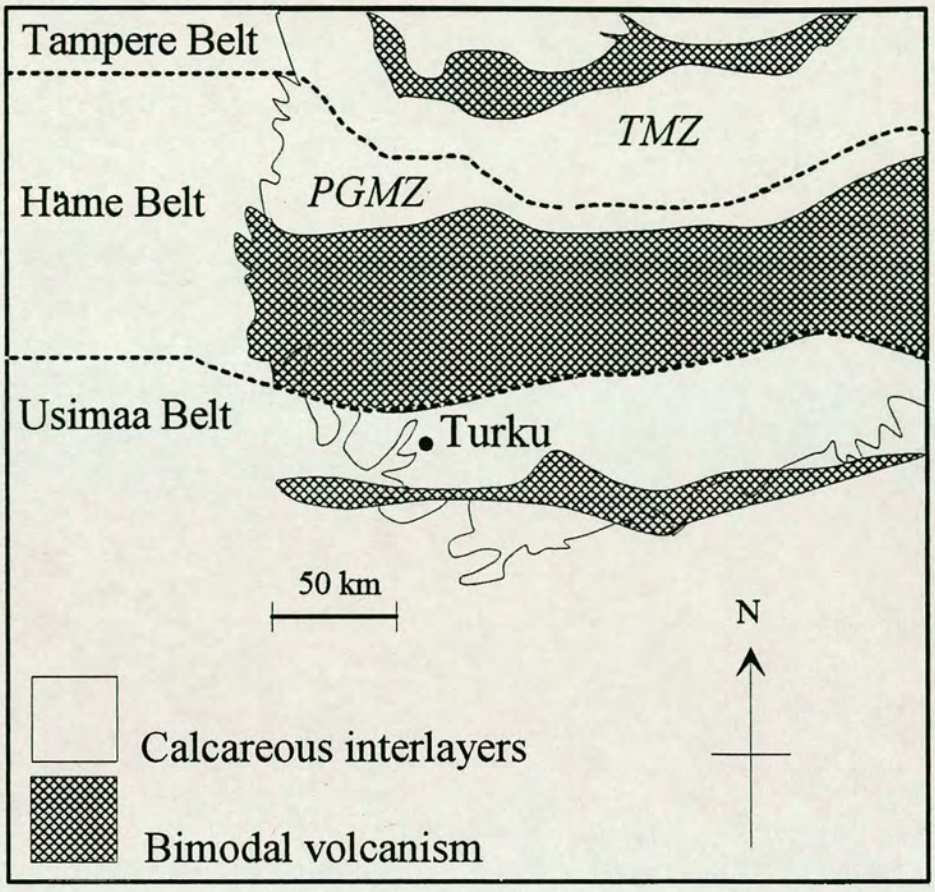

Figure 1.20 - Supracrustal belts of southern Finland, after Nironen (1996). The boundary between the Tampere Belt and the Häme Belt is also a palaeosuture between the Tonalite Migmatite Zone and the Potassium Granite Migmatite Zone which represent the northern and southern arc complexes respectively.

It is difficult to correlate the different structural episodes of the Svecofennian orogeny as a whole because it consists of a number of tectonically distinct terrains that underwent deformation at different stages of accretion and collision. In the broadest terms the terrain underwent two main events, a collisional period followed by an episode of extension. The Svecofennian is typified by thick crust, 40-65 km thick in comparison to the Karelian maximum of 40 km, with the bulk of the thickness heterogeneity occurring in the lower crust (Korja et al., 1994). Deep seismic reflective surveys have identified dipping bands of strong reflectors in the upper-middle crust, with some extending into the lower crust, that have been identified as potential compressional and extensional structures (Korja et al., 1993; Korja, 1995).

D1 varies in intensity throughout the Svecofennian. Within the Turku area D1 is overprinted by late deformation fabrics and is not associated with any mesoscopic folds. Within the Tampere-Vammala area, (Tampere Schist Belt), D1 is defined by large-scale recumbent folds. D2 in both Turku and the Tampere-Vammala terrains is associated with recumbent folding. In the Tampere/Vammala area this D2 folding is associated with the peak of metamorphism in the terrain whereas the Turku area experienced a later thermal event that is not recorded in the north. Both Van-Duin and Nieman (1992) and Ehlers (1993) group D1 and D2 across the Svecofennian as a single D1, occurring 1.8-1.7 Ga.

D3 of Väisänen et al. (1993) is responsible for the east-west trend of the Svecofennian. It is important to note that this deformation fabric is termed D2 by Van Duin and Nieman (1993) and Ehlers (1993). The structural definitions of the SSB are shown in Table 1.3. D3 folds are open to tight and slightly overturned indicating movement to the north. Early in D3 the Turku terrain was affected by a thermal event linked to the production of potassic granites and migmatites (Väisänen et al., 1994). Later D3 shear zones truncated D3/F3 folds but occurred at continuing high temperatures as they contain remobilised melt. Much later D4 shear zones have been dated at 1.81 Ga by Lindroos et al., (1996) by dating minerals in the associated

Väisänen et al., 1994; Väisänen and Höltta, (in press). The structural framework used by this study. ***(Data from Turku terrain)***	**Ehlers et al., 1993** ***(Data from the Late Svecofennian Granite Migmatite zone)***	**Van Duin and Nieman, 1993** ***(Data from the Turku terrain)***	**Koistinen et al., 1996** ***(Data from southern Finland)***
>1.89 Ga - D1	>1.89 Ga	>1.89 Ga	
S1 foliation seen as inclusion trails	No early deformation fabrics discussed.	No early deformation fabrics discussed.	No early deformation fabrics discussed.
1.89-1.87 Ga - D2	1.89-1.87 Ga - D1	D1	D1
Tight folds, often recumbent with NW/SE trending axial traces.	Tight folds, often recumbent with NW/SE trending axial traces.	Tight folds, often recumbent with NW/SE trending axial traces.	Tight folds, often recumbent with NW/SE trending axial traces.
1.87-1.83 Ga - Early D3	1.87-1.83 Ga - D2	D2	D2
Open/tight folds with NE/SW trending axial traces. Some shearing.	Open/tight folds with NE/SW trending axial traces. Some shearing.	Open/tight folds with NE/SW trending axial traces. Some shearing.	Open/tight folds with NE/SW trending axial traces.
1.83-1.80 Ga - Late D3	1.83-1.80 Ga - Late D2		D3
Late shear zones, present in conjugate sets. Shearing started when melting was occuring.	Late shear zones, present in conjugate sets. Shearing started when melting was occuring.	Not discussed	Large-small upright or north-verging folds (Not seen in Turku area except as early upright shear zones.
<1.80 Ga - D4			
Brittle shearing containing pseudotachylite.	Not discussed	Not discussed	Not discussed

Table 1.3 - Structural definitions from different papers. This project picked the work of Väisänen et al. (1994) and Väisänen and Höltta (in press) as a template as it was felt that their observations were based on the most thorough structural work and were particular to the Turku area.

pegmatites. Koistinen et al. (1996) defines a later stage of folding as D5, but as none of the other authors report this deformation it is possible that it is confined to certain localities.

1.7.4 - Granitoid emplacement

Plutonic igneous activity in the Svecofennian orogenic domain has been split into four main groups which are outlined in Table 1.4, with ages and broad chemical affinities given in Figure 1.21. The positions of these intrusives can be seen in Figure 1.1. They are distributed across the Svecofennian with the north typified by Early Svecofennian granitoids (CFGC) and the south by the Late Svecofennian potassic granitoids (Figure 1.19).

Group/name	Description.	Locality (tectonic unit)	Dates (author/method)
Synorogenic granitoids and related rocks Syn D1	Granites and granodiorites to gabbros. Mostly I type.	In the CFGC S and I type signatures are recorded which suggests mixing of mantle derived material and crustal magma. In the surrounding schist belts the signature is just of I-type magmas.	1.89-1.87 Ga Zircon U-Pb ages (Huhma, 1986; Patchett and Kuovo, 1986)
Late orogenic intrusives. D2-syn-D3	Mostly potassium rich granites that are garnet and cordierite bearing, S-type signatures	PGMZ of southern Finland where they occur in rocks of a high metamorphic grade (Ehlers et al., 1993)	1.84-1.83 Ga, zircon U-Pb ages (Huhma 1986; Suominen, 1991)
Post orogenic intrusives. D4	Tonalites, monzonites and granitic intrusions.	These mostly occur within southern Finland in a WSW-ENE zone that broadly coincides with the PGMZ.	1.77-1.81 Ga, zircon U-Pb ages (Suominen, 1991).
Anorogenic intrusives	Rapakivi granites, diabase dykes and anorthosites	Distributed regularly throughout southern Finland and northern Estonia.	1.6±0.1 Ga U-Pb zircon ages (Laitakari, 1969)

Table 1 4 - Granitoids of the Finnish Svecofennian.

1.7.5 - Metamorphic conditions

The Svecofennian Domain is typified by low-pressure/high-temperature metamorphism, extensive migmatite areas and zonal metamorphic field gradients (Höltta, 1986; Van Duin and Nieman, 1993; Ehlers et al., 1993; Koistinen et al., 1996). The lowest grade metasediments usually belong to the staurolite zone,

although there are localised areas of greenschist facies. Within the pelites a biotite and sillimanite assemblage of the uppermost amphibolite facies is stable over large areas, but locally granulite facies conditions were reached and are expressed by a garnet and cordierite assemblage, associated with migmatites. As mentioned previously the Svecofennian is spilt into two areas, on the basis of the chemistry of their associated migmatites; the tonalite migmatite zone (TMZ) in the north and the potassium granite migmatite zone (PGMZ) in the south (Ehlers et al., 1993; Korja et al., 1994). This mainly reflects differences in the original protoliths. In the TMZ the protoliths were semi-pelites whereas the pelites within the PGMZ are richer in aluminium relative to calcium and alkalis (Korja et al., 1994).

Peak metamorphism in the PGMZ post-dates that in the TMZ (Kähkönen et al., 1994). The TMZ reached peak temperatures of 670-800°C and 5 kbar and underwent partial melting. The resulting tonalitic melting is now represented by migmatites which have been dated at 1.89 Ga from U-Pb zircon dating (Korja et al., 1994). No further high-grade metamorphism occurred in the TMZ after this time. By contrast the PGMZ underwent a later thermal pulse where the terrain attained its peak conditions of 700-800°C and 4-6 kbar at around 1.85-1.83 Ga (U-Pb date from the migmatite zircons). This produced large quantities of potassic granitic melts (Korja et al, 1994; Väisänen et al., 1994).

1.7.6 - Reconstruction of the Svecofennian orogeny

Hietanen (1975) suggested that an island arc system, the Svionian, formed to the south of the Karelian continent due to subduction under the Archaean craton. Continued subduction led to collision of this arc against the continent when "all sediments were folded and intruded by plutonic magmas" (Hietanen, 1947). Since this first simple model it has been recognised that the Svecofennian orogeny was somewhat more complicated than initially thought (Korja, 1995). The following account of the Svecofennian is essentially a summary of the evolutionary models developed by Korja (1995), Nironen (1997) and Lahtinen and Huhma (1997)

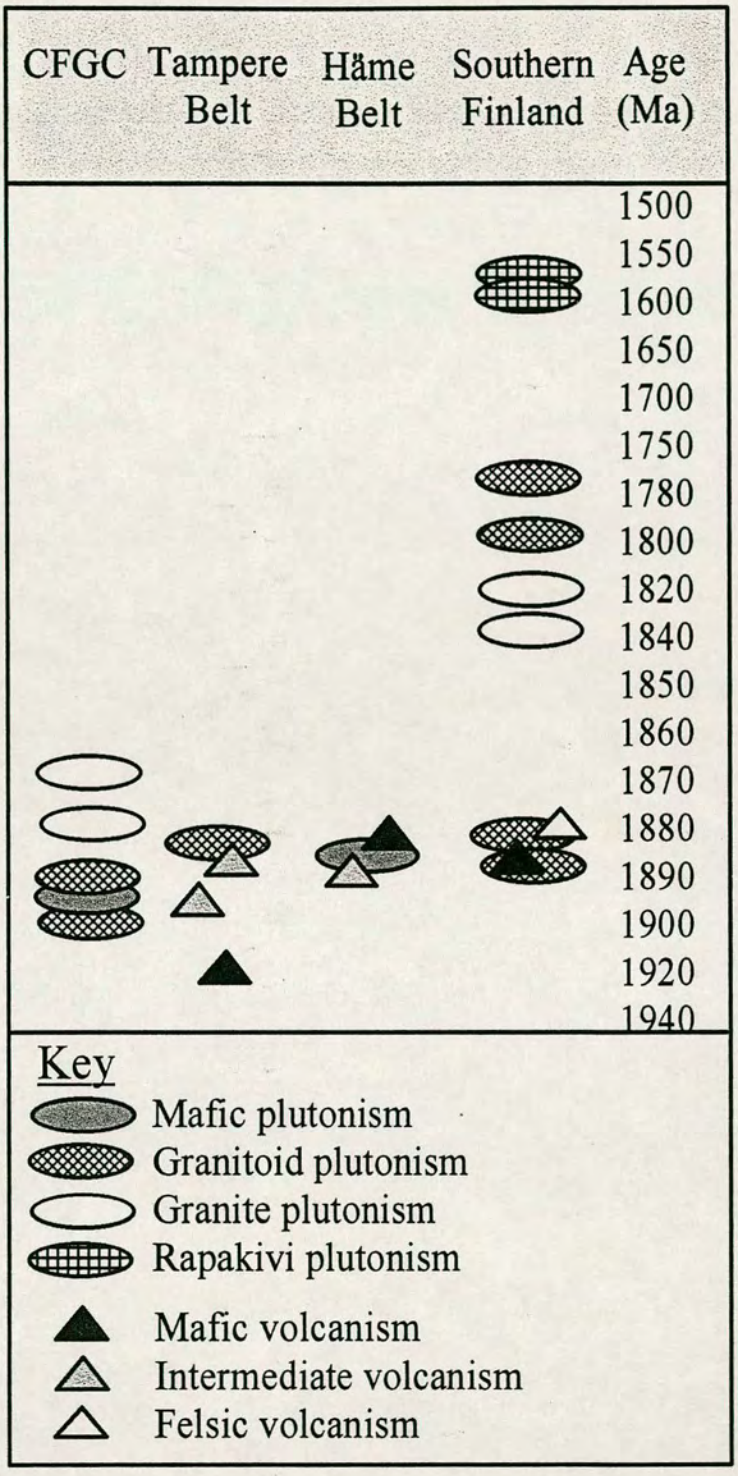

Figure 1.21- Main magmatic episodes in the southern Svecofennian of Finland (after Nironen, 1996)

The western margin of the Archaean Karelian continent underwent rifting 2.1 to 2.2 Ga, and the Jatulian dykes that cross-cut the Archaean and the overlying Karelian metasediments have been interpreted as reflecting the opening of the Svecofennian ocean (Korja et al., 1993). The final stages of the opening of this ocean, are dated at 1.95 Ga by Nironen (1997). Within the newly-formed Svecofennian ocean, an island arc complex grew to the south of the Archaean continent. This consisted of several arcs, basins and subduction zones, which slowly accreted juvenile crust. This is represented today by acid to intermediate plutonics that retain geochemical characteristics of juvenile arc magmatism (Nironen, 1997). Work by Lahtinen and Huhma (1997) suggests that there may have been an older palaeoproterozoic crustal input into this largely juvenile material. The Central Finland Granitoid Complex (CFGC) that now represents these accreted areas and earlier nucleii, is thought to have formed through several cycles of crustal addition during the Palaeoproterozoic with a metamorphic event preceding the plutonism at 1.91 Ga.

Island arc basalts, andesites, volcanics and plutonics formed at the active margin of this nucleus, represented today by the Savo Belt (Figure 1.19) intrusives and extrusives. The rocks of southern Finland are thought to have belonged to a second more distal arc system which formed further south and was separated from the first arc by the Bothnian sea.

Through continued subduction of the oceanic crust, the first arc accreted to the Archaean continent around 1.91 Ga (Figure 1.22a). Thus there was a 40 My time gap between rifting and accretion. The Archaean continent and the arc system met along what has been termed a palaeosuture, the Ladoga-Bothnian Bay zone which runs NW-SE across Finland (Koistinen et al., 1996). As there is no evidence of subduction-related magmatism on the Archaean craton it is proposed that subduction took place to the south-west of the arc complex in Nironen's models.

This collisional event (1.91 Ga) led to the emplacement of ophiolites (Jormua and Outokumpu associations), and marine strata onto the Karelian basement (Koistinen et

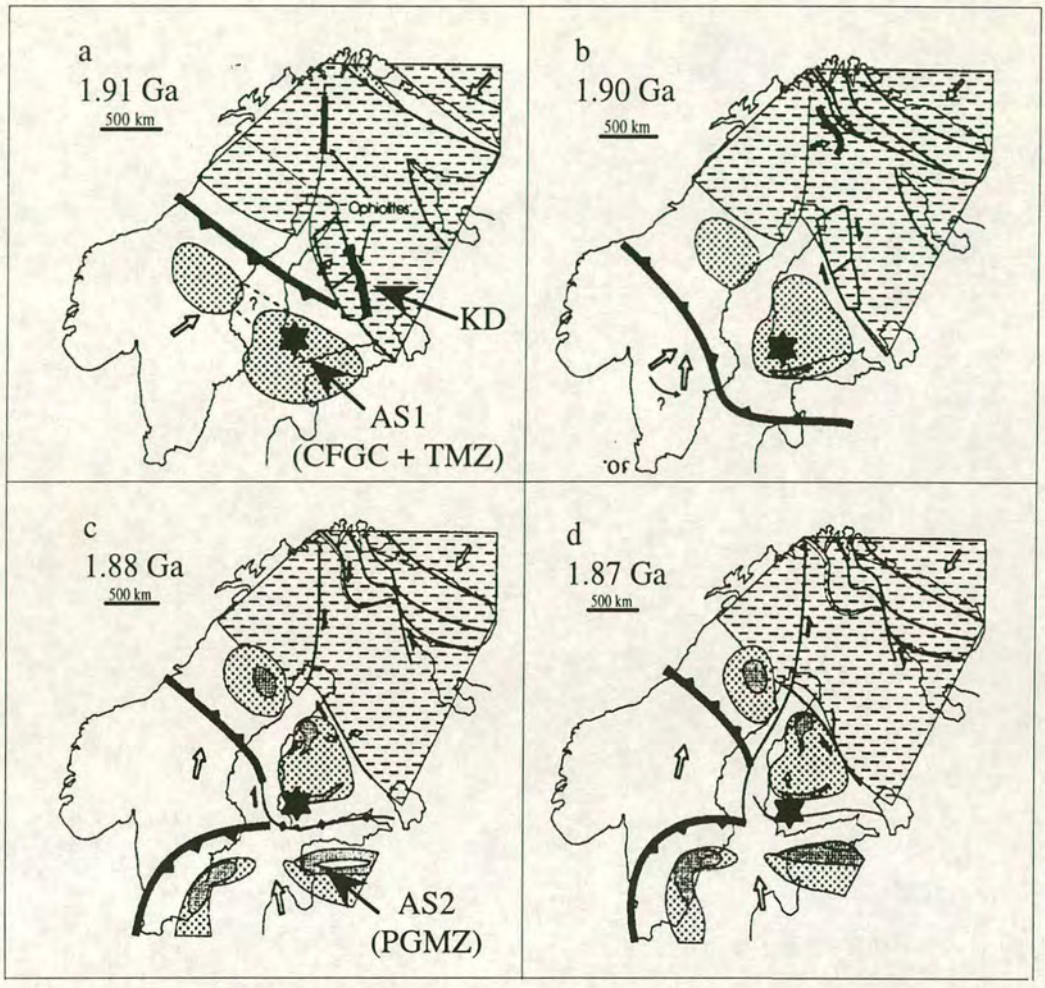

Dashes represent the Archaean Cration.
Dotted and shaded areas are the newly formed Svecofennian crust.

Figure 1.22 Reconstruction of the Svecofennian orogeny, after Nironen (1996) (a) - Collision of an island arc system against the Karelian continent. Subduction took place under the arc system. The Archaean margin starts to thicken in the east due to accretion whilst subduction continued to the west. The Jormua and Outokumpu ophiolites were thrust NE onto the Archaean crust. (b) - Subduction started to the SW of the newly accreted Karelian continent and the primary arc system. (c) - Another microplate and island arc system approached from the SW and convergence was then accommodated by and E-W trending subduction zone. This produced the E-W trending folds of D3. (d) - The eastern part of the Svecofennian crust was largely stabilised and deformation was partitioned into ductile shear zones. The southern arc complex continued to curve until the complex doubled and caused lithospheric thickening.

al., 1996). To the south the second island arc complex that had formed during and after accretion of the first arc against the Archaean craton (Figure 1.22b), also collided and closed the Bothnian Basin, (Figures 1.22c+d). Plate convergence was oblique to the craton edge at this point (Nironen, 1997). The suture between the two arcs is thought to be an E-W trending zone now exposed between the Tampere Schist Belt and the Häme Volcanic Belt, which also corresponds to the southern edge of the Tonalite Migmatite Zone. The collision of the two arc systems led to thickened lithosphere with movement along dextral megashears, and magma underplating with large-scale granitoid magmatism. The geochemical signatures of these granitoids are I-type with a mixing of mantle-derived and remelted arc complex material (Nironen, 1997; Lahtinen and Huhma, 1997). Late stage shearing formed a block structure within the Savo Belt in which slices of rock with different metamorphic assemblages were emplaced next to each other (Nironen, 1997).

The accreted rocks underwent a low P-high T metamorphism event, which in the northern Savo and Tampere Belts culminated between 1.88-1.89 Ga (Korja et al., 1993; Koistinen et al., 1996; Nironen, 1997). Both of these belts belong to the northern arc system. The rocks of the southern arc system also underwent granulite facies metamorphism in this time interval, but peak temperatures and migmatisation occurred during a later thermal event which was coeval with the late orogenic granitoids of Ehlers et al. (1993), around 1.84-1.83 Ga (Van Duin and Nieman, 1993; Korja et al., 1993; Koistinen et al., 1996; Nironen, 1997).

The present day crust in the SSB is thinner than the crust in the northern CFGC (Korja et al., 1993; Korja et al., 1994; Korja et al., 1995; Korja, 1995) and it is proposed that the originally thickened, relatively cool base of the crust was pushed into the hot asthenosphere immediately after accretion. This was gravitationally unstable compared to the surrounding asthenosphere because of density differences, and around 1.89 Ga the lower part of the lithosphere was thinned by delamination, which led to decompression melting of the asthenosphere based on the models of Houseman and McKenzie (1981), Loosveld and Etheridge (1990), and Sandiford and

Powell (1991). The mantle melts that were produced rose and helped to re-melt the lower crust which produced a variety of magmas depending on the degree of crustal assimilation (Nironen, 1997; Lahtinen and Huhmaa, 1997). This crustal under- and intra-plating caused high heat flow in the crust and helped cause the high temperature-low pressure metamorphism mentioned previously. This mafic underplating may be shown by high velocity zones in seismic sections (Korja et al., 1993; Korja et al., 1994; Korja et al., 1995; Korja, 1995; Nironen, 1997).

As mentioned previously the rocks of southern Finland were metamorphosed during an additional, younger thermal pulse and this is associated with the intrusion of potassium granites. The geochemistry of these intrusives suggests that they are S-type granites that are a product of partial melting of the crust. These later granites are emplaced along transpressional structures that initially formed during the compressional episode, although some of the shear zones directly associated with the granites are thought to represent crustal extension (Väisänen et al., 1994). It is postulated that late-D3 the southern Svecofennian crust underwent extension along low angle faults which led to an increase in heat flow through the crust. This enhanced the dry melting of the crust and led to the emplacement of potassium granites and migmatites along earlier transpressional features (Väisänen et al., 1994, Korja, 1995, Nironen, 1997), at 1.84-1.83 Ga.

The stress field during D3 had NNW-SSE compression and WSW-ENE dextral drag which led to wide E-W striking ductile shear zones. Deformation continued during extension and uplift until the crust entered the field of brittle deformation. Later shearing is dated by the emplacement of pegmatites at 1.8 Ga. Deformation was then concentrated into NE-SW and E-W margins of rhomboidal blocks (Lindroos et al., 1996). This extension is due to uplift and collapse of the orogen.

The youngest features of the Svecofennian are anorogenic intrusives, including a rapakivi granite suite, that were emplaced at 1.58 Ga during crustal thinning and rifting. It is thought that the crust underwent mafic underplating leading to crustal

melting and emplacement of intrusives into the upper crust along low angle listric shear zones (Stel et al., 1993; Korja and Heikkinen, 1995). This deformation took place within the brittle field and at higher crustal levels than the previous high-grade deformation. For example, a contact aureole formed around the Vehmaa rapakivi batholith within the Turku terrain at pressures and temperatures of 800°C and 2 kbar, implying that the crust was exhumed by 10 km between 1.83 Ga (D2) and the emplacement of the anorogenic rocks at 1.58 Ga (Väisänen et al., 1994).

1.8 - Section 2 - Brief introduction to the Turku terrain

The Turku terrain is one of three low-pressure granulite terrains within the Svecofennian Schist Belt of Southern Finland (Van Duin and Nieman, 1993), (Figure 1.19). It is characterised by low P and high T upper amphibolite-granulite facies metamorphism, extensive migmatisation and the emplacement of volumetrically important anatectic potassium granites (Höltta et al., 1994). Younger anorogenic rapakivi granites also intrude a large amount of the terrain (Hietanen, 1947; Van Duin and Nieman, 1993; Väisänen et al., 1994; Väisänen and Höltta, in press).

The earliest rocks in the terrain are a supracrustal sequence of predominantly pelitic and psammitic gneisses with interlayered volcanic rocks (Van Duin and Nieman, 1993). One of the first detailed examinations of the terrain was by Hietanen (1947), who refers to the pelitic migmatites as kinzigites. The pelites are reported as bedded except where the migmatites disrupt the layering. This bedding is termed compositional layering by Väisänen and Höltta (in press) and is represented in the field as an alternation of pelitic garnet-mica schists with quartzo-feldspathic gneisses (Van Duin and Nieman, 1993).

The meta-volcanics are discussed in detail by Hietanen (1947) and are represented by amphibolites and fine grained mafic layers. On the north edges of some layers are amygdaloidal structures, which would suggest the top side of a lava flow. Within the volcanic rocks are large lenticular bodies that have been interpreted to represent relict volcanic bombs. These volcanics alternating with pelitic/psammitic bands are

considered to be indicative of the island arc system described previously (Väisänen et al, 1993; Väisänen and Höltta, in press).

1.8.1 - Structural evolution

The oldest structural feature is S1, a biotite foliation parallel to compositional layering (Väisänen et al., 1994; Väisänen and Höltta, in press). Later deformation has meant that S1 is only preserved in the hinge zones of some later folds and as inclusion trails within K-feldspar, cordierite and garnet pophyroblasts (Väisänen et al., 1994, Väisänen and Höltta, in press). As no F1 folds have been found it is difficult to extrapolate the kinematics and tectonic setting of the first deformation event. It may be that D1 was an early phase of D2.

The second deformation, D2 (D1, Ehlers et al., 1993) has deformed the compositional layering and S1 into isoclinal to tight folds with subhorizontal axial planes and strong axial planar foliations, S2 (Väisänen et al., 1993; Väisänen and Höltta, in press). S2 is the dominant foliation in the area and is parallel to bedding and S1, except in fold hinges where it can be seen to be axial planar. The recumbent nature of F2 is attributed to layer parallel shear and over or under-thrusting during D2. Garnet and cordierite were developed within pelites throughout most of the terrain during D2, with both minerals present as elongate ellipses parallel to S2 (Väisänen et al., 1994; Väisänen and Höltta, in press). Hence it is inferred that granulite facies conditions were reached early in D2.

S2 has since been folded into open to tight folds that can be seen on a regional scale, (Hietanen, 1947; Van Duin and Nieman, 1993; Ehlers et al., 1993; Väisänen et al., 1994; and Väisänen and Holtta, in press). This phase of folding has deformed the subhorizontal S1+2 fabrics into upright or asymmetrically inclined F3 folds (F2, Ehlers et al., 1993; Van Duin and Nieman, 1993). The axial traces are generally orientated E-W or NE-SW. The intensity of this folding varies from open to tight, with some limbs attenuated by shearing (Väisänen et al., 1994; Väisänen and Holtta, in press). S3 is only developed in the tight F3 folds. Some cases of recumbent or

overturned F3 folds are also found within the terrain and are linked to continuing crustal thickening early in D3 (Väisänen and Höltta, in press).

D3 shear zones can be seen attenuating and reactivating F3 fold limbs, indicating that shearing outlasted the open folding (Väisänen et al., 1993). The early D3 shear zones are characterised by an abundance of leucosome material and large K-feldspar megacrysts (Väisänen et al., 1994; Väisänen and Höltta, in press). These subvertical to steep SE-dipping shear zones range in size from one metre to several tens of metres in width, and are generally subparallel to S3 (Väisänen et al., 1994; Väisänen and Höltta, in press). Later D3 shear zones have deformed the late-orogenic granites (1.83-1.84 Ga, Patchett and Kuovo, 1986; Suominen, 1991) to a range of mylonite textures (Väisänen and Höltta, in press). Chlorite and epidote crystallise within these late shear zones indicating much lower metamorphic grades than the early D3 shear zones that contain leucosome. Nevertheless, these shear zones are D3 because their dextral kinematics are consistent with the D3 folding. This deformation has been linked to the beginning of extensional tectonics rather than the compressional regime that dominated through D1, 2 and early D3 (Väisänen and Höltta, in press).

The youngest structural features to be seen within the study area are small, localised shear zones that cut through all previous tectonic features (Väisänen et al., 1994; Väisänen and Höltta, in press) which generally trend N-S and NE-SW. They are generally metres in width but several can occur in a wider sheared region (Väisänen and Höltta, in press). Some zones have a ductile mylonitic fabric but others contain brittle pseudotachylites (e.g. Vellua shear zone in the north of the terrain, Väisänen and Höltta, in press).

1.8.2 - Metamorphic evolution

As noted above, the rocks have undergone metamorphism in the upper amphibolite to granulite fields (Van Duin and Nieman, 1993). In the pelitic rocks the incoming of granulite facies is marked by a cordierite + garnet assemblage and in the metavolcanics by the appearance of orthopyroxene (Van Duin and Nieman, 1993),

The range of temperatures recorded in the terrain are illustrated in Figure 1.23. The supracrustals of the terrain have undergone various degrees of anatectic melting.

The general pelitic assemblage is bt + qtz + plag + kfs + opaque ± grt ± crd ± sil ± gr. Garnet and cordierite is the stable peak mesosome assemblage throughout most of the terrain, except to the north of the Vehmaa rapakivi pluton, where Väisänen et al. (1994) have reported a bt + qtz + kfs + crd + sil assemblage. Throughout most of the terrain sillimanite is not a stable phase with garnet and cordierite, except near the isograd between bt + sil and crd + grt assemblages.

More than one generation of garnet and cordierite is present. The early generation has been deformed into ellipses parallel to S2 placing their formation at late D1 or early D2. Biotite and sillimanite occur included in cordierite and K-feldspar (Höltta, 1986; Väisänen et al., 1993; Väisänen and Höltta, in press). These inclusions form an internal foliation along with quartz blebs that are oblique to S2. This may correlate with S1 and would suggest that sillimanite, K-feldspar, biotite and cordierite were stable during D1. In the middle and southern parts of the terrain the sillimanite inclusions are limited to the cores of the cordierites (Höltta, 1986; Väisänen et al., 1994; Väisänen and Höltta, in press). The presence or absence of garnet or cordierite within the pelites is also linked to compositional differences, as deduced by Hietanen (1947).

Garnet and cordierite are also both present in later textural generations of crystals. These include undeformed porphyroblasts that mostly have poikiloblastic textures. Later garnet overgrows F3 folds and preserves S2 as inclusion trails (Väisänen et al., 1993). These garnets are often large, contain rounded quartz inclusions, and are sometimes rimmed by quartz which forms crystal faces with adjacent K-feldspar and cordierite (Väisänen and Höltta, in press). This texture is generally interpreted as a typical melt texture and supports the interpretation that some of the leucosome

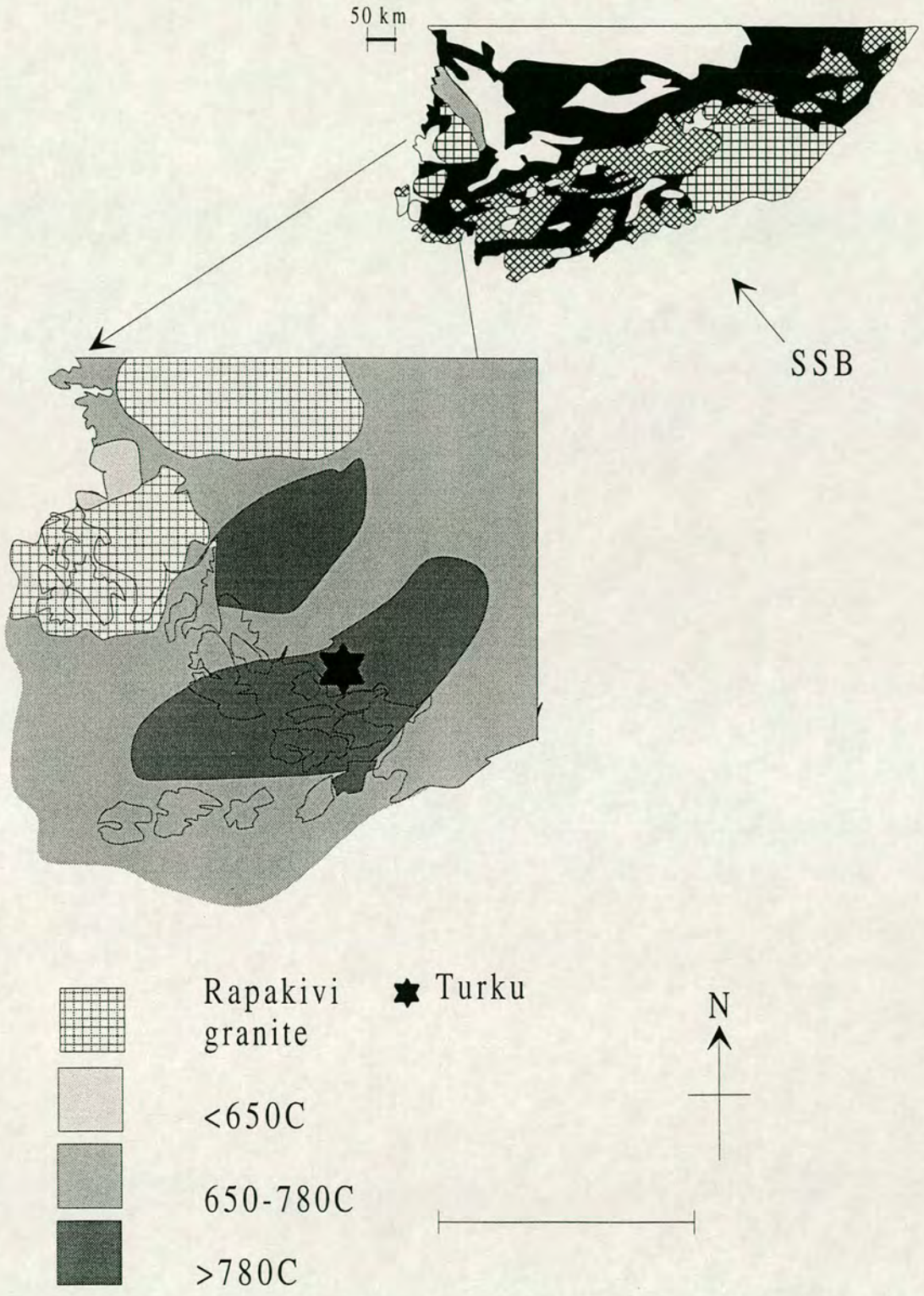

Figure 1.23 The metamorphic gradient across the Turku terrain (after Väisänen and Höltta, in press).

patches are representative of melt that formed during the dehydration melting reaction:-

biotite + sillimanite + quartz = garnet + cordierite + K-feldspar + melt (1.1)

The Turku terrain does record some retrogression. Garnet is often altered to biotite on its rims with quartz (Höltta, 1986). Cordierite is also a retrogressive phase around garnet and so is chlorite. The retrogression is strongest in the north where cordierite is altered to a green biotite, aluminosilicate and white mica. In some cases andalusite is a retrogressive product around cordierite (Höltta, 1986; Väisänen et al., 1994; (Väisänen and Höltta, in press). White mica and chlorite are also retrogressive on K-feldspar and biotite.

A characteristic of the Turku terrain is the presence of migmatites and the late-Svecofennian granites which form part of the late-Svecofennian granite-migmatite zone, the LSGM, (Ehlers et al., 1993). Hietanen (1947) has identified two main leucosome types throughout the terrain. Her 'early leucosomes' are described as having penetrated the rocks parallel to the main foliation (S2 Väisänen et al., 1994), as veins ½ to 2 cm in width and regularly distributed. These 'normal' migmatites are sometimes cut by broader pegmatitic leucosomes which raise the amount of granitic material to 80% or more. These observations are generally confirmed in the more recent work, (e.g. Koistinen et al., 1996).

Recent studies (Höltta, 1986; Väisänen et al., 1994; Väisänen and Höltta, in press) have suggested that the production of granitic melt occurred following biotite dehydration reactions (Thompson, 1982; Waters and Whales, 1984; Le Breton and Thompson, 1988; Waters, 1989). Textures within the leucosomes such as myrmekite feldspars and poikiloblastic garnet and cordierite, are indicative of the leucosome representing crystallised melts (Höltta, 1986; Waters, 1988; Powell and Downs, 1991; Väisänen and Höltta, in press), potentially formed through melting reaction 1.1.

Partial melting also took place within the metavolcanics which generated melts that were compositionally different to those generated from the pelitic lithologies (Väisänen and Höltta, in press). However both leucosome types are confined to their source rock which is seen as evidence for in-situ crystallisation of melts. Little detailed work has been done on the generation of the leucosomes within the Turku terrain and on potential links to the larger granitic sheets found at the same localities.

1.8.3 - Turku intrusives

The Turku terrain is typified by a number of intrusives. Work on these by Väisänen et al. (1994), Koistinen et al. (1996), and Väisänen and Höltta (in press) has agreed with the work of Sederholm (1934) who separated the intrusives into four groups, early orogenic, late orogenic, post-orogenic and anorogenic. The different groups have been dated by later workers on the terrain and the dates and descriptions are detailed in Table 1.4 below.

Group	Description	Dates (Ga)
Early orogenic type Hietenen's first cycle.	1) I type, gneissic tonalite with mafic enclaves. Also trondjhemites, granodiorites, diorites and gabbros. 2) Enderbites (A general name for an Opx bearing, compositionally tonalitic-dioritic igneous rock e.g. opx + hbl + bt + plag + qtz. (Höltta, 1997).	1) 1.89-1.87 Ga U-Pb zircon ages (Patchett and Kuovo, 1986; Suominen, 1991) 2) 1.86-1.82 Ga U-Pb zircon ages (Patchett and Kuovo, 1986; Suominen, 1991)
Late-orogenic granitoids Hietanen's second cycle	S-type coarse grained granites. Large garnet and cordierite bearing intrusions and leucosomes. Dating from the east end of the LSGM shows that small leucosomes and the larger granites are the same age.	1.84-1.83 Ga (Patchett and Kuovo, 1986; Suominen, 1991; Ehlers, 1993) 1.85-1.81 Ga (Korsman et al., 1984)
Post orogenic intrusions Hietanen's third cycle	Small undeformed granitoids that cut all folding although in places they are deformed by later shear zones.	1.82-1.77 Ga (Patchett and Kuovo, 1986; Suominen, 1991; Korsman et al., 1984)
Anorogenic magmatism Hietanen's 'young post tectonic intrusives'	Late intrusives are represented by Laitila and Vehmaa rapakivi plutons and the Kolinummi anorthosite.	1.57 Ga (Suominen, 1991)

Table 1.5. - Intrusive characteristics after Väisänen and Höltta, (in press)

1.8.4 - Tectonic reconstruction

The SSB was a Palaeoproterozoic extensional basin that followed a zone of inherited weakness in the crust (Ehlers et al., 1993). This then underwent transpressional deformation as the rocks were thickened by thrusting towards the NW. This

Time (Ga)	Intrusives	Deformation	Metamorphism
2.0-1.8 Ehlers et al., 1993.		**S0** deposition and extrusion of volcanics in an island arc system.	
1.88±0.11 Vaasjoki, 1994.		**S1** foliation formed parallel to S0.	**Bt 1 Kfs 1 Sil 1** Upper amphibolite facies.
1.89-1.87 Ehlers et al., 1993.	Cycle 1 - tonalites	**F2** folding is coeval with the intrusion of the early orogenic intrusives. The flat lying nature of F2 is linked to collision and thickening of the crust. Folds are overturned towards the NW, indicating movement to the N-NW (Ehlers et al., 1993) In the northern Tampere belt extension had begun so the tectonic regime was variable across the Svecofennian.	**Bt 2 Crd 1 Grt 2** Some sillimanite is consumed and early anatectic melts are formed due to dehydration melting (Holtta 1986, Väisänen and Höltta, in press). Granulite facies.
1.84-1.83 Ehlers et al., 1993	Cycle 2 - late orogenic potassium granitoids	During **D3**, F2 was refolded into open to tight folds whose axes were overturned towards the NW. This was due to continued crustal thickening. The LSGM's translation direction was oblique to the strike of the zone (Ehlers et al., 1993).	**Crd 1 Grt 2** This generation is unaltered and poikiloblastic in texture. The thickened crust lead to melting and the formation of migmatites and the late orogenic granites.
1.8-1.77 Suominen, 1991	Cycle 3 - post orogenic granites	Some **D4** shear zones are coeval with the post orogenic granites but shearing carried on after the intrusions. These later shear zones can be mapped into the lower crustal boundary and are linked to crustal extension.	**Crd 3 Sill 2 Bt 3 And 1** From late D3 to D4 decompression and cooling had lead to retrogression of the peak assemblages.
1.57 Suominen, 1991 Vaasjoki, 1977	Cycle 4 - anorogenic intrusions-rapakivi	Some shear zones have been reactivated such as the shearing of the Kolinummi anorthosite. The granites intruded through extended crust that was controlled by listric faults (Väisänen et al., 1994).	**Crd 4 Opx 1** Contact metamorphism around the late intrusives. 2 kbar and 800°C Vaisanen et al. (1994).

Table 1.6 - Tectonic summary of the Turku area after Hietanen, 1947; Väisänen et al., (1993); Väisänen and Höltta, (in press).

thickening of the already hot rock pile due to compression during D2 and early D3, lead to granulite facies conditions enhanced by crustal delamination (Korja et al.,

1993, Väisänen et al., 1994). Melting of the Turku rocks and the peak of metamorphism were reached mid to late D3 when the crust begin to undergo extension (Väisänen et al., 1994) due to lithospheric delamination (Korja et al., 1993, Korja, 1995). Extensional collapse of the terrain late-D3 led to thinning of the crust and the subsequent uplift of the Turku terrain when the post orogenic potassium granites were intruded. Much later renewed extension led to the intrusion of the rapakivi suites (Väisänen et al., 1994).

The peak metamorphic temperature attained in the terrain is 800°C at 6 kbar, with an inferred evolution from 610°C and 4.3 kbar on the prograde path (Van Duin and Nieman, 1993) to the peak via a clockwise P-T path (Van Duin and Nieman, 1993). The main deformation, intrusive and metamorphic episodes that occurred within the Turku terrain during the Svecofennian orogeny are outlined in Table 1.6. above.

Chapter 2

Fieldwork

Chapter 2 - Fieldwork

2.1 - Objectives

As mentioned in the previous chapter, the main aim of the field study was to construct a basic model for the metamorphic, deformation and melting history of the Turku terrain. Once this basic framework had been derived more detailed petrological methods could be employed to build up a fuller picture. Thus at the beginning of the field seasons the basic field objectives were to:

1. Document leucosome characteristics, size, mineralogy, grain size and relation to the deformation fabric.
2. Document the amount of leucosome material present at any one outcrop.
3. Decipher relationships of different leucosomes and determine crosscutting relationships.
4. Observe and interpret the mesosome assemblages and textures.
5. Check structural observations against previous studies.

2.2 - Methods

Outcrops varied in size from a few square metres up to two hundred metres long and 20 metres high, although on average each outcrop examined in detail was approximately 10 m by 10 m in size. They were either horizontal, smooth, glaciated humps or vertical, craggy road/quarry cuttings. At each outcrop observations were made on the 3-dimensional distribution of leucosome material, its mineralogy and its relationship to the structure. In order to reconstruct the metamorphic history, observations were made of mesosome mineralogy and textural relations. To systematically catalogue this information certain techniques were used and are briefly described below.

2.2.1 - Mapping

In order to record the features of each outcrop detailed maps were constructed. One metre grid squares were measured out onto the outcrop and the details were then

copied onto 1 cm grid paper. These field slips were then made into final compilation maps with the aid of photomontages. The scale of the maps varies, but generally 1 cm is equal to 10 cm.

2.2.2 - Tracing

Specific features of interest in individual outcrops were documented directly by tracing onto tracing paper placed onto the actual outcrop. This produced a scaled diagram of features such as leucosome relationships, leucosome margins and mesosome textures.

2.3 - Previous work and structural framework.

2.3.1 - Regional structure

As detailed regional structural work was outside the scope of this project, the structural observations made herein have been based on the structural framework of Väisänen et al. (1994) and Väisänen and Höltta (in press), which was discussed in Chapter 1 (summary in Table 1.4). This study aims to evaluate the timing and continuity of melting and melt segregation within this structural context. The structural framework is summarised below.

S0 - >1.89 Ga

This refers to the lithological layering that can still be seen at some localities in the form of compositionally different layers in the mesosome. SO is best preserved in weakly deformed outcrops with a low percentage of leucosome material. Original sedimentary bedding can be seen as pelitic and semi-pelitic layers.

D1 – 1.89 Ga

S1 is the earliest fabric but is only seen very rarely on an outcrop scale where it has formed parallel to bedding (Väisänen et al., 1994). Generally it is only present as biotite and sillimanite inclusion trails within porphyroblasts of cordierite, garnet and

K-feldspar. As there are no folds associated with D1 it may be that S1 reflects an early stage of a progressive D1-D2 deformation (Väisänen and Höltta, in press).

D2 – 1.89 to 1.87 Ga

S2 is the dominant foliation in the study area and is characterised by isoclinal folds with axial planar cleavage and sub-horizontal axial planes (Väisänen and Höltta, in press). The intensity of S2 varies from crenulated S1 to a penetrative S2 biotite foliation (Väisänen et al., 1994). The fact that S2 is parallel to bedding suggests that it may be described as composite S1 and S2. Generally the axial traces are oriented N-S to NW-SE.

D3 – 1.87 to 1.83 Ga

F3 is found from outcrop to regional scale as open to tight folds with E-W or NE-SW orientated fold axial traces. The fold axes are generally horizontal or slightly plunging, but there is no dominant plunge direction (Väisänen et al., 1994). At localities where original layering is visible (localities 2 and 3 of this study), F3 can clearly be seen refolding F2 folds (see Figure 2.1 for locations). F3 folds can be isoclinal, often with sheared limbs as seen at locality 4 (location in Figure 2.1). In the north and centre of the terrain the axial planes are vertical or inclined towards the NW.

Late D3 – 1.83 to 1.80 Ga

Shearing took place throughout D3 with later shear zones reorienting F3 fold axes. These later shear zones contain leucosome material, which represents once mobile melt. Some of the leucosomes contain entrained schlieren of mesosome material.

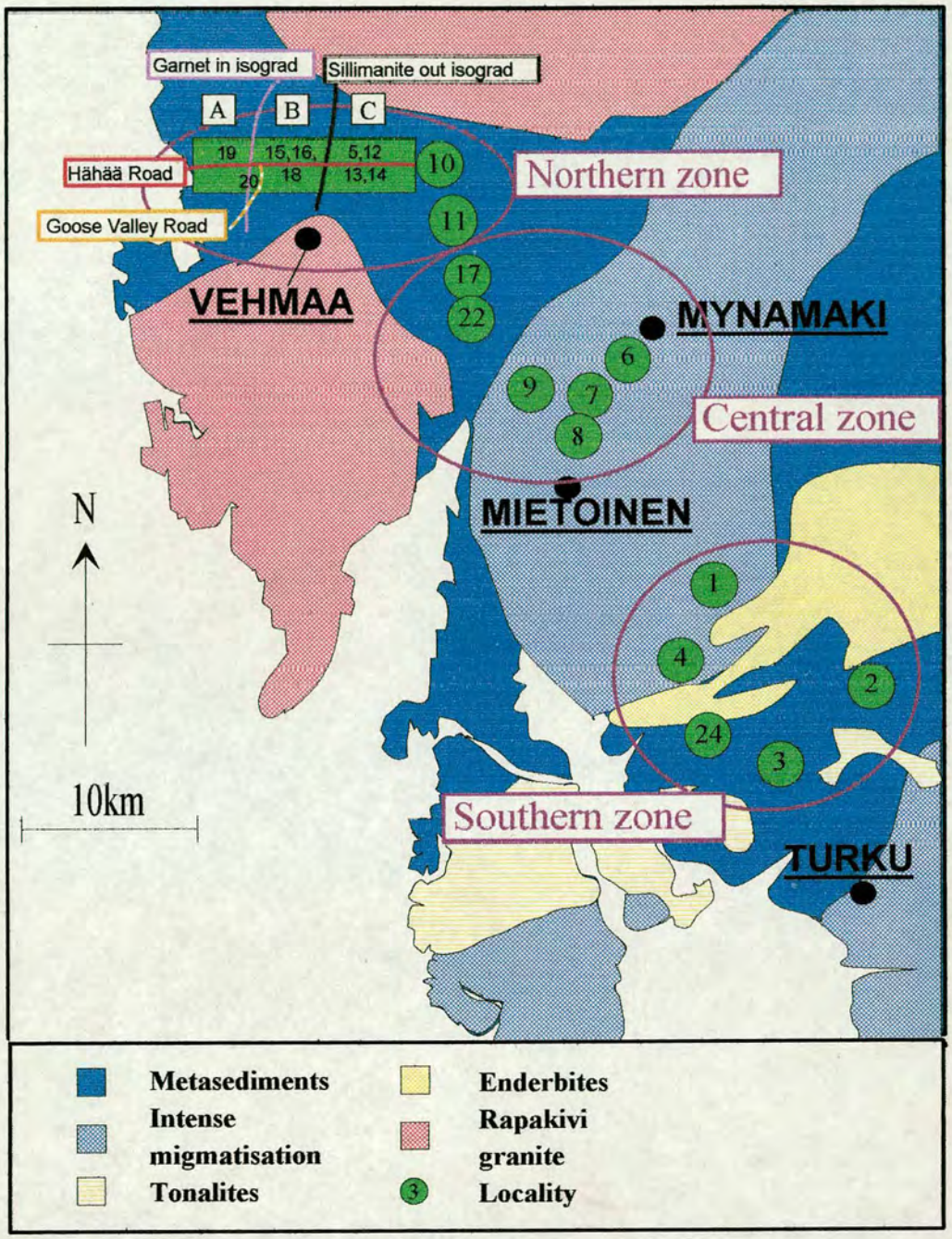

Figure 2.1 - Metamorphic map of the Turku terrain (After Väisänen et al. 1994).
A - Cordierite+sillimanite+biotite assemblage
B - Garnet+cordierite+sillimanite+biotite assemblage
C - Garnet+cordierite assemblage

D4 – 1.80 Ga

During D4 the deformation regime was brittle and localised shear zones cut through all previous fabrics and granitic material. The only shear zone observed in this study is found on the Goose Valley Road transect, locality 20 (see Figure 2.1), where a strongly deformed fabric and pseudotachylite are found. The pseudotachylite is indicative of brittle deformation. No PT estimate have been made by previous workers on the terrain but muscovite and biotite porphyroblasts have been found parallel to and crosscutting the mylonitic fabric (Väisänen et al., 1994; Väisänen and Höltta, in press).

2.3.2 - Metamorphic regime

Previous work on the area by Höltta (1989), Van Duin and Nieman (1993), Väisänen et al. (1994), and Väisänen and Höltta (in press) has indicated a metamorphic gradient throughout the terrain. A peak of 800°C and 6 kbar (Höltta, *pers. comm.*) has been measured in the middle of the terrain, with a minimum of 670-720°C and 5 kbar (Väisänen et al., 1994) from the north. In order to observe the effects of metamorphic grade on the type and quantity of leucosomes present, localities were concentrated into three areas, the northern, middle and southern zones that are illustrated in Figure 2.1 and discussed below. Whilst 24 localities were studied, 11 were chosen as key localities: 1, 2, 3 and 4 (southern localities); 6 and 7 (middle localities); and 5, 12, 15, 19 and 20 (northern localities).

Northern zone

The northern localities are principally spread out along the Hähää road, north of Vehmaa (Figure 2.1). Moving from east to west along this transect the mineral assemblage in the pelites changes from garnet + cordierite + biotite to garnet + cordierite + biotite + sillimanite, and finally to cordierite + biotite + sillimanite. The sillimanite-out and garnet-in isograds have been mapped out by Väisänen et al. (1994) and Väisänen and Höltta (in press), who interpret the change in mineral assemblages as a P-T gradient. Thus the road outcrops were studied intensively in

order to observe the possible effects that this gradient may have had on the proportion and composition of leucosome material.

Central zone

Localities in the central zone are within an area of intensely migmatised rocks. Peak metamorphic conditions of 800°C and 6 kbar have been recorded from one of the middle localities (Väisänen et al., 1994; Väisänen and Höltta, in press). The area was studied to see if there was a link between the PT conditions and the proportion of leucosome material (i.e. whether the observed apparent extents of melting correlate with peak temperatures). As discussed in chapter 1, the bulk composition would also influence the amount of melting that could have taken place.

Southern zone

The southern area encompasses features of both the other two areas. There are outcrops with high volumes of leucosome material and also those with scarcer leucosomes. The south of the terrain has yielded similar PT conditions to the north (Väisänen et al., 1994; Väisänen and Höltta, in press) and so the area was studied for comparison of melting regimes with ostensibly identical grades of metamorphism.

Table 2.1. Summary of the structural and metamorphic evolution of the Turku terrain. After Väisänen et al. (1994). The different generations of phases are discussed on the following page.

T (Ma)	Deformation	Mineral growth				Metamorphism
>1890	S0 D1	Sill 1	Kfs1		Bt 1	Amphibolite facies metamorphism
1890-1870	D2	Sill 2	Crd 1	Grt 1	Bt 2	Granulite facies metamorphism 750°C and 5 kbar
	D3		Crd 2	Grt 2		
1830	Late-D3					
1800	D4					

2.3.3 - Definition of terms

For field descriptions the definition of materials are after Ashworth (1985).

Leucosome - A pale feldspathic segregation that is, in this instance, representative of melt material.

Mesosome - Mafic schist which is full of aluminous phases i.e. garnet, cordierite and biotite. This can be foliated or granuloblastic.

Melanosome - Dark schistose material that is found intimately associated with leucosome material at localities where the amount of leucosome material is >60%.

Selvage - A coarse biotite and cordierite mantle on leucosomes, sandwiched between mesosome material and the leucosome. Its thickness is generally linked to the width of the leucosome.

2.4 - Results

2.4.1 - Structure

The following abbreviations have been used as a classification scheme for the structural features observed in the field. Table 2.2 illustrates the structural feature observed at key localities.

S0 - Original compositional layering, semi-pelite and pelite bands.

S2 - D2 deformation fabric axial planar to F2 folds, usually defined by biotite + cordierite + garnet.

F2 - D2 folds, isoclinal to recumbent with axial traces orientated N-S or NW-SE.

F3 - D3 folds that gently refold F2. E-W to NE-SW orientated axial traces.

D3Sz - D3 shear zones that contain remobilised melt.

D4Sz - Later brittle shear zone.

Grt 1 - Garnet elongate along S2.

Grt 2 - Undeformed garnet, generally porphyroblasts.

Crd 1 - Cordierite elongate along S2.

Crd 2 - Undeformed cordierite porphyroblasts.

Crd 3 - Elongate cordierite grains parallel to the axial trace of F3 folds.

	S0	S2	F2	F3	D3Sz	D4Sz	Grt 1	Crd 1	Crd 3
Southern Localities (N-S)									
Locality 3	*	*	*	*			*	*	
Locality 2	*	*	*	*			*	*	*
Locality 4		*		*	*				
Locality 1		*		*	*		*	*	
Middle Localities (N-S)									
Locality 7		*		*					
Locality 6		*		*					
Northern Localities (E-W)									
Locality 12	*	*		*					
Locality 5		*		*					
Locality 15	*	*		*					
Locality 20	*	*	*	*		*			
Locality 19	*	*	*	*	*			*	

Table 2.2 - Table of structural features observed at key localities.

In the following section examples of these structural features are presented with reference to key localities, not all localities are described as they have been picked as key localities because of leucosome or mesosome features. These outcrops will therefore be discussed in later sections. The locations of all the key localities are shown in Figure 2.1 but they are arranged in the text in geographical order from south to north. The northern localities are then described from east to west

Locality 3 - Hauninen Reservoir

Compositionally banded mesosome is folded into F2 isoclinal folds, with axial planar S2 orientated E-W. F3 has refolded S2, and the F3 axial traces strike NE-SW. These refolded folds are very distinctive at this locality and an example can be seen in Figure 2.2.

Locality 2 - Rusko Gravel Pits

The gravel pits cover an area approximately 1 km^2 (Figure 2.3) and four outcrops (labelled 2.1 through 2.4) were studied from this locality. The outcrops are smooth, glaciated hummocks that are surrounded by loose glacial gravel.

Locality 2.1

S0 is present as compositional layering. The dominant fabric at locality 2 is S2 which is mostly parallel to S0 and is axial planar to isoclinal F2 folds. F2 axial traces are aligned NW-SE. D1 garnets and cordierites are parallel to S2. F3 has gently refolded S2 and F2 into gentle folds with axial traces orientated NE-SW. These features are illustrated in Figure 2.4.

Locality 2.2

Repeated pelite and semi-pelite layers are folded into isoclinal F2 folds. F3 gently refolds S2 with axial traces aligned NE-SW (Figure 2.5)

Locality 2.3

S2 has been folded into a large open F3 fold with an axial trace trending NE-SW. Primary garnet and cordierite are elongate along S2 within pelite bands. Interesting features at this outcrop are the later elongate cordierites aligned parallel to the F3 axial trace, thus defining S3. These cordierite are found within a metre of a large pink leucosome that is has been deformed by F3 (Figure 2.6).

Locality 2.4

S2 is orientated NW-SE but has gently been refolded by NE-SW orientated F3 axial traces. Within the pelite layers and within a metre of a large pink leucosome are cordierites parallel to F3 axial traces (Figure 2.7), as seen at locality 2.3.

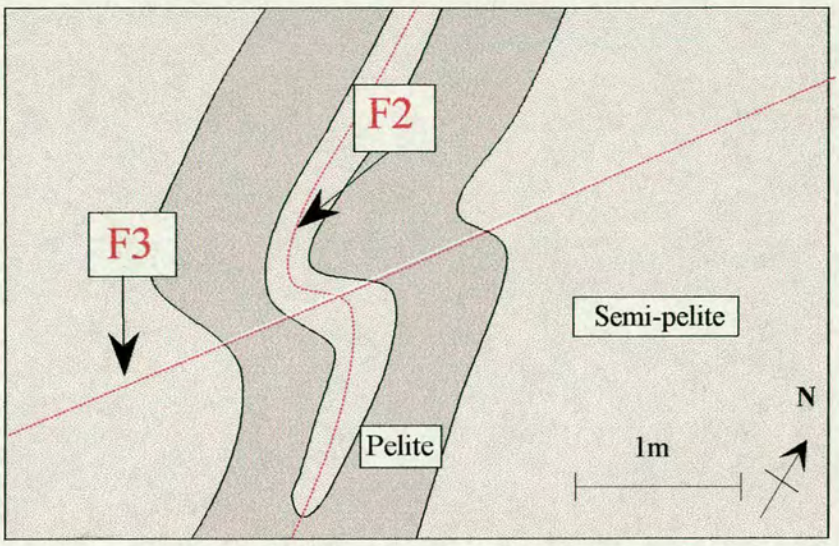

Figure 2.2 - Sketch of refolded F2 folds at locality 3, Hauninen reservoir.

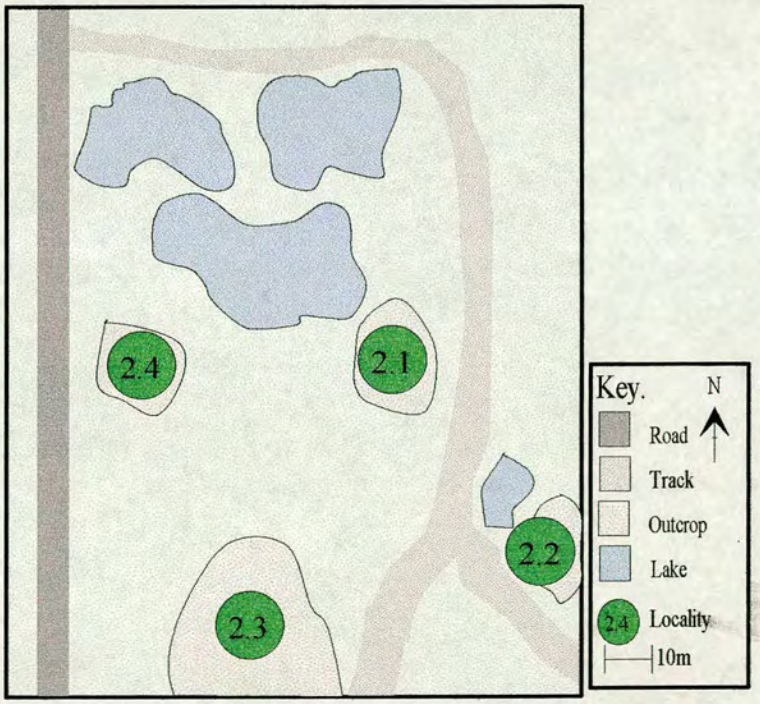

Figure 2.3 - Map of outcrop locations at locality 2, Rusko Gravel Pits.

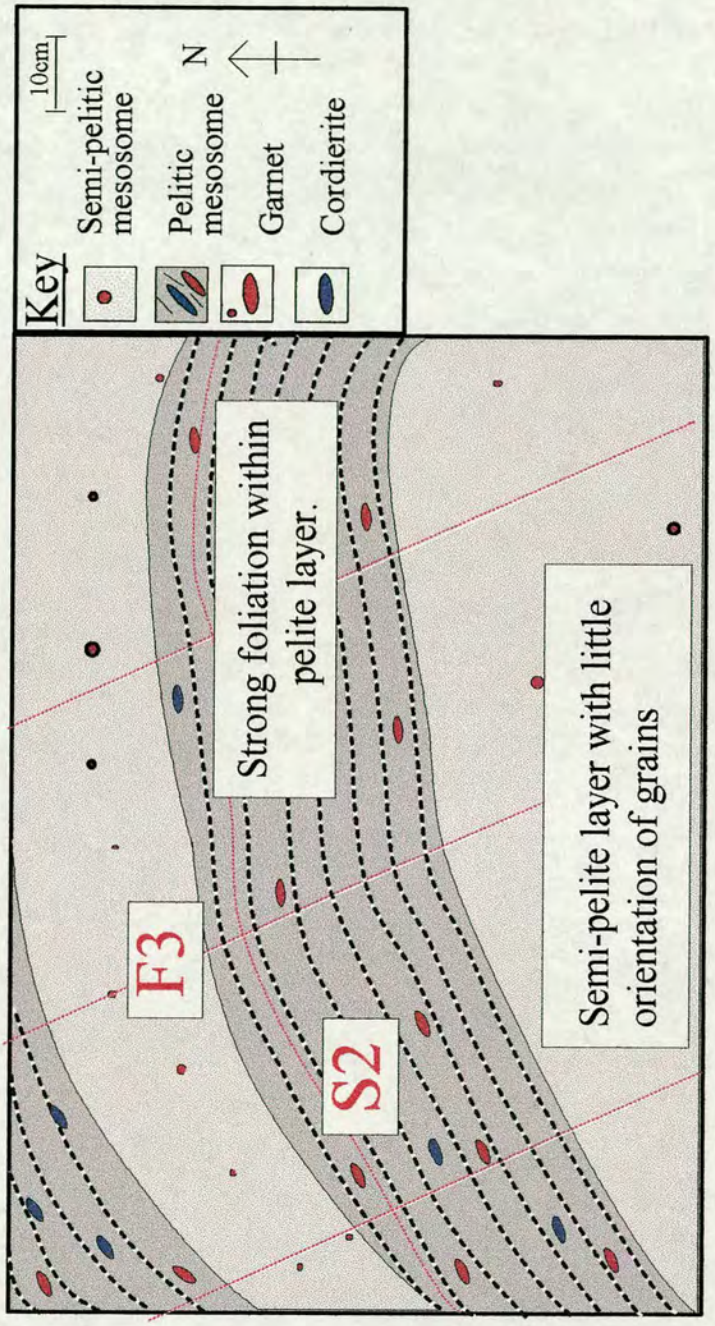

Figure 2.4 - Structural features within mesosome at locality 2.1 and how these are affected by compositional layering. Pelite layers preserve stronger foliation than the semi-pelite layers.

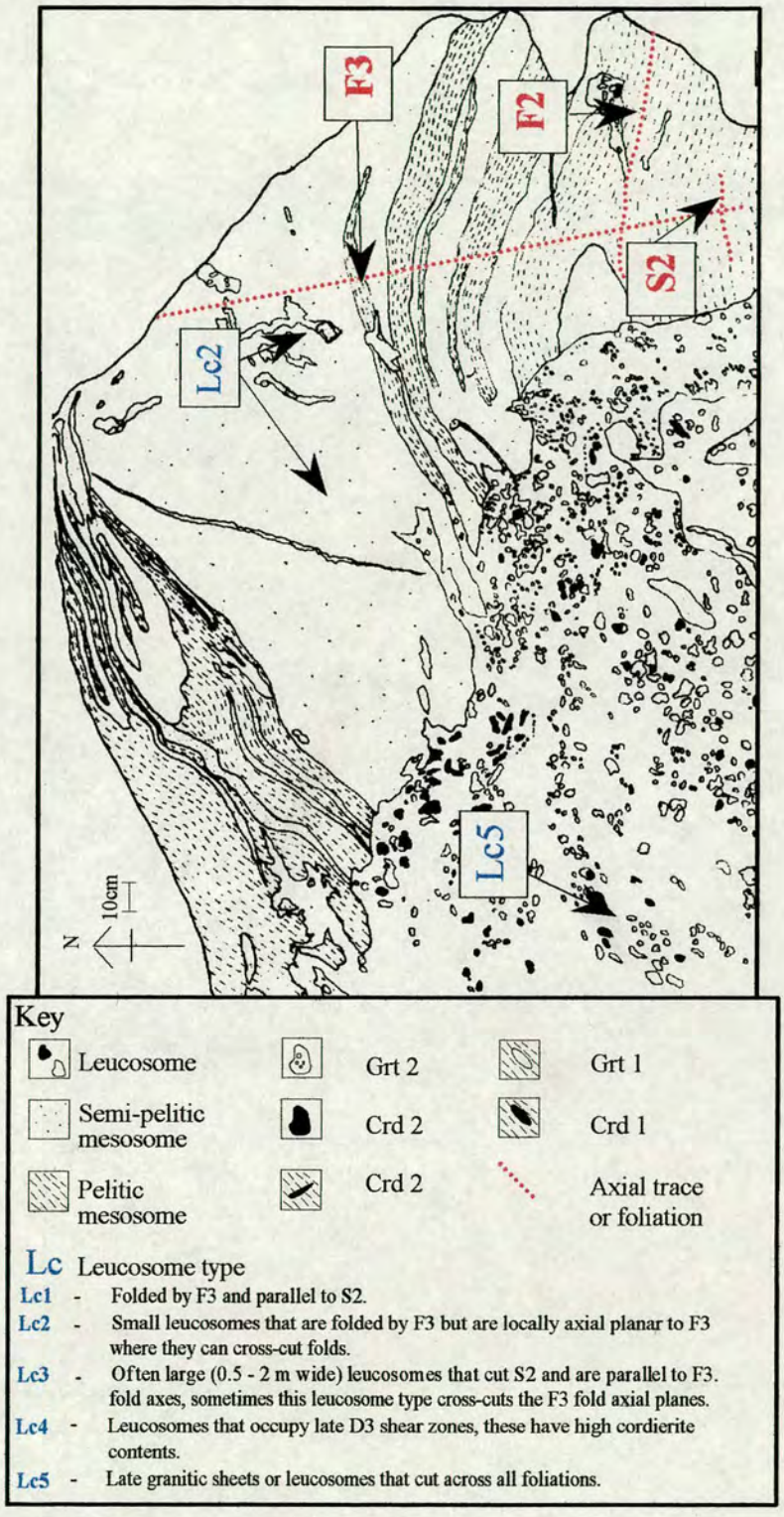

Figure 2.5 - Outcrop map of locality 2.2 encompassing the structural features and leucosome

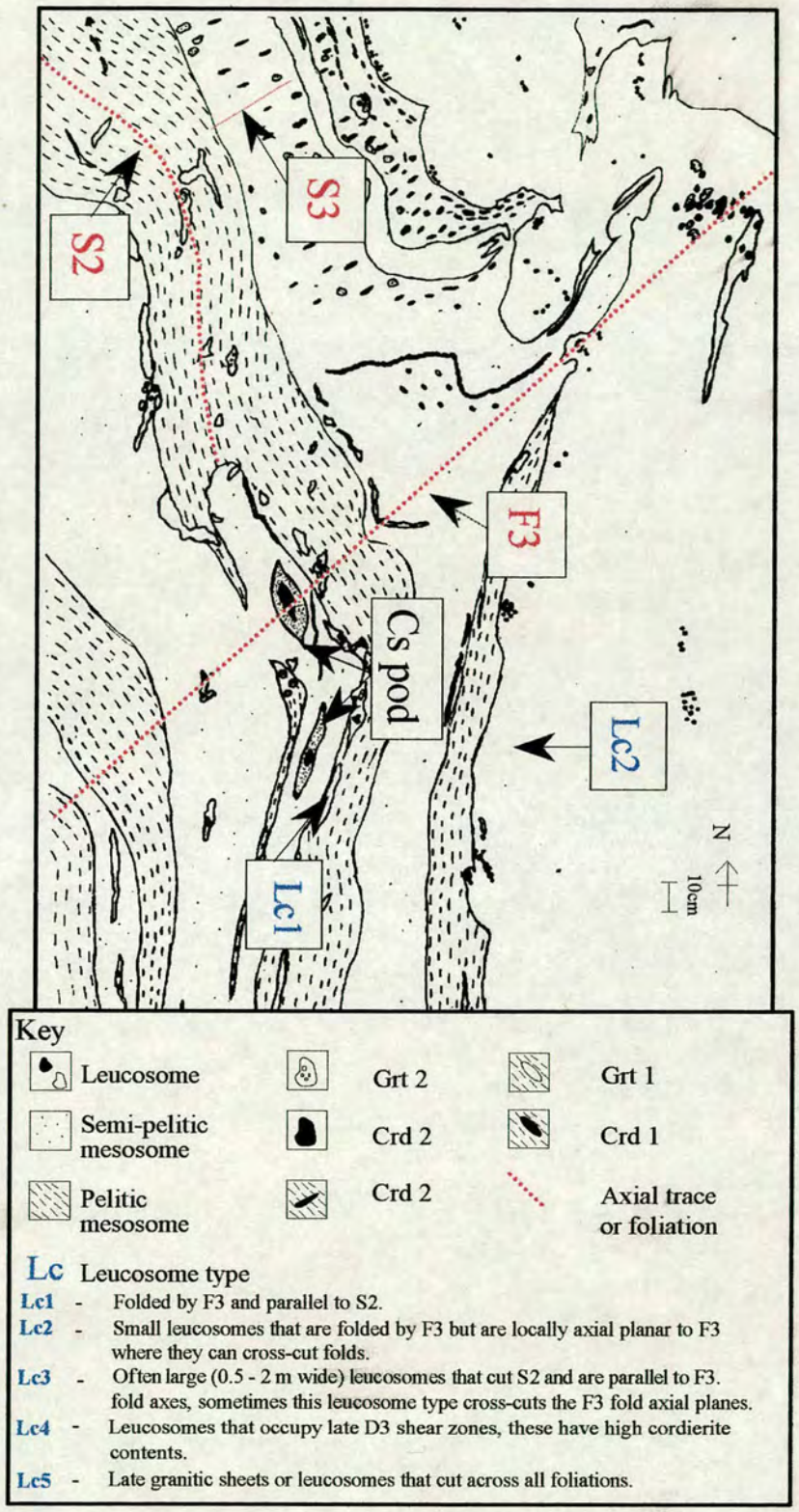

Figure 2.6 - Outcrop map of locality 2.3 with relevant structural and leucosome features. Cs pod - compositionally layered boudin.

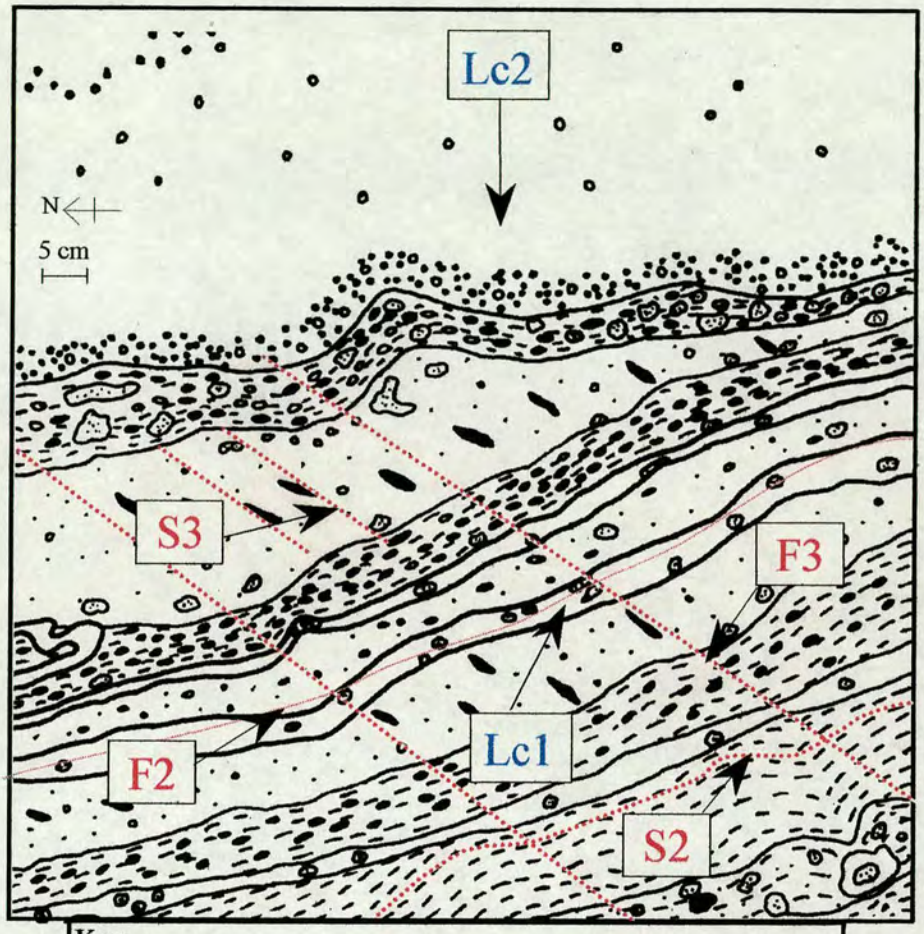

Key

Leucosome	Grt 2	Grt 1
Semi-pelitic mesosome	Crd 2	Crd 1
Pelitic mesosome	Crd 2	Axial trace or foliation

Lc Leucosome type

- Lc1 - Folded by F3 and parallel to S2.
- Lc2 - Small leucosomes that are folded by F3 but are locally axial planar to F3 where they can cross-cut folds.
- Lc3 - Often large (0.5 - 2 m wide) leucosomes that cut S2 and are parallel to F3. fold axes, sometimes this leucosome type cross-cuts the F3 fold axial planes.
- Lc4 - Leucosomes that occupy late D3 shear zones, these have high cordierite contents.
- Lc5 - Late granitic sheets or leucosomes that cut across all foliations.

Figure 2.7 - Outcrop map of locality 2.4 with relevant structural and leucosome features.

Locality 4 - Road cutting on M8

This locality is a large road cutting approximately 100 m long and 20 m high. There is a large percentage of leucosome (granitic material) present, >70%. At the SE end of the outcrop S2 is gently folded by F3 folds (Figure 2.8). F3 fold traces dip gently to the SW, but further NW along the outcrop F3 steepens and tightens until it becomes vertical. The fabric is very strong and most of the leucosome material is aligned with the F3 fabric (Figure 2.9). This deformation is consistent with localised shearing affecting the F3 fold limbs (Väisänen, *pers. comm.*). There is no compositional banding at this outcrop and the non-leucosome material that is scarce is termed melanosome due to the high percentage of leucosome material, and the lack of clear contact between leucosome and schistose portions. Occasional Grt 1 garnets occur aligned along sheared S2.

Locality 1 - Riviera

The dominant fabric at this outcrop is S2 but this has been refolded into close/tight F3 folds. S2 is evident in the aligned biotite and Grt 1 garnets seen within the mesosomes. The F3 close/tight folding within the comparatively competent mesosome has lead to ptygmatic folding within the less competent leucosomes. Late-D3 shear zones containing remobilised leucosome are present in two conjugate sets oriented N-S and E-W. One such shear zone is illustrated in Figure 2.10.

Locality 6 - Mynamaki quarry

This outcrop is a large abandoned quarry and is where Höltta *(pers. comm)* has recorded peak PT conditions of 800°C and 6 kbar. The north of the quarry is typified by gentle F3 folds that refold NNE dipping S2. Väisänen (*pers. comm.*) has shown that in places previously vertical folds have been overfolded into gentle box folds (Figure 2.11). F3 folding causes S2 to steepen until it reaches an area of high

2.8

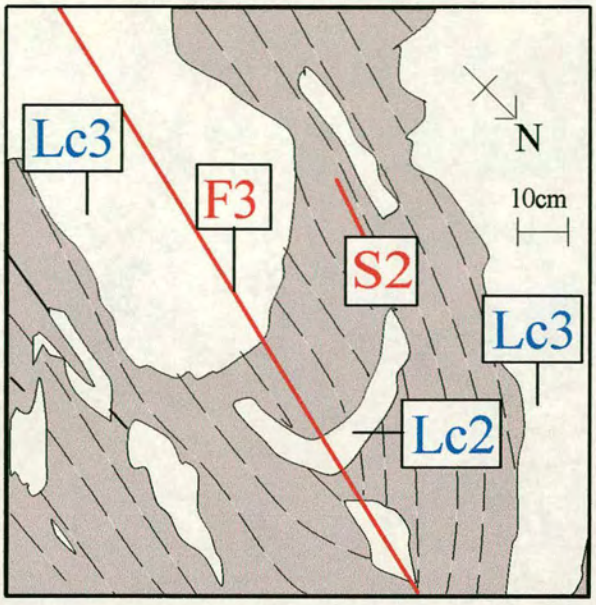

2.9

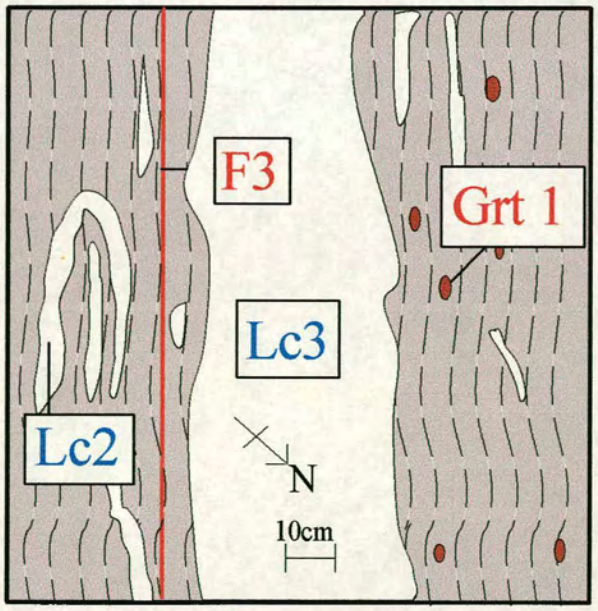

Figure 2.8 - Gentle F3 folds at the SE end of locality 4.

Figure 2.9 - Vertical F3 folds due to strong D3 shearing locality 4.

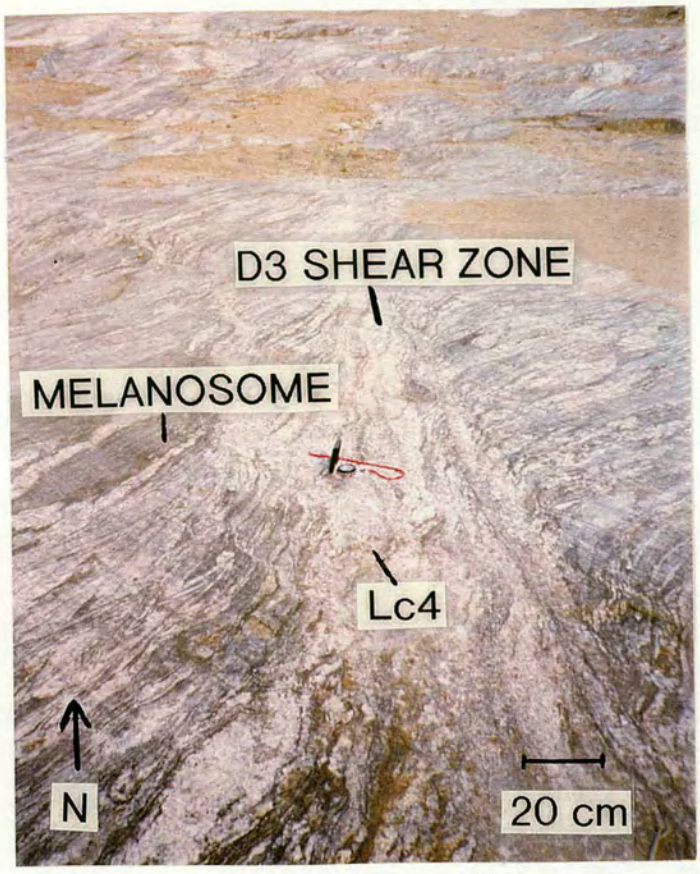

Figure 2.10 - D3 shear zone cutting through F3 folded S2. The shear zone contains cordierite rich leucosome material and some entrained mesosome material. The leucosome is representative of mobile melt during shearing.

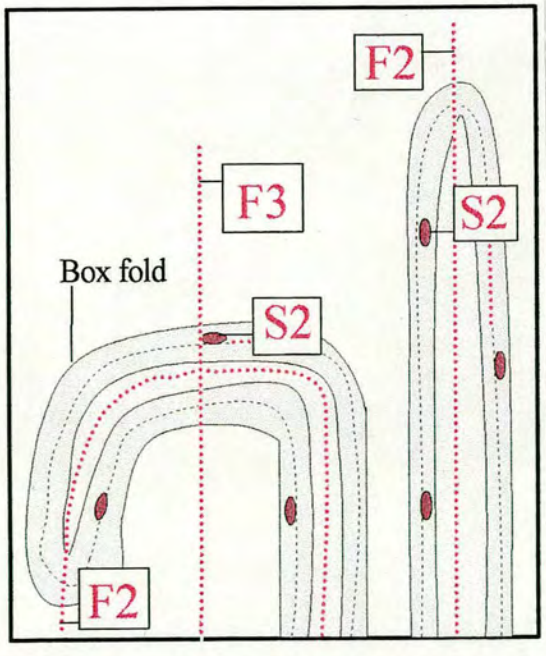

Figure 2.11 - Representative sketch of refolded box folds at locality 6.

leucosome content, where it is difficult to see a strong foliation direction. S2 in the rest of the quarry dips gently to the SSW (Figure 2.12).

Locality 20 - Goose Valley Road transect

The localities along the transect show compositional banding and, as at other localities, S2 is parallel to S0 and axial planar to F2. D2 garnets and cordierite are aligned along S2 as is sillimanite. F2 is refolded by F3 but the intensity of the folding varies. The distinctive feature along this transect is the outcrop of the large D4 shear zone that runs NE-SW through the area (Väisänen, *pers. comm.*). It is up to 100 m wide and contains a pseudotachylite (Figure 2.13). The leucosomes within the shear zone have been deformed in the brittle field and not remobilised as at locality 1.

Locality 19 - Vellua road cutting

At this locality S2 is delineated by elongate cordierite (Crd1) within the compositionally banded mesosome. The locality is at the west end of the Häähä road transect, west of the garnet-in isograd (Väisänen et al., 1994) and the mesosome has a bt + crd + sill + Kfs assemblage. S2 is gently folded by F3 fold axes oriented NE-SW. A shear zone aligned NE-SW also cuts across the mapping area with its orientation parallel to the F3 fold axes (Figure 2.14).

.2.4.2 - Mesosome characteristics

The mesosome provides information on PT conditions through its mineral assemblage and the textures of the phases present. The key mesosome features and their abbreviations are outlined below with descriptions from key localities

S0 - Compositional layering within the mesosome, psammitic and pelitic layers.

Mes - Mesosome material as defined previously (section 2.3.3).

Mel - Melanosome material as defined previously (section 2.3.3).

Grt1 - 1st generation of garnet, elongate along D2.

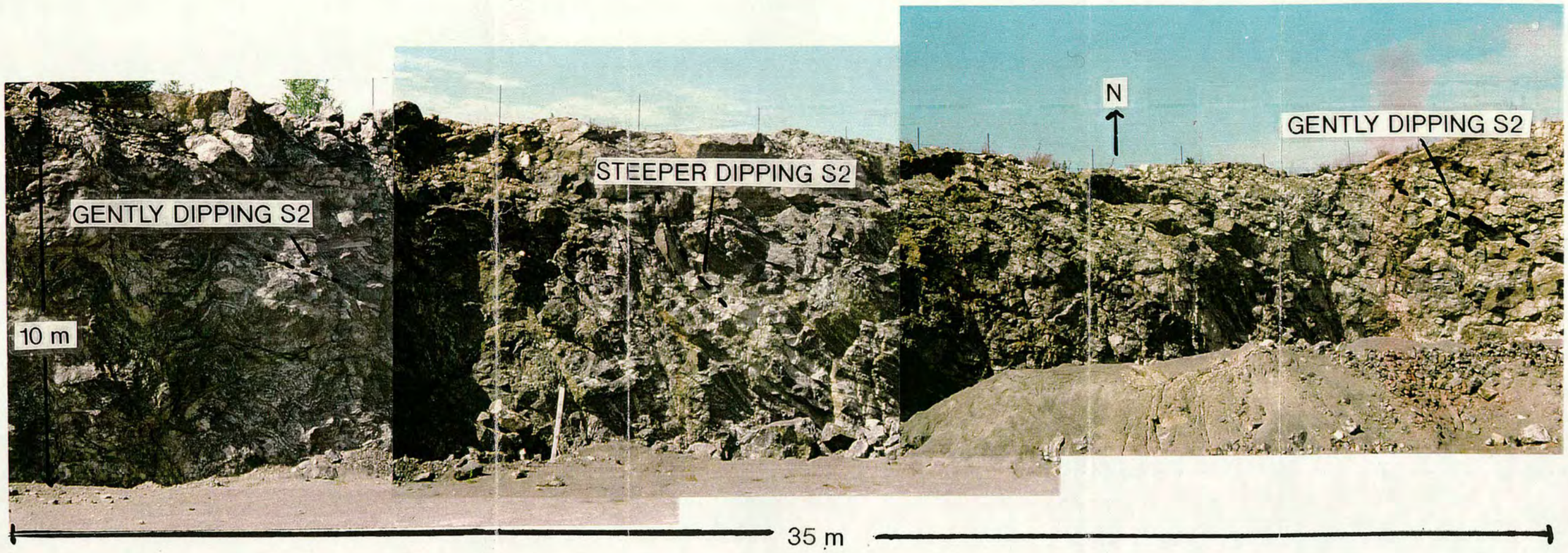

Figure 2.12 - Locality 6, Mynamaki quarry. S2 is dipping gently in the right of the photograph due to gentle F3 folding. This steepens to the centre of the of the outcrop before becoming shallower again as you move towards the back wall of the quarry.

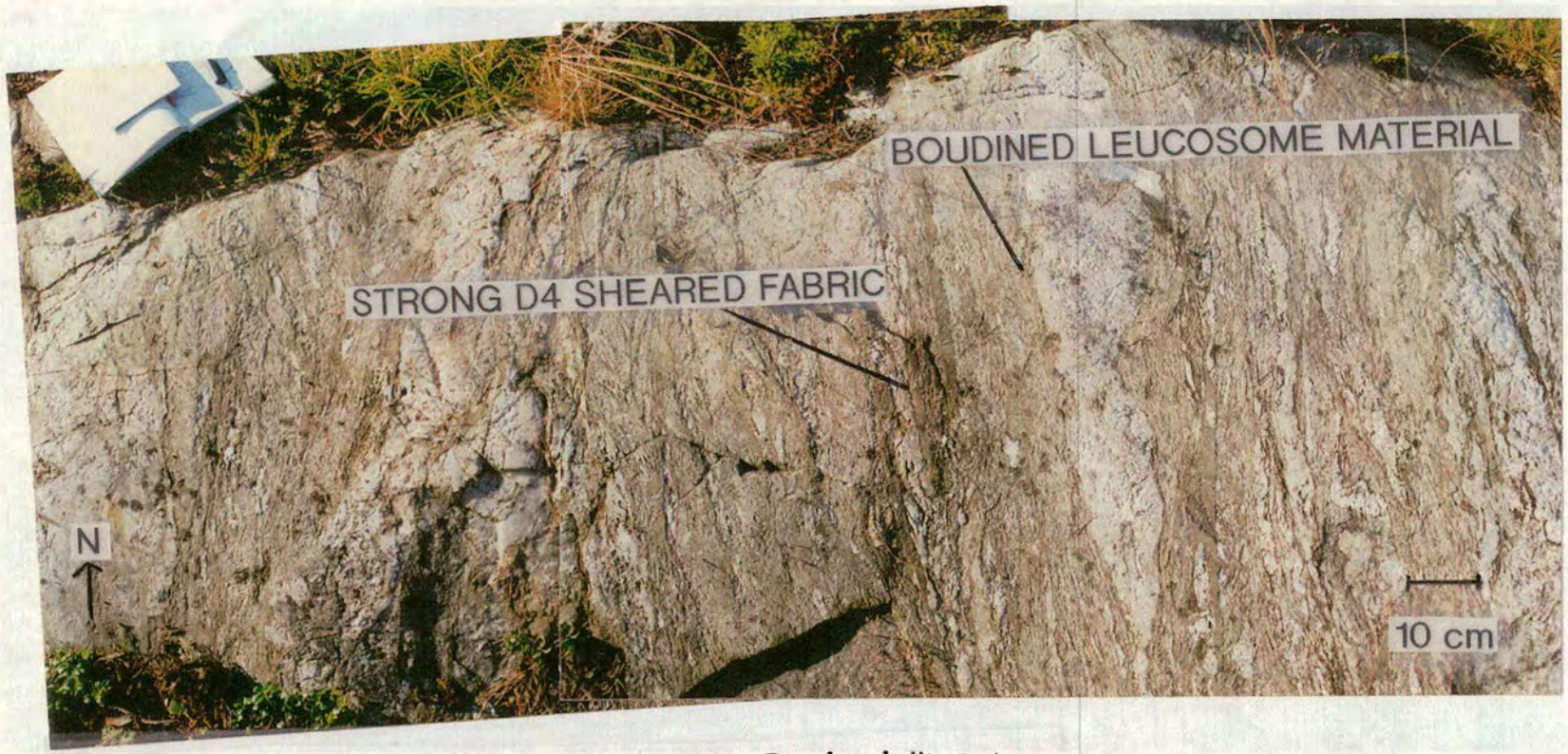

Figure 2.13 - Locality 20, Goose Valley Road transect. Pseudotachylite texture within a D4 shear zone. The width of the shear zone is approximately 100 m wide (Väisänen et al, 1994).

Key

Leucosome
Semi-pelitic mesosome
Pelitic mesosome
Grt 2
Crd 2
Crd 2
Grt 1
Crd 1
Axial trace or foliation

Lc Leucosome type

- **Lc1** - Folded by F3 and parallel to S2.
- **Lc2** - Small leucosomes that are folded by F3 but are locally axial planar to F3 where they can cross-cut folds.
- **Lc3** - Often large (0.5 - 2 m wide) leucosomes that cut S2 and are parallel to F3. fold axes, sometimes this leucosome type cross-cuts the F3 fold axial planes.
- **Lc4** - Leucosomes that occupy late D3 shear zones, these have high cordierite contents.
- **Lc5** - Late granitic sheets or leucosomes that cut across all foliations.

Figure 2.14 - Locality 19, Vellua road cutting. S2 is deformed by F3 folds and shear zones that are aligned NE/SW.

Crd1 - 1st generation of cordierite, elongate along D2.

Grt2 - 2nd generation of garnet, equigranular and poikiloblastic.

Crd2 - 2nd generation of cordierite, equigranular and poikiloblastic and mostly constrained to leucosomes.

Crd3 - 3rd generation of cordierite, parallel to F3 fold traces.

P - Compositionally different layers that have been boudined along D2.

Locality	S0	Mes	Mel	Grt 1	Grt 2	Crd 1	Crd 2	Crd 3	Sill	P
Southern Localities (N-S)										
3	*	*		*	*	*	*			
2	*	*		*	*	*	*	*		*
4		*	*	*	*		*			
1	*	*	*	*	*	*	*			
Middle Localities (N-S)										
7		*	*	*	*	*	*			*
6		*	*	*	*		*			
Northern Localities (E-W)										
12	*	*		*	*		*			
5		*								
15	*	*		*	*	*	*		*	
20	*	*		*	*	*	*		*	
19	*	*				*			*	

Table 2.3 - Table of mesosome features observed at key localities.

Locality 3 - Hauninen Reservoir

The mesosome characteristics at this locality are very like those at locality 2. The mesosome is compositionally banded, D2 garnet and cordierite occur along S2 and later garnet poikiloblasts cut the fabric. The unusual feature at this locality are mesosome patches that are rich in tourmaline. Within these are long thin D2 garnets that have been folded by F3. Figure 2.15 is a trace of an F3 fold refolding S2 and distinct compositional layers.

Locality 2 - Rusko Gravel Pits

Figure 2.16 illustrates most of the mesosome features observed at locality 2.1. At the left of the photograph is a layer of semi-pelitic mesosome; most of the mesosome in

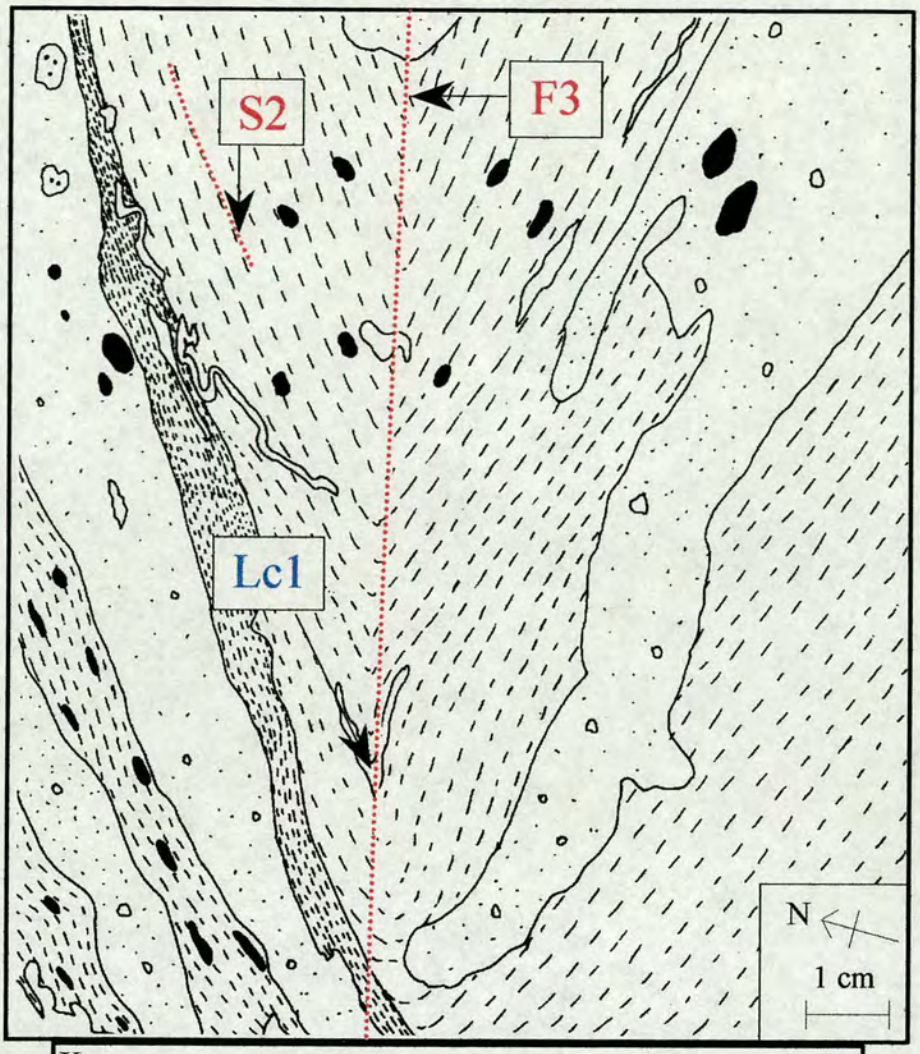

Key

Leucosome
Semi-pelitic mesosome
Pelitic mesosome
Grt 2
Crd 2
Crd 2
Grt 1
Crd 1
Axial trace or foliation

Lc Leucosome type

Lc1 - Folded by F3 and parallel to S2.

Lc2 - Small leucosomes that are folded by F3 but are locally axial planar to F3 where they can cross-cut folds.

Lc3 - Often large (0.5 - 2 m wide) leucosomes that cut S2 and are parallel to F3. fold axes, sometimes this leucosome type cross-cuts the F3 fold axial planes.

Lc4 - Leucosomes that occupy late D3 shear zones, these have high cordierite contents.

Lc5 - Late granitic sheets or leucosomes that cut across all foliations.

Figure 2.15- F3 fold at locality 3, Hauninen Reservoir.

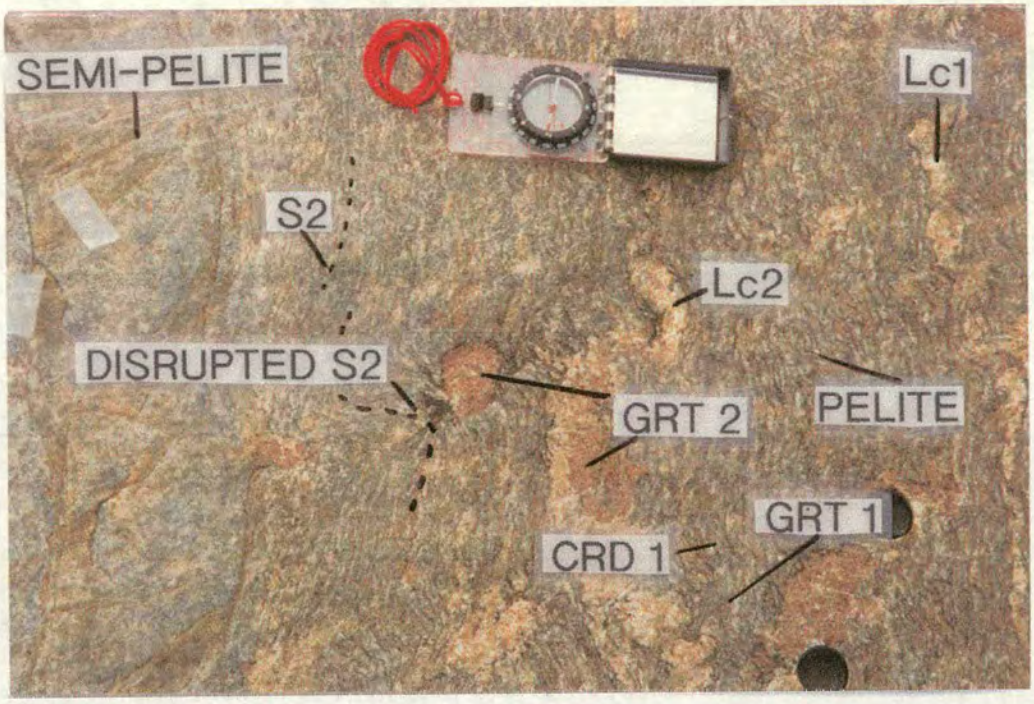

Figure 2.16 - Mesosome features at locality 2.

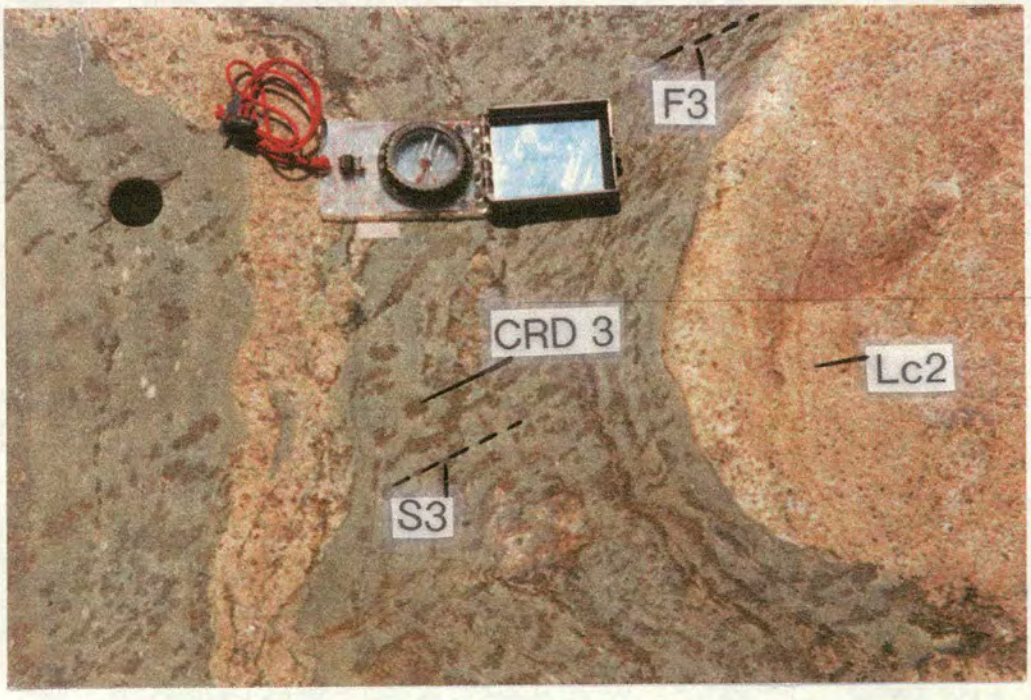

Figure 2.17 - Elongate cordierites aligned along F3 axial traces defining S3, locality 2.3, Rusko Gravel pits. Lc2 leucosomes have been boudined by F3.

the photo is pelitic. Within the mesosome the elongate, elliptical cordierites and garnets can be seen orientated along S2. However, running NE-SW is a second fabric that gently folds S2: this is F3. Another generation of garnet is present as large poikiloblastic crystals, often present in small patches of leucosome not much larger than the garnet itself. The garnet appears to grow across the main foliation locally disrupting it, and so may have formed later than the elongate garnets. The garnets contains many quartz inclusions that are coarser than the surrounding mesosome, none of these inclusions indicate any preferred orientation in hand specimen.

A later generation of cordierite is seen within the Gravel Pits, at locality 2.3, aligned axial planar to a large F3 fold (Figure 2.17). Another feature at locality 2 is the presence of compositionally zoned boudins, deformed by D2. One of these pods can be seen in Figure 2.18: this particular pod has a pink core, a green layer, white layer and grey shell. These compositionally different pods are seen at other localities but not as clearly as here.

Locality 4 - Road cutting on M8

This road cutting has a high percentage of leucosome material that ranges in size from small intimate leucocratic segregations on a centimetre scale, to metre wide granitic sheets. There is upwards of 70 % leucosome material and the melanosome here is coarse with large (3-4 mm) biotite flakes, cordierite and garnet. There is no clear boundary between mafic and leucocratic material (Figure 2.19).

Locality 1 - Riviera

Due to the generally high percentage of leucosome at this outcrop the schistose portion can be described as melanosome. Figure 2.20 illustrates the intimate nature of melanosome and leucosome. There are also patches of mesosome material in areas where leucosomes do not dominate and this is compositionally banded. Early generations of garnet and cordierite are aligned along S2, within melanosome and mesosome. Garnet also grows as later equigranular poikiloblasts, with rounded

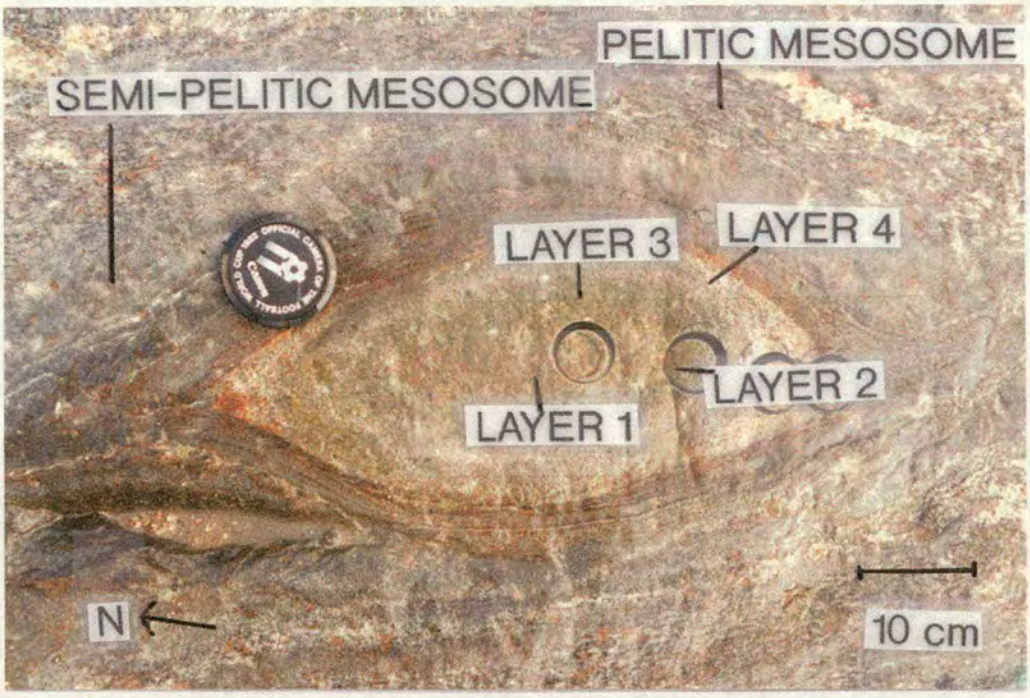

Figure 2.18 - Compositionally banded pod at locality 2.1 surrounded by mesosome of pelitic and semi-pelitic composition.

Figure 2.19 - Intimately associated leucosome and melanosome material, locality 4.

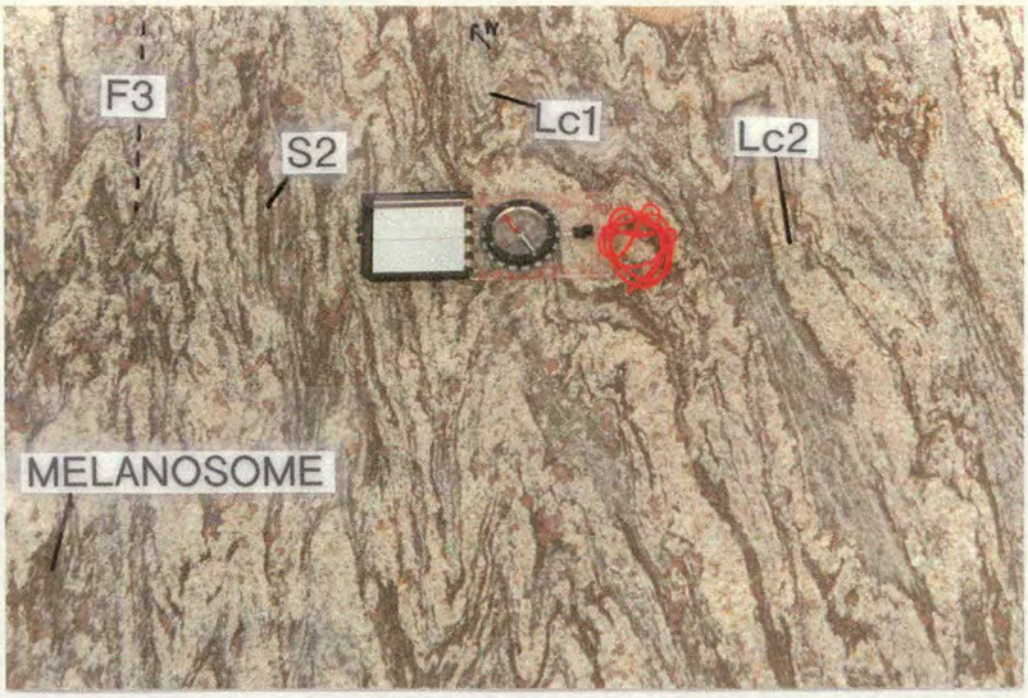

Figure 2.20 - Melanosomes and Lc1/Lc2 leucosomes gently folded by F3 at locality 1, Riviera.

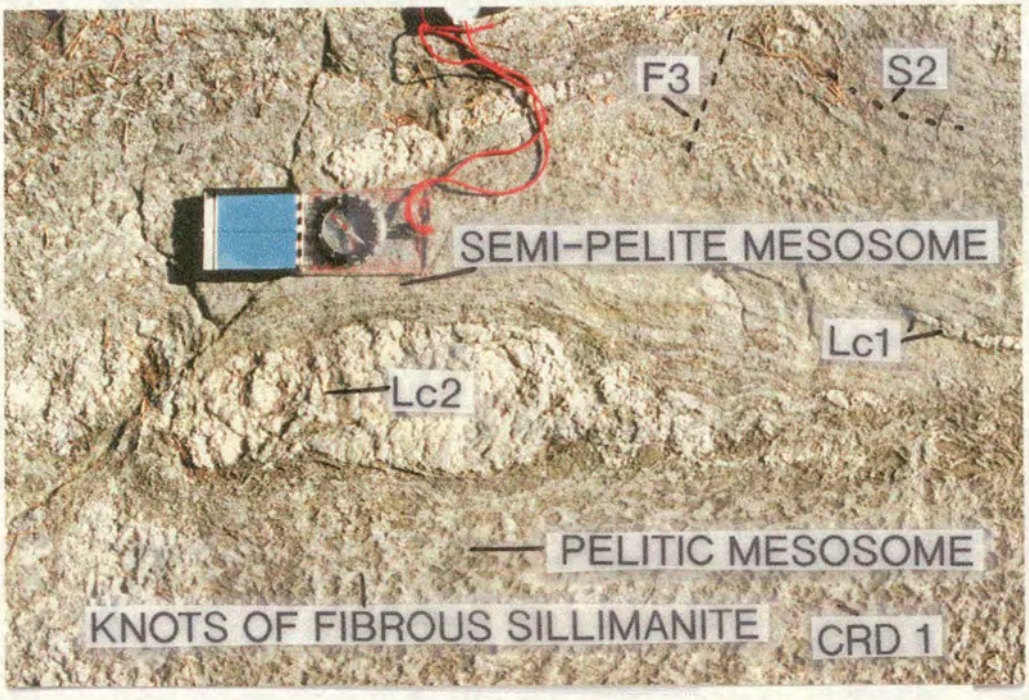

Figure 2.21 - Cordierite + sillimanite + biotite pelitic mesosome, locality 19. Lc1 and Lc2 leucosomes can be seen in the bottom half of the photo.

quartz inclusions that range in size from 1-3 cm in diameter. These garnets appear to overprint the S2 fabric.

Hääh ä road transect - localities 12 to 19

Locality 12 is located at the west end of this road where garnet + cordierite is a stable assemblage. The fabric at this locality is dominantly S2, defined by biotite + cordierite. The fabric has been gently crenulated by F3 with an S3 fabric oriented NE-SW. Compositional layering can be seen and there is a low percentage of leucosome material.

At locality 15, the centre of the Hääh ä road, the mesosome is compositionally banded and similar in appearance to that at locality 12. The difference at this outcrop is that sillimanite can now be seen within the mesosome assemblage.

At the west end of the road is locality 19, which is on the lower grade side of the garnet in isograd. Cordierite and sillimanite are stable without garnet. The pelitic mesosome is dominated by elongate pits, which are weathered cordierites, surrounded by raised knots of sillimanite. This is alternately banded with layers of a semi-pelite composition (Figure 2.21).

2.4.3 - Leucosome characteristics

Due to the high leucosome percentage at some outcrops and the varied characteristics of the leucosomes present, a categorisation scheme was made in the field and is outlined below. Five leucosome types were identified and examples are outlined in Table 2.4 and described below.

Lc1 - Folded by F3 and parallel to S2.

Lc2 - Small leucosomes that are folded by F3 but are locally axial planar to F3 where they can crosscut folds.

Lc3 - Often large (0.5 - 2 m wide) leucosomes that cut S2 and are parallel to F3 fold axes, sometimes this leucosome type cross-cuts the F3 fold axial planes.

Lc4 - Leucosomes that occupy late D3 shear zones, these have high cordierite contents.

Lc5 - Late granitic sheets or leucosomes that cut across all foliations.

Locality	Lc1	Lc2	Lc3	Lc4	Lc5
Southern Localities (N-S)					
3	*		*		
2	*	*			*
4	*		*		
1	*	*	*	*	
Middle Localities (N-S)					
7	*	*	*		
6	*	*	*		*
Northern Localities (E-W)					
12	*	*	*		
5	*		*		
15	*	*	*		
20	*				
19	*	*	*		

Table 2.4 - Table of leucosome types observed at key localities.

Locality 3 - Hauninen reservoir

Lc1 leucosomes at this locality are 2-3 mm thin, elongate and concordant to S2 and are folded by F3 into ptygmatic folds (Figure 2.22). Lc2 type leucosomes often truncate F3 folds and some are found in F3 fold hinges. At the reservoir edge is a white pegmatitic leucosome that cuts across S2 and F3 folds and thus can be categorised as a Lc5 leucosome. It covers approximately 3-4 m^2 of the outcrop.

Locality 2.1 - Rusko Gravel Pits

Lc1 leucosomes at this locality range in size from 1-2 cm long leucocratic foliae, aligned along S2, to 1-3 cm by 30 cm elongate leucosomes. These are sometimes coalesced into larger leucosomes. There is some interconnectivity between these two leucosome types (Figure 2.23).

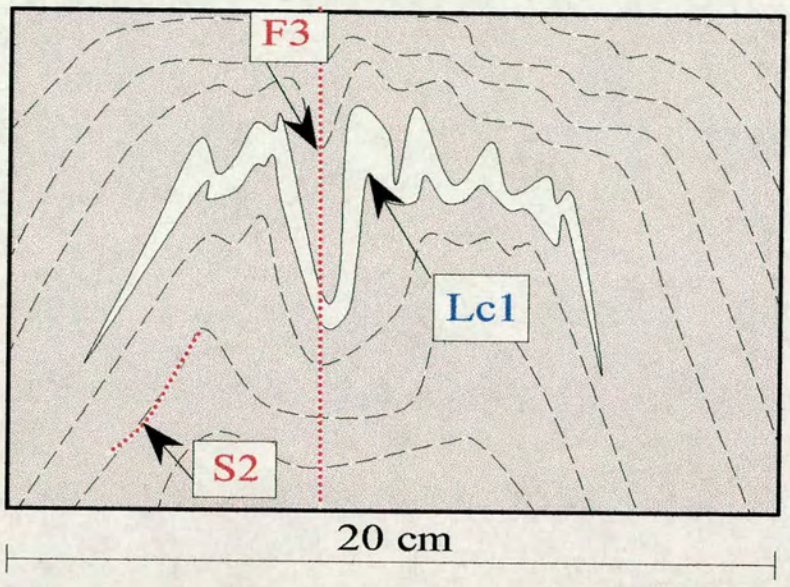

Figure 2.22 - Lc1 leucosome folded by F3, at locality 3.

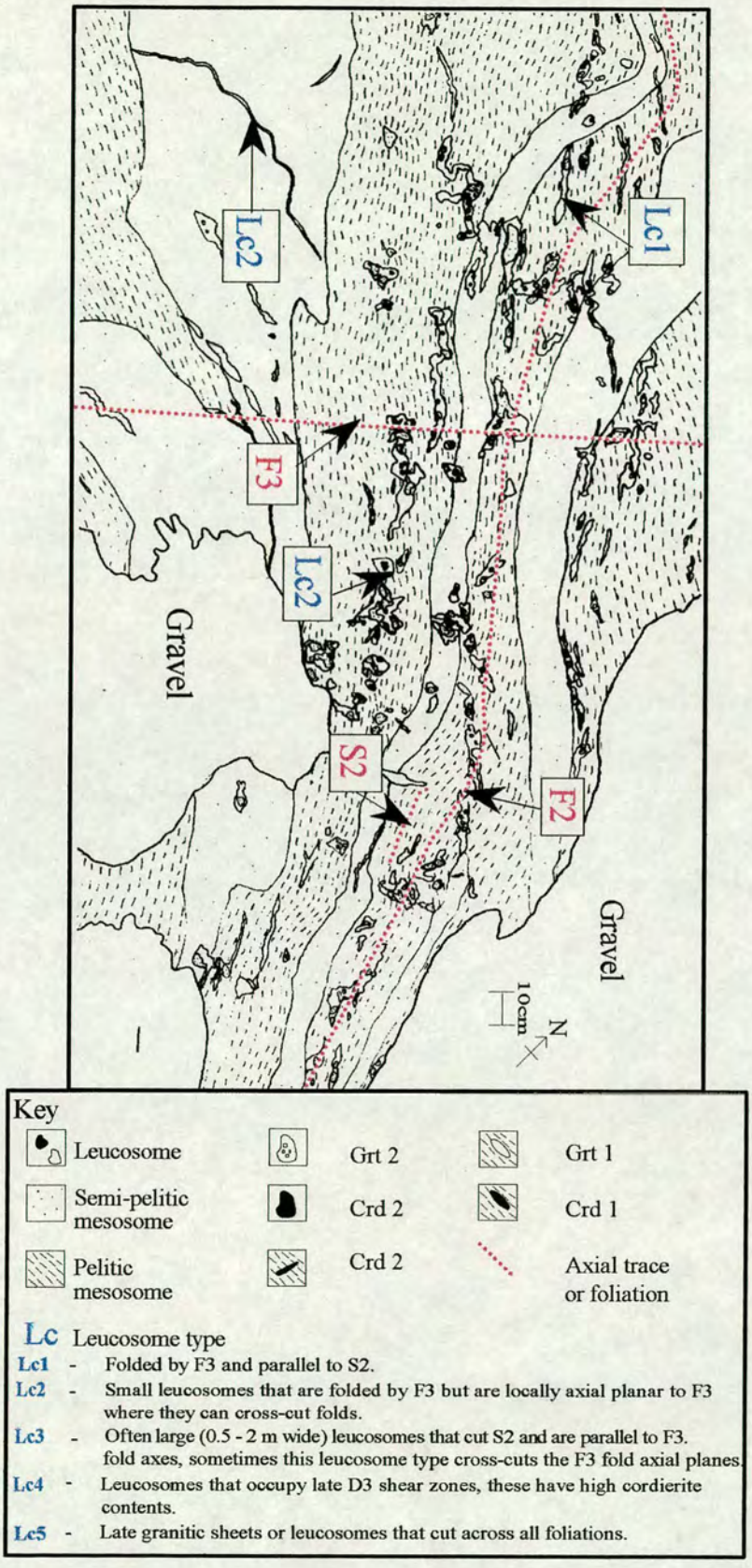

Figure 2.23 - Outcrop map locality 2.1, Rusko Gravel pits. Compositional layering is folded into isoclinal F2 folds and then gently refolded by F3.

Lc2 leucosomes are generally 3 cm by 1 m, elongate leucosomes which are orientated roughly parallel to S2. They can be ptygmatically folded with axial traces parallel to F3 or oblique to S2 and F3. Some are patchy leucosomes that grow across the foliation associated with the poikiloblastic garnets (Figure 2.24).

Figure 2.24 shows an area just to the north of Figure 2.23 where wider Lc2 leucosomes are encountered. The leucosomes are broadly concordant to S2 but, as will be seen from other outcrops at locality 2, they are deformed by F3. Garnet is the dominant mafic phase in these pale pink leucosomes and is found either as small (<1 cm) euhedral crystals or as large (>2 cm) poikiloblastic crystals. The smaller garnets are often found clustered together.

Locality 2.2 - Rusko Gravel Pits

Lc2 are often thin elongate leucosomes, slightly oblique to S2 within pelite layers or roughly parallel to F3 axial traces within semi-pelite layers. They can be patchy in association with poikiloblastic garnets. Larger Lc1 type leucosomes are seen that are orange/pink in colour and have been deformed by F3

A large, pervasive Lc5 leucosome that contains large patches of poikiloblastic garnet and cordierite, cuts across all deformation fabrics present within this outcrop. This contains clusters of garnet and cordierite both at the edges of the leucosome but also about 10 cm into the mesosome (Figure 2.7).

There is another leucosome type at this locality that is difficult to classify: these leucosomes are located at the top of the outcrop (Figure 2.25). They are oblique to S2 and are clearly discordant to compositional layering, but appear to be folded into isoclinal folds.

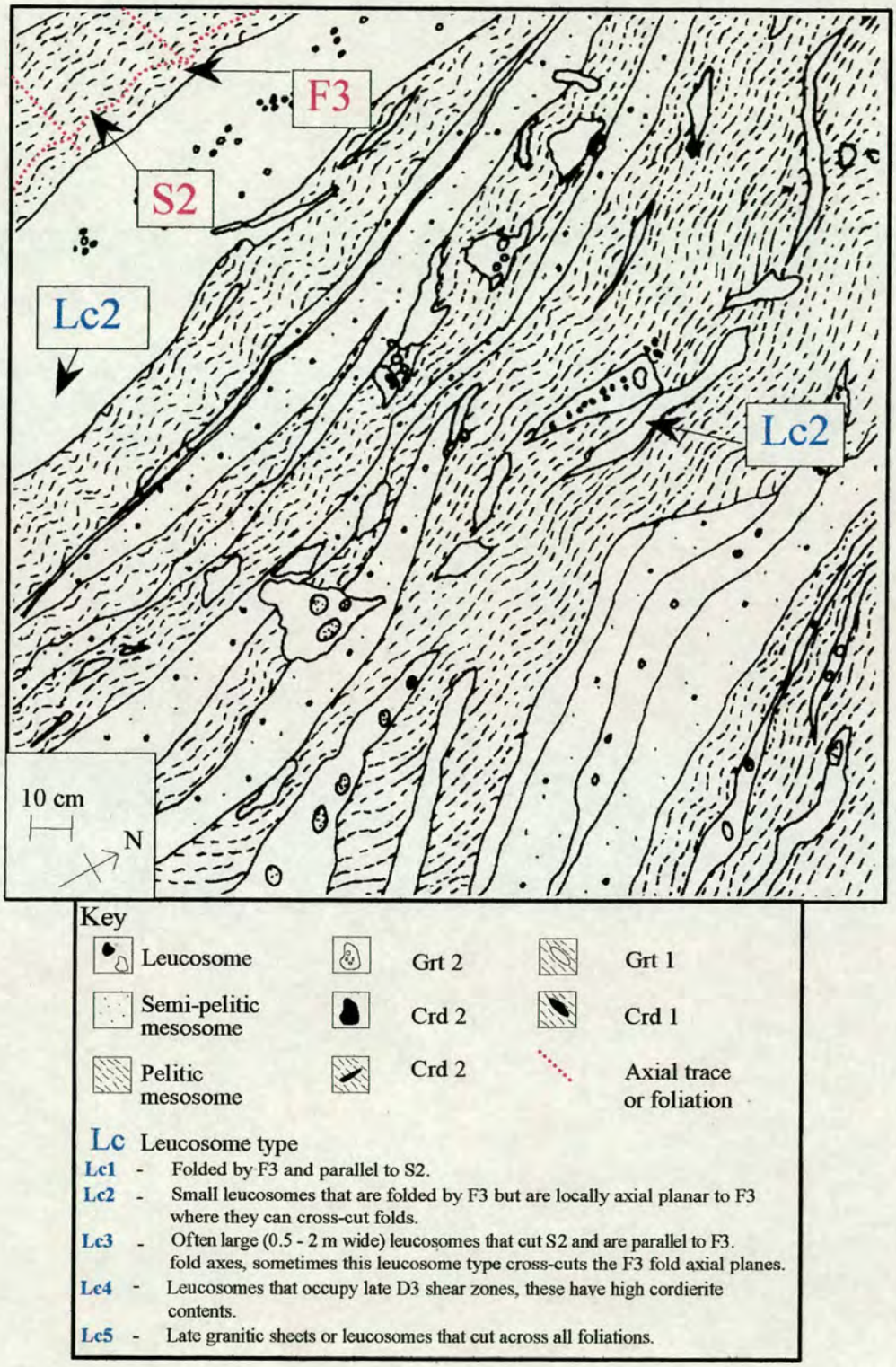

Figure 2.24 - Outcrop map of locality 2.1 (vertical section), Rusko Gravel Pits. Lc2 leucosomes are wider than within Map 2.1 and contain clusters of euhedral garnets.

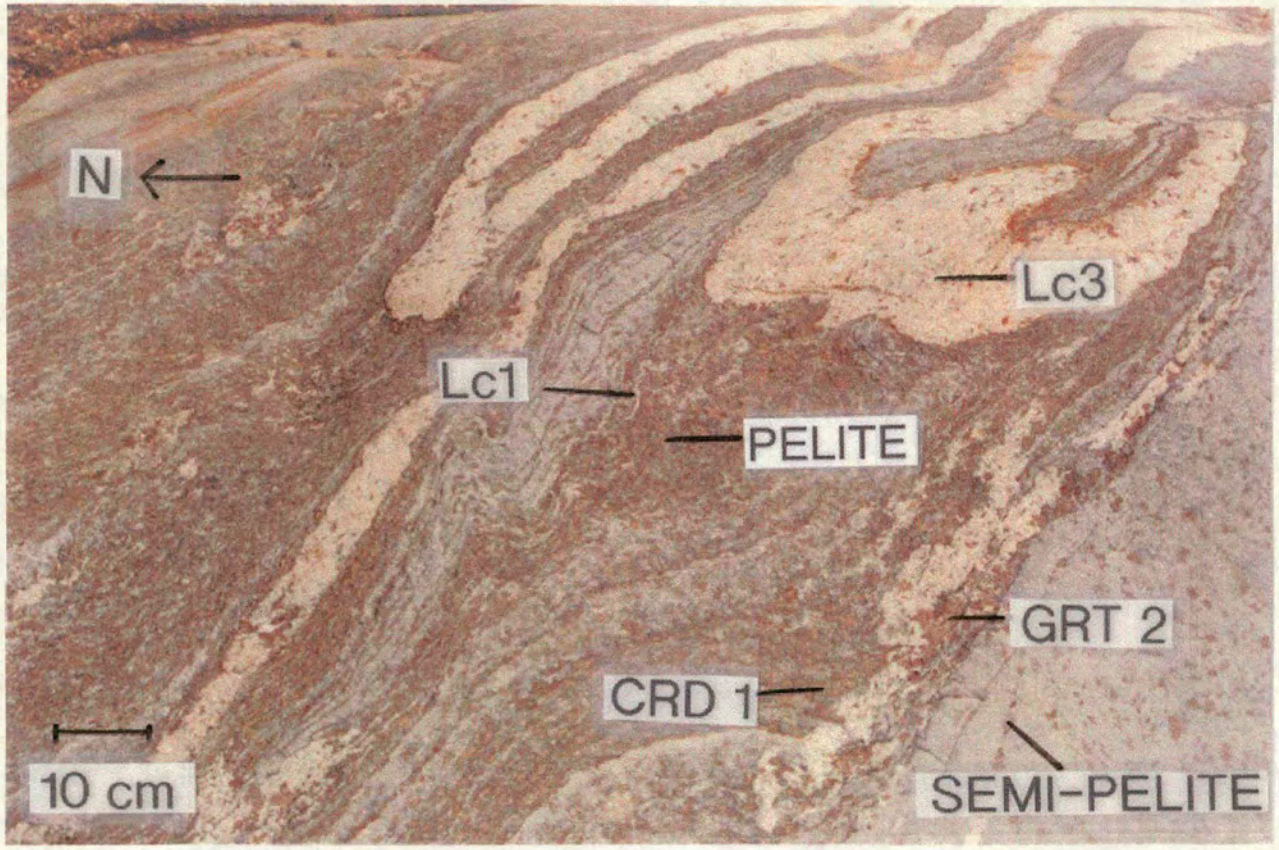

Figure 2.25 - Apparently folded leucosomes at Locality 2.2 (field of view approximately 3 m)

Locality 2.4 - Rusko Gravel Pits

Present within this outcrop are small Lc1 leucosomes that are up to 5 cm wide and 1 m long. These leucosomes, however, are bound by a biotite and cordierite selvage that is approximately 5-15 mm wide (Figure 2.26).

Locality 1 - Riviera

Locality 1 contains four of the main leucosome types categorised above (Table 2.4), all of which can be seen in Figure 2.27. The smallest leucosomes Lc1 and Lc2, 1-3 cm in width and tens of centimetres long, have an intimate relationship with the S2 fabric and generally follow it around F3 fold hinges. Lc2 are not always totally concordant with the early structures, and in detail often show some evidence of crosscutting parts of F3 fold hinges. The largest leucosomes Lc3, 50-200 cm in width and tens of metres long, have a different relationship with local structures. Leucosomes of this size clearly crosscut the folded S2 fabric of the mesosome but are slightly oblique to the axial traces of the F3 folds.

Another leucosome type at this locality is Lc4, which can be found within late, 1830 Ma, D3 shear zones (Väisänen et al., 1994). Shear zone leucosomes contain a much higher proportion of cordierite and garnet than any other leucosome at this locality. There is no brittle deformation of leucosomes at the edges of the shear zone, and the contact is quite diffuse suggesting that the leucosome material was present as melt whilst the shear zone was active (Figure 2.28).

Figure 2.29 illustrates the effect that the later shear zones had on the larger Lc3 leucosomes. Where the shear zone cuts the leucosomes, trails of cordierite occur and are oriented parallel to the shear zone margins. The large leucosomes also contain patches of cordierite with schlieren of mesosome material. The shear zone in Figure 2.28 has sinistral movement whilst that in Figure 2.29 has dextral movement. Thus at this locality the shear zones are present in a conjugate set.

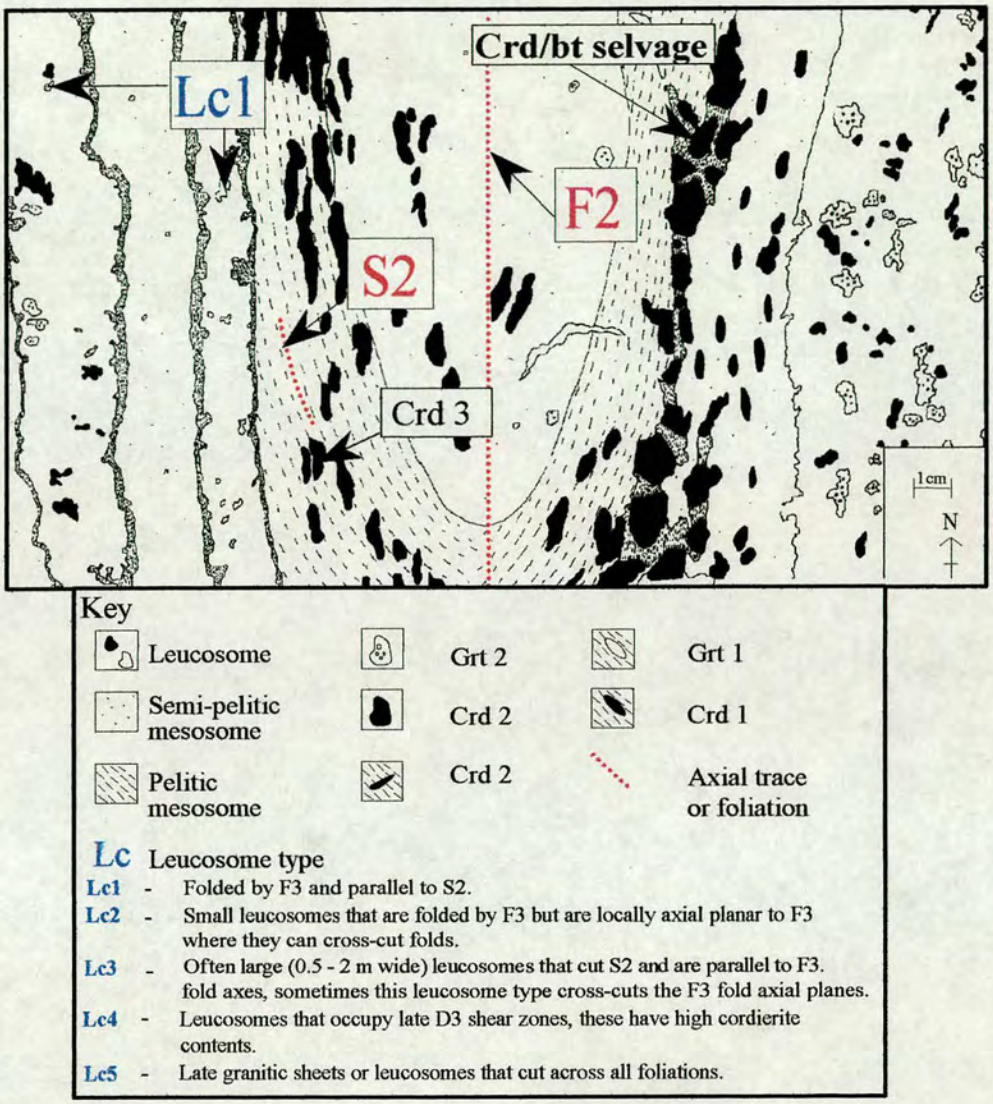

Figure 2.26 - F2 fold with associated selvage bound Lc1 leucosomes at locality

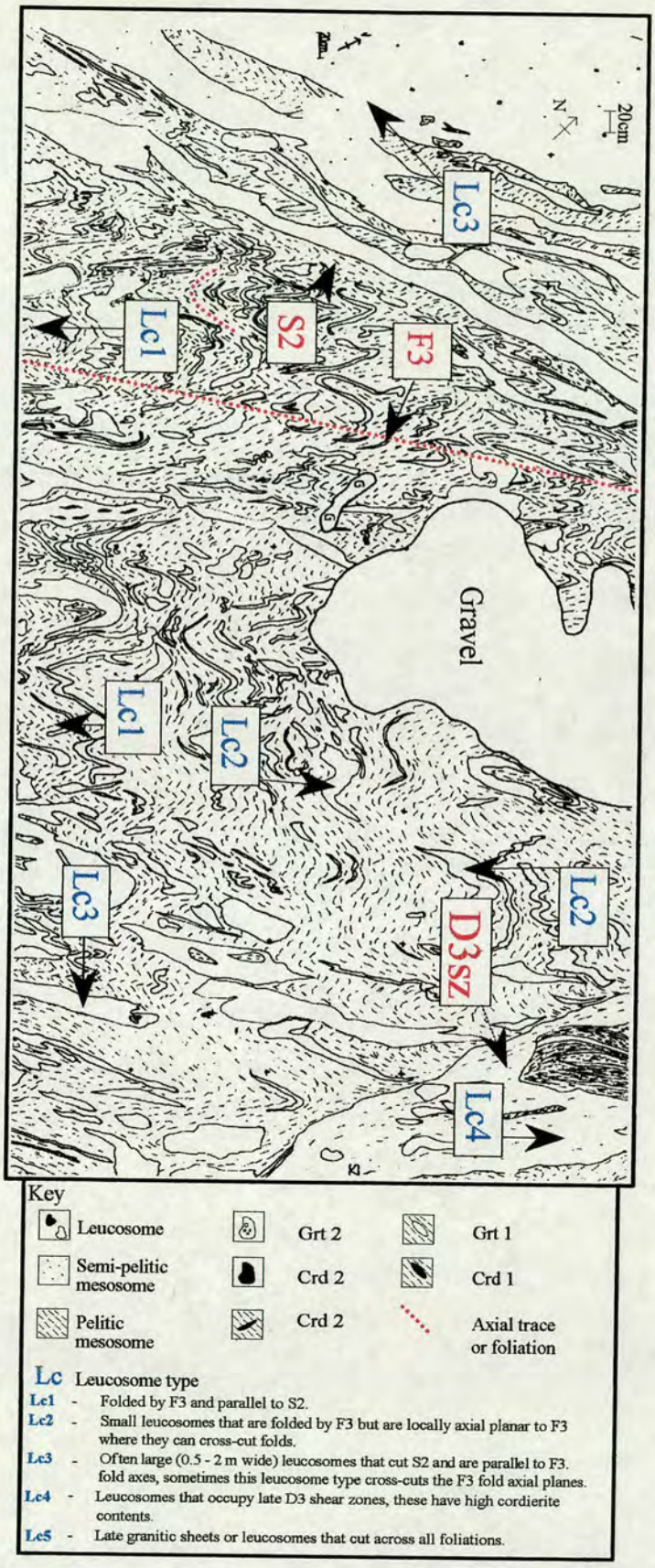

Figure 2.27 - Outcrop map of locality 1, Riviera, illustrating the relationships of leucosome material to F3 folding and shearing.

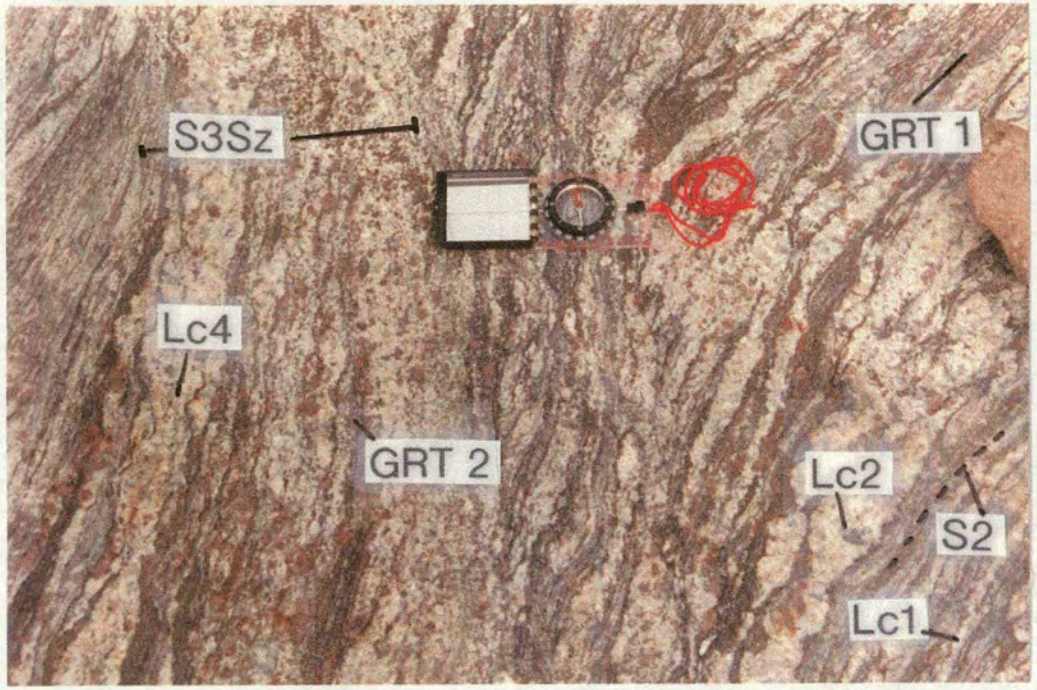

Figure 2.28 = Photograph of the edge of a D3 shear zone at locality 1, Riviera. There is a diffuse contact between Lc4 leucosomes within the shear zone and Lc1/Lc2 leucosomes on the outside. The leucosome material within the shear zone is though to represent remobilised melt.

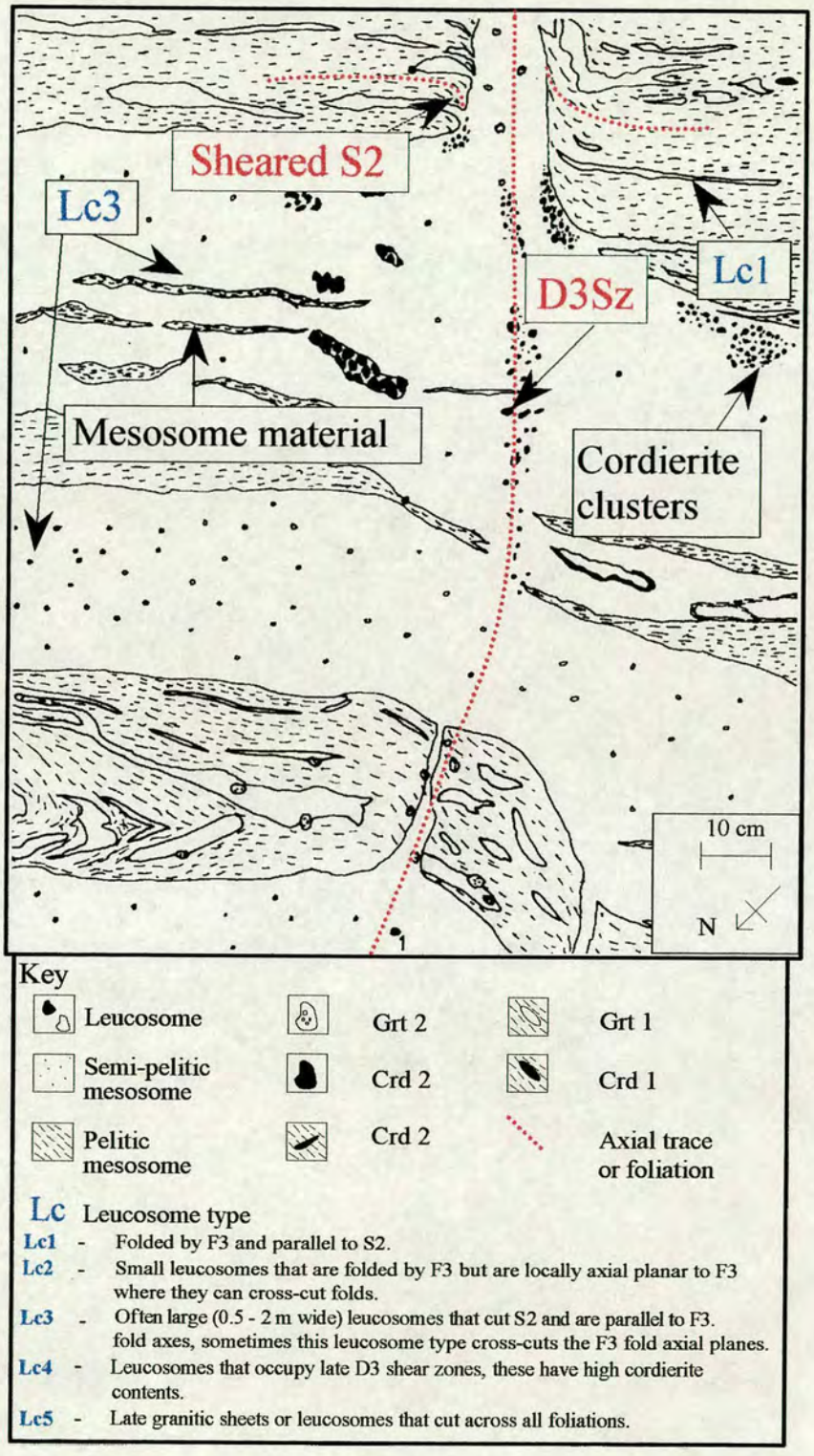

Figure 2.29 - Outcrop map (Map 1.2) showing a D3 shear zone cutting Lc3 leucosomes at locality 1.

Locality 6 - Mynamaki quarry

This quarry contains a high percentage of leucosome material and displays a range of leucosome types. Lc1 leucosomes are 1 cm by 1 m and concordant to S2. They are only found in areas where there is a low percentage of leucosome material. Later Lc2 leucosomes can be elongate (3-4 cm by 40-100 cm) and roughly concordant to S2, whilst some are patchy. In some parts of the quarry there is a high percentage of large Lc3 leucosomes that crosscut S2, and are approximately 50 cm by 3-4 metres. These leucosomes are pink in overall colour with large K-feldspar tablets. Lc5 leucosomes are present in two forms:

1. A brick red granitic sheet that has a sheared, intrusive contact and is 6-7 metres wide, cuts vertically through all deformation fabrics (Figure 2.30).
2. Fine grained, cream granitic sheets with strong intrusive contacts, approximately 30 cm by 20 m . They are either layer parallel with S2 or cut across all fabrics.

Locality 7 - Raukka road cutting

Lc2 leucosomes are present at this locality and are small (2-3 cm wide), elongate and roughly concordant to S2. In cross section it could be seen that they are folded by F3 and can be shown to be slightly oblique to S2. In addition, there are longer 20-30 cm wide leucosomes that are roughly concordant to S2, classified as Lc2/3. They contain cordierite in elongate clusters and entrained mesosome material. All of these leucosome types are illustrated in Figure 2.31.

Within one of the larger leucosomes is a sillimanite-rich patch. Further west the amount of leucosome material decreases. The leucosomes there are either patchy and very rich in large pink garnets, or small discrete leucosomes with cordierite and graphite.

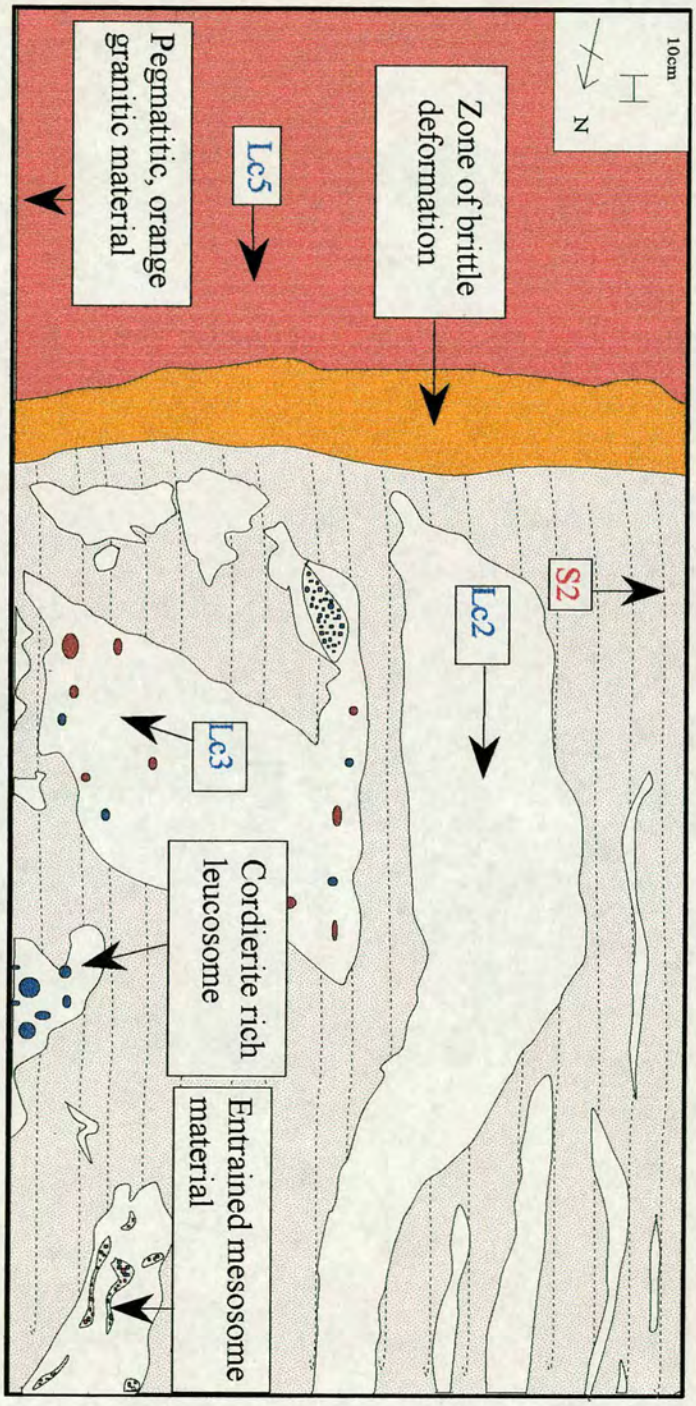

Figure 2.30 Outcrop map of leucosome types in the south wall of the quarry, locality 6, including the large pegmatitic granite sheet that has brittly deformed the surrounding rocks.

Figure 2.31 - Outcrop map of locality 7, Raukka road cutting. This is a middle locality and contains a high percentage of leucosome material. The leucosomes contain a high proportion of garnet and biotite with some entrained leucosome material.

Locality 12 - Road cutting at the east of the Häähä road

Although there is a relatively low percentage of leucosome material at this locality, there are a range of leucosome types from Lc1 to Lc5. Small leucocratic foliae (Lc1) that are up to 2 cm long are aligned along S2, whilst elongate Lc2 leucosomes are roughly concordant to S2 but ptygmatically folded in some places. Lc2 leucosomes are associated with a coarse biotite selvage that is orientated N-S and is approximately 10-15 cm by 1.6 m (Figure 2.32)

Lc3 leucosomes are elongate or patchy leucosomes that cut across S2 and are orientated NE-SW, parallel to F3 axial traces. These leucosomes are associated with poikiloblastic garnets or smaller idiomorphic cordierites. One leucosome cuts across all deformation fabrics (Figure 2.32) and can therefore be identified as Lc5, although it does not have the same characteristics of the granitic sheets seen at localities 2, 3 and 6.

Locality 5- Outcrop near Rapakivi granite contact

There is a low percentage of leucosome material at this outcrop in comparison to localities 4 and 6, (Figure 2.30). The leucosomes are up to 10 cm wide and 20-30 cm long. They are white with a 2-3 mm wide biotite rich selvage, mostly parallel to S2 and are gently folded by F3. They are rich in clear, blue-violet cordierite.

Locality 15 - Central road cutting along the Häähä road

S2 is parallel to the surface of the outcrop so that there is an apparent high volume of S2 leucosome material (Figure 2.34). Lc3 leucosomes are 3-4 cm wide and cut through S2. One Lc3 leucosome has a tourmaline and garnet rich selvage, and 30% of the leucosome is composed of tourmaline. The associated garnets contain tourmaline as inclusions (Figure 2.35).

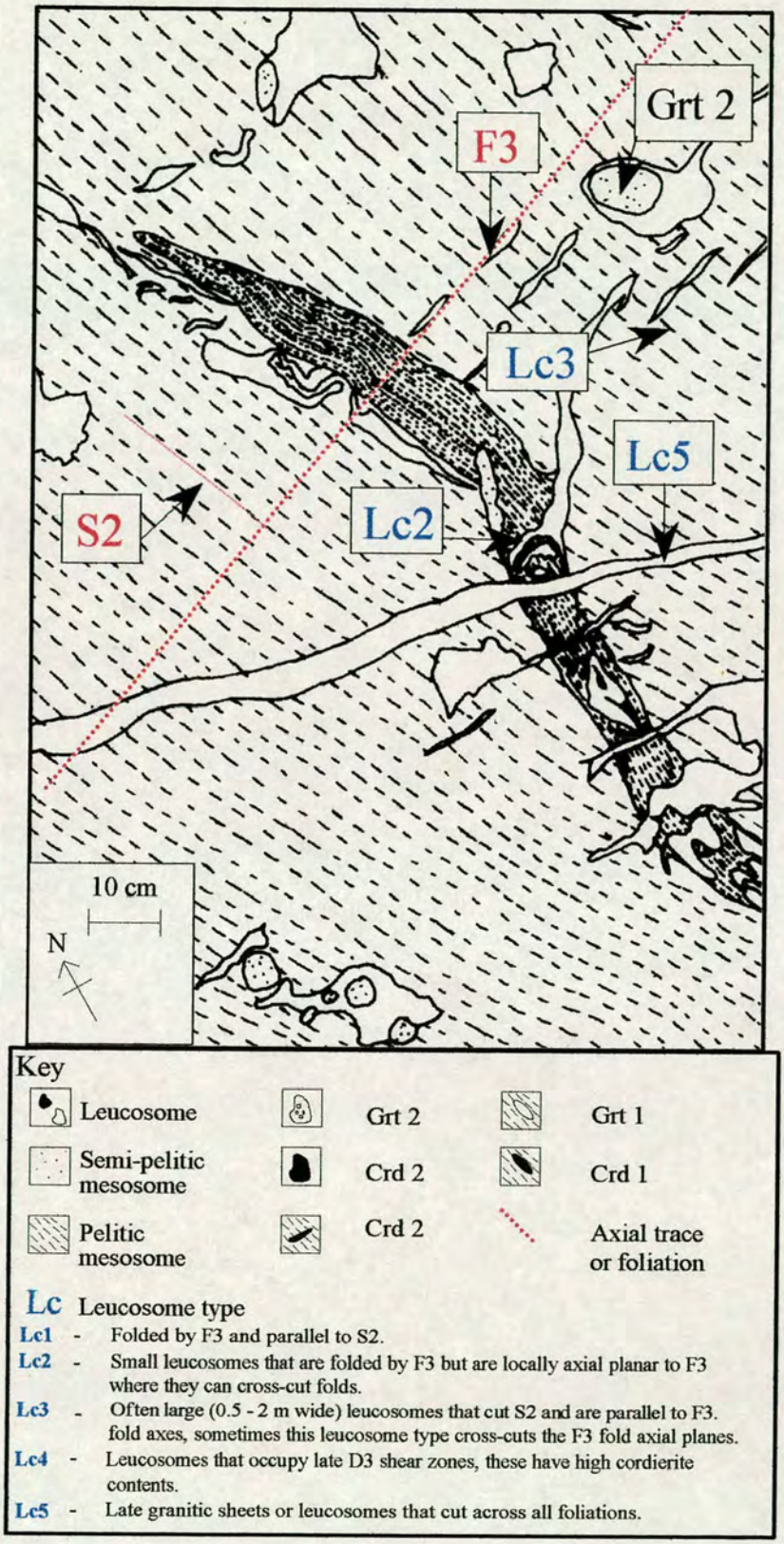

Figure 2.32 - Outcrop map of locality 12. Lc2 leucosomes are associated with coarse biotite rich patches.

Figure 2.33 - Locality 5, this outcrop is approximately 1 km south of the Häähä road transect. The outcrop contains a low percentage of leucosome material. The leucosomes are interpreted as Lc1 type with 2 mm wide biotite selvages and a high proportion of clean , violet cordierite.

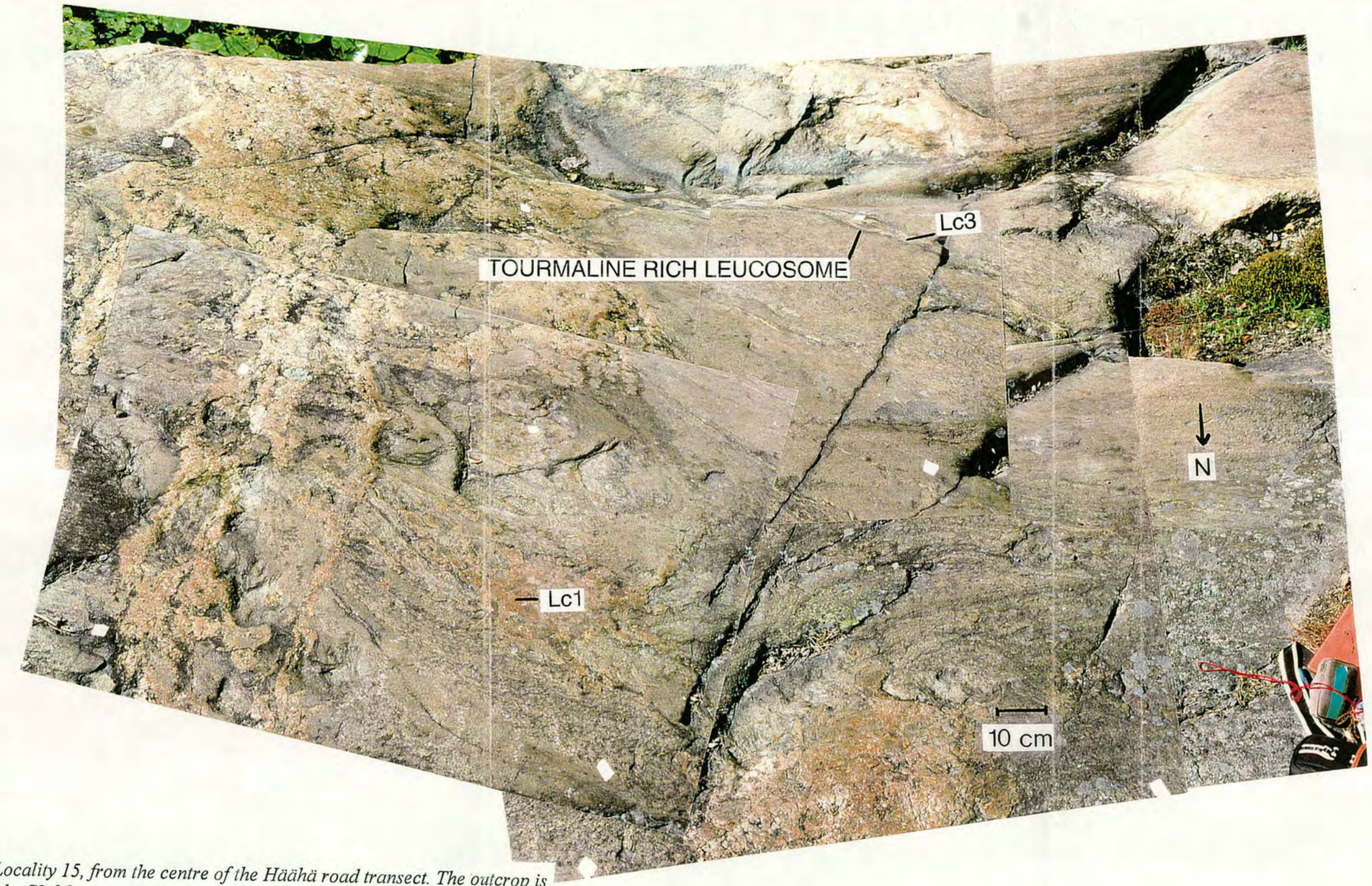

Figure 2.34 – Locality 15, from the centre of the Häähä road transect. The outcrop is in the plane of the S2 foliation. The high percentage of leucosome material observed is due to the orientation of the outcrop. The small selvage banded leucosome (top right) is shown in detail in figure 2.35.

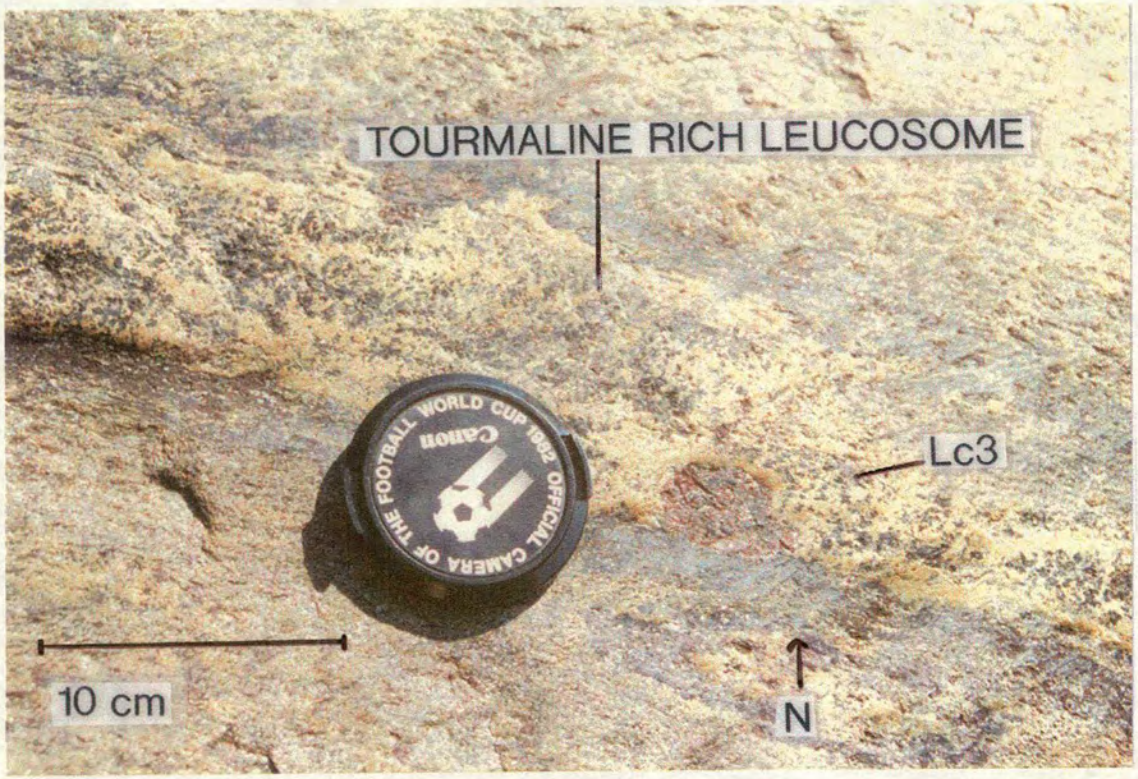

Figure 2.35 - Tourmaline rich leucosome at locality 15. The selvage and inclusions within the garnet are also mostly tourmaline with some biotite. This is a distinctive leucosome characteristic and is particular to this locality.

Locality 20 - Goose valley road transect

Lc1 leucosomes are small and elongate (2-3 cm by 1m), folded by F3 and orientated along S2 (Figure 2.36). Slightly larger Lc2 leucosomes have a similar appearance to Lc1 leucosomes but can either be roughly concordant along S2 or aligned with F3 axial traces. Patchy leucosomes are also present and are garnet- or cordierite-bearing. Some leucosomes have biotite and cordierite rich-selvages.

2.5 - Geological history of the Turku terrain

2.5.1 - Structural evolution

SO

The first recognisable event in the Turku terrain is the deposition of sediments. Bedding is now preserved as compositional layering of semi-pelitic and pelitic bands in the mesosome. This layering is laterally discontinuous on an outcrop scale and the layers are of varied thickness. Their origin is thought to be turbiditic (Väisänen et al., 1994). The more aluminous pelite bands contain a strongly foliated assemblage of biotite + garnet + cordierite, and a higher percentage of these phases than the semi-pelite bands, where these phases are mostly equigranular (Figure 2.37). As semi-pelite layers become more aluminous the grain size of garnet increases (Figure 2.38). This may be representative of original graded bedding in the turbidite sequence, i.e. the base of the bed would have contained less clay fines than the top due to density settling. The grain size is now reversed: the garnets are coarser near the top of the band because there is more aluminous material for them to nucleate from.

The other original feature to be observed is the small, layered, boudined pods seen at locality 2. From field observations their origin is not clear but they may represent calc-silicate pods. This can be determined from thin section observations of the mineral assemblage. Compositional layering is a feature that is present at localities

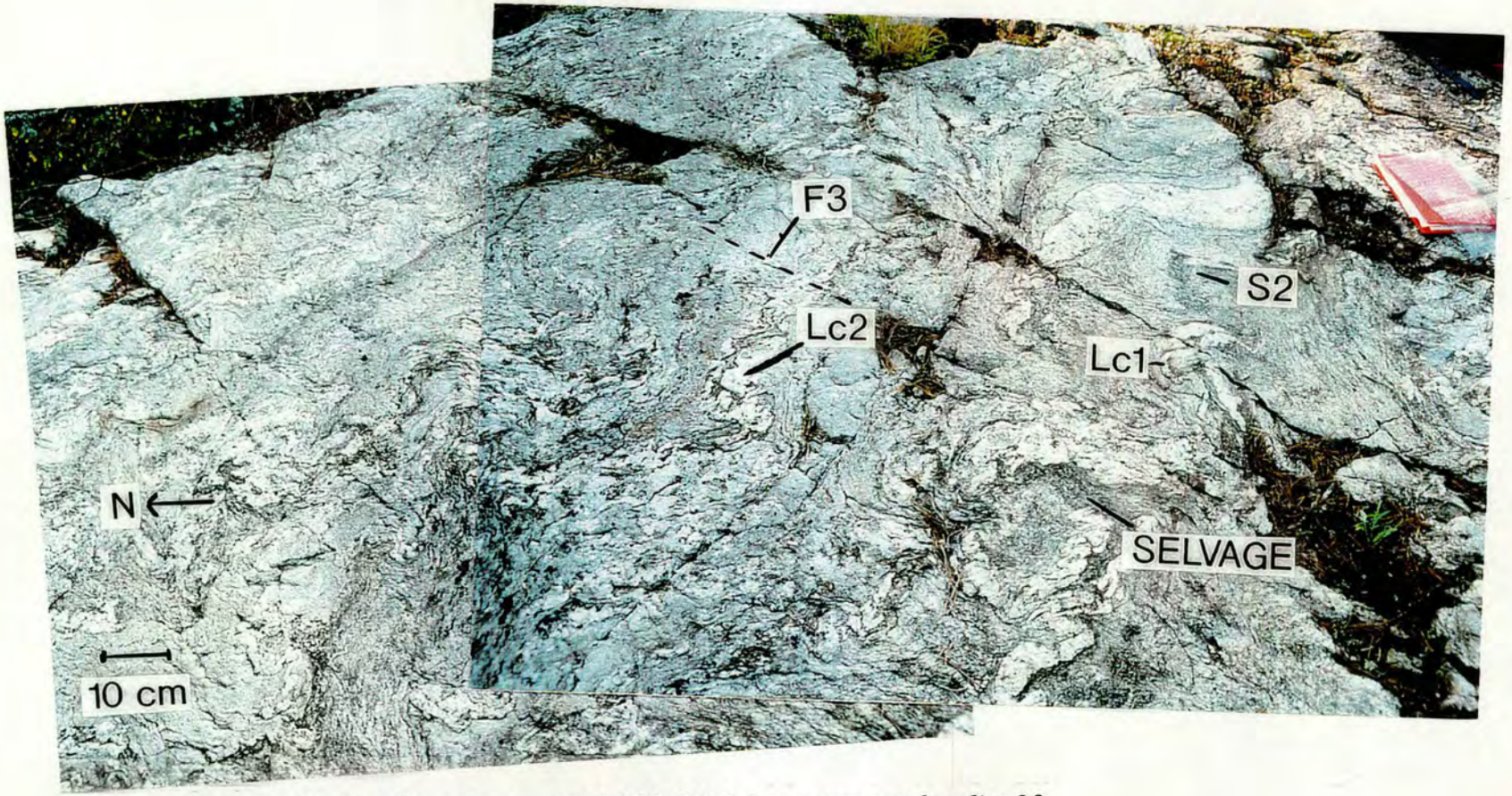

Figure 2.36 - S2 folded by F3 and associated folded Lc1 leucosomes at locality 20. Lc2 leucosomes are also present and are patchy rather than elongate within lower strain areas.

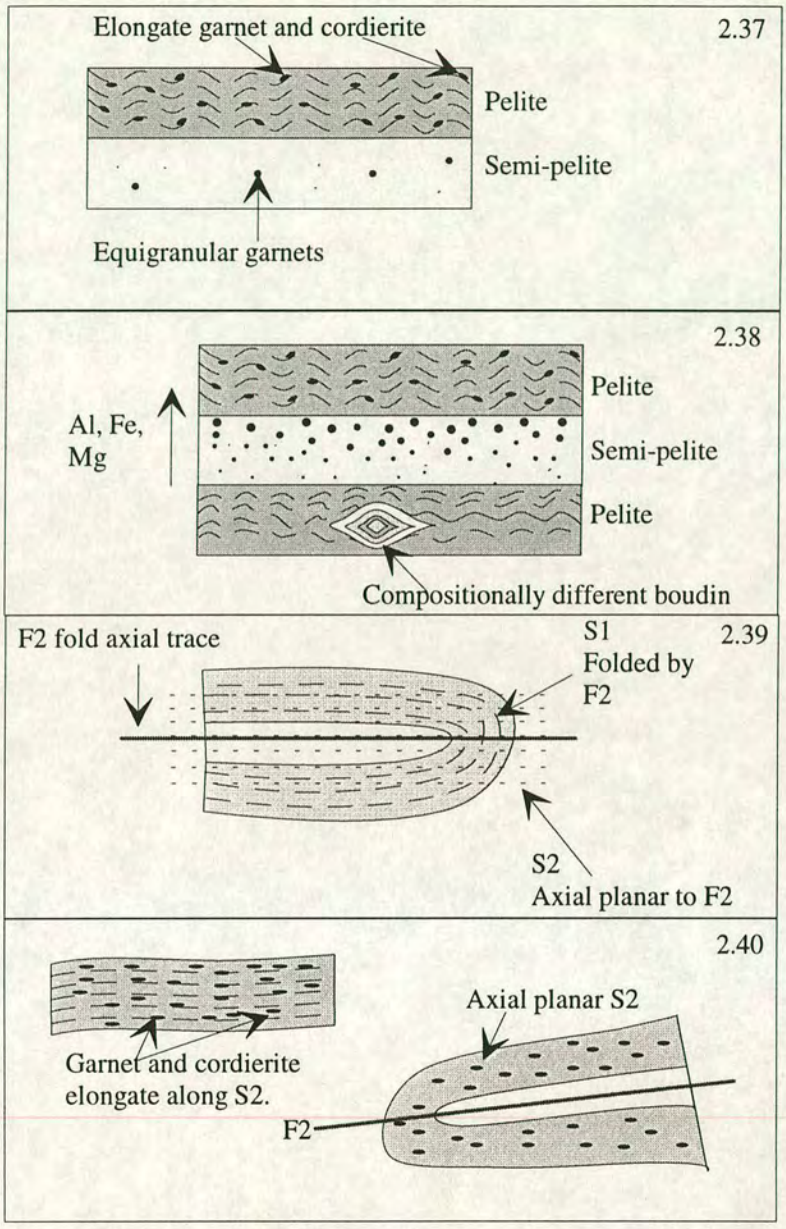

Figure 2.37 - Characteristic features of the compositionally layered mesosome observed at localities across the Turku terrain.

Figure 2.38 - Repeated layers of pelitic and semi-pelitic mesosome layers are thought to indicate a turbiditic protolith. Original graded bedding is now indicated by an increase in the size and abundance of garnet towards the top of semi-pelite layers. Small layered boudins are thought to be calc-silicate pods and so may be indicative of a deposition of more calcic material.

Figure 2.39 - The relationship between S1 and S2.

Figure 2.40 - S2 is axial planar to F2 and Grt 1 and Crd 1 have been deformed into ellipses that are aligned parallel to S2.

across the terrain except at localities with a high proportion of leucosome material, where the melanosome is homogeneous.

S1 + S2

The primary tectonic fabric of S1 was not seen in the field during this study, but work by Väisänen et al. (1994) and Väisänen and Höltta (in press) has shown that it is visible in some F2 fold hinges. S1 formed layer-parallel to bedding and was subsequently folded during D2 by F2 folds. S2 overgrew S1 and is axial planar to F2 but also layer-parallel to SO, like S1. In some F2 fold hinges S1 may still be preserved where it is wrapped around the nose of the fold rather than being axial planar like S2 (Figure 2.39).

F2 folds are isoclinal with a general axial trace orientation NW-SE. At localities across the terrain cordierite and/or garnet are aligned along S2 as elongate ellipses (Figure 2.40) and thus these phases must have been stable during early D2-late D1 for them to be deformed during D2. This assemblage indicates that granulite facies conditions were stable across the Turku terrain during early D2, and this is coeval with the appearance of orthopyroxene in the relic volcanic layers discussed in Chapter 1 (Hietanen, 1947; Van Duin and Nieman, 1993; Väisänen et al., 1994).

D3

F2 and S2 were refolded by F3. F3 folding varies from a gentle crenulation of S2 to tighter refolded F2 folds, e.g. the box folds observed at locality 6 (Figure 2.41). F3 folds have axes orientated NE-SW. There is no observable S3 foliation except at locality 2 where elongate cordierites have grown axial planar to F3 axial traces (Figure 2.42a).

F3 was sheared during late-D3, and late-D3 shear zones are found at a number of localities across the terrain (e.g. localities 1, 4 and 19 of this study) They crosscut earlier deformation fabrics (Figure 2.42b). At locality 4 shear zones have deformed

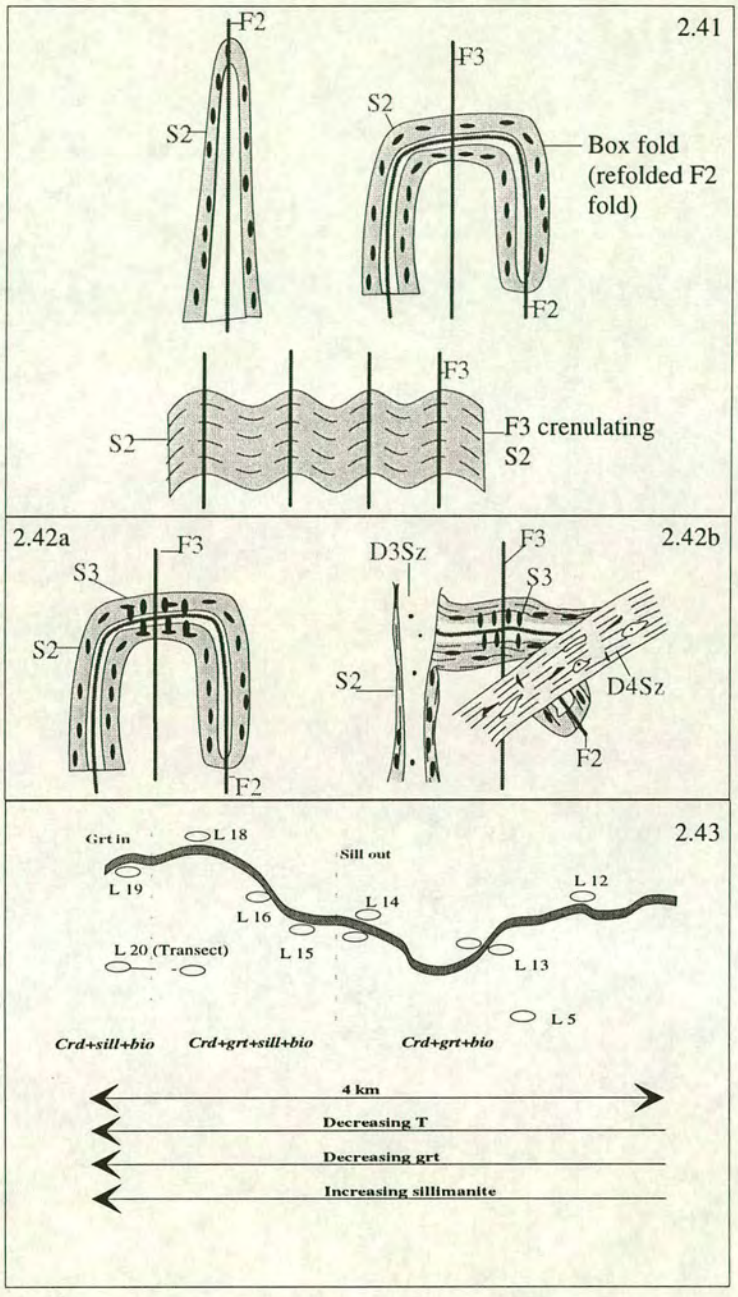

Figure 2.41 - F2 shows D3 deformation across the terrain although it varies in intensity from refolded folds to a slight crenulation of S2.

Figure 2.42a - Although there is no pervasive S3 fabric across the whole Turku terrain, at locality 2 it is manifest in elongate cordierites that formed parallel to F3 axial traces.

Figure 2.42b - During and after D3 folding, deformation began to take place along shear zones. Late D3 shear zones contain leucosome material that is indicative of once mobile melt during ductile shearing. Later D4 shear zones contain pseudotachylites, evidence for brittle deformation.

Figure 2.43 - The Hähää Road transect with the changes in mineral assemblage, garnet in and sillimanite out isograds and the inferred decrease in metamorphic grade relevant to the localities of this study.

F3 fold limbs into vertical structures, whilst at locality 1 they are present as conjugate sets. D3 shear zones contain leucosome material, suggesting that they may have provided pathways for melt movement throughout the terrain.

D4

The last stage of deformation linked to the Svecofennian orogeny is the set of later shear zones that are typified by brittle deformation (Figure 2.42b). These shear zones are classified as D4 and dated at 1800 Ma (Väisänen et al., 1994). The only D4 shear zone observed in the field is located at locality 20 and contains a pseudotachylite. There is no remobilised leucosome in the D4 shear zones, and the pseudotachylite texture points towards much lower temperatures during D4 than the earlier deformation periods.

2.5.2 - Metamorphic evolution

As mentioned earlier, granulite facies conditions were obtained during early D2 when garnet + cordierite became a stable assemblage at the southern and middle localities. However in some northern localities, garnet is unstable relative to sillimanite. This transition is clearly seen along the Hähää Road transect (Figure 2.43) where a grt + crd + bt assemblage is stable in the east, and a crd + bt + sil assemblage is stable towards the west. In between these extremes, sillimanite is stable with garnet + cordierite + biotite. Thus previous workers have mapped in garnet in and sillimanite out isograds (Figure 2.43) to delineate between these different assemblages. The difference in assemblages from the north of the terrain compared with the rest of the terrain, has been attributed to lower local PT conditions by Van Duin and Nieman (1993), Väisänen et al. (1994), Väisänen and Höltta (in press). The lowest temperatures in the terrain have been recorded from the northern localities (650-670°C) whilst a temperature of 800°C has been derived for locality 6 in the middle of the terrain (Väisänen et al., 1994), Väisänen and Höltta, in press).

The fieldwork of this study has enabled identification of a second generation of garnet and cordierite. These phases are not deformed like Grt 1 and Crd 1 and often crosscut S2. As such, these phases probably crystallised during D3. They are often found within leucosome patches where they form poikiloblasts with coarse quartz inclusions. This texture generally indicates that the phase is the peritectic product of a dehydration melting reaction such as: biotite + sillimanite + quartz = garnet + cordierite + K-feldspar + melt (Waters, 1988; Powell and Downes, 1991). This second generation of garnet and cordierite is coeval with the second thermal pulse that the terrain reportedly underwent during D3 (Väisänen et al., 1994). The finer textures of these phases that were identified with an optical microscope are catalogued in Chapter 3.

2.5.3 - Leucosome characteristics

This study has identified five key leucocratic segregation types across the terrain although they are not all present at every locality.

Lc1

Lc1 leucosomes are seen at most localities but good examples are found at localities 2, 3 and 5. They are generally small, elongate and concordant to S2 and have been folded by F3 (Figure 2.44). Their size and relationship to S2 suggests that they may represent small in-situ melts that have formed through dehydration melting of the local protolith (Le Breton and Thompson, 1988; Stevens and Clemens, 1987). It is difficult to assess the amount of melt that was produced during D2 because of the volume of later leucosome material. Initial melt volumes may have been small, or melt could have been remobilised during later melting or removed from the system entirely.

Lc2

This second generation of leucosomes is more ambiguous as they are often partially folded by F3 but not totally concordant to S2 (Figure 2.44). They are usually small

and elongate or patchy. However the 1 m wide, pink leucosomes at locality 2 were classified as Lc2 as they were also strongly deformed by F3. The Lc2 leucosomes may be representative of late D2 melts that were not concordant to S2 in the first instance and some may be early D3.

Lc3

These leucosomes are totally discordant to S2 and cut across earlier leucosomes, although the contacts are mostly diffuse. Often this leucosome type is orientated parallel to F3 axial traces and so must have formed during early to mid-D3. These leucosomes range in size from small (cover 100 cm^2 of the outcrops surface), patchy or elongate leucosomes, to large granitic sheets (cover few square metres of the outcrops surface). The small patchy leucosomes that cut across S2 are often associated with the large poikiloblastic garnets discussed previously. There is often only a very small amount of leucosome material found in association with the garnets and the foliation is usually disrupted around these patches (Figure 2.45). These textures may suggest that the leucosome and the garnet were products of dehydration melting, but that some melt has escaped leaving the garnet rich patches behind as a form of restite. The removal of melt may have caused the local fabric to fold itself into the void behind.

Lc4

This leucosome type is characterised as being located within the late D3 shear zones. The leucosome material within these shear zones contains schlieren of mesosome and a high percentage of cordierite and garnet crystals. There is little continuation of wall rock mesosome and leucosome material into the shear zone, which suggests that there was movement of melt and entrained material during shearing (Figure 2.46). The cordierite is present as elongate patches of small rounded grains that are

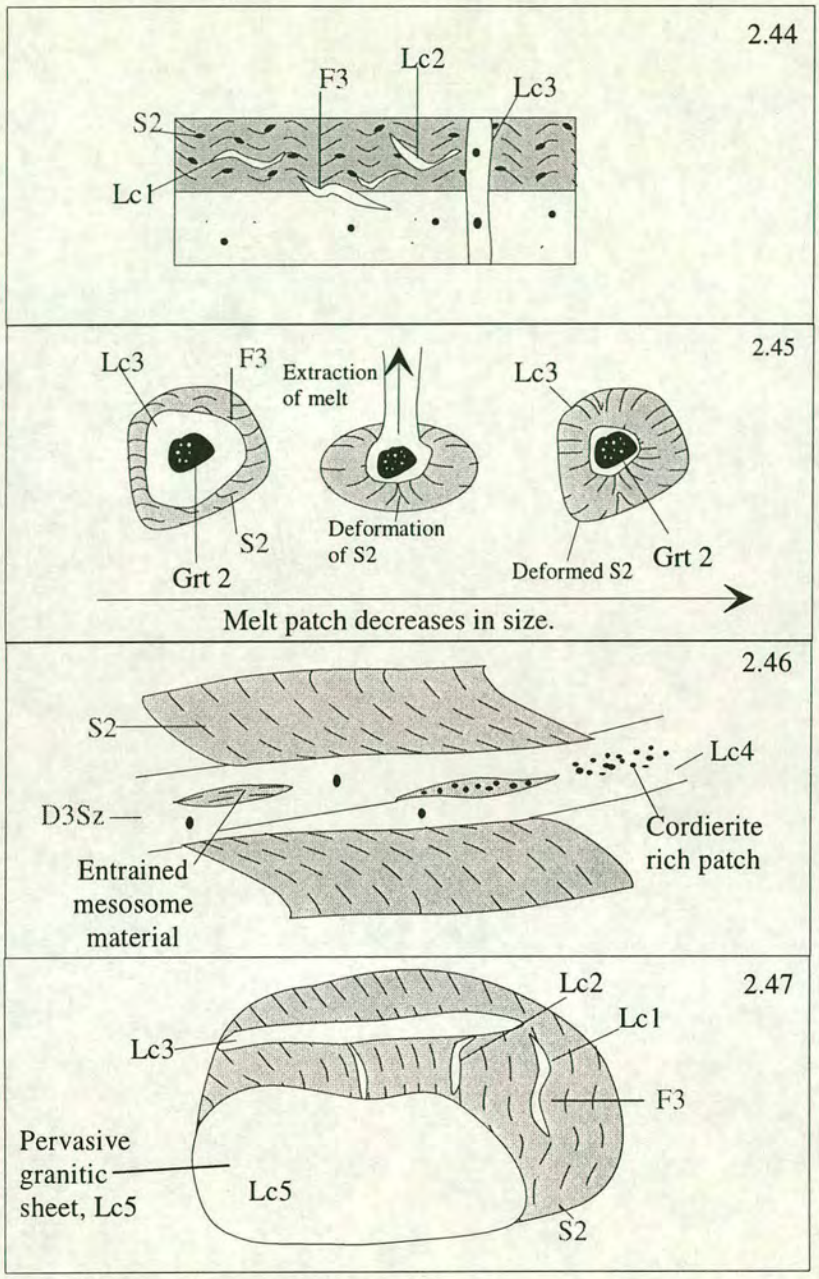

Figure 2.44 - The relationship between leucosome types Lc1, Lc2 and Lc3, and the structural framework of this study and that of Väisänen et al. (1994) and Väisänen and Höltta (in press).

Figure 2.45 - A model for the development of patchy garnet-rich Lc3 leucosomes and associated deformation of S2 by the extraction of melt from a once larger melt patch.

Figure 2.46 - An example a D3 shear zone containing an Lc4 leucosome, entrained mesosome and associated cordierite-rich patches. These shear zones could have provided pathways for melt movement out of the terrain.

Figure 2.47 - The relationship of Lc5 leucosomes to previous leucosome types. These granitic sheets may be linked to emplacement of post-orogenic, S-type granitoids across the Svecofennian Schist Belt.

associated with entrained mesosome. These patches may represent the remnants of mesosome material that has undergone some dissolution in the melt.

Lc5

The final identifiable leucosome type is again found in a range of sizes, but the overall distinguishing characteristic of this leucosome type is that it crosscuts all deformation fabrics that are associated with periods of melting. This leucosome type encompasses large granitic sheets that can be up to 30 m^2 in dimension and these may represent the late-orogenic granitic intrusions documented by Hietanen, (1947), Ehlers et al. (1993), and Väisänen et al. (1994). These cross cutting granitic sheets are usually garnet- and/or cordierite-bearing. Their size and cross-cutting nature means that classifying these granitic sheets as leucosomes is slightly erroneous. However their peraluminous composition suggests that their origins are linked to the same period of crustal melting that produced the smaller granitic segregations. These leucosomes can be seen to be cut by D4 shear zones (Väisänen and Höltta, in press).

2.6 - Preliminary models.

The observations from this field study have demonstrated that the Turku terrain does display three main deformation events on a macro-scale, D2, D3 and D4. There are two generations of a garnet + cordierite, granulite facies assemblage, one early D2 the other during D3. However the crd + sill + bt assemblage in the north of the terrain suggests that there is a metamorphic gradient across the terrain.

Melting of the Turku terrain seems to have taken place during D2 and D3, but it is difficult to constrain the extent and timing of early melting because of the presence of later leucosomes and granitic sheets. There are some leucosomes that do not fit all of the criteria for a particular classification i.e. the apparently folded leucosomes at locality 2.2. This could support an argument that melting was a continuous process from D2-onwards, through D3. As the principal stress field changes during the transition from D2 to D3, the melt would have segregated aligned to the principal

stress field at the time. Therefore not all leucosomes will be perfectly aligned to a NW-SE S2 fabric or a NE-SW F3 axial trace. Thus there is no evidence for clearly defined migmatisation pulses from the relationship of the deformation regime to the leucosomes present today.

It is possible to make some assumptions about the timing of melting from field evidence, but information is also needed about the style of melting. A feature common to many leucosomes is the high content of garnet and cordierite, occasionally up to 40%. A minimum melt that formed through dehydration melting of a pelitic protolith would contain a maximum of 3 wt % total Fe-Mg (Patinô Douce and Johnston, 1991) and this is too low to produce the garnet and cordierite contents observed in most leucosomes. The presence of mesosome schlieren within some leucosomes may suggest that the source of some of these phases is the entrainment and dissolution of Fe-Mg-rich restite. The poikiloblastic texture of some garnets and cordierites is indicative that the phases are the peritectic products of a dehydration melting reaction and grew in the presence of melt (Waters and Whales; 1984, Waters, 1988; Powell and Downes, 1991). Therefore, there are two possible sources for the large percentage of garnet and cordierite within the granitic leucosomes.

As discussed in Chapter 1 there is a limit to the amount of melt that can be extracted from dehydration melting of a pelitic assemblage (Clemens and Vielzeuf, 1987; Le Breton and Thompson, 1988), generally <40%. However at some southern and middle localities there is upwards of 70% leucosome material (qualitative estimate based on the percentage of the outcrop that consists of leucosome material in m^2). This suggests that either not all of the leucosome is internally derived, i.e. there was introduction of external melt material, or there may have been an H_2O-rich fluid introduced into the terrain during D3 which would have enhanced melting. This could have been introduced within external melts or channelled through shear zones.

The northern localities generally contain a much lower percentage of leucosome material than the middle and southern localities. The leucosome types present (Lc1,

Lc2 and Lc3) also tend to be much smaller and often selvage-bound. There are none of the large granitic sheets and pervasive leucosome types that are seen further south, present along the Hähää Road. The presence of a hydrous selvage may indicate that there was limited extraction of fluids upon melt crystallisation, with the local mesosome being rehydrated along the contact with leucosomes. This factor together with limited interconnectivity of leucosomes points towards the northern zone being typified by dehydration melting of the local protolith throughout D2 and D3 without the introduction of either external melt or fluid.

From the field evidence it can be postulated that melting was a continuous process throughout the whole of the Turku terrain with a large percentage of leucosomes produced through dehydration melting of the local pelitic protolith. This continued in the north whilst the middle and southern zones underwent a higher degree of melting at the expense of sillimanite, with the possible introduction of external melt and/or fluid. The differences between the north and south of the terrain are illustrated by Figures 2.48 and 2.49, two model outcrops typifying the range of features observed across the terrain. Further chapters will add petrographical and compositional data to this framework, together with information on any potential PT differences and the inferred volatile regime present at the time of melting.

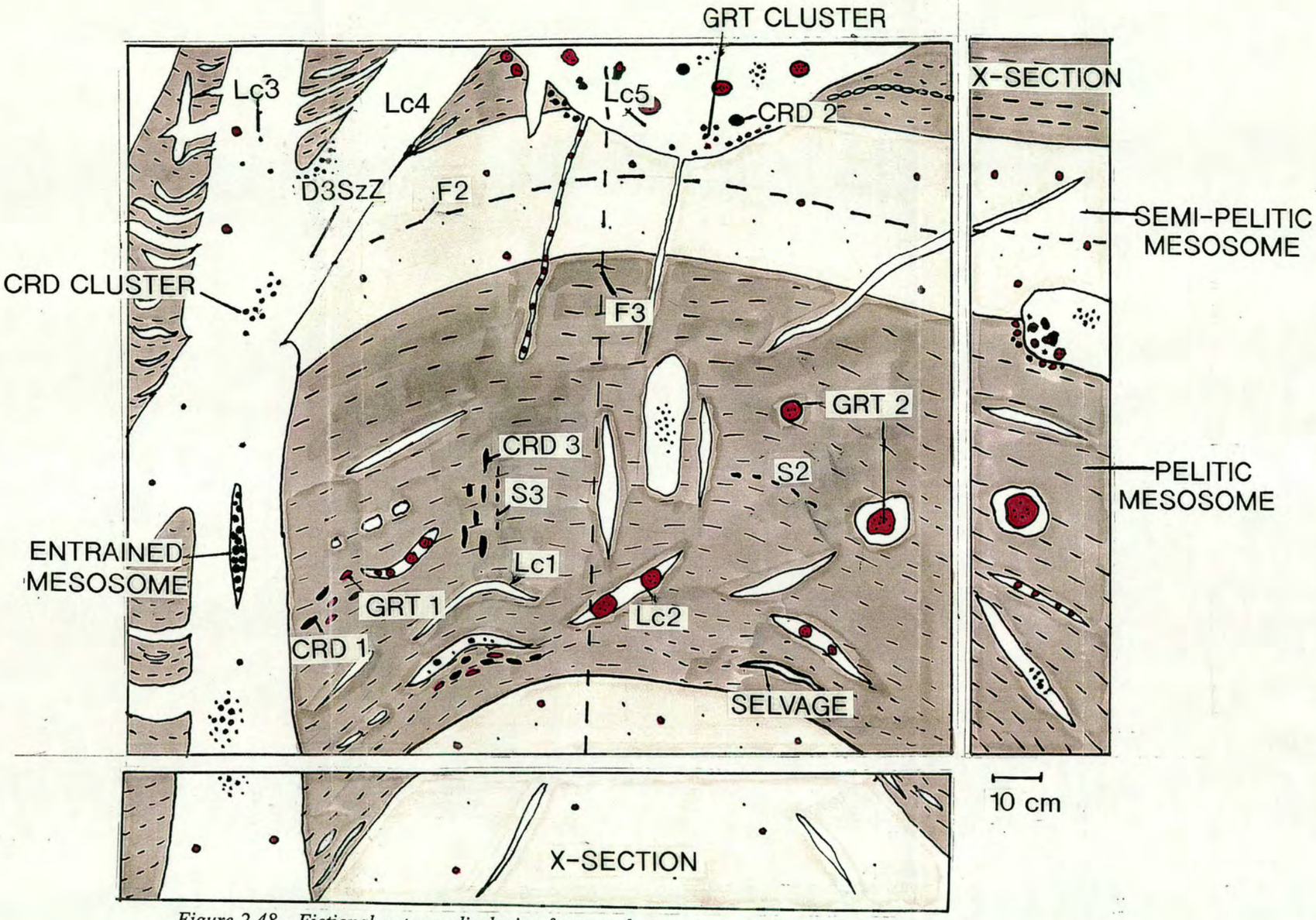

Figure 2.48 - Fictional outcrop displaying features that are typical of southern and middle localities with the Turku terrain. Some southern and middle localities contain much higher percentages of leucosome material than is shown in this diagram.

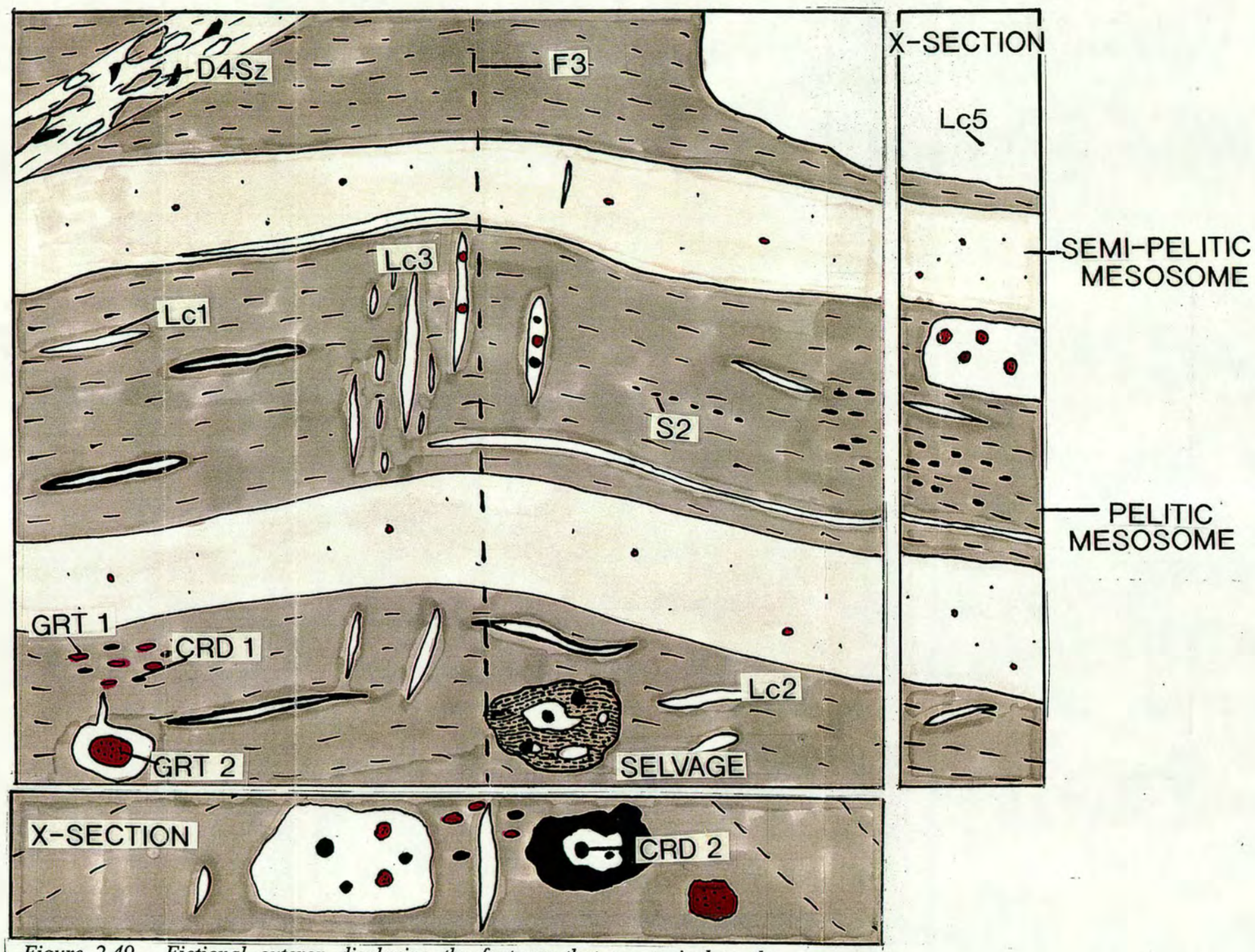

Figure 2.49 - Fictional outcrop displaying the features that are typical to the northern localities, particularly those that are located along the Hähää road transect.

Chapter 3

Petrography

Chapter 3 - Petrography

3.1 - Introduction and rationale

In this chapter, the key phases and textures of representative leucosome, mesosome and melanosome material from across the Turku terrain area are described. Field observations have shown that most of the terrain is typified by the stability of garnet and cordierite within rocks having pelitic mesosome compositions. Sillimanite does not occur co-existing with both phases in southern and middle localities, though it is a common inclusion within early generations of cordierite and more rarely garnet. In the north of the terrain, the grt + crd assemblage passes into a crd + sil assemblage through a transitional zone where garnet and cordierite are found co-existing with sillimanite. The stability of sillimanite within the mesosome assemblages in the north is mirrored by a decrease in garnet occurrence. This assemblage transition and relevant sillimanite out and garnet out isograds are marked on Figure 3.1. This transition has been inferred to show lower PT conditions in the northern localities than in the rest of the terrain (Väisänen et al., 1994; Väisänen and Höltta, in press).

Field observations provide a basic model for the sequence of metamorphic events and also for the melting regime. However in order to properly understand the metamorphic history of the Turku terrain, a knowledge is needed of the assemblages present and the textural relations between phases. To investigate the possible metamorphic gradient across the terrain detailed petrographic knowledge is essential to pick the right the samples for geothermobarometry. This chapter aims to describe and interpret the petrography of representative mesosome and leucosome samples taken from key localities.

3.2 - Definition of terms

The classifications used for the migmatite components studied are the same as for the field descriptions in the previous chapter (and are after Ashworth, 1985). This

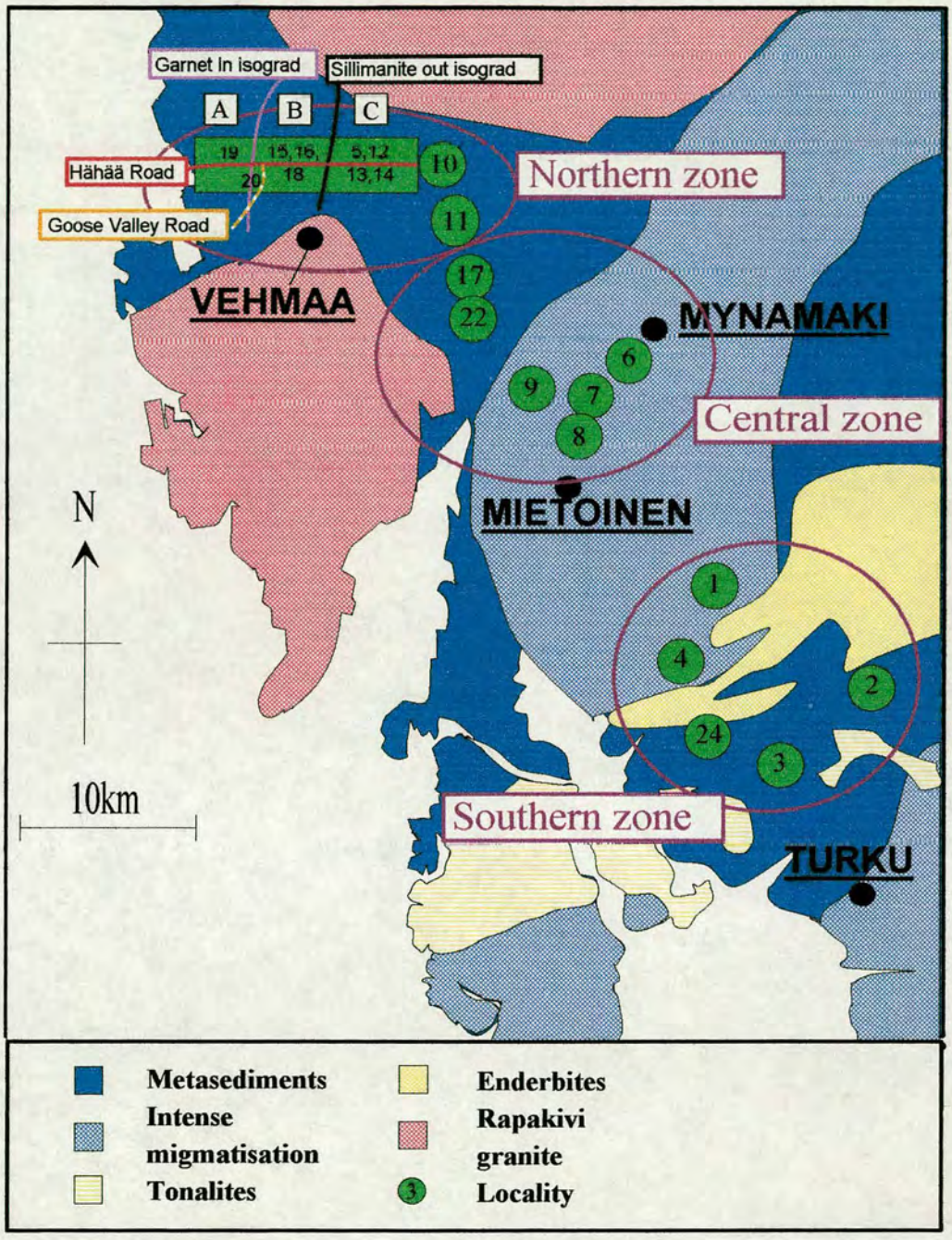

Figure 3.1 - Metamorphic map of the Turku terrain (After Väisänen et al. 1994).
A - Cordierite+sillimanite+biotite assemblage
B - Garnet+cordierite+sillimanite+biotite assemblage
C - Garnet+cordierite assemblage

chapter aims to add the full mineral assemblage and textural information to these previous definitions. All of the following descriptions are illustrated in Figure 3.2.

3.2.1 - Mesosome

The mesosome is often granuloblastic with biotite crystals having either a decussate texture or strong S2 foliation. The general assemblage is pl + qtz + kfs + bt ± grt ± crd ± sil. The mesosome consists of aluminous layers which are rich in bt + crd + grt ± sil and less aluminous layers that are more leucocratic.

3.2.2 - Melanosome

This is found in the localities where there is a high percentage of leucosome material and is generally coarser grained and has less leucocratic phases than mesosome material. The melanosome was defined by Ashworth (1985) as 'a body of the dark coloured lithology present in some migmatites, rich in mafic minerals, complementary to leucosome'. A typical melanosome assemblage is bt + crd + grt + qtz ± pl + kfs + gr and is often strongly foliated.

3.2.3 - Selvage

Where an outcrop has a low percentage of leucosome material, a coarse grained selvage may be observed mantling a leucosome, composed dominantly of biotite and cordierite. The cordierite may contain sillimanite inclusions and often occurs as clustered grains within the edge of the leucosome itself. Selvages are mostly found in the north of the terrain although some are seen at southern localities 2 and 24.

3.2.4 - Leucosome

The leucosome is the leucocratic segregation that is thought in this instance to represent a site of crystallised granitic melt. It is characterised by large tabular crystals of potassium feldspar, quartz and plagioclase, plus a mafic component of garnet, cordierite and rarely biotite. Leucosomes are usually much coarser grained

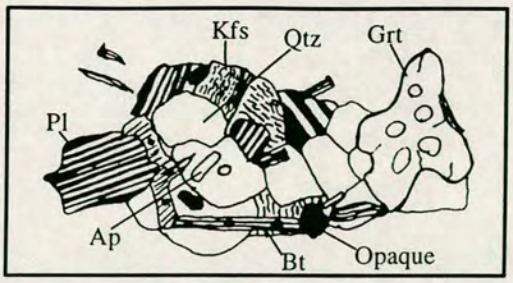

Granuloblastic mesosome with decussate biotite.

Mesosome with strong S2 fabric

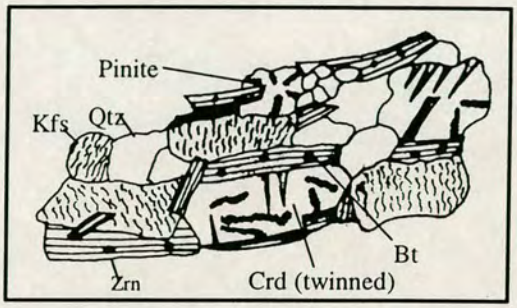

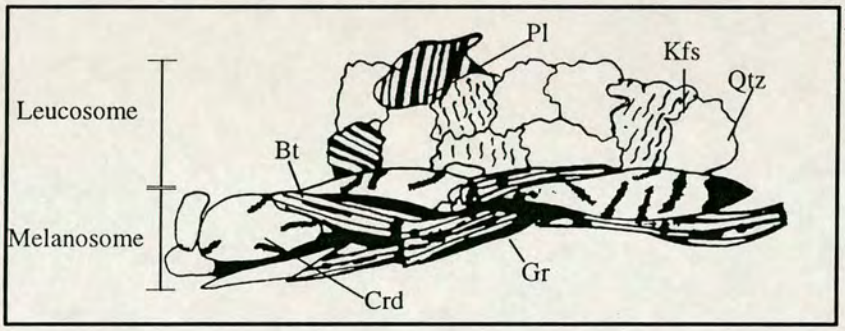

Melanosome

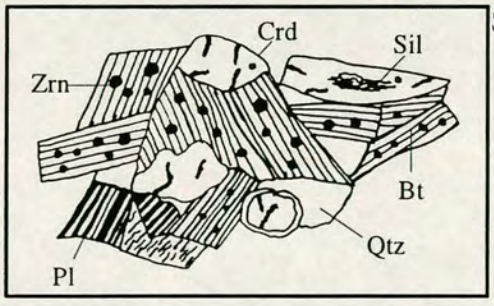

Selvage

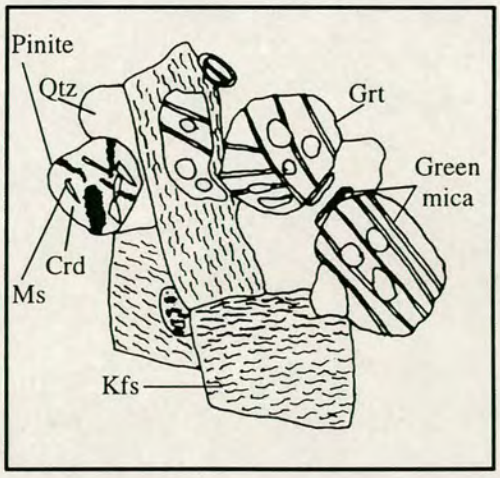

Leucosome

Figure 3.2 - Textural features and mineral assemblages of mesosome, melanosome leucosome, and selvage materials.

(5-20 mm) than the surrounding mesosome and can have a granulose but not granuloblastic texture. Grain boundaries between minerals generally are not straight, and are often embayed or lobate.

3.3 - Mesosome assemblages and textures

The mineral assemblages in the mesosomes from southern, middle and northern localities are summarised in Tables 3.1 to 3.3, and a brief description of all the samples studied can be found in Appendix 3. The aim of this section is to explore the differences in assemblages throughout the terrain and their implications for metamorphic isograds and reaction boundaries. The positions of localities referred to in the following descriptions may be found in Figure 3.1.

3.3.1 - Garnet

Garnet is generally present as two generations: (1) Firstly, there are elongate porphyroblasts that are parallel to S2 (Grt 1) but do not appear to be wrapped by S2. As these garnets have been deformed by D2 and can be seen in the field and thin sections to have been folded by F3, they are inferred to have grown during early/mid-D2. Grt 1 occasionally contain biotite, quartz and sometimes sillimanite (Figure 3.3) but they are only rarely poikiloblastic; (2) The second generation garnets (Grt 2) are commonly poikiloblastic and generally contain large quartz inclusions that can be rounded or rib-like, usually coarser than the mesosome matrix. These garnets are sometimes surrounded by K-feldspar and quartz with a similar coarse grain size to the inclusions (Figure 3.4).

Around garnets within mesosome material, or at the edges of leucosomes, there is some retrogression of garnet to biotite + quartz and sometimes cordierite. Often this reaction is present as a symplectite of elongate biotite with worm-like quartz inclusions.

Table 3.1 - Petrographic composition of mesosomes in the Southern Turku terrain.

Cp pinnitised cordierite, *D2* early, elongate phase, *D3p* later poikiloblastic phase, *D3NP* later non-poikiloblastic, idiomorphic phase, *GM* general mesosome phase, *1* inclusion in *1* garnet, *2* cordierite, *3* K-feldspar, *4* biotite, *My* myrmekitic texture, *P* porphyroblast, *R* retrograde phase of $_1$ garnet, $_2$ cordierite, $_3$ K-feldspar, $_4$ biotite, *S* selvage phase * phase is a minor component

Locality	Sample	Access	And	Amph	Bt	Chl	Crd	Grt	Gr	Kfs	Ms	Opaque	Pl	Pyx	Qtz	Sil	Spl	Tur
3.a	AV1	Mnz, Zrn, Ap			GM $R_{1,2}$ $I_{1,2}$	R_1	P D_2 D_{3NP} Cp R_1	P D_{3P}	I_1	GM	R_2		GM		GM I_1			I_1
3.a	AV3	Mnz, Zrn			GM I_1 $R_{1,2}$		GM Cp D3 R_1	P D_{3P} $I_{2,3}$	*	P			GM P		GM I_1 $_R$ I	I_2 D_3	I_2	
3.a	AV4	Mnz, Zrn, Ap			GM R_1 $I_{1.2,3}$		P D_2 R_1 I_1	P D2 D_{3P} D_3		GM P			GM My		BM R_1 I_1	I_2	I_2	
3.a	AV5	Mnz, Zrn			GM R_1 I_1		D_3 Cp	P D_{3P}	*	GM			GM		I_2			
3	D26	Mnz, Zrn			GM $R_{1,2}$ I_1		GM Cp	P D_{3P} D_2	$I_{1,4}$	GM			GM		GM R_1 I_1		R_4	
3	D28	Mnz, Zrn			GM R_1 I_1		P D_{3P} D_2	P D_{3P}	*	GM			GM		GM R_1 $I_{1,2}$	I_1		
3	AV88	Mnz, Zrn, Ap			D_2 GM $I_{1,2}$ R_1		P D_2	P D_2		GM			GM		GM	$I_{1,2}$		D_2 $I_{1,2}$ GM
3	AV89	Mnz, Zrn, Ap			GM		P D_{3P} Cp	P D_{3P}		GM			GM		GM I_2			
3	AV90				GM I_1 R_1	R_1	P D_2 D_3 CP I_1	P D_{3P}		GM		*	GM		GM R_1 I_1	I_2		I_1
2.1	D8	Mnz, Zrn			GM R_1		GM Cp	P D_{3p}		GM			GM		GM R I_1			
2.1	AV82	Mnz, Zrn			GM $R_{1,2}$ I_1	R_1	P D_3 Cp R_1	P D_2 D_{3p}		GM p			GM		GM $I_{1,2,3}$ R_1	I_2		
2.1	AV83	Mnz, Zrn			GM $R_{1,2}$ I_1	R_1	PD_2	P D_{3P}		P GM		*	GM		GM $I_{1,2}$ R_1	$I_{1,2}$		
2.2	D13	Mnz, Zrn, Ap			GM $R_{1,2}$ I_3	$R_{1,4}$	P D_2 R_1	P D_{3p}	*	P GM		*	GM		GM $R_{1,2}$ $I_{1,2,3}$	I_2 F	I_2	
2.2	D14	Zrn, Ap			GM							*	P GM		GM			
2.2	D15	Zrn, Ap			GM			GM		GM		*	GM		GM			
2.2	D16	Mnz, Zrn, Ap		R		R amph			*			*	GM	P	GM			
2.3	D19	Mnz, Zrn, Ap			GM R_1 I_1	R_1		P D_{3P}		P GM			GM		GM $I_{1,2}$ R_1			
2.3	D20	Mnz, Zrn			GM R_2 I_2		P D_{3P} Cp			GM			GM		GM I_2	I_2		
2.3	D22	Mnz, Zrn			GM R_2 S	R_4	P GM D_2 S		*	GM			GM		GM			
2.3	AV78	Mnz, Zrn			GM $R_{1,2}$ $I_{1,2,3}$	R_4	P D_{3P} Cp	P D_{3P}		P GM			GM		GM $I_{1,2,3}$			
2.3	AV79	Mnz, Zrn			GM S R_2	$R_{2,4}$	P GM D_{3P} S		*	P GM			GM		P GM S $I_{2,3}$			
2.4	D3	Mnz, Zrn, Ap			GM $I_{2,3}$			P D_{3P}	*	GM			GM		GM I_1			
2.4	D4	Mnz, Zrn, Ap			GM		D_{3P}	P D_{3P}		GM			GM		GM $I_{1,2}$			
2.4	D5	Mnz, Zrn, Ap			GM S				*	GM			GM		GM			
2.4	D6	Ap			GM		GM Cp	P D_{3P}				*	GM			*	*	
2.4	D7	Ap			GM I_1 R_1			P D_{3P}		GM			GM		GM I_1			
4	AV7	Mnz, Zrn			GM $R_{1,2}$	$R_{1,2,4}$	P D_2 Cp R_1	P D_{3P}	*	P					GM 1_1 $R_{1,2}$	I_2		
4	AV8	Zrn, Ap			GM		GM	P D_{3P}		P GM		* I_1	GM		GM I_1			
4	AV12	Mnz, Zrn			GM R_1	$R_{1,2}$	P D_2 Cp R_1	P D_{3P}	* I_1	P			GM		GM R_1 I_1	I_2		
4	AV14	Mnz, Zrn			GM R_2	R_2	GM D_{2NP} Cp					* R_2	GM		GM	I_2		
4	AV15	Mnz, Zrn			GM S R1		GM S Cp	P D_{2P} D_{3P}					GM		GM I_1	I_2		
4	AV101	Mnz, Zrn			GM S R_1	R2	GM S Cp	P D_{2P} D_{3NP}		GM			GM My		GM I_1	I_2		

Table 3.2 - Petrographic composition of mesosomes in the Middle Turku terrain.

Cp pinnitised cordierite, *D2* early, elongate phase, *D3p* later poikiloblastic phase, *D3NP* later non-poikiloblastic, idiomorphic phase, *GM* general mesosome phase, *I* inclusion in *1* garnet, *2* cordierite, *3* K-feldspar, *4* biotite, *My* myrmekitic texture, *P* porphyroblast, *R* retrograde phase of $_1$ garnet, $_2$ cordierite, $_3$ K-feldspar, $_4$ biotite, *S* selvage phase * phase is a minor component

Locality	Sample	Access.	And	Bt	Chl	Crd	Grt	Gr	Kfs	Ms	Opaque	Pl	Qtz	Sil	Spl	Tur
8	D31	Mnz, Zrn	R_2	GM R_2 I_2		GM Cp		*	P GM	R_4		PGM My	GM R_2	I_2 R_2		
7	D34	Mnz, Zrn		GM				*	GM			GM	GM			
7	D37			GM		P GM D_2	PD_{3P}	*		R_2		GM	GM	I_2		
7	AV35	Mnz, Zrn		GM	R_1	P GM	P D_{3P}		GM	R_2	*	GM	GM	I_2		
7	AV120	Mnz, Zrn		R_1	R_4	P GM	P D_{3P}	*	GM	R_2		GM	GM	I_2		
7	AV148	Mnz, Zrn	*	GM $R_{1,3}$			P $D_{3NP/P}$	*	P $R_{1,4}$			GR My	GM I_1			
6	AV17B	Mnz, Zrn, Ap	P	GM R_2		GM P D_2 D_{3NP}		*	P GM				GM R_2 I_1	I_2		
6	AV114	Mnz, Zrn	R_2	GM $R_{1,2}$ I_1		GM P D_{3NP} Cp R_1	P D_{3P}	*				P GM	GM $R_{1,2}$ I_1			
17	AV145	Zrn, Ap	R_2	GM R_2		P D_2 Cp	P D_{3NP}			$R_{3,4}$				GM		

Table 3.3 - Petrographic composition of mesosomes in the Northern Turku terrain.

Cp pinnitised cordierite, *D2* early, elongate phase, *D3p* later poikiloblastic phase, *D3NP* later non-poikiloblastic, idiomorphic phase, *GM* general mesosome phase, *I* inclusion in *1* garnet, *2* cordierite, *3* K-feldspar, *4* biotite, *My* myrmekitic texture, *P* porphyroblast, *R* retrograde phase of $_1$ garnet, $_2$ cordierite, $_3$ K-feldspar, $_4$ biotite, *S* selvage phase * phase is a minor component

Locality	Sample	Access.	And	Bt	Chl	Crd	Grt	Gr	Kfs	Ms	Opaque	Pl	Qtz	Sil	Spl	Tur
11	**AV129**	Mnz, Zrn	R2	GM R_2	R_4	P D2 D_{3P} Cp		I_4	P GM	$R_{2,3}$			P GM	GM $R_{2,3}$		
5	**AV102**	Mnz, Zrn		GM S I_2 R_2		P GM D_2 D_{3P} S		*				GM	GM	I_2		
5	**AV103**	Mnz, Zrn		GM S $R_{1,2}$ $I_{1,2}$		P GM Cp D_2 S	P D_{3P}	*	GR My	R_3			GM	I_2		
5	**AV104**	Mnz, Zrn		GM S $R_{1,2}$ $I_{1,2}$		P GM Cp D_2 S	P D_{3P}	*					GM	I_2 R_2		
12	**D44**	Mnz, Zrn		GM $R_{2,3}$ I_3		GM Cp R_1	P D_{3P}	*	P GM	R_4			P GM I_3	GM		
12	**AV18**	Mnz, Zrn, Ap		GM $I_{2,3}$		P D2 Cp D_{3P}			P GM	$R_{3,4}$		GM	GM $I_{2,3}$	GM $I_{2,3}$		
15	**AV25**	Mnz, Zrn, Ap			$R_{2,4}$	P GM D_2			GM	$R_{3,4}$		GM	GM	GM R_2		
16	**AV136**			GM R_1 I_3			P D_2 D_{3P}					P	GM R_1 I_3	GM I_1		
20	**AV27**	Mnz, Zrn		GM		P $D_{3P/NP}$			GM	$R_{2,3,4}$		GM	GM I_2			
20	**AV28**	Mnz, Zrn		GM		P D_2 $D_{3P/NP}$	P D_2		GM	R_4		GM	GM I_2	R_2 I_2		
20	**AV29**	Mnz, Zrn		GM		P D_{3P}			GM	$R_{2,4}$		GM	GM I_2 R_4	GM R_2		
20	**AV31**	Mnz, Zrn		GM		P D_{3P}			GM My	$R_{2,4}$			GM I_2 R_4			
20	**AV32**	Mnz, Zrn		GM R_2		P D_2 Cp		*	GM	$R_{2,4}$		GM	GM	R_2		
20	**AV33**	Mnz, Zrn		GM $R_{1,2}$	R_1	P D_{3NP} R_1	PD_{3P}	*	GM			GM	GM $R_{1,2}$	R_1		
19	**AV22**	Zrn, Ap		GM R_2 $I_{2,3}$		P D_2 Cp			GM	R_3		GM	GM $R_{2,4}$	GM $R_{2,4}$		
19	**AV23**	Zrn, Ap		GM R_2 $I_{2,3}$		P D_2 Cp			GM	$R_{2,3,4}$		GM	GM $R_{2,4}$ I_4	GM $R_{2,4}$		
19	**AV24**	Zrn, Ap	R_2	GM R_2 $I_{2,3}$		P D_2 D_{3P} Cp		*	GM	$R_{2,3,4}$		GM	GM $R_{2,4}$	GM $R_{2,4}$		

As discussed in Chapter 2, the poikiloblastic (Grt 2) garnets are often associated with patchy Lc3 leucosomes, e.g. at locality 2, large 3-4 cm wide garnets are sometimes found in small leucosome patches but also isolated within the mesosome. Around these small patches and garnets the foliation is disturbed, a feature attributed to deformation due to melt extraction (Chapter 2).

3.3.2 - Cordierite

As with garnet, there is more than one generation of cordierite. Early syn-D2 cordierites are also elongate and often parallel to S2 (Crd 1). These may contain biotite, quartz and sillimanite inclusions. Those with sillimanite inclusions have this mineral confined to their core, whereas biotite and quartz inclusions are found throughout the phase (Figure 3.5). The biotite crystals show an earlier foliation that is slightly oblique to S2, and may represent S1 (Väisänen et al., 1994). The cordierites as a whole show an ellipsoid shape elongate along S2, which suggests that they are coeval with early garnet. In the north and south of the terrain, elongate cordierite crystals are found within selvage assemblages with sillimanite inclusions. Another cordierite type observed is sub-idiomorphic (Crd 2) with large quartz inclusions. These are common in semi-pelite mesosome assemblages and also within leucosomes.

At locality 2, elongate cordierites were observed aligned parallel to the general orientation of F3 axial traces and so appear to have grown syn-F3. Under the microscope these crystals contain aligned biotite and quartz inclusions that are slightly oblique to the main foliation and so may reflect S2 before F3 re-folding. Cordierite is also found as a retrogressive phase on garnet in association with a biotite and quartz symplectite. This cordierite is generally quite pinitised and is yellow under plane polarised light.

3.3.3 - Biotite

The earliest generation of biotite is present within large K-feldspar and cordierite grains as oriented inclusions. These orientated inclusion trails are oblique to S2 and as such may be representative of S1 (Figure 3.5). Biotite is the main component of the D2 mineral assemblage, either as orientated or decussate grains. D3 orientated biotite growth was not observed in this study but is restricted to tight F3 folds (Väisänen et al., 1994). The last form of biotite to crystallise in the mesosome assemblage is a retrogressive phase of both garnet and cordierite, where it is sometimes pale green in colour. Often this retrograde biotite crystallises with quartz, and sometimes cordierite, to give a rib like symplectite (Figure 3.6). The retrograde reaction responsible will be discussed later (Section 3.6.2).

Within melanosomes the biotite is frequently coarser grained than mesosome biotite. It is often found in association with acicular graphite, which is located along the edges and cleavage planes of the biotite (Figure 3.7). Also, within these assemblages the biotite is split along its cleavage planes and later in filled by quartz.

3.3.4 - K-feldspar

Within the mesosome, K-feldspar is present either as small, granuloblastic, matrix grains or larger porphyroblasts. It often has a perthitic texture over crystals of orthoclase and occasionally microcline twinning is also observed. Some larger K-feldspar porphyroblasts contain possible S1 biotite inclusions, suggesting its stability is syn-D1 or early D2. It is also associated with the large commonly poikiloblastic garnets mentioned previously, and occurs on the edges of melanosomes/mesosomes.

3.3.5 - Plagioclase

This phase is dominantly granuloblastic and equi-dimensional within the main mesosome assemblage or slightly elongate where S2 is strong. It may occasionally have a myrmekitic texture, but this is mostly associated with leucosome assemblages (see Section 3.4.3).

3.3.6 - Quartz

Quartz is a dominant mesosome mineral, but is also present as inclusions with D1 biotite within K-feldspar, garnet and cordierite. Later quartz occurs within symplectites around garnet and cordierite.

3.3.7 - Aluminosilicates

Sillimanite is the dominant aluminosilicate. Throughout most of the terrain sillimanite is not in equilibrium with the D2 mesosome assemblage and is only present as inclusions within cordierite and, less commonly, garnet. However, in the north of the terrain (localities 15, 16, 18) sillimanite is stable with garnet and cordierite as a mesosome phase. In total three generations of sillimanite can be distinguished: (1) D1 sillimanite present as inclusions, (2) a mesosome generation in the north, (3) a later retrogressive generation. Andalusite is only found as a retrogressive phase after cordierite.

3.3.8 - Spinel

Spinel is a rare phase and is usually found associated or included within a sillimanite-free patch of cordierite (Figure 3.8).

3.3.9 - Chlorite

Chlorite is present mostly as a retrogressive phase on garnet, cordierite and biotite. On garnet it mostly appears as a thin halo but is also present in cracks within the garnet crystal. It tends to replace cordierite along with pinite, and often replaces biotite. This replacement of biotite is mostly constrained to the north of the terrain.

3.3.10 - Graphite

Graphite is a rare mesosome phase but is quite common at localities 4 and 6 in the melanosome, where it is found as radiating clusters of acicular crystals or along the edges and cleavage planes of biotite (Figure 3.7).

3.3.11 - White mica

White mica is present as sericite alteration of feldspars and as fine-grained fringes around cordierite across the terrain. White mica alteration is minor in the southern and middle localities but in the north it is quite extensive. K-feldspar, cordierite and biotite all show alteration to radiating crystals of white mica (Figures 3.9 and 3.10).

3.3.12 - Accessory phases

These are monazite and zircons with occasional apatite. Zircons are found dominantly within biotite with their distinctive dark haloes. Monazites are often inclusions within cordierites where they have pale birefringent haloes. Apatite is not constrained to any mineral but is mostly found in granulose mesosomes (Figure 3.11). Opaque phases mostly consist of magnetite and ilmenite (Höltta, 1986).

3.4 - Leucosome assemblages and textures

The mineral assemblages in the leucosomes, and the significant textural reactions are summarised in Tables 3.4 to 3.6. Brief descriptions of all the samples studied can be found in Appendix 3.

3.4.1 - Garnet and cordierite

Garnets within the leucosomes are always poikiloblastic, ranging in size from 3-4 mm to 1.5 cm. The dominant inclusions are rounded or rib-like quartz grains. As in the mesosome the garnets show some alteration, usually to chlorite, green biotite and often cordierite. The alteration and breakdown of garnet rims is more noticeable at

Table 3.4 - Petrographic compositions of leucosomes in the Southern Turku terrain.

Cp pinnitised cordierite, *D2* early, elongate phase, *D3p* later poikiloblastic phase, *D3NP* later non-poikiloblastic, idiomorphic phase, *Gm* green mica, *GR* granular texture
I inclusion in $_1$ garnet, $_2$ cordierite, $_3$ K-feldspar, $_4$ biotite, *IN* interstitial phase, *LP* general leucosome phase,
Myrmekite boundaries (*K* K-feldspar boundaries, *Q* quartz boundaries, *Pl* plagioclase boundaries), *P* porphyroblast,
R retrograde phase of $_1$ garnet, $_2$ cordierite, $_3$ K-feldspar, $_4$ biotite, * phase is a minor component, SER sericite, *TA* tabular leucosome phase

Locality	Sample	Access.	And	Bt	Chl	Crd	Grt	Gr	Kfs	Ms	Myrm	Opaque	Pl	Qtz	Sil	Tur
3.a	**AV1**	Mnz, Zrn, Ap		I_2	R_1	R_1 Cp	D_{3P}	*	TA PER				TA	TA INT		
3.a	**AV2**	Mnz		LP		P Cp			TA				TA	TA INT		
3.a	**AV4**			I_1 R_1	R_1	P Cp	D_{3P} INT		TA PER INT					TA I_1		
3	**D23**				R_2	P Cp				$R_{2,3}$	P/P		TA PER	TA	R_3	
2.1	**D8**	Mnz					D_{3P}		TA PER		K/K			TA IN I_1		
2.2	**D18**	Mnz, Zrn, Ap		$R_{1,2,3}$	$R_{1,3,4}$	R_1	$D_{3NP/P}$	*	TA PER MIC		K/K	*		TA INC		
2.2	**D19**	Mnz, Zrn		INT			D_{3P}		TA PER/MPER				TA	TA INT I_1		
2.2	**AV81**	Mnz		R_1		D_{3P} Cp	D_{3P}		TA PER	SER				INT $I_{1,2}$		
2.3	**D21**	Mnz, Zrn		$R_{1,2}$ I_1	$R_{1,3}$	R_1 Cp	D_{3P}		TA PER	R_2	K/K	*	TA	TA INT I_1 R_1		
2.3	**D22**					P Cp							TA	TA		
2.3	**AV80**			R_3					TA GR	SER	P/Q		TA GR			
2.4	**D1**	Mnz, Zrn					D_{3P}		GR PER	SER	K/Q		GR	TA GR I_1	I_3 LP	
2.4	**D5**	Ap		S		P Cp			TA PER/MPER	SER			GR	TA GR		
4	**AV6**	Mnz		INT I_3	$R_{1,2}$	P Cp	D_{3P}		TA PER/MPER MIC R_3	R_2	K/K			TA INT R_1 I_3	I_3	
4	**AV7**	Mnz, Zrn	TA	LP $R_{1,3}$ I_3	R_4	P Cp	D_{3P}	*	TA PER MIC	SER			LP	TA INT		
4	**AV10**		R_2	$R_{1,2}$ I_3	R_2	P Cp R_1	D_{3P}		TA PER MIC R_1	R_2	Pl/Q		TA	TA I_3 R_1		
4	**AV11**			Gm	R_1		D_{3P}		TA PER MIC	SER				INT $I_{1,3}$		
4	**AV12**	Mnz, Zrn	TA	INT $R_{2,5}$	R_1	P Cp R_1	D_{3P}	*	TA PER MIC	SER		* R_1		TA INT		
4	**AV13**		R_2	$R_{1,2,5}$ Gm I_2	$R_{1,2}$	P Cp R_1	D_{3P}	*	TA PER MIC	R_2				TA I_1 $R_{1,2}$		
4	**AV14**	Mnz, Zrn	TA	$R_{2,5}$ Gm		Cp	D_{3P}		TA PER MIC	R_2	K/Q		LP	INT I_3		
4	**AV60**	Mnz, Ap		R_2 I_2 Gm	R_2	P Cp I_3			TA MPER MIC	SER			TA	TA INT	I_2	
4	**AV92**		LP	INT I_3			D_{3P}		TA PER MIC	SER	K/Q		LP	TA INT		
4	**AV97**	Ap	R_2	INT I_2 R_2		P Cp		*	TA PER MIC	SER R_2			TA	TA INT		
4	**AV98**			INT I_3	R_2	P Cp			TA PER MIC	SER R_2		R_4	TA	TA INT R_4		

Table 3.5 - Petrographic compositions of leucosomes in the Southern Turku terrain.

Cp pinnitised cordierite, *D2* early, elongate phase, *D3p* later poikiloblastic phase, *D3NP* later non-poikiloblastic, idiomorphic phase, *Gm* green mica, *GR* granular texture
I inclusion in $_1$ garnet, $_2$ cordierite, $_3$ K-feldspar, $_4$ biotite, *IN* interstitial phase, *LP* general leucosome phase,
Myrmekite boundaries (*K* K-feldspar boundaries, *Q* quartz boundaries, *Pl* plagioclase boundaries), *P* porphyroblast,
R retrograde phase of $_1$ garnet, $_2$ cordierite, $_3$ K-feldspar, $_4$ biotite, * phase is a minor component, SER sericite, *TA* tabular leucosome phase

Locality	Sample	Access	And	Bt	Chl	Crd	Grt	Gr	Kfs	Ms	Myrm	Opaque	Pl	Qtz	Sil	Tur
8	D29	Coarse Mnz		* R_2		P Cp R_2	D3P		TA MIC		K/K		TA	INT	I_2	*
8	D30	Mnz, Zrn	R_2	$R_{2,3}$ Gm	R_2	P Cp			TA	SER	K/K		TA	TA	R_2	
8	AV122								TA PER/MPER	SER	K/K			TA GR I_3	*	
7	D33	Mnz	R_2	Lp Gm		P Cp			TA PER R_4	SER R_2	K/Q			TA GR	R_2	
7	D34	Mnz		*					TA PER	R_2			TA	TA		
7	D35	Mnz, Zrn, Ap		R_1 Gm			D_{2P}		TA PER		K/K		TA	TA I_1		
7	D36	Mnz		* I_1		P D_{3P}			TA PER R_3	R_2			TA	INT I_1		
7	D37	Mnz		*		P Cp			TA MPER R_4		K/Pl		TA	TA INT		
7	D41	Mnz, Zrn		$R_{1,2}$	R_2	D_2 Cp R_1 I_1	D_{3P}	*	INT MPER		K/K		TA	$R_{1,2}$ I_1	I_2	
6	AV16	Mnz, Zrn	R_2	$R_{1,3}$ Gm	$R_{1,2}$	P Cp R_1	D_{3P}	*	TA MPER	SER		* I_1		TA GR I_1		
6	AV17A	Mnz	R_2	$R_{1,3}$ Gm	R_2	P Cp			TA PER	SER	K/K			TA GR		
6	AV105	Mnz		R_1	$R_{1,4}$		D_{3P}		TA PER R_4	SER			TA	TA GR		
6	AV107	Coarse Mnz	TA	LP		Cp LP			TA MPER R_4	SER	K/K	*	LP	TA INT		
6	AV110	Mnz, Zrn, Ap	TA	$R_{1,3}$ $I_{1,3}$	$R_{1,2}$	P Cp R_1	D_{3P}		TA MPER	SER			TA	INT	*	
6	AV112	Mnz, Zrn, Ap	TA R_2	R_1 I_3	$R_{1,2}$	P Cp R_1	D_{3P}	*	TA MPER	R_2 SER	Gr K/K		TA	INT	I_2	
6	AV117	Mnz, Zrn	R_2	LP		Lp Cp			TA PER	SER	Gr/MYRM		TA	TA INT		
17	AV137			R_3	R_4				TA PER	R_3 SER		R_4	TA	INT	LP	
17	AV138			R_3	$R_{3,4}$				TA PER R_4	$R_{3,4}$ SER			TA	INT	LP	
17	AV140				$R_{3,4}$				TA PER GR	SER				INT	LP	
17	AV145			R_3	$R_{3,4}$	EDGE	D_{3NP}		TA	R_3				TA INT	R_3	
22	AV154				R_1		D_{3P}	*	TA PER	R_3				TA INT I_3		

Table 3.5 - Petrographic compositions of leucosomes in the Southern Turku terrain.

Cp pinnitised cordierite, *D2* early, elongate phase, *D3p* later poikiloblastic phase, *D3NP* later non-poikiloblastic, idiomorphic phase, *Gm* green mica, *GR* granular texture
I inclusion in $_1$ garnet, $_2$ cordierite, $_3$ K-feldspar, $_4$ biotite, *IN* interstitial phase, *LP* general leucosome phase,
Myrmekite boundaries (*K* K-feldspar boundaries, *Q* quartz boundaries, *Pl* plagioclase boundaries), *P* porphyroblast,
R retrograde phase of $_1$ garnet, $_2$ cordierite, $_3$ K-feldspar, $_4$ biotite, * phase is a minor component, SER sericite, *TA* tabular leucosome phase

Locality	Sample	Access	And	Bt	Chl	Crd	Grt	Gr	Kfs	Ms	Myrm	Opaque	Pl	Qtz	Sil	Tur
11	AV129	Mnz, Zrn	R_2	R_3	R_4	P Cp			TA PER	SER R_2				TA	LP	
11	AV131	Mnz, Zrn		LP	$R_{3,4}$			*	TA PER	SER	K/Q	*	TA	TA INT	LP R_4	
5	AV102	Mnz, Zrn, Ap		LP		P							TA	TA GR I_2	$I_{2,3}$	
5	AV103	Mnz, Zrn, Ap		$R_{1,2}$		P Cp R_2	D_{3P}	*		R_2			TA	TA	R_2	R_2
5	AV104	Mnz, Zrn		R_2 Gm		P Cp		*		$R_{2,3}$		*	TA	TA	R_2	
12	D43	Mnz, Zrn		R_1 I_1 Gm	R_1		D_{3P}	*						R_1 I_1		
12	D46			R_2 EDGE		P Cp			TA PER	R_2	Pl/Q/K		TA GR	TA GR	I_2 *	
12	D47	Mnz			R_2	P Cp D_{3P} D_2			TA PER		Pl/K		TA GR	GR	I_2 *	
12	AV19	Mnz, Zrn		LP R_2	$R_{2,3,4}$	P Cp R_1	D_{3NP}	R_4	TA PER R_4	$R_{2,3}$				TA	I_2	
16	AV136			R_1			D_2 D_{3P}		TA PER					INT R_1	LP R_1 I_1	
18	AV143	Mnz, Zrn		LP $R_{1,2}$		R_1	D_{3P}		TA PER R_4	SER	K/K		TA MY	INT		
20	AV30	Mnz, Zrn		$R_{2,3}$	$R_{2,3}$	P Cp			TA PER	SER $R_{2,3}$				INT $R_{2,3}$		
19	AV21	Zrn		$R_{2,3}$ Gm	$R_{2,4}$	P Cp		*	TA PER MIC	SER $R_{2,3,4}$	K/Q		TA	INT	$R_{3,4}$	LP

the edges of the leucosomes where a symplectite of brown biotite and quartz occurs. One texture to note is within sample 4 where garnet is interstitial between quartz grains (Figure 3.12).

Cordierite is present as porphyroblasts within most leucosomes. It may be present as large idiomorphs with sillimanite inclusions in the cores, or as patches in association with quartz. The cordierites with sillimanite-rich cores often form in clusters at the edges of the large leucosomes or are present throughout the smaller (3-4 cm) leucosomes, and may represent entrained mesosome material. Other cordierites are riddled with quartz inclusions and are non-idiomorphic, comparable to garnets with similar net textures (Figure 3.13).

Most cordierites within the leucosomes have suffered some degree of pinitisation, which is usually more pronounced than in mesosome cordierites. In addition to the alteration of cordierite to pinite, the minerals chlorite, green biotite, white mica and andalusite are all retrogressive after cordierite (Figure 3.14). As with feldspars, the degree of alteration of cordierite increases northwards in the terrain, until only coarse white mica crystals are found within a fine grained, altered ground mass. Heavily pinitised cordierite also replaces garnet. Field observations indicate that some leucosomes have preferentially crystallised cordierite, others garnet, and still others contain both phases.

3.4.2 - Biotite

In small intimate segregations and in the very large granitic sheets, biotite is a leucosome phase. It also often occurs as an alteration phase around garnet where it often forms symplectitic growths with quartz, cordierite and sometimes K-feldspar. In some heavily altered leucosomes, biotite has been replaced by a chlorite with anomalous blue or purple polarisation colours (Figure 3.15).

3.4.3 - Felsic minerals

Leucosome feldspars are mostly perthites or micro-perthites. These generally occur as large tablets that have irregular contacts with other crystals. Often the boundaries are curved, embayed and sometimes lobate. Microcline is also seen at some localities, notably locality 4 where a perthite texture has exsolved after the development of the microcline twinning (Figure 3.16). Potassium feldspars are the dominant feldspars in these leucosomes but plagioclase is often present in smaller quantities. In one or two leucosomes large plagioclase tablets with fine lamellar twinning dominate (Figure 3.17).

Both feldspars often have a twinkly appearance in crossed polars from sericite alteration, which also gives the crystals a turbid appearance under plane polarised light. In the far north of the area, white mica alteration becomes much coarser up to the western end of the Hähää road (Figure 3.1), where coarse plates of white mica replace K-feldspar (Figure 3.18). In some cases new biotite replaces feldspar along with chlorite and occasionally sillimanite.

Quartz is usually interstitial between the larger feldspar grains, but may also form large tabular crystals. In some leucosomes it forms rims of much smaller grains around larger crystals (Figure 3.19) and the presence of the smaller grain mantles on the larger tabular crystals is indicative of some deformation after a melt has crystallised. It often has undulose extinction and some crystals appear strongly cracked. Together with the breakdown into much smaller grains, this may be indicative of deformation whilst solid. Quartz is ubiquitous as inclusions within feldspars and other poikiloblastic phases.

Myrmekites, a symplectite of quartz and sodic plagioclase (Smith and Brown, 1988), are a major feature of the Turku leucosomes (Figure 3.20). These mostly form as small patches on the edge of large K-feldspar grains adjacent to plagioclase, quartz or other K-feldspar tablets. These myrmekite textures can be categorised as textures B (intergranular myrmekites) and D (megacryst margin myrmekites) according to the classification of Philips (1974). At locality 6 (from the middle of the terrain), one of

the leucosomes displays a granophyric texture formed by quartz and K-feldspar intergrowth (Figure 3.21).

3.4.4 - Aluminosilicates

Sillimanite is only present within southern leucosomes and most middle localities as inclusions in entrained mesosome cordierite. However it is present as a leucosome phase in localities further south than those in which it is seen as a mesosome phase. In the northern localities sillimanite becomes a major leucosome phase that often grows over the grain boundaries of cordierite from the inclusion rich core. In some places it is retrogressive on K-feldspar and, rarely, biotite.

Andalusite is sometimes retrogressive on cordierite but it is also a leucosome phase in its own right where it forms crystals with square basal sections and rectangular long sections (Figure 3.22). This is seen at both localities 4 and 6 where there is a high degree of leucosome material in the outcrops.

3.4.5 - Graphite

As within the mesosome assemblages, graphite is a common phase within leucosomes. It is generally associated with other minerals such as garnet, cordierite and biotite and is usually present as platelets (Figure 3.14).

.

3.4.6 - Muscovite

White mica is common in leucosomes as sericite alteration in association with feldspars. Most of the feldspar crystals have a speckly appearance from variable sericite. The northern leucosomes are typified by a high degree of white mica alteration, with many K-feldspar tablets being consumed by coarse needles of muscovite (Figure 3.18). Muscovite also grows as a retrogressive phase around cordierite and biotite (Figure 3.23).

3.4.7 - Tourmaline

Crystals of tourmaline are rare. They can be seen growing on the edge of large cordierite crystals in association with quartz at locality 5 (Figure 3.24). These tourmaline crystals are coarser than the smaller basal sections seen elsewhere and this texture is not seen anywhere else.

3.4.8 - Accessories

The accessory phases are the same as in the mesosome but apatite is not as common. Monazite and zircon are mostly found within cordierite, garnet and biotite. Leucosomes without these major mafic phases are generally poor in accessories. However, in two of the orange granitic sheets from the middle localities, coarse 2 mm monazites can be found in felsic minerals as a leucosome phase (Figure 3.25 - black material is K-feldspar in extinction).

3.5 - Selvage assemblages

At northern and some southern localities, selvages may be found bordering individual leucosomes. They are mostly 2-5 mm wide on small (2-5 cm) leucosomes, but at localities 12 and 20 coarse selvages up to 20 cm wide are observed. Figure 3.26 illustrates a typical selvage showing coarse laths of biotite orientated roughly parallel to the mesosome edge. This is often found together with elongate cordierites, and sometimes quartz. These selvages are often seen in conjunction with more rounded cordierites that have formed at the very edge of the leucosome and main biotite-rich selvage. Both the elongate and more rounded cordierites contain sillimanite-rich cores which suggest that the cordierite in the leucosomes is a mesosome phase mantling the edge of the leucosome.

One feature observed during field work (Chapter 2) was the presence of compositionally layered pods that were boudinaged out along S2. Two pods were sampled from locality 2 (samples D6 and D16). One had a plagioclase + quartz + diopside assemblage with tremolite retrogressive on the diopside. This assemblage is

representative of a calcium rich protolith. The second sample, however, contains a garnet + spinel + sillimanite + cordierite assemblage which is more suggestive of an aluminous, silica-poor protolith. As these assemblages are rare they will not be discussed in this study in the context of the metamorphic evolution of the Turku terrain.

3.6 - Discussion

The petrographic descriptions provide information on the structural and metamorphic evolution of the Turku terrain. The textures observed within the leucosomes also give clues to the conditions under which melting took place and the crystallisation of the melt material.

3.6.1 - Structural evolution

Clues to the earliest metamorphic fabric are the mineral inclusions of sillimanite, biotite and quartz within later generations of cordierite, K-feldspar and garnet. Whilst the fibrous sillimanite inclusions show no particular orientation, quartz and biotite are oblique to the dominant foliation, identified in the field as S2 following the structural classification of Väisänen et al. (1994). Thus these inclusions may be remnants of an S1 fabric.

S2 can generally be seen in thin section by the orientation of biotites in the compositionally more aluminous layers. As could be seen in the field, there are early generations of garnet and cordierite that are elongate along S2, containing the aforementioned inclusion trails.

The gentle F3 folding that is seen on an outcrop scale is sometimes evident as a slight crenulation of S2. The deformation does not generally manifest itself in any new generations of mineral growth, but S3 is evident in the form of elongate cordierites at locality 2, which grew parallel to an F3 axial trace trapping S2 as inclusion trails across the crystal.

3.6.2 - Metamorphic evolution

During D1, sillimanite (Sil 1) and biotite (Bt 1) appear to have been stable throughout the terrain as they are found as inclusions within cordierite, K-feldspar and garnet, with the biotite inclusions indicating a relict S1 foliation. Late in D1 or early in D2, garnet (Grt 1), cordierite (Crd 1) and K-feldspar (Kfs 1) became a stable assemblage over a large part of the terrain by general stabilisation of this assemblage in place of sillimanite and biotite. Melting also occurred during this time so the following reactions 3.1-3.3 occurred, depending upon bulk composition.

biotite + sillimanite + quartz = cordierite + K-feldspar + melt (3.1)

biotite + sillimanite + quartz = garnet + K-feldspar + melt (3.2)

biotite + sillimanite + quartz = garnet + cordierite + K-feldspar + melt (3.3)

These relationships appear similar to those formed in samples showing garnet and cordierites with sillimanite and biotite inclusions from the Reynolds Range, Australia (Buick et al., 1999). Buick et al. (1999) attribute the textures to garnet and cordierite forming as peritectic phases through the above reactions. The products of these reactions are dependent upon the bulk composition of the rocks undergoing melting, as shown by experimental data of partial melting within pelitic rocks (Thompson, 1982; Le Breton and Thompson, 1988; Vielzeuf and Holloway, 1988; Patino Douce and Johnston, 1991). Cordierite is preferentially crystallised in highly magnesian bulk compositions or at low pressures, whereas higher pressures favour garnet and Fe-rich bulk compositions.

Spinel is present at both localities 2 and 3 as inclusions within cordierite along with sillimanite. This texture is seen in rocks from the Bohemian Massif, Germany where Kalt et al. (1999) considered it to be a product of the following reaction:

biotite + sillimanite + quartz = spinel + K-feldspar + cordierite + melt (3.4)

This garnet-absent reaction emanates from the [Opx] invariant point of Fitzsimons (1996) in the petrogenetic grids related to the pelites of the Brattstrand Bluffs and is a lower pressure melting reaction than 3.1-3.3.

During late D2 to early D3 the Turku terrain suffered a late thermal pulse (Van Duin and Nieman, 1993; Väisänen et al., 1994) coinciding with the formation of recumbent F3 folds. Later generations of garnet, cordierite and melt were the products of further melting reactions with sillimanite being totally consumed in most localities. This melting produced large poikiloblastic garnets with coarse quartz inclusions in contact with coarse K-feldspar. This generation of garnet (Grt 2) has the textural appearance of a garnet formed in the presence of melt through melting reactions 3.2 and 3.3 (Waters and Whales, 1988; Powell and Downes, 1990; Whales, 1990). Second generations of cordierite (Crd2) and K-feldspar were also products of partial melting following equations 1 and 3. There is, however, a limit to the amount of melt produced following these dehydration melting reactions as sillimanite is completely consumed by earlier melting in the southern and middle localities. This points towards a conclusion that some of the melt found at these localities may have an external source or that melting was enhanced by the introduction of an H_2O-rich fluid during this later thermal episode.

In the middle of the Hähää road in the north of the terrain, sillimanite is stable with garnet and cordierite. This sillimanite, a later generation than the inclusions within cordierite, is most abundant to the west end of the Hähää road. At locality 19, garnet is not present and the mesosome assemblage is crd + sil + bt + kfs + qtz. Cordierite dominates this assemblage and is present as large weathered ellipsoids, which in thin section can be seen to contain biotite and quartz inclusions. As this texture is also seen in cordierites from garnet- bearing assemblages in the north, it is inferred that the cordierite + sillimanite assemblage was coeval with the garnet + cordierite

assemblage, suggesting a temperature gradient from locality 12 to 19, and from the north to the middle/south of the terrain.

By late D3, conditions had cooled slightly (Väisänen et al., 1994; Väisänen and Höltta, in press) and the terrain suffered some retrogression of both mesosome and leucosome assemblages. Retrogression is particularly pronounced in the north, where melt extraction and separation was not as advanced as in other parts of the terrain. Across the terrain garnet is mantled by biotite + quartz symplectites (Figure 3.6) and altered cordierite. This is especially true for those poikiloblastic garnets that grew in or near melt. Therefore this texture may be representative of a back reaction (equation 3.5) with any fluid that has remained in the system after the crystallisation of the melt (Powell and Downes, 1990).

garnet + K-feldspar + V/melt = biotite + quartz + cordierite (3.5)

Whilst alteration of cordierite to pinite is common across the whole terrain, further retrogression is seen in the alteration of cordierite, and of K-feldspar, to first biotite and sillimanite and then to lower temperature muscovite. Cordierite also shows later alteration to fine grained andalusite. Thus evidence for the occurrence of reactions 3.6 and 3.7 exists in the Turku terrain, especially within the northern zone.

cordierite + K-feldspar + H_2O/melt = biotite + sillimanite + quartz (3.6)

K-feldspar + sillimanite + H_2O = muscovite + quartz. (3.7)

The metamorphic history of the Turku terrain is outlined in Table 3.7 with reference to the timing of the associated structural events of Väisänen et al. (1994).

Table 3.7 - Mesosome assemblages linked to major deformation periods.

Time Ma (Väisänen et al., 1994)	**Deformation period** (Väisänen et al., 1994)	**Mineral generations**
Pre 1890	D1	Sil 1 Bt 1 Qtz 1
1890-1870	D2	Grt 1 Crd 1 Kfs 1 Bt 2 Sil 2 Pl 1 Qtz 2 Gr **Tur** Spl
1870-1830	D3	Grt 2 Crd 2 Kfs 2 Bt 3
1830-1800	Late D3 to D4	Bt 4 Crd 3 And 1 Chl 1 Ms 1 Sil 3

Tur Tourmaline is found sporadically throughout the terrain both as a mesosome and leucosome phase.

3.6.3 - Leucosome generation

As discussed in Chapter 1, migmatite formation in many different terrains has been attributed to a number of mechanisms: the most commonly accepted is by partial melting of the surrounding protolith by dehydration melting, producing melts under low a_{H2O} conditions (Philips, 1980; Powell, 1982; Waters and Whales, 1984; Waters 1988; 1990; Harley, 1989). As well as the previous textural information that supports the occurrence of melting reactions 3.1-3.3, textures within the leucosomes also support the theory that they represent sites of segregated melt material:

1. The phases in the leucosome portions often have irregular grain contacts, i.e. lobate or embayed, unlike the straight contacts of mesosome or melanosome phases (Figure 3.2). The leucosome phases are also coarser grained and these textures are characteristic of originally molten material (Ashworth, 1985; Ashworth and McLellan, 1985).
2. In the field it can be seen that most leucosomes are oblique to the main foliation, S2 (Väisänen et al., 1994). This supports intrusion of the material rather than metamorphic segregation (Johannes, 1983).
3. Myrmekitic and granophyric textures are found within the Turku leucosomes. Myrmekites are features of many plutonic rocks (Smith, 1974, Garcia et al, 1991), such as the Rapakivi granites of southern Scandinavia, the Ambaspitya granitoids of Sri Lanka and the Velay granites of France (Eskola, 1914; Mathavan, 1991; Vernon, 1991). Becke (1908) suggested that myrmekites were the product of metasomatism after fluids were expelled upon crystallisation of the melt. Recent models still utilise this basic premise (Mathavan, 1991). Garcia et al (1991)

suggested that when a late, magmatic fluid came into contact with the Kfs + plag + qtz assemblage of the Velay granites, its relatively sodic composition reacted with the calcium content in the plagioclase. The fluid moved towards higher CaCl2 and KCl contents to maintain equilibrium with the feldspars. The plagioclase was replaced by more sodic plagioclase and the K-feldspar by quartz and plagioclase intergrowths. Vernon (1991) points out that deformation indirectly aids the production of myrmekitic textures by facilitating access of fluids to growth sites.

4. As mentioned previously, poikiloblastic textures of garnet and cordierite mantled by K-feldspar and quartz are indicative of growth within a melt (Powell and Downes, 1990).

Melting as a method for lowering the a_{H2O} of a terrain is linked to the supposition that the melts and dissolved volatiles leave the system (Powell, 1982; Waters, 1984; Water and Whales, 1988). In the north of the Turku terrain, the presence of selvages on leucosomes and the replacement of anhydrous leucosome assemblages by hydrous phases, may suggest that some of the fluids expelled upon melt crystallisation were not removed from the system. In the middle and south of the terrain, retrogression is not seen to the same extent although there is a much larger proportion of leucosome material at these localities (see Chapter 1). The presence of melt-filled shear zones in the middle and south may indicate that these zones acted as conduits for melt and fluid extraction in a more open system. Later chapters will provide insights into the fluid regime present at the time of melting.

Figure 3.3 - Sample 88a: an aluminous layer with D2 elongate garnets, biotite and basal sections of tourmaline. The garnets contain elongate sillimanite inclusions, biotite and tourmaline. S2 has been gently refolded by an F3 fold. Field of view = 6mm. Locality 3

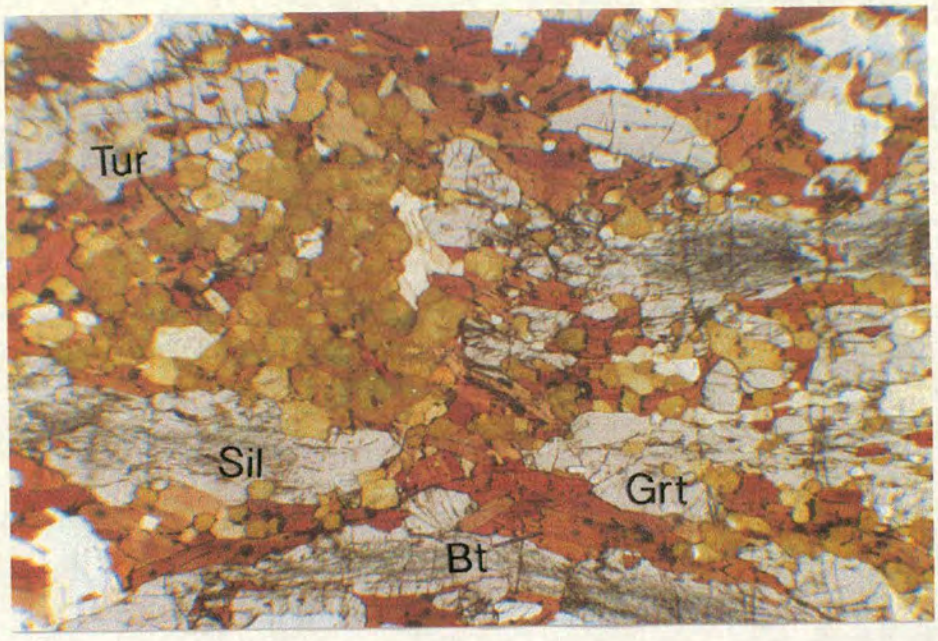

Figure 3.4 - Sample 83: large D3 poikiloblastic garnet with quartz inclusions and coarse biotite and cordierite crystallising on the edges. This texture may be interpreted as a retrogression texture; the garnet is interpreted as a product of dehydration melting. Field of view = 4mm. Locality 2.

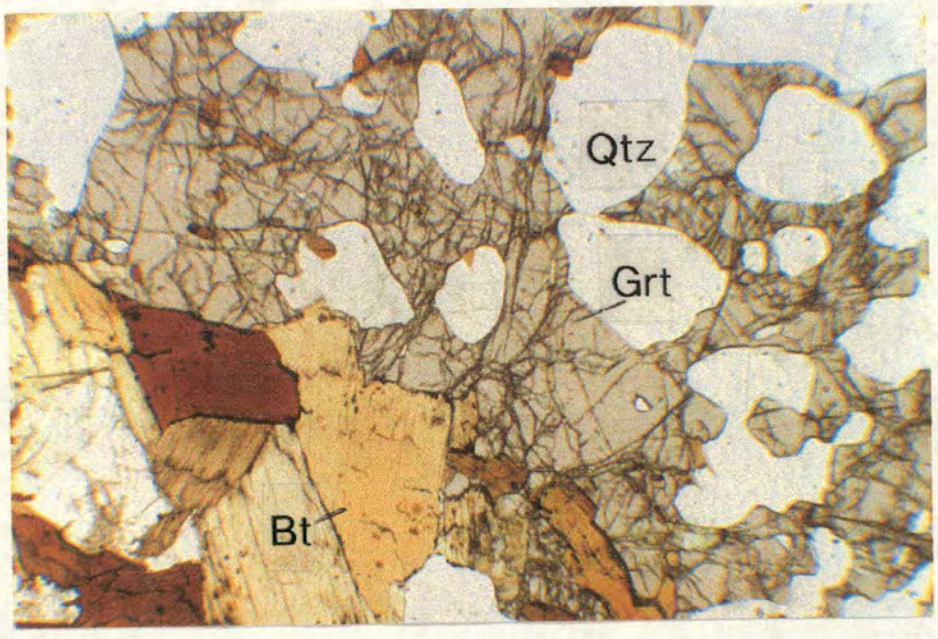

Figure 3.5 - Sample 22: large mesosome cordierite with foliated biotite and quartz aligned in S1. Field of view = 4mm. Locality 19.

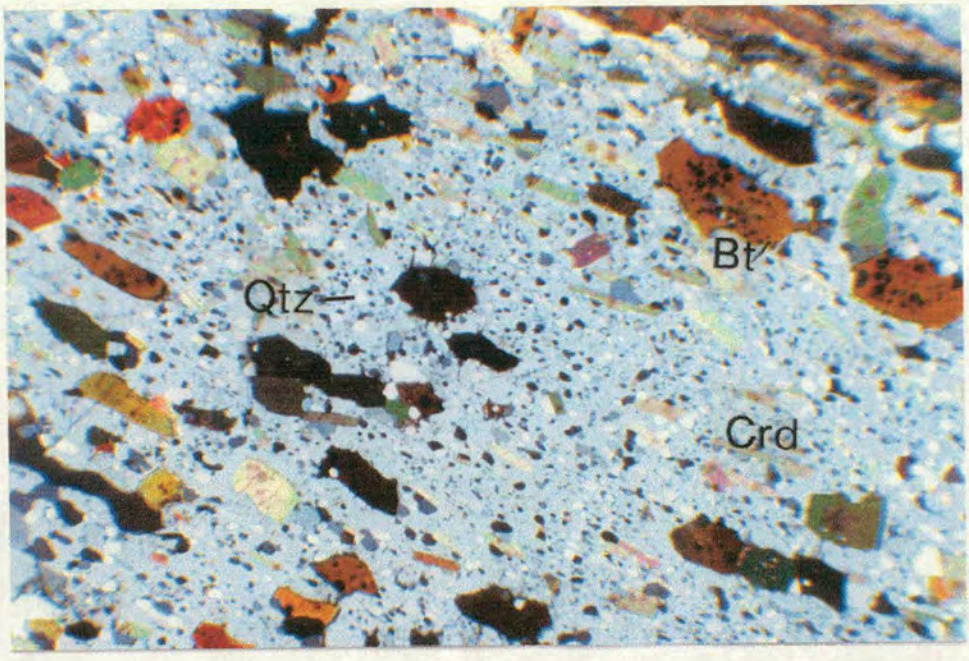

Figure 3.6 - Sample D41: biotite and quartz symplectite at the edge of a D3 garnet. Cordierite and acicular graphite are also crystallising on the garnet edge. Field of view = 1mm. Locality 7.

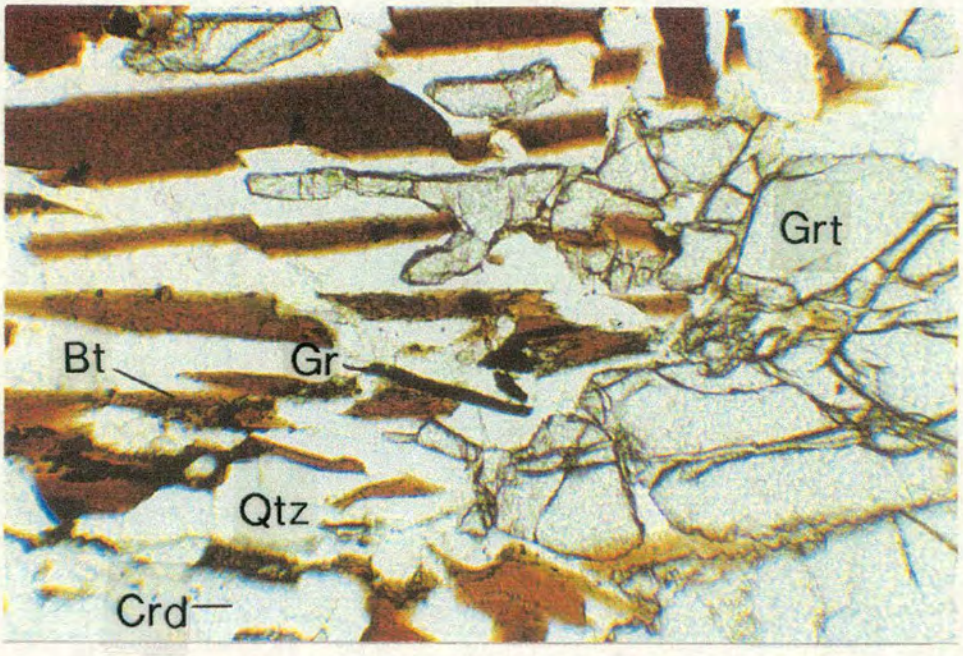

Figure 3.7 - Sample 6b: melanosome biotite with graphite along cleavage planes. This is a common association throughout the terrain. Field of view = 2 mm. Locality 4

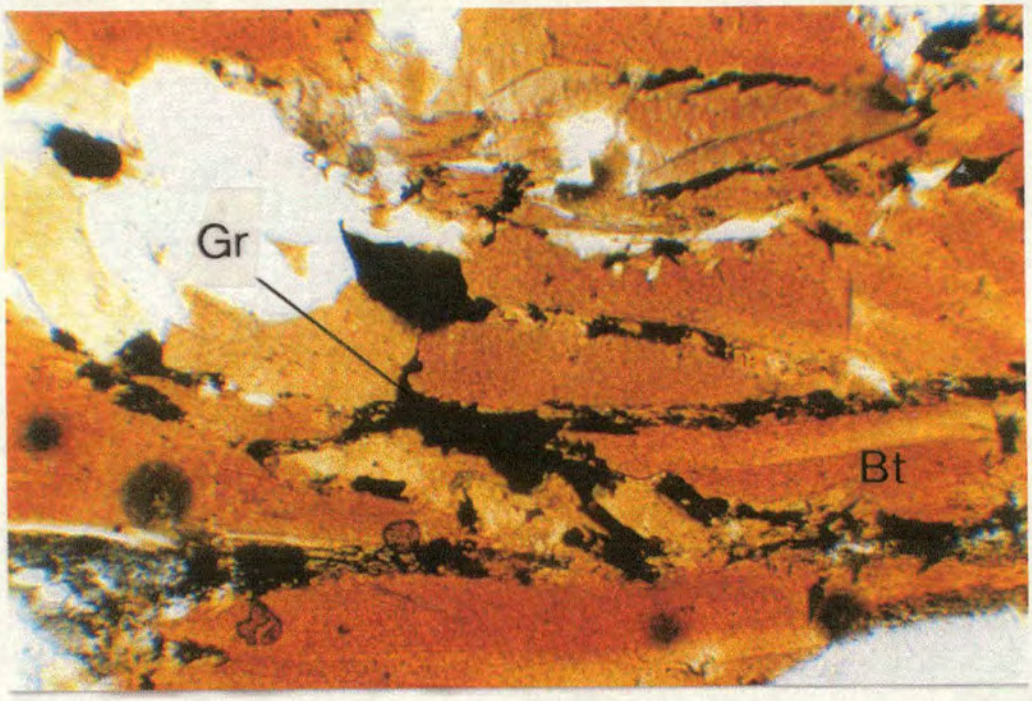

Figure 3.8 - Sample D13: cordierite with green spinel inclusions and foliated sillimanite within a mesosome sample. Spinel is a rare phase that is normally found associated with cordierite. Field of view = 1 mm. Locality 2.

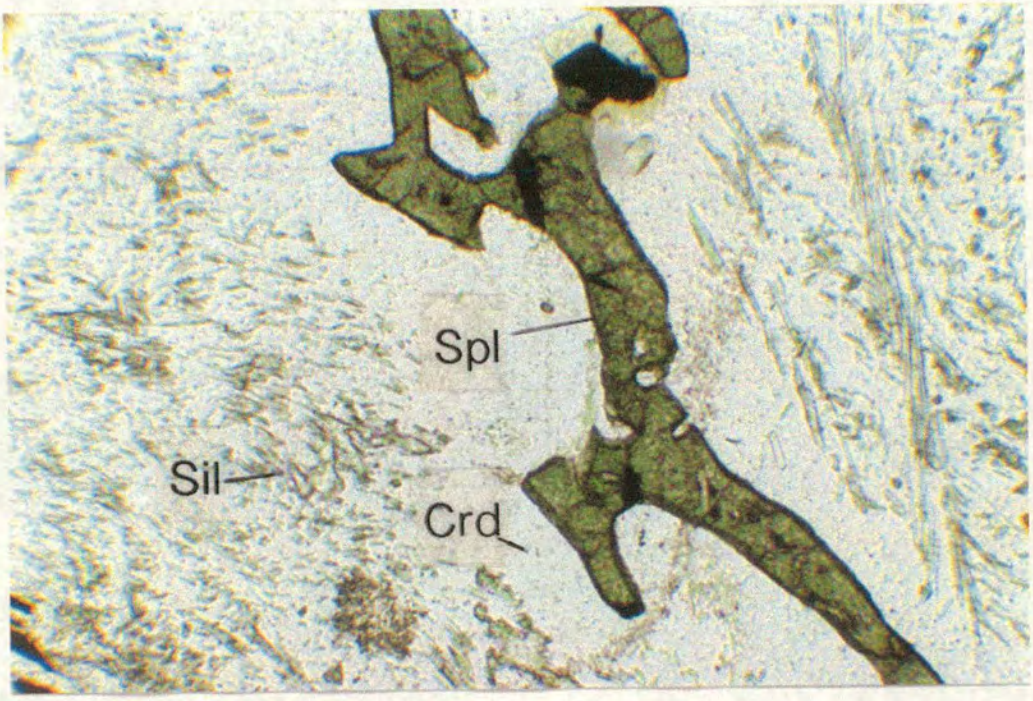

Figure 3.9 - Sample D37: white mica alteration of twinned mesosome cordierite along cracks in the crystal. Cordierites in the north of the terrain are particularly affected by this form of alteration. Field of view = 0.5 mm. Locality 7

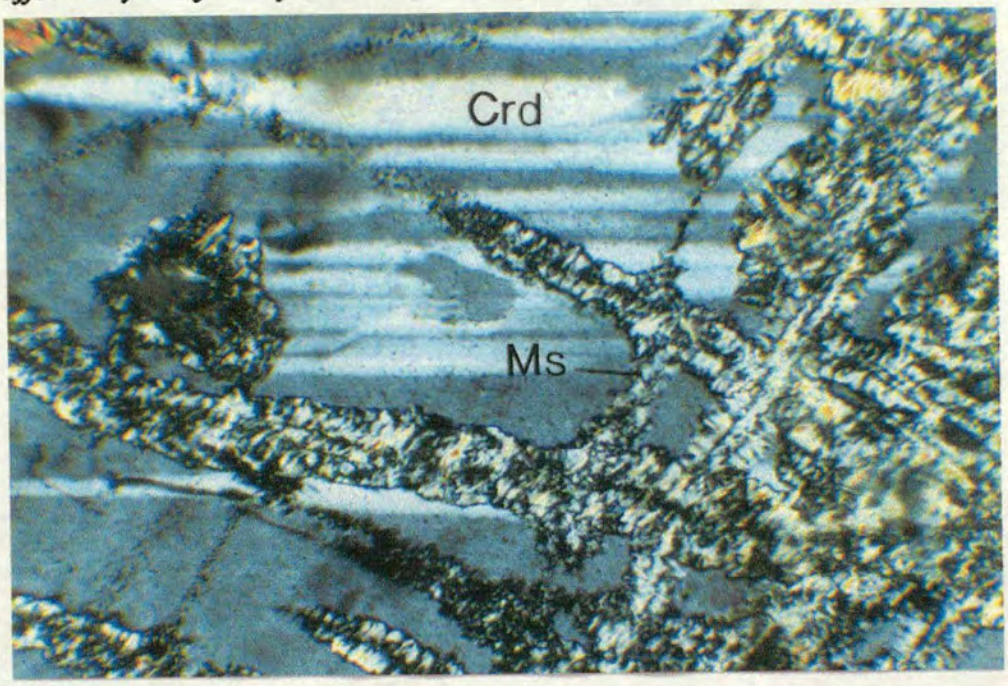

Figure 3.10 - Sample 21: white mica alteration at the edges of mesosome biotite, a common retrogression feature from the northern localities. Field of view = 1 mm.

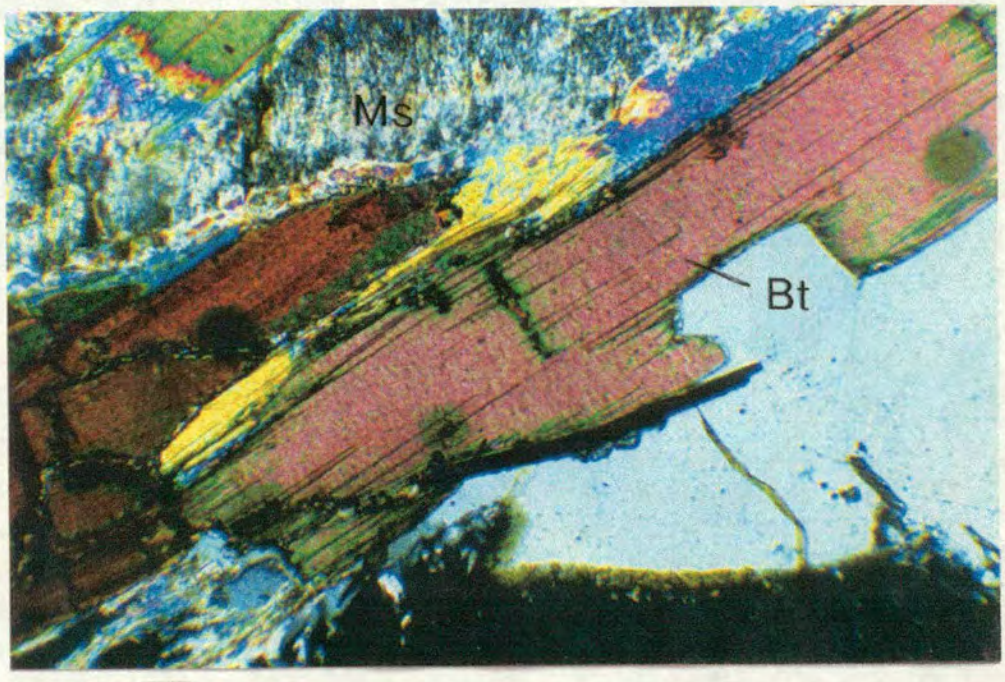

Locality 19

Figure 3.11 - Sample D40: granuloblastic mesosome with abundant apatites. Field of view = 1 mm. Locality 7

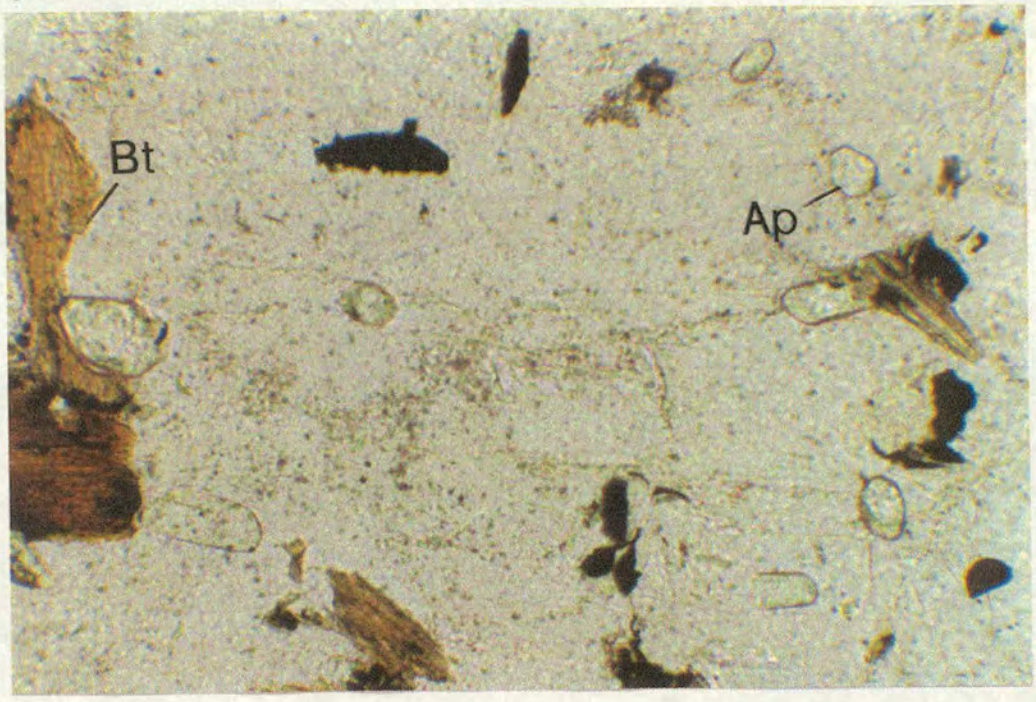

Figure 3.12 - Sample 4 : a small leucosome with garnet that has grown interstitial between quartz. This sieve texture is an extreme version of a poikiloblastic texture. Field of view = 5 mm. Locality 3.

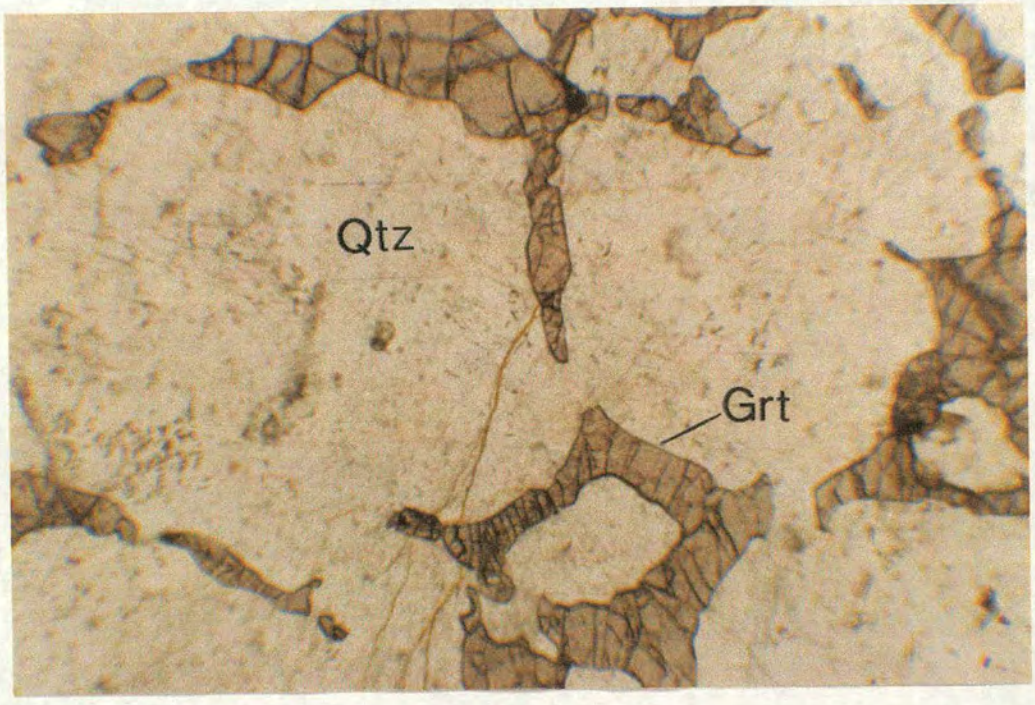

Figure 3.13 - Sample 81b: poikiloblastic cordierite near to garnet with the same texture from a large leucosome with a high proportion of both minerals. Field of view = 4 mm. Locality 2.

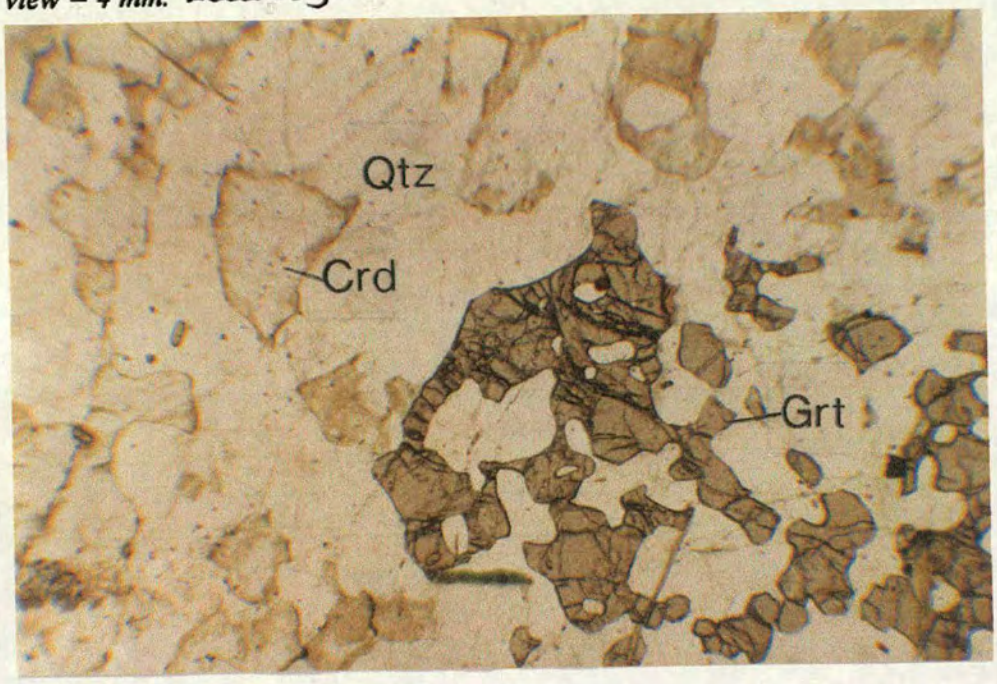

Figure 3.14 - Sample 20: badly pinitised cordierite within a small leucosome. The cordierite is also altered to green and brown biotite with radiating, acicular needles of graphite in association. Field of view = 6 mm. Locality 12.

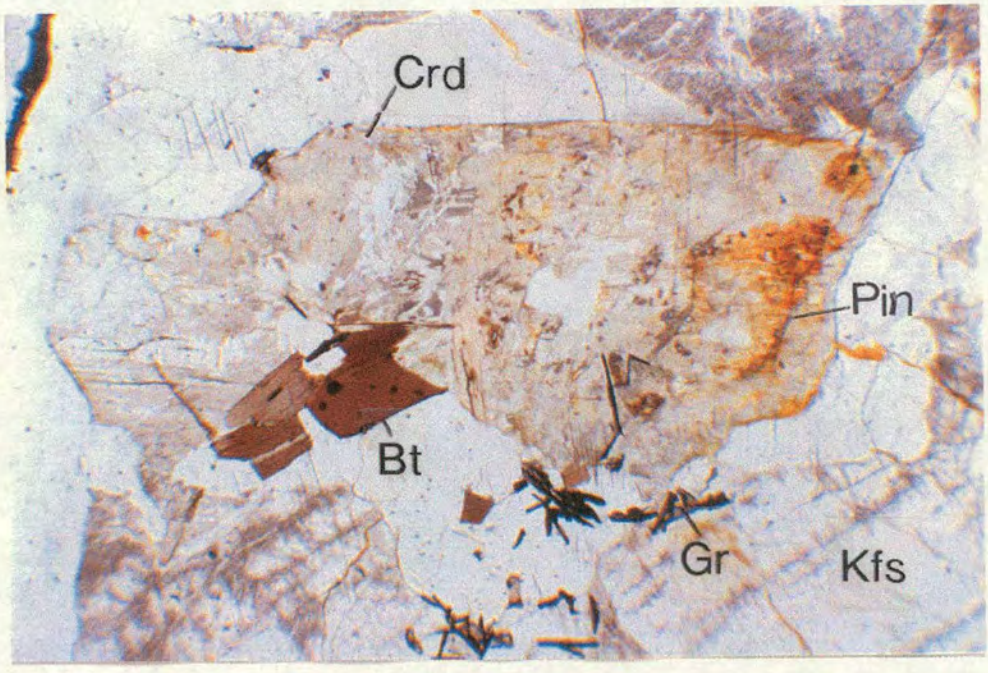

Figure 3.15 - Sample 19: altered biotite crystal from within a patchy leucosome. Chlorite has almost totally replaced the original biotite. This sample is highly altered, as can be seen by the white mica replacement of the potassium feldspars. Field of view = 1 mm. Locality 12.

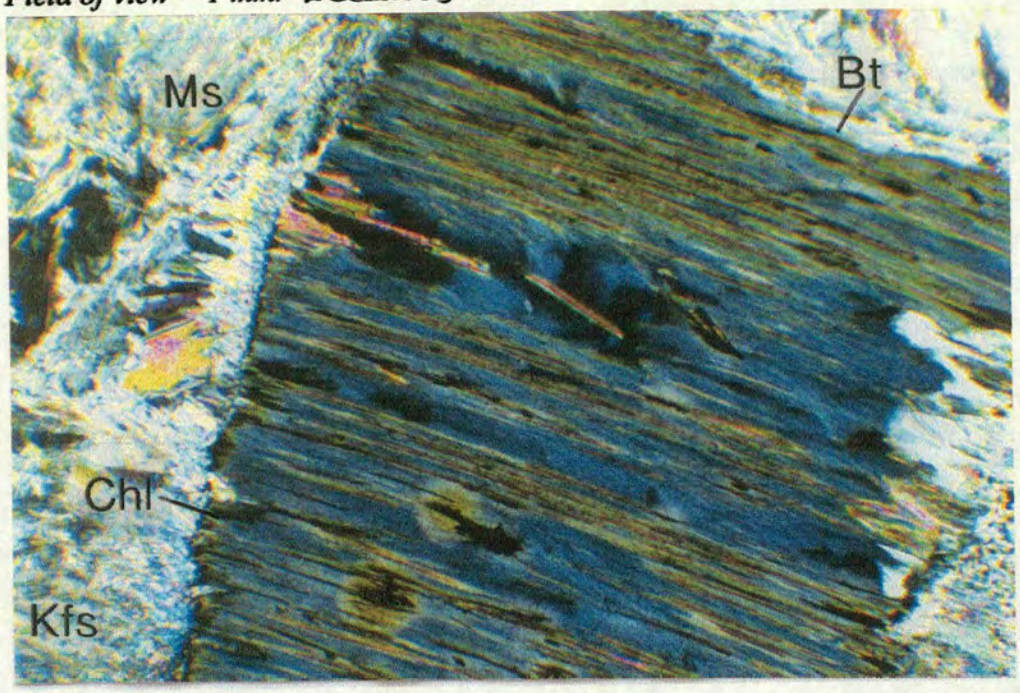

Figure 3.16 - Sample 12a: perthite texture overgrowing microcline feldspar, surrounded by quartz with undulose extinction. Field of view = 1 mm. Locality 4

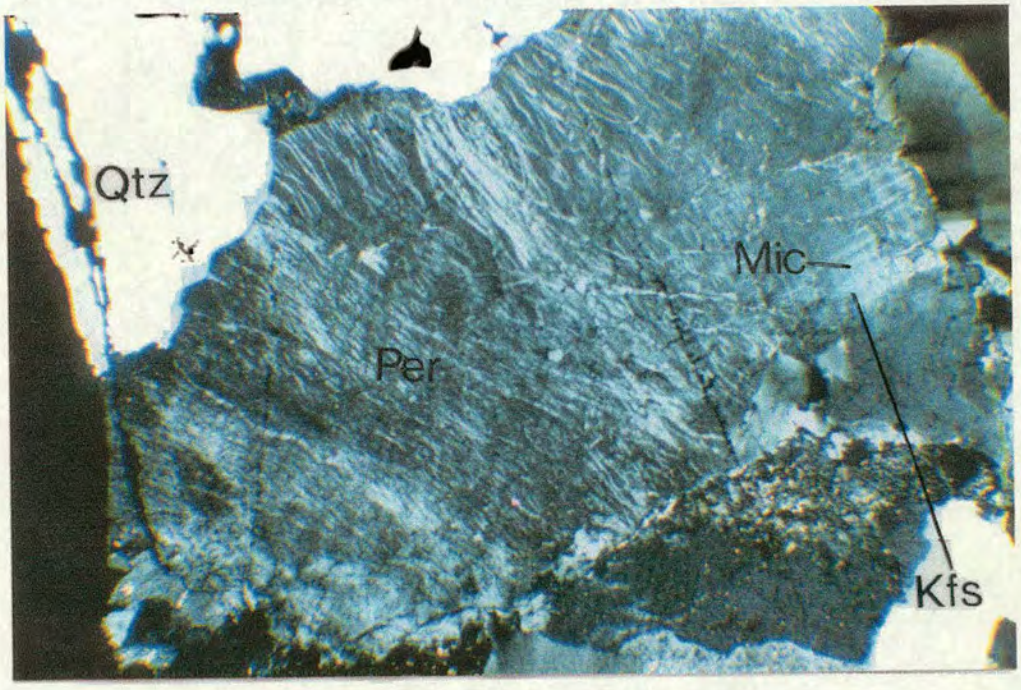

Figure 3.17 - Sample 103: plagioclase crystal within a small, selvage-bound leucosome. The plagioclase has very thin lamellae and some sericite alteration. Field of view = 1 mm. Locality 5

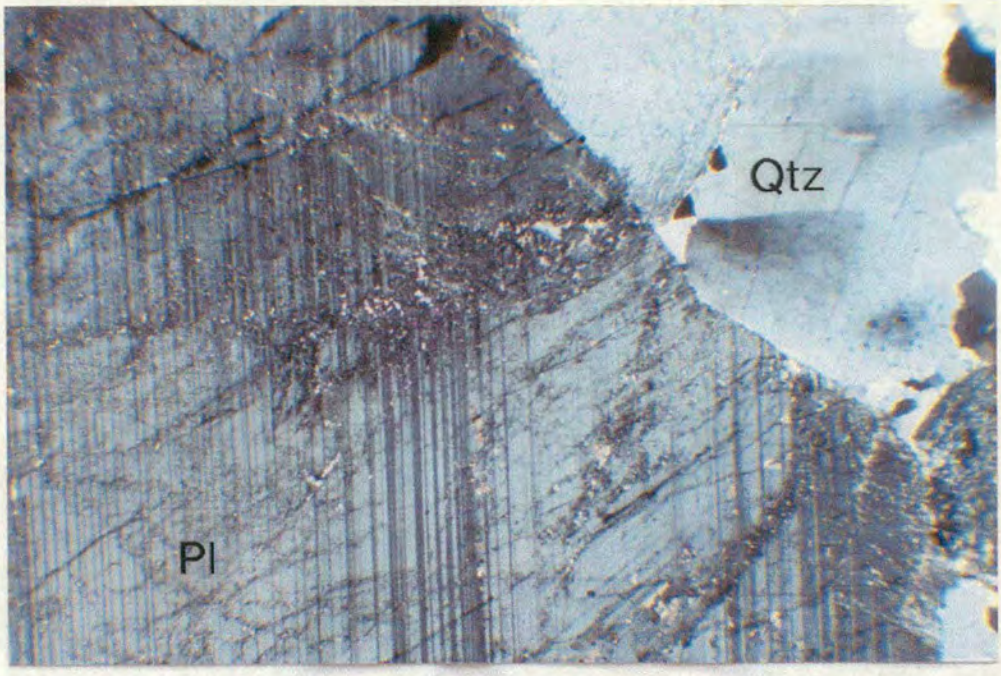

Figure 3.18 - Sample 30: strong alteration of K-feldspar to white mica and quartz within a small leucosome. Field of view = 4 mm. Locality 20.

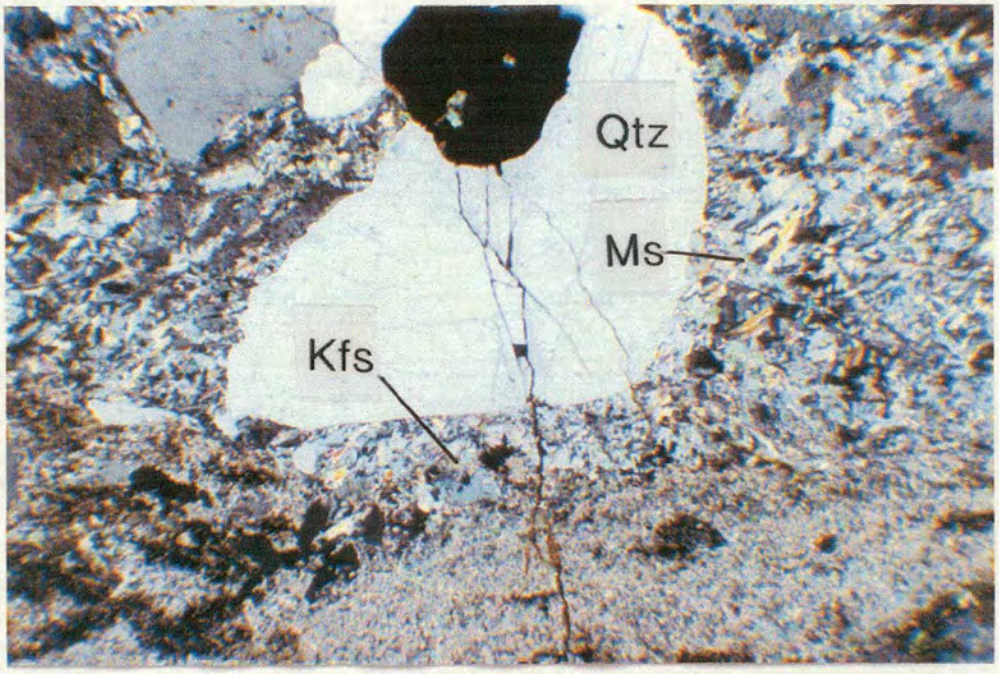

Figure 3.19 - Sample 99: small quartz grains that are growing on the edge of much larger quartz and feldspar crystals. Field of view = 1 mm. Locality 4.

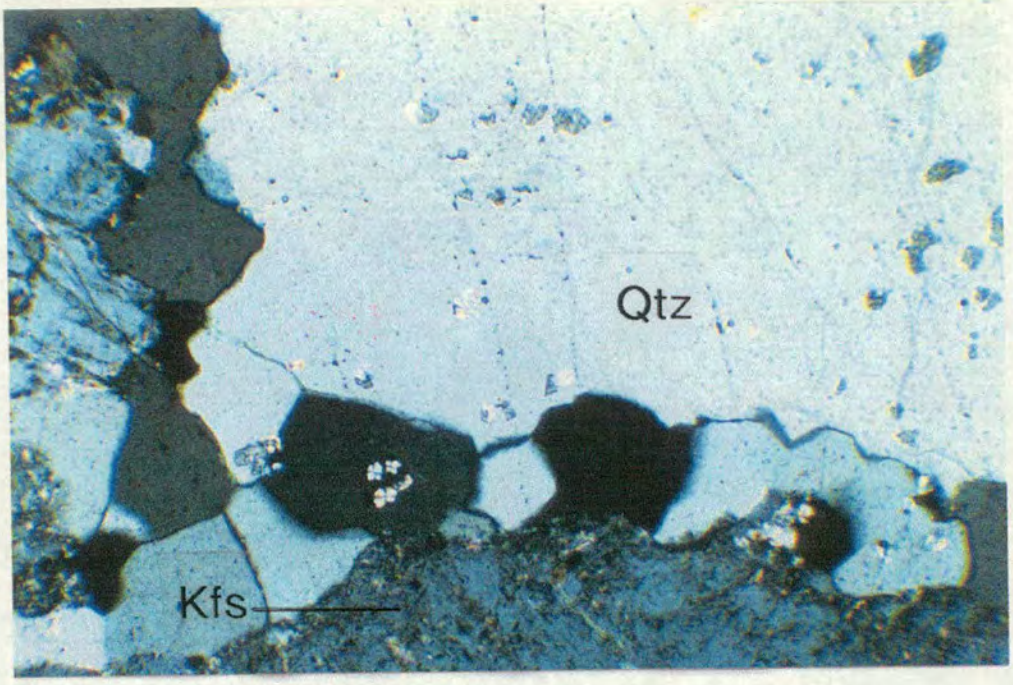

Figure 3.20 - Sample D18: myrmekite growing on the edges of perthite and quartz crystals within a small leucosome. Field of view = 0.5 mm. Locality 2.

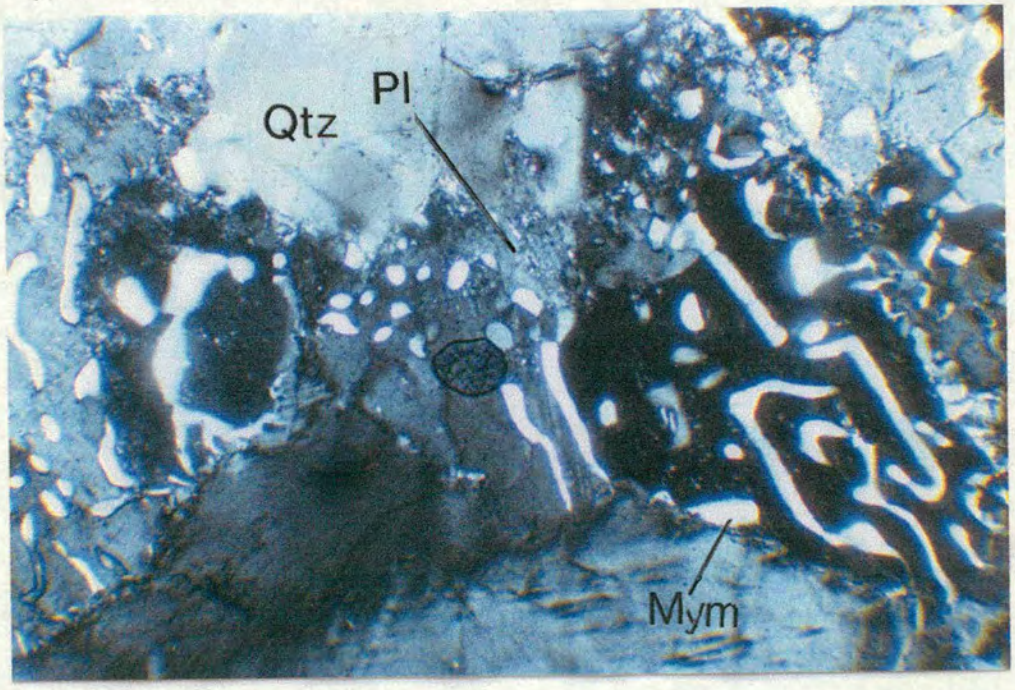

Figure 3.21 - Sample 117: granophyric texture over K-feldspar crystals. This texture is particular to locality 6. Field of view = 4 mm. Locality 6.

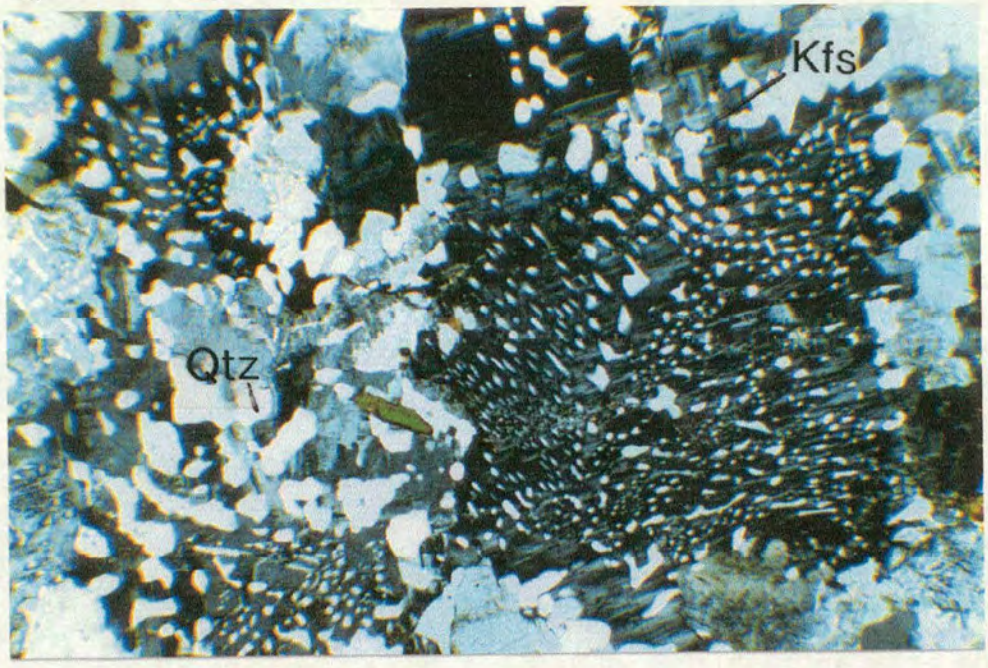

Figure 3.22 - Sample 14b: square, high relief crystals of andalusite. These have crystallised out of the melt, indicating a peraluminous melt. Field of view = 6 mm.

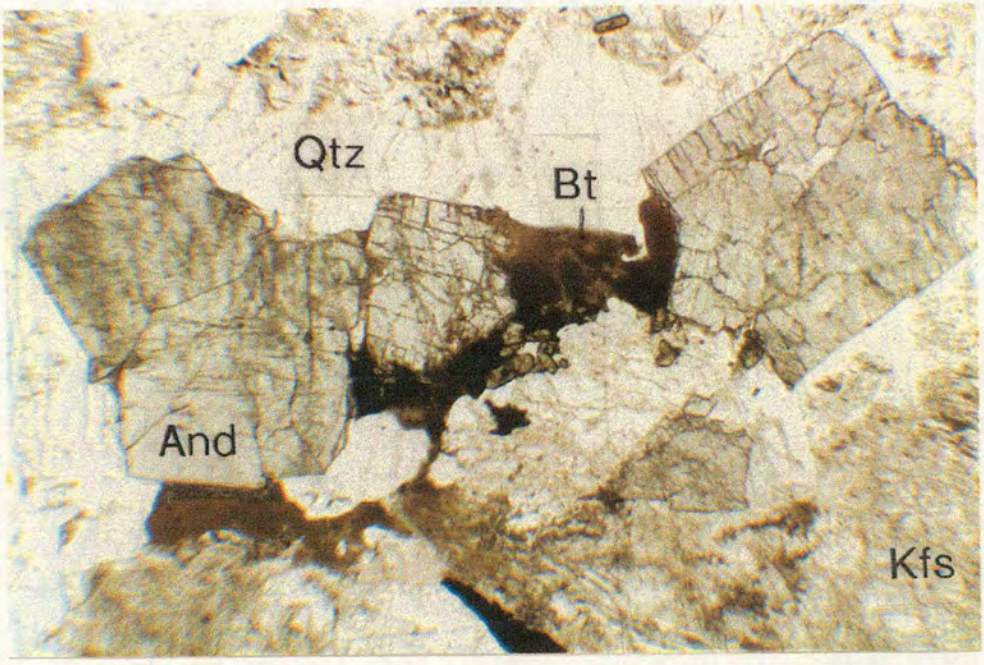

Locality 4

Figure 3.23 - Sample 20: coarse white mica crystallising from leucosome cordierite. The white mica is also replacing biotite at the edges of elongate crystals. Field of view = 6 mm. Locality 12.

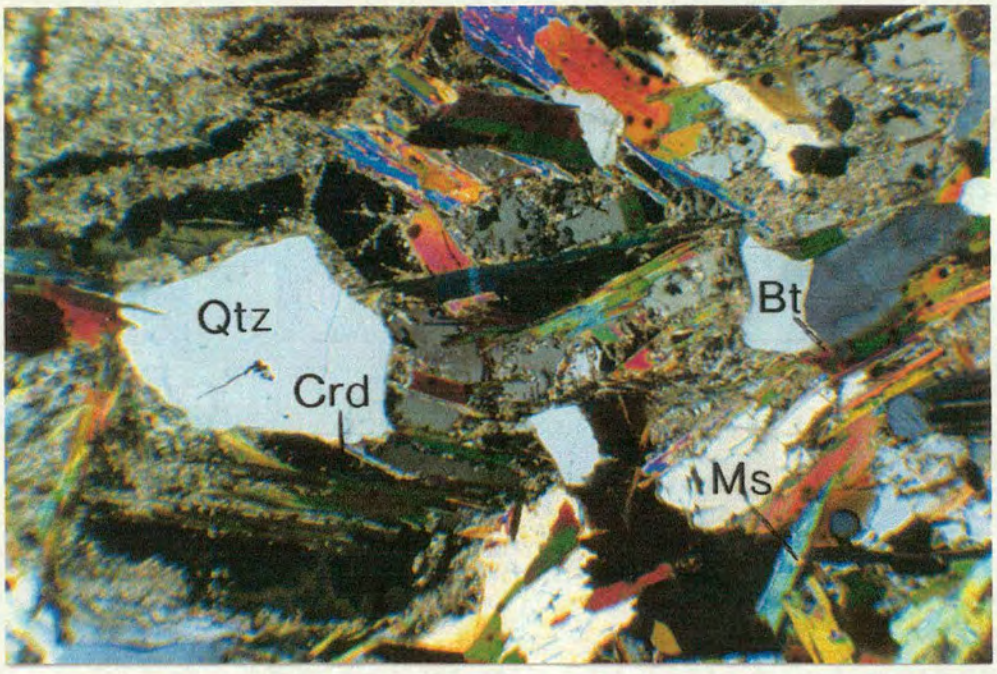

Figure 3.24 - Sample 103: tourmaline is growing around the edges of cordierite within this thin selvage-bound leucosome. Field of view = 1 mm. Locality 5.

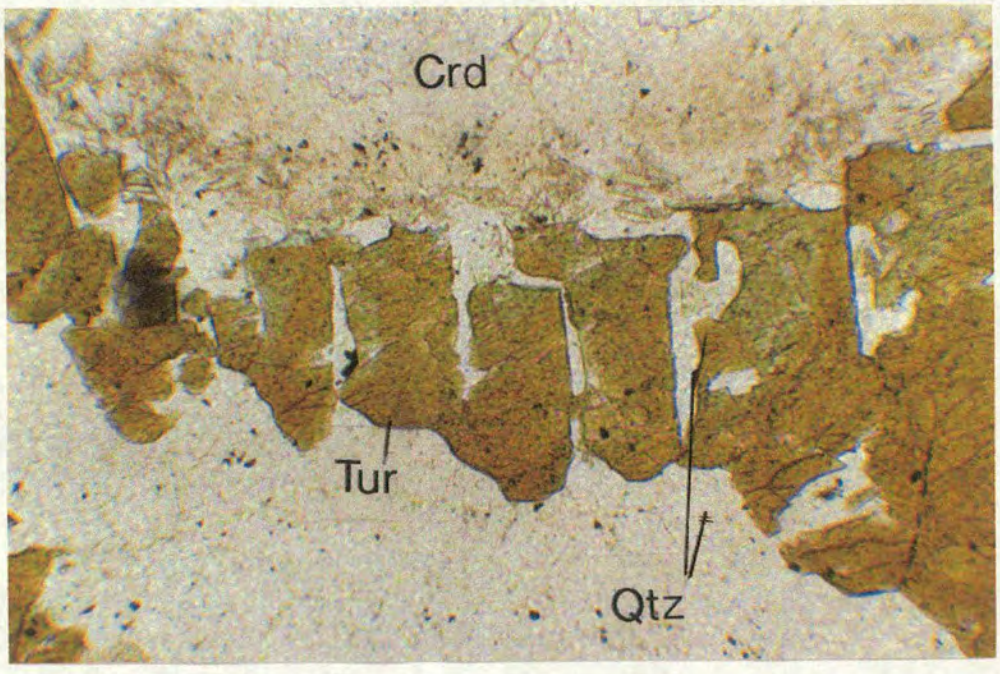

Figure 3.25 - Sample 107: large (2 mm) monazites from within an orange granitic sheet. Monazites are also seen at another locality from the middle of the terrain within a similarly coloured leucosome. Field of view = 0.25 mm. Locality 6.

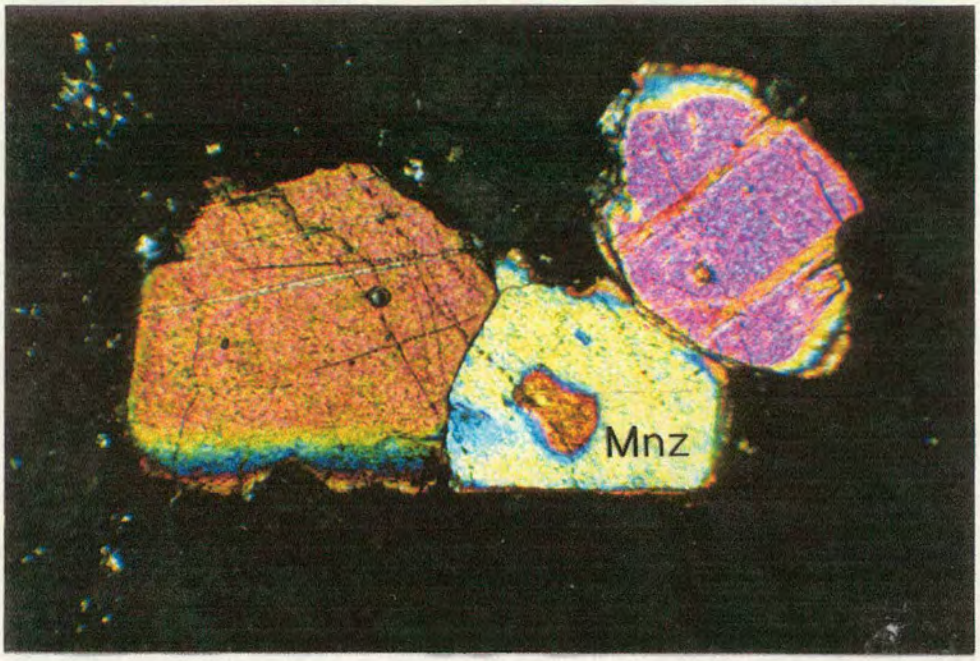

Figure 3.26 - Sample D47: selvage on a small folded leucosome, composed of coarse biotite and cordierite crystals. This is a 'typical' selvage assemblage. Field of view = 1 mm. Locality 12.

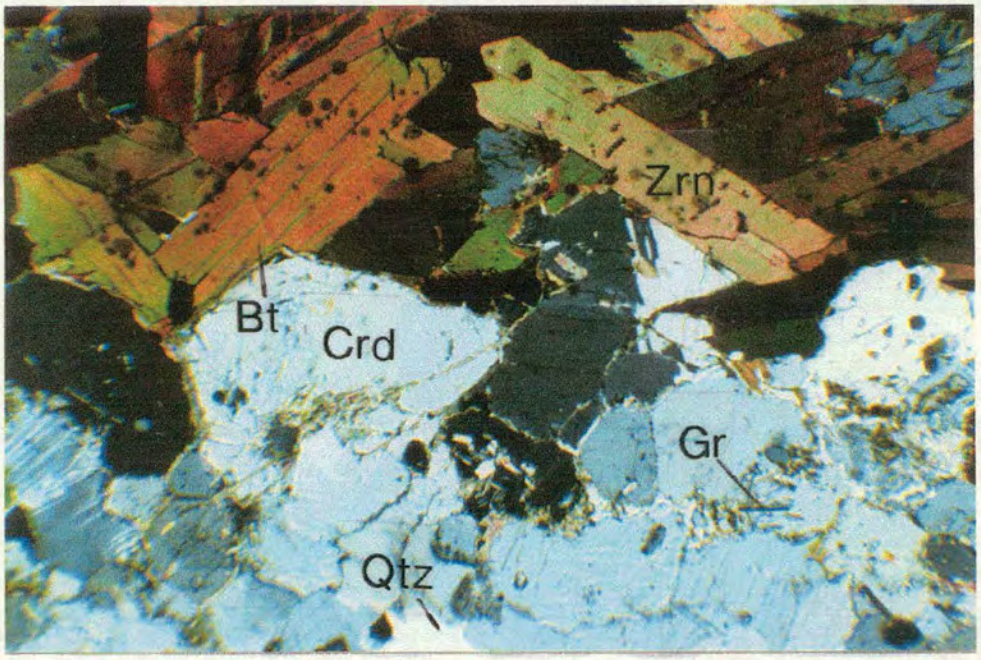

Chapter 4

Mineral chemistry

Chapter 4 - Mineral chemistry

4.1 - Introduction

In order to investigate mineral compositions across the Turku terrain, phases were analysed by wavelength dispersive electron probe microanalysis. Phases were analysed from core to rim to provide information about any mineral zoning formed either during the prograde P-T-t path, or during later post-peak retrogression, e.g. Fe-Mg exchange. Leucocratic phases within leucosomes were also analysed to see if there was a link between the leucosome types derived in Chapter 1 and the composition of their phases. Operating conditions, errors and detection limits, and normalisation procedures are given in Appendices 4.1-4.4. Tables of example analyses from each sample studied, in wt% and calculated cations, are presented in Appendices 4.4-4.6 along with a list and description of the samples used.

4.2 - Previous work

The compositions of phases from the Turku terrain have been reported by previous authors (Hietanen, 1947; Höltta, 1986; Van Duin and Nieman, 1993; Väisänen et al., 1994; Väisänen and Höltta, in press), although there is no distinction in the composition of different generations of the same mineral, e.g. Grt 1 and Grt 2. The range of X_{Mg} (Mg/Mg+Fe) values for garnet, cordierite and biotite provided by their work is plotted in Figure 4.1.

4.3 - Phase compositions

4.3.1 - Mafic phases

Across the majority of the Turku terrain, garnet + cordierite + biotite is the stable D3 assemblage within the mesosome. Biotite is present as a dominant mesosome matrix phase either having a decussate texture in more granulose mesosomes, or often orientated along S2. Biotite is also present as a retrogressive phase around some garnets

where it can form biotite + quartz symplectites. Both garnet and cordierite are present as two generations: an early D2 assemblage where the phases are elongate along S2 (Grt 1 and Crd 1) and a later non-deformed, often poikiloblastic D3 generation (Grt 2 and Crd 2). In this study all generations of garnet, cordierite and biotite from across the terrain have been analysed, as well as the leucocratic phases that make up the rest of the mesosome assemblage and that are the main components of leucosomes.

Biotite

Average X_{Mg} values range between 0.40-0.65 with those biotites that are within or near to garnet (INC/NGT) having the widest range of values (Figure 4.2). When analysing biotites in contact with garnet, care was taken to avoid those biotites that were obviously retrogressive after garnet. Those biotites labelled matrix (MAT) phases, i.e. those that are part of the general mesosome assemblage and not in contact with garnet within the same section, have a much narrower X_{Mg} range (between 0.40-0.52). All of the biotites shown in Figure 4.2 are from garnet-bearing localities but garnet is not present in all samples.

X_K (K/(Na + K) values range from 0.95 to 0.99 apart from one lone sample point whose X_K is 0.94 (Figure 4.2). Biotite inclusions or biotites in contact with garnet are generally lower in their X_K values than matrix phases. Titanium contents are on average 3-4 wt% and are slightly lower in northern localities (Table 4.1). Biotites found within leucosomes generally show no appreciable compositional differences from mesosome phases apart from sample 97 (locality 4) which has comparably low TiO_2 contents and higher Al values (Appendix 4.5).

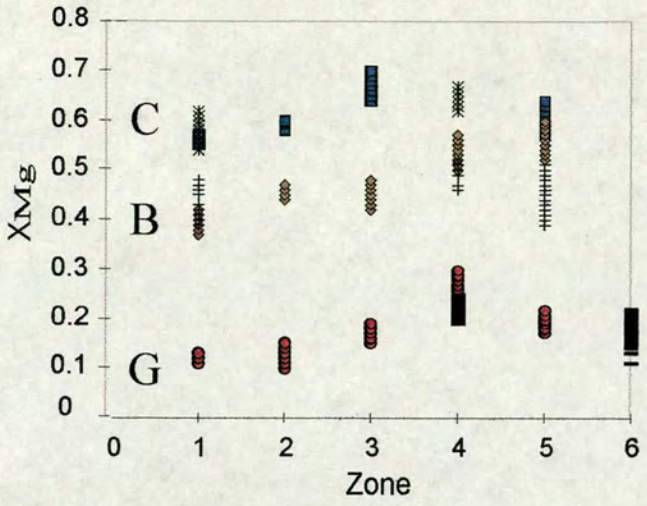

Figure 4.1 - Previous workers XMg ranges of mafic phases within Turku pelites. G = garnet, B = biotite, C = cordierite. Zones 1-2 represent northern localities, 3-4 - middle localities, and 5-6 the southern localities of this study. Black unfilled symbols refer to data collected by this study. There is no distinction between generations of phases and thus equilibrium assemblages.

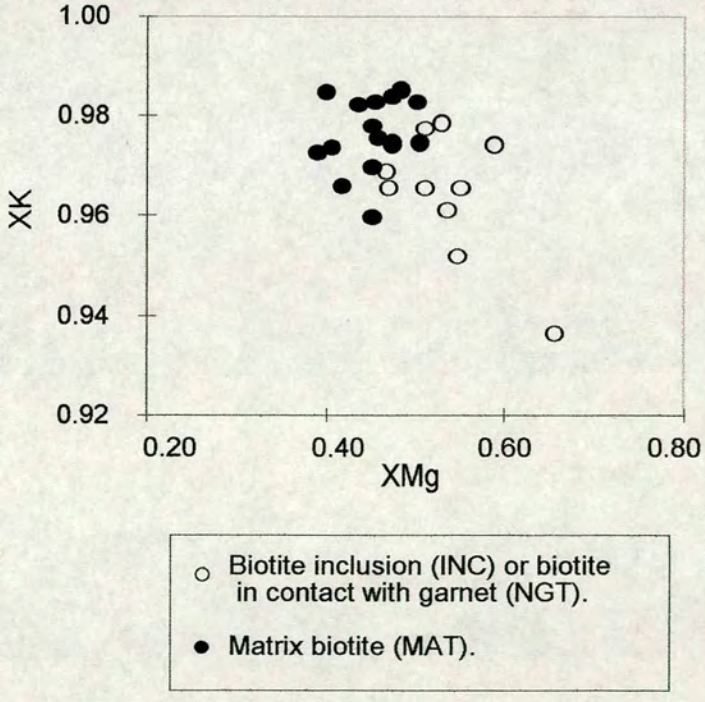

Figure 4.2 - Plot of biotite XMg's against XK for mesosome samples throughout the Turku terrain.

Cordierite

The X_{Mg} values of cordierite range from 0.52 to 0.68 across the terrain but there is no zoning within single crystals. These compositions fall within the range of compositions proposed by previous workers. Generally there is no difference in the X_{Mg} of matrix cordierites to those found near garnet, or between Crd 1 cordierites (e.g. Samples 12, 88, and 154) and Crd 2 cordierites (e.g. samples 90 and 118). MnO is present in amounts up to 0.1 wt%, whereas TiO_2, Cr_2O_3, CaO, Na_2O and K_2O only constitute 0.2-0.3 wt%. As with biotite there are no differences in composition between leucosome and mesosome phases, although under the microscope it can be seen that leucosome cordierites are usually more highly altered. There are also no compositional differences between D2 and D3 generations of cordierite.

Garnet

X_{Mg} values of the garnets analysed in this study range from 0.10 to 0.24, with southern localities having a slightly higher range of X_{Mg} values than middle localities. Many garnets have higher X_{Mg} values in their cores than in their rims and so are zoned with respect to Fe-Mg. CaO and MnO contents range from 0.6 to 0.9 and 0.4 to 1.10 wt% respectively. The Turku garnets are generally almandine-rich with X_{alm} values of 0.74 to 0.86, X_{prp} values of 0.1 to 0.23, X_{grss} values of 0.017 to 0.024 and X_{spss} values of 0.007 to 0.20. X_{uvr} values are negligible (<0.005). These end members are plotted on ternary diagrams in Figure 4.3. As with cordierite there are no compositional differences between different generations of garnet.

Spinel

Spinel is present as inclusions within cordierite across the Turku terrain. All spinel analyses have been obtained from one sample taken from an outcrop from the middle of the terrain (locality 8). Figure 4.4 shows that the spinel is dominantly hercynite with X_{hc} values of around 0.72 and X_{spl} values of around 0.13. The sample also contains a considerable ZnO component (6.2 wt%) so that X_{gah} is around 0.13.

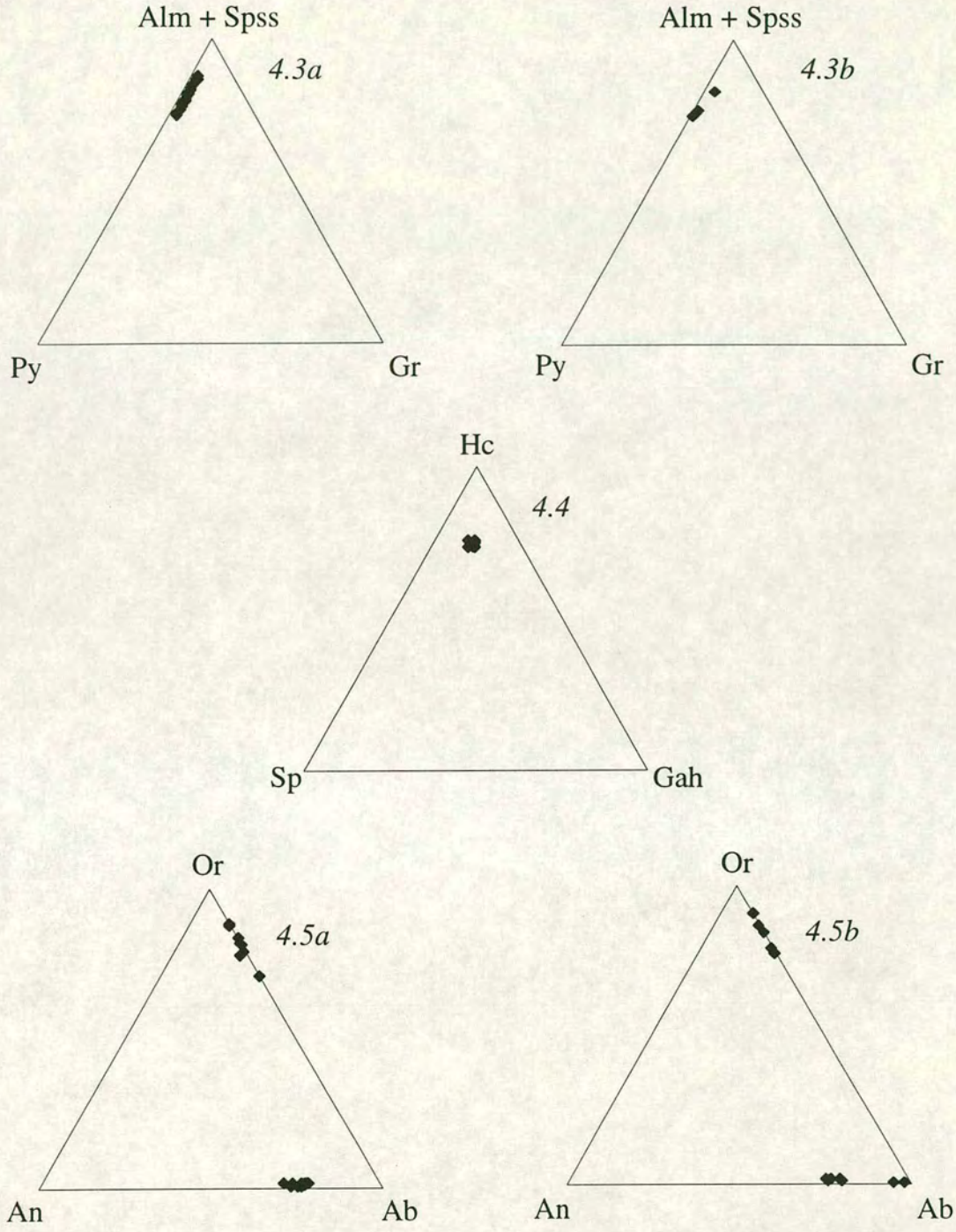

Figure 4.3 - Garnet end member proportions for a) - mesosome and b) - leucosome assemblages across the terrain.

Figure 4.4 - Spinel end member proportions from an inclusion within cordierite, sample 123, locality 8.

Figure 4.5 - Endmember feldspar compositions for K-feldspar and plagioclase from a) - mesosome and b) leucosome assemblages.

Table 4.1 - Representative analyses of mafic mesosome phases.

Locality	3 (SL)	2 (SL)	4 (SL)	8 (ML)	7 (ML)	6 (ML)	5 (NL)	22 (NL)	13 (NL)	14 (NL)	18 (NL)
Garnet											
X_{Mg}	0.149	0.206	0.224	0.164	0.188	0.236	na	na	na	na	na
X_{alm}	0.824	0.763	0.749	0.806	0.785	0.741	na	na	na	na	na
X_{prp}	0.145	0.199	0.216	0.158	0.182	0.229	na	na	na	na	na
X_{grs}	0.017	0.023	0.024	0.022	0.020	0.020	na	na	na	na	na
X_{sps}	0.013	0.014	0.010	0.013	0.011	0.011	na	na	na	na	na
X_{uvr}	0.001	0.001	0.002	0.001	0.001	0.000	na	na	na	na	na
Biotite											
TiO_2	3.614	4.017	3.781	3.514	3.861	3.409	3.757	3.567	3.177	2.908	2.952
X_{Mg}	0.513	0.439	0.455	0.478	0.490	0.480	0.392	0.422	0.392	0.407	0.402
X_K	0.975	0.983	0.978	0.975	0.985	0.984	0.974	0.967	0.974	0.975	0.985
Cordierite											
X_{Mg}	0.588	0.600	0.594	0.627	0.636	0.615	0.545	0.582	0.543	na	0.567
Spinel											
X_{hc}	na	na	na	0.717	na	na	na	na	na	na	na
X_{sp}	na	na	na	0.138	na	na	na	na	na	na	na
X_{chr}	na	na	na	0.006	na	na	na	na	na	na	na
X_{usp}	na	na	na	0.000	na	na	na	na	na	na	na
X_{gal}	na	na	na	0.001	na	na	na	na	na	na	na
X_{gah}	na	na	na	0.114	na	na	na	na	na	na	na
X_{mag}	na	na	na	0.023	na	na	na	na	na	na	na

(na - not analysed because the phase is not present within the sample)

Sillimanite

A couple of sillimanite inclusions within a cordierite from sample 83 were analysed, yielding FeO contents of 0.5 wt%. In samples from the south and middle localities sillimanite is only present as inclusions within cordierite and some garnets.

4.3.2 - Leucocratic phases

Plagioclase

Plagioclases within mesosome assemblages show a wider range of compositions than those located within leucosomes. Generally the X_{ab} values of plagioclases from mesosomes range from 0.6 to 0.8 (Figure 4.5). Those samples from the northern Hähää

exposures have higher X_{ab} values than the rest of the localities (Table 4.2). In most cases the plagioclase in the corresponding leucosomes is richer in albite. Two leucosome samples preserve much lower X_{ab} values of 0.5 to 0.10. Both of these samples are from a southern locality (locality 4) with a large quantity of cross-cutting leucosome generations, some of which may represent granitic material with an external source. Generally, however, there are no links between feldspar composition and leucosome type.

K-feldspar

Values of X_{or} for potassic feldspar values range from 0.8 to 0.95 and there are no compositional differences between leucosome and mesosome feldspars. The feldspars are therefore dominantly orthoclase, but as most samples are perthitic in texture the Xab is around 0.2. Typical values are presented in Table 4.2 and plotted on ternary diagrams in Figure 4.5.

Table 4.2 - Representative analyses of leucocratic mesosome and leucosome phases.

Locality	3 (SL)	2 (SL)	4 (SL)	8 (ML)	7 (ML)	6 (ML)	5 (NL)	22 (NL)	13 (NL)	14 (NL)	18 (NL)
K-feldspar -mesosome											
X_{an}	0.004	na	na	na	na	0.005	0.006	0.001	0.003	0.020	0.002
X_{ab}	0.122	na	na	na	na	0.289	0.204	0.188	0.183	0.200	0.179
X_{or}	0.874	na	na	na	na	0.706	0.790	0.811	0.814	0.780	0.820
K-feldspar - leucosome											
X_{an}	na	0.004	0.004	na	0.003	na	na	na	na	na	na
X_{ab}	na	0.156	0.130	na	0.092	na	na	na	na	na	na
X_{or}	na	0.840	0.866	na	0.905	na	na	na	na	na	na
Plagioclase mesosome											
X_{an}	0.246	0.224	0.266	0.238	0.215	0.256	0.229	0.212	0.206	0.277	0.235
X_{ab}	0.747	0.765	0.728	0.750	0.766	0.730	0.756	0.772	0.775	0.703	0.757
X_{or}	0.008	0.011	0.006	0.012	0.019	0.015	0.015	0.016	0.020	0.020	0.008
Plagioclase leucosome											
X_{an}	na	0.198	0.048	na	0.199	na	na	na	na	na	na
X_{ab}	na	0.792	0.947	na	0.783	na	na	na	na	na	na
X_{or}	na	0.010	0.005	na	0.018	na	na	na	na	na	na

4.4 - Chemical trends and compositional relationships

As mentioned previously, there are differences in the X_{Mg} of garnet, biotite and cordierite across the terrain, and generally the X_{Mg} of crd $\geq$ bt > grt. As well as these general trends there are differences between garnet cores and rims, and between cordierites and biotites that are either in contact with garnet or are general matrix phases. Work by Höltta (1986) showed that the Turku garnets are strongly zoned with their cores typified by much higher X_{Mg} values than their rims. Traverses were taken across garnets as part of this study to investigate this zoning. Those ferromagnesian phases found as inclusions or at the edges of garnets (biotite and cordierite) were also analysed to study the possible effects of retrogressive Fe-Mg exchange.

Figure 4.6 plots the X_{Mg} of biotite inclusions in garnet or biotite in contact with garnet, against the X_{Mg} of garnet rims or garnets in contact with the relevant biotite inclusions. The compositions of matrix biotite phases against garnet core compositions are plotted onto the same diagram for comparison. These two combinations will be used in garnet - biotite thermometry, discussed in Chapter 6. The biotites show clear groupings where the inclusions or rim biotites have a higher range of X_{Mg} values than matrix biotites (Figure 4.6). This relationship is not seen for garnet and cordierite pairings as there is little compositional difference between matrix cordierites and those in contact with garnet.

4.4.1 - Garnet traverses

Four garnet traverses are illustrated in Figures 4.7 through 4.10 where garnet is plotted as its end-member components, and the composition of any biotite inclusion is represented by its X_{Mg}. Sample 120 (Figure 4.7) taken from a leucosome sample from locality 6 shows no zoning in any end-member. A mesosome sample from the same locality (sample 118) (Figure 4.8) shows a slight increase in its X_{alm} component and corresponding decrease in its X_{pyp} component at the rim. X_{grss} and X_{spss} have patterns

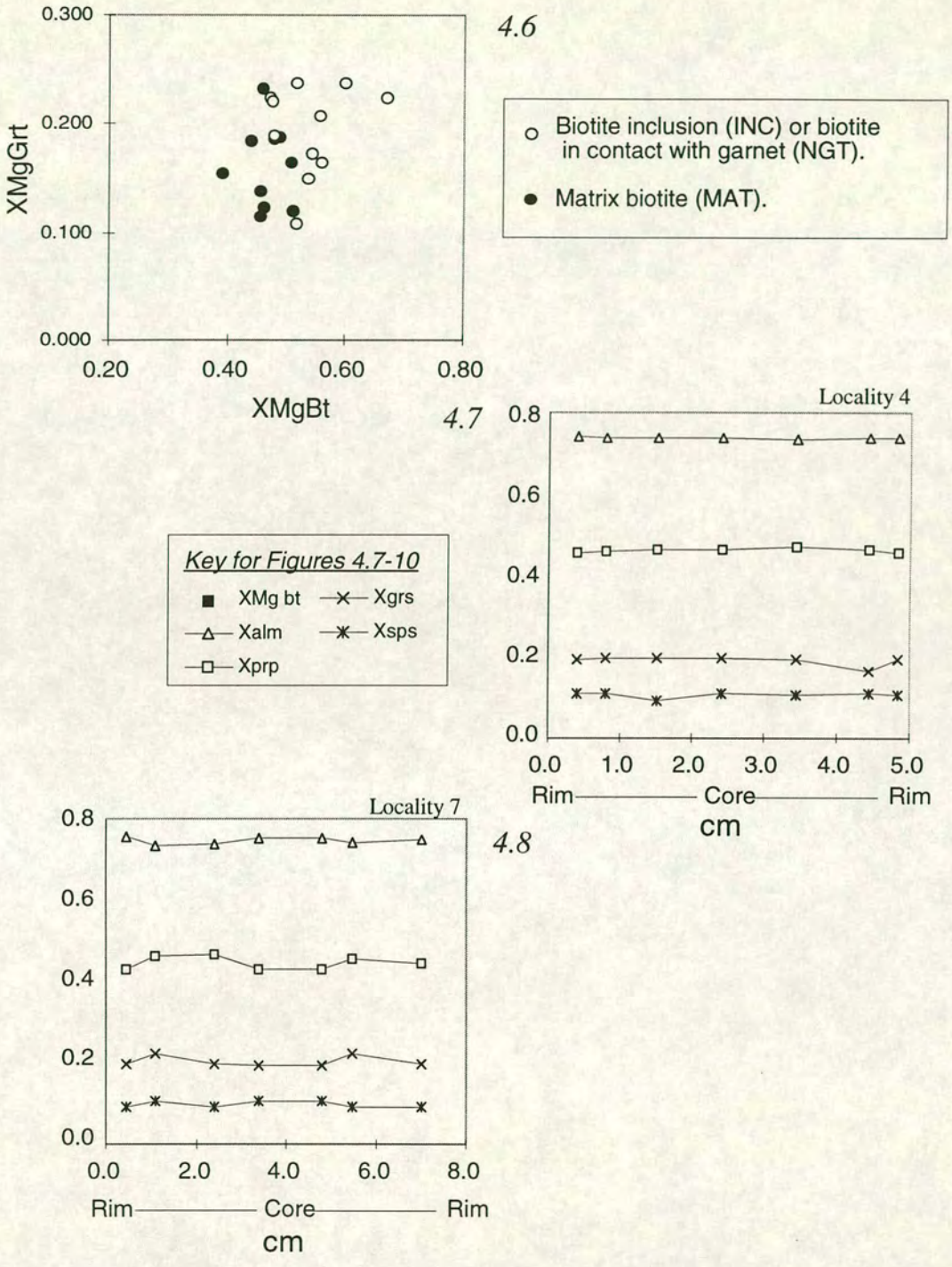

Figure 4.6 - Plot of biotite XMg against garnet XMg for mesosome samples throughout the terrain.

Figure 4.7 - Profile across a leucosome garnet (sample 10) which has no compositional zoning between rim and core. For Figures 4.7-4.9 the Xpyp component has been doubled and the Xspss and Xgrs components have both been increased by a factor of 10 for clarity.

Figure 4.8 - This sample shows a slight increase in Xalm at the rims accompanied by a decrease in Xprp, Xgrs and Xspss. This garnet (sample 120) was found within a mesosome and so may have undergone Fe-Mg exchange with neighbouring biotite or cordierite as discussed in the text.

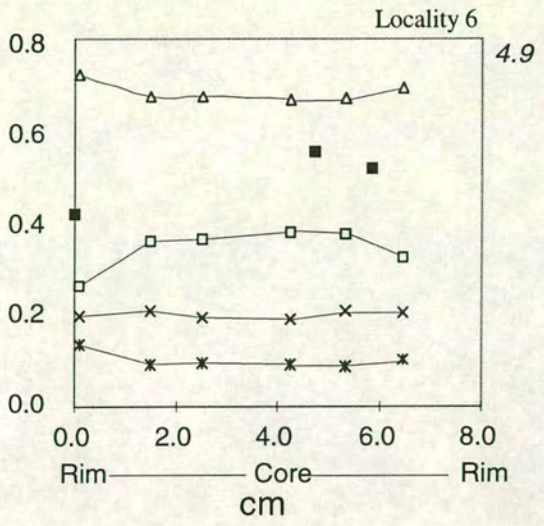

Figure 4.9 - Traverse across a mesosome garnet sample (118) which has stronger Fe-Mg zoning at its rims seen in the Xprp and Xalm components. The black squares represent biotite inclusions within the garnet and their XMg. There is no apparent Fe-Mg exchange between the garnet and its inclusions.

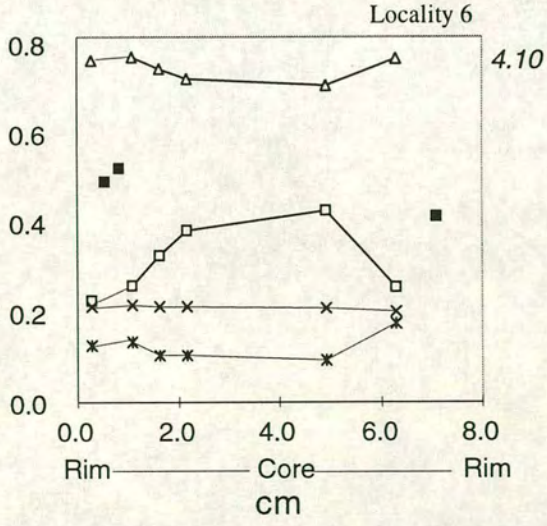

Figure 4.10 - The garnet featured in this traverse (sample 114) is also zoned and in this case the garnet in contact with the biotite inclusions has suffered Fe-Mg exchange so that Xalm increases relative to Xprp. Xspss mirrors Xalm but their is no variation in the Xgrss component. In this case the Xprp end member was multiplied by 2.5 for clarity.

mirroring the X_{prp} components. Stronger zoning in X_{alm} and X_{prp} components is seen in sample 114 (Figure 4.9) but biotite inclusions have no influence on garnet composition. The opposite is seen in sample 15 (Figure 4.10) which shows strong compositional differences both at its rims and near to the biotite inclusions. X_{prp} increases towards the core, X_{adr} and X_{spss} show a reversed pattern whilst X_{grss} is constant across the grain.

This zoning of garnets, and their relationship to biotite in the Turku terrain, is attributed to Fe-Mg exchange during cooling (Höltta, 1986; Väisänen and Höltta, in press). Höltta (1986) proposed that large garnets may preserve peak assemblage compositions at their cores. Smaller garnet cores and rims with much lower X_{Mg} ratios are indicative of later cooler conditions where the garnets underwent Fe-Mg exchange with other phases such as biotite and cordierite.

4.4.2 - AFM plots

It is assumed that each generation of garnet and cordierite was in equilibrium with the matrix biotite (this study; Höltta, 1986; Van Duin and Nieman, 1993; Väisänen and Höltta, in press). However, the rims and cores of some garnets have been modified by Fe-Mg exchange with biotite. As such, the cores of Grt 2 garnets together with matrix biotite and D3 generations cordierite are here interpreted as the peak D3 compositions. Garnet rims, biotite inclusions and biotite + cordierite in contact with garnet are interpreted as having retrogressive compositions due to Fe-Mg exchange upon cooling. These assumptions will be discussed in Chapter 6 together with their implications for garnet-biotite thermometry. For this reason D3 generations of garnet, cordierite and biotite have been plotted onto AFM diagrams (Figure 4.11). The compositions plotted are from southern and middle localities.

D3 garnet, cordierite and biotite are tightly clustered with respect to their Fe-Mg ratios (Figures 4.11a and b), especially in samples from the middle of the terrain. Cordierites

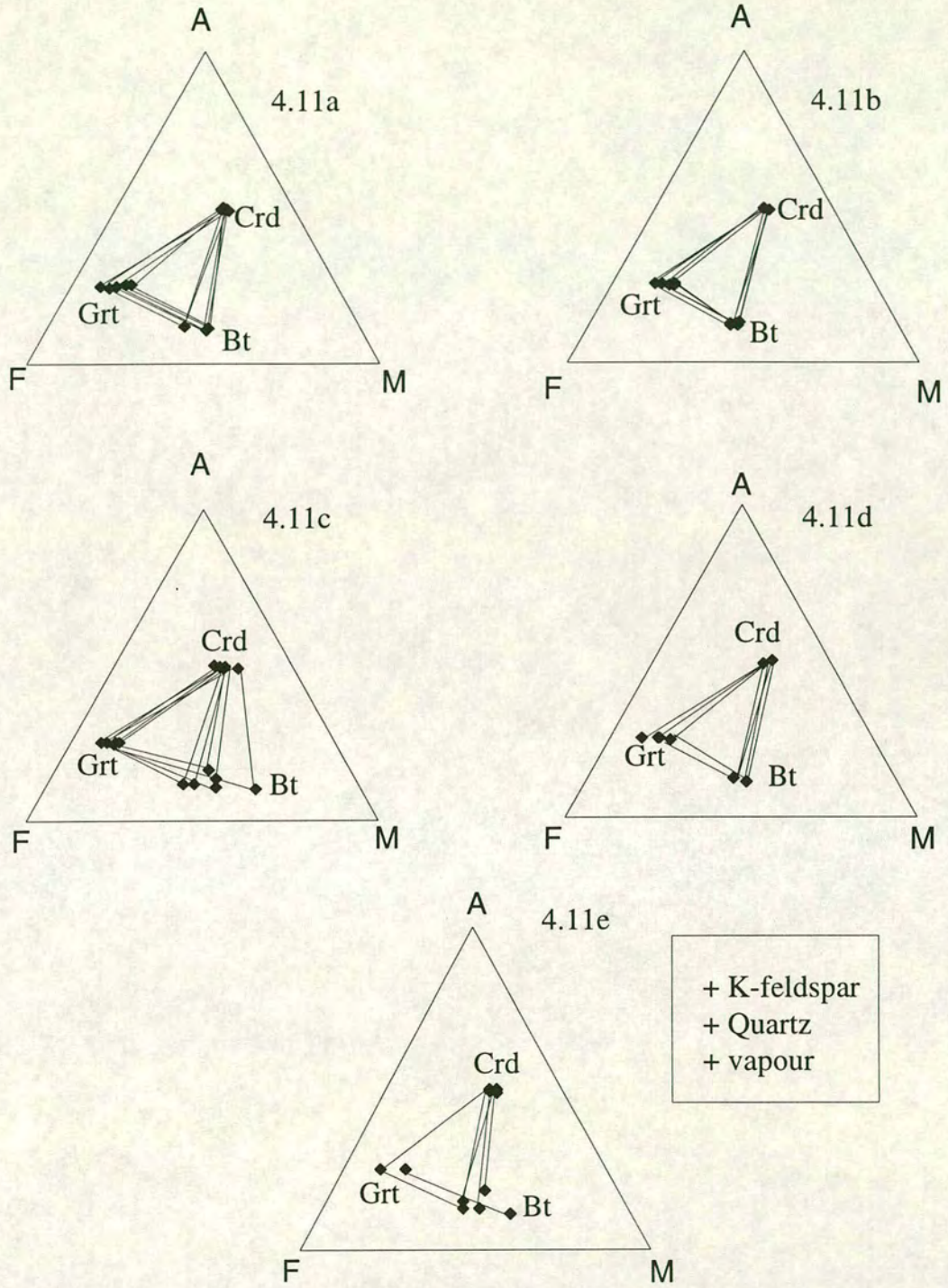

Figures 4.11 - AFM plots for Turku pelitic assemblages, tie lines are drawn between equilibrium phases within the same sample. (a) D3 assemblages for southern localities (garnet cores, matrix biotite and cordierite). (b) D3 assemblages for middle localities. (c) Post peak retrogression assemblages for southern localities (garnet rims, and biotite inclusions or biotite + cordierite in contact with garnet). (d) Post peak retrogression assemblages for northern localities. (e) Leucosome garnet, cordierite and biotite.

and biotites in contact with garnet from the southern localities show much greater Fe-Mg variation than matrix phases (Figure 4.11c). Leucosome biotites also have a large spread of Fe-Mg values. This spread of values coincides with variation in the alumina component of biotites (Figures 4.11d and e). Phases from the southern localities show much less range in their FM and A components for peak and retrogressive assemblages than phases from the south of the terrain.

4.5 - Discussion

Based on compositional and textural evidence some reactions can be inferred that constrain the metamorphic history of the Turku terrain. There is no zoning in Turku garnets and so they provide no information about the prograde path. However textural evidence shows that there are two generations of garnet and cordierite and thus two separate metamorphic events. The early generation is deformed by D2 and contains sillimanite inclusions. Both lines of evidence therefore indicate that garnet and cordierite formed along reaction 4.1 during late D1/early D2:

biotite + sillimanite + quartz = K-feldspar + garnet + melt (4.1)

The D2 mesosome assemblage is therefore grt + sill + bt, crd + sill + bt or grt + crd + sill + bt, depending upon bulk composition and PT conditions (Yardley, 1989). The compositions of the phases are projected onto an AFM plot from K-feldspar in Figure 4.12a. During D3 sillimanite was exhausted over most of the terrain following melting reactions, and the bulk composition of the Turku pelites favoured a grt + bio + crd assemblage (Figure 4.12b). Although the garnets analysed showed no prograde zoning, the decrease in X_{Mg} at their rims suggests that after D3 they underwent Fe-Mg re-equilibration due to retrogression. Biotites in contact with garnet have increased X_{Mg} values whilst cordierites are mostly homogeneous, which suggests that most Fe-Mg exchange was between garnet and biotite.

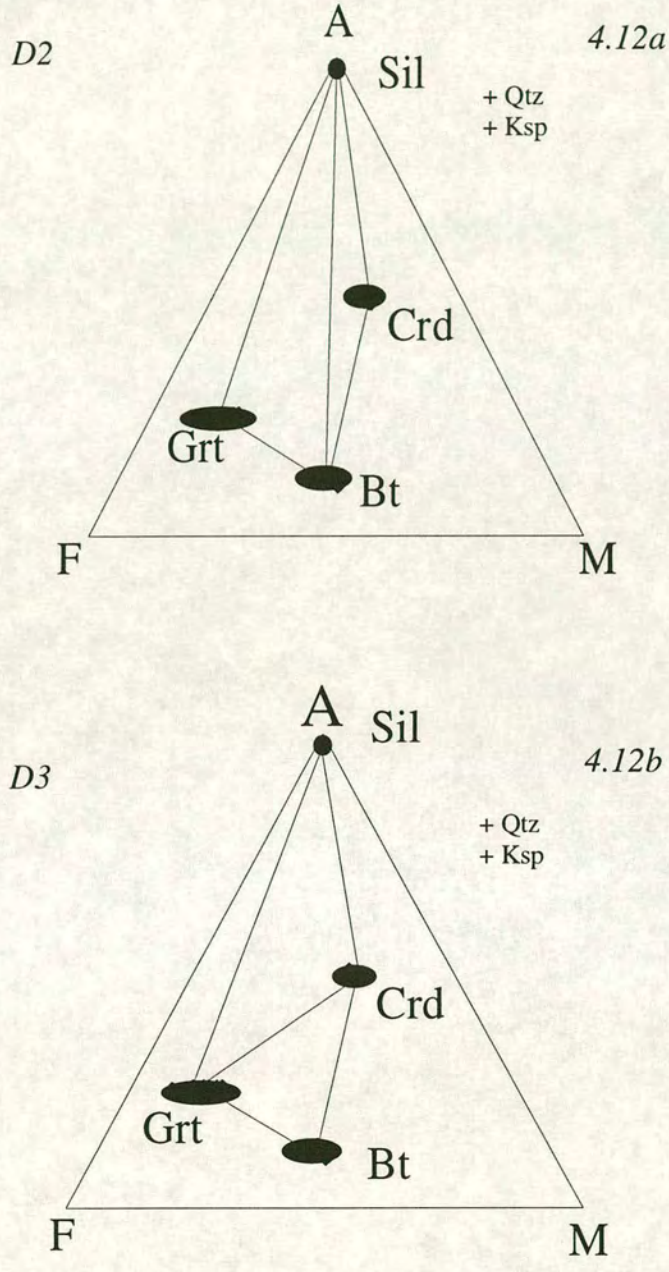

Figure 4.12 - AFM plots representing assemblage changes throughout the metamorphic history of the Turku terrain., projected from K-feldspar. (a) Following melting reactions 4.1 to 4.3 garnet and cord formed during early D2. Bulk composition controls whether biotite + sillimanite + garnet, biotite + sil + cordierite or biotite + sillimanite + cordierite are stable. (b) Garnet + biotite + cordierite is a stable assemblage in southern and middle localities following the consumption of sillimanite.

Chapter 5

Leucosome geochemistry

Chapter 5 - Leucosome geochemistry

5.1 - Introduction

Fieldwork has determined that leucosome characteristics vary across the Turku terrain. Leucosomes range in size from a few millimetres to a few metres wide, vary in their mineral assemblage, the texture of their phases and their relationship to the structural regime. Fieldwork and petrography have suggested that a large percentage of the leucosome material is indicative of melt formed from partial melting of the surrounding schists. Melts formed through this process should have a characteristic bulk and trace geochemistry as discussed below.

Experimental work has shown that under H_2O saturation, melting can take place at relatively low temperatures and produce melts with compositions near to the granite minimum (Johannes and Holtz, 1996). In low a_{H2O} granulite terrains (Harley, 1989, Waters 1988; 1994) melting occurs under water-undersaturated conditions through the breakdown of hydrous phases, i.e. biotite in pelitic rocks (Thompson 1982; Clemens and Vielzeuf, 1987; Le Breton and Thompson, 1988; Waters, 1988; Patino Douce and Johnston, 1991; Thompson, 1996). The resulting melts are strongly water undersaturated and may have modal proportions of phases that differ from the minimum melt compositions (Johannes and Holtz, 1996)

Melts formed from the partial melting of biotite have low a_{H2O}, high wt% SiO_2, A/CNK (Al_2O_3/CaO + NaO +K_2O) ratios >1.1, and low Na/K (White and Chappell, 1977; Patino Douce and Johnston, 1991; Sawyer, 1996). The peraluminous composition of experimentally derived melts is shown by the high values of wt% normative corundum (2-5 wt%) as demonstrated by Patino Douce and Johnston (1991), whose melts also have low wt% FeO and MgO (<3 wt%) even at temperatures above 1000°C. Under equilibrium conditions the X_{Mg} of these partial melts is marginally greater than garnet but much less than biotite (Thompson, 1982).

Trace element studies (Watt and Harley, 1993; Sawyer, 1996) show that felsic and peraluminous partial melts produced by biotite dehydration melting have low Zr, Th, P_2O_5 and REE concentrations relative to other crustal granitoids. The REE signatures within crustal partial melts are strongly controlled by the degree of dissolution of accessory phases, notably zircon and monazite (Watt and Harley, 1993, Watt, 1993, Sawyer, 1996). As REE's are essential structural components in these phases, the low Zr, Th and REE's of granulite facies partial melts is therefore linked to the limited dissolution of accessory phases in melts with low H_2O contents (Bea, 1996, Sawyer, 1996 and Watson, 1996). REE contents in partial melts are also controlled by major phases such as garnet and K-feldspar.

Thus to try to identify whether leucosomes are representative of partial melting within a terrain, their major and trace element geochemistry can be studied. Geochemical analysis of leucosomes from the Brattstrand Bluff granulites, Antarctica, identified two main suites, LG1 and LG2 (Watt and Harley, 1993, Fitzsimons 1996). LG1 leucosomes have more aluminous (A/CNK = 1.22) bulk compositions than LG2 (A/CNK = 1.17) and have low total Zr, Th and LREE, whilst LG2 leucosomes are enriched in the latter elements as well as in Fe-Mg, plotting below the garnet-cordierite tie-line on AFM projections (Fitzsimons, 1996). It was suggested by Watt and Harley (1993) and Fitzsimons (1996) that the LG2 leucosome types represent mixing of melt with restitic material, rich in accessory and ferro-magnesian phases. Therefore the leucosomes are not representative of melt compositions but instead reflect melt-solid mixtures. The solids may be undissolved entrained restite material, residual phases after melt extraction or peritectic minerals produced during incongruent melt reactions.

Leucosomes produced under dehydration melting can therefore retain a range of compositions and trace element signatures depending upon a_{H2O}, pressure, temperature (discussed in chapter 1) and the degree of mixing with restitic material.

5.2 - Aims

Previous work has concentrated on the metamorphic and structural evolution of the Turku granulite terrain (Höltta, 1986; Van Duin and Nieman, 1993; Väisänen et al., 1994; Väisänen and Höltta, in press). There is as yet little information on, or classification of, Turku leucosome types present in any of the literature. Höltta (1986) carried out bulk analysis on some granitic material but did not attempt to differentiate leucosome characteristics. The one main aim of this study has been to provide insight into the nature of the melts produced at the peak of metamorphism, 1870-1830 Ma (Väisänen et al., 1994).

This study and earlier work (Höltta, 1986; Van Duin and Nieman, 1993; Väisänen et al., 1994; Väisänen and Höltta, in press) has suggested that the leucocratic material observed within the Turku terrain is the product of partial melting following the dehydration of biotite. If the leucosomes are the products of partial melting of the surrounding pelites then they would have distinctive geochemical signatures, as discussed in the beginning of this chapter. However as discussed in Chapter 2 the leucosome material studied at each outcrop varied in volume, geometry, mineralogy and size and was categorised on the basis of these variations (Lc1 – 5). In order to see if the different categories of leucosome had the bulk geochemistry of partial melts as well as being geochemically different from each other, the major and trace elements of 24 leucosome samples were analysed for their bulk geochemistry.

5.3 - Methodology

The 24 leucosome and 5 mesosome samples (Appendix 5.1) were analysed by X-ray fluorescence using the Phillips PW 1450 automatic X-ray spectrometer at the University of Edinburgh. Samples weighing approximately 0.5-0.8 kg were crushed and powdered. Trace elements were analysed from pressed-powder samples made from 6 g of material. Major elements were measured from glass disks prepared by fusing with Spectroflux 105. Standards were a range of natural rock standards and

were analysed at stages throughout the analysis session in order to check for instrument drift.

5.4 - Results

The major and trace element compositions of leucosome and mesosome samples are presented in Appendix 5.2. A representative selection of analyses are presented in Table 5.1.

5.4.1 - Major elements

SiO_2 contents range from 65-80 wt% with most leucosomes containing 70-75 wt%, similar to the SiO_2 values of S-type granites (White and Chappell, 1977) and partial melt experiments (Patino Douce and Johnston, 1991). Al_2O_3 ranges from 10-18 wt% with typical values of 14-17 wt%. The molecular A/CNK values of the leucosomes are ≥ 1.10 and are therefore typical of peraluminous granitoids (White and Chappell, 1977, Clarke, 1992).

On a QAP normative plot (Figure 5.1) the leucosomes show a wide spread of values from granodiorite to syenogranite (Clarke, 1992). Most of the data points are clustered within the syenogranite-monzogranite fields with no real distinction between different leucosome types. When the data are presented on a ternary feldspar plot (Figure 5.2), the samples all have low modal anorthite, <20 wt%. Orthoclase contents range from 75-25 modal wt% with most of the data clustered between 75-50 wt%. Corundum normative values range between 0.14-10.45 wt% with an average of 2.88 wt%. These compositions are typical of peraluminous partial melts (Patino Douce and Johnston, 1991).

On the corundum-quartz-total feldspar plot in Figure 5.3 it can be seen that the type 1 leucosomes (Lc1) contain the highest normative corundum on average 6 wt%. Leucosome types 3 (Lc3) and 5 (Lc5) are richer in total feldspars than quartz, >60 wt%. Type 1 and 2 (Lc2) leucosomes show a range of values from 40-60 wt% total

Table 5.1 – Representative major and trace element data and normative values for four leucosome types and from one mesosome sample for comparison.

Sample	2/D1 Lc1	3/D24 Lc2	4/97 Lc3	7/D41 Lc5	5/102A Meso
Major oxides (wt%)					
SiO_2	75.16	73.80	67.93	65.89	45.60
Al_2O_3	13.61	14.80	17.67	14.12	22.90
Fe_2O_3	2.17	1.51	1.98	10.02	15.48
MgO	0.20	0.18	0.51	1.94	6.15
CaO	0.70	1.40	2.55	0.52	0.21
Na_2O	3.03	4.94	5.95	1.33	0.35
K_2O	3.89	2.08	2.83	5.01	4.23
TiO_2	0.01	0.02	0.08	0.22	1.59
MnO	0.35	0.04	0.02	0.13	0.09
P_2O_5	0.12	0.16	0.09	0.10	0.09
Total	99.23	98.92	99.59	99.28	96.68
Fe_2O_3+MgO	2.37	1.69	2.49	11.96	21.63
(A/CNK)	1.30	1.15	1.01	1.65	4.14
X_{Fe}	0.86	0.82	0.69	0.74	0.59
Trace elements (ppm)					
U	0	0.6	0.4	0.9	1
Ba	0.8	1.4	3.6	4.9	53.6
Rb	57.1	9.7	71.4	152.5	331.8
Th	11.6	9.5	12.6	47.7	19.9
Nb	45.4	64	195	132.1	41.1
La	15.9	4.3	4.3	1.7	-0.6
Ce	149.3	62.1	86.6	152.6	419.7
Sr	-0.8	-2	8	19.8	31.9
Nd	18.4	16.7	28.5	41.8	1.6
Zr	14.9	14.2	26	49.1	300
Y	1.8	13.1	11.2	43.3	125.8
Pb	-0.1	9.5	6.9	27.9	128.6
Zn	6.1	13.4	21.9	62.8	373.7
Cu	9.2	13.4	49.1	63.5	74.2
Ni	0.2	3.9	15.8	26.1	48.4
Sc	0.4	2.9	21.9	29.5	12.6
V	0	6.2	15.1	43.4	394.5
Cr	139.6	96	252.9	756.3	399.4
Mo	3.9	2.7	6.9	32.8	38.7
Example wt% normative leucosome values					
Quartz	41.5	34.66	16.58	35.51	
Corundum	3.46	2.28	0.4	5.85	
Orthoclase	23.16	12.42	16.79	29.82	
Albite	25.83	42.25	50.54	11.34	
Anorthite	2.71	5.96	12.11	1.94	

$A/CNK = Al_2O_3/(CaO + Na2O + K_2O)$

$X_{Fe} = Fe_2O_3/(Fe_2O_3 + MgO)$

feldspar. The mesosome samples are richer in aluminium (16-23 wt%) and poorer in normative quartz (45-61 wt%) and so the A/CNK ratio was subsequently higher, 1.45-4.14.

Normative compositions are also plotted on a Qz-Ab-Or diagram in Figure 5.4 (Inger and Harris, 1993). A melt a_{H2O} of 0.3 was chosen as being representative of water undersaturated melts formed through partial melting and is based upon undersaturated cordierite water contents calculated in chapter 7 of this study. Minimum melts formed at higher water activities would be displaced towards the quartz apex (Inger and Harris (1993). Whilst a subset of samples plot in the near minimum region (e.g. 99, 100, 101a, 11, 115, 117, D36), some are clearly displaced away from minimum melt compositions being enriched in normative quartz (e.g. D41, 116, 20, 144) or albite (e.g. D24, 97, 111) and less commonly in normative K-feldspar (e.g. 99, 107, 18). Leucosome types 3 and 5 are generally richer in feldspars compared to type 1 and 2 leucosomes which are located nearer the quartz apex. Many of the displaced samples are also anomalously high or low in normative corundum (e.g. D41, 18, 20, 144).

The Fe_2O_3+MgO values of the leucosomes (Figure 5.5) are mostly <3 wt%, in keeping with the experiments of Patino Douce and Johnston (1991), but several contain much higher Fe_2O_3 and MgO. This is correlated with decreasing SiO_2, and also with important trace element variations (e.g. Y and Sc) to be described below. These high Fe_2O_3+MgO leucosomes probably reflect incorporation of garnet, biotite and/or cordierite as residual or peritectic phases in the bulk analysis.

5.4.2 - Redefinition of leucosome types

As there is no clear link between the major geochemistry and the five leucosome types identified in the field, the major element data can be used to define leucosome generations, and act as a filter to help identify patterns in the trace element data.

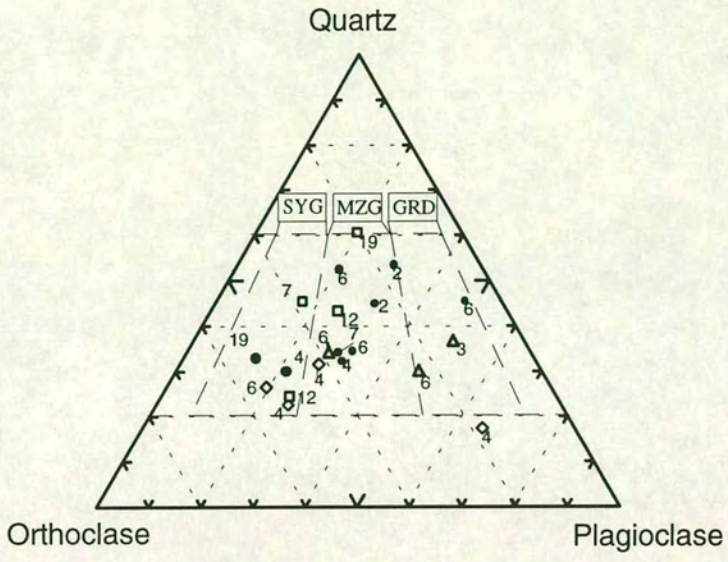

Figure 5.1 - Quartz-Orthoclase-Plagioclase normative plot of Turku leucosomes. All modal values have been normalised to 100. The classification of granitoids is after Clarke (1992). Numbers refer to the localities described in chapter 2

Key for figures 5.1 to 5.5

SYG	Syenogranite	□	Type 1 leucosomes
MZG	Monzogranite	●	Type 2 leucosomes
GRD	Granodiorite	◇	Type 3 leucosomes
		△	Type 5 leucosomes

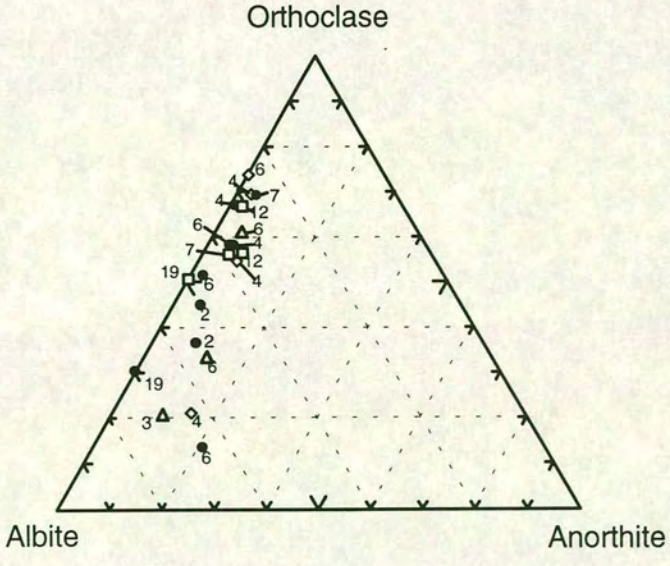

Figure 5.2 - Orthoclase-Albite-Anorthite normative plots of Turku leucosomes. Numbers refer to the localities described in chapter 2

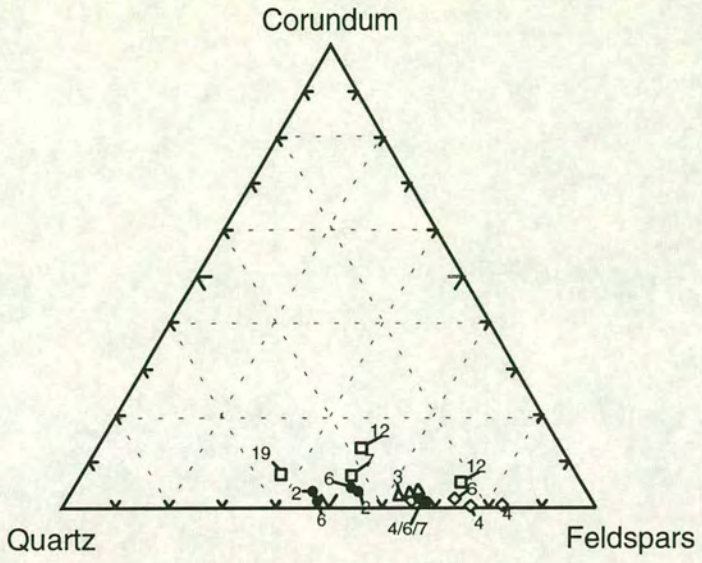

Figure 5.3 - Corundum-Quartz-Total feldspar normative plot of Turku leucosomes. Numbers refer to the localities described in chapter 2

Key for figures 5.1 to 5.5

SYG	Syenogranite	Type 1 leucosomes
MZG	Monzogranite	Type 2 leucosomes
GRD	Granodiorite	Type 3 leucosomes
		Type 5 leucosomes

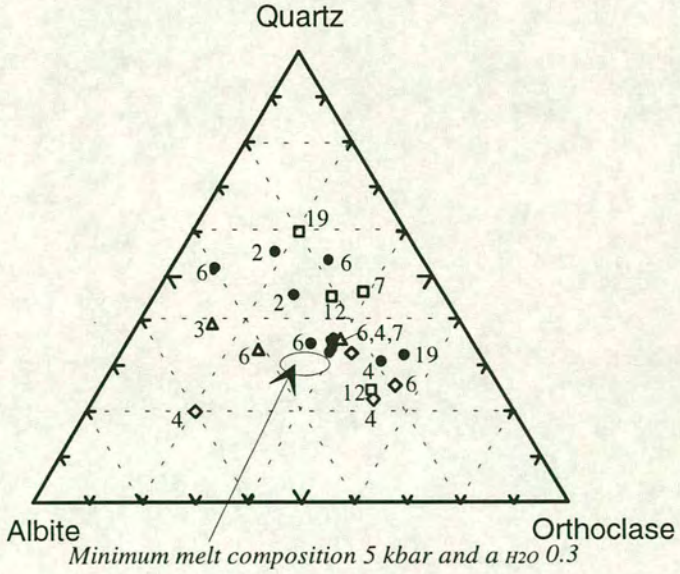

Figure 5.4 - Quartz-Albite-Orthoclase normative plot. Minimum melt compositions are extracted from Inger and Harris (1993). Numbers refer to the localities described in chapter 2

Leucosome compositions that most closely approximate to minimum melts are defined to have normative corundum < 3%, A/CNK ratios between 0.95 and 1.2, Fe_2O_3+MgO <3 wt%, CaO <2 wt% and low Ti. These are hereafter termed Leuc A. Other samples may represent crystal cumulates after some melt extraction (e.g. rich in normative quartz and plagioclase); melt and peritectic phase mixtures (e.g. cordierite or garnet rich); or melt and entrained or adjacent mesosome/restite material. The leucosomes will be termed Leuc B hereafter.

The effects of incorporation of mesosome material can be seen from an AFM plot of the bulk compositions (Figure 5.6). Whilst many leucosomes (Leuc A and some Leuc B) plot above the garnet-biotite and garnet-cordierite tie-lines, several (Leuc B) show the effects of probable incorporation of these phases into the bulk analysis and so plot on or between such tie-lines with mesosome bulk compositions.

5.4.3 - Trace element data

Trace elements can be utilised to examine the effects of minerals or mesosome material mixing with potential melt, and also to evaluate the probable melting reactions (Inger and Harris, 1993). Trace element data for all samples are presented in ppm in Appendix 5.2 along with chondrite normalised equivalents and plots. On the basis of their Rb and Nb+Y contents (Figure 5.7) Leuc A leucosomes mostly plot on the boundary between the COLG (syn-collision granites) and VAG (volcanic arc granite) fields on the discrimination diagram of Pearce et al. (1984). This is the same positions as the Himalayan Leucogranites studied by Inger and Harris (1993). Only Leuc A leucosomes were plotted as these were thought to most closely represent uncontaminated partial melts.

The extent of relative depletion and enrichments in the incompatibles can be evaluated using Rb/Sr ratios. The Rb/Sr ratio can vary as a result of the type of melting reaction involved and also as a result of the fractionation of minerals such as K-feldspar, plagioclase and biotite. Figures 5.8 and 5.9, previously used by Harris et al. (1993), can distinguish between these alternatives. Turku leucosomes (Leuc A)

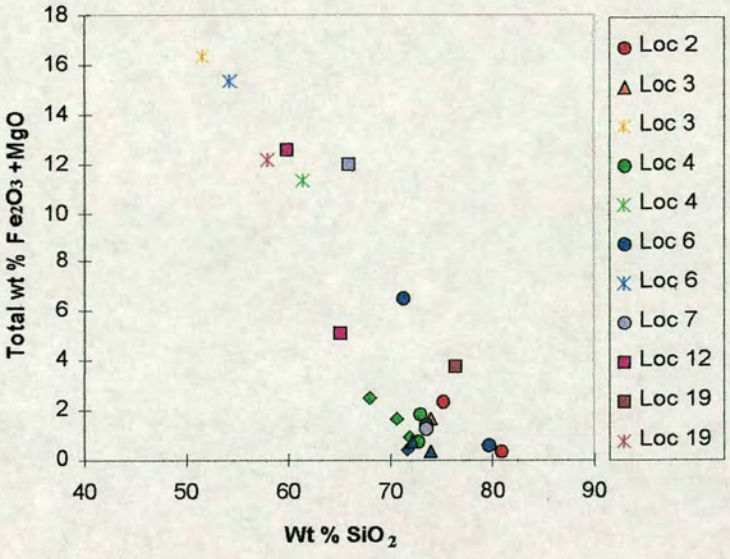

Figure 5.5 - Total wt % Fe 2O3 and MgO against SiO 2 for leucosome and mesosome samples. The leucosome symbols are as for previous diagrams the ✳ symbol represents mesosome samples.

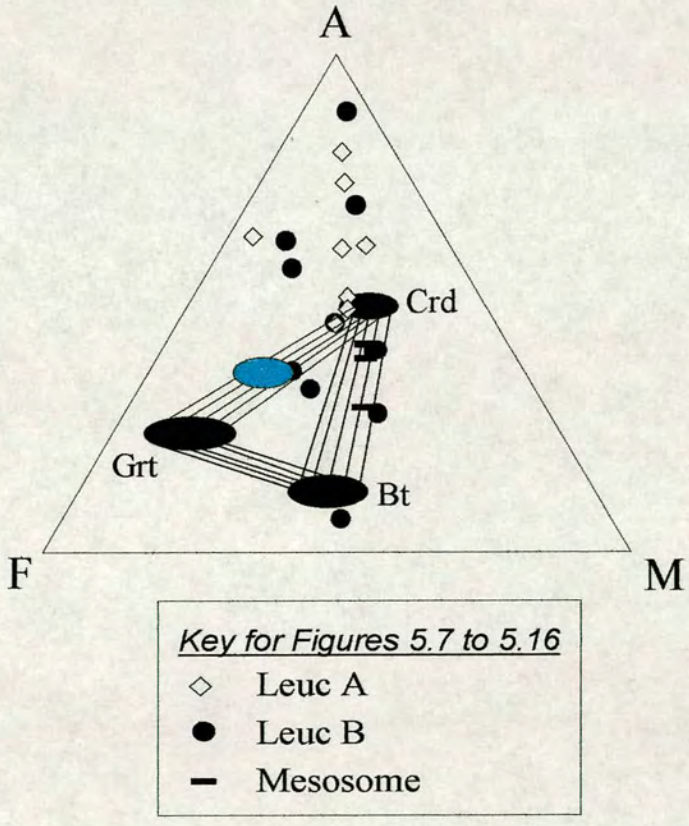

Figure 5.6 - Leucosome and mesosome compositions projected onto an AFM plot along with typic AFM ranges of D3 mesosome phases. The leucosome and mesosome compositions have been adjusted to account for all feldspar components, hence A = Al 2O3-K2O-Na2O-CaO). The mesosome phases have also had K2O-Na2O-CaO removed for direct comparison. The blue elipse represents a melt composition calculated from Namaqualand metapelites by Waters (1988).

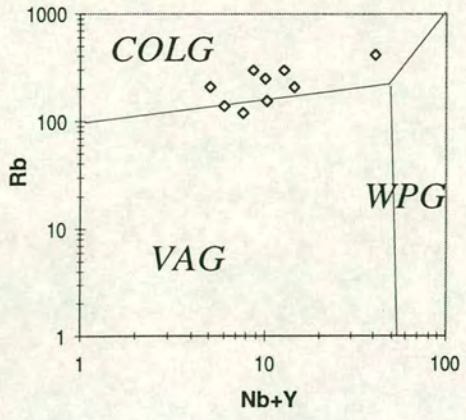

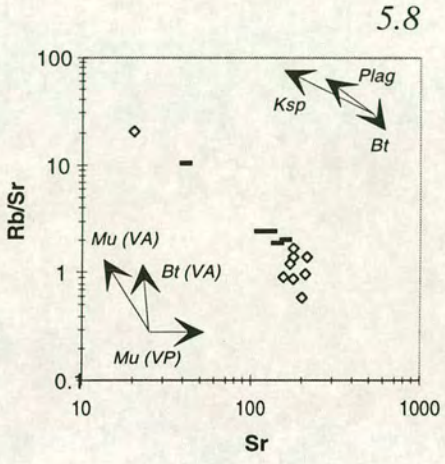

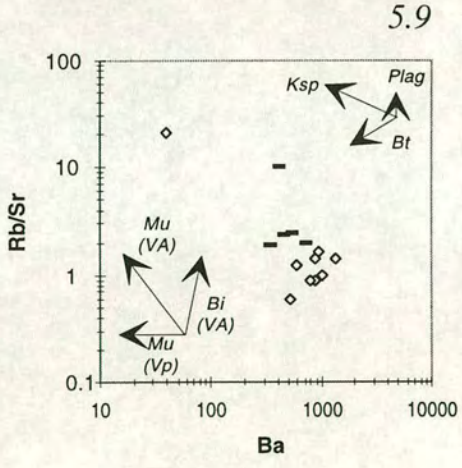

Figure 5.7 - Position of Leuc A leucosomes on the tectonic discrimination diagram of Pearce et al., (1984). COLG - syn-collision granites, WPG - within plate granites, VAG - volcanic arc granites.

Figure 5.8 - Variation In Rb/Sr ratio relative to Sr for Leuc A leucosomes relative to mesosome compositions. The vectors in the top right corner are representative of 10% fractionation of relevant phases. Other arrows reflect partial melting reactions (Harris et al., 1993). The decrease in Rb/Sr of leucosomes can represent accumulation of K-feldspar and plagioclase in the melt, and fractionation or loss of biotite into the mesosome which would become enriched in Rb/Sr.

Figure 5.9 - Variation in Rb/Sr ratio relative to Ba. The lower Rb/Sr ratios and slightly higher Ba content of the leucosomes relative to mesosome suggests enrichment in K-Feldspar. Vectors and symbols are as for Figure 5.8.

move away from mesosomes to lower Rb/Sr ratios with little change in Ba or Sr. This pattern is representative of biotite fractionation rather than typical melting trends, allowing the restite to become relatively enriched in Rb. It is therefore difficult to compare the Rb/Sr ratio of the leucosomes to the source rock as the source has been modified and enriched in Rb. On a Ba (ppm)/K_2O (wt%) plot (Figure 5.10), Leuc A leucosomes are mostly enriched in both elements in comparison to the mesosome. Leuc B leucosomes have a range of K_2O contents with values below those of the mesosome and others comparable to Leuc A leucosomes. This pattern may be representative of final or late melt extraction leaving some leucosomes depleted in K-feldspar, suggesting that the leucosomes are accumulations of feldspars rather than having actual melt compositions.

The contributions of garnet and other Fe-Mg phases, as well as accessory phases such as zircon to the analyses can be evaluated from the plots of Figure 5.11 and 5.12. Increasing Fe_2O_3 and MgO correlates well with Sc, consistent with garnet incorporation in several samples. For this reason the mesosome samples contain the highest contents of both elements. There is a less clear link for Y with some leucosomes containing higher Y contents than mesosome samples, there may therefore be another Y bearing phase present in these leucosomes. This phase however is not zircon as the mesosomes are enriched in Zr in comparison with leucosomes (Figure 5.13). As with Fe+Mg there is a range of Zr contents from depleted up to mesosome values which suggests some degree of restite entrainment in these leucosomes.

The relative roles of entrained/incorporated zircon and garnet can be evaluated further using the normalised Ce/Y (Ce(n)/Y(n) versus Zr (Figure 5.14) and versus Sc (Figure 5.15) plots. Leuc A leucosomes generally have higher Ce(n)/Y(n) and low Zr and Sc whilst the reverse is true for Leuc B leucosomes. The clearest correlation is found to be with Sc and this parallels the relationship between Ce(n)/Y(n) and total Fe+Mg (Figure 5.16) These relationships suggests that some Leuc B leucosomes contain excess garnet and zircon. Those leucosomes with high Ce(n)/Y(n) and low

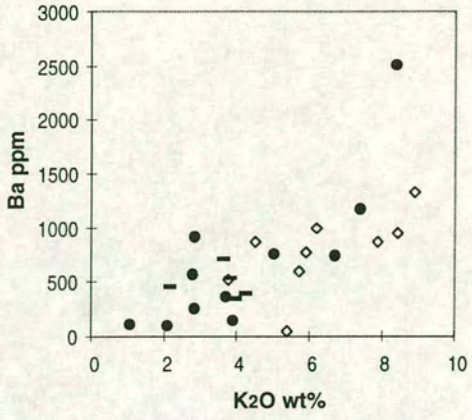

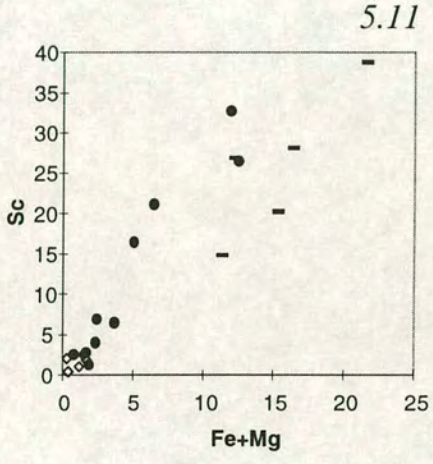

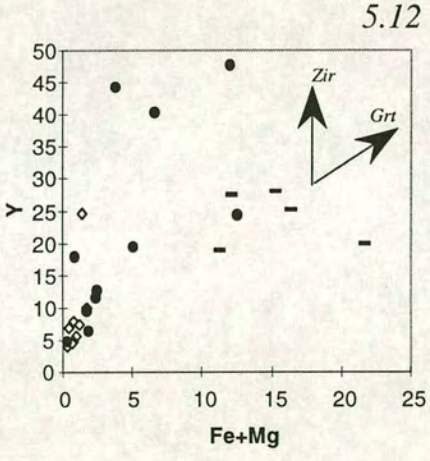

Figure 5.10 - Ba against K2O plot for all Turku leucosomes and mesosomes. The low Ba and K2O leucosomes are depleted in K-feldspar and may represent plagioclase rich cumulates.

Figure 5.11 - Positive trend between Sc and Fe+Mg. Sc is preferentially held within garnet but is not incorporated in zircon.

Figure 5.12 - There is less correlation between Fe+Mg and Y. Some Leuc 2 leucosomes are enriched in Y and not Fe+Mg, which would suggests that these leucosomes are enriched in a Y bearing phases other than garnet.

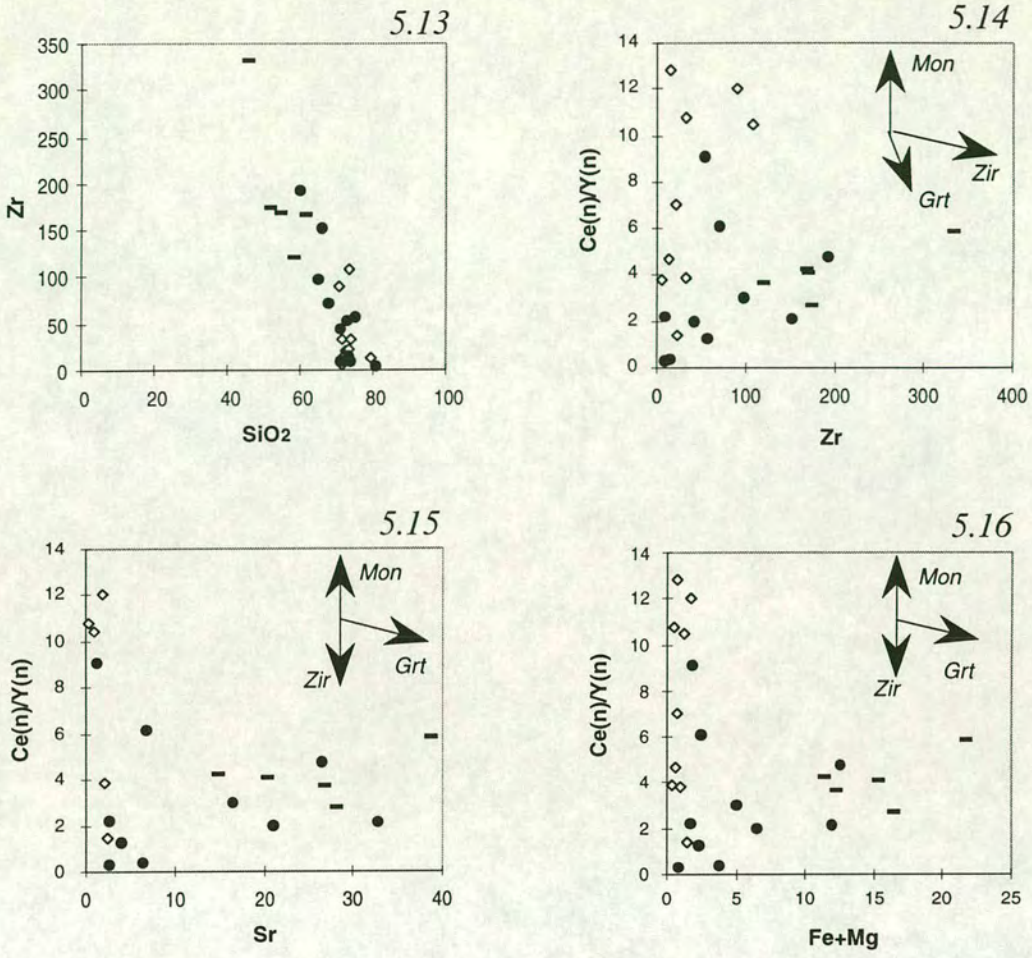

Figure 5.13 - Zr against SiO2 plot. There is a negative correlation between the two elements with mesosomes enriched in Zr relative to most leucosomes

Figure 5.14 - Normalised Ce/Y ratio against Zr plot with some leucosomes enriched in Ce/Y and others in Zr.

Figure 5.15 - Normalised Ce/Y ratio against Sr plot. The Sc contents of some Leuc A leucosomes were too low to detect.

Figure 5.16 - Normalised Ce/Y ratio against Fe+Mg plot which mirrors the pattern observed in the previous diagrams.

Fe-Mg (Sc, Zr) may indicate the presence of monazite which typically has high Ce(n)/Y(n) ratios (Watt, 1993).

5.5 - Discussion

The major element contents and normative values of the Turku granulites are within the compositional range of S-type granitoids, although there is a spread of values from granodiorite to syenogranitic compositions within a QAP plot (Figure 5.1). On a quartz-albite-orthoclase plot (Figure 5.4) it can be seen that several of the analysed leucosomes have compositions that approximate minimum melts. These observations are irrespective of the leucosome types that the samples were assigned from field observations. The Rb/Sr ratio suggests that as melting occurred biotite fractionated from the melt into the restite, depleting the melt in Rb. Biotite has high Rb and low Sr and as such removal of biotite leads to depletion of melt in Rb driving it to lower Rb/Sr ratios. This depletion is seen as a case for disequilibrium melting by Inger and Harris (1993). A further observation from the Rb/Sr data is that the leucosomes (even the clean ones) may be in part accumulations of feldspars, deviating from true melts by having lost a final fraction of late crystallising melt rich in incompatibles.

The Fe_2O_3 and MgO wt% contents of Leuc B leucosomes are higher than the experimental values of Patino Douce and Johnston (1991), i.e. >3 wt%. This enrichment in Fe-Mg correlates with high Sc, Y and Zr values which is consistent with the melt having entrained some restitic material (White and Chappell, 1977; Patino Douce and Johnston, 1991; Sawyer, 1996) that is comparatively enriched in Fe-Mg phases such as biotite, garnet and cordierite.

Ce(n)/Y(n) ratio variations between samples reflect both garnet and zircon entrainment as well as preferential 'entrainment' of monazite in some cases. The accessory phases monazite and zircon can contain 60 % of the REE mass budget of a melt but they have limited dissolution in low a_{H2O} melts (Watt and Harley, 1996; Bea, 1996; Watson, 1996). Therefore during the segregation of melt, the restite

becomes positively enriched in these phases, but if some restitic material is entrained or mixed in the melt then the sum of the two become comparatively enriched in these elements.

Further evidence for entrained material in some of the Turku leucosomes is the presence of cordierites with sillimanite rich cores, a common texture in mesosomes (Chapter 3 this study). Poikiloblastic crystals of garnet and cordierite present within Turku leucosomes are interpreted as peritectic products of dehydration melting (Waters and Whales, 1984; Waters, 1988; 1994; Powell and Downes, 1991). Therefore the enrichment in Fe+Mg, Zr, Sc and Y in Leuc B leucosomes can be seen to result from a combination of entrained restitic material and the presence of peritectic melt phases (solid phases produced during incongruent melting.

Those leucosomes with low total Fe-Mg could be seen as efficiently segregated melts (White and Chappell, 1977; Sawyer, 1996), but their low Rb/Sr ratios suggest that they do not represent melts formed in equilibrium with the preserved mesosome. This low Rb/Sr could reflect the loss of a final minimum melt fraction, leaving behind a leucosome that is itself slightly residual or 'cumulate', consisting of peritectic phases plus minerals that crystallised prior to final melt freezing. Leuc 2 leucosomes of the Turku terrain are also representative of partial melts, but their major and minor element geochemistry is indicative of varying degrees of restitic entrainment. Low K-feldspar values in some leucosomes may indicate that there may have been some melt extraction, leaving the leucosomes as a form of 'restite', increasing the proportion of Fe-Mg phases, as well as already crystallised feldspars.

5.6 - Conclusions

Of the leucosome samples studied, despite superficial similarities in field features, modal mineralogy, textures and general appearance, very few have chemical features (majors, trace and REE) completely compatible with simple minimum/haplogranitic melts. Important deviations from ideal melt compositions may reflect combinations of the following:

1. Incorporation or entrainment of restite and/or peritectic phases (Fe+Mg, Zr, Sc, Y contents)
2. Fractionation and reaction with wall rocks.
3. Accumulation of crystals and loss of a final small percentage of melt (drive to low Rb/Sr, low K_2O, Ba and Zr (i.e. fractional crystallisation).

Chapter 6

Geothermobarometry

Chapter 6 - Geothermobarometry

6.1 - Previous work

The significance of melting in a terrain has to be assessed in light of the peak pressures and temperatures attained, as they influence the fertility of rocks (Clemens and Vielzeuf, 1987; Le Breton and Thompson, 1988; Johannes and Holtz, 1996). The metamorphic evolution of the Turku terrain has been closely studied by previous workers (Höltta, 1986; Van Duin and Nieman 1993; Väisänen et al., 1994; 1999). The results of their thermobarometric studies are presented in Table 6.1.

Work by Höltta (1986) and Van Duin and Nieman (1993) has indicated that there is a gradient in metamorphic temperature and pressure across the Turku terrain. Van Duin and Nieman (1993) observed a transition from amphibolite to granulite facies conditions around the Turku area. Väisänen et al. (1994) and Väisänen and Höltta (in press) suggest the peak in temperature and pressure (800°C and 6 kbar) is located around the town of Mynamaki in the middle of the terrain. Similar temperatures are also recorded in the Parainen area south east of the town of Turku, an area not studied within this project. Temperatures in the south and north of the terrain are reported to range from 650 to 730°C.

Höltta (1986), Van Duin and Nieman (1993) and Väisänen et al. (1994) utilised only the cores of large garnets and matrix biotite phases to obtain temperature estimates, as it was believed that these would preserve the peak temperatures. When Höltta (1986) analysed garnet rims against biotite inclusions or biotites next to the garnet, he derived much lower temperatures due to the phases having undergone Fe-Mg exchange upon retrogression, as discussed in Chapter 4. For their pressure estimates, the peak in values is also obtained from outcrops near the towns of Mynamaki and Parainen. Values calculated by previous workers (Höltta, 1986; Van Duin and Nieman, 1993; Väisänen et al., 1994; Väisänen and Höltta, in press) range from 3.5 to 6.5 kbar across the terrain.

Table 6.1 – Previous pressure and temperature estimates for the Turku terrain.

Höltta, 1986	
Temperature estimates	
641-775	Garnet-cordierite, Holdaway and Lee (1977)
448-876	Garnet-biotite, Ferry and Spear (1978)
528-730	Garnet-biotite, Perchuk and Lavrent'eva (1983)
Pressure estimates	
4.8-5.8	Garnet-cordierite, Holdaway and Lee (1977)
6.3-6.5	Garnet-plagioclase, Newton and Haselton (1981)
Van Duin and Nieman, 1993	
Temperature estimates (pressure - 5 kbar)	
627-743	Garnet-biotite, Holdaway and Lee (1977)
652-845	Garnet-biotite, Ferry and Spear (1978)
595-714	Garnet-biotite, Perchuk and Lavrent'eva (1983)
649-732	Garnet-biotite, Perchuk and Aranovich (1986)
713-781	Garnet-cordierite, Thompson (1976)
688-744	Garnet-cordierite, Holdaway and Lee (1977)
684-740	Garnet-cordierite, Perchuk and Lavrent'eva (1983)
Pressure estimates (temperature - 750°C, X_{H2O} - 0.4)	
5.2-6.5	Garnet/cordierite/sillimanite/quartz, Holdaway and Lee (1977)
5.0-5.9	Garnet/cordierite/sillimanite/quartz, Newton and Wood (1979)
4.3-5.2	Garnet/cordierite/sillimanite/quartz, Aranovich and Podlesskii (Fe basis) (1983)
3.9-5.2	Garnet/cordierite/sillimanite/quartz, Aranovich and Podlesskii (Mg basis) (1983)
Väisänen and Höltta (in press)	
Temperature estimates calculated by THERMOCALC v 2.4 (Holland and Powell, 1990) and GEOPATH (Gerya and Perchuk, 1992)	
North	660-730
Middle	800-825
South	640-720
Pressure estimates calculated by THERMOCALC v 2.4 (Holland and Powell, 1990) and GEOPATH (Gerya and Perchuk, 1992)	
North	T 3.7-3.9/G 3.5-3.7
Middle	6.3-6.7
South	3.7-4.7

6.2 - Aims for this study

Samples were taken from the key localities throughout the terrain in order to assess the presence of the temperature and pressure gradient reported by the earlier work of Höltta 91986); Van Duin and Nieman (1993), Väisänen et al. (1994) and Väisänen and Höltta (in press).

6.3 - Methodology

The geothermometric approach of this study was to utilise Fe-Mg exchange thermometers involving reactions between garnet and cordierite, and between garnet and biotite. Pressure is calculated from garnet-cordierite-sillimanite-quartz barometers, all listed below. Both pressures and temperatures are also derived from the internally consistent data set of Holland and Powell (1990) using the associated computer software THERMOCALC.

Samples were taken from across the terrain but the thermobarometric data are concentrated within the southern and middle zones. Samples without garnet from the northern assemblages could not fix a temperature or pressure using THERMOCALC. Following the same approach of earlier workers on the area, care was taken to select sample points from garnet cores and corresponding matrix phases in order to attain near-peak temperatures and pressures. As a comparison, and to try to constrain conditions of lower grade retrogression, sample points from garnet rims and the corresponding phases in contact with the garnet were also analysed.

Thermometers and **B**arometers used:

T Garnet-biotite, Ferry and Spear (1978).	(F&S)
T Garnet-biotite, Perchuk and Lavrent'eva (1983).	(PLGB)
T Garnet-biotite, Thompson (1976).	(Thompson)
T Garnet-cordierite, Aranovich and Podlesskii (1983).	(A&P)
T Garnet-cordierite, Perchuk and Lavrent'eva (1983).	(PLGC)
B Garnet-cordierite-sillimanite-quartz, Carey (1995).	(CA and CH)
B Garnet-cordierite-sillimanite-quartz, Waters and Whales (1984).	(WW)
B Garnet-cordierite-sillimanite-quartz, Mukhopadyay and Holdaway (1994).	(MHA and MHH)

6.3.1 - Thermometry

Garnet-biotite and garnet-cordierite thermometers are based on the following Fe-Mg exchange reactions:

$$\text{Fe-grt} + \text{Mg-bt} = \text{Mg-grt} + \text{Fe-bt} \qquad (6.1)$$

$$\text{Fe-crd} + \text{Mg-grt} = \text{Mg-crd} + \text{Fe-grt.} \qquad (6.2)$$

The thermodynamic calculations used by each thermometer can be found in Appendix 6.1. In the case of equation 6.1, the biotite becomes more Fe-rich with an increase in temperature following the continuous exchange reaction. As the ΔV of this reaction is small, it is in theory an excellent thermometer (Chipera and Perkins, 1988). The Thompson (1976) thermometer was derived by correlating the K_D values of natural biotite- and garnet-bearing assemblages against estimated temperatures based upon experimental phase equilibria. The thermometer of Ferry and Spear (1978) was based on experiments in a system with an X_{Fe} (Fe/Fe+Mg) of 0.9 compared to the 0.6 of the system used by Perchuk and Laverent'eva (1983). Some thermometers have tried to incorporate other elements that may affect the PT position of the reaction, for example Ca in garnet and Ti in biotite (e.g. Indares and Martignole, 1985). However work by Chipera and Perkins (1988) has shown that it is the straightforward Fe-Mg thermometers that yield the most consistent temperatures. Also, as discussed by Schreurs (1985) and Höltta (1986) and as shown by this study, the grossular content of the garnet is low enough to have a negligible effect.

As an alternative to using simple Fe-Mg exchange, the thermodynamics for a given reaction can be derived from an internally consistent thermodynamic dataset, in this study the dataset of Powell and Holland (1988) and Holland and Powell (1990) were used. All reactions within a given assemblage are calculated using available experimental information on phase end members (Powell and Holland, 1994). From this information a best fit average P/T can be calculated using a least squares method to average the data for an independent set of reactions within a rock (Powell and Holland 1993; 1994). These calculations are carried out using the computer programme THERMOCALC, which utilises the dataset of 123 end members to calculate a reaction position appropriate to the compositions of complex solid solutions. Textural relations must be understood so that the peak assemblages can be

defined. For the Turku pelites the assemblage used was grt + crd + bio + kfs + plag + qtz. A detailed description of THERMOCALC calculations and example files can be found in Appendix 6.3.

In order to extract as near to peak temperatures as possible it is important to select the sample points that are least affected by obvious re-equilibration and exchange during cooling. Garnets that show growth zoning preserve an artefact of the prograde path during growth. In these circumstances the rim of the garnet should be used because this should yield the highest temperatures (Chipera and Perkins, 1988). However the

Turku granulites do not preserve such zoning (see Chapter 4) but rather show a decrease in X_{Mg} at their rims. Previous workers on the terrain (Höltta, 1986; Van Duin and Nieman, 1993; Väisänen and Höltta, in press) have attributed this to Fe-Mg exchange between the garnet and any biotite or cordierite it is in contact with upon cooling or later retrogression. In this case, the centre of the garnet should be used in conjunction with a matrix biotite or cordierite that is not in contact with the garnet. This is the approach taken by previous workers on the terrain and by Chipera and Perkins (1988) when they compared garnet and biotite thermometers.

In all of the samples used in this chapter the garnet and cordierite are second generation, D3 phases. It is assumed that the matrix biotite was in equilibrium with this generation of garnet and cordierite even though it was still aligned along S2, because matrix biotite was used up in the dehydration melting reactions that formed these phases. Diffusion is fast in biotite at high temperatures (Spear, 1993) and as the Turku rocks saw another thermal peak during D3 (Väisänen and Höltta, in press) it has been assumed that Grt 2 and Crd 2 were stable with matrix biotite. However it is also possible that since this peak the biotite has suffered mass transfer reactions which have changed its composition (Spear, 1993). As it is possible that the compositions of the phases analysed have been affected by post-peak Fe-Mg exchange reactions, the results should be treated with some degree of caution.

6.3.2 – Barometry

The barometers used are based on the reaction below:

$3(Fe\text{-}Mg)Cordierite.H_2O = 2(Fe\text{-}Mg)Garnet + 4Sillimanite + 5Quartz$ (6.3)

Cordierite-Garnet-Sillimanite-Quartz barometers have been used by previous workers to calculate pressures, even though sillimanite is not stable across all of the terrain (Höltta, 1986; Van Duin and Nieman, 1993). Pressures in this study were also calculated using the database of Powell and Holland (1988) and Holland and Powell (1990) in case the above approach produced erroneous results. The thermodynamic calculations of the individual barometers can be found in Appendix 6.2. The position of this barometer is dependent upon the H_2O content of the cordierite, this n value (n moles of H_2O per formula unit) is calculated experimentally by the two barometers of Carey (1995) as a function of pressure and temperature.

These values are then input into equation 6.3 to derive a pressure. The barometer of Mukhopadyay and Holdaway (1994) experimentally calibrates the position of the reaction in PT space inputting various values of wt% H_2O. In both cases the two barometers were devised for hydrous and anhydrous cordierite. The barometer of Waters and Whales (1984) is calculated using the experiments of Holdaway and Lee (1977) for their cordierite H_2O content.

6.4 - Results

6.4.1 - Thermometry

The equilibration temperatures obtained using the garnet-biotite and garnet-cordierite thermometers are listed in Table 6.2, along with the stated errors. Figure 6.1 is a plot showing the temperatures calculated from the five conventional thermometers along with those calculated by THERMOCALC v 2.4 (Powell and Holland, 1988; Holland and Powell, 1990). The thermometers of Thompson (1976) and Perchuk and Lavrent'eva (1983) show fairly consistent ranges of peak temperatures of 600-800°C. These temperatures are consistent with those of previous workers shown in Table 6.1. The errors are also shown in Table 6.1 although they haven't been added to

Figures 6.1 and 6.2 as they hid the data points. Thus for errors refer to Table 6.1. The garnet-cordierite thermometers yield a wider range of estimates down to 500°C (Figure 6.1). The other agreement with previous temperature estimates is that the maximum values of the Ferry and Spear (1978) thermometer are too high, up to 900°C. The peak values of the other thermometers range from 750-800°C.

The retrogressive temperatures of Ferry and Spear (1978) are the lowest with a minimum of 300°C. The retrogressive temperatures for the Perchuk and Lavrent'eva (1983) and Thompson (1976) thermometers range from 700-300°C. The maximum retrogressive values of the cordierite thermometers are equal to the average values for the peak assemblages, around 600°C with a much smaller total temperature range of about 50°C.

Some of the 'peak' pairings of garnet core and matrix biotite or cordierite, actually produce temperatures as low as 500°C which may indicate that the core of some garnets have been affected by re-equilibration upon cooling (Spear, 1993). The hat[1] values produced by THERMOCALC are highest for the pyrope end member which illustrates the dependence of temperature on garnet composition (Holland, 1998, *pers. comm.*) Samples 88 and 90 preserve garnet-biotite temperatures up to 140°C lower than those calculated from garnet-cordierite thermometers. Therefore the biotite may have suffered a net transfer or Fe-Mg exchange with garnet or cordierite causing an increase in X_{Mg} within the biotite, i.e. down temperature (retrograde) re-equilibrium. This has the effect of lowering the temperatures calculated by garnet-biotite thermometry (Spear, 1992).

[1] The hat value is a numerical measure of the dependence of the pressure or temperature estimate of the composition of 1 particular end-member.

Table 6.2 – Equilibration temperature estimates in °C using five Fe-Mg exchange thermometers. C/M – Temperature calculated from garnet core combined with matrix biotite or cordierite. R/I NGT – Temperature calculated form garnet rim composition combined with biotite inclusion compositions, or from biotite or cordierite in contact with garnet rim. L - Locality, S - Sample. Errors are quoted at the 2σ level, the propagation of errors is discussed in Appendix 6.

BT-GRT	F&S	PLGB	TH	CD-GRT	A&P	PLGC
Southern Localities						
L3/S88				**L3/S88**		
C/M	552 ±89	577 ±43	552 ±61	C/M	740 ±62	708 ±60
R/NGT	329 ±89	433 ±43	372 ±61	R/NGT	632 ±62	605 ±60
L3/S90				**L3/S90**		
C/M	556 ±89	579 ±43	555 ±61	C/M	808 ±62	773 ±60
R/I	385 ± 89	473 ±43	419 ±61	R/NGT	658 ±	629 ±60
L2/S83				**L2/S83**		
C/M	848 ±89	722 ±43	757 ±61	C/M	756 ±62	721 ±60
R/I	566 ±89	585 ±43	562 ±61		Na	na
L2/SD18				**L2/SD18**		
C/M	749 ±89	678 ±43	692 ±61	C/M	734 ±62	702 ±60
R/I	476 ±89	532 ±43	493 ±61	R/NGT	648 ±62	620 ±60
L4/S10				**L4/S10**		
C/M	868 ±89	730 ±43	769 ±61	C/M	798 ±62	763 +60
R/NGT	565 ±89	584 ±43	561 ±61	R/NGT	613 ±62	585 +60
L4/S15				**L4/S15**	na	Na
C/M	696 ±89	653 ±43	656 ±61			
R/NGT	430 ±89	503 ±43	456 ±61			
Middle Localities						
L8/S123				**L8/S123**	517 ±62	487 ±60
C/M	633 ±89	621 ±43	611 ±61	C/M	639 ±62	605 ±60
R/I	432 ±89	504 ±43	458 ±61	R/NGT	517 ±62	487 ±60
L6/S114				**L6/S114**		
C/M	848 ±89	722 ±43	756 ±61		na	na
R/NGT	614 ±89	611 ±43	597 ±61		na	na
L6/S118				**L6/S118**		
C/M	852 ±89	723 ±43	759 ±61	C/M	793 ±62	758 ±60
R/I	751 ±89	679 ±43	693 ±61	R/NGT	772 ±62	736 ±60
L7/S36				**L7/S36**		
C/M	685 ±89	648 ±43	648 ±61	C/M	676 ±62	641 ±60
R/NGT	698 ±89	654 ±43	657 ±61		681 ±62	647 ±60
L7/SD41				**L7/SD41**		
C/M	904 ±89	744 ±43	791 ±61	C/M	775 ±62	739 ±60
R/I	523 ±89	561 ±43	530 ±61		na	na

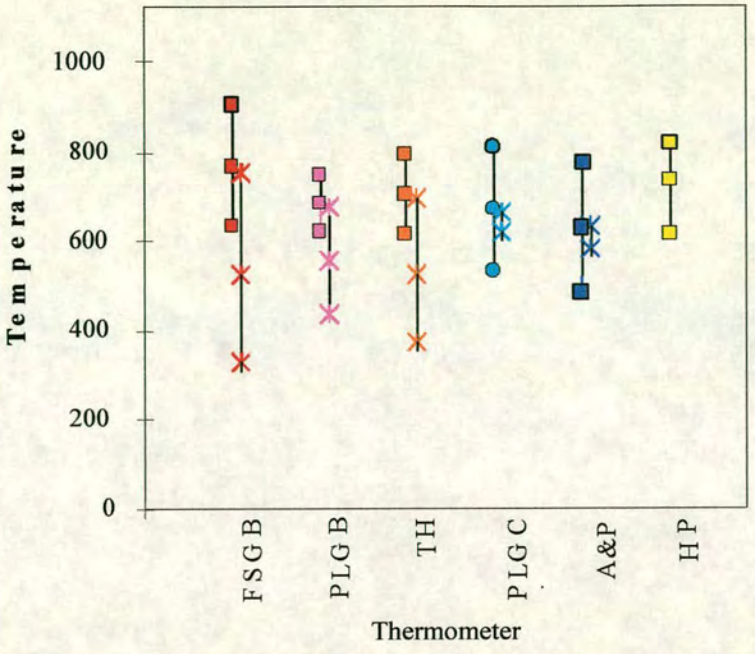

Figure 6.1 - Equilibration temperature ranges (in °C) of the Turku granulites calculated using the 5 Fe-Mg exchange thermometers and THERMOCALC. Solid symbols represent prograde T estimates, crosses represent retrogressive T estimates. Abbreviations: F&S = Ferry and Spear (1976) grt-bt; PLGB = Perchuk and Lavrent'eva (1983) grt-bt; TH = Thompson (1976) grt-bt; PLCB = Perchuk and Lavrent'eva (1983) grt-crd; A&P = Aranovich and Podlesskii (1983); HP = THERMOCALC.

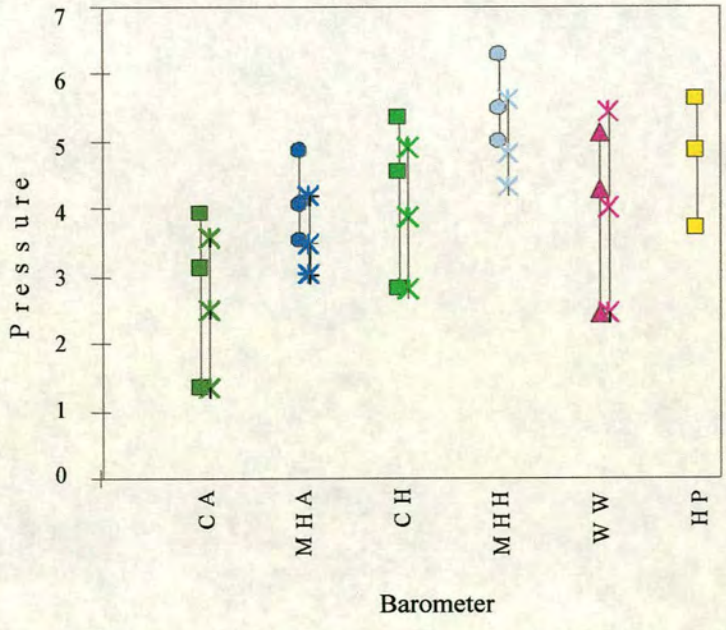

Figure 6.2 - Equilibration pressure ranges calculated using the following geobarometer calibrations: CA = Carey (1995), anhydrous cordierite; MHA = Mukhopadyay and Holdaway (1994), anhydrous; CH = Carey (1995), hydrous cordierite; MHH = Mukhopadyay and Holdaway (1994), hydrous; WW = Waters and Whales (1984); HP = THERMOCALC.

6.4.2 - Barometry

Calculated equilibration pressures are presented in Table 6.3 and illustrated in Figure 6.2, again for errors refer to Table 6.3. The barometers do not show particularly consistent results.

Table 6.3 – Equilibration pressures estimated using various workers calibrations of the cordierite + garnet + sillimanite + quartz barometer. C/M – Pressure calculated from garnet core combined with matrix biotite or cordierite. R/I NGT – Pressure calculated from garnet rim composition combined with biotite inclusion compositions, or from biotite or cordierite in contact with garnet rim. L - Locality, S - Sample. Errors are quoted at the 2σ level, the propagation of errors is discussed in Appendix 6.

	PCarey	P Muk	PHCarey	PH-Muk	PWaters
Southern Localities					
L3/S88					
C/M	3.03 ±0.53	3.54 ±0.71	4.49 ±0.65	4.97 ±0.91	4.20 ±0.91
R/NGT	2.10 ±0.53	3.02 ±0.71	3.41 ±0.65	4.31 ±0.91	3.89 ±0.91
L3/S90					
C/M	3.88 ±0.53	3.78 ±0.71	5.34 ±0.65	5.21 ±0.91	5.09 ±0.91
R/NGT	2.68 ±0.53	3.33 ±0.71	4.00 ±0.65	4.62 ±0.91	4.50 ±0.91
L2/S83					
C/M	3.57 ±0.53	3.90 ±0.71	5.02 ±0.65	5.37 ±0.91	4.76 ±0.91
L2/SD18					
C/M	3.04 ±0.53	3.61 ±0.71	4.50 ±0.65	5.05 ±0.91	4.21 ±0.91
R/NGT	2.29 ±0.53	3.04 ±0.71	3.60 ±0.65	4.33 ±0.91	4.08 ±0.91
L4/S10					
C/M	3.84 ±0.53	3.82 ±0.71	5.30 ±0.65	5.26 ±0.91	5.05 ±0.91
R/NGT	2.27 ±0.53	4.17 ±0.71	3.73 ±0.65	5.61 ±0.91	3.40 ±0.91
Middle Localities					
L8/S123					
C/M	1.54 ±0.53	4.87 ±0.71	3.00 ±0.65	6.30 ±0.91	2.64 ±0.91
R/NGT	1.55 ±0.53	3.98 ±0.71	2.86 ±0.65	5.27 ±0.91	3.31 ±0.91
L6/S118					
C/M	3.91 ±0.53	3.94 ±0.71	5.37 ±0.65	5.37 ±0.91	5.12 ±0.91
R/NGT	3.59 ±0.53	3.21 ±0.71	4.90 ±0.65	4.51 ±0.91	5.44 ±0.91
L7/S36					
C/M	3.08 ±0.53	4.30 ±0.71	4.55 ±0.65	5.74 ±0.91	4.26 ±0.91
L7/SD41					
C/M	3.86 ±0.53	4.06 ±0.71	5.32 ±0.65	5.49 ±0.91	5.06 ±0.91

The anhydrous barometer of Carey (1995) has a range of values down to 1 kbar which is much lower than the estimates of previous workers. However the hydrous barometer of Carey (1995) ranges from 3 to 5.5 kbar which is in agreement with the

barometer of Waters (1984). THERMOCALC also produces similar peak and average pressures but has a smaller range with minimum values of 3.5 kbar. The barometers of Mukhopadyay and Holdaway (1994) have a much smaller pressure range, with anhydrous pressures calculated from 3.5 to 5 kbar and hydrous pressures 5 to 6.5 kbar. The barometers of Carey (1995), Waters and Whales (1984) and THERMOCALC have an average value ≤1 kbar from their maximum values whilst the average pressures of Mukhopadyay and Holdaway (1994) are only 0.5 kbar above their minimum values. There is therefore a clustering of values from 3 to 5 kbar which is in agreement with the values of previous workers (Höltta, 1986; Van Duin and Nieman, 1993; Väisänen and Höltta, in press).

6.5 - Discussion

6.5.1 - Comparison of geothermometers

Temperatures obtained with the thermometer of Ferry and Spear (1978) are consistently higher than the other thermometers at high temperatures. It also produces the lowest temperatures at the low temperature end of the range. This pattern has also been observed by Schreurs (1985); Höltta (1986); Van Duin and Nieman (1993). In their comparison of thermometers Chipera and Perkins (1988) also found that the temperatures of Ferry and Spear (1978) were too high. The thermometers of Perchuk and Lavrent'eva (1983) and of Thompson (1976) are very similar to each other, and to the calculations of THERMOCALC. These show garnet core temperatures of 600 to 800° which is in agreement with previous work on the terrain. The garnet-cordierite thermometers of Perchuk and Lavrent'eva (1983) and of Aranovich and Podlesskii (1983) are very similar to each other and to the garnet-biotite thermometers, although they show a slightly larger variation between their minimum and maximum values. The range of retrogressive values however is much less, <100°C. This may be linked to the larger retrogressive X_{Mg} range displayed by biotite in contact with garnet in comparison to cordierite, as discussed in chapter 4.

Thus the thermometers are in agreement with each other with the exception of the Ferry and Spear (1978) calibration. This may be linked to the X_{Mg} of the system in

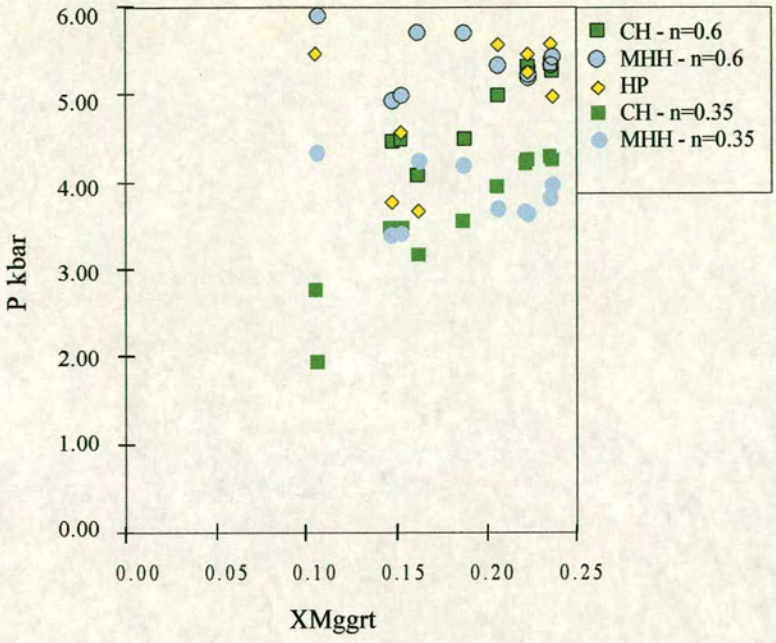

Figure 6.3 - Plot of pressure (in kbar) versus garnet X $_{Mg}$ illustrating the effect of varying the n value of the hydrous barometers of Mukhopadyay and Holdaway (1994) and Carey (1995). Outlined symbols refer to pressures calulated using an n value of 0.6. Symbols without outlines are values calculated assuming an n value of 0.35.

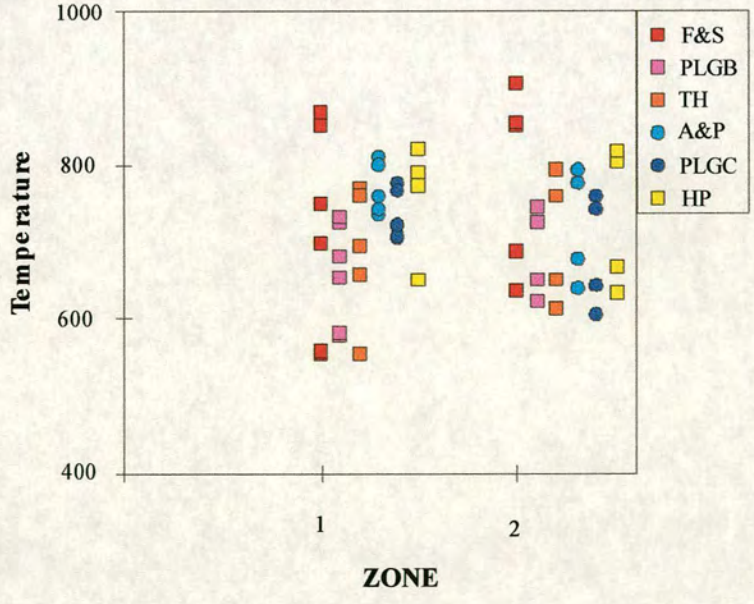

Figure 6.4 - Calculated temperature ranges (in °C) for the southern (1) and middle (2) zones in the study.

which these workers carried out their experiments, (>0.1). The thermometers of Perchuk and Lavrent'eva (1983) used compositions analogous to natural phases and Thompson (1976) calibrated his thermometer using K_D values of natural assemblages against experimental data. Perchuk and Lavrent'eva (1983) did have problems producing biotites and garnets experimentally with a variance in X_{Mg} at all temperatures. Thus they assumed ideal distribution between phases above 600°C which may have led to a slight underestimation of temperature in comparison to the other thermometers.

6.5.2 - Comparison of geobarometers

In all cases the anhydrous barometers of Carey (1995) and of Mukhopadyay and Holdaway (1994) produce the lowest pressures, whilst the hydrous barometer of Mukhopadyay and Holdaway (1994) or THERMOCALC gives the highest. Those samples with garnet X_{Mg} >0.2 have slightly higher pressures.

The difference between the barometers is probably linked to their differing a_{H2O} models, which has an effect on the position of the reaction in PT space. The hydrous barometers produce pressures that fit the assemblages and previous estimates better than their anhydrous counterparts. The hydrous barometers of Mukhopadyay and Holdaway (1994) and Carey (1995), use an estimate of the amount of H_2O in mole per formula unit within the channels of cordierite at saturation (n), based upon an estimate of pressure and temperature. Using pressures and temperatures calculated by previous workers on the terrain (Höltta, 1986; Väisänen et al., 1994; and Väisänen and Höltta, in press), an n value of 0.6 was used in this study. These pressure estimates can be compared to those calculated from n values of 0.35, which are obtained from Turku cordierites using the model of Harley and Carrington (in press), (Chapter 7), in Figure 6.3. The pressures calculated with the lower values of n are on average 1 kbar lower than previous pressure estimates and those pressures calculated by THERMOCALC. As will be discussed in later chapters this difference is due to the Turku cordierites being undersaturated with respect to H_2O.

6.5.3 - Comparison to earlier PT estimates

Previous work has suggested that there is a peak of temperature and pressure in the central zone of the Turku terrain (Höltta, 1986; Väisänen et al., 1994; Väisänen and Höltta, in press), as discussed in the beginning of the chapter. To this end the data were split into two, southern zone/middle zone temperatures and southern zone/middle zone pressures (Figures 6.4 and 6.5). Figure 6.4 shows that samples from both zones yield temperatures up to 800°C with no maximum peak for data from the middle localities. Also, there is virtually no difference in the range of pressures (Figure 6.5) between the two areas, certainly not a difference of 3 kbar as reported by Väisänen and Höltta (in press).

6.6 - Conclusions

The choice of sample points has a strong bearing on the pressure and temperature calculated. The rims of some garnets as well as in some cases the cores, and the biotite or cordierite in contact with them, produce lower temperatures and pressures due to later retrogressive Fe-Mg exchange (Höltta, 1986).

Although there are some problems associated with the thermometers used, as discussed earlier, the peak temperatures for the two zones averages 750 to 800°C in agreement with the estimates of Höltta (1986); Van Duin and Nieman (1993) Väisänen and Höltta (in press). Temperatures calculated for retrograde exchange average 550 to 650°C with minimum temperatures of 450 to 500°C. Pressure decreases from an average peak of 5 kbar to just under 4 kbar and thus the terrain underwent cooling with no significant decrease in pressure. This isobaric cooling path fits with the gentle slope of Höltta (1986) (Figure 6.6). Väisänen et al. (1994) suggest that peak metamorphism occurred during D3, around 1840 Ma. Later generations of sillimanite are a retrogressive phase found mostly in the north of the terrain, which would fit with the beginnings of the retrograde path. Andalusite has been found as a retrogressive phase around cordierite in this study (middle and northern zones) and by Höltta (1986) and Väisänen and Höltta (in press). This would

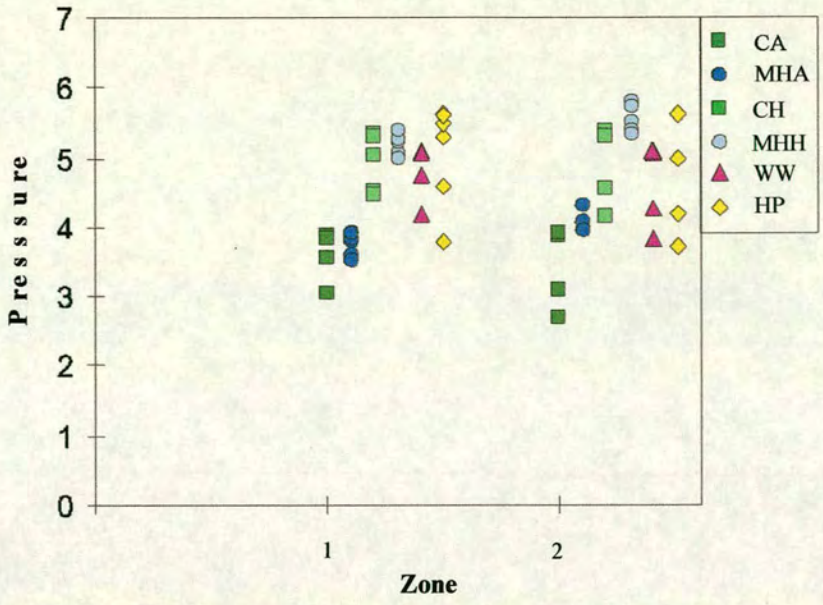

Figure 6.5 - Calculated pressure ranges (in kbar) for the southern (1) and middle (2) zones in the study. As with temperature, no pressure gradient is observed, contrary to the observations of Väisänen et al. (1994) and Väisänen and Höltta (in press).

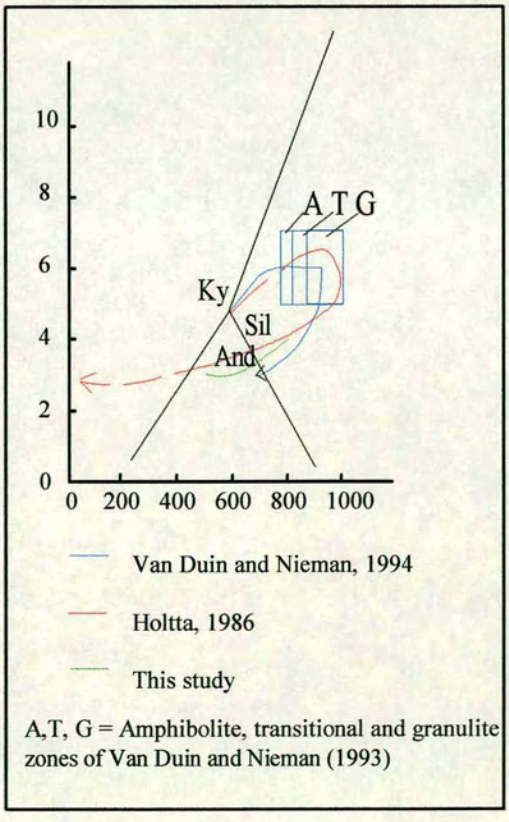

Figure 6.6 - PT path derived by previous workers (in red and blue) compared to that derived in this study (green). Pressure in kbar, temperature in °C.

represent the edge of the P-T path in Figure 6.6 at temperatures less than 500°C and pressures just below 4 kbar. Work done by previous workers has suggested that exhumation was very slow. Geothermobarometry on assemblages within the metamorphic aureoles of Rapakivi granite plutons have yielded PT conditions of 800°C and 2 kbar (Väisänen et al., 1994; 1999). The intrusion of the granites occurred 1580 Ma, thus pressure had decreased by 3 kbar in approximately 260 My.

As with many granulite terrains it is difficult to give any indication of a prograde path (Harley, 1989). Sillimanite is the only aluminosilicate found as an inclusion phase in this study, and no other work claims to have found either kyanite or andalusite as an early phase. However Van Duin and Nieman (1993) and Höltta (1986) have derived clockwise paths. That of Van Duin and Nieman (1993) is based on the transition from amphibolite to granulite facies conditions at the edges of the Turku terrain, (Figure 6.6). The slope of their retrograde path is fairly steep whereas that of Höltta (1986) is gentler which fits with the section of the path that has been determined by this study. The path of Van Duin and Nieman (1993) was calculated using GEO-CALC whereas that of Höltta (1986) was calculated by the separate exchange thermometers and barometers, combined with textural evidence. Neither these earlier studies, or this study could distinguish between the two thermal pulses reported in the literature because of the lack of equilibrium D2 assemblages.

This study has not investigated the temperatures to the north of the terrain where the grt-crd assemblage passes into the amphibolite assemblage of sil + crd + bt (as discussed in earlier chapters). For future calculations the temperatures of Väisänen and Höltta (in press) will be used.

Chapter 7

SIMS analysis of cordierite

Chapter 7 - SIMS analysis of cordierite

7.1 - Introduction

The Turku granulite terrain has undergone varying degrees of partial melting (Höltta, 1986; Van Duin and Nieman, 1993; Väisänen et al., 1994; Väisänen and Höltta, in press). In earlier chapters it has been suggested that the melting took place under conditions of low a_{H2O}, and by dehydration of the pelites following the breakdown of biotite. In order to test this model it is essential to constrain whether melting was indeed fluid-absent, or whether an external fluid was present, and if so what its composition may have been.

The generation of melt along a given divariant reaction is governed by a_{H2O} which is a function of temperature, pressure and the activities of any other volatile species that may be present (Le Breton and Thompson, 1988; Thompson, 1982; 1996; Vielzeuf and Holloway, 1988; Johannes and Holtz, 1996; Shmulovich and Graham, 1996). Granulite facies rocks typically preserve low values of a_{H2O} (Powell, 1982; Waters, 1988; Harley, 1989; Waters and Whales 1984) in comparison to amphibolite facies conditions. Therefore it is often considered that melting within granulites takes place through the breakdown of hydrous phases which liberate their volatile contents into the melt (Clemens and Vielzeuf, 1987; Le Breton and Thompson, 1988; Stevens and Clemens, 1993).

The concentration of water within a melt is a function of pressure, temperature and the X_{H2O} of the system (Johannes and Holtz, 1996): analysis of the volatile content of the melt provides information about the fluid regime at the time of melting. This is not possible where one is now looking at the solid products and remains of former melting reactions, unless inclusions of the melt itself are preserved. The only alternative methods for determining the volatile content of the melt is to either:

A) Define the melting reaction and independently estimate the precise PT conditions under which it occurred,

B) Measure the volatile contents of minerals that are associated with the melts and whose volatile contents depend systematically on a_{H2O}.

Melting within a pelitic system is analogous to the haplogranitic system (Johannes and Holtz, 1996) where the presence of free water means that the production of granitic melt can take place at temperatures as low as 630°C. However, under low a_{H2O} granulite conditions, partial melting involving the breakdown of hydrous minerals (e.g. biotite) produces fluid-undersaturated granitic segregations above 750°C (Clemens and Vielzeuf, 1987; Stevens and Clemens, 1993; Le Breton and Thompson, 1988). At the PT conditions of metamorphism in the Turku terrain the amount of melt that could be produced through such a mechanism is about 29 wt% based upon a biotite content of >50% (Le Breton and Thompson, 1988). However as mentioned in Chapter 2 some Turku outcrops can be dominated by leucosome material. Qualitative estimates suggest that leucosome material can cover >70% of the area of an outcrop and that > 30% is quite common.

One of the products of biotite-dehydration melting reactions within a pelitic system is cordierite (Waters, 1988; Bucher Nurminen and Ohta, 1993; Stevens et al., 1995; Fitzsimons, 1996; Raith and Harley, 1998; Kalt et al., 1999), and it is well documented that cordierite can retain volatiles within its framework (Newton and Wood, 1979; Johannes and Schreyer, 1981; Armbruster and Bloss, 1982; Schreyer, 1985; Santosh et al., 1993; Vry et al., 1988; 1990; Fitzsimons and Mattey, 1994; Carrington and Harley, 1996).

The cordierite crystal structure consists of six membered rings of corner-sharing tetrahedra stacked along the *c*-axis, linked by corner sharing with other tetrahedra both vertically and horizontally to form a framework structure (Figure 7.1). Within this structure are cages and bottlenecks, and within the cages volatile species can reside (Armbruster and Bloss, 1982; Schreyer, 1985; Vry et al., 1990). H_2O is incorporated into the structure in two orientations: with H-H vibrating parallel to *c* (type 1 water molecules) and with H-H parallel to *b* (type 2 water molecules). The

larger CO_2 molecule is found in one site orientation aligned on average along *a* within the widest channel cage dimension (Vry et al., 1990) (Figure 7.1). As cordierite can incorporate both H_2O and CO_2 into its crystal structure, it is a potential monitor of lower crustal fluids (Armbruster and Bloss, 1982; Schreyer, 1985; Harley, 1994; Fitzsimons and Mattey, 1994). It can, in principle, monitor the absolute amount and ratio of the two species in any co-existing fluid or melt (Fitzsimons, 1994; Fitzsimons and Mattey, 1994; Harley, 1994; Carrington and Harley, 1996). Where an external fluid is present, the amount of volatiles trapped within a crystal of cordierite, along with the X_{CO2} (CO_2/CO_2+H_2O), is a function of P, T and X_{CO2} in the co-existing fluid. Under fluid-absent conditions, the cordierite channel volatiles will instead depend upon the distribution of H_2O and CO_2 between cordierite and melt (Harley, 1994; Carrington and Harley, 1996).

Granulite facies cordierites generally preserve high X_{CO2} values and this evidence has been used in support of the argument that granulites form through CO_2 flushing (Johannes and Schreyer, 1981; Armbruster et al., 1982). However when the volatile contents of the cordierites are analysed, they are often well below the saturation curves calculated for cordierite, arguing against cordierite growth in equilibrium with a free fluid (Vry et al., 1990; Harley, 1994). Analysis of the carbon isotope values from cordierite channel CO_2 has shown that many preserve $\delta^{13}C$ values that are low (certainly <-15‰, some down to -30‰), consistent with an organic source for much of the carbon (Vry et al., 1988; 1990; Fitzsimons and Mattey, 1994). The substantial number of granulite terrains that preserve these values argue against CO_2 flushing as a method for granulite formation, as only a small amount of CO_2-rich fluid would be required to reset these to heavier isotopic compositions. The $\delta^{13}C$ values of cordierites from the Turku terrain have been measured and are discussed in Chapter 8.

Another explanation for the high X_{CO2} ratios measured in granulite facies cordierites is that of H_2O leakage during cooling or retrogression of the terrains (Vry et al., 1990). Carrington and Harley (1996) investigated the distribution of water between

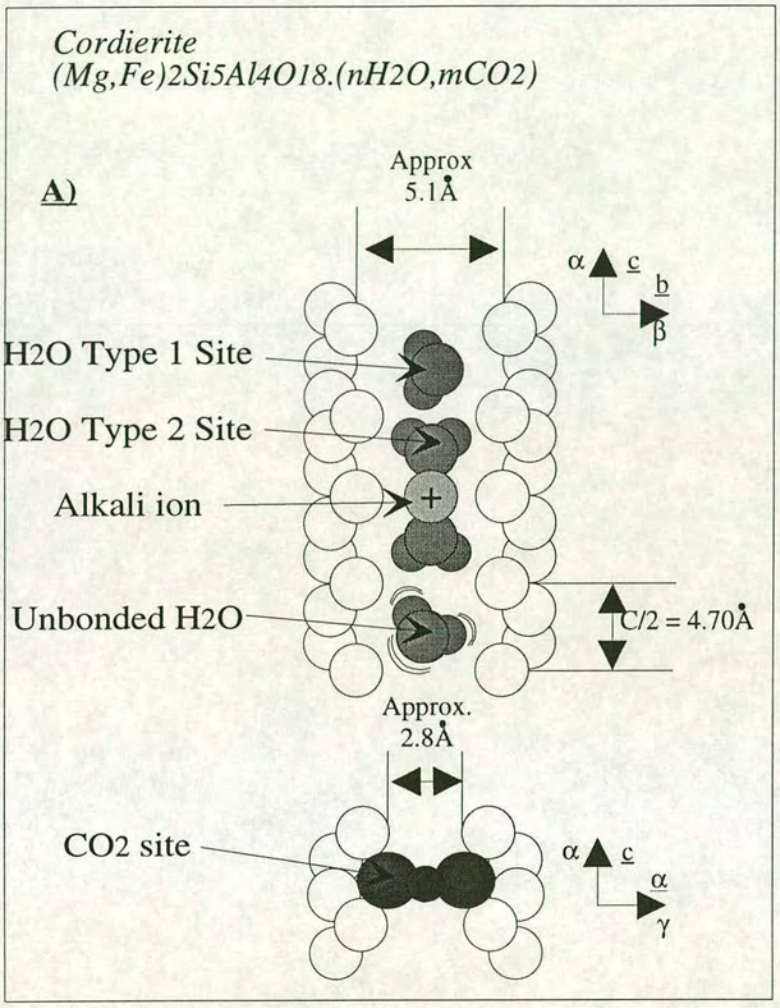

Figure 7.1 - (a) The structure of cordierite projected along (100) showing the location of volatiles within its structure, After Santosh et al. (1993) and Vry et al. (1990). (b) cordierite is viewed along (001) showing the same cages relative to the crystal lattice, After Deer, Howie and Zussman (1992).

cordierite and co-existing melt from saturation down to highly H_2O-undersaturated conditions at 900°C and 5 kbar. These experiments have shown that the abundance of channel H_2O actually depends upon the distribution of H_2O between the cordierite and melt, with lower cordierite H_2O contents co-existing with H_2O-undersaturated melt at a single P-T condition. Their analysis of natural cordierite grains has also shown higher H_2O contents at rims as well as a consistency of H_2O contents within samples from the same structural setting. The values of H_2O contents are different over a range of structural settings, suggesting that the volatile ratios measured have undergone little leakage on local scales.

In order to relate the amount of water within a cordierite to that in the co-existing melt, Carrington and Harley (1996) defined and calculated D_w, the distribution coefficient for H_2O = H_2O (melt)/H_2O (cordierite), in wt%. D_w was shown to decrease from 5.9±0.3 to 4.4±0.6 as the system moved from H_2O saturation towards the maximum degree of undersaturation. The experiments show that equilibrium with a volatile-poor melt is an alternative explanation to volatile leakage for the low H_2O contents measured in cordierite in migmatites and granulites. Therefore a knowledge of the water content within a cordierite can discriminate between growth under fluid-absent, melt-present or fluid-present conditions.

The X_{CO2} of the system may affect the D_w term as the maximum solubility of CO_2 in granitic melts is much lower than it is in cordierite (Carrington and Harley, 1996). However, further experiments (Harley et al., *unpubl. data*) demonstrate that D_w at a given P, T and wt% H_2O (i.e. a_{H2O}) in cordierite is not significantly affected by the CO_2 content of the cordierite. For fluid-saturated conditions, the presence of CO_2 within cordierite decreases the total channel occupancy of both volatile species, as shown in Figure 7.2 (Vry et al., 1990), but the D_w is still primarily dependent only on a_{H2O}.

Previous analyses of H_2O and CO_2 contents of cordierite have used stepped heating (Vry et al., 1988; Santosh et al., 1993; Fitzsimons and Mattey, 1994) or IR spectra

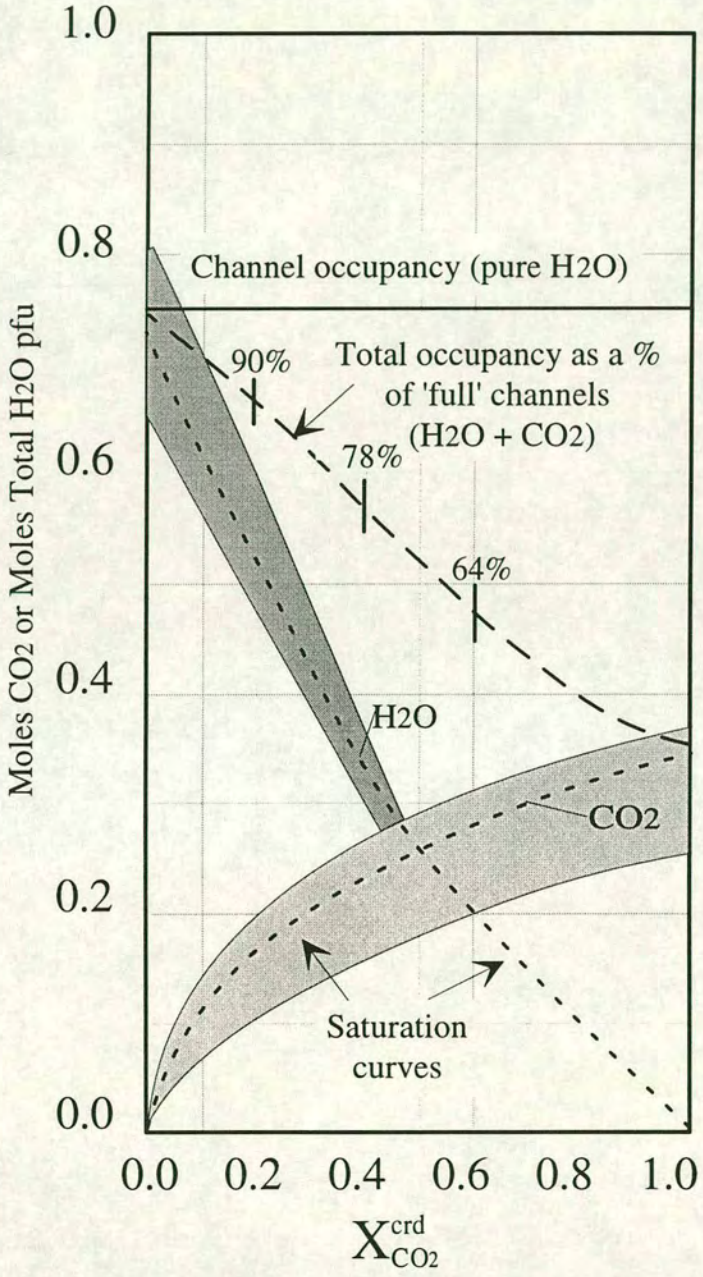

Figure 7.2 - Comparison of experimentally derived H_2O and CO_2 contents of cordierite using the data of Vry et al. (1990) at 5 kbar and 600°C. The upper solid and dashed lines show channel occupancy by H_2O and the effects of CO_2 upon total channel occupancy. The shaded areas show the experimental data of Johannes and Schreyer (1981).

(Armbruster and Bloss, 1982; Schreyer, 1985; Vry et al., 1990). However the cordierite volatile contents reported by Harley (1994), Fitzsimons (1994), and Carrington and Harley (1996) were measured using SIMS (secondary ion mass spectrometry) analysis. This method enables both hydrogen and carbon to be measured in the same analysis and with the same 25μm spot beam, which allows for the analysis of small samples and also for variation in volatile ratios across a sample. The C/Si and H/Si ratios were checked against natural reference grains analysed by independent means (stepped heating and H extraction) in order to obtain wt% values for CO_2 and H_2O equivalents.

This method has been applied to a number of granulite terrains by Harley (1994). The values of m.p.f.u (moles per formula unit) range from 0.2-0.8 (wt% values of 0.3-1.6) for H_2O and 0.5-1.0 for CO_2, often well below the saturation curves of Vry et al. (1990) for appropriate P-T conditions. For example volatile contents in cordierite from the Brattstrand Bluffs, Antarctica, are in the range 0.05-0.5 wt% H_2O and 0.1-1.0 wt% CO_2, the equivalent of 0.08-0.25 total volatiles in m.p.f.u of cordierite. These values are only about 15-50% of the experimental values determined by Johannes and Schreyer (1981) for saturated cordierite at relevant pressures and temperatures (Fitzsimons, 1994). Thus it is likely that the cordierite in the Brattstrand Bluffs migmatitic granulites grew in equilibrium with volatile undersaturated melts.

A further example of the utility of the cordierite volatile content approach is work on the low pressure granulite terrain of the Reynolds Range in Australia, which underwent peak metamorphism of around 5 kbar and 750-800°C (Buick et al., 1998). Cordierites produced through the melting reactions preserve X_{CO2} values of 0.3-0.4 and contain a total of 0.28-0.35 m.p.f.u volatiles. The calculated volatile activities in this case were a_{H2O} 0.13-0.19 and a_{CO2} 0.48-0.67, suggesting that partial melting progressed under vapour-absent conditions and highly reduced a_{H2O} (Harley et al., *unpubl. data*). As discussed in Chapter 1 the presence and effect of other volatile species such as NaCl on the local a_{H2O} cannot be discounted. Crustal brines are

capable of lowering water activity and buffering and limiting crustal melting (Shmulovich and Graham, 1996). This chapter uses the experiments and models of Carrington and Harley (1996), Harley and Carrington (in press) and Harley et al (unpubl. data) and their models do not take account of other crustal volatiles. For this reason this chapter will mostly discuss low water activities in relation to fluid undersaturated melting.

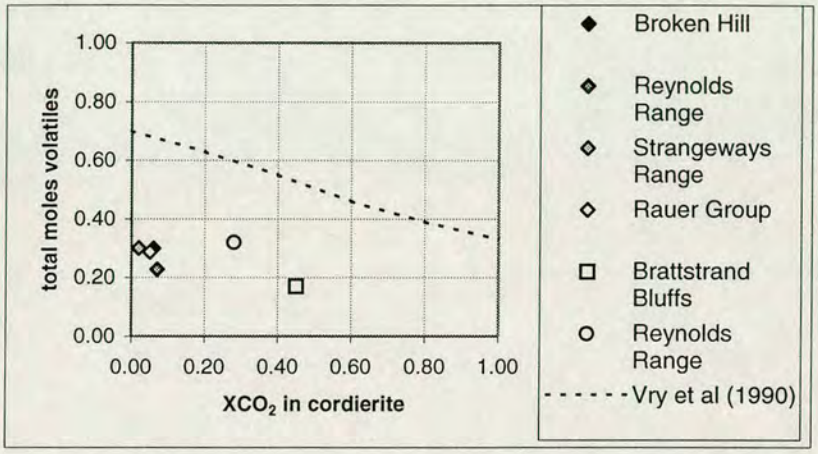

Figure 7.3 – Total moles of volatiles (H_2O and CO_2) per formula unit of cordierite, vs XCO2 of the channel volatiles for a range of granulite terrains. Total m.p.f.u and X_{CO2} values were calculated at 5 kbar and 750°C using the model of Harley et al (unpubl.data)*. Total moles of volatiles in cordierite at fluid saturation and at 5 kbar and 750°C are recalculated from Vry et al (1990).*

- *Carrington and Harley (1996)*
- *Fitzsimons (1994)*
- *Buick et al (1998)*

7.2 - Methods

The H_2O and CO_2 contents of 20 samples from the Turku granulites were measured by SIMS analysis using the Cameca ims-4f ion microprobe at the University of Edinburgh. $^{12}C/^{30}Si$ and $^{1}H/^{30}Si$ ratios were obtained from standards and unknowns using a negative secondary beam of 25μm after a 3 minute burn-in time. The instrument was operated with an 8.0nA beam current, 10kV primary voltage and a 4.5kV secondary voltage. The isotope ratios were converted to wt% H_2O and CO_2 by plotting them against calibration lines determined from two standards with known wt% values, 8-90 and AMNH. AMNH contained 0.66 wt% H_2O and 1.56 wt % CO_2,

whilst 8-90 contained H_2O values of 0.8 wt% and CO_2 values of 1.25 wt%. A list and descriptions of the samples used can be found in Appendix 7.1. Appendices 7.2-7.4 contain operating conditions, error calculations and raw data.

7.3 - Results

7.3.1 - Wt% values

Table 7.1 contains the average wt% H_2O and CO_2 values calculated for each cordierite sample (for calculations see Appendix 7.3). The average H_2O wt% values range from 0.74 to 1.27 across the terrain, whilst the average CO_2 wt% values extend from 0.09 to 0.98 wt%. The CO_2 values therefore have a wider range. The lowest values of wt% CO_2 are found in northern localities, 5, 12, 17 and 20, but there is no such variation visible for the H_2O data. There is no correlation between leucosome type/volume or between leucosome and mesosome fractions at a given locality, and the volatile contents recorded. The wt% values can be further manipulated to provide information on the volatile regime present at the peak of metamorphism. The wt% data have been recast in terms of moles of H_2O (n) and CO_2 (m) per formula unit of cordierite (m.p.f.u), using the expressions:

$$n = \left(\frac{Wt\%H_2O}{MWH_2O} \right) \Big/ \left(\frac{Wt\%hydrousCrd - wt\%anhydrousCrd}{MWCrd} \right) \qquad (7.1)$$

$$m = \left(\frac{Wt\%CO_2}{MWCO_2} \right) \Big/ \left(\frac{Wt\%hydrousCrd - wt\%anhydrousCrd}{MWCrd} \right) \qquad (7.2)$$

MW is molecular weight. Hydrous cordierite is fully hydrous cordierite.

With these parameters it is then possible to define the X_{CO2} of the channel volatiles $X_{CO2}(ch)$, thus:

$$X_{CO_2(ch)} = \frac{m}{n+m} \qquad (7.3)$$

with total volatiles in m.p.f.u = n+m.

7.3.2 - H_2O and CO_2 activity values

In order to calculate a_{H2O} and a_{CO2} from the cordierite data, an independent estimate of pressure and temperature is needed: a_{H2O} or a_{CO2} can then be solved from equations which define the PT dependence of n and m. The relationships between water activity, D_w and the H_2O contents of cordierite and melt previously discussed by Carrington and Harley (1996), have been thermodynamically modelled by Harley and Carrington (in press). This modelling is discussed in the section below.

Modelling of the H_2O melt-cordierite system

H_2O is only incorporated into cordierite as a molecular species into the channels (1 mole p.f.u, Carey, 1994), but H_2O can be incorporated into melts through the breaking of Si-O linkages, producing -(OH) and (H)O- pairs, and as molecular water (Johannes and Holtz, 1996). Studies of the thermodynamics of cordierite hydration by Carey (1995) yield the following expression:

$$a_{H2O} = z_w[n/(1-n)], \qquad (7.4)$$

where z_w is a P-T (fugacity) dependent term and n is moles of H_2O per formula unit.

Harley and Carrington (in press) used the Burnham (Burnham and Nekvasil, 1986), model of solubility of H_2O in granitic melt to derive the relationship between a_{H2O} and melt wt% H_2O contents. This relationship can be expressed as:

$$a_{H2O} = k_w(X_w^2) \qquad (7.5)$$

where X_w is the mole fraction of water in a melt (expressed in terms of an 8-oxygen unit) and k_w is a PT (fugacity) dependent variable.

Therefore both expressions 7.4 and 7.5 define a_{H2O}, which is the same in each phase at equilibrium. Plots of n/(1-n) against X_w^2(melt) for the cordierite-melt data of

Harley and Carrington (in press) yielded linear relations with slopes (k_w/ z_w) that were solely dependent on the P-T condition of the experiment. Simultaneous solution of equations 7.4 and 7.5 predicts that D_w is an asymmetric parabolic function of k_w/z_w with a minimum in D_w occurring between 0.6-1.2 wt% H_2O in cordierite. The results and modelling of Harley and Carrington (in press) show that water activity and pressure are the main controls on D_w in the cordierite-melt system.

The cordierite H_2O saturation data obtained by Harley and Carrington (in press) were combined with data taken from previous studies of Mg-, Fe- and Fe-Mg cordierites (Mirwald et al., 1979; Carey, 1994; Boberski and Schreyer, 1990; Mukhophadyay and Holdaway, 1994), and were regressed to evaluate z_w. This analysis yielded the following expression for the relation between maximum cordierite H_2O content, pressure and temperature:

$$\ln K_H = [4203\ (\pm 320)/T] - 11.75\ (\pm 0.33) \qquad [r^2 = 0.87] \qquad (7.6)$$

where

$$K_H = (n_{sat}/(1-n_{sat}))/f_{H2O(P,T)} \qquad (7.7)$$

and n_{sat} is n at saturation (in moles p.f.u) in H_2O system.

These equations can be used to calculate n_{sat} and hence z_w at appropriate PT conditions, and thus z_w can be input into equation 7.4 to yield estimates for water activity. At a given PT, $a_{H2O} = 1$ when n equals n_{sat}. Therefore:

$$1 = Z_w\left[\frac{n_{sat}}{1-n_{sat}}\right] \qquad (7.8)$$

and

$$Z_w = \frac{(1-n_{sat})}{n_{sat}} \qquad (7.9)$$

Equation 7.5 can be solved for a given water activity, provided k_w is known from experimental saturation data, to give melt water content and a D_w value.

H_2O-CO_2 system and CO_2 system

Saturation H_2O-CO_2 data obtained by Harley et al. (*unpubl. data*) for cordierite are coupled with a_{H2O} estimated from both the H_2O content of cordierite and of melt in their experiments to demonstrate that:

$$a_{CO2} = z_c[m/(1\text{-}m)]_{crd} \qquad (7.10)$$

where z_c is a P-T sensitive coefficient that is extracted by regression and is the CO_2-system analogue of z_w, and m is the number of moles of CO_2 p.f.u in cordierite.

Harley et al. (*unpubl. data*) derived the following expression for the relationship between the maximum cordierite CO_2 content, and P, and T:

$$\ln K_C = [962\ (\pm 150)/T] - 11.91\ (\pm 0.75) - (0.2020)P \qquad (7.11)$$

where

$$K_C = (m_{sat}/(1\text{-}m_{sat}))/f_{CO2(P,T)} \qquad (7.12)$$

A solids volume change, ΔV_s, of +1.679 J/mol was required in these calculations. The maximum predicted CO_2 contents at 800°C are 0.6, 1.15 and 1.7 wt% for pressures of 3, 5 and 7 kbar respectively. At 900°C the values are 0.6, 1.2 and 1.8 wt% for the same pressures. The saturation curves for H_2O-CO_2 channel volatiles in cordierite produced using the equations 7.6 and 7.12 of Harley et al. (*unpubl. data*) differ significantly from previous models. They are consistent with the 600-800°C H_2O-CO_2 data obtained by Johannes and Schreyer (1981) and hence suggest that equation 7.6 provides a good approximation to estimate the CO_2 contents of natural cordierites. Equations 7.6, 7.7, 7.11 and 7.12 have been used to estimate H_2O and CO_2 activities from the cordierite volatile analyses obtained in this study. For the

middle localities a PT condition of 750°C and 5 kbar has been used, whereas for the northern localities 650°C and 5 kbar have been adopted, based upon the pressure and temperature data of this and previous studies (Van Duin and Nieman, 1993; Väisänen et al., 1994; Väisänen and Höltta, in press). The calculations for each sample point are presented in Appendix 7.5 and discussed in Section 7.3.3.

Calculated cordierite volatile values

Across any given sample the a_{H2O} can vary by 0.17 and the a_{CO2} by as much as 1.0. Within a given sample there are no differences in the range of values taken from a mesosome or leucosome cordierite. There is also no zoning seen in any individual cordierite grain.

As can be seen from Table 7.1 and Figures 7.3 through 7.5, the obvious difference across the Turku terrain in terms of cordierite volatiles, is the variation in channel X_{CO2}, from 0.03-0.22 at northern localities to up to 0.3 at southern localities. The actual CO_2 contents (in m.p.f.u.) vary from 0.01 to 0.16 across the terrain. There is no similar trend for the H_2O contents of Turku cordierites, which all lie within a range of 0.2-0.5 m.p.f.u. When volatile m.p.f.u values are plotted against X_{CO2}(ch) it can be seen that there is a negative relationship for H_2O and a positive .3.3 - Results of cordierite calculations

relationship for CO_2 (Figure 7.3) consistent with previous models of volatile relations in cordierite (Vry et al., 1990; Johannes and Schreyer, 1981; Harley and Carrington, in press). The total volatile contents (CO_2 + H_2O m.p.f.u) of the cordierites studied range from 0.25 to 0.60 in the southern and middle localities, whilst total volatile contents from northern localities are slightly more tightly grouped between 0.35 and 0.60 (Figure 7.4).

Table 7.1 - Average calculated cordierite data, see appendix 7.5 for all analyses points. Pressure variations were calculated using the saturation isopleths of Harley and Carrington (in press).

Units	Wt%		m.p.f.u		activity		activity		Wt%	
Sample (L Locality S Sample)	H_2O	CO_2	$n(H_2O)$	$m(CO_2)$	aH_2O	aCO_2	$(a_{H2O}+a_{CO2})$	$X_{CO2}(ch)$	H_2O melt	Dw
Errors based upon propagation of ion probe analysis errors										
	± 0.01	± 0.01	± 0.01	± 0.01	± 0.01	± 0.02	± 0.03	± 0.01	± 0.11	± 0.08
Errors based upon ½ kbar variation on pressure										
					± 0.02	± 0.08	± 0.1		±0.07	±0.7
Southern localities										
L3/SD26	0.91	0.53	0.31	0.07	0.23	0.50	0.73	0.18	2.89	3.17
L2/SD18	1.09	0.54	0.37	0.08	0.29	0.50	0.79	0.16	3.46	3.18
L2/S79	1.02	0.66	0.35	0.09	0.26	0.61	0.87	0.21	3.22	3.16
L2/SD22	1.06	0.61	0.36	0.09	0.29	0.57	0.86	0.19	3.42	3.22
L2/SD5	0.87	0.45	0.30	0.06	0.21	0.41	0.62	0.18	2.73	3.15
L4/S10	1.00	0.98	0.35	0.13	0.26	0.92	1.18	0.28	3.17	3.16
L4/S12	0.86	0.72	0.29	0.10	0.20	0.68	0.88	0.26	2.69	3.13
L4/S60	0.74	0.73	0.25	0.10	0.17	0.70	0.87	0.28	2.35	3.18
L4/SX	0.86	0.83	0.29	0.12	0.21	0.79	0.99	0.29	2.74	3.18
Middle localities										
L7/S148	1.11	0.59	0.38	0.08	0.31	0.54	0.85	0.18	3.59	3.22
L7/SD35	1.10	0.49	0.38	0.07	0.30	0.45	0.75	0.16	3.54	3.20
L6/S17	0.99	0.64	0.34	0.09	0.26	0.60	0.86	0.21	3.18	3.20
L17/S145	1.27	0.40	0.44	0.06	0.31	0.33	0.63	0.11	3.44	2.69
Northern Localities										
L12/S18	1.15	0.11	0.40	0.02	0.26	0.09	0.37	0.04	3.02	2.64
L12/S19	1.27	0.14	0.44	0.02	0.31	0.12	0.43	0.05	3.43	2.70
L12/SD45	0.83	0.56	0.29	0.08	0.16	0.48	0.64	0.22	2.18	2.63
L12/S47	1.25	0.36	0.43	0.05	0.30	0.30	0.60	0.10	3.39	2.70
L5/S103	0.99	0.21	0.34	0.03	0.21	0.17	0.38	0.08	2.58	2.59
L5/S104	1.08	0.48	0.38	0.07	0.24	0.41	0.65	0.15	2.84	2.61
L19/S31	1.11	0.09	0.38	0.01	0.25	0.07	0.32	0.03	2.93	2.63

The average activities of a_{H2O} range from 0.17 to 0.29 in the north, 0.26 to 0.31 in the centre and 0.16 to 0.31 in the south of the terrain (Figure 7.5). Thus the water activity is fairly constant across the terrain. However a wide range of a_{H2O} values can be seen within a single outcrop (e.g. locality 12) and so there is local heterogeneity.

Using the model of Harley and Carrington (in press) the D_w and consequent wt% H_2O melt values were calculated. The middle and northern localities preserve D_w values of 3.1±0.05 whilst the northern localities have an average D_w value of 2.6±0.1 (Figure 7.6). The lower values of D_w derived from the northern localities are due to the different pressures and temperatures used in the calculations, and is therefore a function of the model of Harley and Carrington (in press). The resulting estimate of

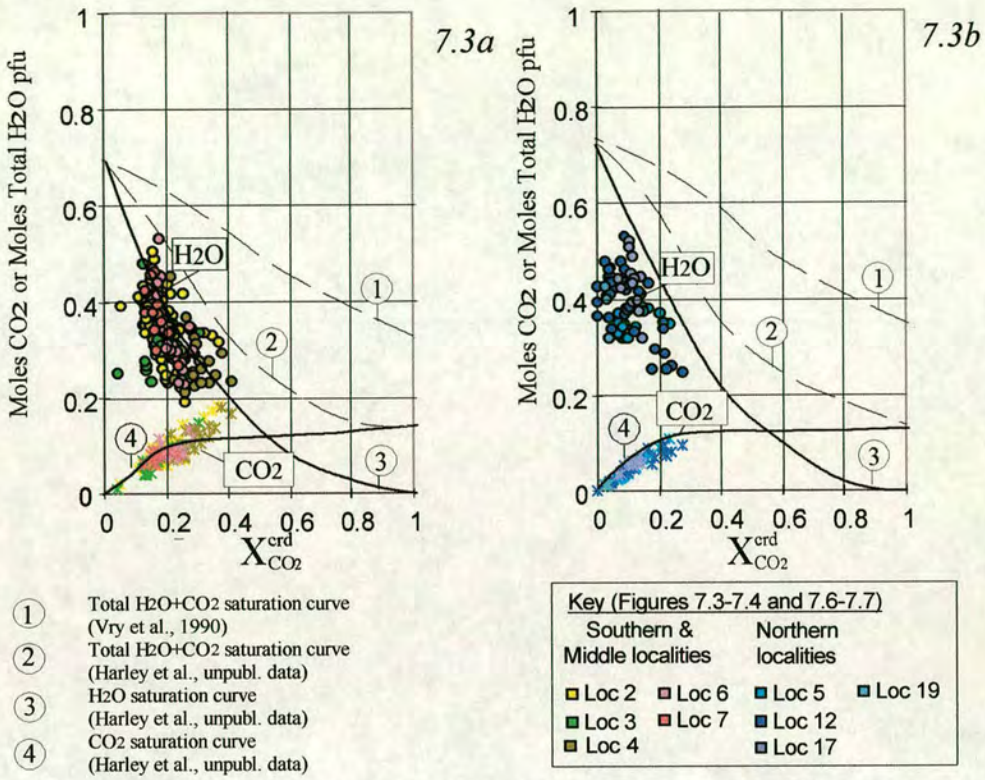

Figure 7.3 - The H2O and CO2 contents of Turku cordierites in m.p.f.u. (a) Southern and middle localities (calculated at 750°C and 5 kbar) (b) Northern localities (650° and 5 kbar). The H2O CO2 and total H2O+CO2 saturation curves of Harley et al. (unpubl. data) for 5 kbar and 750°C or 650°C are superimposed on to the data, as are the total H2O+CO2 saturation curves of Vry et al. (1990) for the same PT. An increase in pressure will lead to the saturation curves moving to higher values of total mpfu according to the model of Harley et al (unpubl. data).

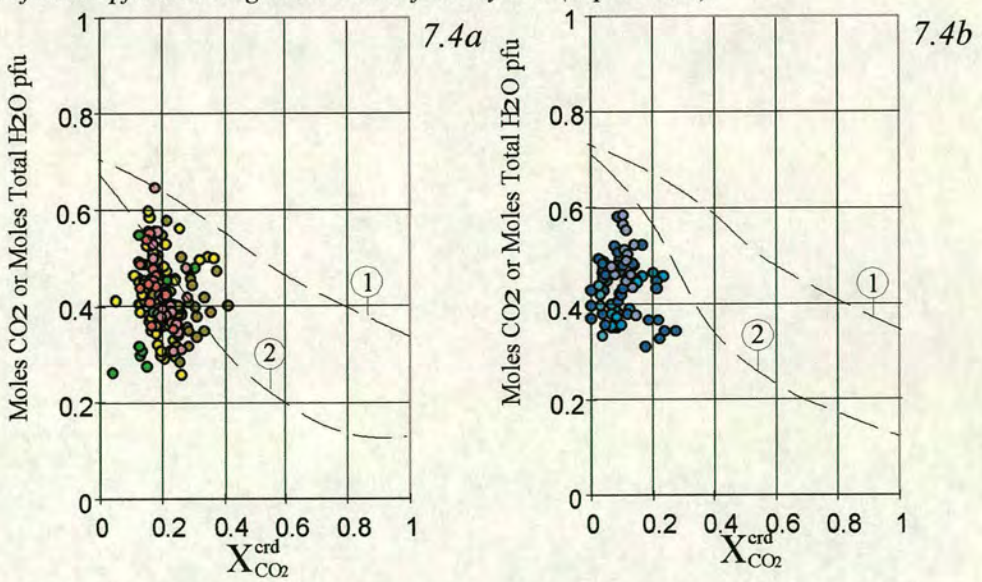

Figure 7.4 - H2O + CO2 m.p.f.u. of Turku cordierites from (a) southern and middle localities (calculated at 750°C and 5 kbar), and (b) northern localities (650° and 5 kbar). The total H2O + CO2 saturation curves of Harley et al. (unpubl. data) and Vry et al. (1990) were calculated at 5 kbar and 650°C and 750°C as in Figure 7.3.

the water content of the melt is on average 3.0±1.0 wt% (Figure 7.7). Although the water contents of cordierite in m.p.f.u were at near water saturation, the actual activities were low. These melt water contents, attained at low a_{H2O}, are significantly less than the saturation H_2O contents possible at 5 kbar, (10 wt%, Johannes and Holtz, 1996). Such low H_2O contents would imply increased viscosity of the melts, compared with H_2O-saturated ones, but conversely would allow the melts to move considerable distances vertically through the crust before they would intersect the H_2O-saturated solidus (for 3 wt% H_2O the vapour-saturated solidus is intersected at 2 kbar).

7.4 - Description and discussion of data

The saturation curves for the H_2O, CO_2 and H_2O+CO_2 contents of cordierite (in m.p.f.u) of Vry et al. (1990) and Harley et al. (*unpubl. data*) are overlain onto the Turku data in Figures 7.3 and 7.4. The curves of Vry et al. (1990) and Harley et al. (*unpubl. data*) are calculated at 750° and 5 kbar or 650° and 5 kbar. From these plots it can be seen that the total volatile contents of the Turku cordierites (in m.p.f.u) range from saturation values to relatively under-saturated. The H_2O contents of cordierite are typically under-saturated at northern localities, although some are near saturation as seen from their positions near to the reference H_2O saturation curves of Harley et al. (*unpubl. data*). CO_2 contents in cordierite from the north range from undersaturated values to just saturated, whilst cordierites from the southern and middle localities have CO_2 contents that are mostly at or above the saturation curve of Harley et al. (*unpubl. data*). The CO_2 trend is mirrored for H_2O in the southern and middle localities with many values at and above the H_2O saturation curve.

The total contents of CO_2+H_2O in cordierite from the northern localities are typically undersaturated with respect to both saturation curves, although some do lie near to the saturation curve of Harley et al. (*unpubl. data*). The data from the southern localities is typically clustered on the saturation curve of Harley et al. and some points approach the saturation curve of Vry et al. (1990). The curves of Harley et al. (*unpubl. data*) are most relevant to this study. as their model has been used to

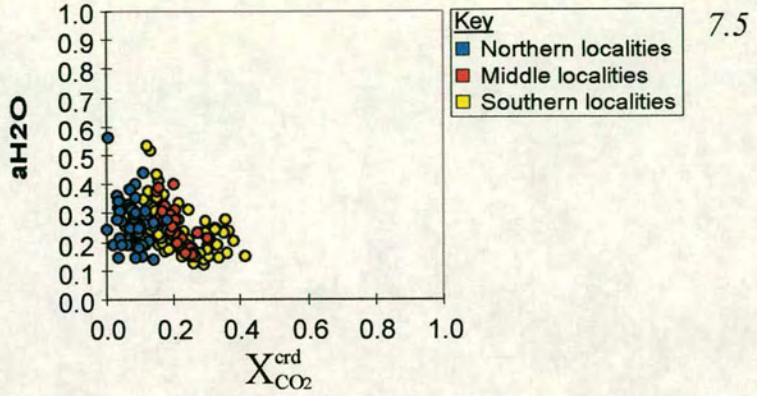

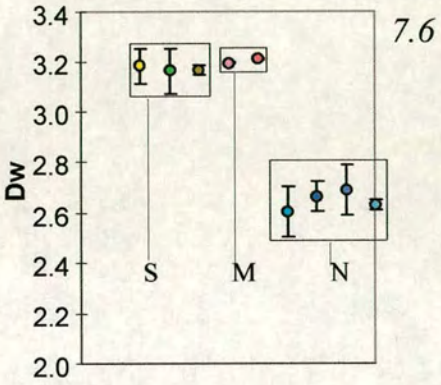

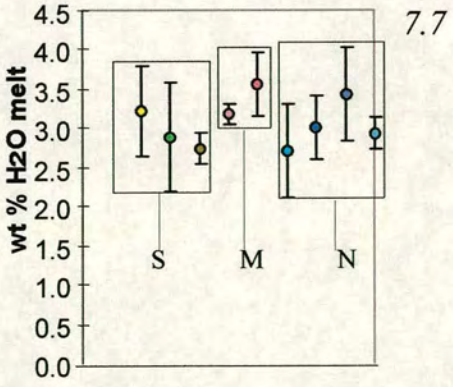

Figure 7.5 - Plot of XCO2(ch) against aH2O for Turku cordierites.

Figure 7.6 - Dw values across the Turku terrain. The difference between northern localities and middle and southern zone is a function of the model of Harley et al. (unpubl. data). N = northern localities, M= middle localities and S = southern localities.

Figure 7.7 - Melt H2O contents in wt % calculated from Dw (Harley et al., unpubl. data). N = northern localities, M= middle localities and S = southern localities.

calculate the volatile contents of the Turku cordierites. Thus many cordierite samples from the southern and middle localities are saturated with respect to total volatiles, whereas cordierite samples from the north are generally undersaturated.

As shown in Figures 7.5 to 7.7 the a_{H2O}, wt% H_2O in melt and D_w term are not affected by X_{CO2}, in agreement with the experimental work of Harley et al. (*unpubl. data*). The amounts of H_20 present in cordierite are therefore a function of aH_2O. Thus some melts, e.g. those in the northern terrain where leucosome material is typically <25% of the outcrop, are evidence of dehydration melting, producing water-undersaturated melts. The heterogeneity within localities is indicative of local control of a_{H2O} typical of dehydration melting (Waters, 1988; 1994). However, the high activities and near saturation values of CO_2 at middle and southern localities, where the percentage of leucosome material is high, may indicate that a CO_2 dominated fluid was also introduced to the Turku terrain perhaps within externally-derived melts. This would help to explain the very high CO_2 activities observed within samples from the southern outcrops.

The similarity of calculated a_{H2O} and wt% H_2O in melts throughout the Turku terrain could be explained by two main processes:

(a) H_2O availability was largely controlled by biotite breakdown via dehydration melting, so that a_{H2O} was buffered by the local, quite homogeneous, rocks.

(b) H_2O in all cordierite, whether in leucosomes or mesosome and whether early or late, was reset to near constant values reflecting a closure temperature post melting and potentially after cooling and decompression.

The data could be explained by a combination of both processes. (a) is consistent with field data (Chapter 2) but (b) is possible as an overprint. For example if conditions stayed at high temperatures the water values may exchange with water in the melt or they may be reset with any later infiltrating fluid. The presence of an infiltrating late crustal brine would have the effect of decreasing the water activity recorded, increasing the a_{CO2} (Jacobs and Kerrick, 1981; Aranovich and Newton,

1996; Shmulovich and Graham, 1996; Aranovich and Newton, 1997; Aranovich and Newton, 1999; Shmulovich and Graham, 1999).

The fact that calculated $a_{CO2+}a_{H2O}$ values approach unity in the south and middle of the terrain, suggests that an excess fluid phase may have been present. This is particularly the case at locality 4, where an a_{CO2} of > 0.7 implies that the cordierite grew in the presence of either a free CO_2-rich fluid, or that CO_2 that was transported in a melt that was saturated or near-saturated with a free fluid phase. The other possibility is the presence of an NaCl rich brine. It is difficult to assess the effect of NaCl as there have as yet been no experiments in the NaCl-H_2O-CO_2 system relative to cordierite. However as discussed in Chapter 1, NaCl drives the activity of water down and that of CO_2 up (Jacobs and Kerrick, 1981; Aranovich and Newton, 1996; Shmulovich and Graham, 1996; Aranovich and Newton, 1997; Aranovich and Newton, 1999; Shmulovich and Graham, 1999).. This may be one method for gaining the high CO_2 values found in the southern and middle localities.

The primary differences between the south and north of the terrain are the lower CO_2 contents and less melting apparent in the latter. In order to evaluate whether the CO_2 in the south and middle of the terrain was introduced as an additional free fluid, or whether it was only present transported at 10^3 ppm levels in melt, $\delta^{13}C$ data and mass balance calculations must be considered. These are discussed in chapters 8 and 9.

Chapter 8

Carbon isotope signatures of cordierite volatile contents

Chapter 8 - Carbon isotope signatures of cordierite volatile contents

8.1 - Introduction

As discussed in the previous chapter, cordierite has an open framework structure with channels that can trap volatiles (Newton and Wood, 1979; Johannes and Schreyer, 1981; Armbruster and Bloss, 1982; Schreyer, 1985; Vry et al., 1990; Harley, 1994; Carrington and Harley, 1996). The SIMS work carried out as part of this study identified ratios and quantities of CO_2 and H_2O within the channels of cordierites from across the Turku terrain. Experimental work by Carrington and Harley (1996) has shown that the amount and ratio of these volatiles can indicate the environment in which the cordierite was formed. In this chapter, CO_2 is analysed for its carbon isotopic composition as it is a potential monitor of melt volatile regimes (Fitzsimons and Mattey, 1994).

Vry et al. (1988) have shown that cordierites can preserve peak metamorphic carbon isotopes and channel gas compositions. Studies of cordierite co-existing with graphite indicates that $\delta^{13}C$ values for channel CO_2 are not in general modified by processes post-dating peak metamorphism (Vry et al., 1990). Carbon isotopes can help to evaluate the extent of modification of the CO_2 compositions in natural cordierites. $\delta^{13}C$ values representing original sedimentary values are on average -35‰ (Vry et al., 1988; 1990)..

For this study only cordierite was used, as analysable flakes of graphite were not available from the samples studied. However, the textures and CO_2-H_2O volatile contents of most of the cordierite studied suggests that they are the product of a dehydration-melting reaction at the peak of metamorphism. Therefore, the isotopic composition of the cordierite should be representative of this dehydration-melting during peak metamorphism.

8.2 - Methods

This study analysed the isotopic composition of 14 samples (for sample list see Appendix 8.1) taken from six localities throughout the Turku granulite terrain. Analyses were made using a VG PRISM mass spectrometer at the Stable Isotope Laboratory, Royal Holloway, University of London. Fresh crushed cordierite was picked out under a binocular microscope, with care being taken to avoid fragments showing alteration or cracks. The sample was then weighed, washed and run through the low blank, high vacuum, gas extraction line (see Appendix 8.2 for details). The samples were first heated at 400°C, where the 30 minute step was carried out in the presence of 500 mbar of oxygen to burn off any surface contaminants. Subsequently the sample was heated in 30 minute steps of 100°C up to 1200°C under high vacuum. The 1200°C step was repeated until volatile release dropped. The CO_2 was collected with the aid of liquid nitrogen and a variable temperature finger. The $\delta^{13}C$ of the CO_2 was measured to an accuracy ±3‰ with a Baratron capacitance manometer (Fitzsimons and Mattey, 1994).

8.3 - Results

Example step release profiles from the six localities studied are shown in Figure 8.1. In each case the first few steps produce a low yield of isotopically light carbon ($\delta^{13}C$ = -19 to -30‰), which is thought to represent surface organic contamination (Fitzsimons and Mattey, 1994). The bulk carbon yields depend upon the CO_2 concentration in each sample and the weight of the sample.

Carbon yields (ppm C per °C) from the southern and central localities (localities 3, 4, 6, 7) all feature a smooth stepped profile with a peak from 900-1200°C. Localities 3, 4 and 7 record a peak ppm C of 400 whilst locality 6 records a higher value of 800 ppm C. Both northern localities (localities 5 and 12) have much lower carbon yields, with maximums of 200 ppm C found at much lower temperatures (700-800°C).

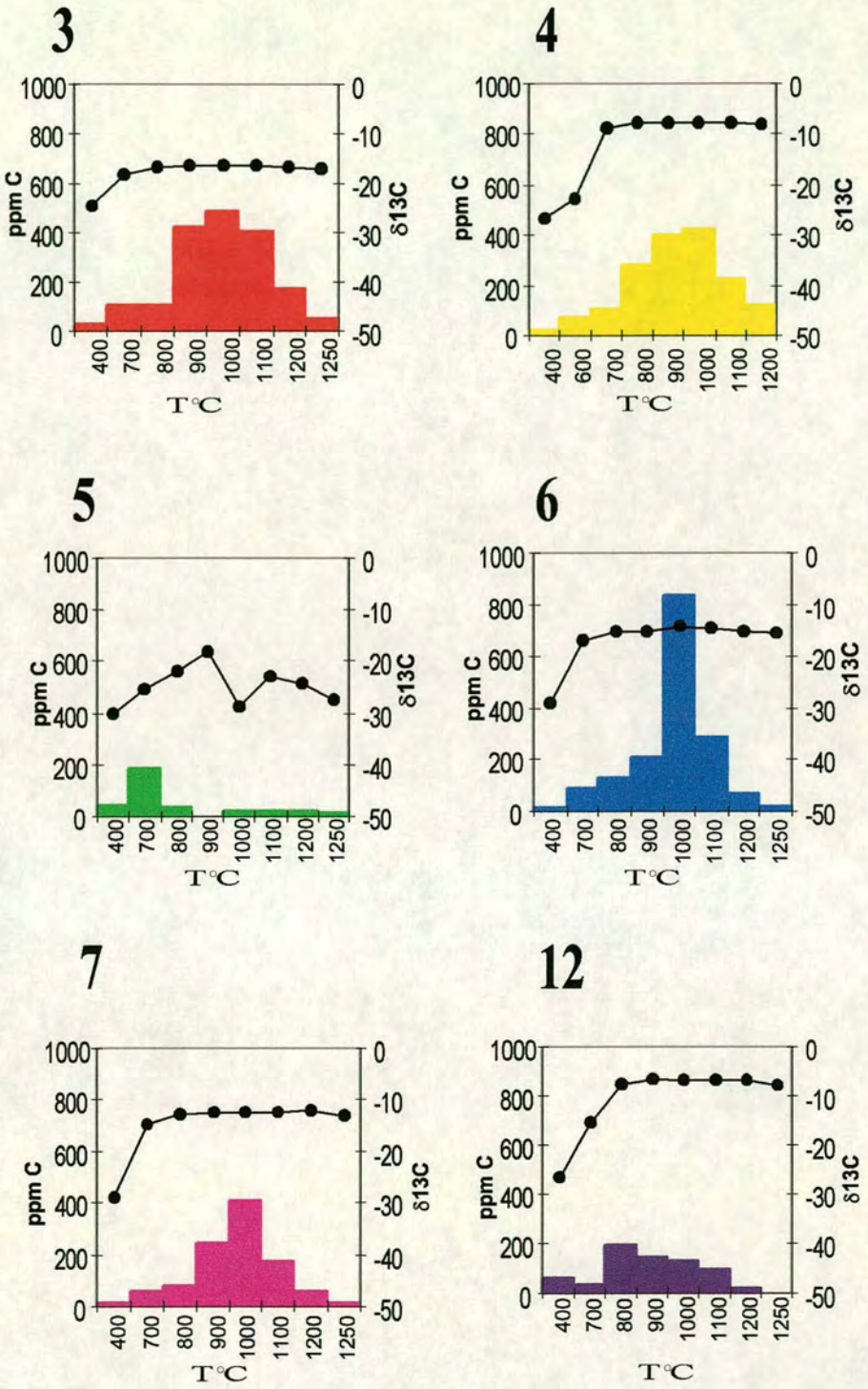

Figure 8.1 - Example step release profiles for CO_2 released from cordierite from the six localities studied (3, 4, 5, 6, 7 and 12). Each graph shows the amount of carbon released during each step (in ppm C, bar chart), as well as the bulk isotope composition ($\delta^{13}C$ in ‰, black circles).

This shape of T-yield graph is attributed by Fitzsimons and Mattey (1994) and Santosh et al. (1993) to the decrepitation of fluid inclusions, where the related $\delta^{13}C$ values show a rapid increase to heavy isotopic signature before levelling out at lighter values. This pattern of variation may fit the graph from locality 5 but not those from locality 12. The presence and abundance of fluid inclusions within the Turku granulites is not known from any previous work and has not been investigated in this study.

Average wt% CO_2 values calculated from the six localities range from 0.2-0.58, as shown in Table 8.1. This range fits into the average granulite CO_2 abundances of 0.1-2 wt% (Santosh et al., 1993). Very CO_2-rich cordierite has been found in Valjok, Norway, with an average wt% CO_2 of 2.2 and an X_{CO2} of 0.75 (Armbruster et al., 1982).

Wt% CO_2 yields from stepped heating analysis are mostly in agreement with SIMS analysis of the same samples (Table 8.1). Any differences may be due to the fact that the first few steps are not included in the total wt% CO_2 calculated because they may include surface contaminants. The calculated values may therefore miss out some channel volatiles (Table 8.1). The large difference from locality 5 is linked to errors in analysing very low volumes of gas with SIMS analysis (Craven, 1999, *pers. comm.*).

Isotopic compositions from localities 4 and 12 record heavy $\delta^{13}C$ values of around -7‰. Localities 3, 6, and 7 all record lighter signatures of -12 to -14‰. However, locality 5 from the north retains much lighter $\delta^{13}C$ ratios of -24‰. The $\delta^{13}C$ values from the six localities are quite different, with no patterns relating to the geographical position of the outcrops and thus inferred grade (Väisänen et al., 1994; Väisänen and Höltta, in press). Localities 4 and 12 come from the southern and northern zones respectively and these record the heaviest isotope signatures. Locality 5, which is under a kilometre away from locality 12, records the lightest signature. As Figure 8.2 shows, there is no relation between isotopic composition and wt% CO_2 which is consistent with observations made from other studies (Fitzsimons and Mattey, 1994).

Table 8.1 - Average (Ave) Wt% CO_2 and $\delta^{13}C$ values from stepped heating (SH) and secondary ion mass spectrometry (SIMS).

Method	Locality	3	4	5	6	7	12
SH	Ave $d^{13}C$	-16.61	-7.88	-24.12	-14.89	-12.54	-7.16
SH	Ave wt% CO_2	0.58	0.47	0.03	0.56	0.38	0.22
SIMS	Ave wt% CO_2	0.54	0.70	0.30	0.64	0.56	0.22

Samples used.
3 = SH: Ave 1, SIMS: Ave D26
4 = SH: Ave XA-D, SIMS: Ave X
5 = SH: Ave 103/104, SIMS: 103/104
6 = SH: Ave 17, SIMS: Ave 17
7 = SH: Ave 148, SIMS: Ave 148
12 = SH: Ave D44, SIMS: Ave D45

8.4 - Discussion

The cordierite in the Turku terrain is mostly the product of dehydration-melting and so was often in equilibrium with a volatile undersaturated melt. Therefore, the $\delta^{13}C$ values from the cordierite must be representative of the CO_2 within the melt (Fitzsimons and Mattey, 1994). Given the variation in isotopic signatures found throughout the terrain it is worthwhile considering the possible sources of carbon in the crust:

1. Reduced organic matter in sediments has a range of values from -20 to -30‰ (average = -25‰) (Fitzsimons and Mattey, 1994). This range of values is indicative of the isotopic variation in the Earth's biomass. A range of $\delta^{13}C$ values from -31 to -35‰ represent original Archean carbon values (Vry et al., 1988).
2. Sedimentary carbonate is another possible source, and has a $\delta^{13}C$ value of 0‰ (Fitzsimons and Mattey, 1994).

3. Finally, an external source for $\delta^{13}C$ is from mantle fluids, with a $\delta^{13}C$ value of around -7‰, permeating the lower crust; many mantle-derived magmas have $\delta^{13}C$ values of -5‰ (Vry et al., 1988).

The values from the Turku terrain stretch from characteristic sedimentary reduced carbon values to mantle-like values (-25 to -7‰). As with the results of Fitzsimons and Mattey (1994), this wide range of values may represent mixing of an original light sedimentary carbon source with varied amounts of a heavier carbon reservoir, i.e., carbonate or mantle-derived fluids. $\delta^{13}C$ values from this study are plotted with those of Fitzsimons and Mattey (1995), Vry et al. (1988; 1990) and Santosh et al. (1993) in Figure 8.2. The data from Vry et al. (1990) are thought to represent original sedimentary values, whereas data from Fitzsimons and Mattey (1995) are centred around -10 to 20‰. Localities 3, 6 and 7 all fall within the range of data from Fitzsimons and Mattey (1994). Data from localities 4 and 12 lie within the range of $\delta^{13}C$ values from Santosh et al. (1993) and, as they are characteristic of a mantle fluid signature, may require another explanation. Cordierites from Valjok (Armbruster et al., 1982) have similar values and are attributed to a local fluid influx which resulted from the intrusion of mantle derived magmas into the lower Scandinavian shield. Cordierite from locality 5 has very low wt% CO_2 yields but the $\delta^{13}C$ values are within the range of data from Vry et al. (1988; 1990).

None of the rocks studied from the Turku terrain contain any carbonates, and none are reported by previous workers (Hietanen, 1947; Väisänen et al., 1994). Väisänen et al (1993). This study did report sporadic calc-silicate boudins but their origins are unclear. The quantity and distribution of these boudins are unknown but they could locally contribute to the carbon isotope composition. In their study of the Brattstrand Bluffs, Fitzsimons and Mattey (1994) propose that even though there is now no longer carbonate in existence, some original sedimentary carbonate could have devolatised during prograde metamorphism.

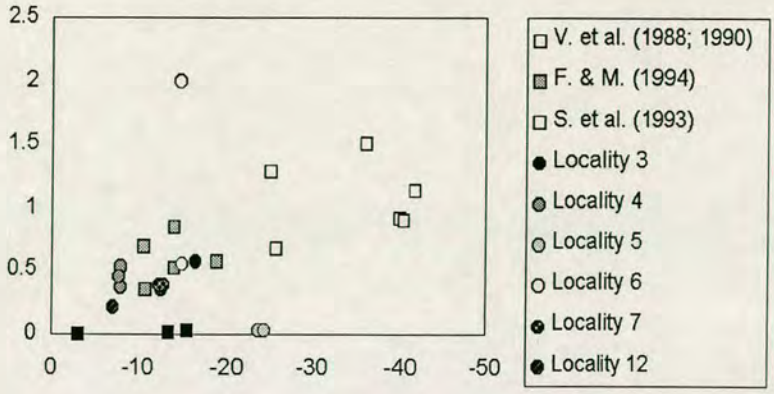

Figure 8.2 - Yields of wt% channel CO_2 plotted against $\delta^{13}C$ of channel CO_2 for cordierite from six localities, compared with data from Vry et al. (1988; 1990), Fitzsimons and Mattey (1994) and Santosh et al. (1993).

The alternative carbon mixing source to carbonate is an external, mantle-derived fluid. As discussed in Chapter 1, CO_2 flushing is one of the possible mechanisms for producing granulite facies conditions. However it is unlikely that the Turku terrain had undergone a pervasive CO_2 influx due to the heterogeneity of the isotope signatures. Vry et al. (1988, 1990) argue that the presence of light $\delta^{13}C$ values is evidence against large amounts of CO_2 infiltration and that $\delta^{13}C_{crd} < -15$ is evidence against large scale fluid infiltration, as only a small amount of a heavy isotope fluid is needed to homogenise isotopic compositions within a terrain. Further evidence for a pervasive CO_2-rich fluid would be the presence of fluid inclusions (Santosh et al., 1993). However most Turku CO_2 release patterns do not have peaks around lower temperature steps attributed to thermal decrepitation of fluid inclusions (Santosh et al., 1993; Fitzsimons and Mattey, 1994), apart from sample 103 (from locality 5) which has lower yields than seen anywhere else. In addition, the previous chapter shows that the volatile contents of cordierite are in fact dominated by H_2O, with X_{CO2} varying between 0.01 to 0.4.

The cordierites in this study do not have $\delta^{13}C$ values from different leucosomes within the same outcrop (unlike Fitzsimons and Mattey (1994) and so, therefore, it is difficult to

make any comments on isotope heterogeneity on an outcrop scale but there are clearly large differences on the regional scale.

8.5 - Conclusions

Analysis of the limited samples from Turku suggests a similar situation to that reported for the Brattstrand Bluffs by Fitzsimons and Mattey (1994). The $\delta^{13}C$ signature for the Turku cordierites is a mixture of either a sedimentary source and local carbonate- or externally-derived fluid. The near-saturation volatile contents of some cordierites (Chapter 7) points towards the introduction of externally derived melts carrying CO_2 in 10^3 ppm levels. The amount of CO_2 needed to attain the range of values seen within Turku cordierites will be assessed within chapter 9.

Chapter 9

Summary and conclusions

Chapter 9 - Summary and conclusions

9.1 - Main aim and approaches of the study

Previous work on the Turku granulite terrain has established a well-constrained metamorphic history and structural framework (Hietanen, 1947; Höltta, 1986; Van Duin and Nieman, 1993; Väisänen et al. 1994; Väisänen and Höltta, in press). The terrain represents a slice of an island arc system that collided with the Baltic shield 1890 Ma. During collision the resulting compression and deformation of the terrain lead to amphibolite to granulite facies metamorphism (Van Duin and Nieman, 1993; Väisänen et al. 1994; Väisänen and Höltta, in press). This metamorphic event is associated with large volumes of granitic material (leucosomes) now found at many Turku localities. Whilst previous work on the terrain has suggested that the leucosomes represent melts formed through dehydration melting of the local pelites, there has been no previous attempt to try and classify the range of leucosome types, or to define quantitatively the conditions under which melting and melt segregation took place. This study aimed to constrain these features and derive a model for melting within the Turku terrain.

The melting model for the Turku terrain proposed in this study is based upon three approaches;

1. Classification of the temporal relationships of leucosomes within the structural framework defined by Väisänen et al. (1994).
2. Petrological evidence for partial melting and a compositional classification of leucosome types based upon mineral assemblages, bulk compositional data and trace element geochemistry.
3. A definition of the conditions of melting governed by external factors such as P, T a_{H2O} and a_{CO2}.

9.1.1 - Relationship of melting to the structural history

In the field two main deformation events were observed, consistent with the definitions of Väisänen et al. (1994) and Väisänen and Höltta (in press). D2

deformed the Turku rocks into recumbent F2 isoclinal folds, with axial traces striking NW-SE. S2 is the dominant fabric seen in the field and is typically axial planar to F2 folds. D2 was followed by a gentler period of compression (D3) that produced folds with axial traces orientated NE-SW. These separate deformation events are associated with two generations of garnet and cordierite that are present both in mesosomes and some leucosomes. The poikiloblastic texture of some of these phases suggest that they are the peritectic products of biotite dehydration melting reactions (Waters and Whales, 1984; Waters, 1988, 1994; Powell and Downes, 1991; Kalt et al, 1999). Early garnets and cordierites are seen as ellipsoids that are elongated parallel to S2. and hence must have been deformed during D2. Later generations show no such deformation but are associated with D3 melting.

The relationship of the leucosomes to the two main foliations was studied to determine if two separate periods of melting could be distinguished. Melts that were formed in association with early Grt 1 and Crd 1 might be expected to be consistently aligned along S2, and to be subsequently folded by F3. Leucosomes that formed syn-F3 would cross cut S2 but may be controlled by compression during D3. However, field observations do not support the model for two distinct melting episodes, but rather indicate that melting was a continuous (or quasi-continuous) process from syn-post D2 to post D3. Five leucosome types were identified in the field based on their relationship to both periods of deformation, as well as by their size, colour and mineral assemblage:

pre-D3 Lc1 - Folded by F3 and parallel to S2

syn-D3 Lc2 - Small leucosomes that are folded by F3 but are locally axial planar to F3 where they can cross cut fold hinges

syn/late D3 Lc3 - Generally large (0.5 - 2 m wide) leucosomes that cut S2 and are parallel to F3 fold axes. Sometimes this leucosome type cross cuts the F3 folds

late D3 Lc4 - Leucosomes that occupy late D3 shear zones with high cordierite contents (i.e. late D3)

post D3 Lc5 - Late granitic sheets that cross cut all foliations. Technically not migmatitic leucosomes but these granitic sheets share a similar mineralogy and are thought to be linked to the same melting event.

Whilst the five identified leucosome types were observed across the terrain, they were not present at every locality, e.g. Lc4 leucosomes were only seen at localities 1 and 4 (Riviera outcrops and Sojerma road cutting). The southern and middle localities were typified by a high percentage of leucosome material, and at some localities (4, 6, 7, 9) there was >70%. The actual percentage was not quantitatively measured but the values quoted are based on qualitative estimates after comparison of all outcrops. A common feature of these outcrops is the presence of large granitic sheets that cut across earlier leucosomes with diffuse contacts i.e. Lc3 and some Lc5 leucosome types.

The northern localities, especially along the Häähä road, typically had much lower percentages of leucosome material and the dominant leucosome types were Lc1 and Lc2. At northern localities, and southern localities with a relatively low amount of melt material present, some leucosomes were selvage-bound which may indicate that the melt produced did not move far into or out of the system, and that the fluids expelled upon melt crystallisation rehydrated the immediate country rock. If this is the case then phases that formed in the melt as the peritectic products of melting reactions may have partially back-reacted with the retained fluids.

9.1.2 - Evidence for partial melting and compositional variations in leucosome type

Dehydration melting involving the breakdown of hydrous phases is the main process ascribed to the production of melts within low a_{H2O} granulite terrains (Thompson, 1982; Waters, 1984; Le Breton and Thompson, 1988; Vielzeuf and Holloway, 1988; Patino Douce and Johnston, 1991). The melting of pelitic compositions will produce peraluminous S-type melts leaving behind a residuum rich in Al-, Fe- and Mg-

bearing minerals, e.g. biotite, cordierite, garnet (Patino Douce and Johnston, 1991). However there is a limit on the amount of melt that can be produced through this process (Clemens and Vielzeuf, 1987; Le Breton and Thompson, 1988; Patino Douce and Johnston, 1991), generally <50 % in pelitic rocks. As mentioned previously, there is often a much higher percentage of leucosome material observed at some southern and middle Turku localities. There is therefore evidence that some leucosomes are not solely the products of dehydration melting reactions occurring on the local scale.

Petrographical evidence

Evidence for partial melting of the pelites can be seen in the mesosome assemblages. The mesosome has a bt + qtz + kfs + plag + grt + crd assemblage over much of the terrain. The presence of sillimanite, biotite and quartz inclusions within cordierite, K-feldspar and garnet in Turku mesosomes have also been observed in rocks from the Reynolds Range, Australia. Buick et al. (1999) suggested that this texture indicated that the garnets and cordierites were the products of the following dehydration melting reaction:

Biotite + quartz + sillimanite = garnet + cordierite + K-feldspar + quartz (9.1)

The presence of poikiloblastic garnets and cordierites within leucosomes are thought to represent the peritectic products of dehydration melting. There is evidence for this in the large poikiloblastic garnets found in leucosomes across the terrain, but it is particularly well documented at locality 2 where large (3-4 cm diameter) garnets can be seen in association with small K-feldspar and quartz leucosome patches (Chapters 2 and 3). This texture in other terrains has been attributed to garnet being a peritectic phase within the leucosome (Waters and Whales, 1984; Powell and Downes, 1991; Waters, 1994). Cordierite can also form poikiloblasts with quartz inclusions, and it is this textural feature and lack of sillimanite inclusions that identifies them as peritectic phases (Kalt et al, 1999).

Other evidence for the presence of melt in the Turku terrain are textures found in the leucosomes that are also common in plutonic granites:

- The phases in the leucosomes often have irregular grain contacts i.e. lobate or embayed, unlike the straight contacts of mesosome or melanosome phases (Ashworth and McLellan, 1988).
- The leucosome phases are coarser grained than mesosome assemblages (Ashworth, 1985, Ashworth and McLellan).
- Myrmekitic and granophyric textures are found within the Turku leucosomes. Myrmekites are features of many plutonic rocks (Smith, 1974), such as the Rapakivi granites of southern Scandinavia (Eskola, 1914) where they form through the exsolution of adjoining K-feldspar with the incorporation of primary quartz (Smith, 1974, Smith and Brown, 1986).

Melting will lower the a_{H2O} of a terrain if the melt is extracted to higher crustal levels (Thompson, 1982; Waters, 1988; Le Breton and Thompson, 1988; Vielzeuf and Holloway, 1988; Patino Douce and Johnston, 1991). However if melt stays in-situ then fluid will be released upon melt crystallisation which may cause a back reaction with the leucosome phases (Powell and Downes, 1991). The presence of selvages on some leucosomes may suggest local rehydration of the mesosome as discussed earlier. Petrographic descriptions have shown the replacement of K-feldspar and cordierite by biotite and sillimanite, and later by white mica and chlorite, in northern localities. Pinitisation of cordierite is also very strong in northern localities. Recent work on myrmekite formation has suggested that this process involves interaction with a fluid phase upon crystallisation of the melt (Mathavan, 1991; Garcia et al., 1996), as discussed in Chapter 3

Thus there is evidence to indicate retrogression in a fluid-present or high a_{H2O} system, which may suggest that fluids expelled upon melt crystallisation were not entirely removed from the system. In the middle and south of the terrain this retrogression is not seen to the same extent but cordierite is frequently altered to pinite. Garnet is often mantled by biotite and quartz (±cordierite) symplectites which represents a

conversion towards more hydrous phases upon retrogression. This lack of strong retrogression in southern and middle localities may be due to the presence of the D3 shear zones which could have removed melt from the system to higher crustal levels.

Leucosome composition

The bulk geochemistry of the leucosomes analysed shows that there is no obvious link between leucosome types observed in the field and their major and trace element contents. Some leucosomes may represent crustal melts formed through the dehydration melting of pelitic compositions, based upon the major element criteria of White and Chappell (1977), Vielzeuf and Holloway (1988), and Patino Douce and Johnston (1991):

1. Silica rich (68-73 wt%)
2. Strongly peraluminous (2-5 normative wt% corundum and an A/CNK ratio of >1.1)
3. Low in total magnesium and iron (<3 wt%) following the experimental work of Patino Douce and Johnston (1991).
4. The mesosome (restite) is rich in garnet and biotite (White and Chappell, 1977, Vielzeuf and Holloway, 1988).

On a normative Qz-Ab-Or plot, a subset of leucosome samples plot in a near granite minimum region, whereas others are displaced away from the minimum melt region towards normative quartz and less commonly, normative orthoclase. Those leucosomes with near minimum melt compositions (Leuc A) can be classified as COLG (syn-collision granites) to VAG (volcanic are granite) on the basis of their Rb and Nb+Y contents (Inger and Harris, 1993).

Leuc B leucosomes often have too high total Fe-Mg contents than would typical for melts formed through the breakdown of biotite i.e. they are >3 wt % (White and Chappell, 1977; Vielzeuf and Holloway, 1988; Patino Douce and Johnston, 1991). These Fe-Mg totals are consistent with excess garnet and cordierite being incorporated into the leucosomes. As discussed earlier, mesosome cordierites often

contain cores of fibrous sillimanite inclusions, whilst some contain inclusions of biotite and quartz. A petrographic analysis of leucosomes has shown that some cordierites found within the mesosome have sillimanite inclusions. This suggests that some of the leucosomes contain entrained mesosome material (restite). Garnet and cordierite formed as the peritectic products of dehydration melting will also increase total Fe-Mg.

Further evidence for the entrainment of restite comes from trace element data. The aforementioned enrichment in Fe-Mg correlates with high Sc, Y and Zr values which are consistent with the melt having entrained some restitic material (White and Chappell, 1977; Patino Douce and Johnston, 1991; Sawyer, 1996) that is comparatively enriched in Fe-Mg phases such as biotite, garnet and cordierite. Ce(n)/Y(n) ratio variations between samples reflect both garnet and zircon entrainment as well as preferential entrainment of monazite in some cases.

The accessory phases monazite and zircon can contain 60 % of the REE mass budget of a melt but they have limited dissolution in low a_{H2O} melts (Watt and Harley; 1996, Bea, 1996; Watson, 1996), which allows the restite to become relatively enriched in these phases. At mesosome-leucosome contacts there are abundant zircon and monazite inclusions in cordierite and biotite; entrainment of such mesosome material into a melt would increase the proportion of these phases relative to a melt that segregated cleanly from its source. Thus many leucosomes are typified by the entrainment of some restitic material and as such, garnet, cordierite, zircon and monazite.

The Rb/Sr ratio of leucosomes suggest that as melting occurred biotite fractionated from the melt into the restite depleting the melt in Sr, this depletion is seen as a case for disequilibrium melting by Inger and Harris (1993). A further observation from the Rb/Sr data is that the leucosomes (even the clean ones) may be in part accumulations of feldspars, deviating from true melts by having lost a final fraction of late crystallising melt rich in incompatibles. The concentration of garnet and

cordierite, zircon and monazite could therefore also have been enhanced by the removal of a later melt fraction.

9.1.3 - External factors controlling melting

Thus evidence so far suggests that partial melting of the local pelites occurred from D2 through to late D3, with varied extraction of melt material. The volume of leucosome material at some localities however has still not been clarified, although field relations do suggest an external input of granitic material. The next section will therefore concentrate on the external factors that govern melt production.

P-T data

The composition of mesosome phases, notably garnet, cordierite and biotite were used to extrapolate PT data. The cores of some garnets preserve an X_{Mg} of ≥0.20 but this can decrease to 0.11 in some garnet rims. Biotite X_{Mg} increases from 0.4-0.55 in matrix phases, to >0.6 in some biotite inclusions and biotite in contact with garnet. This decrease of garnet and biotite X_{Mg} when the two phases are in contact, provided further evidence for later retrogression in the form of Fe-Mg exchange. As there was moderate to extensive modification of the Fe-Mg compositions of garnet and biotite, garnet cores with matrix biotite and cordierite were used to try and calculate peak PT conditions.

The peak temperatures and pressures attained by the Turku terrain are 750-800°C and 5-5.5 kbar based on the geothermobarometry carried out by this study and by previous workers (Höltta, 1986; Van Duin and Nieman, 1993; Väisänen et al., 1994; Väisänen and Höltta, in press). Typical errors range from ± 89-40°C for the thermometers and ± 0.91-0.53 kbar for the barometers, based on errors of the FeO and MgO content of the phases concerned. Although the studies of Väisänen et al. (1994) and Väisänen and Höltta (in press) have indicated a P-T gradient between the middle localities and the southern localities, no such gradient was observed in this study. The P-T conditions of the northern localities was not assessed in this study but the average P-T calculated by the previous studies is 650° and 5 kbar (actual

range 725-625°). (Le Breton and Thompson, 1988) The maximum amount of melt that could be formed purely through dehydration melting at the PT conditions of the Turku terrain is <40 vol% (Clemens and Vielzeuf, 1987; Le Breton and Thompson, 1988; Patino Douce and Johnston, 1991).

Fluid regime

As well as the P-T conditions present, the melting is dependent upon a_{H2O}, as the amount of water within a melt is a function of pressure, temperature and the X_{H2O} of the system (Johannes and Holtz, 1990). Therefore an analysis of the volatile content of the melt would provide information on the fluid regime at the time of melting. The method employed by this study was to measure the volatile contents of a mineral that is associated with the melts and whose volatile contents depend systematically on a_{H2O}. Cordierite can incorporate both H_2O and CO_2 into its crystal structure and is a potential monitor of lower crustal fluids (Armbruster and Bloss, 1982; Schreyer, 1985; Harley, 1994; Fitzsimons and Mattey, 1994). It can therefore, in principle, monitor the absolute amount and ratio of the two species in any co-existing fluid or melt (Fitzsimons 1994; Fitzsimons and Mattey, 1994; Harley, 1994; Carrington and Harley, 1996).

The cordierite volatile contents reported by Harley (1994), Fitzsimons (1994), and Carrington and Harley (1996) were measured using SIMS (secondary ion mass spectrometry) analysis which allows both hydrogen and carbon to be measured in the same analysis within 25μm. This method yielded wt% H_2O and CO_2 contents of the cordierite samples. Using the models of Harley and Carrington (in press) and Harley et al. (*unpubl. data*), water activity was calculated based on the thermodynamics of hydration and the fugacity of both volatile species. These models then allowed both a D_w term (H_2O melt/ H_2O cordierite), and a consequent melt water content to the calculated.

The H_2O values in m.p.f.u cordierite from the northern localities, are typically undersaturated with respect to the H_2O saturation curves of Vry et al. (1991) and

Harley et al. (*unpubl. data*). However some southern and middle localities are at or above the saturation curves of Harley et al (*unpubl. data*). Water activity is fairly homogeneous across the terrain within the average range of values (0.2-0.4), but there is heterogeneity in a_{H2O} within a locality (i.e. 0.16-0.30 at locality 12). This is indicative of local control of a_{H2O} in agreement with melting occurring to varying extents along dehydration-melting reactions. (Powell, 1982; Waters and Whales, 1984; Waters 1988, 1994; Harley, 1989).

Under the range of a_{H2O} values, melts were found to have an average D_w of 3.1±0.05 in the middle and southern localities, whilst the northern localities have an average D_w value of 2.6±0.1. The standard deviation on the D_w data varies from nearly zero to ±0.1. The lower values of D_w derived from the northern localities are due to the different pressure and temperatures used in the calculations, and are therefore a function of the model of Harley and Carrington (in press). The resulting estimate of the water content of the melt is on average 3±1.0 wt%, with little variation shown across the terrain. These values are typically undersaturated compared to 11 wt % H_2O present in saturated melts at the same PT (Johannes and Holtz, 1996).

Variation occurs in X_{CO2}(ch) from nearly 0 in the north of the terrain to 0.4 in the southern localities. This variation in X_{CO2}(ch) has no affect on the average a_{H2O} across the terrain. High CO_2 activities and saturation values of CO_2 (in m.p.f.u) in the middle and southern localities, where the percentage of leucosome material is high, may indicate that a CO_2-dominated fluid was introduced to the Turku terrain within externally-derived melts. This hypothesis could be further constrained with a knowledge of the isotopic composition of the CO_2 included within the channels of cordierite.

The $\delta^{13}C$ values recorded from the Turku terrain range from sedimentary carbon values (-25‰) to mantle-like values (-7‰) (Vry et al, 1988; 1990, Fitzsimons and Mattey, 1994). This wide range in $\delta^{13}C$ may represent mixing of an original light sedimentary carbon source with varied amounts of a heavier carbon reservoir, e.g. a

mantle derived fluid. It is unlikely that the Turku terrain underwent a pervasive CO_2 influx because of the heterogeneity of the isotope signatures. Vry et al. (1988, 1990) argue that the presence of $\delta^{13}C_{crd}$ <-15‰ is evidence against large scale fluid infiltration, as only a small amount of a heavy isotope fluid is needed to homogenise isotopic compositions within a terrain. In addition, the volatile contents of cordierites analysed in chapter 7 are dominated by H_2O.

However if mantle derived CO_2 could have been introduced into the system within externally derived melts in ppm levels, then there would be some mixing of isotope values, and saturation of melt borne cordierite with respect to CO_2. Some melting took place due to dehydration reactions, as shown by the low and variable a_{H2O}, and low wt% water contents of the leucosomes, but all of the leucosome material present could not have been derived from this method alone and was probably supplemented by an input of externally derived melts. In order to see how much external CO_2 would be needed to change original sedimentary values, a few hypothetical mass balance calculations can be carried out (Figure 9.1).

Curve 1 in Figure 9.1 was calculated assuming that an original carbon content in the mesosome of 1000 ppm ($\delta^{13}C$ -25‰), was mixed with an external carbon source (-7‰) at varying concentrations from 100-9000 ppm. Curve 2 was calculated using an original carbon content of 200 ppm and the same varied external carbon concentrations. 200 ppm is a good estimate for an original carbon concentration in the Turku pelites as it based on samples 103 and 104 from the north of the terrain. The possible sedimentary $\delta^{13}C$ values of -25‰ (Vry et al, 1988; 1990), and very low values of total ppm C from 103 and 104 in comparison to other samples, may be indicative of cordierite that grew with no external input. This second curve shows that it is possible to derive $\delta^{13}C$ values down to -8 with no more than 3000 ppm external carbon. However these figures are just estimates and the values of original carbon could vary across the terrain.

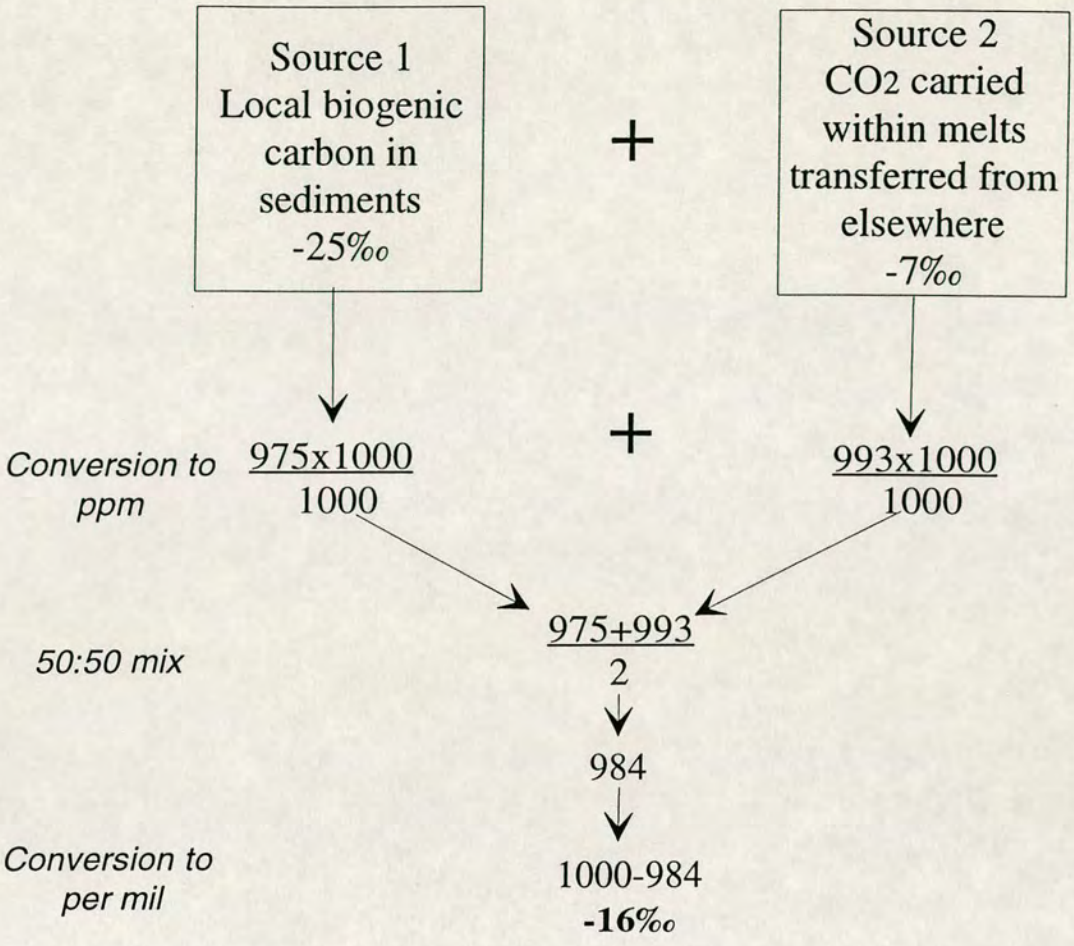

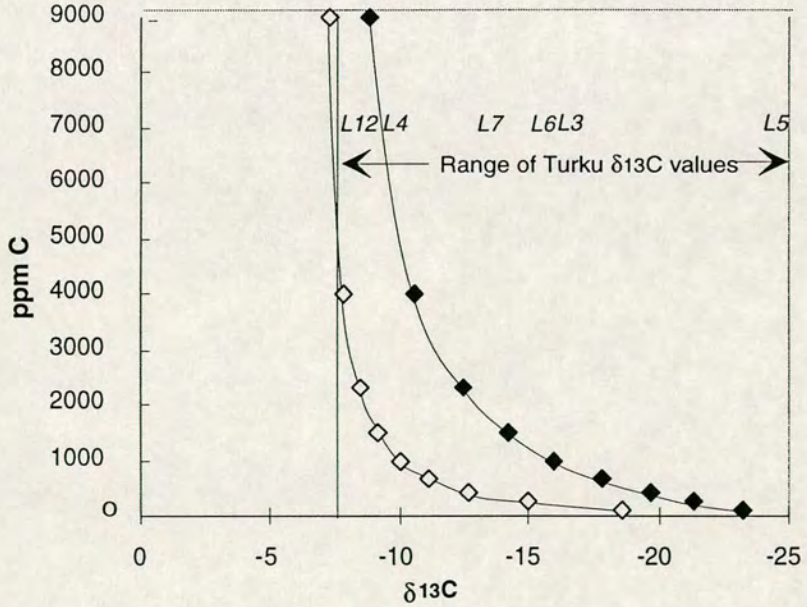

Figure 9.1 - The results of mixing original sedimentary carbon ($\delta^{13}C$ = -25‰) with an external carbon source ($\delta^{13}C$ = -7‰). The calculation assumes a 50:50 mix of 1000 ppm of each source. Curve 1 (black diamonds) was calculated using 1000 ppm in the source and varied ppm levels of external carbon. Using data collected from samples 103 and 104, curve 2 (grey diamonds) was calculated assuming 200 ppm in the source but the same variation in external carbon.

Therefore the saturated values of cordierite in the southern and middle localities, the varied $\delta^{13}C$ values across the terrain and the excess of leucosome material at some localities could be explained by the introduction of external melts that are carrying up to 3000 ppm C, possibly with an original mantle origin.

9.2 - Conclusions and model for melting

The Turku terrain was at granulite facies conditions (700-800° and 5-5.5 kbar) from 1890-1830 Ma, although the grade varied through the terrain. During metamorphism the terrain suffered two periods of ductile deformation. Two generations of garnet + cordierite are present in the mesosome, and both generations contain textures that suggest the phases were the product of dehydration melting following the break down of biotite and sillimanite. The melting of the terrain lead to the production of granitic melts that are now represented by leucosome material. The geochemistry and mineralogy of the leucosomes suggest that the degree of segregation, and subsequent extraction of melt, was varied across the terrain with some entrainment of mesosome material. The melting was continuous through D2 and D3, but during D3 later granitic sheets were introduced from outside of the Turku terrain., dominantly into southern and middle localities. These external melts contained varying amounts of CO_2 at concentrations of 10^3 ppm, with typical mantle $\delta^{13}C$ values of <-7. Mixing of this carbon with original sedimentary carbon lead to a heterogeneous variation in $\delta^{13}C$ from cordierite CO_2 across the terrain. Some cordierites therefore became saturated with respect to CO_2, and total volatiles in m.p.f.u.

The terrain then underwent retrogression in the form of hydrous assemblages replacing anhydrous assemblages, and in Fe-Mg exchange between mafic phases. The retrogression was stronger in the north where the presence of selvages and strong white mica, pinite and chlorite overprint of phases may suggest back reaction with fluid released upon melt crystallisation. The terrain was slowly uplifted along an isobaric cooling path until the terrain saw brittle deformation in the form of D4 shear zones containing pseudotachylites..

At the end of chapter 2 two diagrams were constructed of 'typical' localities seen in the north and in the south/middle of the terrain. At the end of this study representative data has been added to these figures to summarise the geological history of the Turku terrain.

9.3 - Links to wider granulite and crustal melting studies.

Although it is possible to derive a model for melting in the Turku granulite terrain, how does the study of this area contribute towards the main issues of granulite and crustal melting studies discussed in the literature. In chapter 1 some key problems associated with granulites were discussed,

1. P-T-t paths
2. Low a_{H2O} values in granulites
3. Melting in granulite facies metapelites.

Although this project did not attempt to solve any of these problems, it can have some positive input into these ongoing discussions.

P-T-t paths

Lack of definitive prograde inclusions, growth zoning and major retrogressive textures means that producing a P-T-t path is difficult for the Turku terrain. Geothermobarometry from this and earlier studies (Väisänen et al. (1994), Väisänen and Höltta (in press) does suggest that temperature decreased faster than pressure. Sillimanite is the primary retrogressive aluminosilicate which also suggests that pressure decreased slowly. Thus the Turku terrain probably followed an IBC path.

Fluid regime

The volatile contents of the Turku cordierites help to argue against CO_2 flushing as a method for stabilising granulite facies. Mixed H_2O-CO_2 fluid compositions with X_{CO2} typically lower than 0.4, varied CO_2 contents from 0.09-0.9 and a range of $\delta^{13}C$ values from -7 to -24‰ all rule out the presence of a pervasive CO_2 rich fluid at the peak of metamorphism. These results agree with the work of Lamb et al. (1987),

Lamb (1990), Valley et al. (1990) and Bhowmik et al. (1995) for the Adirondacks and Eastern Ghats respectively.

The other crustal volatiles that were discussed in relation to stabilising the low water activities of granulites, were salts such as NaCl, KCl etc. The only volatile ratios measured in this study were H_2O and CO_2 and so the effect of introducing NaCl is not quantitatively known. However NaCl will decrease a_{H2O} and increase a_{CO2} within a fluid (Jacobs and Kerrick, 1981; Aranovich and Newton, 1996; Shmulovich and Graham, 1996; Aranovich and Newton, 1997; Aranovich and Newton, 1999; Shmulovich and Graham, 1999). This relative increase and decrease of CO_2 and H_2O respectively, would decrease the D*w* value and thus the calculated water content of the melt. The high a_{CO2} in the southern and middle localities could indicate that CO_2 was in equilibrium with a saline fluid. However this would not explain the heterogeneous $\delta^{13}C$ values across the terrain, especially the near mantle values (-7‰), unless there was an alternative heavy $\delta^{13}C$ source. There may have been some mixing with a local sedimentary carbonate source (0‰) if the calc-silicate pods observed at locality 2 were more widespread. Thus in order to properly constrain and calculate fluid compositions within such a terrain care needs to be taken to:

- Determine PT conditions as absolutely as possible by collecting samples across any reported gradients, establishing equilibrium assemblages and by using a good range of geothermobarometers.
- Collect CO_2+H_2O samples from a variety of structural settings in order to assess the composition of a fluid, the activity of its phases and any variation in isotopic composition over a range of scales.
- Look carefully for the presence of any heavy $\delta^{13}C$ source in the surrounding rocks, i.e. carbonates or calc-silicate pods.

Melting in low pressure granulite terrains

The presence of cordierite and garnet as the interpreted products of biotite dehydration melting agrees with the conclusions of workers on other low pressure granulite terrains such as Namaqualand, S Africa (Waters and Whales, 1984; Waters,

1988) and Broken Hill, Australia (Powell and Downes, 1991). It also agrees with the theoretical and experimentally constrained grids of Hensen and Harley (1990), Powell and Downes (1990), Carrington and Harley (1995) and Holland et al. (1996), in that the reaction bt + sil + qtz = grt + crd + kfs + melt takes place at low pressures within the KFMASH system.

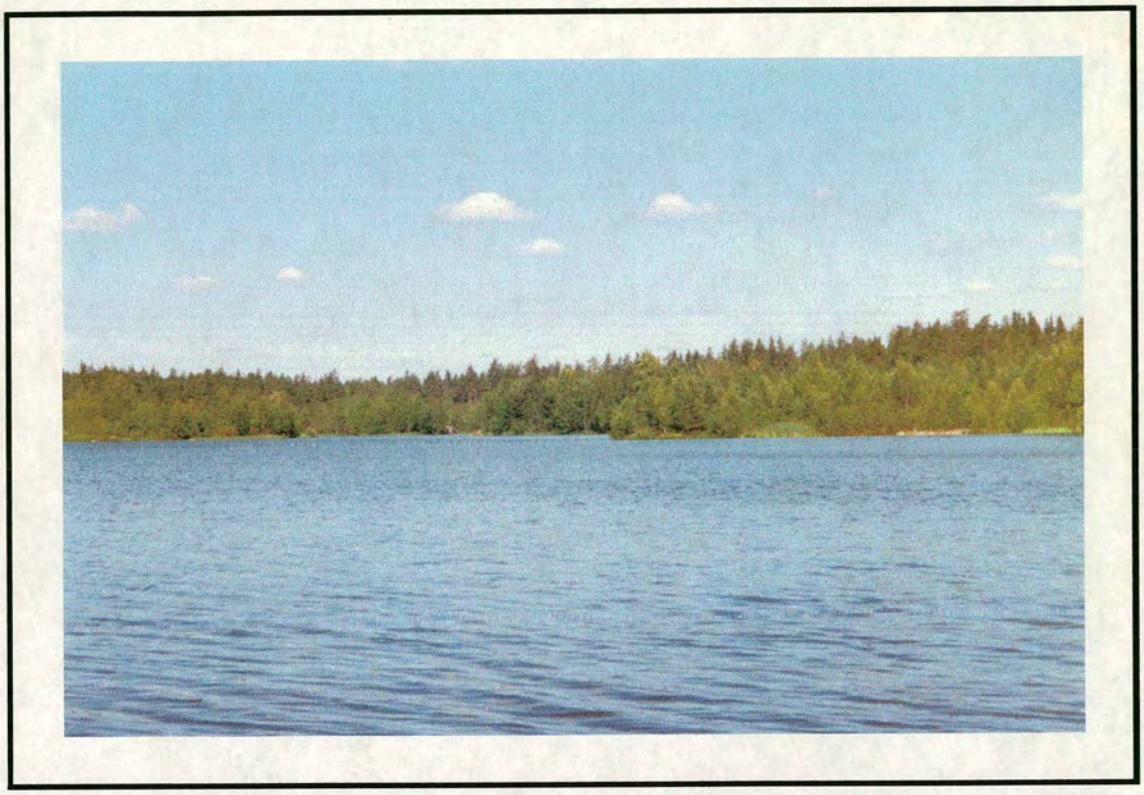

"Finland, Finland, Finland,

Finland has it all.....

References

Aranovich, L.Y. and Podlesskii, K.K. 1983. The cordierite-garnet-sillimanite-quartz equilibrium: experiments and applications. In: Saxena, S.K. (ed) *Kinetics and equilibrium in mineral reactions.* Advances in Physical Geochemistry 3, Springer, Berlin, pp. 173-198.

Aranovich, L.Y. and Newton, R.C. 1996. H_2O activity in concentrated NaCl solutions at high pressures and temperatures measured by the brucite-periclase equilibrium. *Contributions to Mineralogy and Petrology*, **125**, 200-212.

Aranovich, L.Y. and Newton, R.C. 1997. H_2O activity in concentrated KCl and KCl-NaCl solutions at high temperatures and pressures measured by the brucite-periclase equilibrium. *Contributions to Mineralogy and Petrology,* **127**, 261-271.

Aranovich, L.Y. and Newton, R.C. 1999. Experimental determination of CO_2-H_2O activity-composition relations at 600-1000°C and 6-14 kbar by reversed decarbonation and dehydration reactions. *American Mineralogist*, **84**, 1319-1332.

Appel, P., Möller, A. and Schenk, V. 1998. High-pressure granulite facies metamorphism in the Pan-African belt of eastern Tanzania: P-T-t evidence against granulite formation by continent collision. *Journal of Metamorphic Geology*, **16**, 491-509.

Armbruster, T. and Bloss, F.D. 1982. Orientation and effects of channel H_2O and CO_2 in cordierite. *American Mineralogist*, **67**, 284-291.

Armbruster, T., Schreyer, W. and Hoefs, J. 1982. Very high CO_2 cordierite from Norwegian Lapland: mineralogy, petrology, and carbon isotopes. *Contributions to Mineralogy and Petrology*, **81**, 262-267.

Ashworth, J.R. 1985. Introduction. In: Ashworth, J.R. (ed) *Migmatites.* Blackie and Son, Glasgow, pp. 1-35.

Ashworth, J.R. and McLellan, E.L. 1985. Textures. In: Ashworth, J.R. (ed) *Migmatites.* Blackie and Son, Glasgow, pp. 180-203.

Atherton, M.P. and Gribble, C.D. (eds) 1983. *Migmatites, Melting and Metamorphism.* Proceedings of the Geochemical Group of the Mineralogical Society, Shiva Publishing, Nantwich.

Baba, S. 1998. Proterozoic anticlockwise P-T path of the Lewisian Complex of South Harris, Outer Hebrides, NW Scotland. *Journal of Metamorphic Geology*, **16**, 819-841.

Barth, A.P. and May, D.J. 1992. Mineralogy and pressure-temperature-time path of Cretaceous granulite gneisses, south-eastern San Gabriel Mountains, southern California. *Journal of Metamorphic Geology*, **10**, 529-544.

Bea, F. 1996. Controls on the trace element composition of crustal melts. *Transactions of the Royal Society of Edinburgh: Earth Sciences,* **87,** 33-41.

Becke, F. 1908. Ueber Myrmekite. *Schweizerische Mineralogische und Petrographische Mitteilungen*, **27**, 377-390.

Bhowmik, S.K., Dasgupta, S., Hoernes, S. and Bhattacherva, P.K. 1995. Extremely high-temperature calcareous granulites from the Eastern Ghats, India: Evidence for isobaric cooling, fluid buffering, and terminal channelised fluid flow. *European Journal of Mineralogy*, **7**, 689-703.

Blumenfield, P. and Bouchez, J-L. 1988. Shear criteria in granite and migmatite deformed in the magmatic and solid states. *Journal of Structural Geology*, **10**, 361-372.

Boberski, C. and Schreyer, W. 1990. Synthesis and water content of Fe^{2+}-bearing cordierites. *European Journal of Mineralogy,* **2,** 565-584.

Bohlen, S.R. 1987. Pressure-temperature-time paths and a tectonic model for the evolution of granulites. *Journal of Geology*, **95**, 617-632.

Bohlen, S.R. 1991. On the formation of granulites. *Journal of Metamorphic Geology*, **9**, 223-229.

Brown, M., Averkin, Y.A., McLellan, E.L. and Sawyer, E.W. 1995. Melt segregation in migmatites. *Journal of Geophysical Research*, **100**, 15655-15679.

Bucher-Nurminen, K. and Ohta, Y. 1993. Granulites and garnet-cordierite gneisses from Dronning Maud Land, Antarctica. *Journal of Metamorphic Geology*, **11**, 691-703.

Buick, I.S., Cartwright, I. and Harley, S.L. 1998. The retrograde P-T-t path for low-pressure granulites from the Reynolds Range, central Australia: petrological constraints and implications for low-P/high-T metamorphism. *Journal of Metamorphic Geology*, **16**, 511-529.

Burnham, C.W. and Nekvasil, H. 1986. Equilibrium properties of granite pegmatite magmas. *American Mineralogist,* **71,** 239-263.

Carey, J.W. 1995. A thermodynamic formulation of hydrous cordierite. *Contributions to Mineralogy and Petrology*, **119**, 155-165.

Carrington, D.P. and Harley, S.L. 1995. Partial melting and phase relations in high grade metapelites: an experimental petrogenetic grid in the KFMASH system. *Contributions to Mineralogy and Petrology*, **120**, 270-291.

Carrington, D.P. and Harley, S.L. 1996. Cordierite as a monitor of fluid and melt H_2O contents in the lower crust: An experimental calibration. *Geology*, **24**, 647-650.

Carson, C.J., Powell, R., Wilson, C.J.L. and Dirks, P.H.G.M. 1997. Partial melting during tectonic exhumation of a granulite terrain: an example from the Larsemann Hills, East Antarctica. *Journal of Metamorphic Geology*, **15**, 105-126.

Chipera, S.J. and Perkins, D. 1988. Evaluation of biotite-garnet geothermometers: application to the English River sub-province, Ontario. *Contributions to Mineralogy and Petrology*, **98**, 40-48.

Clarke, D.B. 1992. *Granitoid Rocks.* Chapman and Hall, London.

Clemens, J.D. and Vielzeuf, D. 1987. Constraints on melting and magma production in the crust. *Earth Planetary Science Letters*, **86**, 287-306.

Clemens, J.D. and Droop, G.T.R. 1998. Fluids, *P-T* paths and the fates of anatectic melts in the Earth's crust. *Lithos*, **44**, 21-36.

Collins, W.J. and Sawyer, E.W. 1996. Pervasive granitoid magma transfer through the lower-middle crust during non-coaxial compressional deformation. *Journal of Metamorphic Geology*, **14**, 565-579.

Dawson, J.B., Harley, S.L., Rudnick, R.L. and Ireland, T.R. 1997. Equilibration and reaction in Archean quartz – sapphirine granulite xenoliths from the Lace Kimberlite pipe, South Africa. *Journal of Metamorphic Geology*, **145**, no 2, 253-266.

Deer, W.A., Howie, R.A. and Zussman, J. 1992. *An introduction to the rock-forming minerals.* Longman Scientific and Technical, Harlow.

Dempster, T.J., Harrison, T.N., Brown, P.E. and Hutton, D.H.W. 1991. Low-pressure granulites from the Ketilidian Mobile Belt of southern Greenland. *Journal of Petrology*, **32**, 979-1004.

Ehlers, C, Lindroos, A. and Selonen, O. 1993. The late Svecofennian granite-migmatite zone of southern Finland - a belt of transpressive deformation and granite emplacement. *Precambrian Research*, **64**, 295-309.

Ellis, D.J. 1987. Origin and evolution of granulites in normal and thickened crusts. *Geology*, **1**, 167-170.

Eskola, P. 1914. On the petrology of the Orijärvi region in south-western Finland. *Geological Survey of Finland Bulletin,* **40.**

Etheridge, M.A., Wall, V.J. and Cox, S.F. 1984. High fluid pressures during regional metamorphism and deformation: implications for mass transport and deformation mechanisms. *Journal of Geophysical Research*, **89**, 4344-4358.

Ferry, J.M. and Spear, F.S. 1978. Experimental calibration of the partitioning of Fe and Mg between biotite and garnet. *Contributions to Mineralogy and Petrology*, **66**, 113-117.

Fitzsimons, I.C.W. 1991. *The metamorphic histories of some Proterozoic granulites from East Antarctica.* PhD Thesis, University of Edinburgh, Edinburgh.

Fitzsimons, I.C.W. 1994. Cordierite migmatites from East Antarctica: geochemical constraints on volatile distribution during crustal anatexis. *Goldschmidt Conference Abstract Volume, Mineralogical Magazine,* **58A,** 274-275.

Fitzsimons, I.C.W. 1996. Metapelitic migmatites from Brattstrand Bluffs, East Antarctica - metamorphism, melting and exhumation of the mid crust. *Journal of Petrology*, **37**, 395-414.

Fitzsimons, I.C.W. and Mattey, D.P. 1994. Carbon isotope constraints on volatile mixing and melt transport in granulite-facies migmatites. *Earth and Planetary Science Letters*, **134**, 319-328.

Front, K. and Nurmi, P.A. 1987. Characteristics and geological setting of Synkinematic Svecokarelian Granitoids in Southern Finland. *Precambrian Research*, **35**, 207-224.

Frost, B.R. and Frost, C.D. 1987. CO_2, melts and granulite metamorphism. *Nature*, **327**, 503-506.

Garcia, D., Pascal, M-L. and Roux, J. 1996. Hydrothermal replacement of feldspars in igneous enclaves of the Velay granite and the genesis of myrmekites. European *Journal of Geology*, **8**, 703-717.

Gerya, T.V. and Perchuk, L.L. 1992. GEOPATH – a thermodynamic database for geothermobarometry and related calculates with the IBM PC AT/TX computer. *29th International Geological Congress, Kyoto, Volume 2,* 1026.

Gibson, G.M. and Ireland, T.R. 1995. Granulite formation during continental extension in Fiordland, New Zealand. *Nature*, **375**, 479-482.

Guiraud, M., Kienast, J-R. and Rahmani, A. 1996. Petrological study of high-temperature granulites from In Ouzzal, Algeria: some implications on the phase relationships in the FMASTOCr system. *European Journal of Mineralogy*, **8**, 1375-1390.

Southern Localities

Structural features

D1 – Inclusion trails in cordierite
D2 – S2 fabric and F2 folds
D3 – F3 folds and shear zones that contain leucosome material.

Leucosome features

Small Lc1 and Lc2 leucosome are present but generally they are swamped by large, intrusive Lc3 and Lc5 leucosomes. Some leucosomes contain large poikiloblastic garnets (a) that are thought to be peritectic products of dehydration melting reactions within local pelites. K-feldspars often have a perthitic texture (b) whilst at the grain boundaries of leucosome phases myrmekite textures are common (c)

1) Leuc A – near minimum melt compositions, A/CNK > 1, normative corundum < 2, Fe-Mg< 3 wt, low Zr, Sc.
2) Leuc B – too Or or Qtz normative rich to be minimum melts. Also total Fe-Mg ranges up to 11 wt%. Sc, Zr and Th contents have positive correlations with Fe-Mg, and are high in comparison to Leuc A leucosomes. This suggests some entrainment of local restite.

Mesosome characteristics.

Garnet and cordierite are present as elongate D2 phases and later D3 poikiloblasts. Spinel is found as inclusions within cordierite (d). Cordierite is also found as a D3 phases, growing parallel to S3 (e)

PT conditions

750-800°C and 5-5kbar

Volatile regime

a_{H2O} - 0.17 to 013
a_{CO2} – 0.4 to 0.9
Wt % H2O melt – 2.4 to 3.6
$\delta^{13}C$ - -7 to -16‰

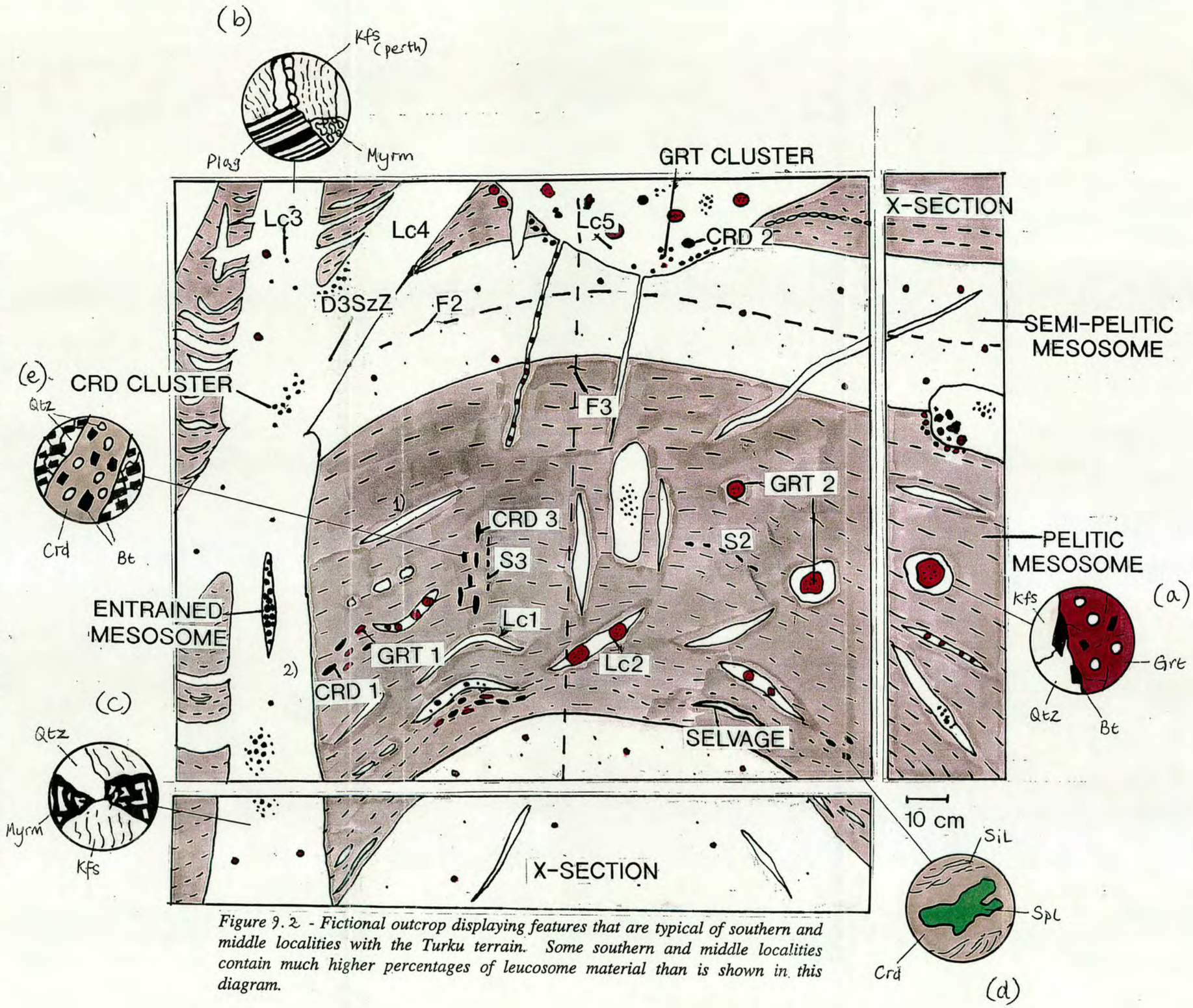

Figure 9.2 - Fictional outcrop displaying features that are typical of southern and middle localities with the Turku terrain. Some southern and middle localities contain much higher percentages of leucosome material than is shown in this diagram.

Northern Localities

Structural features

D1 – Inclusion trails in cordierite (a+b)

D2 – S2 fabric and F2 folds

D3 – F3 folds and shear zones.

D4 – Brittle D4 shear zones.

Leucosome features

Lc1, Lc2, Lc3 and Lc5 leucosome types. Leucosomes are generally small and present in low volumes, they are often selvage bound (b). Cordierite within and near leucosomes is heavily altered to pinite (c), whilst white mica replaces cordierite, biotite and K-feldspar (d). Garnet can be altered to a biotite-quartz simplectite, and cordierite is also present as a retrogressive phase on garnet (e)

Leucosome compositions

1) Leuc A – near minimum melt compositions, A/CNK > 1, normative corundum < 2, Fe-Mg< 3 wt, low Zr, Sc.
2) Leuc B – too Or or Qtz normative rich to be minimum melts. Also total Fe-Mg ranges up to 11 wt%. Sc, Zr and Th contents have positive correlations with Fe-Mg, and are high in comparison to Leuc A leucosomes. This suggests some entrainment of local restite.

Mesosome characteristics.

Garnet and cordierite are present as elongate D2 phases (f) and later D3 poikiloblasts (e). Along the Hähää Rd sillimanite is a stable mesosome phase.

PT conditions

650-725°C and 5 kbar

(Väisänen and Höltta, in press)

Volatile regime

a_{H2O} - 0.16 to 0.31

a_{CO2} – 0.07 to 0.4

Wt % H2O melt – 2.2 to 3.4

$\delta^{13}C$ - -7 to -25‰

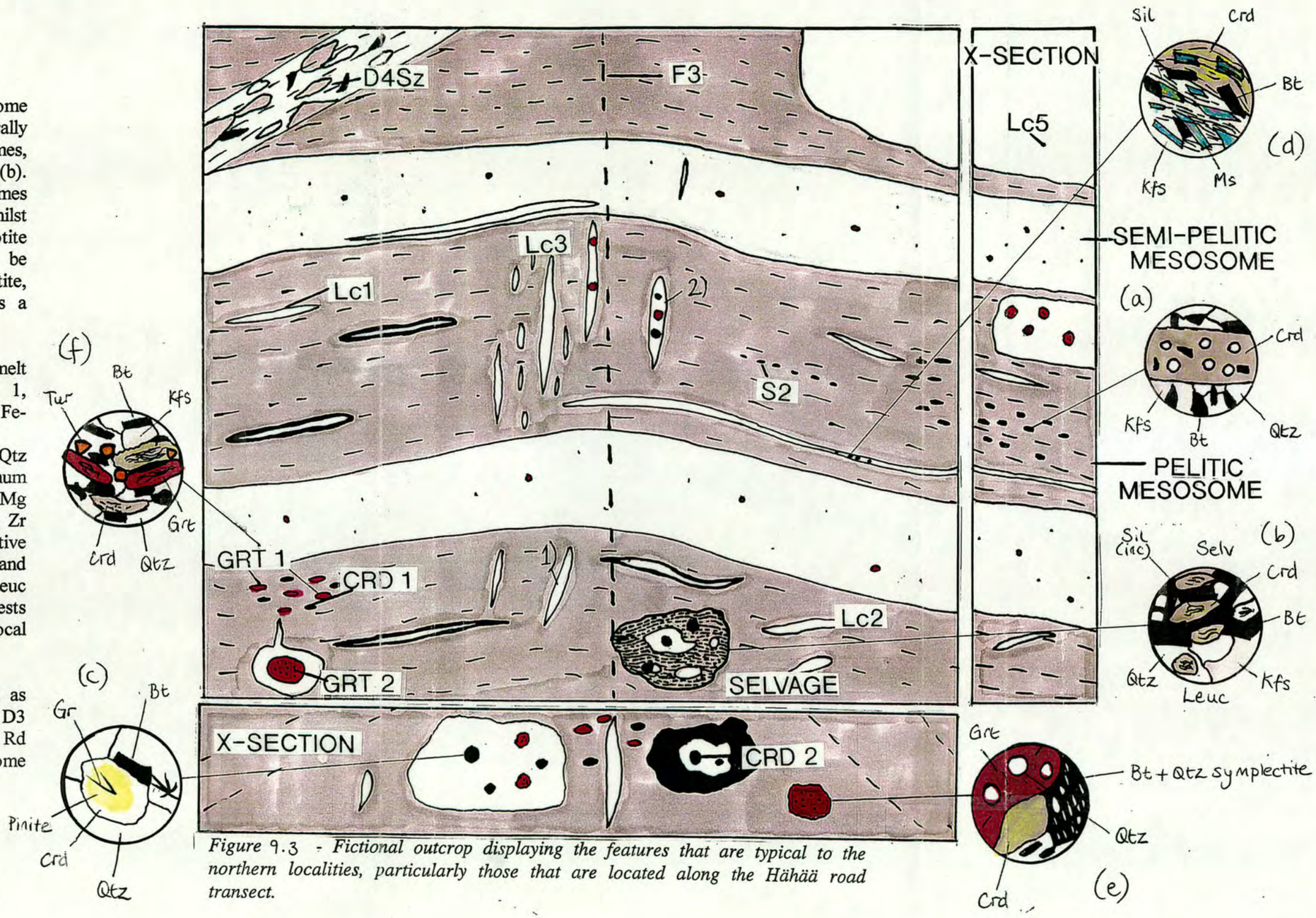

Figure 9.3 - Fictional outcrop displaying the features that are typical to the northern localities, particularly those that are located along the Hähää road transect.

2466

Hand, M. and Dirks, P.H.G.M., Powell, R. and Buick, I.S. 1992. How well established is isobaric cooling in Proterozoic orogenic belts? An example from the Arunta inlier, central Australia. *Geology*, **20**, 649-652.

Hand, M., Scrimgeour, I., Powell, R., Stüwe, K. and Wilson, C.J.L. 1994. Metapelitic granulites from Jetty Peninsula, east Antarctica: formation during a single event or by polymetamorphism. *Journal of Metamorphic Geology,* **12**, 557-573.

Harley, S.L. 1989. The origins of granulites: a metamorphic perspective. *Geological Magazine*, **126**, 215-247.

Harley, S.L. and Hensen, B.J. 1990. Archean and Proterozoic high-grade terranes of East Antarctica (40-80°E): a case study of diversity in granulite facies metamorphism. In: Ashworth, J.R. and Brown, M. (eds) *High-temperature Metamorphism and Crustal Anatexis*. Mineralogical Society Series 2, Unwin Hyman, London, pp. 320-370.

Harley, S.L. and Fitzsimons, I.C.W. 1991. Pressure-temperature evolution of metapelitic granulites in a polymetamorphic terrane: the Rauer Group, East Antarctica. *Journal of Metamorphic Geology*, **9**, 231-243.

Harley, S.L. 1992. Proterozoic granulite terranes. In: Condie, K. (ed*) Proterozoic Crustal Evolution.* Elsevier, Amsterdam, pp. 301-359.

Harley, S.L. 1994. Cordierite as a sensor of fluid and melt distribution in crustal metamorphism. *Goldschmidt Conference Abstract Volume, Mineralogical Magazine,* **58A**, 374-375.

Harley, S.L. 1998. Ultrahigh temperature granulite metamorphism (1050°C, 12 kbar) and decompression in garnet (Mg70)-orthopyroxene-sillimanite gneisses from the Rauer Group, East Antarctica. *Journal of Metamorphic Geology*, **16**, 541-562.

Harley, S.L. and Carrington D.P. (in press) The distribution of H_2O between cordierite and granitic melt: Improved calibration of water incorporation in cordierite. Applications to high grade metamorphism and crustal melting. *Journal of Petrology.*

Hensen, B.J. and Green, D.H. 1973. Experimental study of the stability of cordierite and garnet in pelitic compositions at high pressures and temperatures, III. Synthesis of experimental data and geological applications. *Contributions to Mineralogy and Petrology,* **38,** 151-166.

Hensen, B.J. and Harley, S.L. 1990. Graphical analysis of *P-T-X* relations in granulite facies metapelites. In: Ashworth, J.R. and Brown, M. (eds) *High-temperature Metamorphism and Crustal Anatexis.* Mineralogical Society Series 2, Unwyn Hyman, London, pp. 105-123.

Hensen, B.J. and Zhou, B. 1995. Retention of isotopic memory in garnets partially broken down during an overprinting granulite-facies metamorphism: Implications for the Sm-Nd closure temperature. *Geology,* **23,** 225-228.

Hietanen, A. 1947. Archean geology of the Turku district south-western Finland. *Bulletin of the Geological Society of America*, **58**, 1019-1084.

Hietanen, A. 1975. Generation of potassium-poor magmas in the northern Sierra Nevada and the Svecofennian of Finland. Journal of Research, US Geological Survey, **3**, 631-645.

Holdaway, M.J. and Lee, S.M. 1977. Fe-Mg cordierite stability in high-grade pelitic rocks based on experimental, theoretical and natural observations. *Contributions to Mineralogy and Petrology,* **63,** 175-198.

Holland, T.J.B., Babu, E.V.S.S.K. and Water, D.J. 1996. Phase relations of osumilite and dehydration melting in pelitic rocks: a simple thermodynamic model for the KFMASH system. *Contributions to Mineralogy and Petrology*, **124**, 383-394.

Holland, T.J.B. and Powell, R. 1990. An enlarged and updated internally consistent thermodynamic dataset with uncertainties and correlations: the system K_2O-Na_2O-CaO-MgO-MnO-FeO-Fe_2O_3-Al_2O_3-Al_2O_3-TiO_2-SiO_2-C-H_2-O_2. *Journal of Metamorphic Geology*, **8**, 89-124.

Hollister, L.S. and Crawford, M.L. 1986. Melt-enhanced deformation: A major tectonic process. *Geology*, **14**, 558-561.

Hollister, L.S. 1988. On the origin of CO_2-rich fluid inclusions in migmatites. *Journal of Metamorphic Geology*, **6**, 467-474.

Höltta, P. 1986. Observations on the metamorphic reactions and PT conditions in the Turku Granulite area. *Geological Survey of Finland Bulletin,* **339,** 43-58.

Höltta, P. 1997. Geochemical characteristics of granulite facies rocks in the Archean Varpaisjärvi area, central Fennoscandian Shield. *Lithos*, **40**, 31-53.

Holtz, F. and Johannes, W. 1994. Maximum and minimum water contents of granitic melts: implications for chemical and physical properties of ascending magmas. *Lithos*, **32**, 149-159.

Houseman, G.A. and McKenzie, D.P. 1981. Convective instability of a thickening boundary layer and its relevance for the thermal evolution of continental convergent belts. *Journal of Geophysical Research*, **86**, 6115-6132.

Huhma, H. 1986. Sm-Mn, U-Pb and Pb-Pb isotopic evidence for the origin of the Early Proterozoic Svecokarelian crust in Finland. *Geological Survey of Finland Bulletin,* **337.**

Ibarguchi, J.I.G. and Martinez, F.J. 1982. Petrology of Garnet - Cordierite - Sillimanite Gneisses from the El Tormes Thermal Dome, Iberian Hercynian Foldbelt (W Spain). *Contributions to Mineralogy and Petrology*, **80**, 14-24.

Indares, A. and Martignole, J. 1985. Biotite-garnet geothermometry in the granulite: the influence of Ti and Al in biotite. *American Mineralogist,* **70**, 272-278.

Indares, A. 1997. Garnet-kyanite clinopyroxenites and garnet-kyanite restites from the Manicouagan Imbricate zone: A case of high-P - High-t metamorphism in the Grenville Province. *The Canadian Mineralogist*, **35**, 1161-1171.

Inger, S. and Harris, N.B.W. (1993) Geochemical constraints on leucogranite magmatism in the Langtang Valley, Nepal Himalaya. *Journal of Petrology,* **34,** 345-368.

Johannes, W. 1988. What controls partial melting in migmatites? *Journal of Metamorphic Geology*, **6**, 451-465.

Johannes, W. and Gupta, L.N. 1982. Origin and evolution of a migmatite. *Contributions to Mineralogy and Petrology,* **79,** 114-123.

Johannes, W. and Holtz, F. 1996. *Petrogenesis and experimental petrology of granitic rocks.* Mineral and Rocks 22, Springer Verlag, Berlin.

Johannes, W. and Schreyer, W. 1981. Experimental introduction of CO_2 and H_2O into Mg-cordierite. *American Journal of Science,* **281,** 299-317.

Kalt, A., Berger, A. and Blümel, P. 1999. Metamorphic evolution of cordierite bearing migmatites from the Bayerische Wald (Variscan Belt, Germany). *Journal of Petrology*, **40**, 601-627.

Kilpeläinen, T. and Korikovsky, S., Korsman, K. and Nironen, M. 1994. Tectono-metamorphic evolution in the Tampere-Vammala area. *Geological Survey of Finland Guide,* **37**, 27-34.

Koistinen, T., Klein, V., Koppelmaa, H., Korsman, H., Lahtinen, R., Nironen, M., Puura, V., Saltykova, T., Tikhomirov, S. and Yanovsky, A. 1996. Paleoproterozoic Svecofennian Orogenic Belt in the surroundings of the Gulf of Finland. *Geological Survey of Finland Special Paper*, **21**, 21-57.

Korja, A. 1995. *Structure of the Svecofennian Crust - growth and destruction of the Svecofennian Orogen.* Academic Dissertation, Report s31, Institute of Seismology, University of Helsinki, Helsinki.

Korja, A., Korja, T., Luosto, U. and Heikkinen, P. 1993. Seismic and geoelectric evidence for collisional and extensional events in the Fennoscandian Shield - implications for Precambrian crustal evolution. *Tectonophysics,* **219,** 129-152.

Korja, T., Luosto, U., Korsman, K. and Pajunen, M. 1994. Geophysical and metamorphic features of Palaeoproterozoic Svecofennian orogeny and Palaeoproterozoic overprinting on Archean Crust. *Geological Survey of Finland Guide,* **37**, 11-20.

Korja, A. and Heikkinen, P. J. 1995. Proterozoic extensional tectonics of the central Fennoscandian Shield: Results from the Baltic and Bothnian Echoes from the lithosphere experiment. *Tectonics,* **14**, 504-517.

Korsman, K., Höltta, P., Hautal, T. and Wasenius, P. 1984. Metamorphism as an indicator of evolution and structure of the crust in Eastern Finland. *Geological Survey of Finland Guide*, **37**, 11-20.

Kraus, J. and Menard, T. 1997. A thermal gradient at constant pressure: implications for low- to medium-pressure metamorphism in a compressional tectonic setting, Flin Flon and Kisseynew domains, Trans-Hudson Orogen, Central Canada. *The Canadian Mineralogist*, **35**, 1117-1136.

Laajoki, K. 1986. The Precambrian supracrustal rocks of Finland and their tectono-exogenic evolution. *Precambrian Research*, **33**, 67-85.

Lahtinen, R. and Huhma, H. 1997. Isotopic and geochemical constraints on the evolution of the 1.93-1.79 Ga Svecofennian crust and mantle in Finland. *Precambrian Research*, **82**, 13-34.

Laitakari, I. 1969. On the set of olivine diabase dykes in Häme, Finland. *Geological Survey of Finland Bulletin,* **241,** 65p.

Lamb, W.M. 1990. Fluid inclusions in granulites: peak vs. retrograde metamorphism. In: Vielzeuf, D. and Vidal, Ph. (eds) *Granulites and Crustal Evolution.* Kluwer, Dordrecht, pp. 419-434.

Lamb, W.M., Valley, J.W. and Brown, P.E. 1987. Post-metamorphic CO_2-rich fluid inclusions in granulites. *Contributions to Mineralogy and Petrology*, **96**, 485-495.

Le Breton, N. and Thompson, A.B. 1988. Fluid-absent (dehydration) melting of biotite in metapelites in the early stages of crustal anatexis. *Contributions to Mineralogy and Petrology*, **99**, 226-237.

Lindroos, A., Romer, R.L., Ehlers, C. and Alviola, R. 1996. Late-orogenic Svecofennian deformation in SW Finland constrained by pegmatite emplacement ages. *Terra Research*, **8**, 576-574.

Loosveld, R.J.H. and Etheridge, M.A. 1990. A model for low-pressure facies metamorphism during crustal thickening. *Journal of Metamorphic Geology*, **8**, 257-267.

Markl, G. and Bucher, K. 1999. Composition of fluids in the lower crust inferred from metamorphic salt in lower crustal rocks. *Nature*, **391**, 781-783.

Mathavan, V. 1991. The origin of Myrmekites in the Granitic Rocks of Ambaspitya, Sri Lanka. *Journal of the Geological Society of India*, **38**, no3, 319-325.

McDonough, W.F. and Sun, S-s. 1995. The composition of the Earth. *Chemical Geology,* **120,** 223-253.

McLellan, E.L. 1983. Problems of structural analyses in migmatite terrains. In: Atherton, M.P. and Gribble, C.D. (eds) *Migmatites, melting and metamorphism.* Proceedings of the Geochemical Group of the Mineralogical Society, Shiva Publishing, Nantwich, pp. 299-303.

Mirwald, P.W., Maresch, W.V. and Schreyer, W. 1979. Der wassergehalt von Mg-cordierit zwischen 500°C and 800°C sowie 0.5 und 11 kbar. *Fortschritte Mineralogie,* **57,** 101-102.

Mukhopadhyay, B. and Holdaway, M. 1994. Cordierite-garnet-sillimanite-quartz equilibrium: New experimental calibration in the system $FeO-Al_2O_3-SiO_2-H_2O$ and certainP-T-XH_2O relations. *Contributions to Mineralogy and Petrology*, **116**, 462-472.

Newton, R.C. and Haselton, H.T. 1981. Thermodynamics of the garnet–plagioclase–Al_2SiO_5–quartz geobarometer. In: Newton, R.C., Navrotsky, A. and Wood, B.J. (eds) *Thermodynamics of minerals and melts.* Advances in Physical Geochemistry 1, Springer, Berlin, pp. 131-148.

Newton, R.C., Smith, J.V. and Windley, B.F. 1980. Carbonic metamorphism, granulites and crustal growth. *Nature,* **288,** 45-50.

Newton, R.C. and Wood, B.J. 1979. Thermodynamics of water in cordierite and some petrologic consequences of cordierite as a hydrous phase. *Contributions to Mineralogy and Petrology*, **68**, 391-405.

Nironen, M. 1997. The Svecofennian Orogen: a tectonic model. *Precambrian Research*, **86**, 21-44.

Oliver, R.L., Lawrence, R.W., Goscombe, B.D., Ding, P., Sivell, W.J. and Bowyer, D.G. 1988. Metamorphism and crustal considerations in the Harts Range and neighbouring regions, Arunta Inlier, Central Australia. *Precambrian Research*, **40-1**, 277-295.

Osanai, Y. and Kagami, H. 1998. Sapphirine-bearing granulites and related high-temperature metamorphic rocks from the Higo metamorphic terrane, west-central Kyushu, Japan. *Journal of Metamorphic Geology*, **16**, 53-66.

Pajunen, M. (ed) 1994. *High temperature-low pressure metamorphism and deep crustal structure. . Geological Survey of Finland Guide*, **37,** 7-10.

Park, A.F. 1991. Continental growth by accretion: A tectonostratigraphic terrane analysis of the evolution of the western and central Baltic Shield, 2.50 to 1,75 Ga. *Bulletin of the Geological Society of America*, **103**, 522-537.

Patchett, J. and Kuovo, O. 1986. Origin of continental crust of 1.9-1.7 Ga age: Nd isotopes and U-Pb zircon ages in the Svecokarelian terrain of South Finland. *Contributions to Mineralogy and Petrology*, **92**, 1-12.

Patiño Douce, A.E. and Johnston, A.D. 1991. Phase equilibria and melt productivity in the pelitic system: implications for the origin of peraluminous granitoids and aluminous granulites. *Contributions to Mineralogy and Petrology*, **107**, 202-218.

Patiño Douce, A.E. 1996. Effects of pressure and H_2O content on the compositions of primary crustal. *Transactions of the Royal Society of Edinburgh: Earth Sciences,* **87**, 11-21.

Pearce, J.A., Harris, N.B.W. and Tindle, A.G. 1984. Trace element discrimination diagrams for the tectonic interpretation of granitic rocks. *Journal of Petrology*, **25**, 956-983.

Perchuk, L.L. and Aranovich, L.Y. 1986. Improvement of the biotite-garnet geothermometer: correction for the Fe content of biotite. *Doklady Akademi Nauk SSSR*, **277**, no2, 471-475.

Perchuk, L.L. and Lavrent'eva, I.V. 1983. Experimental investigation of exchange equilibria in the system cordierite-garnet-biotite. In: Saxena, S.K. (ed) *Kinetics and Equilibrium in Mineral Reactions.* Advances in Physical Geochemistry 3, Springer, Berlin, pp. 199-239.

Philips, E.R. 1974. Myrmekite – one hundred years later. *Lithos,* **7,** 181-194.

Phillips, G.N. 1980. Water activity changes across an amphibolite-granulite facies transition, Broken Hill, Australia. *Contributions to Mineralogy and Petrology*, **75**, 377-386.

Powell, R. 1978. *Equilibrium Thermodynamics in Petrology an Introduction.* Harper and Row, London.

Powell, R. 1982. Processes in granulite-facies metamorphism. In: Atherton, M.P. and Gribble, C.D. (eds) *Migmatites, melting and metamorphism*. Proceedings of the Geochemical Group of the Mineralogical Society, Shiva Publishing, Nantwich, pp.127-142.

Powell, R. and Downes, J. 1990. Garnet porphyroblast-bearing leucosomes in metapelites: mechanisms, phase diagrams, and an example from Broken Hill, Australia. In: Ashworth, J.R. and Brown, M. (eds) *High-temperature Metamorphism and Crustal Anatexis*. Mineralogical Society Series 2, Unwyn Hyman, London, pp. 105-123.

Powell, R. and Holland, T.J.B. 1988. An internally consistent dataset with uncertainties and correlations: 3. Applications to geobarometry, worked examples and a computer program. *Journal of Metamorphic Geology*, **6**, 173-204.

Powell, R. and Holland, T. 1993. The applicability of least squares in the extraction of thermodynamic data from experimentally bracketed mineral equilibria. *American Mineralogist,* **78,** 107-112.

Powell, R. and Holland, T. 1994. Optimal geothermometry and geobarometry. *American Mineralogist,* **79,** 120-133.

Raith, M., Karmakar, S. and Brown, M. 1997. Ultra-high-temperature metamorphism and multistage decompressional evolution of sapphirine granulites from the Palni Hill Ranges, southern India. *Journal of Metamorphic Geology,* **15,** 379-399.

Raith, J.G. and Harley, S.L. 1998. Low-P/high-T metamorphism in Okiep Copper District, western Namaqualand. South Africa. *Journal of Metamorphic Geology*, **16**, 281-305.

Reimer, T.O. 1984. Graphite in Pre-Cambrian rocks of Southern Africa: implications on the carbon content of metamorphic rocks. *Precambrian Research*, **26**, 223-234.

Ring, U., Kröner, A. and Toulkerdis, T. 1997. Paleoproterozoic granulite-facies metamorphism and granitoid intrusions in the Ubendian-Usagaran Orogen of northern Malawi, east-central Africa. *Precambrian Research*, **85**, 27-31.

Sandiford, M. and Hand, M. 1998. Controls on the locus of intraplate deformation in central Australia. *Earth and Planetary Science Letters*. **162**, 97-110.

Sandiford, M. and Powell, R. 1986. Deep crustal metamorphism during continental extension: modern and ancient examples. *Earth and Planetary Science Letters*. **79**, 151-158.

Sandiford, M. and Powell, R. 1991. Some remarks on high-temperature - low-pressure metamorphism in convergent orogens. *Journal of Metamorphic Geology*, **9**, 333-340.

Santosh, M., Jackson, D.H. and Harris, N.B.W. 1993. The significance of channel and fluid-inclusion CO_2 in cordierite: evidence from carbon isotopes. *Journal of Petrology*, **34**, 233-258.

Sawyer, E.W. 1996. Melt segregation and magma flow in migmatites: implications for the generation of granite magmas. *Transactions of the Royal Society of Edinburgh: Earth Sciences,* **87**, *85-94.*

Schreurs, J. 1985. Prograde metamorphism of metapelites, garnet-biotite thermometry and prograde changes of biotite chemistry in high-grade rocks of West Uusimaa, southwest Finland. *Lithos*, **19**, 69-80.

Schreyer, W. 1985. Experimental studies on cation substitutions and fluid incorporation in cordierite. Bulletin de Mineralogie, **108,** 273-291.

Schumacher, R., Schenk, V., Raase, P. and Vitanage, P.W. 1990. Granulite facies metamorphism of metabasic and intermediate rocks in the Highland Series of Sri Lanka. In: Ashworth, J.R. and Brown, M. (eds) *High-temperature Metamorphism and Crustal Anatexis.* Mineralogical Society Series 2, Unwin Hyman, London, pp. 235-271.

Selverstone, J. and Chamberlain, C.P. 1990. Apparent isobaric cooling paths from granulites: Two counterexamples from British Columbia and New Hampshire. *Geology*, **18**, 307-310.

Seyler, M., Paquette, J-L., Ceuleneer, G., Kienast, J-R. and Loubert, M. 1998. Magmatic underplating, metamorphic evolution and ductile shearing in a Mesozoic lower crustal-upper mantle unit (Tinaquillo, Venezuala) of the Caribbean Belt. *The Journal of Geology*, **106**, 35-58.

Shmulovich, K.I. and Graham, C.M. 1996. Melting of albite and dehydration of brucite in H2O-NaCl fluids to 9 kbar and 700-900°C: implications for partial melting and water activities during high pressure metamorphism. *Contributions to Mineralogy and Petrology*, **124**, 370-382.

Shmulovich, K.I. and Graham, C.M. 1999. An experimental study of phase equilibria in the system H_2O-CO_2-NaCl at 800°C and 9 kbar. *Contributions to Mineralogy and Petrology*, **136**, 247-257.

Smith, J.V. 1974. *Feldspar minerals 2: Chemical and Textural Properties.* Springer-Verlag, Berlin.

Smith, J.V. and Brown, W.L. 1988. *Feldspar Minerals 1: Crystal Structures, Physical, Chemical, and Microtextural Properties,* Springer-Verlag, Berlin.

Spear, F.S. 1993. *Metamorphic Phase Equilibria and Pressure-Temperature-Time paths.* Monograph Series, Mineralogical Society of America, Washington D.C.

Stel, H., Cloetingh, S., Heeremans, M. and van der Beek, P. 1993. Anorogenic granites, magmatic underplating and the origin of intracratonic basins in a non-extensional setting. *Tectonophysics*, **226**, 285-299.

Stevens, G., Clemens, J.D. 1993. Fluid-absent melting and the roles of fluids in the lithosphere: a slanted summary? *Chemical Geology,* **108**, 1-17.

Stevens, G., Clemens, J.D. and Droop, G.T.R. 1995. Hydrous cordierite in granulites and crustal magma production. *Geology*, **23,** 9325-9328.

Stüwe, K. and Powell, R. 1989. Metamorphic evolution of the Bunger Hills, East Antarctica: evidence for substantial post-metamorphic peak compression with minimal cooling in a Proterozoic orogenic event. *Journal of Metamorphic Geology*, **7**, 449-464.

Suominen, V. 1991. The chronostratigraphy of south-western Finland with special reference to Postjotnian and Subjotnian diabases. *Geological Survey of Finland Bulletin,* **356.**

Thompson, A.B. 1976. Mineral reactions in pelitic rocks: II Calculations of some P-T-X (Fe-Mg) phase relations. *American Journal of Science*, **276**, 425-454.

Thompson, B.T. 1982. Dehydration melting of pelitic rocks and the generation of H_2O-undersaturated granitic liquids. *American Journal of Science*, **282**, 1567-1595.

Thompson, A.B. 1996. Fertility of crustal rocks during anatexis. *Transactions of the Royal Society of Edinburgh: Earth Sciences*, **87**, 1-10.

Touret, J.R.L. 1985. Fluid regime in southern Norway: the record of fluid inclusions. In: Tobi, A.C. and Touret, J.R.L (eds). *The Deep Proterozoic Crust in the North Atlantic provinces*, Reidel, Dordrecht, 517-549.

Treloar, P.J. and Kramers, J.D. 1989. Metamorphism and geochronology of the granulite and migmatitic granulites from the Magondi Mobile Belt, Zimbabwe. *Precambrian Research*, **45**, 277-289.

Vaasjoki, M., Huhma, H. and Karhu, J. 1994. Evolution of the continental crust in Finland with special reference to the Svecokarelian orogeny. *Geological Survey of Finland Guide*, **37**, 21-26.

Väisänen, M. and Höltta, P. (in press) Structural and metamorphic evolution of the Turku Migmatite Complex, south-western Finland. *Bulletin of the Geological Society of Finland.*

Väisänen, M., Höltta, P., Rastas, J., Korja, A. and Heikkinen, P. 1994. Deformation, metamorphism, and the deep structure of the crust in the Turku area, Southwestern Finland. *Geological Survey of Finland Guide*, **37**, 35-41.

Van Duin, J.A. and Nieman, P. 1993. Pressure and temperature history of a low-pressure transitional granulite area, Turku, SW Finland. *Geologie en Mijnbouw*, **71**, 259-280.

Vernon, R.H. 1991. Questions about myrmekite in deformed rocks. *Journal of Structural Geology*, **13**, no9, 979-985.

Vielzeuf, D. and Holloway, J.R. 1988. Experimental determination of the fluid-absent melting relations in the pelitic system. Consequences for crustal differentiation. *Contributions to Mineralogy and Petrology*, **98**, 257-276.

Vry, J., Brown, P.E., Valley, J.W. and Morrison, J. 1988. Constraints on granulite genesis from carbon isotope compositions of cordierite and graphite. *Nature*, **332**, 66-68.

Vry, J., Brown, E.B. and Valley, J.W. 1990. Cordierite volatile content and the role of CO_2 in high-grade metamorphism. *American Mineralogist*, **75**, 71-88.

Warren, R.G. 1983. Metamorphic and tectonic evolution of granulites, Arunta Block, central, Australia. *Nature*, **305**, 300-303.

Warren, R.G. and Ellis, D.J. 1996. Mantle underplating, granite tectonics, and metamorphic P-T-t paths. *Geology*, **24**, no 7, 663-666.

Waters, D.J. 1988. Partial melting and the formation of granulite facies assemblages in Namaqualand, South Africa. *Journal of Metamorphic Geology*, **6**, 387-404.

Waters, D.J. 1994. Textural studies of migmatitic granulites: solid-melt reactions and the role of fluids. *Goldschmidt Conference Abstract Volume, Mineralogical Magazine,* **58A,** 957-958.

Waters, D.J. and Whales, C.J. 1984. Dehydration melting and the granulite transition in metapelites from southern Namaqualand, S. Africa. *Contributions to Mineralogy and Petrology*, **88**, 269-275.

Watson, E.B. 1996. Dissolution, growth and survival of zircons during crustal fusion: kinetic principles, geological models and implications for isotopic inheritance. *Transactions of the Royal Society of Edinburgh: Earth Sciences,* **87,** 43-56.

Watt, G.R. 1993. *A geochemical study of processes in granulite facies migmatites from Prydz Bay, eastern Antarctica.* PhD Thesis, University of Edinburgh, Edinburgh.

Watt, G.R. and Harley, S.L. 1993. Accessory phase controls on the geochemistry of crustal melts and restites produced during water-undersaturated partial melting. *Contributions to Mineralogy and Petrology*, **114**, 550-566.

White, A.J.R. and Chappell, B.W. 1977. Ultrametamorphism and granitoid genesis. *Tectonophysics,* **43,** 7-23.

Williams, M.L. and Karltstrom, K.E. 1996. Looping *P-T* paths and high-T, low-P middle crustal metamorphism: Proterozoic evolution of the south-western United States. *Geology*, **24**, 1119-1122.

Windley, B.F. 1991. Phanerozoic granulites. *Journal of the Geological Society of London*, **138**, 745-751.

Yardley, B.W.D. 1989. *An Introduction to Metamorphic Petrology.* Longman Scientific and Technical, Harlow.

Appendices

Appendices 1 - 8

Appendix 1 - Localities

Table A1.1 - Location and description of outcrops studied.

Locality	Description	Grid reference
Locality 1	Riviera - smooth, flat outcrops. Southern locality.	6715.27/1562.76
Locality 2	Rusko gravel pits - smooth, rounded outcrops. Southern locality.	6712.56/1567.53
Locality 3	Hauninen reservoir - smooth, rounded outcrops. Southern locality.	6710.74/1565.87
Locality 4	Sojerma road cutting, 20 m by 100 m. Southern locality.	6712.82/1563.00
Locality 5	Small road cutting, 2 km south of the Häähä road. Northern locality.	6737.90/1535.87
Locality 6	Large quarry near to Mynamaki. Middle locality.	6727.24/1555.34
Locality 7	Raukka road cutting, smooth rounded outcrop. Middle locality.	1552.56/6726.06
Locality 8	Small road cutting between Nousianen and Mietoinen. Middle locality.	1551.28/6723.79
Locality 9	High road cutting between Mietoinen and Mynamaki. Middle locality.	6724.40/1551.45
Locality 10	Pauläteenpolku, small roadcutting. Middle locality.	6737.54/1537.98
Locality 11	Small roadcutting on the road from Välitä to Vehmaa. Northern locality.	6735.90/1539.76
Locality 12	Small road cutting at the east end of the Häähä road. Northern locality.	6739.40/1536.98
Locality 13	Small road cutting west from locality 12. Northern locality.	6738.96/1535.78
Locality 14	Small road cutting west from locality 13. Northern locality.	6738.98/1535.13
Locality 15	Big Häähä lake, smooth, flat outcrop. Northern locality.	6739.20/1534.46
Locality 16	Small roadcutting, fifth stop along the Häähä road. Northern locality.	6739.56/1533.84
Locality 17	Large quarry near Paavalinkallio. Northern locality.	6733.10/1540.25
Locality 18	Small road cutting, sixth stop along the Häähä road. Northern locality.	6739.87/1535.25
Locality 19	Smooth, flat Vellua road cutting, east end of Häähä road. Northern locality.	6740/05/1532.75
Locality 20	Smooth flat outcrops along the Goose valley road transect. Northern locality.	6737.15/1531.90
Locality 21	Transect along the E18. No data from here is used in this study.	Unknown
Locality 22	Small outcrop on the 12375 to Heikla. Northern locality.	6732.90/1541.51
Locality 23	Flat outcrop 2 km south of the Häähä road, Rapakivi contact. Northern locality.	6738.87/1535.90
Locality 24	Flat outcrop near the Koivisto turn off on the M8. Southern locality.	6710.22/1564.28

Appendix 2 – Extra locality descriptions

A2.1 - Introduction

Key localities were included in the main body of the chapter, this appendix will describe other localities which have helped to build up the fieldwork results and conclusions.

A.2.2 - Locality 8: Outcrop on Nousianen - Mietoinen road

Feature	Description
Structure	Strong S2 fabric, axial planar to isoclinal F2 folds. S2 crenulated by F3.
Mesosome description	Coarse and homogeneous especially around leucosomes. Garnets are elongate along S2
Leucosomes Lc1	1 cm wide folded leucosomes with axial traces parallel to F3 folds.
Lc2	1. 1 cm wide and 50 cm long leucosomes that are rich in pink K-feldspar and contain rounded garnets which have often grown on the edge of a leucosome. 2. Cream in colour and up to 30 cm thick. These leucosomes contain both garnet and cordierite with the cordierite forming in patches with interstitial quartz.
Lc3	Large, patchy leucosomes that cut across S2.
Lc5	K-feldspar rich pegmatite that cuts diagonally across all foliations.

A2.3 - Locality 9: Road cutting on Mynamaki/Mietoinen road

Feature	Description
Structure	The strongest fabric here is S2, slightly deformed by F3. In some areas there are F2 isoclinal folds. The mesosome has a homogeneous appearance which is typical of outcrops in this band of high grade rocks.
Leucosomes Lc2	5-6 cm by 1-2 m roughly concordant to S2 and elongate whilst larger leucosomes are more patchy.
Lc5	Metres wide granitic sheet that is pink and K-feldspar-rich. Cordierite is in patches with interstitial quartz.

Another feature at this locality is a boudined quartz rich leucosome. It is 90% quartz, with interstitial pink K-feldspar. Rounded garnet crystals are also present.

A2.4 - Locality 10: Päulateenpölku

Feature	Description
Structure	S2 is axial parallel to F2 fold axes which has been refolded by gentle F3 folds. Garnet is sparse and neither cordierite nor garnet are seen elongate along S2.
Leucosomes Lc1	One face of the outcrop is perpendicular to S2 and one is parallel, therefore the leucosomes are seen as either elongate or patchy, but are parallel to S2. Leucosomes are cordierite-rich, in some places: the cordierite is present in elongate patches.

A2.5 - Locality 11: Road cutting on the Välilä - Vehmaa road

Feature	Description
Structure	S2 is strong and axial planar to S2 folds. There has been some crenualtion by F3.
Leucosomes Lc1	1-5 cm by 40-100 cm elongate leucosomes that are layer parallel to S2. Some are folded into F3 folds. They are often boudined along S2 and bound by 2 mm selvages.
Lc2	As type 2 but wider and slightly discordant to S2.
Lc3	Metres wide granitic sheet with coarse grain size, K-feldspar tablets. Cordierite is common and found in patches with interstitial quartz. Garnet is rare and where found has a halo of garnet. This sheet has offshoots of thinner leucosomes which can be distinguished from type 1 and 2 leucosomes by colour, grain size and cross-cutting nature.

A2.6 - Locality 13: Locality on Häähä road

This road cutting is about 1.2 km along the road from locality 12.

Feature	Description
Structure	S2 is slightly deformed by F3 folds. The outcrop lies parallel to the main foliation. This gives an impression of a greater percentage of leucosome than is actually present.
Mesosome description	The mesosome is quite coarse and homogeneous, it is dark and bioite rich. No large garnet porphyroblasts.
Leucosomes Lc1	Thin smears, parallel to S2 that are cream in colour.
Lc5	Pink pegmatitic leucosome, with large K-feldspar tablets that cut across all the foliation.

A2.7 - Locality 14: Midway along Häähä road

Feature	Description
Structure	The outcrop is dominated by a large F2 fold, which folds the compositional banding. S2 is axial planar to F2 and has been refolded by a series of smaller F3 folds with their axial trace NE/SW.
Leucosomes Lc2	Elongate, roughly concordant to S2
Lc3	Patchy, cut across S2, associated with poikiloblastic garnets.

A2.8 - Locality 16: Eastern Häähä outcrop

Feature	Description
Structure	S2 gently refolded by F3.
Mesosome description	The mesosome is compositionally banded, garnet is rare and only found in leucosomes. The biotite-rich pelitic layers also contain fibrous sillimanite.
Leucosomes Lc1	There is a low percentage of leucosome, <20%. Most leucosomes are present as small patches that are concordant to S2.

A2.9 - Locality 17: Quarry on the Rhalmala road

Feature	Description
Structure	F3 folds have deformed S2.
Leucosomes Lc2	3-4 mm to 3-4 cm by 2-3 cm to 25 cm leucosomes that are slightly oblique to S2, with some patchy types.
Lc5	1. Large granitic sheet covering approximately 60% of the quarry that is bound by a coarse pegmatite with biotites 20 cm long. 2. Pink elongate leucosomes that cross-cut all foliations and so are probably offshoots of type 5 leucosome. They have muscovite at their edges.

There is also an elongate (30 cm by 6 m) intrusive feature with a sharp contact that may be even later than the type 5 sheets. Dents de cheval leucosomes are also present and are strung out along S2 like the beads of a necklace.

A2.10 - Locality 18: West end of the Häähä road

Feature	Description
Mesosome description	The mesosome is coarse grained and shows little orientation of grains. On a weathered surface it can be seen to be orientated in a NW/SE direction, S2.
Leucosomes Lc2	The amount of leucosome material at this outcrop is low, the leucosomes are small and there is little inter-communication between leucosomes. They are generally cream in colour, and some are rich in garnet and cordierite. These melts are seen to be oblique to S2.
Lc5	20 metres to the west is a large pegmatite consisting of orange K-feldspar, quartz and biotite. The K-feldspar tablets reach up to 3-5 cm in length. This cuts vertically up through the outcrop, across all foliations.

A2.11 - Locality 22: Outcrop on the 12375 to Heikola

Feature	Description
Structure	S2 dips into the outcrop, to the SE. This has been crenulated by F3 axial traces although F3 is weak at this outcrop.
Mesosome description	The mesosome is very dark and homogeneous. Garnet is rare but may be present as some pale pink flecks.
Leucosomes Lc1	Elongate along S2, 2-6 cm by 30-40 cm with sharp contacts with the mesosome.
Lc2	Larger, 10-20 cm by 2-3 m leucosome which contains rafts of mesosome material and patches of cordierite with biotite and quartz. It is oblique to S2 and it forms a large patch in the centre of the outcrop.

A2.12 - Locality 24: Outcrop on the M8, near Koivisto

Work on this outcrop (Höltta, *pers. comm.*) has yielded a metamorphic grade similar to those in the north of the area. However this outcrop does not contain sillimanite.

Feature	Description
Structure	The mesosome is compositionally banded and the layers are picking out gentle to tight folds. These fold S2 but it is not possible to see if this fabric is axial planar to any isoclinal F2 folds.
Mesosome description	In the case of both maps the mesosome has pelite layers that are rich in biotite with elongate garnets present along S2. The psammite layers show no orientation of grains and the garnets are small and rounded.
Leucosomes Lc1	White elongate leucosomes aligned along S2, folded by F3, approximately 2-3 cm by 3-4 m
Lc2	Patchy leucosomes associated with poikiloblastic garnets.
Lc3	1. Similar to Lc1 in dimensions but not orientation. Most are roughly NNE/SSW to NE/SW, parallel to F3 axial traces. Some are perpendicular to the strain that is causing psammite layers to boudin. 2. A pegmatitic white leucosome that follows the limb of the F3 fold.

Appendix 3 - Sample descriptions

Table A3.1 - Sample descriptions.

Samples	Locality	Description
1	3	Mostly mesosome sample with a small garnet dominated leucosome patch.
2	3	Patchy, thin leucosome with mesosome.
3	3	Thin, slightly discordant, garnet-rich leucosomes and mesosome.
4	3	Pale leucosome with pokiloblastic garnets and interlayered mesosome.
5	3	Very thin leucosomes and mesosome layers with poikiloblastic garnet.
6	4	Dark foliated mesosome and coarse leucosome layers with large K-feldspar crystals.
7	4	Very thin leucosome segregations and mesosome with elongate garnets.
8	4	Dark mesosome sample with large garnets.
10	4	Melanosome and coarse leucosome with large K-feldspar tablets.
11	4	Large cross cutting leucosome with a high garnet content.
12	4	Mostly fine grained mesosome material, and leucosome layers with large garnets.
13	4	Coarse gained melanosome and intimately layered leucosomes.
14	4	Strongly foliated mesosome with garnet-rich leucosome layer.
15	4	Coarse biotite-rich mesosome and coarse leucosome.
16	6	Coarse leucosme with biotite-rich patches.
17	6	Coarse leucosome with cordierite patches and cordierite-rich mesosome.
18	12	Fine grained mesosome with small leucocratic foliae.
19	12	Fine grained mesosome with patchy, cordierite-rich leucosome.
20	12	Coarse grained leucosome consisting mostly of white K-feldspar.
21	19	White K-feldspar-rich, coarse grained leucosome with cordierite-rich patches.
22	19	Almost entirely made of foliated, sillimanite-rich mesosome with small, thin leucosomes.
23	19	As above but without the leucosome material.
24	19	Coarser mesosome material with elongate prisms.
25	15	Coarse grained mesosome and patchy garnets.
27	20	Coarse grained mesosome.
28	20	Fine grained mesosome with tiny garnet flecks.
29	20	Strongly deformed mesosome sample with boudined leucosome layers.
30	20	Fine grained leucosome and mesosome layers.
31	20	Strongly deformed sillimanite-rich mesosome and deformed leucosome layers.
32	20	Foliated mesosome with fine grained quartz-rich leucosome.
33	20	Fine grained small leucosomes with pale mesosome.
34	7	Dark biotite and garnet-rich mesosome layered with pale garnet-rich leucosomes.
35	7	As above.
36	7	Very dark mesosome with thin leucosome veins.
78	2.3	Elongate cordierites that are parallel to an F3 axial trace.
79	2.3	Pink boudined wide leucosome with rounded garnets and the neighbouring mesosome.

80	**2.3**	Pink boudined wide leucosome with rounded garnets.
81	**2.2**	Poikiloblastic garnet and cordierite-rich leucosome.
82	**2.1**	Pelitic mesosome band with elongate cordierite ellipses.
83	**2.1**	Large D3, poikiloblastic garnet.
88	**3**	Elongate D2 garnets, gently folded by F3.
89	**3**	F2 fold hinge within psammitic mesosome.
90	**3**	F2 fold hinge within psammitic mesosome.
94	**4**	Leucosome and mesosome sample, pale pink thin leucosomes apparently folded by F3.
95	**4**	Patchy garnetiferous leucosome sample.
96	**4**	Sample of the mafic dyke.
97	**4**	Mesosome and leucosome sample, wide cordierite-rich leucosome.
98a	**4**	Smaller, finer grained leucosome.
98b	**4**	Smaller, finer grained leucosome.
99	**4**	Large, patchy leucosome with large K-feldspar crystals.
100	**4**	Large pale pink, coarse leucosome that runs vertically through the outcrop.
101	**4**	Smaller pale pink, cordierite-rich leucosome.
102	**5**	Mesosome sample containing a 2 cm wide leucosome with a 5 mm thick selvage.
103	**5**	As above but the sample contains more leucosome material that is very rich in cordierite.
104	**5**	As above.
105	**6**	Pale pegmatitic leucosome in the north of the quarry.
106	**6**	Pale pink patchy leucosome near to a large quartz-rich vein.
107	**6**	Dark pink K-feldspar-rich leucosome up to 2 metres in length.
108	**6**	Pale cream leucosome, intimate to the mesosome material.
109	**6**	Pale cream leucosome, intimate to the mesosome material.
110	**6**	Orange/pink leucosome.
111	**6**	Wide orange granitic sheet from the south of the quarry.
112	**6**	Leucosome and mesosome, coarse grained cream leucosome.
113	**6**	Smaller, finer cream leucosome.
114	**6**	Leucosome and mesosome, a pale pink/orange in colour.
115	**6**	Thick, white leucosomes, metres in length.
116	**6**	White, small, elongate leucosome.
117	**6**	Generally concordant, coarse grained white leucosome.
118	**6**	Mesosome sample taken for the high garnet content.
119	**7**	Small thin leucosomes in a large leucosome sample.
120	**7**	Edge of a large leucosome containing big garnets.
121	**8**	Large ponded pink leucosome.
122	**8**	Paler leucosome with a high cordierite content.
123	**8**	Mesosome sample.
124	**9**	Large metres wide leucosome containing garnet and cordierite with mesosome.
125	**9**	Thin, roughly concordant, cream leucosome.
126	**9**	Thin garnetiferous leucosome.

127	**9**	Quartz-rich leucosome.
128	**11**	Large, fat leucosome, pale pink with cordierite and quartz.
129	**11**	Pale pink, roughly concordant leucosome with mesosome.
130	**11**	Large sample composed of mostly of mesosome from locality 11.
131	**11**	Cream, elongate leucosome.
132	**9**	Possible calc silicate pod - grossular garnet.
133	**13**	Patchy, thin leucosome.
134	**13**	Mesosome sample from the left hand side of the road.
135	**13**	Mesosome sample from the right hand side of the road.
136	**16**	Patchy, small, pale leucosome.
137	**17**	Mesosome and small, elongate leucosome sample.
138	**17**	Mesosome and small, elongate leucosome sample.
139	**17**	Granitic dyke cutting across the foliation.
140	**17**	Granitic sheet.
141	**17**	Large disconcordant leucosome sample.
142	**18**	Mesosome and pegmatite sample.
143	**18**	Pegmatite sample.
144	**19**	Thin, white, elongate leucosome with mesosome.
145	**17**	Granite and mesosome contact with sillimanite trails.
146	**17**	Mesosome and small, elongate leucosomes.
147	**17**	Mesosome sample from the quarry.
148	**7**	Cordierite/graphite sample from a very thin leucosome.
149	**17**	Layered leucosome/mesosome sample.
150	**17**	Layered leucosome/mesosome sample.
151	**9**	Grossular-rich sample, possible calc-silicate pod.
152	**14**	Small, elongate leucosome with mesosome.
153	**14**	Mesosome sample.
154	**22**	Mesosome and small, elongate leucosome.
155	**22**	Larger, patchy leucosomes with cordierite.
173	**10**	Small thin leucosome and mesosome.
174	**10**	Part of larger leucosome and mesosome material.

Drill samples

D1	**2.4**	Sample from centre of pale pink large melt.
D2	**2.4**	Contact of granite with neighbouring pelite.
D3	**2.4**	Psammitic leucosome containing garnet.
D4	**2.4**	Psammitic leucosome containing cordierite.
D5	**2.4**	Selvage-rich leucosome.
D6	**2.4**	Core of calc silicate pod.
D7	**2.4**	Edge of calc silicate pod.
D8	**2.1**	Small 1 cm wide leucosome in metapelite.

D9	**2.1**	Core of 3-3 cm wide leucosome.
D10	**2.1**	Edge of leucosome containing garnet and cordierite.
D11	**2.2**	'Folded' leucosome with sharp edges from MA2.2.
D12	**2.2**	Edge of same leucosome with mesosome.
D13	**2.2**	Mesosome next to the same leucosome.
D14	**2.2i**	Edge of calc silicate pod, white area.
D15	**2.2i**	Next layer which is pale grey in colour.
D16	**2.2i**	Third greenish layer.
D17	**2.2i**	Core of pod that is pale pink.
D18	**2.2i**	Thin leucosome that is very garnetiferous.
D19	**2.2i**	Thin folded leucosome that is folded by F3.
D20	**2.3**	Axial planar mesosome cordierite.
D21	**2.3**	Garnet in leucosome that is next to mesosome cordierite.
D22	**2.3**	Slightly oblique leucosome and mesosome that both contain cordierite.
D23	**3**	Garnet within large leucosome from PC3.
D24	**3**	Mostly leucosome from the edge.
D25	**3**	Leucosome/mesosome from the same boundary as above.
D26	**3**	Mesosome near to large leucosome.
D27	**3**	Cordierite within mesosome.
D28	**3**	Small garnet-rich leucosome near D27.
D29	**8**	Cross cutting pegmatitic leucosome.
D30	**8**	Cross cutting leucosome and mesosome boundary.
D31	**8**	Small offshoot from x-cutting leucosome.
D32	**8**	Small concordant leucosome.
D33	**7**	Wide syn-F3 leucosome containing euhedral cordierite.
D34	**7**	Wide syn-F3 leucosome boundary with mesosome .
D35	**7**	Wide syn-F3 leucosome boundary with a garnet patch.
D36	**7**	Wide syn-F3 leucosome boundary with a cordierite patch.
D37	**7**	Small concordant leucosome that is 3-4 mm wide.
D38	**7**	Core of calc silicate pod.
D39	**7**	Next layer in of possible calc silicate pod..
D40	**7**	Outside rim of the possible calc silicate pod..
D41	**7**	Sillimanite-rich pod.
D42	**7**	Sillimanite-rich pod.
D43	**12**	Core of large poikiloblastic garnet from within a ponded leucosome.
D44	**12**	Edge of large garnet and leucosome.
D45	**12**	Small oblique leucosome.
D46	**12**	Folded leucosome in general concordant orientation.
D47	**12**	Folded leucosome boundary with biotite-rich selvage.

Appendix 4 - Electron microprobe analyses

A4.1 - Instrument

The compositions of the mineral phases used in Chapters 4, 6, 7 and 8 were all analysed by wavelength dispersive electron microprobe analysis. The data was collected on a Cameca CAMEBAX Microbeam microprobe within the Department of Geology and Geophysics, Edinburgh University.

A4.2 - Operating conditions

Electrons were emitted at an accelerating voltage of 20 keV with a beam current of 25 nA. The concentrations of oxides were calculated using the Cameca PAP correction programme.

Table A4.1- Conditions for electron probe WDS analysis. The four diffracting crystals used were TAP, PET and LiF, thallium acid phthalate, penaerythritol and lithium fluoride respectively.

Element	Crystal	Count times		Standard
		Peak	Background	
Na	TAP	30	15	jadeite
Si	TAP	30	15	wollastonite
K	PET	30	15	orthoclase
Fe	LiF	30	15	Fe metal
Mg	TAP	30	15	periclase
Al	TAP	30	15	corundum
Ca	PET	30	15	wollastonite
Mn	LiF	30	15	Mn metal
Cr	LiF	30	15	Cr metal
Ti	PET	30	15	rutile

A4.3 - Error and detection limit calculation

In order to monitor the stability of the instrument over time and also check the calibration of Si, Fe, Ca and Al, a well characterised andradite standard was analysed. An adequate analysis of accuracy is difficult to quantify and it dependent on a number of factors. Precision can be analysed from the counting statistics of an analysis following equation 1

$$\%error = \frac{100}{\sqrt{T((\sqrt{Rp}) - (\sqrt{Rb}))}} \quad (1)$$

where T = count time on the peak

Rp = counts per second on the peak

Rb = counts per second on the background

Representative samples are presented in Table A4.2 along with their errors in wt%. Detection limits can be calculated for each element to a 3σ confidence level following equation 2

$$\text{Detection limit} = 3\sqrt{\text{Tb}(\text{Rp} - \text{Rb})} \quad (2)$$

where Tb = count time on the background in seconds.

Table A4.2 - Example electron probe analyses of phases in wt% oxides, plus the errors and detection limit for each element, calculated from raw peak and background count rates per second following equations 1 and 2. Using the equation above an average of 5% error was determined.

Cordierite 123			***Biotite AV 123***	
	wt % oxides ± errors	**detection limits**	**wt % oxides ± errors**	**detection limits**
Na_2O	0.10 ± 0.005	0.00	0.12 ± 0.006	0.00
SiO_2	47.49 ± 2.374	0.12	33.97 ± 1.698	0.10
K_2O	0.01 ± 0.000	0.00	9.38 ± 0.469	0.05
FeO	8.64 ± 0.432	0.03	19.43 ± 0.971	0.04
Al_2O_3	32.26 ± 1.613	0.11	17.21 ± 0.961	0.07
CaO	0.02 ± 0.001	0.00	0.00 ± 0.000	0.00
MnO	0.05 ± 0.002	0.00	0.02 ± 0.001	0.00
MgO	8.15 ± 0.407	0.05	9.57 ± 00.478	0.05
TiO_2	0.02 ± 0.001	0.00	3.81 ± 0.190	0.04
Cr_2O_3	0.01 ± 0.000	0.00	0.19 ± 0.010	0.01

Garnet 90			***Plagioclase AV 102***	
	wt % oxides ± errors	**detection limits**	**wt % oxides ± errors**	**detection limits**
Na_2O	0.02 ± 0.001	0.01	9.18 ± 0.459	0.04
SiO_2	36.62 ± 1.831	0.11	62.18 ± 3.109	0.14
K_2O	0.01 ± 0.001	0.00	0.29 ± 0.014	0.01
FeO	36.26 ± 1.813	0.07	0.02 ± 0.001	0.00
Al_2O_3	20.49 ± 1.024	0.08	22.65 ± 1.132	0.09
CaO	0.83 ± 0.042	0.02	4.55 ± 0.228	0.04
MnO	0.43 ± 0.022	0.01	0.00 ± 0.000	0.00
MgO	4.57 + 0.228	0.03	0.02 ± 0.001	0.00
TiO_2	0.03 ± 0.002	0.00	0.02 ± 0.001	0.00
Cr_2O_3	0.03 ± 0.001	0.00	0.00 ± 0.000	0.00

K-feldspar 102		
	wt % oxides ± errors	**detection limits**
Na_2O	1.55 ± 0.078	0.02
SiO_2	63.82 ± 3.191	0.15
K_2O	14.19 ± 0.710	0.06
FeO	0.03 ± 0.002	0.00
Al_2O_3	18.54 ± 0.927	0.09
CaO	0.03 ± 0.002	0.00
MnO	0.02 ± 0.001	0.00
MgO	0.02 ± 0.001	0.00
TiO_2	0.05 ± 0.003	0.00
Cr_2O_3	0.01 ± 0.001	0.00

A4.4 - Normalisation procedures

Representative probe analyses from mesosome and leucosome phases are presented in Appendix 4.6. The analyses are displayed in their weight per cent and cation

proportions. The cation proportions are determined using Appendix 1 of Deer et al. (1992) where the cations are formulated on the basis of the number of oxygens in the standard mineral formula. All Fe is assumed to be Fe^{2+} for garnet, biotite and cordierite, but in spinel Fe^{3+} is calculated based on a site balance calculation (Fitzsimons, 1991) where:

$$Fe^{3+} = 2-(Al + Cr + Ti).$$

A4.4.1 - X_{Mg}

X_{Mg} has been calculated for all mafic phases and is derived as follows:

$$X_{Mg} = Mg / (Mg + Fe)$$

A4.4.2 - Biotite

Biotite formulas are calculated based on 20 oxygens. X_K was calculated using the following calculation (Fitzsimons, 1991):

$$X_K = K / (Na + K)$$

A4.4.3 - Garnet

Mole fractions of almandine, pyrope, uvarovite, spessertine and grossular were calculated as follows:

$$X_{alm} = Fe / 3$$

$$X_{prp} = Mg / 3$$

$$X_{uvr} = Cr / 2$$

$$X_{spss} = Mn / 3$$

$$X_{grs} = (Ca / 3) - (Cr / 2) - (Fe^{3+} / 2)$$

and then re-normalised to a total of 1.

A4.4.4 - Spinel

Spinel was calculated on the basis of 4 oxygens. Mole fraction of end members hercynite, spinel, chromite, ulvöspinel, galaxite, gahnite and magnetite were calculated by the following equations after Ti, Al, Cr, Fe^{total}, Mn, Mg and Zn were normalised to 3:

$$X_{hc} = Fe^{total} - 1.5Fe^{3+} - 2Ti - (Cr / 2)$$

$X_{spl} = Mg$

$X_{chr} = Cr / 2$

$X_{usp} = Ti$

$X_{gal} = Mn$

$X_{gah} = Zn$

$X_{mag} = Fe^{3+} / 2$

A4.4.5 - Feldspar

Feldspar end members were calculated thus:

$X_{an} = Ca / (Ca + Na + K)$

$X_{ab} = Na / (Ca + Na + K)$

$X_{or} = K / (Ca + Na + K)$

A4.5 - Samples and sample descriptions

The following samples were analysed and their phase compositions are used in chapters 4, 6 and 8.

Table A4.3 - Samples used for electron probe analysis.

LOCALITY	SAMPLE	DESCRIPTION
2.1	83	POIKILOBLASTIC GARNET IN MESOSOME
2.2	81	LEUCOSOME GARNET/CORDIERITE INTERGROWTH
2.2	D18	THIN GARNETIFEROUS LEUCOSOME
2.3	D22	OBLIQUE LEUCOSOME/MESOSOME SAMPLE BOTH CONTAIN CORDIERITE
2.4	D5	SELVAGE RICH LEUCOSOME
3	88	F3 FOLDED GARNET
3	90	GARNET WITHIN LARGE LEUCOSOME
4	10	LAYERED MESOSOME WITH SMALL, FINE GRAINED LEUCOSOME
4	12	MESOSOME/LEUCOSOME SAMPLE WITH MESOSOME CORDIERITE
4	60	COARSE GRAINED CORDIEIRITE RICH LEUCOSOME.
4	97	MESOSOME/LEUCOSOME SAMPLE
5	102	MESOSOME SAMPLE, THIN (2 CM) SELVAGE BOUND LEUCOSOME
6	114	LEUCOSOME AND MESOSOME SAMPLE
6	118	DARK, GARNET RICH MESOSOME WITH COARSE BIOTITE
7	36	MESOSOME CUT BY VERY SMALL LEUCOSOMES
7	120A	EDGE OF A LARGE GARNET BEARING LEUCOSOME
7	D41	SILL RICH PATCH
8	123	MESOSOME SAMPLE
13	135	MESOSOME SAMPLE
14	152	SMALL ELONGATE LEUCOSOME AND MESOSOME
18	142	MESOSOME AND ELONGATE LEUCOSOME
22	154	MESOSOME WITH SMALL ELONGATE LEUCOSOME

A4.5.1 - Locality 2.1

Sample 83

This sample consists mostly of a large poikiloblastic garnet with rounded inclusions of bioite and quartz. Pinitised cordierite is present as an inclusion phase. The inclusions are all coarser grained than the matrix. Some of the garnet edges are altered to biotite, both brown and green. The matrix is composed of bioitite, twinned unaltered cordierite, microperthite, myrmekite, quartz and biotite.

A4.5.2 - Locality 2.2

Sample 81

This sample originates from the large, coarse leucosome that cross cuts the foliation at locality 2.2. The leucosome contains a very high proportion of garnet and cordierite. In the field this sample was taken from what appeared to be a garnet/cordierite intergrowth but under the microscope it is obvious that the two

minerals grew separately. The poikiloblastic garnet dominates. There is a high proportion of biotite in the rock and much of this is associated with the garnet and cordierite and so may be retrogressive. The cordierite is altered to pinite but this varies in its intensity. The other minerals are K-feldspar and quartz.

Sample D18

Again the cordierite is in various stages of alteration, with that associated with the garnets highly pinitised and in some places altered to chlorite and biotite that form a symplectite. Quartz and K-feldspar dominate and garnet is present as euhedral crystals that are weakly poikiloblastic, containing some biotite and quartz inclusions. Granuloblastic mesosome edges the sample containing quartz, plagioclase and biotite

Sample D22

The cordierite in the leucosome is much coarser than that in the mesosome and is dominantly surrounded by quartz with some K-feldspar. The boundary of the mesosome is again rich in biotite and cordierite. Cordierite is mostly equant, though it may be elongate in the mesosome. The biotite that has crystallised around the elongate cordierites defines a foliation, whereas the main matrix biotite is mostly decussate in texture.

A4.5.3 - Locality 2.4

Sample D5

This leucosome is fairly fine grained, probably due to the small size of the leucosome. The mineralogy is dominated by K-feldspar and quartz. The cordierite is altered to pinite on all rims and in cracks that traverse into the centre of the crystals.

A4.5.4 - Locality 3

Sample 88

An F3 fold can be seen folding S2, garnet and cordierite are elongate along S2 and contain sillimanite needles. The sample has layers rich in garnet, cordierite, biotite and tourmaline, and more quartz-rich layers contain microperthite, quartz and biotite.

The dominant mineral in the slide is tourmaline, which is also present as inclusions within most other phases.

Sample 90

This is a mesosome sample with poikiloblastic garnets containing quartz and biotite inclusions, up to 1 cm in length. There are relatively unaltered cordierite porphyroblasts as well as granular plagioclase, quartz, perthite, cordierite and biotite.

A4.5.5 - Locality 4

Sample 10

Half of the slide is dominated by a large poikiloblastic garnet with coarse quartz inclusions. Biotite and cordierite grow at the edges. Various areas are rich in quartz and cordierite with either plagioclase or K-feldspar and biotite, and a quartz and biotite dminated domain also occurs.

Sample 12

This mesosome preserves some layers that are dominated by quartz and contain no other leucosome minerals. Cordierite occurs within biotite-rich layers, elongated parallel to the main D2 fabric, with sillimanite inclusions within the cores. Granular quartz and plagioclase dominate the mesosome assemblage.

Sample 60

This leucosome is dominated by a large (1 cm in length) untwinned cordierite that is only pinitised at it's edges. The rest of the slide is composed of altered K-feldspar and interstitial quartz.

Sample 97

The leucosome is composed dominantly of altered cordierite crystals up to 2-3 mm long. The cordierite is strongly altered in some places to isotropic pinite, sillimanite and bioitite. Plagioclase, perthite and quartz also occur.

A4.5.6 - Locality 5

Sample 102

Overall the sample is fine grained but there are very large cordierite crystals with foliated biotite and quartz inclusions. These cordierite crystals dominate the slide but the matrix is also composed of quartz, plagioclase and perthite.

A4.5.7 - Locality 6

Sample 114

This slide contains a large garnet that is free from the large quartz inclusions seen in other garnets but does contain some small biotite inclusions. The garnet alters to cordierite and green and brown biotite-quartz symplectites on its margins. The rest of the slide consists of plagioclase, perthite, quartz and biotite. Most of the cordierite is altered to pinite.

Sample 118

The slide is dominated by a large (1 cm) garnet with a small number of quartz and biotite inclusions. The garnet alters to biotite + quartz symplectites and to cordierite, on its margins. The mesosome is composed of biotite, plagioclase, perthite, cordierite and quartz.

A4.5.8 - Locality 7

Sample 36

This dominantly mesosome sample preserves a 6 mm wide plagioclase and quartz discordant leucosome. At the leucosome edge is a cordierite and biotite selvage. The cordierite is totally pinitised and contains sillimanite as an alteration phase. Poikiloblastic garnets are present with quartz inclusions and K-feldspar around the edges. The mesosome consists of perthite, plagioclase, quartz biotite and cordierite.

Sample 120A

A garnet-bearing leucosome, with garnets containing few quartz inclusions which aren't so badly cracked. The garnets are found with altered K-feldspar and interstitial quartz but also some clusters of graphite.

Sample D41

This garnet bearing leucosome features garnets with a few large quartz inclusions, biotite inclusions and altered cordierite (pinite, green mica and graphite). At its margins the garnet breaks down to cordierite and biotite + quartz symplectites. Coarse biotite occurs at the edge of the slide. The rest of the slide consists of altered perthite, quartz and monazites.

A4.5.9 - Locality 8

Sample 123

This is a granular sample dominated by cordierite that is surrounded by decussate biotite. There's also granular plagioclase, perthite and quartz. The large cordierites and garnets have a large number of sillimanite inclusions. The garnet is patchy and contains only biotite inclusions. The cordierite also contains spinel inclusions.

A4.5.10 - Locality 13

Sample 135

This is a mesosome sample that contains large inclusion filled cordierites, the inclusions being biotite, sillimanite and quartz. There are also small granular patches composed of quartz, cordierite and plagioclase.

A4.5.11 - Locality 14

Sample 152

This sample is similar to that described above with large cordierites in patches but there are no inclusions. The matrix is made of granular plagioclase, quartz, cordierite and decussate biotite.

A4.5.12 - Locality 18

Sample 142

This is a very fine grained sample with a granoblastic texture. Decussate biotite, quartz, plagioclase and a small amount of K-feldspar. There are a couple of poikiloblastic cordieirites that are totally altered to yellow pinite.

A4.5.13 - Locality 22

Sample 154

This is a foliated sample with very dark brown biotite forming the foliation. In between the biotite are elongate cordierites with fibrous sillimanite and rounded biotite inclusions. The matrix is of granular quartz, plagioclase, cordierite and K-feldspar. Also there are larger perthites and quartz in a small 2 mm leucosome.

A4.6 - Analyses of mesosome and leucosome assemblages

This section contains example analyses from the samples described previously. The abbreviations seen at the top of each analysis are as follows:

C - core analysis
R - rim analysis
INC - inclusion
NGT - near garnet (<5mm)
MAT - general mesosome matrix phase

For each mesosome analysis, the activities of the phase end-members are added at the base of each column. These were calculated using AX, a programme that calculates the activities of end members from raw electron probe data (Holland, *pers. comm.*). These are present for garnet, biotite cordierite, K-feldspar and plagioclase as these phases are used for thermobarometric calculations in Chapter 6 of this study. Tables A4.4 and A4.5 contain electron probe analyses of phases in the mesosomes and leucosomes respectively.

Table A4.4 - Analyses from mesosome assemblages.

	Garnets											
Sample	**83C**	**83R**	**D18C**	**D18R**	**88C**	**88R**	**90C**	**90R**	**10C**	**10R**	**12C**	**15C**
SiO2	36.48	36.22	36.78	36.58	35.40	35.93	36.23	36.30	36.87	36.23	36.32	35.65
TiO2	0.03	0.03	0.03	0.02	0.03	0.04	0.04	0.02	0.03	0.02	0.03	0.00
Al2O3	20.87	20.83	20.83	20.60	19.90	20.47	21.13	20.50	20.97	20.56	20.37	20.66
Cr2O3	0.04	0.04	0.04	0.04	0.04	0.03	0.05	0.05	0.05	0.06	0.17	0.03
FeO	34.65	35.40	35.10	36.24	37.37	38.23	34.24	36.77	34.34	37.32	39.01	36.25
MnO	0.75	0.65	1.02	1.10	0.72	0.74	0.40	0.52	0.54	0.86	0.53	0.64
MgO	5.06	4.46	4.99	4.18	3.68	2.89	5.54	4.05	5.54	3.32	2.63	4.22
CaO	0.86	0.81	0.73	0.76	0.65	0.63	0.86	0.86	0.90	0.88	0.84	0.86
Na2O	0.00	0.00	0.01	0.01	0.03	0.03	0.05	0.06	0.05	0.02	0.03	0.03
K2O	0.01	0.00	0.00	0.00	0.02	0.02	0.01	0.01	0.01	0.00	0.01	0.00
Totals	98.74	98.44	99.53	99.51	97.82	99.00	98.54	99.14	99.29	99.27	99.93	98.35
Oxygens	12	12	12	12	12	12	12	12	12	12	12	12
Si	2.960	2.958	2.967	2.971	2.950	2.961	2.937	2.963	2.964	2.966	2.970	2.933
Ti	0.002	0.002	0.002	0.001	0.002	0.002	0.002	0.001	0.002	0.001	0.002	0.000
Al	1.995	2.005	1.981	1.971	1.954	1.988	2.019	1.972	1.987	1.983	1.964	2.003
Cr	0.002	0.003	0.003	0.002	0.002	0.002	0.003	0.003	0.003	0.004	0.011	0.002
Fe2	2.351	2.418	2.368	2.461	2.604	2.635	2.320	2.510	2.309	2.554	2.668	2.494
Mn	0.042	0.036	0.057	0.061	0.042	0.042	0.023	0.029	0.030	0.049	0.030	0.036
Mg	0.612	0.544	0.600	0.506	0.457	0.355	0.669	0.492	0.665	0.405	0.320	0.518
Ca	0.075	0.071	0.063	0.066	0.058	0.056	0.074	0.075	0.078	0.077	0.074	0.076
Na	0.000	0.000	0.001	0.001	0.004	0.005	0.007	0.010	0.008	0.002	0.004	0.005
K	0.001	0.000	0.000	0.000	0.002	0.002	0.001	0.001	0.001	0.000	0.001	0.000
Totals	8.040	8.036	8.041	8.042	8.075	8.048	8.056	8.057	8.046	8.042	8.044	8.068
XMg	0.206	0.184	0.202	0.171	0.149	0.119	0.224	0.164	0.224	0.137	0.107	0.172
Xalm	0.763	0.788	0.767	0.795	0.824	0.853	0.752	0.808	0.749	0.828	0.863	0.798
Xprp	0.199	0.177	0.194	0.164	0.145	0.115	0.217	0.159	0.216	0.131	0.104	0.166
Xgrs	0.023	0.022	0.019	0.020	0.017	0.017	0.023	0.022	0.024	0.023	0.019	0.023
Xsps	0.014	0.012	0.018	0.020	0.013	0.014	0.007	0.009	0.010	0.016	0.010	0.012
Xuvr	0.001	0.001	0.001	0.001	0.001	0.001	0.002	0.002	0.002	0.002	0.005	0.001
Activities												
prp	0.01070	0.00770	0.00005	0.00005	0.00430	0.00220	0.01500	0.00560	0.01400	0.00320	0.00160	0.00680
grs	0.00002	0.00002	0.00330	0.00190	0.00001	0.00001	0.00003	0.00002	0.00003	0.00002	0.00002	0.00002
alm	0.39000	0.44000	0.50000	0.54000	0.45000	0.54000	0.35000	0.44000	0.36000	0.50000	0.56000	0.42000
sps	0.00000	0.00000	0.00001	0.00002	0.00000	0.00000	0.00000	0.00000	0.00000	0.00001	0.00000	0.00000

Sample	15R	114C	114R	118C	118R	36C	36R	D41C	D41R	123C	123R
SiO2	36.11	36.72	36.52	37.30	37.20	36.72	36.70	36.94	36.66	36.37	36.03
TiO2	0.00	0.02	0.03	0.00	0.00	0.00	0.00	0.04	0.02	0.04	0.02
Al2O3	20.72	20.63	20.61	21.10	21.00	20.93	21.03	21.01	21.03	20.58	20.58
Cr2O3	0.04	0.00	0.05	0.00	0.10	0.04	0.02	0.05	0.04	0.05	0.11
FeO	38.26	34.29	36.62	34.00	34.30	35.38	35.50	34.32	36.09	36.25	37.25
MnO	1.05	0.55	0.82	0.60	0.60	0.62	0.66	0.56	0.75	0.72	0.74
MgO	2.78	5.42	3.76	5.90	5.80	4.61	4.54	6.01	4.69	3.97	2.92
CaO	0.83	0.81	0.84	0.70	0.80	0.75	0.79	0.83	0.86	0.82	0.86
Na2O	0.02	0.03	0.02	0.00	0.00	0.01	0.00	0.09	0.07	0.02	0.02
K2O	0.00	0.00	0.01	0.00	0.00	0.02	0.01	0.02	0.01	0.00	0.01
Totals	99.82	98.47	99.28	99.60	99.80	99.07	99.24	99.85	100.21	98.82	98.53
Oxygens	12	12	12	12	12	12	12	12	12	12	12
Si	2.955	2.978	2.975	2.978	2.971	2.974	2.968	2.953	2.948	2.972	2.971
Ti	0.000	0.001	0.002	0.000	0.000	0.000	0.000	0.002	0.001	0.003	0.001
Al	1.998	1.972	1.979	1.985	1.977	1.997	2.005	1.979	1.994	1.981	2.000
Cr	0.003	0.000	0.003	0.000	0.006	0.002	0.001	0.003	0.003	0.003	0.007
Fe2	2.618	2.326	2.495	2.270	2.291	2.396	2.401	2.294	2.427	2.477	2.568
Mn	0.059	0.031	0.046	0.033	0.033	0.035	0.037	0.031	0.042	0.041	0.042
Mg	0.339	0.655	0.457	0.702	0.691	0.556	0.547	0.716	0.562	0.484	0.358
Ca	0.073	0.070	0.073	0.060	0.068	0.065	0.069	0.071	0.074	0.072	0.076
Na	0.003	0.005	0.003	0.000	0.000	0.002	0.000	0.014	0.011	0.004	0.004
K	0.000	0.000	0.001	0.000	0.000	0.002	0.001	0.002	0.001	0.000	0.001
Totals	8.048	8.038	8.035	8.029	8.037	8.029	8.029	8.065	8.062	8.036	8.028
XMg	0.114	0.220	0.155	0.236	0.232	0.188	0.186	0.238	0.188	0.164	0.122
Xalm	0.848	0.755	0.812	0.741	0.743	0.785	0.786	0.737	0.782	0.806	0.844
Xprp	0.110	0.213	0.149	0.229	0.224	0.182	0.179	0.230	0.181	0.158	0.118
Xgrs	0.022	0.023	0.022	0.020	0.019	0.020	0.022	0.021	0.022	0.022	0.021
Xsps	0.019	0.010	0.015	0.011	0.011	0.011	0.012	0.010	0.013	0.013	0.014
Xuvr	0.001	0.000	0.002	0.000	0.003	0.001	0.001	0.002	0.001	0.001	0.004
Activities											
prp	0.00190	0.01250	0.00450	0.01500	0.01500	0.00810	0.00780	0.01700	0.00850	0.00530	0.00230
grs	0.00002	0.00002	0.00002	0.00001	0.00002	0.00002	0.00002	0.00002	0.00002	0.00002	0.00002
alm	0.53000	0.38000	0.48000	0.37000	0.36000	0.44000	0.44000	0.32000	0.39000	0.47000	0.55000
sps	0.00001	0.00000	0.00001	0.00000	0.00000	0.00000	0.00000	0.00000	0.00000	0.00000	0.00000

Sample	Biotite 83INC	83MAT	D18INC	D18MAT	88NGT	88MAT	90INC	90MAT	10NGT	10MAT	12INC	12MAT	15NGT
SiO2	34.95	34.07	34.82	34.57	34.95	34.79	35.75	34.79	33.84	34.41	34.36	34.51	35.62
TiO2	3.87	4.02	4.01	4.11	3.77	3.61	3.19	3.75	3.64	3.78	0.17	3.12	2.25
Al2O3	17.05	17.13	18.14	17.56	16.25	16.27	16.47	16.81	17.01	17.04	20.62	17.81	18.64
Cr2O3	0.10	0.10	0.08	0.11	0.03	0.09	0.05	0.15	0.13	0.18	0.02	0.11	0.07
FeO	16.94	20.18	14.55	18.89	17.55	18.30	13.70	18.37	19.56	19.75	19.00	20.46	17.51
MnO	0.02	0.03	0.03	0.03	0.06	0.03	0.01	0.02	0.03	0.05	0.01	0.02	0.01
MgO	12.00	8.85	12.79	9.64	11.48	10.80	15.56	10.67	9.85	9.24	11.44	9.64	11.67
CaO	0.00	0.00	0.01	0.01	0.02	0.04	0.00	0.00	0.01	0.00	0.01	0.00	0.02
Na2O	0.29	0.11	0.29	0.11	0.13	0.15	0.40	0.11	0.19	0.14	0.21	0.18	0.24
K2O	9.12	9.65	8.91	9.81	9.19	8.95	8.98	9.59	9.36	9.34	9.12	9.15	9.28
Totals	94.33	94.14	93.63	94.84	93.43	93.03	94.10	94.24	93.63	93.93	94.95	95.00	95.29
Oxygens	20	20	20	20	20	20	20	20	20	20	20	20	20
Si	4.954	4.945	5.094	5.090	5.022	5.032	4.994	4.988	4.921	4.980	4.860	4.936	4.990
Ti	0.413	0.439	0.442	0.455	0.408	0.393	0.335	0.404	0.399	0.411	0.018	0.335	0.237
Al	2.848	2.930	3.128	3.047	2.752	2.773	2.711	2.840	2.915	2.905	3.438	3.003	3.077
Cr	0.011	0.012	0.009	0.013	0.003	0.010	0.005	0.017	0.015	0.020	0.002	0.013	0.007
Fe2	2.008	2.449	1.780	2.326	2.109	2.214	1.601	2.202	2.378	2.390	2.247	2.447	2.051
Mn	0.002	0.003	0.003	0.003	0.006	0.003	0.001	0.001	0.003	0.005	0.001	0.002	0.001
Mg	2.536	1.914	2.004	1.521	2.460	2.329	3.240	2.280	2.135	1.993	2.411	2.055	2.436
Ca	0.000	0.000	0.002	0.001	0.003	0.007	0.000	0.000	0.002	0.001	0.001	0.000	0.003
Na	0.078	0.032	0.083	0.031	0.036	0.042	0.109	0.031	0.054	0.038	0.056	0.050	0.064
K	1.648	1.787	1.663	1.843	1.684	1.651	1.600	1.754	1.736	1.724	1.645	1.669	1.658
Totals	14.499	14.510	14.206	14.330	14.483	14.453	14.595	14.518	14.558	14.468	14.679	14.511	14.523
XMg	0.558	0.439	0.530	0.395	0.538	0.513	0.669	0.509	0.473	0.455	0.518	0.457	0.543
XK	0.955	0.983	0.953	0.984	0.979	0.975	0.936	0.983	0.970	0.978	0.967	0.971	0.963
Activities													
phl	0.057	0.026	0.068	0.032	0.053	0.045	0.126	0.043	0.034	0.029	0.050	0.032	0.058
ann	0.032	0.065	0.018	0.050	0.040	0.047	0.007	0.047	0.058	0.059	0.024	0.062	0.037
east	0.048	0.030	0.069	0.038	0.040	0.037	0.060	0.040	0.036	0.032	0.081	0.037	0.059

Sample	15MAT	102MAT	114NGT	114MAT	118INC	118MAT	36NGT	36MAT	D41INC	D41MAT	123INC	123MAT	135MAT
SiO2	34.55	33.66	34.37	34.70	34.74	34.78	34.65	34.43	35.58	34.14	34.64	34.20	33.71
TiO2	2.87	3.76	3.57	4.03	2.66	3.41	3.85	3.86	1.36	3.78	3.20	3.51	3.18
Al2O3	18.25	17.84	17.47	17.11	17.25	17.34	17.29	17.00	17.03	17.48	16.78	17.27	18.86
Cr2O3	0.09	0.12	0.21	0.20	0.04	0.07	0.17	0.16	0.05	0.19	0.15	0.16	0.13
FeO	20.09	21.64	19.50	19.59	18.64	19.38	19.43	18.90	16.52	19.88	16.92	19.46	21.31
MnO	0.01	0.06	0.01	0.04	0.04	0.03	0.04	0.05	0.01	0.03	0.03	0.02	0.08
MgO	9.42	7.81	9.87	9.28	11.29	10.03	9.98	10.17	13.84	9.55	12.07	9.99	7.70
CaO	0.01	0.00	0.01	0.00	0.00	0.00	0.01	0.03	0.00	0.03	0.00	0.03	0.00
Na2O	0.25	0.16	0.21	0.11	0.14	0.10	0.15	0.09	0.16	0.15	0.20	0.16	0.17
K2O	9.32	8.98	9.35	9.56	9.42	9.53	9.17	8.68	9.23	9.44	8.96	9.24	9.24
Totals	94.85	94.02	94.57	94.62	94.23	94.67	94.72	93.35	93.76	94.67	92.95	94.03	94.37
Oxygens	20	20	20	20	20	20	20	20	20	20	20	20	20
Si	4.945	4.901	4.932	4.982	4.979	4.979	4.951	4.963	5.053	4.909	4.983	4.934	4.883
Ti	0.309	0.411	0.385	0.435	0.286	0.367	0.413	0.419	0.145	0.409	0.346	0.381	0.346
Al	3.078	3.060	2.955	2.895	2.914	2.926	2.910	2.888	2.849	2.963	2.844	2.936	3.219
Cr	0.011	0.014	0.024	0.023	0.005	0.008	0.019	0.018	0.005	0.021	0.017	0.018	0.015
Fe2	2.405	2.634	2.340	2.352	2.234	2.320	2.321	2.279	1.962	2.390	2.035	2.347	2.581
Mn	0.001	0.006	0.001	0.004	0.004	0.003	0.004	0.005	0.001	0.003	0.003	0.001	0.008
Mg	2.010	1.696	2.112	1.986	2.412	2.141	2.124	2.185	2.930	2.046	2.588	2.149	1.663
Ca	0.002	0.000	0.002	0.000	0.001	0.000	0.001	0.004	0.000	0.004	0.000	0.004	0.000
Na	0.068	0.045	0.058	0.031	0.039	0.029	0.042	0.024	0.043	0.042	0.056	0.044	0.046
K	1.701	1.667	1.712	1.751	1.722	1.740	1.670	1.596	1.671	1.732	1.644	1.700	1.708
Totals	14.529	14.435	14.521	14.460	14.596	14.514	14.456	14.380	14.660	14.520	14.516	14.515	14.470
XMg	0.455	0.392	0.474	0.458	0.519	0.480	0.478	0.490	0.599	0.461	0.560	0.478	0.392
XK	0.961	0.974	0.967	0.983	0.978	0.984	0.975	0.985	0.975	0.976	0.967	0.975	0.974
Activities													
phl	0.032	0.018	0.034	0.029	0.052	0.037	0.034	0.036	0.092	0.030	0.062	0.035	0.019
ann	0.060	0.075	0.054	0.057	0.045	0.055	0.052	0.048	0.017	0.058	0.033	0.055	0.071
east	0.039	0.026	0.038	0.032	0.048	0.038	0.036	0.037	0.071	0.035	0.051	0.038	0.031

Sample	152MAT	142MAT	154MAT
SiO2	34.16	34.31	34.09
TiO2	2.91	2.95	3.57
Al2O3	18.80	19.43	17.88
Cr2O3	0.14	0.07	0.12
FeO	20.80	20.28	19.95
MnO	0.03	0.09	0.04
MgO	8.02	7.65	8.16
CaO	0.02	0.01	0.03
Na2O	0.16	0.10	0.21
K2O	9.31	9.33	9.27
Totals	94.35	94.22	93.32
Oxygens	20	20	20
Si	4.931	4.939	4.967
Ti	0.316	0.320	0.391
Al	3.198	3.296	3.070
Cr	0.016	0.008	0.014
Fe2	2.511	2.440	2.431
Mn	0.003	0.009	0.004
Mg	1.727	1.642	1.773
Ca	0.003	0.002	0.005
Na	0.045	0.027	0.058
K	1.714	1.713	1.722
Totals	14.465	14.395	14.435
XMg	0.407	0.402	0.422
XK	0.975	0.985	0.967
Activities			
phl	0.022	0.021	0.023
ann	0.067	0.061	0.061
east	0.033	0.033	0.031

Cordierites

Sample	83MAT	D18NGT	D18MAT	88NGT	88MAT	90NGT	90MAT	10NGT	10MAT
SiO2	47.06	47.61	47.90	47.19	46.87	47.52	47.47	47.29	47.48
TiO2	0.01	0.02	0.01	0.03	0.01	0.01	0.02	0.02	0.02
Al2O3	32.49	32.37	32.46	31.66	32.00	32.54	32.16	32.11	32.36
Cr2O3	0.01	0.01	0.02	0.02	0.02	0.01	0.02	0.04	0.00
FeO	9.14	8.80	9.18	9.25	9.59	7.49	8.88	9.45	9.52
MnO	0.06	0.06	0.11	0.07	0.08	0.04	0.05	0.06	0.10
MgO	7.67	8.22	7.98	7.99	7.68	9.31	8.36	7.82	7.81
CaO	0.00	0.01	0.01	0.02	0.02	0.01	0.00	0.00	0.02
Na2O	0.08	0.07	0.07	0.08	0.08	0.09	0.09	0.12	0.12
K2O	0.01	0.01	0.01	0.00	0.01	0.01	0.02	0.01	0.02
Totals	96.52	97.18	97.75	96.31	96.35	97.02	97.06	96.92	97.44
Oxygens	18	18	18	18	18	18	18	18	18
Si	4.961	4.977	4.986	4.992	4.965	4.950	4.974	4.976	4.971
Ti	0.001	0.001	0.001	0.002	0.001	0.001	0.001	0.001	0.001
Al	4.036	3.988	3.982	3.946	3.994	3.994	3.970	3.981	3.992
Cr	0.001	0.001	0.002	0.002	0.002	0.001	0.002	0.003	0.000
Fe2	0.806	0.769	0.799	0.818	0.849	0.652	0.778	0.832	0.833
Mn	0.005	0.005	0.008	0.005	0.006	0.003	0.003	0.004	0.007
Mg	1.206	1.281	1.239	1.260	1.213	1.445	1.305	1.227	1.219
Ca	0.000	0.001	0.001	0.003	0.002	0.001	0.000	0.000	0.002
Na	0.016	0.014	0.015	0.016	0.017	0.018	0.017	0.024	0.025
K	0.001	0.001	0.001	0.001	0.001	0.002	0.003	0.001	0.003
Totals	11.032	11.038	11.033	11.044	11.049	11.067	11.054	11.050	11.053
T	2.842	2.866	2.878	2.832	2.828	2.876	2.860	2.847	2.862
XMg	0.600	0.625	0.608	0.606	0.588	0.689	0.626	0.596	0.594
Activities									
crd	0.410	0.000	0.000	0.440	0.420	0.550	0.470	0.430	0.430
fcrd	0.160	0.980	0.970	0.140	0.150	0.085	0.120	0.150	0.150

Sample	12MAT	15NGT	102MAT	118NGT	118MAT	36MAT	D41MAT	123NGT	123MAT	135MAT	142MAT	154MAT
SiO2	47.65	47.54	47.15	47.49	46.96	47.21	47.43	47.22	47.49	47.07	47.72	47.22
TiO2	0.00	0.00	0.01	0.01	0.00	0.01	0.03	0.02	0.02	0.01	0.02	0.02
Al2O3	32.37	32.17	31.88	31.69	32.42	32.05	32.16	32.54	32.26	32.29	32.38	32.23
Cr2O3	0.02	0.02	0.01	0.01	0.00	0.03	0.01	0.02	0.01	0.00	0.00	0.00
FeO	8.83	10.14	10.45	8.89	8.96	8.68	8.70	7.60	8.64	10.31	9.58	9.57
MnO	0.05	0.09	0.12	0.09	0.07	0.06	0.05	0.05	0.05	0.10	0.21	0.08
MgO	8.23	7.20	7.01	8.25	8.03	8.50	8.30	8.72	8.15	6.86	7.04	7.48
CaO	0.03	0.01	0.02	0.02	0.02	0.02	0.00	0.02	0.02	0.01	0.03	0.01
Na2O	0.10	0.13	0.23	0.08	0.08	0.09	0.17	0.08	0.10	0.22	0.49	0.10
K2O	0.01	0.01	0.01	0.01	0.02	0.00	0.02	0.01	0.01	0.01	0.00	0.01
Totals	97.28	97.32	96.91	96.54	96.55	96.64	96.86	96.27	96.73	96.88	97.47	96.70
Oxygens	18	18	18	18	18	18	18	18	18	18	18	18
Si	4.978	4.994	4.990	5.002	4.949	4.965	4.977	4.957	4.984	4.976	5.005	4.979
Ti	0.000	0.000	0.001	0.001	0.000	0.001	0.002	0.001	0.002	0.001	0.001	0.001
Al	3.985	3.983	3.975	3.934	4.026	3.972	3.977	4.025	3.990	4.023	4.003	4.005
Cr	0.001	0.002	0.001	0.000	0.000	0.003	0.001	0.002	0.000	0.000	0.000	0.000
Fe2	0.771	0.891	0.925	0.783	0.790	0.763	0.763	0.667	0.758	0.911	0.840	0.844
Mn	0.004	0.007	0.009	0.007	0.005	0.004	0.004	0.004	0.004	0.007	0.015	0.006
Mg	1.281	1.128	1.106	1.296	1.261	1.332	1.298	1.365	1.275	1.081	1.101	1.176
Ca	0.003	0.001	0.002	0.003	0.002	0.002	0.000	0.003	0.002	0.001	0.003	0.001
Na	0.019	0.027	0.048	0.017	0.016	0.018	0.035	0.016	0.021	0.044	0.099	0.020
K	0.001	0.002	0.001	0.001	0.002	0.000	0.002	0.001	0.001	0.002	0.000	0.001
Totals	11.044	11.035	11.058	11.043	11.052	11.060	11.060	11.041	11.035	11.046	11.067	11.032
T	2.868	2.852	2.831	2.844	2.843	2.849	2.855	2.854	2.855	2.834	2.857	2.841
XMg	0.624	0.559	0.545	0.623	0.615	0.636	0.630	0.672	0.627	0.543	0.567	0.582
Activities												
crd	0.460	0.360	0.370	0.460	0.460	0.480	0.480	0.530	0.450	0.360	0.400	0.390
fcrd	0.130	0.190	0.180	0.130	0.130	0.116	0.120	0.096	0.130	0.200	0.160	0.170

	Plagioclase												
Sample	83MAT	D18MAT	90MAT	90MAT	12MAT	102MAT	118MAT	36MAT	123MAT	135MAT	152MAT	142MAT	154MAT
SiO2	61.81	62.25	60.88	61.52	60.45	62.18	61.12	61.09	60.66	62.39	61.05	62.01	61.67
TiO2	0.02	0.01	0.02	0.02	0.01	0.02	0.01	0.02	0.03	0.02	0.03	0.01	0.01
Al2O3	22.86	23.39	23.20	23.62	23.04	22.65	23.32	23.63	23.60	22.99	24.30	23.33	23.16
Cr2O3	0.02	0.03	0.03	0.03	0.00	0.00	0.06	0.01	0.02	0.00	0.02	0.00	0.00
Fe2O3	0.00	0.00	0.00	0.00	0.00	0.00	0.00	0.00	0.00	0.00	0.00	0.00	0.00
FeO	0.04	0.07	0.01	0.10	0.05	0.02	0.04	0.05	0.05	0.03	0.08	0.02	0.07
MnO	0.00	0.02	0.03	0.02	0.02	0.00	0.00	0.00	0.03	0.03	0.03	0.01	0.00
MgO	0.00	4.70	0.01	0.01	0.01	0.02	0.02	0.00	0.02	0.01	0.00	0.00	0.01
CaO	4.77	0.02	5.22	5.13	5.33	4.55	5.16	4.51	5.11	4.38	5.93	5.03	4.78
Na2O	9.00	9.05	8.21	8.62	8.06	9.18	8.13	8.90	8.89	9.11	8.31	8.95	8.72
K2O	0.19	0.19	0.22	0.13	0.10	0.29	0.25	0.34	0.22	0.35	0.36	0.15	0.26
Totals	98.71	99.73	97.82	99.21	97.07	98.90	98.11	98.55	98.61	99.29	100.11	99.51	98.67
Oxygens	8	8	8	8	8	8	8	8	8	8	8	8	8
Si	2.848	2.807	2.823	2.817	2.822	2.861	2.824	2.820	2.805	2.857	2.779	2.833	2.839
Ti	0.001	0.000	0.001	0.001	0.000	0.001	0.000	0.001	0.001	0.001	0.001	0.000	0.000
Al	1.241	1.243	1.268	1.275	1.268	1.228	1.270	1.285	1.286	1.240	1.304	1.256	1.257
Cr	0.001	0.001	0.001	0.001	0.000	0.000	0.002	0.000	0.001	0.000	0.001	0.000	0.000
Fe3	0.003	0.005	0.001	0.008	0.004	0.001	0.003	0.004	0.003	0.002	0.006	0.002	0.005
Fe2	0.000	0.000	0.000	0.000	0.000	0.000	0.000	0.000	0.000	0.000	0.000	0.000	0.000
Mn	0.000	0.001	0.001	0.001	0.001	0.000	0.000	0.000	0.001	0.001	0.001	0.000	0.000
Mg	0.000	0.316	0.000	0.001	0.001	0.002	0.001	0.000	0.001	0.000	0.000	0.000	0.001
Ca	0.235	0.001	0.259	0.252	0.266	0.224	0.255	0.223	0.253	0.215	0.289	0.246	0.236
Na	0.804	0.791	0.738	0.766	0.729	0.818	0.729	0.796	0.797	0.809	0.734	0.793	0.778
K	0.011	0.011	0.013	0.008	0.006	0.017	0.015	0.020	0.013	0.021	0.021	0.009	0.015
Totals	5.144	5.175	5.106	5.128	5.097	5.152	5.099	5.150	5.161	5.145	5.136	5.140	5.130
Xan	0.224	0.001	0.257	0.246	0.266	0.212	0.256	0.215	0.238	0.206	0.277	0.235	0.229
Xab	0.765	0.985	0.730	0.747	0.728	0.772	0.730	0.766	0.750	0.775	0.703	0.757	0.756
Xor	0.011	0.014	0.013	0.008	0.006	0.016	0.015	0.019	0.012	0.020	0.020	0.008	0.015
Activities													
an	0.30	0.00	0.34	0.33	0.35	0.28	0.34	0.29	0.32	0.27	0.37	0.31	0.30
ab	0.77	0.99	0.73	0.75	0.73	0.77	0.73	0.77	0.75	0.77	0.70	0.76	0.76

K-Feldspars

Sample	83MAT	D18MAT	90MAT	102MAT	118MAT	135MAT	152MAT	142MAT	154MAT
SiO2	63.73	63.85	63.85	63.90	64.54	63.80	63.94	63.832	63.76
TiO2	0.01	0.03	0.03	0.01	0.02	0.00	0.02	0.03	0.02
Al2O3	18.41	18.64	17.97	18.33	18.60	18.83	18.68	18.42	18.48
Cr2O3	0.04	0.00	0.02	0.01	0.01	0.00	0.04	0.00	0.01
Fe2O3	0.00	0.00	0.00	0.00	0.00	0.00	0.00	0.00	0.00
FeO	0.06	0.02	0.02	0.04	0.05	0.04	0.03	0.02	0.03
MnO	0.00	0.02	0.02	0.02	0.01	0.03	0.03	0.00	0.00
MgO	0.02	0.13	0.01	0.02	0.02	0.01	0.00	0.01	0.01
CaO	0.08	0.00	0.06	0.01	0.11	0.05	0.40	0.04	0.13
Na2O	1.35	1.82	1.22	2.05	3.13	2.03	2.21	1.98	2.29
K2O	14.67	14.07	14.63	13.46	11.60	13.71	13.11	13.80	13.49
Totals	98.38	98.58	97.83	97.87	98.07	98.49	98.45	98.12	98.22
Oxygens	8	8	8	8	8	8	8	8	8
Si	3.079	3.072	3.098	3.087	3.084	3.068	3.069	3.082	3.076
Ti	0.000	0.001	0.001	0.001	0.001	0.000	0.001	0.001	0.001
Al	1.048	1.057	1.028	1.044	1.047	1.067	1.056	1.048	1.051
Cr	0.002	0.000	0.001	0.000	0.000	0.000	0.002	0.000	0.000
Fe3	0.005	0.001	0.002	0.004	0.004	0.003	0.002	0.002	0.003
Fe2	0.000	0.000	0.000	0.000	0.000	0.000	0.000	0.000	0.000
Mn	0.000	0.001	0.001	0.001	0.000	0.001	0.001	0.000	0.000
Mg	0.001	0.009	0.001	0.001	0.001	0.001	0.000	0.001	0.001
Ca	0.004	0.000	0.003	0.001	0.005	0.003	0.020	0.002	0.007
Na	0.126	0.170	0.114	0.192	0.290	0.189	0.206	0.185	0.214
K	0.904	0.863	0.906	0.829	0.707	0.841	0.802	0.850	0.830
Totals	5.171	5.174	5.153	5.159	5.140	5.172	5.159	5.170	5.182
Xan	0.004	0.000	0.003	0.001	0.005	0.003	0.020	0.002	0.006
Xab	0.122	0.165	0.112	0.188	0.289	0.183	0.200	0.179	0.204
Xor	0.874	0.835	0.885	0.811	0.706	0.814	0.780	0.820	0.790
Activities									
or	0.880	0.850	0.890	0.830	0.760	0.830	0.800	0.830	0.810
ab	0.370	0.470	0.340	0.520	0.700	0.510	0.550	0.500	0.560

Spinel

Sample	123	123
SiO2	0.03	0.02
TiO2	0.00	0.00
Al2O3	56.46	56.76
Cr2O3	0.55	0.22
Fe2O3	0.00	0.00
FeO	32.50	32.44
MnO	0.07	0.08
MgO	3.18	3.00
CaO	0.00	0.00
Na2O	0.18	0.19
ZnO	6.12	6.25
Totals	99.08	98.96
Oxygens	4	4
Si	0.001	0.000
Ti	0.000	0.000
Al	1.941	1.954
Cr	0.013	0.005
Fe3	0.046	0.041
Fe2	0.746	0.751
Mn	0.001	0.002
Mg	0.138	0.131
Ca	0.000	0.000
Na	0.010	0.011
ZnO	0.114	0.117
Totals	3.000	3.000
Xhc	0.717	0.728
Xsp	0.138	0.131
Xchr	0.006	0.003
Xusp	0.000	0.000
Xgal	0.001	0.002
Xgah	0.114	0.117
Xmag	0.023	0.021

Sillimanite

Sample	83INC	83MAT
SiO2	36.53	36.03
TiO2	0.04	0.02
Al2O3	62.81	62.42
Cr2O3	0.02	0.05
FeO	0.54	0.45
MnO	0.01	0.02
MgO	0.05	0.01
CaO	0.01	0.01
Na2O	0.02	0.02
K2O	0.01	0.01
Totals	100.02	99.04
Oxygens	5	5
Si	0.989	0.985
Ti	0.001	0.000
Al	2.004	2.011
Cr	0.000	0.001
Fe2	0.012	0.010
Mn	0.000	0.000
Mg	0.002	0.000
Ca	0.000	0.000
Na	0.001	0.001
K	0.000	0.000
Totals	3.009	3.010

Table A4.5 - Analyses from leucosomes assemblages.

	Garnets		
Sample	81C	120A C	120B R
SiO2	36.57	37.40	37.60
TiO2	0.04	0.00	0.00
Al2O3	20.40	21.10	21.20
Cr2O3	0.35	0.00	0.00
Fe2O3	0.00	0.00	0.00
FeO	36.88	33.60	34.00
MnO	1.62	0.50	0.60
MgO	3.54	5.90	6.00
CaO	0.63	0.80	0.80
Na2O	0.03	0.00	0.00
K2O	0.00	0.00	0.00
Totals	100.07	99.30	100.20
Oxygens	12	12	12
Si	2.973	2.988	2.982
Ti	0.002	0.000	0.000
Al	1.954	1.987	1.981
Cr	0.023	0.000	0.000
Fe3	0.000	0.000	0.000
Fe2	2.507	2.245	2.255
Mn	0.091	0.028	0.033
Mg	0.429	0.703	0.709
Ca	0.055	0.068	0.068
Na	0.005	0.000	0.000
K	0.000	0.000	0.000
Totals	8.040	8.018	8.028
XMg	0.146	0.238	0.239
Xalm	0.813	0.738	0.736
Xprp	0.139	0.231	0.231
Xgrs	0.007	0.022	0.022
Xsps	0.030	0.009	0.011
Xuvr	0.011	0.000	0.000

	Biotites				
Sample	81NGT	D22	D5	97	120A NGT
SiO2	34.66	34.83	36.08	35.90	35.20
TiO2	3.00	3.96	3.98	0.00	2.20
Al2O3	18.98	17.82	18.14	22.20	16.90
Cr2O3	0.29	0.15	0.06	0.00	0.00
Fe2O3	0.00	0.00	0.00	0.00	0.00
FeO	19.23	19.25	17.50	17.30	15.50
MnO	0.06	0.05	0.02	0.00	0.00
MgO	9.28	9.38	10.42	11.30	14.00
CaO	0.01	0.02	0.00	0.00	0.00
Na2O	0.27	0.23	0.16	0.10	0.30
K2O	9.27	9.38	9.61	9.60	8.80
Totals	95.05	95.06	95.97	96.40	92.90
Oxygens	20	20	20	20	20
Si	4.924	4.957	5.024	4.936	5.015
Ti	0.321	0.423	0.417	0.000	0.236
Al	3.177	2.988	2.977	3.597	2.838
Cr	0.033	0.016	0.007	0.000	0.000
Fe3	0.000	0.000	0.000	0.000	0.000
Fe2	2.284	2.291	2.038	1.989	1.847
Mn	0.005	0.005	0.002	0.000	0.000
Mg	1.966	1.991	2.164	2.316	2.974
Ca	0.001	0.003	0.000	0.000	0.000
Na	0.075	0.062	0.043	0.027	0.083
K	1.680	1.703	1.707	1.684	1.599
Totals	14.466	14.441	14.380	14.548	14.592
XMg	0.463	0.465	0.515	0.538	0.617
XK	0.957	0.965	0.975	0.984	0.951

Cordierites

Sample	81	D22	D5	97	60
SiO2	47.61	47.78	48.03	47.60	48.19
TiO2	0.02	0.01	0.02	0.00	0.01
Al2O3	32.37	32.34	32.59	32.20	32.26
Cr2O3	0.00	0.02	0.03	0.00	0.01
Fe2O3	0.00	0.00	0.00	0.00	0.00
FeO	9.57	8.84	8.52	9.40	9.39
MnO	0.15	0.08	0.04	0.10	0.06
MgO	7.65	8.44	8.36	7.80	7.79
CaO	0.01	0.01	0.00	0.00	0.01
Na2O	0.17	0.15	0.11	0.10	0.12
K2O	0.01	0.01	0.00	0.00	0.01
Totals	97.56	97.67	97.69	97.20	97.85
Oxygens	18	18	18	18	18
Si	4.980	4.975	4.986	4.989	5.014
Ti	0.002	0.001	0.001	0.000	0.001
Al	3.991	3.968	3.987	3.978	3.955
Cr	0.000	0.001	0.003	0.000	0.001
Fe3	0.000	0.000	0.000	0.000	0.000
Fe2	0.837	0.770	0.739	0.824	0.816
Mn	0.011	0.005	0.003	0.007	0.004
Mg	1.192	1.310	1.293	1.219	1.208
Ca	0.001	0.001	0.000	0.000	0.002
Na	0.034	0.031	0.022	0.020	0.025
K	0.001	0.001	0.000	0.000	0.001
Totals	11.049	11.064	11.035	11.037	11.027
XMg	0.587	0.630	0.636	0.597	0.597

K-Feldspars

Sample	D18	36	D41	D5	99
SiO2	64.73	65.07	64.58	64.62	63.95
TiO2	0.00	0.00	0.00	0.02	0.01
Al2O3	18.66	18.67	18.85	18.37	18.68
Cr2O3	0.00	0.01	0.03	0.03	0.03
Fe2O3	0.00	0.00	0.00	0.00	0.00
FeO	0.03	0.04	0.01	0.01	0.01
MnO	0.00	0.00	0.02	0.01	0.02
MgO	0.00	0.01	0.00	0.03	0.02
CaO	0.08	0.05	0.10	0.08	0.07
Na2O	1.73	1.01	2.50	2.26	1.49
K2O	14.16	15.18	13.08	13.31	15.05
Totals	99.40	100.05	99.17	98.75	99.32
Oxygens	8	8	8	8	8
Si	3.084	3.088	3.075	3.091	3.071
Ti	0.000	0.000	0.000	0.001	0.000
Al	1.048	1.044	1.058	1.035	1.057
Cr	0.000	0.000	0.001	0.001	0.001
Fe3	0.003	0.003	0.001	0.001	0.000
Fe2	0.000	0.000	0.000	0.000	0.000
Mn	0.000	0.000	0.001	0.000	0.001
Mg	0.000	0.001	0.000	0.002	0.002
Ca	0.004	0.003	0.005	0.004	0.004
Na	0.160	0.093	0.230	0.210	0.138
K	0.861	0.919	0.794	0.812	0.922
Totals	5.159	5.151	5.165	5.157	5.195
Xan	0.004	0.003	0.005	0.004	0.004
Xab	0.156	0.092	0.224	0.204	0.130
Xor	0.840	0.905	0.771	0.792	0.866

	Plagioclase						
Sample	81	15	60	97	99	36	D41
SiO2	63.09	67.00	62.06	62.10	69.03	61.69	62.06
TiO2	0.00	0.00	0.00	0.00	0.00	0.03	0.00
Al2O3	23.03	20.18	23.70	23.90	20.46	23.39	23.33
Cr2O3	0.02	0.03	0.02	0.00	0.02	0.01	0.01
Fe2O3	0.00	0.00	0.00	0.00	0.00	0.00	0.00
FeO	0.01	0.05	0.04	0.00	0.00	0.01	0.03
MnO	0.03	0.03	0.02	0.00	0.02	0.05	0.02
MgO	0.01	0.02	0.01	0.00	0.01	0.02	0.01
CaO	4.24	1.04	5.06	5.00	0.29	4.34	4.72
Na2O	9.37	11.23	8.81	8.70	10.46	9.45	8.93
K2O	0.18	0.09	0.30	0.20	0.11	0.33	0.30
Totals	99.97	99.66	100.02	99.90	100.39	99.31	99.40
Oxygens	8	8	8	8	8	8	8
Si	2.866	3.039	2.823	2.821	3.073	2.833	2.838
Ti	0.000	0.000	0.000	0.000	0.000	0.001	0.000
Al	1.233	1.079	1.270	1.280	1.073	1.266	1.258
Cr	0.001	0.001	0.001	0.000	0.001	0.000	0.000
Fe3	0.001	0.003	0.003	0.000	0.000	0.001	0.002
Fe2	0.000	0.000	0.000	0.000	0.000	0.000	0.000
Mn	0.001	0.001	0.001	0.000	0.001	0.001	0.000
Mg	0.001	0.002	0.001	0.000	0.001	0.001	0.001
Ca	0.206	0.051	0.247	0.243	0.014	0.214	0.231
Na	0.825	0.988	0.776	0.766	0.903	0.842	0.792
K	0.011	0.005	0.017	0.012	0.006	0.019	0.018
Totals	5.144	5.168	5.138	5.122	5.071	5.179	5.141
Xan	0.198	0.048	0.237	0.238	0.015	0.199	0.222
Xab	0.792	0.947	0.746	0.750	0.979	0.783	0.761
Xor	0.010	0.005	0.016	0.011	0.007	0.018	0.017

Appendix 5 - XRF analysis

Appendix 5.1 - Samples and descriptions

Table A5.1 - Sample list

Sample	Locality	L type	Description
Leucosomes			
D1	**2**	**Lc2**	Sample from centre of pale pink large melt.
D9	**2**	**Lc2**	Core of 3cm wide leucosome.
D24	**3**	**Lc5**	Large leucosome from that cross cuts all foliations.
97	**4**	**Lc3**	Wide cordierite rich leucosome.
98b	**4**	**Lc2**	Smaller, finer grained leucosome.
99	**4**	**Lc3**	Large, patchy leucosome with large K-feldspar crystals.
100	**4**	**Lc3**	Large pale pink, coarse leucosome that runs vertically through the outcrop.
101a	**4**	**Lc2**	Smaller pale pink, cordierite rich leucosome.
105	**6**	**Lc2**	Pale pegmatitic leucosome in the north of the quarry.
107	**6**	**Lc3**	Dark pink K-feldspar rich leucosome up to 2 metres in length.
109	**6**	**Lc3**	Pale cream leucosome, intimate to the mesosome material.
110	**6**	**Lc5**	Orange/pink leucosome.
111	**6**	**Lc5**	Wide orange granitic sheet from the south of the quarry.
115	**6**	**Lc5**	Thick, white leucosomes, metres in length.
116	**6**	**Lc2**	White, small, elongate leucosome.
117	**6**	**Lc2**	Generally concordant, coarse grained white leucosome.
D36	**7**	**Lc3**	Wide syn-F3 leucosome boundary with a cordierite patch.
D41	**7**	**Lc2**	Sillimanite-rich pod in a 4 cm wide leucosome.
18	**12**	**Lc1**	Small thin leucosome.
20	**12**	**Lc1**	Coarse grained leucosome consisting mostly of white K-feldspar.
21	**19**	**Lc2**	White K-feldspar rich, coarse grained leucosome with cordierite rich patches.
144	**19**	**Lc1**	Thin, white, elongate leucosome.
Mesosomes			
D25	**3**	**meso**	Leucosome/mesosome from the same boundary as above
101B	**4**	**meso**	Mesosome sample from near 101A.
102	**5**	**meso**	Mesosome sample near to a 2 cm wide leucosome with a 5 mm thick selvage.
118	**6**	**meso**	Mesosome sample with high garnet content.
24	**19**	**meso**	Coarser mesosome material with elongate prisms.

Appendix 5.2 -Results

Table 5.2a - Major element XRF data. (wt%)

Sample	SiO_2	Al_2O_3	Fe_2O_3	MgO	CaO	Na_2O	K_2O	TiO_2	MnO	P_2O_5	Total	Fe+Mg	(A/CNK)	X_{Mg}
Leucosomes														
2/D1	75.16	13.61	2.17	0.20	0.70	3.03	3.89	0.01	0.35	0.12	99.23	2.37	1.30	0.14
2/D9	80.77	12.56	0.22	0.09	0.97	2.95	2.78	0.03	0.00	0.13	100.50	0.31	1.31	0.42
3/D24	73.80	14.80	1.51	0.18	1.40	4.94	2.08	0.02	0.04	0.16	98.92	1.69	1.15	0.18
4/97	67.93	17.67	1.98	0.51	2.55	5.95	2.83	0.08	0.02	0.09	99.59	2.49	1.01	0.31
4/98	72.65	14.26	0.57	0.16	0.59	2.17	7.88	0.04	0.00	0.12	98.44	0.73	1.08	0.33
4/99	70.58	14.29	1.32	0.39	1.05	2.78	5.73	0.10	0.01	0.09	96.36	1.71	1.13	0.34
4/100	71.83	14.19	0.66	0.28	0.31	2.79	8.44	0.11	0.00	0.10	98.69	0.94	0.99	0.43
4/101A	72.93	13.84	1.38	0.50	0.81	2.62	6.68	0.18	0.01	0.09	99.03	1.88	1.06	0.39
6/105	71.21	14.63	5.69	0.86	2.17	3.75	1.08	0.04	0.07	0.10	99.60	6.55	1.30	0.21
6/107	71.66	14.92	0.34	0.11	0.25	2.19	8.88	0.04	0.00	0.17	98.55	0.45	1.09	0.37
6/111	71.98	15.14	0.63	0.16	1.82	4.32	3.78	0.06	0.01	0.12	98.02	0.79	1.04	0.31
6/115	73.96	13.82	0.24	0.07	0.77	2.79	6.20	0.02	0.00	0.14	98.00	0.31	1.09	0.34
6/116	79.61	10.38	0.43	0.18	0.68	1.95	4.51	0.05	0.00	0.11	97.89	0.61	1.11	0.43
6/117	73.44	13.94	1.39	0.06	0.52	3.36	5.40	0.05	0.01	0.14	98.28	1.45	1.13	0.07
7/D36	73.51	13.97	0.94	0.28	0.89	2.86	5.90	0.15	0.01	0.11	98.61	1.22	1.10	0.35
7/D41	65.89	14.12	10.02	1.94	0.52	1.33	5.01	0.22	0.13	0.10	99.28	11.96	1.65	0.26
12/18	59.85	18.02	9.00	3.53	0.71	1.65	3.73	0.85	0.03	0.08	97.45	12.53	2.24	0.41
12/20	65.02	17.36	4.09	1.00	0.52	2.41	7.41	0.19	0.05	0.18	98.23	5.09	1.34	0.30
19/21	71.21	14.71	0.61	0.24	0.49	1.51	8.36	0.03	0.01	0.41	97.58	0.85	1.18	0.41
19/144	73.65	12.93	2.70	1.09	1.18	1.96	2.86	0.14	0.05	0.88	97.45	3.79	1.53	0.42
Mesosomes														
3/D25	51.58	22.27	12.12	4.24	1.21	3.70	2.12	1.07	0.08	0.06	98.43	16.36	2.10	0.38
4/101B	61.33	16.29	8.52	2.77	1.35	2.73	3.96	0.90	0.04	0.07	97.96	11.29	1.45	0.37
5/102A	45.60	22.90	15.48	6.15	0.21	0.35	4.23	1.59	0.09	0.09	96.68	21.63	4.14	0.41
6/118	54.27	20.93	10.91	4.37	0.80	1.94	3.82	1.01	0.09	0.07	98.19	15.28	2.38	0.42
19/24	57.91	19.79	8.92	3.25	1.21	2.24	3.61	0.78	0.08	0.14	97.93	12.17	2.02	0.39

Table 5.2b - Calculated norms for leucosome data.

	Qtz	Cor	Orth	Alb	An
2/D1	41.5	3.46	23.16	25.83	2.71
2/D9	50.87	3.23	16.35	24.84	3.94
3/D24	34.66	2.28	12.42	42.25	5.96
4/97	16.58	0.4	16.79	50.54	12.11
4/98	29.16	1.4	47.31	18.65	2.18
4/99	31.04	1.89	35.15	24.42	4.8
4/100	22.79	0.14	50.53	23.92	0.9
4/101A	30.19	1.05	39.86	22.38	3.46
6/105	39.77	3.6	6.41	31.86	10.15
6/107	25.08	1.68	53.24	18.8	0.13
6/111	29.16	0.94	22.79	37.29	8.41
6/115	33.31	1.48	37.38	24.09	2.96
6/116	50.66	1.35	27.22	16.85	2.71
6/117	32.98	1.99	32.46	28.92	1.69
7/D36	32.73	1.55	35.35	24.54	3.75
7/D41	35.51	5.85	29.82	11.34	1.94
12/18	30.19	10.43	22.62	14.33	3.08
12/20	20.92	4.95	44.58	20.76	1.43
19/21	30.83	3.26	50.64	13.1	0
19/144	50.94	6.74	17.35	17.02	0.11

Table 5.3a - Raw XRF trace element data. (ppm)

Sample	Mo	Nb	Zr	Y	Sr	U	Rb	Th	Pb	Zn	Cu	Ni	Cr	Ce	Nd	La	V	Ba	Sc	S (%)
Leucosomes																				
2/D1	0	0.8	57.1	11.6	45.4	15.9	149.3	-0.8	18.4	14.9	1.8	-0.1	6.1	9.2	0.2	0.4	0	139.6	3.9	-0.01
2/D9	0.6	1.2	4	4.7	99.1	2.7	97.5	-2.3	12.9	8.2	0	0	10.6	-2.7	0.3	-7.1	17.5	567.3	-2.4	-0.02
3/D24	0.6	1.4	9.7	9.5	64	4.3	62.1	-2	16.7	14.2	13.1	9.5	13.4	13.4	3.9	2.9	6.2	96	2.7	0.07
4/97	0.4	3.6	71.4	12.6	195	4.3	86.6	8	28.5	26	11.2	6.9	21.9	49.1	15.8	21.9	15.1	252.9	6.9	0.01
4/98	0.2	2.3	20.5	7.8	178	4.3	249.4	4.5	49.5	11.8	2.9	0.7	8	34.9	4.7	12	5.7	868	-1.5	-0.01
4/99	0.8	4.8	90.1	9.9	171.7	3.3	207.4	18.1	37.7	24.2	6	5.6	18.4	76	27.9	30.4	15.3	597	1.9	-0.01
4/100	0.6	7.2	5.2	5.5	179.8	2.5	298.8	-0.4	46.5	20.6	0.6	3.9	18	13.4	1	2.9	16.3	940.9	-1.2	-0.01
4/101A	0.9	6.8	53.4	6.2	184.1	2.5	216.4	6.5	42.8	54.9	9.9	9.7	33.8	35.8	10.8	16.3	25.4	745.8	1.3	0
6/105	0	1.1	43.2	40.2	157.2	0.9	30.8	2.1	13.7	50.4	6.9	4.1	30.9	22.5	8.4	8.9	8.3	116.7	21.1	0
6/107	0.3	2	32.2	6.7	214.7	3.6	302.7	10.2	46.5	9	4	3.6	3.9	46.1	14.6	17.4	3.6	1323.5	0.4	-0.02
6/109	0.3	2.7	12.5	4.5	213.4	2.8	229.4	0.1	39.5	9.7	0.1	2.3	6.3	16.7	-1	3.3	2.8	1079.8	1	-0.01
6/110	0.1	32.1	207	24.2	60.6	0.8	300.1	19.8	5.7	205.7	7.6	101.6	250.3	43.2	28.8	18.5	223.6	492.8	18.2	-0.02
6/111	0.2	2.9	15.1	4.7	200.9	3.9	120.3	2.3	22.5	11.7	-0.4	1.8	9.3	38.5	11.8	11.2	8.2	527.1	-0.9	-0.02
6/115	0.2	1.1	32.7	4	211	2.4	209.4	-2	39.2	4.6	4.9	2.6	0.8	9.9	-4.5	1.4	1.7	1002.3	2.1	-0.02
6/116	0.3	1.7	13.1	4.4	155.9	3.2	139.2	-0.2	27.6	10.9	3.3	1.7	7.9	13.2	2.2	2.5	10	864.1	-0.1	-0.02
6/117	0.1	15.8	22.6	24.5	20.2	10.9	418.6	6.8	29.9	54.1	3.1	0.4	6.2	22.2	7.6	4.4	0.2	39.7	2.4	-0.02
7/D36	0.8	3.1	107.4	7.3	176.3	4	156.5	10.5	40.9	19.2	2.7	4.6	5.8	48.6	18.8	17.1	16.2	781.1	1	-0.02
7/D41	0.9	4.9	152.5	47.7	132.1	1.7	152.6	19.8	41.8	49.1	43.3	27.9	62.8	63.5	26.1	29.5	43.4	756.3	32.8	0.03
12/18	0.7	18.1	192.2	24.4	101.5	3.1	218.9	19	16.8	160.1	68.8	73.4	169.9	74	40.2	32.4	160.9	358	26.5	0.13
12/20	0.3	5.5	97.6	19.5	204.5	4.9	206.4	8.7	55.6	45.1	20.3	15.4	48.8	37.2	14.2	15.1	48.2	1160.7	16.4	0.02
19/21	0.1	1.7	9.3	17.7	253.1	3	279.4	-2.2	77	12.4	3	1.9	-6.9	3.6	-4.7	-10	4.2	2510.7	2.6	-0.01
19/144	-0.1	7.8	15.2	44.3	118.9	5.6	162.1	-0.1	29.2	37.9	12.3	9.1	16.5	9.4	7.1	-3.7	19.4	911.3	6.5	-0.01
Mesosomes																				
3/D25	2	22.4	173.8	25.2	127.8	-0.1	306.3	14.5	13.1	243.8	95.1	95.9	209.6	44	20.4	14	234.6	454.4	28.1	0.45
4/101B	1.8	33.9	167.1	18.8	142.7	1.2	269	15.5	45.3	320.4	57	73	189	50.7	24.1	21.6	156.9	339.6	14.7	0.14
5/102A	1	53.6	331.8	19.9	41.1	-0.6	419.7	31.9	1.6	300	125.8	128.6	373.7	74.2	48.4	12.6	394.5	399.4	38.7	0.23
6/118	0	21.8	168.8	28.1	112.2	0.9	273.3	21.4	17.8	206.1	6.7	101.1	213	73	40	37.2	210.5	543.3	20.3	-0.01
19/24	0.5	16.4	120.1	27.6	159.5	2.7	320.1	17.1	27.8	138.4	16.1	72.7	169.3	65	31.1	-27.9	171.3	712.6	26.8	-0.01

Table 5.3b - Chondrite normalised trace elements (McDonough & Sun, 1995)

Normalisation factors

U - 7.4		Ba - 2410		Rb - 2.30		Th - 29		Nb - 0.24		La - 237		Ce - 613		Sr - 7.25		Nd - 457		Zr - 3.82	
Y 1.57		Pb - 2470		Zn - 310		Cu - 120		Ni - 10500		Sc - 5.92		V -56		Cr -2560		Mo - 900			
	U	**Ba**	**Rb**	**Th**	**Nb**	**La**	**Ce**	**Sr**	**Nd**	**Zr**	**Y**	**Pb**	**Zn**	**Cu**	**Ni**	**Sc**	**V**	**Cr**	**Mo**
Leucosomes																			
2/D1	2148.6	57.9	64.9		3.3	1.7	15.0	6.3	0.4	14.9	7.4	33.5				0.7			
2/D9	364.9	235.4	42.4		5.0			13.7	0.7	1.0	3.0	23.5					0.3		0.7
3/D24	581.1	39.8	27.0		5.8	12.2	21.9	8.8	8.5	2.5	6.1	30.4		0.1		0.5	0.1		0.7
4/97	581.1	104.9	37.7	275.9	15.0	92.4	80.1	26.9	34.6	18.7	8.0	51.8	0.1	0.1		1.2	0.3		0.4
4/98	581.1	360.2	108.4	155.2	9.6	50.6	56.9	24.6	10.3	5.4	5.0	90.0					0.1		0.2
4/99	445.9	247.7	90.2	624.1	20.0	128.3	124.0	23.7	61.1	23.6	6.3	68.5	0.1	0.1		0.3	0.3		0.9
4/100	337.8	390.4	129.9		30.0	12.2	21.9	24.8	2.2	1.4	3.5	84.5	0.1				0.3		0.7
4/101A	337.8	309.5	94.1	224.1	28.3	68.8	58.4	25.4	23.6	14.0	3.9	77.8	0.2	0.1		0.2	0.5		1.0
6/105	121.6	48.4	13.4	72.4	4.6	37.6	36.7	21.7	18.4	11.3	25.6	24.9	0.2	0.1		3.6	0.1		
6/107	486.5	549.2	131.6	351.7	8.3	73.4	75.2	29.6	31.9	8.4	4.3	84.5				0.1	0.1		0.3
6/109	378.4	448.0	99.7	3.4	11.3	13.9	27.2	29.4		3.3	2.9	71.8				0.2	0.1		0.3
6/110	108.1	204.5	130.5	682.8	133.8	78.1	70.5	8.4	63.0	54.2	15.4	10.4	0.7	0.1		3.1	4.0	0.1	0.1
6/111	527.0	218.7	52.3	79.3	12.1	47.3	62.8	27.7	25.8	4.0	3.0	40.9					0.1		0.2
6/115	324.3	415.9	91.0		4.6	5.9	16.2	29.1		8.6	2.5	71.3				0.4			0.2
6/116	432.4	358.5	60.5		7.1	10.5	21.5	21.5	4.8	3.4	2.8	50.2					0.2		0.3
6/117	1473.0	16.5	182.0	234.5	65.8	18.6	36.2	2.8	16.6	5.9	15.6	54.4	0.2			0.4			0.1
7/D36	540.5	324.1	68.0	362.1	12.9	72.2	79.3	24.3	41.1	28.1	4.6	74.4	0.1			0.2	0.3		0.9
7/D41	229.7	313.8	66.3	682.8	20.4	124.5	103.6	18.2	57.1	39.9	30.4	76.0	0.2	0.4		5.5	0.8		1.0
12/18	418.9	148.5	95.2	655.2	75.4	136.7	120.7	14.0	88.0	50.3	15.5	30.5	0.5	0.6		4.5	2.9	0.1	0.8
12/20	662.2	481.6	89.7	300.0	22.9	63.7	60.7	28.2	31.1	25.5	12.4	101.1	0.1	0.2		2.8	0.9		0.3
19/21	405.4	1041.8	121.5		7.1		5.9	34.9		2.4	11.3	140.0				0.4	0.1		0.1
19/144	756.8	378.1	70.5		32.5		15.3	16.4	15.5	4.0	28.2	53.1	0.1	0.1		1.1	0.3		
Mesosomes																			
3/D25		188.5	133.2	500.0	93.3	59.1	71.8	17.6	44.6	45.5	16.1	23.8	0.8	0.8		4.7	4.2	0.1	2.2
4/101B	162.2	140.9	117.0	534.5	141.3	91.1	82.7	19.7	52.7	43.7	12.0	82.4	1.0	0.5		2.5	2.8	0.1	2.0
5/102A		165.7	182.5	1100.0	223.3	53.2	121.0	5.7	105.9	86.9	12.7	2.9	1.0	1.0		6.5	7.0	0.1	1.1
6/118	121.6	225.4	118.8	737.9	90.8	157.0	119.1	15.5	87.5	44.2	17.9	32.4	0.7	0.1		3.4	3.8	0.1	
19/24	364.9	295.7	139.2	589.7	68.3		106.0	22.0	68.1	31.4	17.6	50.5	0.4	0.1		4.5	3.1	0.1	0.6

Figure A5.1 - Chondrite normalised trace element plot for southern localities 2+3 (McDonough and Sun, 1995)

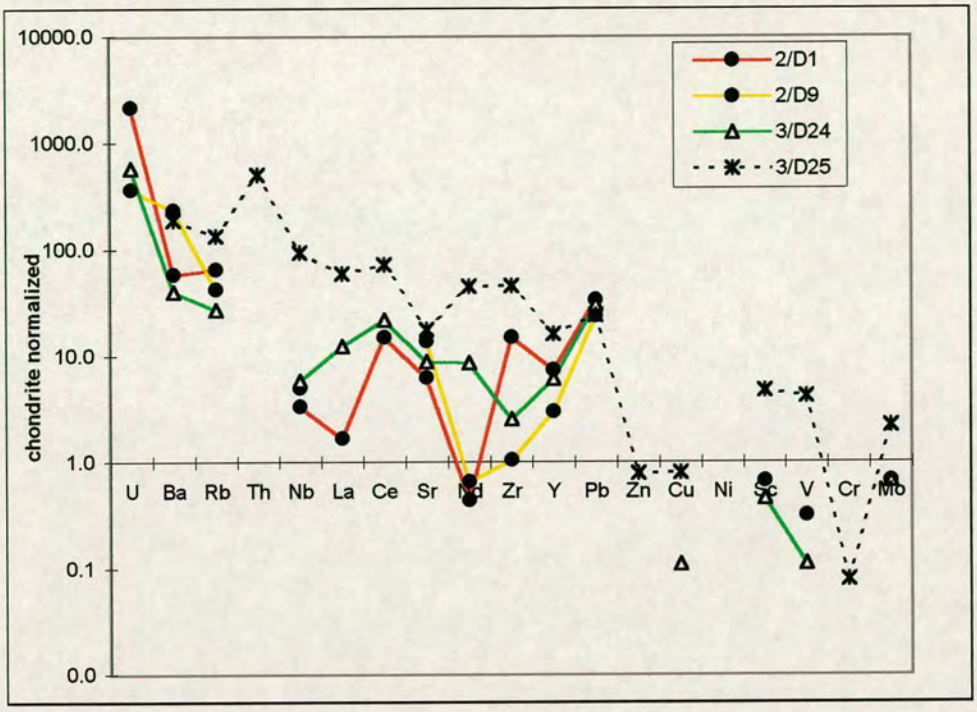

Figure A5.2 - Chondrite normalised trace element plot for southern locality 4 (McDonough and Sun (1995).

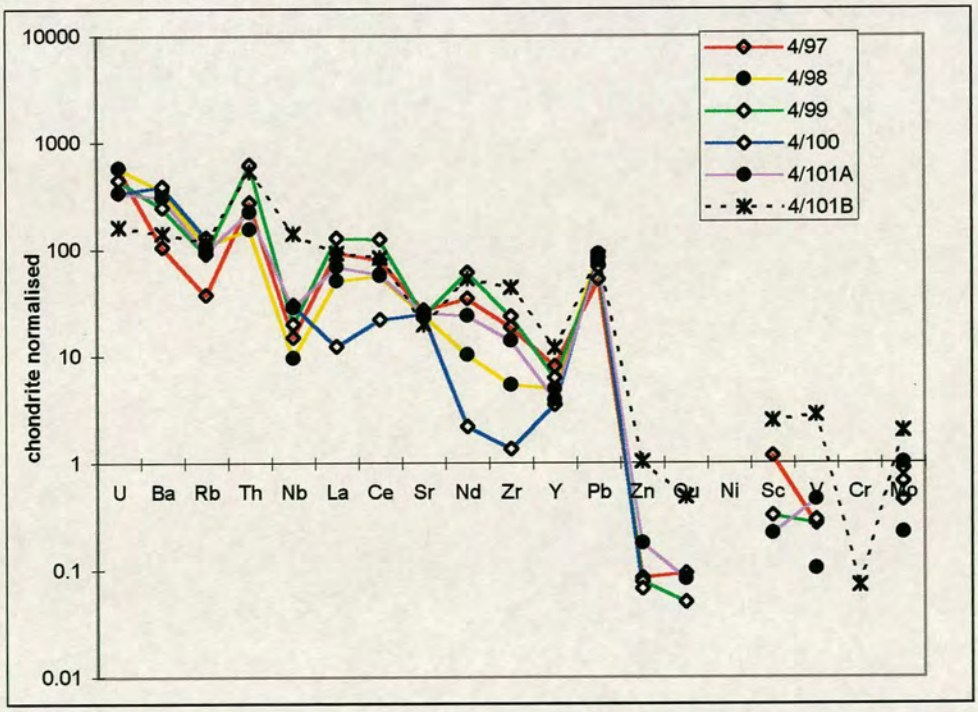

Key
Empty squares = Lc1 Leucosomes, Filled circles = Lc2 Leucosomes
Empty diamonds = Lc3 Leucosomes, Empty triangles = Lc5 Leucosomes

Figure A5.3 - Chondrite normalised trace element plot for middle locality 6 (McDonough and Sun (1995).

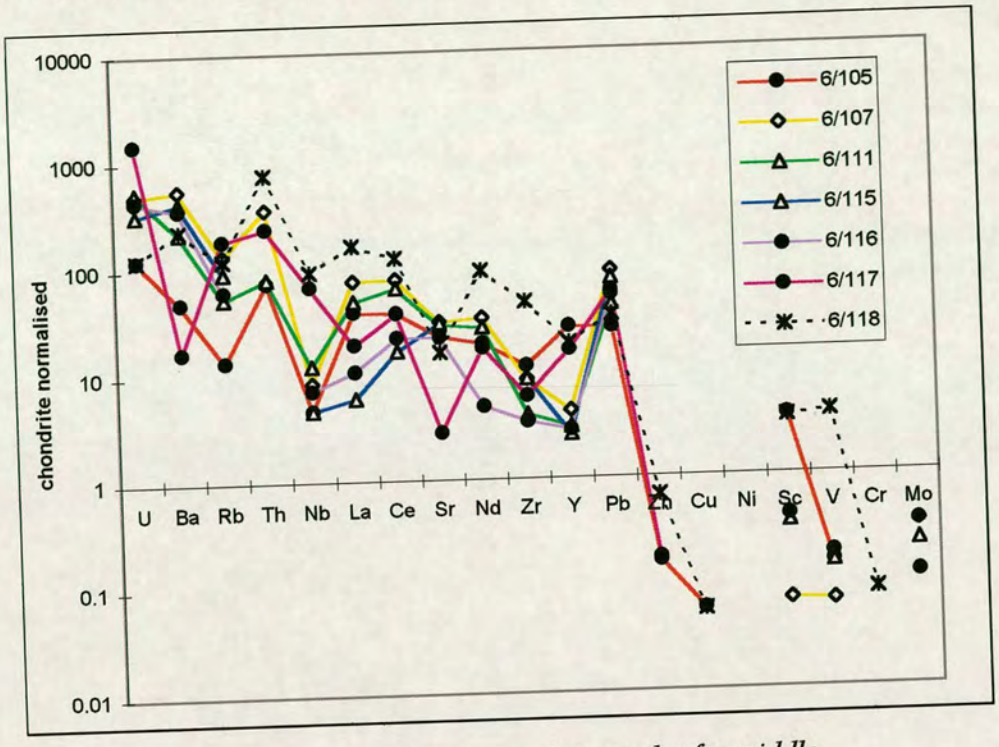

Figure A5.4 - Chondrite normalised trace element plot for middle locality 7 (McDonough and Sun (1995).

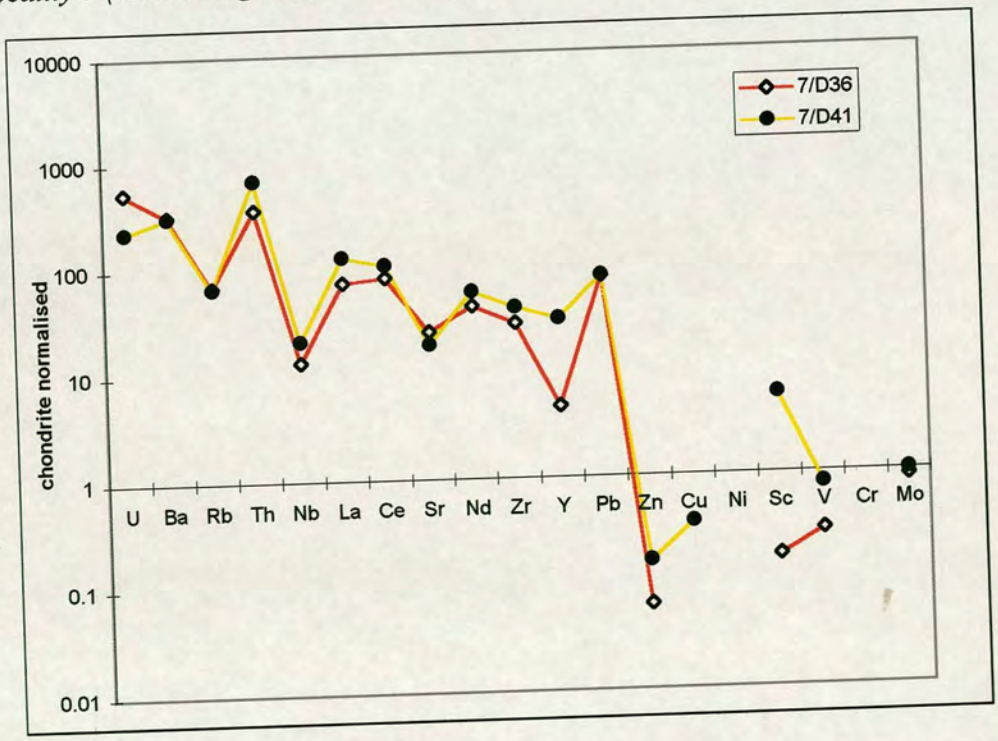

Key
Empty squares = Lc1 Leucosomes, Filled circles = Lc2 Leucosomes
Empty diamonds = Lc3 Leucosomes, Empty triangles = Lc5 Leucosomes

Figure A5.5 - Chondrite normalised trace element plot for northern northern localities 12+19 (McDonough and Sun (1995).

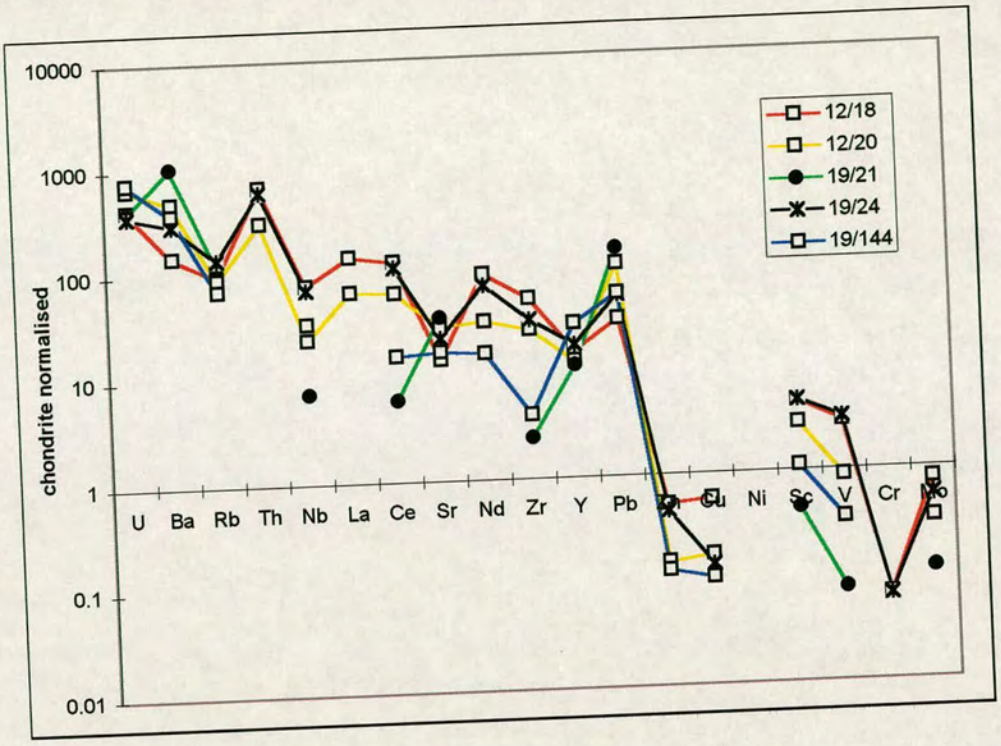

Key

Empty squares = Lc1 Leucosomes, Filled circles = Lc2 Leucosomes
Empty diamonds = Lc3 Leucosomes, Empty triangles = Lc5 Leucosomes

Appendix 6 - Geothermobarometry

A6.1 – Garnet-biotite or garnet-cordierite geothermometers

These two types of thermometer are based upon two exchange reactions:

Fe-cordierite + Mg-garnet = Mg-cordierite + Fe-garnet (a)

Fe-biotite + Mg-garnet = Mg-biotite + Fe-garnet (b)

In order to calculate the K_D values of the reactions, the X_{Mg} of the phases must first be calculated following equation 1 using the wt% oxides of the phases.

$$X_{Mg} = \left(\frac{40.32Mg}{(40.32Mg)(71.85Fe)} \right) \quad (1)$$

From this it is possible to calculate the K_D value of the phases.

Garnet-cordierite

$$K_D = \left(\frac{X_{Mg}}{1 - X_{Mg}} \right)^{crd} \left(\frac{1 - X_{Mg}}{X_{Mg}} \right)^{grt} \quad (2)$$

Garnet-biotite

$$K_D = \left(\frac{1 - X_{Mg}}{X_{Mg}} \right)^{grt} \left(\frac{X_{Mg}}{1 - X_{Mg}} \right)^{bt} \quad (3)$$

The K_D values for Ferry and Spear (1978) are reversed thus:

F&S $$K_D = \left(\frac{1 - X_{Mg}}{X_{Mg}} \right)^{bt} \left(\frac{X_{Mg}}{1 - X_{Mg}} \right)^{grt} \quad (4)$$

The five thermometers used in this study are outlined below.

A6.1.1 - Garnet-biotite thermometers

These exchange thermometers are usually derived by experimentally determining the slope of the reaction in PT space. The two thermometers of Ferry and Spear (1978) and Perchuk and Lavrent'eva (1983) were experimentally determined in systems of different compositions. The former had a bulk composition of X_{Fe} 0.9 whilst that latter favours an X_{Fe} of 0.6. Thompson (1976) calibrated his thermometer with the K_D values of natural assemblages.

Perchuk and Lavrent'eva (1983)

$$T°C = \frac{7843.7}{1.987 \ln K_D + 5.699} - 273 \qquad (5)$$

Thompson (1976)

$$T°C = \left(\frac{2800}{LnK_D + 1.62} \right) - 273 \qquad (6)$$

Ferry and Spear (1978)

$$T°C = \left(\frac{2109}{LnK_D - 0.782} \right) - 273 \qquad (7)$$

A6.1.2 - Garnet-cordierite thermometers

The thermometer of Perchuk and Lavrent'eva (1983) is based on experiments with phase compositions comparable to their natural counterparts. The K_D values for their experiments were consistent over a wide range of X_{Mg}.

Perchuk and Lavrent'eva (1983)

$$T°C = \frac{3020 - 0.018P(bars)}{1.287 + \ln K_D} - 273 \qquad (8)$$

Aranovich and Podlesski (1983)

$$T°C = \left(\frac{3087 + (17.8 * Pkbar)}{1.343 + LnK_D} \right) - 273 \qquad (9)$$

A6.2 – Garnet-cordierite-sillimanite-quartz barometers

These barometers are based on the following reaction:

$3(Fe\text{-}Mg)Cordierite.H_2O = 2(Fe\text{-}Mg)Garnet + 4Sillimanite + 5Quartz$ (c)

The slope has a positive dP/dT slope depending upon the water content of the equilibrium cordierite (Aranovich and Podlesski, 1983; Mukhopadyay and Holdaway, 1994; Carey, 1995). The position of the curve was derived from thermodynamic treatments of experimental data for the barometers of Mukhopadyay and Holdaway (1994) and Carey (1995), whilst Waters and Whales (1984) utilised the experiments of Holdaway and Lee (1977).

By measuring the molar heat capacity and enthalpy of hydration of cordierite under varying PT conditions Carey (1995) was able to derive a thermodynamic formulation of hydrous Mg-cordierite, and thus predict the saturation H_2O contents of cordierite as a function of temperature and fugacity. The equation to derive the range of H_2O contents expresses them as n moles of H_2O per formula unit. Using PT estimates of previous workers an n value of 0.6 was used to derive a final PT for this study. These values can then be inputted into reaction 3 in order to derive pressures and temperatures for a given X_{Crd}^{Mg} and X_{Grt}^{Mg}, assuming $a_{H2O}=1$.

Mukhopadyay and Holdaway (1994) experimentally derived reaction 3 and then analysed the resulting volatile contents of the cordierite. From this they then formulated their own wt% H_2O values and extrapolated their own n values. Both of these barometers produced an equation for hydrous and non-hydrous cordierite. Waters and Whales (1984) used the model of Newton and Wood (1979) for the water content of cordierite.

Carey (1995) - anhydrous barometer

$$P(bar) = 5.2509 * T(K) + 1586 + 6RT \ln\left(\frac{a_{MgCrd}^{Crd}}{a_{Pyrope}^{Grt}}\right) \quad (10)$$

Carey (1995) - hydrous barometer

If equation 10 is termed y then

$$P(bar) = y - (RT(K) * 3\ln(1 - ncrd)) \quad (11)$$

n = moles of H_2O per formula unit of cordierite, n<1

Mukhopadyay and Holdaway (1994) - anhydrous barometer

$$P(bar) = 5.95 * T(K) - 4289 - RT(^{\circ}K)6 * \ln\left(\frac{1 - X_{Mgcrd}}{1 - X_{Mggrt}}\right) \quad (12)$$

Mukhopadyay and Holdaway (1994) - hydrous barometer

If equation 12 is termed x then

$$P(bar) = x - (RT(^{\circ}K) * 3\ln(1 - ncrd)) \quad (13)$$

Waters and Whales (1984)

$$P(bar) = 9500 - T(K) * \left(\frac{4.9 + 6\ln K + 3\ln(1 - ncrd)}{1.842}\right) \quad (14)$$

A6.3 – Error propagation

Many of the papers used in the PT calculations did not quote errors. Thus errors were calculated using an approximation for the standard deviation of a function of several variables:

e.g $y = f(x_1, x_2)$ (15)

$$y = \sigma_{x_1}^2 \left[\frac{\partial f}{\partial x_1}\right] + \sigma_{x_2}^2 \left[\frac{\partial f}{\partial x_2}\right] + 2\sigma x_{x_1 x_2} \left[\frac{\partial f}{dx_1} . \frac{\partial f}{dx_2}\right] \quad (16)$$

where $\sigma_{x_1}^2$ is the variance of x_1 and $\sigma_{x_i x_j}$ is the covariance of x_i and x_j.

For the barometers and thermometers used in this study, the pressures and temperatures are each calculated as functions of several variables, wt% oxides of FeO and MgO in garnet, biotite, cordierite, n_{crd} and estimated pressure and temperature on P_0 and T_0. The variance of each oxide and ncrd was calculated as 5% relative to each oxide with a cut off of 0.01%.

e.g. if $Wt\%_{MgO}^{Grt} = 12\%$ then $\sigma^2_{wt\%_{Mg}^{Grt}} = \left[12 * \frac{5}{100} + 0.01\right]$ (17)

$= 0.61$

An assumed standard deviation of ±50°C and 1 kbar for pressure and temperature gave $\sigma_T = 50^2 = 2500°C$ and σ_P = I kbar. In the absence of a reasonable method of estimating correlation between variables, all $\sigma_{x_i x_j}$ were set at 0. All partial derivatives $\frac{\partial f}{\partial x_i}$ were calculated by finite differences .

Table A6.1 - Example calculation for the garnet/biotite thermometer of Thompson (1976) for sample 83 (Locality 2):

	Grt		Bt	
	MgO	**FeO**	**MgO**	**FeO**
Wt%	5.06	64.65	8.85	20.18
σ^2	0.07	3.04	0.20	1.04
$\frac{\partial f}{\partial x_i}$	74.71	-10.83	-42.41	18.73

Hence $\sigma_T^2 = 0.07 * [74.71]^2 + 3.04 * [-10.83]^2 + 0.20 * [-42.21]^2 + 1.04[18.73]^2$

$\sigma_T^2 = 1475.33$

So $\sigma_T = \pm 38.41°C$ at 1 standard deviation

Or $\sigma_T = \pm 76.82°C$ at 2 standard deviations

Since any correlations between variables are assumed zero (all $\sigma_{x_i x_j} = 0$) it is preferred to express errors at 2 standard deviations. The results off all exchange geothermobarometers and associated errors to two standard deviations can be seen in Table A6.2.

Table A6.2 - PT calculations made using conventional Fe-Mg exchange equilibria Errors are to two standard deviations.

Sample	Locality 3 88C/M		88R/I		90C/M		90R/I		Locality 2 83C/M		83R/I		D18C/M		D18R/I		Locality 4 10C/M	
Thermometer																		
F&S	552	+/-65	329	+/-50	556	+/-101	385	+/-44	848	+/-121	568	+/-68	751	+/-101	477	+/-54	870	+/-125
PLGB	577	+/-37	433	+/-32	579	+/-47	473	+/-30	722	+/-51	586	+/-38	679	+/-47	533	+/-33	731	+/-52
TH	552	+/-49	372	+/-40	555	+/-68	419	+/-36	757	+/-77	564	+/-51	693	+/-68	494	+/-43	770	+/-79
A&P	740	+/-56	632	+/-47	808	+/-68	658	+/-47	757	+/-69	nc	nc	737	+/-66	648	+/-56	800	+/-74
PLGC	708	+/-54	605	+/-45	773	+/-66	629	+/-45	722	+/-67	nc	nc	702	+/-64	621	+/-54	764	+/-72
Barometer																		
PCarey	3.03	+/-0.54	2.10	+/-0.56	3.88	+/-0.52	2.68	+/-0.52	3.56	+/-0.53	nc	nc	3.04	+/-0.53	2.29	+/-0.53	3.84	+/-0.54
P Muk	3.54	+/-0.64	3.02	+/-0.63	3.78	+/-0.72	3.33	+/-0.76	3.93	+/-0.70	nc	nc	3.61	+/-0.71	3.03	+/-0.72	3.82	+/-0.70
PHCarey	4.49	+/-0.71	3.41	+/-0.72	5.34	+/-0.65	4.00	+/-0.61	5.02	+/-0.65	nc	nc	4.50	+/-0.65	3.60	+/-0.63	5.30	+/-0.66
PH-Muk	4.97	+/-0.90	4.31	+/-0.91	5.21	+/-0.91	4.62	+/-0.95	5.37	+/-0.90	nc	nc	5.05	+/-0.90	4.33	+/-0.92	5.26	+/-0.89
PWaters	4.20	+/-0.96	3.88	+/-1.03	5.09	+/-0.86	4.49	+/-0.98	4.76	+/-0.87	nc	nc	4.21	+/-0.88	4.08	+/-0.94	5.05	+/-0.85

Sample	10R/I		15C/M		Locality 8 123C/M		123R/I		Locality 7 36C/M		36R/I		D41C/M		D41C/M		Locality 6 114C/M	
Thermometer																		
F&S	566	+/-68	697	+/-91	634	+/-79	432	+/-48	685	+/-88	698	+/-91	904	+/-133	524	+/-61	849	+/-121
PLGB	584	+/-38	653	+/-44	622	+/-41	504	+/-31	648	+/-44	654	+/-44	745	+/-53	561	+/-36	722	+/-51
TH	561	+/-51	656	+/-63	612	+/-57	458	+/-39	648	+/-62	657	+/-63	792	+/-82	531	+/-47	757	+/-77
A&P	613	+/-52	nc	nc	638	+/-54	518	+/-41	675	+/-58	676	+/-59	nc	nc	681	+/-59	nc	nc
PLGC	586	+/-50	nc	nc	605	+/-52	487	+/-39	641	+/-56	641	+/-54	nc	nc	647	+/-57	nc	nc
Barometer																		
PCarey	2.27	+/-0.54	nc	nc	1.54	+/-0.53	1.55	+/-0.55	3.09	+/-0.52	nc	nc	nc	nc	3.86	+/-0.52	nc	nc
P Muk	4.17	+/-0.71	nc	nc	4.87	+/-0.72	3.98	+/-0.76	4.30	+/-0.73	nc	nc	nc	nc	4.06	+/-0.72	nc	nc
PHCarey	3.73	+/-0.63	nc	nc	3.00	+/-0.63	2.86	+/-0.62	4.55	+/-0.63	nc	nc	nc	nc	5.32	+/-0.63	nc	nc
PH-Muk	5.61	+/-0.91	nc	nc	6.30	+/-0.92	5.27	+/-0.95	5.74	+/-0.92	nc	nc	nc	nc	5.49	+/-0.92	nc	nc
PWaters	3.40	+/-0.99	nc	nc	2.64	+/-0.95	3.31	+/-1.06	4.26	+/-0.92	nc	nc	nc	nc	5.06	+/-0.91	nc	nc

Sample	114R/I		118C/M		118R/I	
Thermometer						
F&S	614	+/-76	852	+/-122	752	+/-101
PLGB	611	+/-40	724	+/-51	680	+/-47
TH	598	+/-55	759	+/-77	694	+/-68
A&P	nc	nc	794	+/-74	773	+/-71
PLGC	nc	nc	758	+/-72	737	+/-69
Barometer						
PCarey	nc	nc	3.91	+/-0.53	3.59	+/-0.52
P Muk	nc	nc	3.94	+/-0.71	3.21	+/-0.71
PHCarey	nc	nc	5.37	+/-0.66	4.90	+/-0.65
PH-Muk	nc	nc	5.37	+/-0.90	4.51	+/-0.91
PWaters	nc	nc	5.12	+/-0.84	5.44	+/-0.85

A6.4 - THERMOCALC calculations

Rather than take a single experimentally derived exchange reaction the thermodynamics for a given reaction can be derived from an internally consistent thermodynamic dataset, in this case that of Powell and Holland (1988) and Holland and Powell (1990). Thus the reactions within a given assemblage can be calculated with all of the available experimental information on phase end members (Powell and Holland, 1994). From all of the data a best fit average PT can be calculated using a least squares method which averages the data for an independent set of reactions within a rock (Powell and Holland 1993; 1994). These calculations are carried out using the computer programme THERMOCALC, which utilising the dataset of 123 end members, can calculate reaction position appropriate to the compositions of complex solid solutions.

The input file for THERMOCALC requires the activities of all the phases in an equilibrium assemblage. Thus textural and compositional data is studied so that the peak assemblages can be defined and in the case of the Turku rocks this is invariably grt + crd + bio + kfs + plag + qtz. The activities of the phase end members are calculated through AX, a program that takes mineral analyses (in oxides) and calculates the activities of the mineral end members. The activities calculated can be found in Appendix 4.6.

Figure A6.1 - Sample AX input file, 118.dat. The columns are wt % oxides derived from the CAMEBAX Electron Microprobe, University of Edinburgh, for operating conditions and errors see Appendix 4.2 and 4.3.

SiO_2	TiO_2	Al_2O_3	Cr_2O_3	Fe_2O_3	FeO	MnO	MgO	CaO	Na_2O	K_2O
cd crd										
46.96	0.00	32.42	0.00	0.00	9.16	0.07	8.03	0.02	0.08	0.02
g grt										
37.30	0.00	21.10	0.00	0.00	34.16	0.60	5.90	0.70	0.00	0.00
fsp k-fe										
64.54	0.02	18.60	0.01	0.00	0.06	0.01	0.02	0.11	3.13	11.60
fsp plag										
61.12	0.01	23.32	0.06	0.00	0.04	0.00	0.02	5.16	8.13	0.25
bi bio										
34.78	3.41	17.34	0.07	0.00	19.38	0.03	10.03	0.00	0.10	9.53
*										

Figure A6.2 – Ax output file and sample THERMOCALC input file with calculated end-member activities (sample- th118.dat).

```
% thermocalc file for C:\AMANDA\THESIS\CHAP6\THERM\AX\118
 crd     0.45   fcrd     0.13
  py    0.015    gr 0.0000129   alm     0.37   spss 0.0000022
 mic     0.76
  an     0.34    ab     0.73
 phl    0.037   ann    0.055  east    0.038
q
*
```

The activities of the end members are calculated at an initially estimated pressure and temperature. In the first case this was 5.5 kbar and 750°C based upon previous geothermobarometry on the terrain (Höltta, 1986; Van Duin and Nieman, 1993; Väisänen et al., 1994). The activities were ran through THERMOCALC once to derive an initial PT which was then put back into the AX file to fun through THERMOCALC a second time. Figure A6.3 is an example output (.log) file from THERMOCALC. The standard deviations used are calculated by THERMOCALC: these are larger for very low activities. As activities decrease they become progressively less well known and thus it is appropriate to make their uncertainties progressively larger (Powell, *pers. comm.*).

Figure A6.3 - Example THERMOCALC file, th118.log.

```
display/print with fixed width font (e.g. Monaco)]
running at 10.54 on Tue 7 Sep, 1999

calculation type :
    0 = table of thermodynamic data of end-members
    1 = phase diagram calculations
    2 = average pressure-temperature calculations
    3 = calculations on all reactions between end-members
    4 = list end-member names and compositions
control code  : 2
data filename: suffix in 'th.dat' : 118
reading phase info from this file ...
```

```
crd fcrd py gr alm spss mic an ab phl ann
east q
log output will be found in "th.log" (from prefs)
(thermodynamic dataset produced at )

standard default uncertainties on activities ? yes

spss is unnecessary and so is excluded
ab is unnecessary and so is excluded
type of rock calculation:
     1 : average P
     2 : average T
     3 : average PT
code : 3
Activity data from input file
         crd    fcrd      py      gr     alm      mic      an
   a   0.450   0.130  0.0150 1.27e-5   0.370    0.750   0.330
 sd(a)  0.0408  0.0319 0.00766 1.63e-5  0.0555   0.0375  0.0444

         phl     ann    east       q
   a  0.0360  0.0550  0.0380    1.00
 sd(a)  0.0142  0.0190  0.0148       0
these data ok ? yes

specification of PT window:
PT window within which average PT is expected to lie
T low, high, P low, high :  300 1000 3 10
for cordierite activity calculation
fixed a(CO2), a(H2O) :  0.684 0.222

Reactions must be reasonably linear within the window;
allowed angle change of reaction per kbar (try 1) : 1
reactions :
|X|0X|00XX

an independent set of reactions has been calculated
print the independent set of reactions and their thermodynamics ? yes

Activities and their uncertainties
             crd    fcrd      py      gr     alm      mic      an
a          0.450   0.130  0.0150 1.27e-5   0.370    0.750   0.330
sd(a)/a    0.09075 0.24533 0.51082 1.28584 0.15000  0.15000 0.13467

             phl     ann    east       q
a          0.0360  0.0550  0.0380    1.00
sd(a)/a    0.39392 0.34563 0.38888       0
```

Independent set of reactions
1) py + east + 3q = crd + phl
2) crd + 2gr + 2east + 3q = 6an + 2phl
3) 3fcrd + 2py + 2east + 6q = 5crd + 2ann
4) crd + 2alm + 2east + 6q = 3fcrd + 2phl

Calculations for the independent set of reactions
(for a(CO2) = 0.684 and a(H2O) = 0.222)

	P(T)	sd(P)	a	sd(a)	b	c	ln_K	sd(ln_K)
1	6.3	1.31	-22.22	3.47	-0.03969	5.189	3.347	0.759
2	3.6	4.12	46.91	7.01	-0.20631	5.695	16.586	2.916
3	5.3	1.48	-74.42	7.47	-0.07690	10.165	11.267	1.695
4	3.8	1.13	92.90	6.99	-0.12887	11.175	-3.442	1.366

print diagnostics only if chi^2 test fails ? yes
Average PT (for a(CO2) = 0.684 and a(H2O) = 0.222)
svd1 ...
svd2 ...
svd3 ...
Single end-member diagnostic information

avP, avT, sd's, cor, fit are result of doubling the uncertainty on ln a :
a ln a is suspect if any are v different from lsq values.
e* are ln a residuals normalised to ln a uncertainties :
large absolute values, say >2.5, point to suspect info.
hat are the diagonal elements of the hat matrix :
large values, say >0.40, point to influential data.
For 95% confidence, fit (= sd(fit)) < 1.73
however a larger value may be OK - look at the diagnostics!

	avP	sd	avT	sd	cor	fit
lsq	5.6	1.4	803	95	0.661	0.77

	P	sd(P)	T	sd(T)	cor	fit	e*	hat
crd	5.69	1.45	812	100	0.692	0.74	0.17	0.04
fcrd	5.78	1.41	844	112	0.665	0.60	-0.52	**0.25**
py	5.13	1.94	763	159	0.846	0.74	0.19	**0.67**
gr	5.51	1.40	801	95	0.664	0.75	-0.26	0.03
alm	5.57	1.38	801	101	0.605	0.77	-0.04	0.10
an	5.55	1.38	803	95	0.662	0.77	0.08	0.00
phl	5.30	1.43	795	96	0.665	0.58	-0.63	0.06
ann	5.84	1.43	798	95	0.617	0.57	0.58	0.12
east	5.64	1.76	804	95	0.551	0.77	-0.04	**0.36**
q	5.57	1.38	803	95	0.661	0.77	0	0

T = 803°C, sd = 95,
P = 5.6 kbar, sd = 1.4, cor = 0.661, sigfit = 0.77

Previous chapters have shown how the metapelites of the Turku terrain have undergone some degree of partial melting. Thus any water present in the assemblage would have partitioned into the melt phase (Powell, 1982; Waters and Whales, 1984; Waters, 1988; Harley, 1989). For this reason H_2O was not put into the input file as a free phase so THERMOCALC asks for cordierite a_{CO_2} and a_{H_2O} values. The derivation of these activities has been calculated for Turku cordierites using methods outlined in chapter 7 of this study.

THERMOCALC was asked to produce an average pressure and temperature from the assemblage inputted. The largest hat values are for pyrope, eastonite and Fe-cordierite end members which means that these had the largest influence on the pressure and temperature generated. (The hat value is a numerical measure of dependence of the pressure or temperature estimate on the composition of one particular end-member.)

A6.5 - Results

A summary compilation of the PT estimates obtained from THERMOCALC are presented in Table A6.1, whilst the PT estimates for the various exchange thermometers and barometers are compiled in Table A6.2.

Table A6.3 - THERMOCALC output, average PT results with standard deviation, for sample 12 temperature was calculated from a given pressure as THERMOCALC could not generate an average pressure or temperature.

Loc 2 - D18
T = *771°C*, sd = 93,
P = *5.6 kbar*, sd = 1.4, cor = 0.687, sigfit = 0.37
Loc 2 - 83
T = *789°C*, sd = 95,
P = *4.6 kbar*, sd = 1.4, cor = 0.649, sigfit = 0.95
Loc 3 - 88
T = *648°C*, sd = 80
P = *3.8 kbar*, sd = 1.3, cor = 0.661, sigfit =0.46
Loc 3 - 90
T = *789°C*, sd = 92
P = *5.3 kbar*, sd = 1.3, cor = 0.645, sigfit = 0.43
Loc 4 - 10
T = *818°C*, sd = 92
P = *5.5 kbar*, sd - 1.4, cor = 0.669, sigfit = 0.83
Loc 6 - 118
T = *803°C*, sd = 95,
P = *5.6 kbar*, sd = 1.4, cor = 0.661, sigfit = 0.77
Loc 7 - 36
T = *667°C*, sd = 79,
P = *4.2 kbar*, sd = 1.2, cor = 0.638, sigfit = 0.61
Loc 7 - D41
T = *816°C*, sd = 165,
P = *5.0 kbar*, sd = 2.3, cor = 0.641, sigfit = 1.69
Loc 8 - 123
T = *632°C*, sd = 76,
P = *3.7 kbar*, sd = 1.2, cor = 0.646, sigfit = 0.50

Appendix 7 - SIMS analysis of cordierite

A7.1 - Sample description and location

20 samples were analysed from 8 localities. Localities 2, 3 and 4 are from the southern zone, 6 and 7 are from the middle of the terrain and 5, 12, 17 and 20 are all northern localities. The main features of the hand specimens are compiled in Table A7.1. Cordierite was analysed within both mesosome and leucosome samples, with a diverse leucosome selection sampled. The descriptions of some of the samples analysed can be found in Appendix 4.5. The samples which were not analysed by electron probe are described in the following sections.

Table A7.1 - Additional samples used for ion probe analysis.

LOCALITY	SAMPLE	DESCRIPTION
2.2	D18	THIN GARNETIFEROUS LEUCOSOME
2.3	79	LARGE LEUCOSOME/MESOSOME BORDER
2.3	D22	OBLIQUE LEUCOSOME/MESOSOME SAMPLE BOTH CONTAIN CORDIERITE
2.4	D5	SELVAGE RICH LEUCOSOME
3	D26	CORDIERITE WITHIN MESOSOME
4	10	LAYERED MESOSOME WITH SMALL, FINE GRAINED LEUCOSOME
4	12	MESOSOME/LEUCOSOME SAMPLE WITH MESOSOME CORDIERITE
4	60	COARSE GRAINED CORDIEIRITE RICH LEUCOSOME.
4	X	CORDIERITE RICH LARGE LEUCOSOME
5	102	MESOSOME SAMPLE, THIN (2 CM) SELVAGE BOUND LEUCOSOME
5	103	CORDIERITE RICH LEUCOSOME
5	104	SMALLER SAMPLE CONTAINING MOSTLY CORDIERITE
6	17	MESOSOME/LEUCOSOME SAMPLE, CORDIERITE RICH
7	35	SMALL LEUCOSOMES LAYERED WITH MESOSOME
7	36	MESOSOME CUT BY VERY SMALL LEUCOSOMES
12	18	SMALL FINE GRAINED LEUCOSOME IN MESOSOME
12	19	MESOSOME/LEUCOSOME - WEATHERED SAMPLE
12	D45	SMALL OBLIQUE LEUCOSOME
12	D47	FOLDED LEUCOSOME BOUNDARY WITH BT RICH SELVAGE
17	145	GRANITE/MESOSOME CONTACT WITH SILLIMANITE TRAILS
20	31	MESOSOME WITH SMALL LEUCOSOMES, SILLIMANITE IS PRESENT IN THE MESOSOME.

A7.1.1 - Locality 2

Sample 79

The leucosome section of this sample contains no cordierite. It mostly consists of K-feldspar and quartz. There is a selvage zone that is rich in biotite, cordierite and quartz. The cordierites within this zone are generally elongate parallel to the edge of the leucosome. Behind the selvage is a coarse zone of cordierite, quartz and K-feldspar. The mesosome is much finer and is granular in texture.

A7.1.2 - Locality 3

Sample D26

The granuloblastic mesosome assemblage consists of quartz, plagioclase, K-feldspar and biotite (some elongate but most orientated) and large quantities of cordierite. This cordierite is not elongate and does not contain sillimanite. A garnet crystal is also present in the mesosome.

A7.1.3 - Locality 4

Sample X

This is a leucosome sample and is dominated by cordierite. The crystals are generally anhedral. At their rounded edges they have altered to a very fine grained mass of white mica. This alteration continues along cracks within the cordierite. Thus these cordierites show the first stages of pinitisation. Some of the crystals contain quartz inclusions and these are surrounded by the same micaceous rim. As well as the cordierite crystals the leucosome assemblage contains tablet like K-feldspars which also have a speckled appearance due to alteration to sericite. In between the cordierite and K-feldspar, grows interstitial quartz with a heterogeneous extinction. There is a small amount of biotite located at the edge of one of the cordierite crystals. The cordierite appears to breaking down to biotite and quartz. The biotite itself has been strongly chloritised.

A7.1.4 - Locality 5

Sample 102

A very fine grained sample of foliated biotite. There are very large cordierite crystals with foliated biotite and quartz inclusions. These cordierite crystals dominate the slide but the matrix is also composed of quartz, plagioclase and perthite.

Sample 103
This sample is dominated by leucosome bound by a selvage. The leucosome assemblage is mainly quartz and plagioclase. The other dominant mineral is the cordierite, which often contains sillimanite within the cores and is found in close association with granular plagioclase crystals. This relationship is also seen near the selvage boundary. The selvage is dominated by biotite that is full of inclusion haloes and less abundant plagioclase is present. After the selvage is the mesosome, composed of equigranular plagioclase and quartz with interstitial biotite and some cordierite.

Sample 104
104 is a leucosome sample consisting of quartz and cordierite. The cordierite shows some break down to white mica, although some crystals are in a further state of alteration than others

A7.1.5 - Locality 6

Sample 17
This sample is very coarse for a mesosome but contains too high a percentage of biotite for a leucosome. The mineralogy is mainly cordierite, biotite, K-feldspar and quartz. The cordierite mostly contains sillimanite and some crystals show twinning. Some of the cordierite is pinitised around the edges. Within one crystal the pinitisation started in the middle and now biotite is forming in a rib like texture.

Sample 148
The sample consists of a large cordierite crystal. Graphite is present within the cordierite and grows as small clusters of acicular needles. The cordierite is unaltered and is twinned.

Sample D35
This leucosome assemblage is predominantly cordierite and quartz. The cordierite has mostly altered along cracks to pinite. In the badly affected areas coarse blades of white mica has started to crystallise. Where cordierite and quartz are in contact, the quartz has recrystallised into clusters of small quartz grains.

A7.1.6 - Locality 12

Sample 18

The leucosome section of the sample has an assemblage of quartz, perthitic K-feldspar and cordierite. The cordierite is present as anhedral grains. The selvage mostly consists of coarse, unoriented biotites. These selvage biotites are rich in inclusion haloes. The selvage also contains oriented cordierite crystals. The mesosome contains cordierite that appears to be growing in biotite-rich zones and as porphyroblasts that contain sillimanite inclusions.

Sample 19b

The mesosome portion of this slide consists dominantly of quartz, plagioclase, orientated biotite and elongate cordierite. Around this, and stretching into the leucosome, is very coarse biotite which appears as a selvage in the field. At the edge of the selvage are cordierites. These appear to have crystallised within the melt but have clustered around the edge of the mesosome. Some of the cordierite within the mesosome has totally pinitised. These are associated with biotite. The rest of the leucosome consists of coarse K-feldspar and quartz. The biotites projecting into the leucosome are partially altered into symplectites within the K-feldspar.

Sample D45

This sample is mostly composed of mesosome but there are small patches that have a leucosomes assemblage of quartz and K-feldspar. Some of these patches contain cordierite, but these appear to be entrained from the mesosome. The mesosome assemblage is equigranular quartz and plagioclase, with interstitial oriented biotite. Cordierite and K-feldspar are present as porphyroblasts. K-feldspar has inclusions of rounded quartz blebs and oriented biotite, whereas the cordierite contains sillimanite inclusions.

Sample D47

The mesosome consists of equigranular quartz, plagioclase and cordierite with interstitial biotite. Coarse biotite with cordierite porphyroblasts make up the selvage assemblage. The cordierite often contains sillimanite inclusions. Some of the cordierite is highly altered whereas some of the cordierite appears to be growing as a

hydrous phase within the selvage. The leucosome is fine grained and is mostly composed of K-feldspar, quartz and cordierite. The cordierite still has sillimanite inclusions and are therefore entrained phases within the leucosome.

A7.1.7 - Locality 17

Sample 145

The leucosome of this sample is mostly quartz with fibrous sillimanite layers parallel to the edge of the leucosome. There are some tablets of perthite at the edges of the leucosome. The mesosome section is mostly made of cordierite, biotite, quartz and plagioclase.

A7.1.8 - Locality 20

Sample 31

The sample consists of mesosome with small leucosome segregations. These leucosomes contain grains of cordierite (2-3 mm) that are altered at the edges to pinite. The feldspars are symplectites, both in the leucosome and mesosome portions of the sample. Fibrous sillimanite is present in this sample, in between layers rich in bioitite. Some of this bioitite is being replaced by brightly birefringent mica and by chlorite.

A7.2 - Methods

Analysis of the H_2O and CO_2 contents of the Turku cordierite were made on the Cameca ims-4f ion microprobe in the Department of Geology and Geophysics, University of Edinburgh.

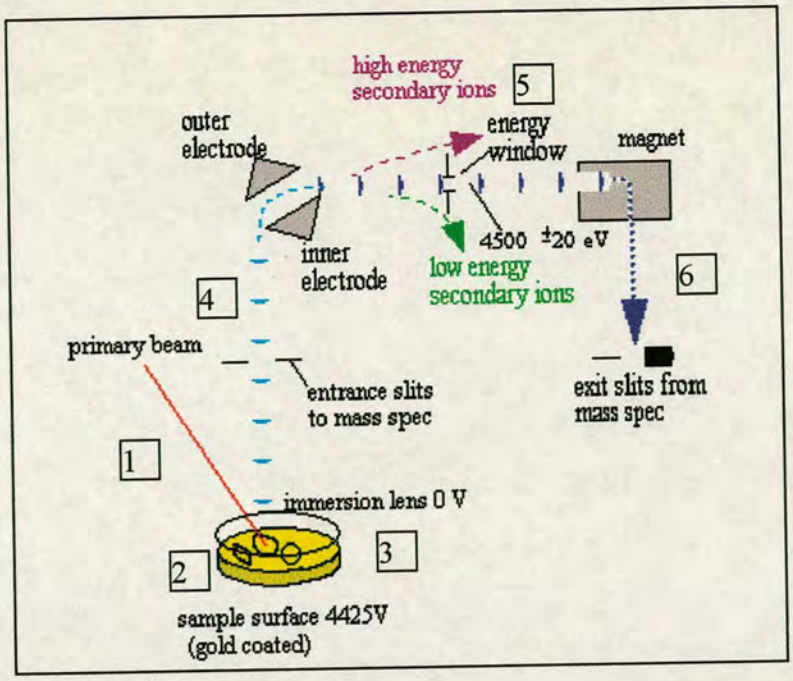

Figure A7.1 - The path of primary and secondary beams to the sample and through to the mass spectrometer where the specific energy of the H, C and Si ions are detected and analysed as $H/^{28}Si$ and $^{12}C/^{28}Si$ ratios.

1. A negative $^{16}O^-$ beam with a current of 8 nA is generated with 10 kV primary voltage. The beam is concentrated by electrostatic lenses onto the sample which results in a beam diameter of 15-25 μm.
2. In order to prevent charging of the sample the surface is given a gold coat, approximately 10-30 nm thick. The negative beam enhances the yield of the positively charged secondary ions and also helps to reduce charging of the sample.
3. Before each analysis started the sample had a burn-in time of three minutes.
4. Secondary ions and other molecules are sputtered from the sample surface. An energy offset (35 V) ensures that only the higher energy species are analysed by the mass spectrometer.
5. The secondary beam is accelerated by a potential difference of 4500 eV, and species within an energy window of 4500 ± 20 eV are transmitted via a magnetic filter to the electron multiplier.
6. Each isotope is counted for ten seconds in a cycle of ten counts. This is repeated three times and the ratio used is the average for the last cycle. C and H are measured as $^{12}C/^{28}Si$ and $H/^{28}Si$ ratios, distinguished by the electron multiplier in

terms of their mass/charge ratios. The ion counts are corrected for the background count rate and dead time of the electron multiplier and counting system

A7.3 - Standards and errors

Two standards (AMNH and 8-90) were used in order to calculate a calibration line for the calculation of wt% H_2O and CO_2 in the unknown samples. AMNH contained 0.66 wt% H_2O and 1.56 wt % CO_2, whilst 8-90 contained H_2O values of 0.8 wt% and CO_2 values of 1.25 wt%. These values were measured by independent analysis including stepped heating mass spectrometry (for CO_2) and hydrogen manometry (for H_2O). The graphs below are representative standard values for one ion probe session, plotted against unknown H/Si and C/Si ratios. Each session (day) generated different regression equations which was applied to the sample analysed in that session. The Si content of the cordierite has a variation underneath the general errors of this method.

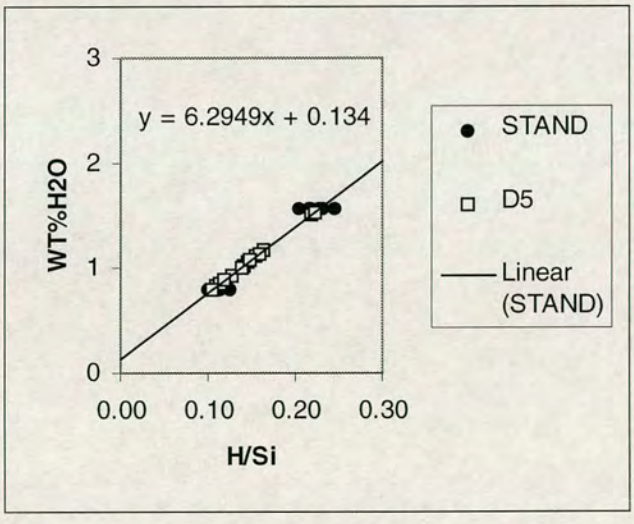

Figure A7.2 - H/Si plotted against wt % H_2O values for cordierite standards and unknown sample D5.

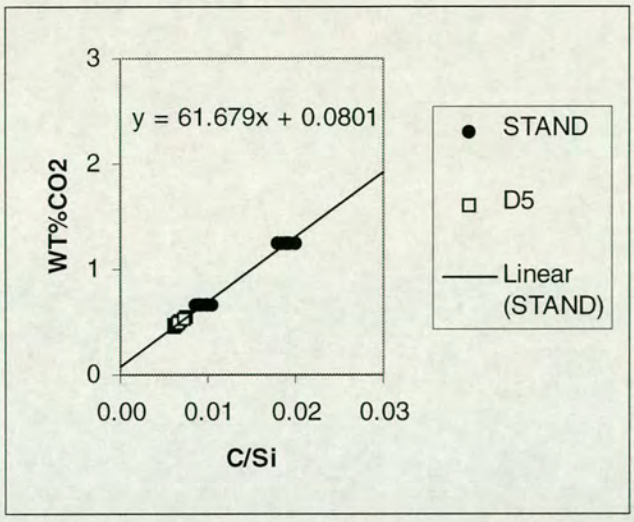

Figure A7.3 - C/Si plotted against wt % CO_2 values for cordierite standards and unknown sample D5.

SIMS analysis gives errors in the form of H/Si and C/Si ratios. In order to convert this to the error of each sample point in wt %, the same regression equation used to calculate the wt % of the sample, is applied to the combined values of the sample ratio and error.

$H / Si = 0.134$

$wt\%H_2O = (0.134 * 6.2949) + 0.134$

$wt\%H_2O = 0.9775$

H/Si error = 0.001

wt% error =((0.134+0.001)*6.2949)+0.134)-0.9775

wt% error = 0.006

This is the error of an analysis of an individual sample point and does not take into account the errors propagated from the regression equation. These errors are typically $\pm$ 0.05 (Carrington and Harley, 1996).

Appendix.7.4 - Raw SIMS data for Turku cordierites with errors.

SAMPLE	H H/Si	error H/Si	H2O wt %	±H2O error wt %	C C/Si	error C/Si	CO2 wt %	±CO2 error wt %
D18								
19//03/98		CALIB	WT%H20 = 5.7487*H/Si+0.2438					
			WT%CO2 = 63.061*C/Si+0.678					
D181	0.156	0.000	1.142	0.030	0.001	0.000	0.147	0.004
D182	0.164	0.003	1.185	0.003	0.005	0.000	0.399	0.004
D183	0.105	0.000	0.850	0.001	0.005	0.000	0.413	0.004
D184	0.178	0.001	1.265	0.003	0.006	0.000	0.439	0.004
D185	0.167	0.001	1.206	0.002	0.005	0.000	0.367	0.003
11/09/98		CALIB	WT%H20 = 5.8356*H/Si+0.2574					
			WT%CO2 = 63.004*C/Si+0.0815					
D181	0.134	0.001	1.042	0.003	0.007	0.000	0.523	0.003
D182	0.153	0.000	1.148	0.003	0.005	0.000	0.408	0.003
D183	0.133	0.001	1.031	0.002	0.004	0.000	0.364	0.002
D184	0.133	0.001	1.032	0.002	0.005	0.000	0.371	0.002
D185	0.121	0.001	0.962	0.003	0.018	0.000	1.244	0.016
D186	0.125	0.001	0.985	0.001	0.004	0.000	0.360	0.002
D188	0.152	0.001	1.143	0.002	0.006	0.000	0.456	0.003
D189	0.148	0.001	1.120	0.001	0.006	0.000	0.448	0.003
D1810	0.165	0.001	1.217	0.003	0.011	0.000	0.803	0.009
D1811	0.141	0.001	1.080	0.001	0.010	0.000	0.721	0.011
D1812	0.125	0.001	0.985	0.002	0.017	0.000	1.134	0.020
Average	***0.144***	***0.001***	***1.087***	***0.004***	***0.007***	***0.000***	***0.537***	***0.006***
79								
20/03/98		CALIB	WT%H20 = 5.8356*H/Si+0.2574					
			WT%CO2 = 64.467*C/Si+0.0116					
791	0.115	0.000	0.931	0.003	0.008	0.000	0.616	0.006
793	0.139	0.000	1.066	0.002	0.007	0.000	0.585	0.005
794	0.145	0.000	1.105	0.003	0.007	0.000	0.546	0.005
795	0.106	0.000	0.878	0.002	0.008	0.000	0.652	0.004
796	0.104	0.000	0.865	0.002	0.008	0.000	0.606	0.006
797	0.128	0.000	1.006	0.000	0.010	0.000	0.782	0.004
798	0.094	0.000	0.804	0.002	0.008	0.000	0.624	0.003
799	0.172	0.000	1.263	0.001	0.010	0.000	0.772	0.005
7910	0.139	0.000	1.069	0.002	0.009	0.000	0.725	0.003
7911	0.145	0.000	1.102	0.002	0.009	0.000	0.700	0.004
7912	0.158	0.000	1.179	0.002	0.008	0.000	0.662	0.006
7913	0.118	0.001	0.947	0.006	0.008	0.000	0.621	0.007
Average	***0.130***	***0.000***	***1.018***	***0.002***	***0.008***	***0.000***	***0.657***	***0.005***

SAMPLE	H H/Si	error H/Si	H2O wt %	±H2O error wt %	C C/Si	error C/Si	CO2 wt %	±CO2 error wt %
D22								
16/03/98		CALIB	WT%H20 = 6.941*H/Si+0.2083					
			WT%CO2 = 67.809*C/Si+0.0927					
D221	0.148	0.001	1.234	0.005	0.008	0.000	0.613	0.007
D222	0.111	0.001	0.977	0.006	0.009	0.000	0.700	0.008
D223	0.177	0.000	1.435	0.003	0.008	0.000	0.660	0.005
D224	0.115	0.001	1.006	0.004	0.010	0.000	0.788	0.005
D225	0.162	0.000	1.331	0.003	0.008	0.000	0.655	0.007
D226	0.183	0.001	1.480	0.006	0.008	0.000	0.666	0.006
D227	0.089	0.000	0.828	0.003	0.007	0.000	0.570	0.004
D228	0.121	0.001	1.046	0.007	0.007	0.000	0.543	0.005
D229	0.159	0.001	1.315	0.005	0.008	0.000	0.638	0.005
D2210	0.148	0.000	1.221	0.002	0.008	0.000	1.026	0.007
D2211	0.154	0.001	1.237	0.006	0.008	0.000	0.632	0.006
D2212	0.141	0.001	1.278	0.004	0.008	0.000	0.628	0.009
D2213	0.163	0.000	1.187	0.003	0.009	0.000	0.655	0.007
D2214	0.076	0.000	1.340	0.003	0.007	0.000	0.695	0.008
D2215	0.101	0.0004	0.738	0.003	0.007	0.0001	0.553	0.004
D2216	0.121	0.0004	0.908	0.003	0.007	0.0001	0.557	0.004
D2217	0.120	0.0003	1.048	0.002	0.019	0.0001	0.554	0.005
D2218	0.131	0.0004	1.044	0.003	0.007	0.0000	0.562	0.002
D2219	0.159	0.0006	1.118	0.004	0.007	0.0001	0.582	0.004
D222	0.112	0.0003	1.310	0.002	0.007	0.0001	0.565	0.005
D223	0.096	0.0003	0.987	0.002	0.007	0.0001	0.541	0.004
08/09/98		CALIB	WT%H20 = 6.1078*H/Si+0.2215					
			WT%CO2 = 58.51*C/Si+0.0142					
D2220	0.132	0.000	0.875	0.003	0.007	0.000	0.523	0.004
D2221	0.101	0.000	1.030	0.002	0.007	0.000	0.428	0.006
D2222	0.103	0.001	0.837	0.003	0.007	0.000	0.449	0.006
D2223	0.140	0.001	0.851	0.004	0.007	0.000	0.416	0.007
D2224	0.055	0.000	1.074	0.002	0.008	0.000	0.416	0.007
D2225	0.078	0.000	0.559	0.001	0.007	0.000	0.479	0.006
D2226	0.100	0.000	0.699	0.002	0.009	0.000	0.417	0.010
D2227	0.115	0.000	0.831	0.002	0.002	0.000	0.525	0.003
D2228	0.116	0.000	0.925	0.002	0.002	0.000	1.301	0.002
Average	***0.124***	***0.000***	***1.058***	***0.003***	***0.008***	***0.000***	***0.611***	***0.006***

SAMPLE	H H/Si	error H/Si	H2O wt %	±H2O error wt %	C C/Si	error C/Si	CO2 wt %	±CO2 error wt %
D5								
17/03/98		CALIB	WT%H20 = 4.9615*H/Si+0.2103					
			WT%CO2 = 65.295*C/Si+0.0203					
D51	0.109	0.005	0.676	0.002	0.006	0.000	0.424	0.004
D52	0.154	0.000	0.899	0.016	0.006	0.000	0.438	0.005
D53	0.114	0.000	0.699	0.002	0.006	0.000	0.420	0.005
D54	0.146	0.001	0.859	0.003	0.007	0.000	0.454	0.005
D55	0.140	0.000	0.829	0.003	0.007	0.000	0.466	0.005
D56	0.141	0.000	0.834	0.004	0.007	0.000	0.445	0.006
D57	0.218	0.001	1.218	0.002	0.007	0.000	0.507	0.005
D58	0.222	0.000	1.235	0.004	0.007	0.000	0.469	0.004
D59	0.155	0.000	0.905	0.003	0.006	0.000	0.428	0.004
D510	0.127	0.000	0.763	0.004	0.006	0.000	0.428	0.005
D511	0.119	0.000	0.722	0.004	0.006	0.000	0.434	0.006
D512	0.164	0.000	0.946	0.006	0.006	0.000	0.423	0.006
D513	0.104	0.000	0.650	0.003	0.007	0.000	0.509	0.004
D514	0.159	0.001	0.921	0.005	0.006	0.000	0.440	0.006
D515	0.139	0.000	0.823	0.006	0.007	0.000	0.447	0.004
D516	0.149	0.000	0.871	0.006	0.007	0.000	0.489	0.003
Average	***0.147***	***0.001***	***0.866***	***0.005***	***0.007***	***0.000***	***0.451***	***0.005***
Locality 3								
D26								
09/09/98		CALIB	WT%H20 = 6.6833*H/Si+0.1636					
			WT%CO2 = 49.615*C/Si+0.2127					
D261	0.111	0.000	0.906	0.002	0.009	0.0002	0.682	0.008
D262	0.131	0.001	1.040	0.004	0.010	0.003	0.705	0.139
D263	0.123	0.000	0.982	0.003	0.016	0.001	0.983	0.027
D265	0.100	0.000	0.834	0.002	0.010	0.000	0.717	0.008
D266	0.122	0.000	0.977	0.003	0.017	0.000	1.047	0.017
D267	0.185	0.007	1.401	0.047	0.006	0.001	0.492	0.051
D268	0.122	0.000	0.976	0.003	0.008	0.000	0.600	0.008
D269	0.117	0.000	0.944	0.002	0.005	0.000	0.468	0.002
10/09/98		CALIB	WT%H20 = 4.9615*H/Si+0.2103					
			WT%CO2 = 65.295*C/Si+0.0203					
D2610	0.109	0.000	*0.751*	0.001	0.005	0.000	*0.280*	0.002
D2611	0.115	0.000	0.779	0.001	0.005	0.000	0.296	0.003
D2612	0.120	0.000	0.806	0.001	0.005	0.000	0.288	0.003
D2613	0.095	0.000	0.682	0.000	0.005	0.000	0.298	0.004
D2614	0.106	0.000	0.734	0.001	0.001	0.000	0.076	0.013
Average	***0.120***	***0.001***	***0.909***	***0.005***	***0.008***	***0.000***	***0.533***	***0.022***
Locality 4								
10								
16/10/97		CALIB	WT%H20 = 4.503*H/Si+0.4605					
			WT%CO2 = 60.717*C/Si+0.1219					
10BIIE	0.118	0.001	0.991	0.004	0.014	0.000	0.946	0.011
10BIIG	0.107	0.000	0.941	0.001	0.013	0.000	0.936	0.006
10BIIH	0.136	0.001	1.072	0.003	0.016	0.000	1.064	0.009
Average	***0.120***	***0.001***	***1.001***	***0.003***	***0.014***	***0.000***	***0.982***	***0.008***

SAMPLE	H H/Si	error H/Si	H2O wt %	±H2O error wt %	C C/Si	error C/Si	CO2 wt %	±CO2 error wt %
12								
16/10/97		CALIB	WT%H20 = 4.503*H/Si+0.4605					
			WT%CO2 = 60.717*C/Si+0.1219					
12A	0.095	0.000	0.886	0.001	0.009	0.000	0.648	0.006
12C	0.083	0.000	0.834	0.001	0.008	0.000	0.637	0.005
12H	0.080	0.000	0.821	0.001	0.010	0.000	0.706	0.005
12I	0.084	0.000	0.840	0.002	0.009	0.000	0.692	0.005
12J	0.100	0.000	0.909	0.002	0.013	0.000	0.936	0.004
Average	***0.088***	***0.000***	***0.858***	***0.001***	***0.010***	***0.000***	***0.724***	***0.005***
60								
07/09/98		CALIB	WT%H20 = 6.0798*H/Si+0.0355					
			WT%CO2 = 62.593*C/Si+0.0157					
601	0.113	0.000	0.724	0.001	0.016	0.000	0.988	0.014
602	0.135	0.000	0.856	0.001	0.020	0.000	1.278	0.026
603	0.105	0.000	0.676	0.001	0.013	0.000	0.830	0.011
604	0.109	0.000	0.695	0.002	0.008	0.000	0.490	0.003
605	0.104	0.000	0.668	0.001	0.009	0.000	0.565	0.004
606	0.096	0.000	0.617	0.001	0.008	0.000	0.527	0.003
607	0.116	0.000	0.742	0.002	0.009	0.000	0.606	0.006
608	0.128	0.000	0.816	0.001	0.009	0.000	0.572	0.005
609	0.108	0.000	0.693	0.001	0.009	0.001	0.558	0.033
610	0.163	0.000	1.028	0.002	0.008	0.000	0.512	0.004
611	0.103	0.000	0.661	0.001	0.010	0.000	0.654	0.004
612	0.108	0.000	0.690	0.002	0.019	0.000	1.179	0.019
Average	***0.116***	***0.000***	***0.739***	***0.001***	***0.011***	***0.000***	***0.730***	***0.011***
X								
15/10/98		CALIB	WT%H20 = 6.3609*H/Si+0.1823					
			WT%CO2 = 63.569*C/Si+0.1029					
X1	0.179	0.001	1.323	0.006	0.012	0.000	0.886	0.013
X2	0.099	0.000	0.813	0.002	0.014	0.000	1.003	0.009
X3	0.078	0.000	0.678	0.002	0.010	0.000	0.749	0.007
X4	0.098	0.001	0.808	0.006	0.012	0.000	0.878	0.005
X5	0.092	0.000	0.766	0.002	0.011	0.000	0.842	0.006
X7	0.085	0.000	0.726	0.003	0.009	0.000	0.710	0.005
X8	0.110	0.000	0.880	0.002	0.009	0.000	0.718	0.005
Average	***0.106***	***0.000***	***0.856***	***0.003***	***0.011***	***0.000***	***0.827***	***0.007***

SAMPLE	H H/Si	error H/Si	H2O wt %	±H2O error wt %	C C/Si	error C/Si	CO2 wt %	±CO2 error wt %
Locality 5								
103								
19//03/98		CALIB	WT%H20 = 5.7487*H/Si+0.2438					
			WT%CO2 = 63.061*C/Si+0.678					
1031	0.130	0.000	0.990	0.002	0.004	0.000	0.340	0.008
1032	0.139	0.000	1.045	0.002	0.002	0.000	0.215	0.002
1033	0.134	0.001	1.014	0.003	0.003	0.000	0.233	0.003
1034	0.119	0.000	0.928	0.002	0.002	0.000	0.211	0.002
1035	0.122	0.000	0.944	0.003	0.002	0.000	0.188	0.003
1036	0.138	0.001	1.035	0.003	0.002	0.000	0.200	0.004
1037	0.138	0.001	1.035	0.003	0.002	0.000	0.216	0.002
1038	0.119	0.000	0.929	0.002	0.003	0.000	0.249	0.004
1039	0.133	0.002	1.006	0.011	0.002	0.000	0.192	0.027
10310	0.145	0.000	1.074	0.002	0.002	0.000	0.191	0.002
10311	0.135	0.001	1.018	0.003	0.002	0.000	0.186	0.003
10312	0.122	0.000	0.945	0.001	0.002	0.000	0.172	0.002
10313	0.124	0.000	0.954	0.001	0.002	0.000	0.172	0.002
Average	***0.130***	***0.001***	***0.994***	***0.003***	***0.002***	***0.000***	***0.213***	***0.005***
104								
17/10/97		CALIB	WT%H20 = 6.7919*H/Si+0.0.1906					
			WT%CO2 = 64.693*C/Si+0.0871					
1041	0.148	0.000	1.192	0.003	0.006	0.000	0.478	0.012
1042	0.118	0.000	0.989	0.002	0.002	0.000	0.216	0.002
1043	0.134	0.000	1.102	0.002	0.007	0.000	0.532	0.009
1044	0.137	0.001	1.119	0.007	0.006	0.000	0.457	0.009
1045	0.121	0.000	1.013	0.002	0.010	0.000	0.755	0.013
1046	0.135	0.000	1.105	0.002	0.003	0.000	0.273	0.003
1047	0.130	0.001	1.074	0.004	0.009	0.000	0.654	0.013
Average	***0.132***	***0.000***	***1.085***	***0.003***	***0.006***	***0.000***	***0.481***	***0.009***
Locality 6								
17								
17/03/98		CALIB	WT%H20 = 6.949*H/Si+0.134					
			WT%CO2 = 61.679*C/Si+0.0801					
171	0.205	0.001	1.558	0.005	0.012	0.000	0.807	0.008
172	0.103	0.001	0.848	0.004	0.008	0.000	0.588	0.005
173	0.127	0.001	1.017	0.005	0.014	0.000	0.951	0.014
174	0.111	0.001	0.905	0.005	0.008	0.000	0.589	0.007
175	0.155	0.001	1.212	0.008	0.008	0.000	0.604	0.003
176	0.171	0.001	1.322	0.006	0.010	0.000	0.726	0.005
177	0.111	0.001	0.905	0.004	0.009	0.000	0.642	0.004
178	0.125	0.001	1.001	0.004	0.008	0.000	0.581	0.005
179	0.121	0.000	0.971	0.003	0.008	0.000	0.598	0.004
1710	0.089	0.000	0.755	0.003	0.009	0.000	0.620	0.005
1711	0.127	0.001	1.016	0.004	0.009	0.000	0.639	0.008
1712	0.178	0.001	1.368	0.009	0.009	0.000	0.624	0.004
1713	0.166	0.001	1.285	0.006	0.009	0.000	0.644	0.005
1714	0.141	0.001	1.112	0.005	0.009	0.000	0.606	0.006
	H/Si	H/Si	wt %	wt %	C/Si	C/Si	wt %	wt %
18/03/98		CALIB	WT%H20 = 4.9615*H/Si+0.2130					

1715	0.099	0.000	0.822	0.003	0.009	0.000	0.606	0.004
1716	0.106	0.000	0.871	0.003	0.009	0.000	0.643	0.004
1717	0.095	0.001	0.797	0.005	0.009	0.000	0.642	0.006
SAMPLE	**H**	**error**	**H2O**	**±H2O error**	**C**	**error**	**CO2**	**±CO2 error**
			WT%CO2 = 65.295*C/Si+0.0203					
1718	0.156	0.001	0.988	0.236	0.010	0.000	0.649	0.030
1719	0.134	0.001	0.877	0.194	0.008	0.000	0.572	0.034
1720	0.091	0.000	0.666	0.104	0.008	0.000	0.575	*0.033*
1721	0.142	0.001	0.919	0.208	0.008	0.000	0.571	*0.036*
1722	0.136	0.000	0.890	0.194	0.008	0.000	0.525	*0.037*
1723	0.134	0.001	0.877	0.192	0.013	0.000	0.844	0.022
1725	0.094	0.000	0.679	0.110	0.008	0.000	0.518	0.036
Average	***0.130***	***0.001***	***0.986***	***0.055***	***0.009***	***0.000***	***0.640***	***0.014***

Locality 7

148								
14/10/97		**CALIB**	**WT%H20 = 8.4412*H/Si+0.0071**					
			WT%CO2 = 65.755*C/Si+0.1295					
7-148A	0.101	0.001	1.098	0.006	0.005	0.000	0.547	0.003
7-148B	0.080	0.000	1.337	0.004	0.005	0.000	0.582	0.004
7-148D	0.116	0.000	1.053	0.003	0.005	0.000	0.573	0.003
7-148E	0.121	0.000	1.354	0.004	0.000	0.000	0.623	0.004
7-148F	0.133	0.001	1.149	0.006	0.005	0.000	0.585	0.003
7-148G	0.088	0.000	0.984	0.001	0.005	0.000	0.634	0.007
7-148H	0.122	0.002	0.785	0.013	0.006	0.001	0.592	0.051
Average	***0.109***	***0.001***	***1.108***	***0.005***	***0.004***	***0.000***	***0.591***	***0.011***

D35								
14/10/97		**CALIB**	**WT%H20 = 8.4412*H/Si+0.0071**					
			WT%CO2 = 65.755*C/Si+0.1295					
D35-2	0.131	0.000	1.098	0.002	0.006	0.000	0.547	0.004
D35-3	0.159	0.000	1.337	0.002	0.007	0.000	0.582	0.004
D35-4	0.126	0.000	1.053	0.003	0.007	0.000	0.573	0.003
D351	0.161	0.000	1.238	0.003	0.007	0.000	0.453	0.003
D352	0.137	0.000	1.108	0.002	0.007	0.000	0.411	0.002
D353	0.117	0.000	1.004	0.003	0.008	0.000	0.466	0.003
D354	0.094	0.000	0.878	0.004	0.007	0.000	0.419	0.004
Average	***0.132***	***0.000***	***1.102***	***0.003***	***0.007***	***0.000***	***0.493***	***0.003***

Locality 12

18								
19/10/97		**CALIB**	**WT%H20 = 6.2554*H/Si+0.257**					
			WT%CO2 = 69.259*C/Si-0.0213					
181	0.149	0.000	1.220	0.004	0.005	0.000	1.188	0.004
182	0.124	0.000	1.053	0.004	0.002	0.000	1.031	0.002
183	0.152	0.001	1.239	0.004	0.000	0.000	1.206	0.002
184	0.113	0.000	0.982	0.002	0.002	0.000	0.964	0.002
185	0.143	0.000	1.183	0.002	0.002	0.000	1.153	0.001
186	0.158	0.001	1.277	0.002	0.002	0.000	1.242	0.002
188	0.125	0.000	1.063	0.005	0.000	0.000	1.040	0.003
Average	***0.138***	***0.000***	***1.145***	***0.003***	***0.002***	***0.000***	***1.118***	***0.002***

SAMPLE	**H**	**error**	**H2O**	**±H2O error**	**C**	**error**	**CO2**	**±CO2 error**
	H/Si	**H/Si**	**wt %**	**wt %**	**C/Si**	**C/Si**	**wt %**	**wt %**

19								
18/03/98		CALIB	WT%H20 = 4.9615*H/Si+0.2130					
			WT%CO2 = 65.295*C/Si+0.0203					
191	0.204	0.000	1.224	0.002	0.002	0.000	0.167	0.002
192	0.218	0.001	1.297	0.003	0.002	0.000	0.123	0.003
193	0.196	0.002	1.187	0.008	0.002	0.000	0.128	0.003
194	0.229	0.000	1.352	0.002	0.002	0.000	0.139	0.003
195	0.220	0.001	1.305	0.004	0.002	0.000	0.140	0.003
196	0.212	0.001	1.264	0.004	0.002	0.000	0.132	0.002
197	0.237	0.000	1.389	0.002	0.001	0.000	0.096	0.003
199	0.228	0.001	1.346	0.003	0.002	0.000	0.125	0.002
1910	0.173	0.001	1.070	0.003	0.004	0.000	0.252	0.002
Average	***0.213***	***0.001***	***1.271***	***0.003***	***0.002***	***0.000***	***0.144***	***0.003***
D45								
10/09/98		CALIB	WT%H20 = 4.9615*H/Si+0.2103					
			WT%CO2 = 65.295*C/Si+0.0203					
D451	0.110	0.001	0.757	0.002	0.006	0.000	0.576	0.019
D452	0.163	0.001	1.018	0.002	0.007	0.000	0.674	0.008
D453	0.155	0.001	0.980	0.003	0.007	0.000	0.648	0.008
D454	0.106	0.000	0.738	0.001	0.005	0.000	0.517	0.007
D455	0.131	0.000	0.862	0.002	0.004	0.001	0.481	0.056
D456	0.103	0.000	0.720	0.003	0.007	0.000	0.666	0.012
D457	0.106	0.001	0.735	0.001	0.003	0.000	0.388	0.002
Average	***0.125***	***0.001***	***0.830***	***0.002***	***0.005***	***0.000***	***0.564***	***0.016***
47								
18/10/97		CALIB	WT%H20 = 7.2422*H/Si+0.181					
			WT%CO2 = 56.079*C/Si+0.1621					
471	0.149	0.001	1.258	0.006	0.009	0.000	0.616	0.004
472	0.187	0.001	1.538	0.008	0.004	0.000	0.359	0.003
473	0.142	0.000	1.211	0.002	0.006	0.000	0.460	0.006
474	0.126	0.001	1.095	0.005	0.002	0.000	0.286	0.023
475	0.167	0.001	1.389	0.010	0.002	0.000	0.279	0.023
476	0.154	0.001	1.299	0.005	0.003	0.000	0.320	0.003
477	0.150	0.001	1.270	0.005	0.003	0.000	0.306	0.002
478	0.109	0.000	0.969	0.002	0.003	0.000	0.316	0.002
479	0.160	0.002	1.339	0.013	0.003	0.000	0.306	0.002
4710	0.130	0.001	1.120	0.004	0.003	0.000	0.318	0.002
Average	***0.147***	***0.001***	***1.249***	***0.006***	***0.004***	***0.000***	***0.357***	***0.007***
Locality 17								
145								
08/09/98		CALIB	WT%H20 = 6.1078*H/Si+0.2215					
			WT%CO2 = 58.81*C/Si+0.0142					
1451	0.167	0.000	1.242	0.002	0.004	0.000	0.249	0.003
1453	0.176	0.000	1.299	0.002	0.004	0.000	0.227	0.004
1454	0.214	0.004	1.528	0.021	0.007	0.000	0.441	0.009
09/09/98	CALIB	WT%H20 = 6.6833*H/Si+0.1636						
		WT%CO2 = 49.615*C/Si+0.2127						

SAMPLE	H H/Si	error H/Si	H2O wt %	±H2O error wt %	C C/Si	error C/Si	CO2 wt %	±CO2 error wt %
1457	0.148	0.001	1.155	0.004	0.003	0.000	0.364	0.003

1458	0.140	0.000	1.097	0.003	0.004	0.000	0.423	0.004
1459	0.174	0.001	1.327	0.003	0.004	0.000	0.405	0.003
14510	0.116	0.000	0.936	0.001	0.004	0.000	0.388	0.002
14511	0.198	0.001	1.486	0.004	0.004	0.000	0.410	0.002
14512	0.171	0.000	1.308	0.003	0.006	0.000	0.530	0.003
14513	0.169	0.000	1.295	0.002	0.004	0.000	0.428	0.004
14514	0.150	0.000	1.165	0.003	0.004	0.000	0.431	0.004
14515	0.189	0.000	1.427	0.003	0.005	0.000	0.446	0.003
Average	***0.168***	***0.001***	***1.272***	***0.004***	***0.004***	***0.000***	***0.395***	***0.004***

Locality 20

31

17/10/97 **CALIB 'T%H20 = 6.7919*H/Si+0.0.1906**

WT%CO2 = 64.693*C/Si+0.0871

L311	0.109	0.000	0.930	0.002	0.002	0.000	0.087	0.005
L312	0.154	0.000	1.237	0.000	0.002	0.000	0.087	0.005
L313	0.144	0.001	1.167	0.003	0.002	0.000	0.087	0.004
Average	***0.136***	***0.000***	***1.111***	***0.002***	***0.002***	***0.000***	***0.087***	***0.005***

Appendix 7.5 - Calculations of aCO_2, aH_2O, XCO_2crd, wt % melt and Dw based on the data of Carrington and Harley (in press).

H_2O fugacity calcs

P(kbar)	T(C)	T(Kelvin)	a-term	b-term	c-term	RTlnf	f
5	660	933.15	-31.85268	0.11735332	-0	63.4656	3569
5	750	1023.15	-31.85268	0.11735332	-0	71.1582	4294

CO_2 fugacity calcs

P(kbar)	T(C)	T(Kelvin)	a-term	b-term	c-term	RTlnf	f
5	660	933.15	3.624401	0.08530393	-0	79.5199	28266
5	750	1023.15	3.624401	0.08530393	-0	86.448	25906

Natural Crd data

Samples	H_2O	CO_2	MW	n(H_2O)	m(CO_2)	P	T	f(H_2O)	f(CO_2)	aH_2O	aCO_2	XCO_2crd	melt wt% sat	Xw(sat)	Xw-samp	wt% melt	Dw
Loc 2																	
D18	1.142	0.147	610.0	0.391	0.021	5	750	4294	25906	0.312	0.127	0.050	10.7	0.63	0.35	3.65	3.19
	1.185	0.399	610.0	0.406	0.056	5	750	4294	25906	0.332	0.357	0.121	10.7	0.63	0.37	3.82	3.22
	0.850	0.413	610.0	0.291	0.058	5	750	4294	25906	0.199	0.370	0.166	10.7	0.63	0.28	2.65	3.12
	1.265	0.439	610.0	0.433	0.062	5	750	4294	25906	0.371	0.395	0.124	10.7	0.63	0.39	4.17	3.29
	1.206	0.367	610.0	0.413	0.051	5	750	4294	25906	0.341	0.326	0.111	10.7	0.63	0.37	3.91	3.24
	1.042	0.523	610.0	0.357	0.073	5	750	4294	25906	0.269	0.476	0.170	10.7	0.63	0.33	3.28	3.14
	1.148	0.408	610.0	0.393	0.057	5	750	4294	25906	0.315	0.366	0.127	10.7	0.63	0.36	3.67	3.20
	1.031	0.364	610.0	0.353	0.051	5	750	4294	25906	0.265	0.324	0.126	10.7	0.63	0.33	3.24	3.14
	1.032	0.371	610.0	0.354	0.052	5	750	4294	25906	0.266	0.330	0.128	10.7	0.63	0.33	3.24	3.14
	0.962	1.244	610.0	0.330	0.174	5	750	4294	25906	0.238	1.271	0.346	10.7	0.63	0.31	3.00	3.12
	0.985	0.360	610.0	0.338	0.050	5	750	4294	25906	0.247	0.320	0.130	10.7	0.63	0.32	3.08	3.13
	1.143	0.456	610.0	0.392	0.064	5	750	4294	25906	0.312	0.411	0.140	10.7	0.63	0.35	3.65	3.20
	1.120	0.448	610.0	0.384	0.063	5	750	4294	25906	0.302	0.403	0.141	10.7	0.63	0.35	3.57	3.18
	1.217	0.803	610.0	0.417	0.113	5	750	4294	25906	0.347	0.763	0.213	10.7	0.63	0.37	3.96	3.25
	1.080	0.721	610.0	0.370	0.101	5	750	4294	25906	0.285	0.677	0.215	10.7	0.63	0.34	3.41	3.16
	0.985	1.134	610.0	0.337	0.159	5	750	4294	25906	0.247	1.137	0.320	10.7	0.63	0.32	3.08	3.13
	1.087	***0.537***		***0.372***	***0.075***					***0.291***	***0.503***	***0.164***	***10.7***	***0.635***	***0.341***	***3.461***	***3.180***
79	0.931	0.616	610.0	0.319	0.086	5	750	4294	25906	0.227	0.569	0.213	10.7	0.63	0.30	2.90	3.12
	1.066	0.585	611.0	0.366	0.082	5	750	4294	25906	0.280	0.538	0.183	10.7	0.63	0.34	3.37	3.16
	1.105	0.546	612.0	0.380	0.077	5	750	4294	25906	0.297	0.500	0.168	10.7	0.63	0.35	3.52	3.19
	0.878	0.652	613.0	0.302	0.092	5	750	4294	25906	0.210	0.609	0.233	10.7	0.63	0.29	2.75	3.14
	0.865	0.606	614.0	0.298	0.086	5	750	4294	25906	0.206	0.563	0.223	10.7	0.63	0.29	2.72	3.14
	1.006	0.782	615.0	0.347	0.111	5	750	4294	25906	0.258	0.748	0.241	10.7	0.63	0.32	3.18	3.16
	0.804	0.624	616.0	0.278	0.088	5	750	4294	25906	0.187	0.583	0.241	10.7	0.63	0.27	2.54	3.16
	1.263	0.772	617.0	0.438	0.110	5	750	4294	25906	0.378	0.740	0.200	10.7	0.63	0.39	4.23	3.35
	1.069	0.725	618.0	0.371	0.103	5	750	4294	25906	0.286	0.691	0.217	10.7	0.63	0.34	3.42	3.20
	1.102	0.700	619.0	0.383	0.100	5	750	4294	25906	0.301	0.666	0.206	10.7	0.63	0.35	3.56	3.23
	1.179	0.662	620.0	0.411	0.094	5	750	4294	25906	0.338	0.627	0.187	10.7	0.63	0.37	3.88	3.29
	0.947	0.621	621.0	0.330	0.089	5	750	4294	25906	0.239	0.585	0.212	10.7	0.63	0.31	3.01	3.18
	1.018	**0.657**		**0.352**	**0.093**					**0.267**	**0.618**	**0.210**	**10.7**	**0.635**	**0.326**	**3.256**	**3.193**
D22	1.234	0.613	609.0	0.422	0.086	5	750	4294	25906	0.355	0.565	0.169	10.7	0.63	0.38	4.02	3.26
	0.977	0.700	609.0	0.334	0.098	5	750	4294	25906	0.243	0.654	0.227	10.7	0.63	0.31	3.05	3.12
	1.435	0.660	609.0	0.491	0.092	5	750	4294	25906	0.468	0.613	0.158	10.7	0.63	0.43	5.03	3.50
	1.006	0.788	609.0	0.344	0.110	5	750	4294	25906	0.255	0.746	0.243	10.7	0.63	0.32	3.15	3.13
	1.331	0.655	609.0	0.455	0.092	5	750	4294	25906	0.405	0.607	0.168	10.7	0.63	0.40	4.47	3.36

	1.480	0.666	609.0	0.506	0.093	5	750	4294	25906	0.497	0.619	0.156	10.7	0.63	0.45	5.29	3.58
	0.828	0.570	609.0	0.283	0.080	5	750	4294	25906	0.192	0.522	0.220	10.7	0.63	0.28	2.58	3.12
	1.046	0.543	609.0	0.358	0.076	5	750	4294	25906	0.270	0.495	0.175	10.7	0.63	0.33	3.29	3.14
	1.315	0.638	609.0	0.450	0.089	5	750	4294	25906	0.397	0.591	0.166	10.7	0.63	0.40	4.39	3.34
	1.221	1.026	609.0	0.418	0.144	5	750	4294	25906	0.348	1.010	0.256	10.7	0.63	0.37	3.96	3.25
	1.237	0.632	609.0	0.423	0.088	5	750	4294	25906	0.356	0.584	0.173	10.7	0.63	0.38	4.03	3.26
	1.278	0.628	609.0	0.437	0.088	5	750	4294	25906	0.377	0.580	0.167	10.7	0.63	0.39	4.22	3.30
	1.187	0.655	609.0	0.406	0.092	5	750	4294	25906	0.332	0.607	0.184	10.7	0.63	0.37	3.82	3.22
	1.340	0.695	609.0	0.459	0.097	5	750	4294	25906	0.411	0.648	0.175	10.7	0.63	0.41	4.52	3.37
	0.738	0.553	609.0	0.252	0.077	5	750	4294	25906	0.164	0.505	0.235	10.7	0.63	0.26	2.33	3.16
	0.908	0.557	609.0	0.311	0.078	5	750	4294	25906	0.219	0.509	0.201	10.7	0.63	0.30	2.83	3.11
	1.048	0.554	609.0	0.359	0.078	5	750	4294	25906	0.271	0.506	0.178	10.7	0.63	0.33	3.29	3.14
	1.044	0.562	609.0	0.357	0.079	5	750	4294	25906	0.270	0.514	0.181	10.7	0.63	0.33	3.28	3.14
	1.118	0.582	609.0	0.383	0.081	5	750	4294	25906	0.301	0.533	0.175	10.7	0.63	0.35	3.55	3.17
	1.310	0.565	609.0	0.448	0.079	5	750	4294	25906	0.394	0.517	0.150	10.7	0.63	0.40	4.37	3.33
	0.987	0.541	609.0	0.338	0.076	5	750	4294	25906	0.247	0.493	0.183	10.7	0.63	0.32	3.08	3.12
	0.875	0.523	609.0	0.299	0.073	5	750	4294	25906	0.207	0.475	0.196	10.7	0.63	0.29	2.73	3.12
	1.030	0.428	609.0	0.352	0.060	5	750	4294	25906	0.264	0.383	0.145	10.7	0.63	0.33	3.23	3.14
	0.837	0.449	609.0	0.286	0.063	5	750	4294	25906	0.195	0.403	0.180	10.7	0.63	0.28	2.61	3.12
	0.851	0.416	609.0	0.291	0.058	5	750	4294	25906	0.199	0.372	0.167	10.7	0.63	0.28	2.65	3.12
	1.074	0.416	609.0	0.368	0.058	5	750	4294	25906	0.282	0.372	0.137	10.7	0.63	0.34	3.39	3.15
	0.559	0.479	609.0	0.191	0.067	5	750	4294	25906	0.115	0.432	0.260	10.7	0.63	0.21	1.85	3.32
	0.699	0.417	609.0	0.239	0.058	5	750	4294	25906	0.152	0.373	0.196	10.7	0.63	0.25	2.22	3.18
	0.831	0.525	609.0	0.284	0.073	5	750	4294	25906	0.193	0.477	0.205	10.7	0.63	0.28	2.60	3.12
	0.925	1.301	609.0	0.316	0.182	5	750	4294	25906	0.224	1.341	0.365	10.7	0.63	0.30	2.88	3.11
	1.058	***0.611***		***0.362***	***0.086***					***0.287***	***0.568***	***0.193***	***10.700***	***0.635***	***0.335***	***3.423***	***3.217***
D5	0.676	0.424	608.5	0.231	0.059	5	750	4294	25906	0.146	0.380	0.204	10.7	0.63	0.24	2.16	3.19
	0.899	0.438	608.5	0.307	0.061	5	750	4294	25906	0.215	0.393	0.166	10.7	0.63	0.29	2.80	3.11
	0.699	0.420	608.5	0.239	0.059	5	750	4294	25906	0.152	0.376	0.198	10.7	0.63	0.25	2.22	3.18
	0.859	0.454	608.5	0.294	0.063	5	750	4294	25906	0.202	0.408	0.178	10.7	0.63	0.28	2.68	3.11
	0.829	0.466	608.5	0.283	0.065	5	750	4294	25906	0.192	0.420	0.187	10.7	0.63	0.28	2.59	3.12
	0.834	0.445	608.5	0.285	0.062	5	750	4294	25906	0.193	0.400	0.179	10.7	0.63	0.28	2.60	3.12
	1.218	0.507	608.5	0.416	0.071	5	750	4294	25906	0.346	0.459	0.146	10.7	0.63	0.37	3.94	3.24
	1.235	0.469	608.5	0.422	0.066	5	750	4294	25906	0.354	0.422	0.134	10.7	0.63	0.38	4.02	3.25
	0.905	0.428	608.5	0.309	0.060	5	750	4294	25906	0.217	0.383	0.162	10.7	0.63	0.30	2.81	3.11
	0.763	0.428	608.5	0.261	0.060	5	750	4294	25906	0.171	0.383	0.187	10.7	0.63	0.26	2.40	3.14
	0.722	0.434	608.5	0.247	0.061	5	750	4294	25906	0.159	0.389	0.198	10.7	0.63	0.25	2.28	3.16
	0.946	0.423	608.5	0.323	0.059	5	750	4294	25906	0.232	0.378	0.155	10.7	0.63	0.31	2.94	3.11
	0.650	0.509	608.5	0.222	0.071	5	750	4294	25906	0.139	0.461	0.242	10.7	0.63	0.24	2.09	3.21
	0.921	0.440	608.5	0.315	0.061	5	750	4294	25906	0.223	0.394	0.163	10.7	0.63	0.30	2.87	3.11
	0.823	0.447	608.5	0.281	0.062	5	750	4294	25906	0.190	0.401	0.182	10.7	0.63	0.28	2.57	3.12
	0.871	0.489	608.5	0.298	0.068	5	750	4294	25906	0.206	0.441	0.187	10.7	0.63	0.29	2.71	3.11
	0.866	***0.451***		***0.296***	***0.063***					***0.209***	***0.406***	***0.179***	***10.700***	***0.635***	***0.287***	***2.730***	***3.151***
Loc 3																	
D26	0.906	0.682	610.3	0.311	0.096	5	750	4294	25906	0.219	0.636	0.235	10.7	0.63	0.30	2.83	3.12
	1.040	0.705	610.3	0.357	0.099	5	750	4294	25906	0.269	0.660	0.217	10.7	0.63	0.33	3.27	3.15
	0.982	0.983	610.3	0.337	0.138	5	750	4294	25906	0.246	0.962	0.290	10.7	0.63	0.32	3.07	3.13

	0.834	0.717	610.3	0.286	0.101	5	750	4294	25906	0.194	0.673	0.260	10.7	0.63	0.28	2.61	3.13
	0.977	1.047	610.3	0.335	0.147	5	750	4294	25906	0.244	1.036	0.305	10.7	0.63	0.31	3.06	3.13
	1.401	0.492	610.3	0.481	0.069	5	750	4294	25906	0.449	0.447	0.126	10.7	0.63	0.43	4.85	3.46
	0.976	0.600	610.3	0.335	0.084	5	750	4294	25906	0.244	0.554	0.201	10.7	0.63	0.31	3.05	3.13
	0.944	0.468	610.3	0.324	0.066	5	750	4294	25906	0.232	0.423	0.169	10.7	0.63	0.31	2.95	3.12
	0.751	0.280	610.3	0.258	0.039	5	750	4294	25906	0.168	0.246	0.132	10.7	0.63	0.26	2.37	3.16
	0.779	0.296	610.3	0.267	0.042	5	750	4294	25906	0.177	0.261	0.135	10.7	0.63	0.27	2.45	3.14
	0.806	0.288	610.3	0.276	0.040	5	750	4294	25906	0.185	0.253	0.127	10.7	0.63	0.27	2.53	3.13
	0.682	0.298	610.3	0.234	0.042	5	750	4294	25906	0.148	0.262	0.152	10.7	0.63	0.24	2.18	3.20
	0.734	0.076	610.3	0.252	0.011	5	750	4294	25906	0.163	0.065	0.041	10.7	0.63	0.26	2.32	3.16
	0.909	***0.533***		***0.312***	***0.075***					***0.226***	***0.498***	***0.184***	***10.700***	***0.635***	***0.298***	***2.888***	***3.166***
Loc 4																	
10	0.991	0.946	615.0	0.342	0.134	5	750	4294	25906	0.252	0.929	0.281	10.7	0.63	0.32	3.13	3.16
	0.941	0.936	615.0	0.325	0.134	5	750	4294	25906	0.234	0.929	0.291	10.7	0.63	0.31	2.96	3.15
	1.072	1.064	615.0	0.370	0.132	5	750	4294	25906	0.285	0.917	0.263	10.7	0.63	0.34	3.42	3.19
	1.001	***0.982***		***0.346***	***0.133***					***0.257***	***0.925***	***0.278***	***10.700***	***0.635***	***0.322***	***3.169***	***3.164***
12	0.886	0.648	611.5	0.304	0.091	5	750	4294	25906	0.212	0.604	0.230	10.7	0.63	0.29	2.77	3.13
	0.834	0.637	611.5	0.286	0.090	5	750	4294	25906	0.195	0.592	0.238	10.7	0.63	0.28	2.61	3.13
	0.821	0.706	611.5	0.282	0.099	5	750	4294	25906	0.190	0.663	0.260	10.7	0.63	0.28	2.57	3.14
	0.840	0.692	611.5	0.289	0.097	5	750	4294	25906	0.197	0.648	0.252	10.7	0.63	0.28	2.63	3.13
	0.909	0.936	611.5	0.312	0.132	5	750	4294	25906	0.220	0.911	0.296	10.7	0.63	0.30	2.84	3.13
	0.858	***0.724***		***0.295***	***0.102***					***0.203***	***0.684***	***0.256***	***10.700***	***0.635***	***0.286***	***2.687***	***3.131***
60	0.724	0.988	611.0	0.249	0.139	5	750	4294	25906	0.161	0.970	0.358	10.7	0.63	0.25	2.30	3.17
	0.856	1.278	611.0	0.294	0.180	5	750	4294	25906	0.202	1.317	0.379	10.7	0.63	0.29	2.68	3.13
	0.676	0.830	611.0	0.232	0.117	5	750	4294	25906	0.146	0.794	0.335	10.7	0.63	0.24	2.16	3.20
	0.695	0.490	611.0	0.239	0.069	5	750	4294	25906	0.152	0.445	0.224	10.7	0.63	0.25	2.22	3.19
	0.668	0.565	611.0	0.229	0.079	5	750	4294	25906	0.144	0.519	0.257	10.7	0.63	0.24	2.15	3.21
	0.617	0.527	611.0	0.212	0.074	5	750	4294	25906	0.130	0.481	0.259	10.7	0.63	0.23	2.01	3.26
	0.742	0.606	611.0	0.255	0.085	5	750	4294	25906	0.166	0.560	0.251	10.7	0.63	0.26	2.35	3.16
	0.816	0.572	611.0	0.280	0.080	5	750	4294	25906	0.189	0.526	0.223	10.7	0.63	0.28	2.56	3.14
	0.693	0.558	611.0	0.238	0.078	5	750	4294	25906	0.151	0.512	0.248	10.7	0.63	0.25	2.21	3.19
	1.028	0.512	611.0	0.353	0.072	5	750	4294	25906	0.265	0.466	0.169	10.7	0.63	0.33	3.24	3.15
	0.661	0.654	611.0	0.227	0.092	5	750	4294	25906	0.142	0.608	0.288	10.7	0.63	0.24	2.12	3.22
	0.690	1.179	611.0	0.237	0.166	5	750	4294	25906	0.150	1.195	0.412	10.7	0.63	0.25	2.20	3.19
	0.739	***0.730***		***0.254***	***0.103***					***0.167***	***0.699***	***0.284***	***10.700***	***0.635***	***0.258***	***2.349***	***3.184***
X	1.323	0.886	610.3	0.454	0.124	5	750	4294	25906	0.403	0.854	0.215	10.7	0.63	0.40	4.45	3.36
	0.813	1.003	610.3	0.279	0.141	5	750	4294	25906	0.187	0.985	0.335	10.7	0.63	0.27	2.55	3.13
	0.678	0.749	610.3	0.232	0.105	5	750	4294	25906	0.147	0.707	0.312	10.7	0.63	0.24	2.17	3.20
	0.808	0.878	610.3	0.277	0.123	5	750	4294	25906	0.186	0.845	0.308	10.7	0.63	0.27	2.53	3.13
	0.766	0.842	610.3	0.263	0.118	5	750	4294	25906	0.173	0.806	0.310	10.7	0.63	0.26	2.41	3.15
	0.726	0.710	610.3	0.249	0.100	5	750	4294	25906	0.161	0.666	0.286	10.7	0.63	0.25	2.30	3.17
	0.880	0.718	610.3	0.302	0.101	5	750	4294	25906	0.210	0.674	0.250	10.7	0.63	0.29	2.75	3.12
	0.856	***0.827***		***0.294***	***0.116***					***0.209***	***0.791***	***0.288***		***0.635***	***0.286***	***2.736***	***3.181***

Loc 5																	
103	0.990	0.340	615.0	0.342	0.048	5	660	3569	28266	0.204	0.279	0.123	9.8	0.61	0.28	2.57	2.59
	1.045	0.215	615.0	0.361	0.030	5	660	3569	28266	0.222	0.174	0.078	9.8	0.61	0.29	2.72	2.60
	1.014	0.233	615.0	0.350	0.033	5	660	3569	28266	0.212	0.188	0.086	9.8	0.61	0.28	2.63	2.59
	0.928	0.211	615.0	0.321	0.030	5	660	3569	28266	0.185	0.170	0.085	9.8	0.61	0.26	2.41	2.59
	0.944	0.188	615.0	0.326	0.027	5	660	3569	28266	0.190	0.151	0.075	9.8	0.61	0.27	2.45	2.59
	1.035	0.200	615.0	0.358	0.028	5	660	3569	28266	0.218	0.161	0.073	9.8	0.61	0.29	2.69	2.60
	1.035	0.216	615.0	0.358	0.031	5	660	3569	28266	0.218	0.175	0.079	9.8	0.61	0.29	2.69	2.60
	0.929	0.249	615.0	0.321	0.035	5	660	3569	28266	0.186	0.203	0.099	9.8	0.61	0.26	2.41	2.59
	1.006	0.192	615.0	0.347	0.027	5	660	3569	28266	0.209	0.155	0.073	9.8	0.61	0.28	2.61	2.59
	1.074	0.191	615.0	0.371	0.027	5	660	3569	28266	0.232	0.154	0.068	9.8	0.61	0.29	2.80	2.60
	1.018	0.186	615.0	0.352	0.026	5	660	3569	28266	0.213	0.150	0.070	9.8	0.61	0.28	2.64	2.59
	0.945	0.172	615.0	0.326	0.024	5	660	3569	28266	0.190	0.138	0.069	9.8	0.61	0.27	2.45	2.59
	0.954	0.172	615.0	0.330	0.024	5	660	3569	28266	0.193	0.138	0.069	9.8	0.61	0.27	2.47	2.59
	0.994	***0.213***		***0.343***	***0.030***					***0.206***	***0.172***	***0.080***		***0.612***	***0.277***	***2.578***	***2.595***
104	1.192	0.478	615.4	0.412	0.068	5	660	3569	28266	0.275	0.402	0.141	9.8	0.61	0.32	3.16	2.65
	0.989	0.216	615.4	0.342	0.031	5	660	3569	28266	0.204	0.175	0.082	9.8	0.61	0.28	2.56	2.59
	1.102	0.532	615.4	0.381	0.075	5	660	3569	28266	0.242	0.451	0.165	9.8	0.61	0.30	2.88	2.61
	1.119	0.457	615.4	0.387	0.065	5	660	3569	28266	0.248	0.383	0.143	9.8	0.61	0.30	2.93	2.62
	1.013	0.755	615.4	0.350	0.107	5	660	3569	28266	0.212	0.662	0.234	9.8	0.61	0.28	2.63	2.60
	1.105	0.273	615.4	0.382	0.039	5	660	3569	28266	0.243	0.223	0.092	9.8	0.61	0.30	2.89	2.61
	1.074	0.654	615.4	0.371	0.093	5	660	3569	28266	0.232	0.565	0.200	9.8	0.61	0.29	2.80	2.61
	1.085	***0.481***		***0.375***	***0.068***					***0.236***	***0.409***	***0.151***		***0.612***	***0.297***	***2.836***	***2.613***
Loc 6																	
17	1.558	0.807	610.3	0.534	0.113	5	750	4294	25906	0.556	0.768	0.175	10.7	0.63	0.47	5.84	3.75
	0.848	0.588	610.3	0.291	0.083	5	750	4294	25906	0.199	0.541	0.221	10.7	0.63	0.28	2.65	3.13
	1.017	0.951	610.3	0.349	0.133	5	750	4294	25906	0.260	0.927	0.277	10.7	0.63	0.32	3.19	3.14
	0.905	0.589	610.3	0.310	0.083	5	750	4294	25906	0.218	0.542	0.210	10.7	0.63	0.30	2.82	3.12
	1.212	0.604	610.3	0.416	0.085	5	750	4294	25906	0.345	0.558	0.169	10.7	0.63	0.37	3.94	3.25
	1.322	0.726	610.3	0.453	0.102	5	750	4294	25906	0.402	0.683	0.184	10.7	0.63	0.40	4.44	3.36
	0.905	0.642	610.3	0.310	0.090	5	750	4294	25906	0.218	0.596	0.225	10.7	0.63	0.30	2.83	3.12
	1.001	0.581	610.3	0.343	0.081	5	750	4294	25906	0.254	0.534	0.192	10.7	0.63	0.32	3.14	3.13
	0.971	0.598	610.3	0.333	0.084	5	750	4294	25906	0.242	0.551	0.201	10.7	0.63	0.31	3.04	3.13
	0.755	0.620	610.3	0.259	0.087	5	750	4294	25906	0.169	0.574	0.252	10.7	0.63	0.26	2.38	3.15
	1.016	0.639	610.3	0.348	0.090	5	750	4294	25906	0.259	0.593	0.205	10.7	0.63	0.32	3.19	3.14
	1.368	0.624	610.3	0.469	0.088	5	750	4294	25906	0.429	0.577	0.157	10.7	0.63	0.42	4.67	3.42
	1.285	0.644	610.3	0.441	0.090	5	750	4294	25906	0.382	0.598	0.170	10.7	0.63	0.39	4.26	3.32
	1.112	0.606	610.3	0.381	0.085	5	750	4294	25906	0.299	0.559	0.182	10.7	0.63	0.35	3.54	3.18
	0.822	0.606	610.3	0.282	0.085	5	750	4294	25906	0.190	0.559	0.232	10.7	0.63	0.28	2.57	3.13
	0.871	0.643	610.3	0.299	0.090	5	750	4294	25906	0.206	0.596	0.232	10.7	0.63	0.29	2.72	3.12
	0.797	0.642	610.3	0.273	0.090	5	750	4294	25906	0.182	0.596	0.248	10.7	0.63	0.27	2.50	3.14
	0.988	0.649	610.3	0.339	0.091	5	750	4294	25906	0.249	0.603	0.212	10.7	0.63	0.32	3.09	3.13
	0.877	0.572	610.3	0.301	0.080	5	750	4294	25906	0.209	0.526	0.211	10.7	0.63	0.29	2.74	3.12
	0.666	0.575	610.3	0.229	0.081	5	750	4294	25906	0.144	0.528	0.261	10.7	0.63	0.24	2.14	3.21
	0.919	0.571	610.3	0.315	0.080	5	750	4294	25906	0.223	0.524	0.203	10.7	0.63	0.30	2.87	3.12
	0.890	0.525	610.3	0.305	0.074	5	750	4294	25906	0.213	0.479	0.195	10.7	0.63	0.29	2.78	3.12
	0.877	0.844	610.3	0.301	0.118	5	750	4294	25906	0.209	0.809	0.283	10.7	0.63	0.29	2.74	3.12

	0.679	0.518	610.3	0.233	0.073	5	750	4294	25906	0.147	0.471	0.238	10.7	0.63	0.24	2.17	3.20
	0.986	***0.640***		***0.338***	***0.090***					***0.259***	***0.595***	***0.214***		***0.635***	***0.318***	***3.177***	***3.198***
Loc 7																	
148	1.098	0.547	610.3	0.376	0.077	5	750	4294	25906	0.293	0.500	0.169	10.7	0.63	0.34	3.48	3.17
	1.337	0.582	610.3	0.458	0.082	5	750	4294	25906	0.410	0.535	0.151	10.7	0.63	0.41	4.51	3.38
	1.053	0.573	610.3	0.361	0.080	5	750	4294	25906	0.274	0.526	0.182	10.7	0.63	0.33	3.32	3.15
	1.354	0.623	610.3	0.464	0.087	5	750	4294	25906	0.420	0.576	0.158	10.7	0.63	0.41	4.60	3.40
	1.149	0.585	610.3	0.394	0.082	5	750	4294	25906	0.315	0.539	0.173	10.7	0.63	0.36	3.68	3.20
	0.984	0.634	610.3	0.337	0.089	5	750	4294	25906	0.247	0.588	0.209	10.7	0.63	0.32	3.08	3.13
	0.785	0.592	610.3	0.269	0.083	5	750	4294	25906	0.179	0.546	0.236	10.7	0.63	0.27	2.47	3.14
	1.108	***0.591***		***0.380***	***0.083***					***0.305***	***0.544***	***0.183***		***0.635***	***0.348***	***3.591***	***3.224***
D35	1.098	0.547	610.3	0.376	0.077	5	750	4294	25906	0.293	0.500	0.169	10.7	0.63	0.34	3.48	3.17
	1.337	0.582	610.3	0.458	0.082	5	750	4294	25906	0.410	0.535	0.151	10.7	0.63	0.41	4.51	3.38
	1.053	0.573	610.3	0.361	0.080	5	750	4294	25906	0.274	0.526	0.182	10.7	0.63	0.33	3.32	3.15
	1.238	0.453	610.3	0.424	0.064	5	750	4294	25906	0.358	0.409	0.130	10.7	0.63	0.38	4.05	3.27
	1.108	0.411	610.3	0.380	0.058	5	750	4294	25906	0.297	0.369	0.132	10.7	0.63	0.35	3.52	3.18
	1.004	0.466	610.3	0.344	0.065	5	750	4294	25906	0.255	0.421	0.160	10.7	0.63	0.32	3.15	3.13
	0.878	0.419	610.3	0.301	0.059	5	750	4294	25906	0.209	0.376	0.163	10.7	0.63	0.29	2.74	3.12
	1.102	***0.493***		***0.378***	***0.069***					***0.299***	***0.448***	***0.155***		***0.635***	***0.345***	***3.539***	***3.201***
Loc 12																	
18	1.220	1.188	615.0	0.422	0.168	5	660	3569	28266	0.286	1.119	0.285	9.8	0.61	0.33	3.25	2.66
	1.053	1.031	615.0	0.364	0.146	5	660	3569	28266	0.225	0.945	0.286	9.8	0.61	0.29	2.74	2.60
	1.239	1.206	615.0	0.428	0.170	5	660	3569	28266	0.294	1.139	0.285	9.8	0.61	0.33	3.31	2.67
	0.982	0.964	615.0	0.339	0.136	5	660	3569	28266	0.202	0.874	0.286	9.8	0.61	0.27	2.55	2.59
	1.183	1.153	615.0	0.409	0.163	5	660	3569	28266	0.271	1.079	0.285	9.8	0.61	0.32	3.13	2.64
	1.277	1.242	615.0	0.441	0.176	5	660	3569	28266	0.310	1.180	0.285	9.8	0.61	0.34	3.44	2.69
	1.063	1.040	615.0	0.367	0.147	5	660	3569	28266	0.228	0.955	0.286	9.8	0.61	0.29	2.76	2.60
	1.145	***1.118***		***0.396***	***0.158***					***0.259***	***1.042***	***0.285***		***0.612***	***0.311***	***3.024***	***2.637***
19	1.224	0.167	615.0	0.423	0.024	5	660	3569	28266	0.288	0.134	0.053	9.8	0.61	0.33	3.26	2.66
	1.297	0.123	615.0	0.448	0.017	5	660	3569	28266	0.319	0.098	0.037	9.8	0.61	0.35	3.51	2.71
	1.187	0.128	615.0	0.410	0.018	5	660	3569	28266	0.273	0.102	0.042	9.8	0.61	0.32	3.14	2.64
	1.352	0.139	615.0	0.467	0.020	5	660	3569	28266	0.344	0.111	0.040	9.8	0.61	0.36	3.72	2.75
	1.305	0.140	615.0	0.451	0.020	5	660	3569	28266	0.322	0.112	0.042	9.8	0.61	0.35	3.54	2.71
	1.264	0.132	615.0	0.437	0.019	5	660	3569	28266	0.305	0.105	0.041	9.8	0.61	0.34	3.40	2.69
	1.389	0.096	615.0	0.480	0.014	5	660	3569	28266	0.363	0.076	0.028	9.8	0.61	0.37	3.87	2.78
	1.346	0.125	615.0	0.465	0.018	5	660	3569	28266	0.341	0.099	0.036	9.8	0.61	0.36	3.69	2.74
	1.070	0.252	615.0	0.370	0.036	5	660	3569	28266	0.230	0.204	0.088	9.8	0.61	0.29	2.79	2.60
	1.271	***0.144***		***0.439***	***0.020***					***0.309***	***0.116***	***0.045***		***0.612***	***0.340***	***3.434***	***2.699***
D45	0.757	0.576	615.0	0.262	0.081	5	660	3569	28266	0.139	0.491	0.237	9.8	0.61	0.23	2.00	2.64
	1.018	0.674	615.0	0.352	0.095	5	660	3569	28266	0.213	0.583	0.213	9.8	0.61	0.28	2.64	2.59
	0.980	0.648	615.0	0.339	0.092	5	660	3569	28266	0.201	0.559	0.213	9.8	0.61	0.27	2.54	2.59
	0.738	0.517	615.0	0.255	0.073	5	660	3569	28266	0.134	0.437	0.223	9.8	0.61	0.22	1.95	2.65
	0.862	0.481	615.0	0.298	0.068	5	660	3569	28266	0.167	0.404	0.186	9.8	0.61	0.25	2.24	2.60
	0.720	0.666	615.0	0.249	0.094	5	660	3569	28266	0.130	0.576	0.274	9.8	0.61	0.22	1.91	2.66

	0.735	0.388	615.0	0.254	0.055	5	660	3569	28266	0.134	0.322	0.178	9.8	0.61	0.22	1.95	2.65
	0.830	***0.564***		***0.287***	***0.080***					***0.160***	***0.482***	***0.218***		***0.612***	***0.243***	***2.177***	***2.626***
47	1.258	0.616	615.0	0.435	0.087	5	660	3569	28266	0.302	0.528	0.167	9.8	0.61	0.34	3.37	2.68
	1.538	0.359	615.0	0.531	0.051	5	660	3569	28266	0.445	0.296	0.087	9.8	0.61	0.41	4.54	2.95
	1.211	0.460	615.0	0.418	0.065	5	660	3569	28266	0.282	0.385	0.135	9.8	0.61	0.33	3.21	2.65
	1.095	0.286	615.0	0.378	0.040	5	660	3569	28266	0.239	0.233	0.096	9.8	0.61	0.30	2.86	2.61
	1.389	0.279	615.0	0.480	0.039	5	660	3569	28266	0.362	0.227	0.076	9.8	0.61	0.37	3.86	2.78
	1.299	0.320	615.0	0.449	0.045	5	660	3569	28266	0.320	0.263	0.092	9.8	0.61	0.35	3.52	2.71
	1.270	0.306	615.0	0.439	0.043	5	660	3569	28266	0.307	0.251	0.090	9.8	0.61	0.34	3.41	2.69
	0.969	0.316	615.0	0.335	0.045	5	660	3569	28266	0.198	0.259	0.118	9.8	0.61	0.27	2.51	2.59
	1.339	0.306	615.0	0.463	0.043	5	660	3569	28266	0.338	0.250	0.085	9.8	0.61	0.36	3.67	2.74
	1.120	0.318	615.0	0.387	0.045	5	660	3569	28266	0.248	0.261	0.104	9.8	0.61	0.30	2.93	2.62
	1.249	***0.357***		***0.431***	***0.050***					***0.304***	***0.295***	***0.105***		***0.612***	***0.335***	***3.389***	***2.702***
Loc 17																	
145	1.242	0.249	610.0	0.426	0.035	5	660	3569	28266	0.291	0.201	0.076	9.8	0.61	0.33	3.28	2.64
	1.299	0.227	610.0	0.445	0.032	5	660	3569	28266	0.315	0.182	0.067	9.8	0.61	0.34	3.48	2.68
	1.528	0.441	610.0	0.524	0.062	5	660	3569	28266	0.432	0.365	0.106	9.8	0.61	0.40	4.43	2.90
	1.155	0.364	610.0	0.396	0.051	5	660	3569	28266	0.257	0.298	0.114	9.8	0.61	0.31	3.01	2.60
	1.097	0.423	610.0	0.376	0.059	5	660	3569	28266	0.236	0.349	0.136	9.8	0.61	0.30	2.84	2.59
	1.327	0.405	610.0	0.455	0.057	5	660	3569	28266	0.328	0.334	0.111	9.8	0.61	0.35	3.58	2.70
	0.936	0.388	610.0	0.321	0.054	5	660	3569	28266	0.185	0.318	0.145	9.8	0.61	0.26	2.41	2.57
	1.486	0.410	610.0	0.509	0.058	5	660	3569	28266	0.408	0.338	0.101	9.8	0.61	0.39	4.23	2.85
	1.308	0.530	610.0	0.448	0.074	5	660	3569	28266	0.319	0.445	0.142	9.8	0.61	0.35	3.51	2.68
	1.295	0.428	610.0	0.444	0.060	5	660	3569	28266	0.313	0.354	0.119	9.8	0.61	0.34	3.47	2.68
	1.165	0.431	610.0	0.399	0.060	5	660	3569	28266	0.261	0.356	0.131	9.8	0.61	0.31	3.04	2.61
	1.427	0.446	610.0	0.489	0.063	5	660	3569	28266	0.376	0.370	0.113	9.8	0.61	0.37	3.97	2.78
	1.272	**0.395**		**0.436**	**0.055**					**0.310**	**0.326**	**0.114**		**0.612**	**0.338**	**3.437**	**2.690**
Loc 20																	
31	0.930	0.087	615.0	0.321	0.012	5	660	3569	28266	0.186	0.069	0.037	9.8	0.61	0.26	2.41	2.59
	1.237	0.087	615.0	0.427	0.012	5	660	3569	28266	0.293	0.069	0.028	9.8	0.61	0.33	3.30	2.67
	1.167	0.087	615.0	0.403	0.012	5	660	3569	28266	0.265	0.069	0.030	9.8	0.61	0.31	3.07	2.63
	1.111	***0.087***		***0.384***	***0.012***					***0.248***	***0.069***	***0.032***		***0.612***	***0.303***	***2.929***	***2.632***

Appendix 8 - Stepped heating analysis of cordierite

A8.1 Samples

Table A8.1 - List of cordierite samples and their weight (Wt) in mg. L stands for locality.

SAMPLE	L	DESCRIPTION	Wt
1	3	Mostly mesosome with a small garnet dominated leucosome patch.	198.4
XA	4	Large, cream, cordierite-rich leucosome.	47.2
XB	4	Large, cream, cordierite-rich leucosome.	36.3
XC	4	Large, cream, cordierite-rich leucosome.	45.3
XD	4	Large, cream, cordierite-rich leucosome.	47.7
103	5	2 cm wide cordierite-rich, selvage bound leucosome.	31.8
104a	5	Smaller sample containing mostly cordierite-rich leucosome.	122.3
16	6	Coarse leucosome with biotite patches.	218.2
17	6	Coarse leucosome with cordierite patches.	122.8
148B	7	Cordierite+graphite sample, predominantly small, pale leucosome.	49.5
148C	7	Cordierite+graphite sample, predominantly small, pale leucosome.	59.3
148bA	7	Cordierite+graphite sample, predominantly small, pale leucosome.	34.8
148bB	7	Cordierite+graphite sample, predominantly small, pale leucosome.	29.2
44	12	Edge of small leucosomes with large poikiloblastic garnet.	51.07

A8.2 - preparation

A8.2.1 - Cleaning procedure

1. Check for carbonates by immersing sample in 10% HCl. Place in ultrasonic bath for 3 minutes.
2. Rinse in distilled water, then place back in the ultrasonic bath for 3 minutes. Repeat.
3. Pour off water and pour in acetone. Place in ultrasonic for 3 minutes. Pour off acetone and place in oven to dry off.
4. Fill beaker with dichloromethane and place in ultrasonic bath for 3 minutes.
5. Empty and then refill to halfway up beaker. Ultrasonic for 3 minutes.
6. Dry out and weigh sample.
7. Load sample into sample finger of the stepped heating line (Figure A8.1)

A8.2.2 - Oxygen production

1. 500 millibars of oxygen are generated by heating a copper oxide coil to 920°C. This is frozen into a molecular sieve with liquid nitrogen. This process takes thirty minutes.
2. The oxygen is liberated and passed into the sample finger.
3. As combustion is only carried out for the 400°C step, excess oxygen is returned to the sieve and up to the copper coil which is reduced to a reabsorption temperature.

Figure A8.1 - Stepped heating line.

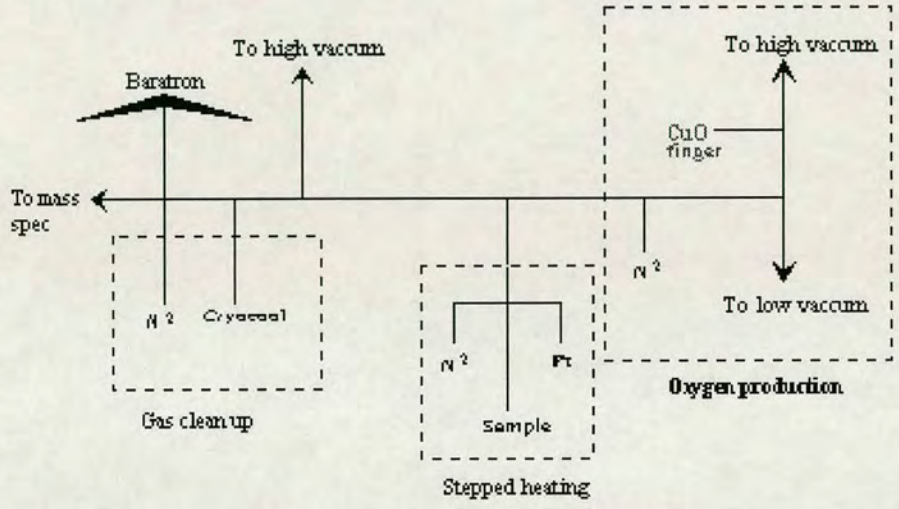

A8.2.3 - Stepped heating

The first step is a combustion step and is carried out in the presence of oxygen, produced as described in A8.2.2.

1. Place a furnace over the sample finger and insert a thermocouple.
2. Heat the furnace to 400°C and leave for thirty minutes whilst the evolving gasses are frozen with liquid nitrogen into a collection finger.
3. The gas clean up procedure (A8.2.4) is carried out for each step. Remaining steps (600, 700, 800, 900, 1000, 1100 and 1200°C) are carried out under vacuum.

A8.2.4 - Gas clean up

1. The line is isolated from the pumps and the gases are transferred to the clean up section of the line (see Figure A8.1).

2. Once fully transferred the sample finger is once again isolated and the temperature is increased for the next step.
3. Once in the clean-up section of the line CO_2 is extracted. CO_2 is liberated around -135°C. Thus a cryocool is used to first take the gas down to -192°C using liquid nitrogen, the gas is then heated to the ambient temperature required for gas extraction by heating the metal coil within the liquid nitrogen.
4. The evolved CO_2 is frozen into a Baratron finger where it is isolated, its volume is measured and then it is passed into the Dual Inlet Mass spectrometer for analysis.

A8.3 Results

The stepped heating data for the samples analysed is shown in Table A8.2.

Table A8.2 - Stepped heating data for 14 samples analysed (samples are described in Table A8.1). Wt% CO_2 yields $d^{13}C$ (in per mil) and carbon yields (in ppm) are shown for each heating step from 400 to 1200°C.
N/D - The step was missed for that sample and so not detected.

T	1	XA	XB	XC	XD	103	104	16	17	148B	148C	148BA	148BB	44
Wt % CO_2														
400	0.01	0.00	0.00	0.01	N/D	0.02	0.01	0.01	0.01	**N/D**	**N/D**	0.01	0.01	0.02
600	**N/D**	0.03	0.02	0.05	0.06	**N/D**	**N/D**	**N/D**	**N/D**	0.01	0.01	**N/D**	**N/D**	**N/D**
700	0.04	0.04	0.00	0.65	0.07	0.07	0.00	0.00	0.03	0.02	0.01	0.01	0.07	0.01
800	0.04	0.10	0.26	0.13	0.12	0.01	0.01	1.04	0.05	0.03	0.02	0.03	0.03	0.07
900	0.16	0.15	0.15	0.11	0.16	0.00	0.00	0.44	0.08	0.09	0.08	0.17	0.17	0.05
1000	0.18	0.15	0.07	0.05	0.10	0.01	0.01	0.40	0.31	0.15	0.20	0.14	0.13	0.05
1100	0.15	0.08	0.04	0.05	0.05	0.01	0.01	0.10	0.10	0.06	0.06	0.04	0.06	0.04
1200	0.06	0.04	0.02	0.03	0.02	0.01	0.02	0.02	0.03	0.02	0.03	0.02	**N/D**	0.01
1200	0.18	**N/D**	**N/D**	0.01	0.01	0.00	0.01	0.01	0.01	0.01	0.01	0.00	**N/D**	0.00
Total	0.58	0.53	0.54	0.37	0.45	0.04	0.03	2.00	0.56	0.35	0.39	0.39	0.38	0.22
$\delta^{13}C$														
400	-24.47	-26.90	-30.00	-20.37	-19.79	-30.01	-31.98	-20.80	-28.92	**N/D**	**N/D**	-23.10	-32.83	-26.66
600	**N/D**	-22.90	-14.45	**N/D**	**N/D**	**N/D**	**N/D**	**N/D**	**N/D**	-28.96	-24.47	**N/D**	**N/D**	**N/D**
700	-18.04	-8.78	-30.00	-8.34	-8.21	-25.32	-25.50	**N/D**	-16.73	-14.78	-15.04	-13.47	-48.48	-15.44
800	-16.69	-7.81	-7.41	-7.63	-7.71	-21.76	-23.41	-14.38	-15.23	-12.86	-13.34	-13.00	-13.19	-7.62
900	-16.40	-7.74	-8.22	-7.61	-7.42	-18.00	-23.77	-14.02	-15.21	-12.65	-12.60	-12.86	-12.22	-6.68
1000	-16.37	-7.63	-7.45	-7.63	-7.32	-28.68	-24.15	-14.05	-14.12	-12.52	-12.45	-12.57	-12.31	-6.92
1100	-16.50	-7.82	-7.78	-7.68	-7.28	-23.11	-25.23	-14.69	-14.60	-12.47	-12.48	-12.75	-12.00	-6.82
1200	-16.69	-8.26	-9.19	-7.40	-7.98	-24.45	-24.77	-15.38	-15.37	-12.15	-12.48	-12.22	**N/D**	-6.99
1200	-16.98	**N/D**	**N/D**	-9.61	-8.58	-27.33	-24.75	-15.90	-15.70	-13.23	-11.04	-12.81	**N/D**	-7.91
ppm C														
400	28.80	17.80	6.20	29.70	162.50	42.30	19.20	26.90	14.10	**N/D**	**N/D**	27.60	19.70	65.00
600	**N/D**	69.60	49.40	**N/D**	**N/D**	**N/D**	**N/D**	**N/D**	**N/D**	12.90	35.50	**N/D**	**N/D**	**N/D**
700	105.60	105.20	0.10	132.70	179.90	185.20	11.20	6.40	89.60	56.90	18.40	27.60	199.50	34.60
800	105.60	281.50	701.40	177.20	328.30	32.20	14.40	2848.00	129.00	78.20	53.40	74.60	83.30	192.00
900	422.40	398.20	415.60	347.40	431.60	0.00	1.80	1203.20	210.20	246.30	223.40	460.30	449.50	147.20
1000	486.40	419.90	195.00	306.40	268.50	21.10	16.60	1078.40	838.40	408.60	540.80	369.20	355.20	134.40
1100	409.60	224.50	110.30	141.20	143.70	23.20	14.70	259.20	281.60	169.40	167.90	119.70	150.20	99.20
1200	169.60	118.70	65.30	77.70	63.10	23.20	42.60	63.40	70.40	61.40	70.70	46.00	**N/D**	21.10
1200	48.00	**N/D**	**N/D**	19.10	15.40	12.10	16.60	19.80	17.00	14.90	16.20	9.20	**N/D**	0.00
	1776.00	1635.40	1543.30	1231.40	1593.00	339.30	137.10	5505.30	1650.30	1048.60	1126.30	1134.20	1257.40	693.50